THE SEAGRASS RHIZOSPHERE

KASPER ELGETTI BRODERSEN

The Seagrass Rhizosphere

Kasper Elgetti Brodersen

MSc. in Eng. Aquatic Science and Technology
Seagrass Health Research Group
Plant Functional Biology and Climate Change Cluster (C3)

Thesis submitted for the degree of Doctor of Philosophy
at the University of Technology Sydney I June 10, 2016

CERTIFICATE OF ORIGINAL AUTHORSHIP

This thesis is the result of a research candidature conducted jointly with another University as part of a collaborative Doctoral degree. I certify that the work in this thesis has not previously been submitted for a degree nor has it been submitted as part of requirements for a degree except as part of the collaborative doctoral degree and/or fully acknowledged within the text.

I also certify that the thesis has been written by me. Any help that I have received in my research work and the preparation of the thesis itself has been acknowledged. In addition, I certify that all information sources and literature used are indicated in the thesis.

Signature of Student:

Date: June 10, 2016

ACKNOWLEDGEMENTS

I would like to thank my supervisors: Michael Kühl, Daniel A. Nielsen, Ole Pedersen and Peter J. Ralph, without whom I would never have been able to complete this PhD thesis and who all provided editorial assistance to this work. Michael you have been the greatest support of all and the best ever imagined mentor during my PhD project. Thank you very much. Daniel you were my solid support at UTS, and patiently helped me sorting my mind especially during the first year of my PhD, which made me stay on track and keep focussed. Thanks. Ole you appeared a bit later in my PhD project, but I will always remember our voyage back to shore at Narrabeen Lagoon (both mentally and physically) with all our sensitive equipment and data in the rubber dinghy; and how you guided me through that challenging phase of my PhD. Peter you have provided the perfect research facility to overcome the challenge of submitting this PhD thesis, and I could not have wished for a better place to undertake my PhD candidature. Thanks.

Friends and colleges: Mads Lichtenberg, Klaus Koren, Jakob Santner, Mathieu Pernice, Nahshon Siboni, Justin Seymour, Paul York, Michael Rasheed, Maria Mosshammer, Kathrine Jul Hammer, Stacey M. Trevathan-Tackett, Laura-Carlota Paz, Sofie L. Jakobsen, Tony Larkum, Anja Frøytrup, Milan Szabo, Katherina Petrou, Dale Radford, Michele Fabris, Joey Crosswell, Jean-Baptiste Raina, Katie Chartrand, Bojana Manojlovic, Peter Davey, Alex Thomson, Jeff Kelleway, Jessica Tout, Daniel Wangpraseurt, Verena Schrameyer, and all the people I have forgotten; thanks for all the fun experiences in the laboratory, good companionships, long scientific and less-scientific talks and nice research. I am looking very much forward to continue our collaborations in the future.

Thanks to my overseas family for supporting me on this personal dream of mine; of both undertaking a PhD, but as much experiencing the adventures and challenges of moving to and living in Australia.

Lastly, in my mind a PhD is like a journey from a to b, where you in the beginning of your PhD stand at the bottom of a mountain, a big impressive mountain with a threatening glacier close to the summit, and you know that somehow in the end of this journey you will have to find yourself on the top of that mountain planting your personal mark, for forever

sight, into the solid rocky ground. But as in all other aspects of life, it is important to remember to focus on the journey itself and not on reaching the final goal, as else you will often find yourself forgetting the purpose of your challenge and thus lose yourself on your way ("journey") to the summit. I therefore dedicate my PhD thesis to my little, much beloved, family. Karla, Rufus and Verena, without you guys I could never have done this, and for that I am you forever grateful. Thanks, with all the love of my heart.

Kasper Elgetti Brodersen

June 10, 2016

"Analysing the below-ground biogeochemical microenvironment of seagrasses to determine how changing environmental conditions affect seagrass health"

Table of Contents

List of Figures

List of Tables

Summary

Seagrass meadows are important marine ecosystems providing an array of ecosystem services to aquatic and terrestrial environments including sediment stabilisation, acting as shelter, feeding and nursery grounds for numerous marine species and even mitigating climate change through their ability to capture and store carbon in the sediment for millennia. However, owing to anthropogenic interference, seagrass meadows worldwide are shrinking, putting essential ecosystem functions at risk. Understanding the basic mechanisms that control the fitness of seagrasses is necessary in order to elucidate how human activities and changing environmental conditions is affecting the seagrass ecosystems and what can be done to better manage them. Through a series of experiments employing high-resolution measuring techniques including luminescence imaging, microsensors and novel optical sensor nanoparticles, this thesis explores the mechanisms of seagrass sediment detoxification and nutrient mobilisation, and the effect of environmental stressors on these essential processes.

We show that radial O_2 loss from the below-ground tissue leads to formation of oxic microshields that re-oxidates phytotoxic H_2S in the rhizosphere and thus results in sediment detoxification; a vital seagrass-derived chemical defence mechanism that is adversely affected by water-column hypoxia. These seagrass-driven alterations of the rhizosphere biogeochemistry modulate the microbial community composition at the plant/sediment interface, potentially increasing the rhizospheric nitrogen availability owing to microbial-mediated nitrogen fixation. We also found that the leaf microenvironment largely controls the intra-plant O_2 conditions and thus the below-ground tissue oxidation capacity, where sediment deposition and epiphyte overgrowth on leaves negatively affects the internal plant aeration through multiple pathways, such as (i) enhancing the thickness of the mass transfer impeding diffusive boundary layer around the leaves, (ii) reducing the light availability/quality for photosynthesis, and (iii) enhancing the over-night respiration rates in the phyllosphere. Finally, we show that seagrass-driven alterations of the rhizosphere pH microenvironment leads to development of low-pH microniches around the below-ground tissue, corresponding to the seagrass-derived oxic microzones, that results in pronounced

rhizospheric phosphorus and iron mobilization for seagrasses colonizing phosphorous-limited carbonate-rich sediments.

The results of this thesis brings to light the overarching importance of internal tissue aeration in seagrasses through its effect on rhizospheric biogeochemical processes and conditions, and thus underlines the need for minimizing environmental stressors leading to inadequate internal aeration, such as water-column hypoxia and sediment re-suspension, for seagrass health in changing oceans.

GENERAL INTRODUCTION

The Seagrass Rhizosphere

GENERAL INTRODUCTION

Seagrass meadows are among the most productive ecosystems on Earth providing a range of key ecological services such as enhancing marine biodiversity by providing feeding grounds and nursery areas for many important marine species such as sea turtles, dugongs, juvenile fish and crustaceans (Larkum et al. 2006; Orth et al. 2006). The seagrass ecosystem also plays a number of important eco-engineering roles in shallow coastal waters by providing wave protection against coastal erosion (Fonseca & Cahalan, 1992), facilitating nutrient cycling, increasing sediment stabilisation, as well as enhancing carbon sequestration (Duarte et al. 2005; Waycott et al. 2009; Ricart et al. 2015). Despite being a high-value ecosystem with an estimated 2-4 times higher ecosystem service value compared to mangroves and coral reefs, respectively (Costanza 1997; Orth et al. 2006), of strong benefit to the commercial fishing industry (Watson et al. 1993), seagrass meadows are currently facing a global decline that is mainly associated with human activity (Orth et al. 2006; Ralph et al. 2006; Waycott et al. 2009).

Seagrass evolved from terrestrial angiosperms and colonized the seafloor about 100 million years ago (Les et al. 1997). There are three dominant genera: *Halophila, Zostera* and *Posidonia*, which typically grow in mono-specific meadows, although multi-species meadows are found especially in the tropics (Larkum et al. 1989; Holmer et al. 2006). Seagrasses have developed unique adaptations to a completely submerged life. These adaptations include hydrophilous pollination, epidermal chloroplasts and an extensive internal lacunar system (aerenchyma), which allows rapid internal gas flow along concentration gradients and interconnects the leaves with the rhizomes and roots, facilitating transport of O_2 to the below-ground tissues (Larkum et al. 1989; Les et al. 1997; Pedersen et al. 1998; Larkum et al. 2006; Figure I).

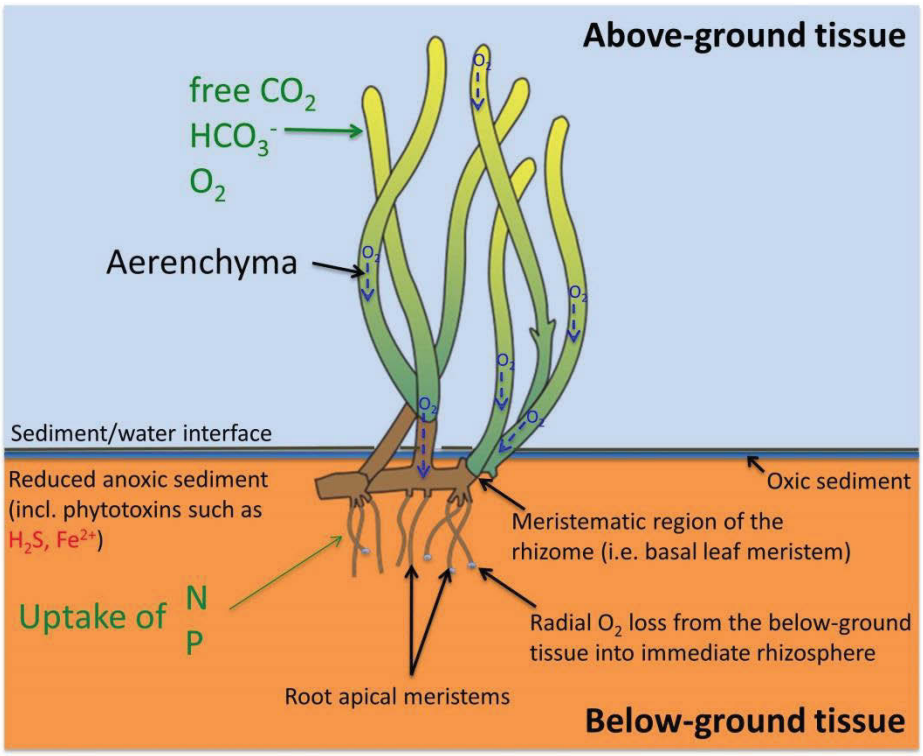

Figure I. Conceptual diagram illustrating the internal O_2 concentration gradient in the aerenchymal tissue of seagrasses. Passive (in darkness, driven by diffusion from the surrounding water-column) or actively (in light, produced via leaf photosynthesis) evolved O_2 is transported down to the below-ground tissue through low-resistance, internal gas channels (i.e. aerenchyma) and is subsequently lost to the immediate rhizosphere, termed radial O_2 loss (ROL).

Diffusive boundary layers and internal plant aeration

Seagrasses get much of their CO_2 and O_2 from the water column. These compounds are mainly taken up through the leaf at a rate, which is determined by the so called diffusive boundary layer (DBL) that is covering the leaves. The DBL is a thin unstirred layer of water at the leaf surfaces impeding the exchange of solutes with the surrounding medium. The DBL thickness is dependent on both the flow-velocity of the surrounding water, as well as the surface microtopography of the tissue, thus increasing in thickness and mass resistance with decreasing flow-velocities and surface roughness (Jørgensen & Des Marais, 1990; Binzer et al. 2005). The flux through the DBL is inversely proportional to the diffusion path length, as seen from Fick's first law of diffusion:

$$J = -D_0 \frac{\partial C}{\partial z}$$

where J is the flux (in mol m^{-2} s^{-1}), D_0 is the respective temperature and salinity dependent diffusion coefficient (in m^2 s^{-1}), $\partial C/\partial z$ is the linear concentration gradient within the DBL (in mol m^{-4}); assuming that the concentration gradient through the DBL, i.e., concentration difference at the leaf surface and the ambient seawater, is kept constant. Diffusion is the only mode of mass transport across DBLs, and in stagnant liquids (e.g., pore-water) this becomes very slow and inefficient over long (cm) distances.

As a result of the DBL, the internal O_2 partial pressure (pO_2) within the lacunar system of seagrasses is affected by the flow-velocity of the water layers surrounding the leaves. This was described in a study by Binzer et al. (2005), that showed a pronounced decline in internal pO_2 with decreasing flow-rates (in darkness) as a result of an increase in the thickness of the DBL. The transport of O_2 through the lacunar system connecting the leaves and rhizome/roots relies primarily on efficient gas-phase diffusion (about 10.000 times faster than in water), which is sufficient to support the O_2 demand of the below-ground tissue (Pedersen et al. 1998, 2004). The internal O_2 transport in seagrasses is driven by partial pressure gradients and is therefore predominantly unidirectional from leaves to rhizomes and finally to the roots (Borum et al. 2006).

The seagrass rhizosphere

Coastal marine sediments typically become anoxic within the first few millimetres of depth due to a combination of microbial respiration and the sediment surface DBL which limit O_2 diffusion from the overlying water column (Jørgensen & Revsbech, 1985; Borum et al. 2005; Glud, 2008). Within this anoxic environment, anaerobic metabolism results in the formation of reduced phytotoxic compounds such as hydrogen sulphide (H_2S). The production of gaseous H_2S results from the activity of sulphate-reducing bacteria (SRB) which uses sulphate (SO_4^{2-}) as an electron acceptor for respiration (e.g. Jørgensen, 1982; Isaksen & Finster, 1996; Lamers et al. 2013). The chemical sulphide speciation in the porewater depends on the porewater pH, where H_2S predominates at pH <7 and HS^- at higher pH levels. To prevent intrusion of phytotoxic H_2S into their tissue, seagrass utilises their internal

lacuna system to transport O_2 from the leaf region to the rhizome and roots (Figure I) where it may be released into the sediment (known as radial O_2 loss or "ROL") and react with H_2S to form non-toxic oxidised sulphur compounds (Pedersen et al. 1998; Jensen et al. 2005; Frederiksen & Glud 2006; Colmer, 2003; Hasler-Sheetal & Holmer, 2015). During day-time, photosynthetically-derived O_2 production results in high ROL to the immediate rhizosphere of the seagrass, resulting in the formation of oxic microshields; i.e. below-ground oxic microzones that surrounds the root apical meristems (the root-caps) of the plant (Pedersen at al. 1998; Jensen et al. 2005; Frederiksen & Glud, 2006). During night-time, the seagrass is totally dependent on passive diffusion of O_2 from the water column into the above-ground tissue in order to provide sufficient O_2 to the below-ground tissues through the lacunar system. The fitness of the seagrass is therefore strongly affected by fluctuations in the night-time bulk water O_2 concentration (Pedersen et al. 1998, 2004; Borum et al. 2005, 2006).

ROL mostly occurs ~1-2 mm behind the root-apex (Jensen et al. 2005, 2007), and has been detected in different seagrass and wetland species, e.g., *Zostera marina* (Jensen et al. 2005; Frederiksen & Glud, 2006), *Halophila ovalis* (Connell et al. 1999), *Phragmites australis* (Armstrong et al. 2000) and *Cymodocea rotundata* (Pedersen et al. 1998), as well as at the rhizome of *Potamogeton perfoliatus* (Caffrey & Kemp 1991). Apart from at the root apex, many of these previous studies have shown an almost complete barrier to ROL across most of the mature part of the roots, especially in older root-bundles (Jensen et al. 2005; Frederiksen & Glud, 2006). This barrier to ROL is believed to serve a two-way function, as it ensures sufficient internal transport of O_2 towards the more distal parts of the plant (Colmer, 2003), but may also function as a protective mechanism against intrusion of phytotoxins, such as H_2S (Armstrong & Armstrong 2001). As such, the barrier to ROL is likely an adaptation to inhabiting highly reduced and anoxic sediments, ensuring that sufficient O_2 supply is provided to the active parts of growing roots to cover both respiration and ROL (Armstrong, 1979). Due to their continued growth, these tissues are unable to form a barrier to block sediment-derived phytotoxic compounds and therefore rely on sufficient O_2 supply and ROL for protection. In general, reducing/anoxic conditions have been shown to induce stronger barriers to ROL in the below-ground tissue (Armstrong & Armstrong 2001), which is likely accomplished through the presence of suberised lamellae in the exodermis of the plant roots (Enstone et al. 2003). This is supported by Barnabas (1996), who suggested that

Casparian band-like structures composed of suberin protect plants from sediment phytotoxins after observing them in the root hypodermis of many marine angiosperms including *Zostera marina*.

The below-ground oxic microshields

The oxic microshields formed around the below-ground tissue as a result of ROL, have been suggested to function as a chemical defence mechanism, preventing H_2S from invading the below-ground tissue as O_2 spontaneously reacts with H_2S in the immediate rhizosphere to form non-phytotoxic compounds (Pedersen et al. 1998; Jensen et al. 2005; Borum et al. 2006; Figure II).

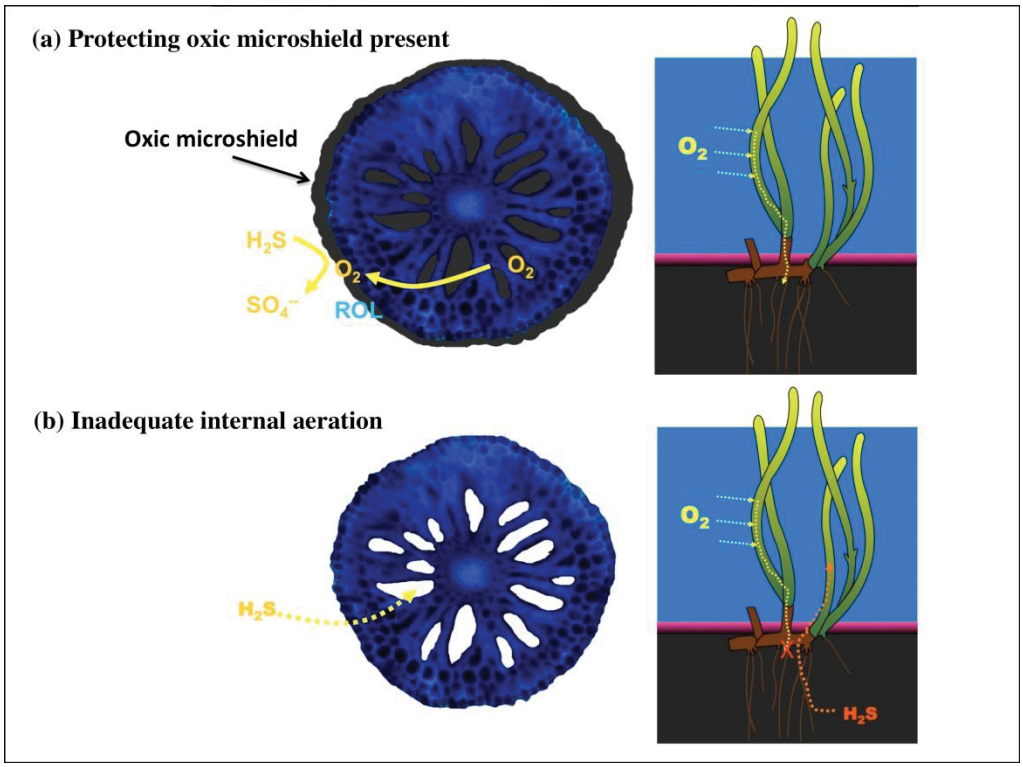

Figure II. Conceptual diagram, illustrating internal aeration, the below-ground oxic microshield and potential hydrogen sulphide (H_2S) intrusion in seagrasses. (a) Rhizospheric oxic microshield present as a result of a sufficient O_2 supply from the leaves. Radial O_2 loss (ROL) from below-ground tissue leads to spontaneous chemical re-oxidation of phytotoxic H_2S to non-toxic sulphate (SO_4^{2-}). (b) Inadequate internal aeration may result in H_2S intrusion, enhancing the risk of seagrass mortality, owing to chemical suffocation. Transversal sections (blue) visualize the extensive internal lacunar system (i.e. aerenchyma) of seagrasses. Black shadow indicates that O_2 is present. Redrawn from Pedersen et al. (1998) with permission from Ole Pedersen (University of Copenhagen, Denmark).

The formation of oxic microshields relies on the ability of the plant to maintain a positive O_2 balance within the tissue, as well as in the rhizosphere. To accomplish this, seagrasses generally require relatively high levels of incident light, with optimal surface photosynthetically active radiation (PAR, 400-700 nm) irradiances up to 6 times higher than what is required for many macroalgae (Ralph et al. 2007). The spatial extent and strength, i.e. the oxidising capacity, of the oxic microshield, is dependent on the balance between: i) the O_2 supply from either passive diffusion, which is dependent on the bulk water O_2 concentration, as well as the thickness of the diffusive boundary layer (Binzer et al. 2005), or photosynthetically-derived O_2 evolution (Pedersen et al. 1998; Pedersen et al. 2004), versus ii) the sediment O_2 demand (including both bacterial respiration and spontaneous chemical reactions with sediment-produced reduced toxic compounds), as well as iii) the plants own respiratory needs (Borum et al. 2006). It has recently been shown that the pO_2 of the meristematic tissue (i.e. the basal leaf meristem) is highly affected by increasing temperatures in the ambient water column (Raun & Borum 2013). Raun and Borum (2013) showed that increasing temperature (especially >25 °C) had substantial negative impacts on meristematic pO_2 as a result of increasing plant tissue respiration, which led to the suggestion that seagrasses are likely more vulnerable to environmental stressors during summer-time when water temperatures generally are higher.

In summary, photosynthetically-derived O_2 evolution is the most important source of O_2 for internal transport, but passive diffusion of O_2 from the water column to below-ground tissue during darkness is necessary for maintaining a constant O_2 supply to rhizomes and roots (Borum et al. 2006). The O_2 budget of seagrasses is thus a complex interaction between several O_2 sources and sinks, and the influence of ROL on rhizospheric biogeochemical processes remains largely unknown, e.g. in terms of whether ROL supports/stimulates bacterial-mediated sediment detoxification in the seagrass rhizosphere.

Rhizospheric plant-microbe interactions

Like most marine sediments, seagrass sediments harbor a diverse microbial community responsible for the biogeochemical cycling of nutrients and carbon (Welsh, 2000; Nielsen et al. 2001; Devereux, 2005). From the plant perspective, both beneficial and harmful bacteria

are present in the seagrass rhizosphere (Devereux, 2005; Jensen et al. 2007). Sulphate-reducing bacteria (SRB) increase the exposure of below-ground tissue to phytotoxic H_2S, but also fix dinitrogen that may become available for plant assimilation (e.g. Hansen et al. 2000; Welsh, 2000; Nielsen et al. 2001). Sulphide-oxidizing bacteria (SOB), on the other hand, may enhance seagrass fitness by detoxifying the surrounding reduced sediment through bacteria-mediated H_2S re-oxidation, a process that can be 10.000-100.000 times faster than chemical oxidation alone (Jørgensen & Revsbech, 1983; Nelson et al. 1986). *Beggiatoa* sp. is an example of a sulphide-oxidizing bacteria (SOB) living within the seagrass rhizosphere (Holmer et al. 2005), potentially supporting seagrasses by re-oxidizing phytotoxic H_2S to its non-phytotoxic counterpart elemental sulphur (S) (Jørgensen & Revsbech, 1983; Nelson et al. 1986). The oxidation of reduced sulphur compounds such as H_2S, results in the release of protons (H^+), which lowers the pH levels of the sediment.

$$2O_2 + H_2S \rightarrow 2H^+ + SO_4^{2-}$$

It is thus intriguing to suggest a possible mutual beneficial relationship between SOB and seagrasses, where seagrasses support SOB with O_2 and root-exudates (dissolved organic carbon secreted from the below-ground tissue; Moriarty et al. 1986) and in return, the SOB oxidize phytotoxic H_2S in the immediate rhizosphere; thereby supporting seagrasses by preventing the influx of phytotoxins into their below-ground tissue.

The seagrass rhizosphere, here focusing on the oxic/anoxic interface, represents an extreme micro-habitat that can oscillate from oxic to anoxic over the diel cycle (Jensen et al. 2005; Frederiksen & Glud, 2006). This is a result of fluctuations in the photosynthetically-derived O_2 supply to below-ground tissues (Borum et al. 2005), as well as a result of possibly decreased water column O_2 concentrations during night time (Greve et al. 2003; Borum et al. 2005, 2006). Such fluctuations in O_2 supply may lead to a shifting oxic/anoxic interface, which in turn may result in shifts in the functionality and composition of the microbial community (Jensen et al. 2007). The interaction between seagrass ROL and the microbial community surrounding the rhizome/roots of the plant remains largely unexplored, and research has mainly focussed on the effects of seagrass-secreted root/rhizome-exudates (e.g., sugars and amino acids) (Moriarty et al. 1986; Pollard & Moriarty, 1991; Badri & Vivanco, 2009). Jensen et al. (2007) investigated the microbial diversity in the seagrass

rhizoplane, showing that rhizospheric O_2 availability can modify the bacterial consortia on seagrass roots by selecting for a distinct bacterial community composition through stimulation of potential symbiotic sulphide-oxidizing bacteria and inhibition of potential harmful sulphate-reducing bacteria (SRB). It is also worthwhile mentioning that a potential mutualistic beneficial relationship between seagrasses and associated, burrowing lucinid bivalves including their endosymbiontic sulphide-oxidizing gill bacteria, has recently been demonstrated by van der Heide et al. (2012). Van der Heide et al. (2012) reported reduced H_2S stress in seagrass meadows inhabited by the lucinid bivalves, as determined from observation of an apparent relative increase in seagrass biomass when lucinid bivalves were present in the seagrass rhizosphere. This three-stage symbiosis was suggested to function as a tripartite mutual beneficial relationship, where the bivalve symbiosis reduces sediment H_2S levels and in return seagrasses provide below-ground oxic micro-habitats.

Mechanisms of stress and H_2S toxicity

Hot calm summer months, enhanced eutrophication, decreased light availability and quality, as well as rapid changes in the water column O_2 level, are all conditions that can lead to physiological stress in seagrass meadows (Borum et al. 2006; Ralph et al. 2006) or even sudden die-off events in seagrass beds (Borum et al. 2005; Raun & Borum, 2013; York et al. 2015). Seagrass die-offs are believed to be triggered by a low intra-plant O_2 status as a result of insufficient O_2 supply from the leaf region leading to inadequate internal plant aeration and subsequent H_2S intrusion (Borum et al. 2006). If H_2S reaches the below-ground tissue surface as a result of a diminished oxic microshield, this may result in high internal H_2S concentrations potentially leading to H_2S poisoning. H_2S has been suggested to function as a broad-spectrum toxin and has been shown to form a complex binding with iron located in the mitochondrial enzyme cytochrome c oxidase, which is essential in the respiratory electron transport chain, thus leading to chemical asphyxiation by preventing cellular respiration (Eghbal et al. 2004; Pedersen et al. 2004; Truong et al. 2006). In combination with increased plant production of reactive oxygen species (ROS) and ethanol from anaerobic respiration, such conditions are highly detrimental and may lead to increased mortality (Eghbal et al. 2004; Pedersen et al. 2004; Borum et al. 2005; Borum et al. 2006; Perez-Perez et al. 2012). H_2S toxicity has, furthermore, been linked to reduced nutrient

uptake and respiration rates, as well as membrane depolarisation (Raven & Scrimgeour, 1997; Eghbal et al. 2004). H_2S toxicity typically results in a poorly developed root-system with blackening of the tissue as a result of the formation of FeS at the tissue surface (also known as iron plaques). In contrast, a healthy root-system will typically appear orange-brown in colour due to a thin coating of iron(III) oxides and hydroxides (Dobermann and Fairhurst 2000).

Although well documented, the direct role of H_2S toxicity on seagrass mortality is complicated and its role in the worldwide die-back events still remains unclear. A recent study by Pulido Pérez and Borum (2010) found that ROS, triggered by H_2S toxicity, kills the seagrass leaf meristem. ROS, which are produced via respiration in the mitochondria, are phytotoxic and can lead to protein degradation and peroxidation of membrane lipids (Eghbal et al. 2004; Perez-Perez et al. 2012). A long-term reduction of the seagrass root surface may thus lead to a dramatic increase in the formation of internal ROS as a result of uncontrolled influx of reduced phytotoxic compounds such as H_2S. In plant cells, ROS are furthermore produced in chloroplasts, peroxisomes, in the endoplasmic reticulum, as well as at the plasma membrane (Perez-Perez et al. 2012) altogether possibly leading to severe oxidative stress inside seagrass tissue, which in turn may cause irreversible oxidative damage to proteins, lipids and nucleic acids, ultimately leading to seagrass death (Perez-Perez et al. 2012).

Anthropogenic-induced stressors

Human activities such as coastal development, eutrophication and boat mooring/activity have resulted in severe loss of seagrass cover across the world (e.g. Hastings et al. 1995; York et al. 2015). Harbour dredging operations causes re-suspension of abiotic and biotic fine sediment particles increasing water turbidity and thus reducing light availability for underwater photosynthesis. This has been shown to cause loss of seagrass meadows likely as a result of reduced photosynthetic O_2 production (Erftemeijer & Lewis 2006; Ralph et al. 2007). Sediment re-suspension, furthermore, has the potential to adversely affect the O_2 conditions in the water column through suspension of reduced metabolites, enhancing the possibility of overnight water-column hypoxia (Erftemeijer & Lewis 2006). Moreover,

sediment re-suspension has been shown to increase the likelihood of algae blooms and bacterial respiration as a consequence of sediment and nutrient dispersion (Ralph et al. 2007). Coastal developments thus represent a severe threat to adjoining seagrass meadows, and further knowledge of dredging impacts on seagrass health is needed in order to enable better coastal management and conservation of this vital marine ecosystem.

Leaf epiphytes are a natural part of the seagrass microbiome, but increased eutrophication e.g. from land run-offs and urban activity has been shown to result in enhanced epiphyte overgrowth on seagrass leaves (Borum, 1985), leading to reduced light availability and quality for the seagrasses and also potentially resulting in competition for dissolved inorganic carbon (DIC) between the seagrass host and the leaf epiphytic assemblage (Drake et al. 2003; Maberly, 2014; Costa et al. 2015). The effect of leaf epiphyte overgrowth on light availability and photosynthetic activity has been described in detail previously (e.g. Drake et al. 2003), but little is known about the effects on the below-ground tissue oxidation capacity and thereby the risk of H_2S intrusion caused by reduced internal plant aeration.

Important knowledge gaps in seagrass research: a rhizospheric perspective

Our current understanding of internal O_2 movement in seagrasses and the dynamics and distribution of rhizospheric O_2 in seagrass meadows, is largely based on planar optode and microelectrode measurements performed in the rhizosphere and internally at the shoot base (i.e. at the basal leaf meristem) (e.g. Pedersen et al. 1998; Connell et al. 1999; Pedersen et al. 2004; Borum et al. 2005; Jensen et al. 2005; Sand-Jensen et al. 2005; Borum et al. 2006; Frederiksen & Glud, 2006; Raun & Borum, 2013; Jovanovic et al. 2015). These recent studies have revealed important information about how seagrasses sustain aerobic metabolism in below-ground tissues despite being situated in a highly reduced anoxic environment, resulting from an accumulation of organic matter in the sediment. Nonetheless, although the intra-plant O_2 status and dynamics are well documented they are also inherently complex (Borum et al. 2006; Lee et al. 2007), and we still lack important knowledge about the effect of seagrass-derived oxic microzones on rhizospheric H_2S levels and distributions, especially at the plant/sediment interface. Other areas that are subject to further investigations include: (i) plant-induced pH changes in the immediate rhizosphere

via excretion of allelochemicals where an increase in rhizospheric pH would e.g. result in chemical sulphide speciation shifts towards non-tissue-permeable and thus non-phytotoxic HS^- ions, (ii) potential plant-driven nutrient mobilization in carbonate-rich tropical sediments, and (iii) possible beneficial relationships with the rhizospheric microbial community through stimulation of rapid bacteria-mediated H_2S re-oxidation in the surrounding sediment.

Outline of PhD project: applied methodology and research aims

The aim of this PhD project was to determine how changing environmental conditions affect the health and performance of seagrasses, with special focus on the dynamics of the below-ground biogeochemical microenvironment (Figure III).

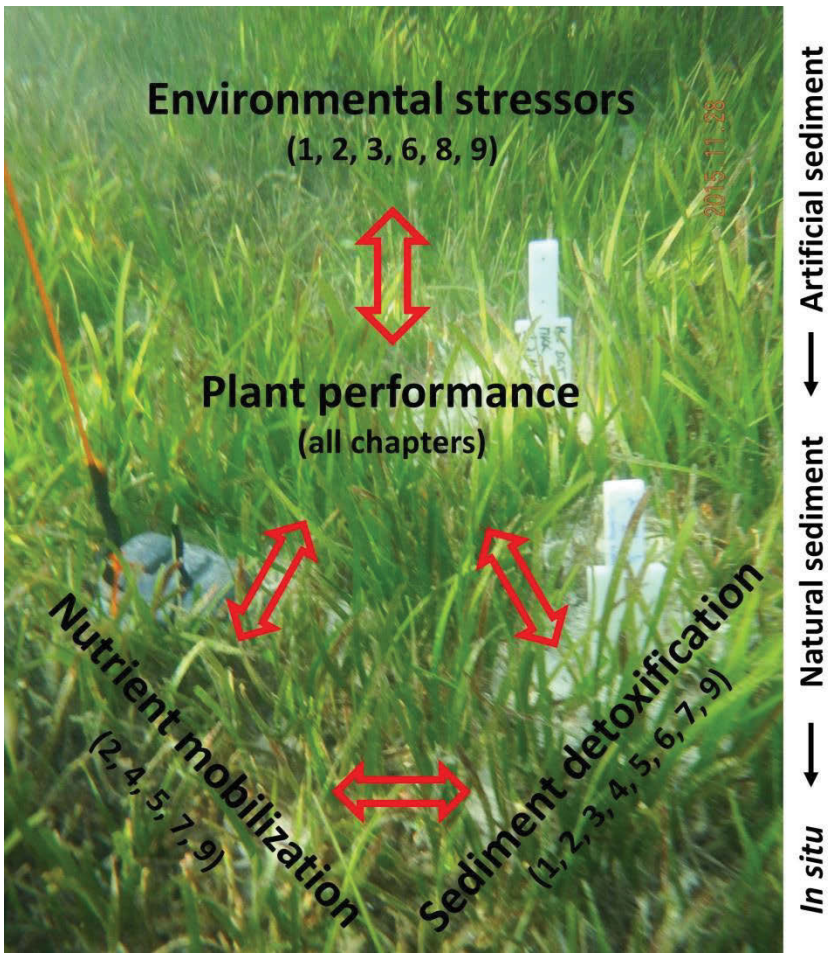

Figure III. Conceptual diagram outlining the major aims of my PhD project, as well as an overview of the chapters that address the different aims specifically. Numbers in brackets refers to the respective data chapters wherein new findings of the respective topic is presented and discusses in detail. The order on the far right (from top to bottom) denotes the general progress in used methodologies as described below.

The major objectives were thus to determine:

(i) Can seagrasses alter the biogeochemical conditions in their rhizosphere and thereby detoxify their surrounding sediment.

(ii) Can seagrasses mobilize nutrients in the immediate rhizosphere through plant-derived allelochemicals.

(iii) How do environmental stressors such as water-column hypoxia, leaf epiphyte overgrowth and sediment re-suspension affect the overall plant performance and thereby the below-ground tissue oxidation capacity.

The seagrass rhizosphere is a highly complex and heterogeneous environment, and to address these aims we therefore choose an experimental approach where we initially limited as many influencing parameters as possible. This was enabled by developing a system based on an artificial, transparent and reduced sediment matrix (deoxygenated seawater-agar amended with H_2S). The artificial sediment matrix allowed us to define at an unprecedented spatial resolution how changing environmental conditions such as light intensity and water column O_2 conditions affects the physiological responses of seagrasses and through that the below-ground biogeochemical microenvironment (described in detail in Chapters 1-4). The dynamics of the chemical microenvironment in the seagrass rhizosphere was primarily determined in high spatio-temporal resolution by advanced microsensor, DET/DGT gel and planar optode technology (e.g. Glud et al. 1996, 1999; Jensen et al. 2005; Robertson et al. 2008; Pagès et al. 2011). As we approached a deeper understanding for how the plants performance and thereby the below-ground biogeochemical microenvironment was affected by individual changes in the surrounding environment, we increased the number of influencing environmental parameters in the seagrass rhizosphere by introducing rhizosphere microbes (i.e. plant-microbe interactions), thereby moving towards more realistic conditions as experienced in natural sediment (Chapter 5). Finally, we performed several studies in natural sediment, addressing the effects of leaf epiphyte overgrowth on plants performance, as well as potential plant-derived rhizospheric nutrient mobilization in carbonate-rich sediments (Chapters 6 & 7). We also carried out an *in situ* assessment of the effects of sediment re-suspension on seagrass health (Chapter 8). The thesis concludes with a review (Chapter 9) describing important plant/sediment interactions in the seagrass rhizosphere largely based on our recent findings.

REFERENCES

Armstrong J, Armstrong W. (2001). Rice and *Phragmites*: effects of organic acids on growth, root permeability, and radial oxygen loss to the rhizosphere. *American Journal of Botany* **88:** 1359-1370.

Armstrong W. (1979). Aeration in higher plants. Academic Press, London.

Armstrong W, Cousins D, Armstrong J, Turner DW, Beckett PM. (2000). Oxygen distribution in wetland plant roots and permeability barriers to gas-exchange with the rhizosphere: a microelectrode and modelling study with *Phragmites australis*. *Annals of Botany* **86:** 687-703.

Badri DV, Vivanco JM. (2009). Regulation and function of root exudates. *Plant, Cell and Environment*, **32**, 666–681.

Barnabes AD. (1996). Casparian band-like structures in the root hypodermis of some aquatic angiosperms. *Aquatic Botany* **55:** 217-225.

Binzer T, Borum J, Pedersen O. (2005). Flow velocity affects internal oxygen conditions in the seagrass *Cymodocea nodosa*. *Aquatic Botany* **83:** 239-247.

Borum J. (1985). Development of epiphytic communities on eelgrass (*Zostera marina*) along a nutrient gradient in a Danish estuary. *Marine Biology*, **87**, 211-218.

Borum J, Pedersen O, Greve TM, Frankovich TA, Zieman JC, Fourqurean JW, Madden CJ. (2005). The potential role of plant oxygen and sulphide dynamics in die-off events of the tropical seagrass, *Thalassia testudinum*. *Journal of Ecology* **93:** 148-158.

Borum J, Sand-Jensen K, Binzer T, Pedersen O, Greve TM. (2006). Oxygen movement in seagrasses. In: Larkum AWD, Orth JR & Duarte CM, Eds., *Seagrass: Biology, Ecology and Conservation*. Springer, Dordrecht, The Netherlands**:** 255-270.

Caffrey JM, Kemp WM. (1991). Seasonal and spatial patterns of oxygen production, respiration and root-rhizome release in *Potamogeton perfoliatus L*. and *Zostera marina L*. *Aquatic Botany* **40:** 109-128.

Colmer TD. (2003). Long-distance transport of gases in plants: a perspective on internal aeration and radial oxygen loss from roots. *Plant, Cell & Environment*, **26**, 17-36.

Connell EL, Colmer TD, Walker DI. (1999). Radial oxygen loss from intact roots of *Halophilia ovalis* as a function of distance behind the root tip and shoot illumination. *Aquatic Botany* **63:** 219-228.

Costa MM, Barrote I, Silva J, Olive I, Alexandre A, Albano S, Santos RO. (2015). Epiphytes modulate *Posidonia oceanica* photosynthetic production, energetic balance, antioxidant mechanisms and oxidative damage. *Frontiers in Marine Science*.

Costanza REA. (1997). The value of the world's ecosystem services and natural capital. *Nature* **387:** 253-260.

Devereux R. (2005). Seagrass rhizosphere microbial communities. In: Erik Kristensen, Ralf R. Haese & Joel E. Kostka, eds. *Coastal and estuarine studies: Interactions between macro- and microorganisms in marine sediments*. American Geophysical Union. Washington, USA.

Dobermann A, Fairhurst T. (2000). Rice. Nutrient disorders & nutrient management. Potash & Phosphate Institute (PPI), Potash & Phosphate Institute of Canada (PPIC) and International Rice Research Institute (IRRI).

Drake LA, Dobbs FC, Zimmerman RC. (2003). Effects of epiphyte load on optical properties and photosynthetic potential of the seagrasses *Thalassia testudinum* Banks ex König and *Zostera marina* L. *Limnology and Oceanography*, **48**, 456-463.

Duarte CM, Middelburg J, Caraco N. (2005). Major role of marine vegetation on the oceanic carbon cycle. *Biogeosciences* **2:** 1–8.

Eghbal MA, Pennefather PS, O'brien PJ. (2004). H_2S cytotoxicity mechanism involves reactive oxygen species formation and mitochondrial depolarisation. *Toxicology* **203:** 69-76.

Enstone DE, Peterson CA, Ma F. (2003). Root endodermis and exodermis: structure, function, and responses to the environment. *Journal of Plant Growth Regulation* **21:** 335-351.

Erftemeijer PLA, Lewis RRR. (2006). Environmental impacts of dredging on seagrasses: a review. *Marine Pollution Bulletin* **52:** 1553-1572.

Frederiksen MS, Glud RN. (2006). Oxygen dynamics in the rhizosphere of *Zostera marina*: A two-dimensional planar optode study. *Limnol. Oceanogr*, **51**, 1072-1083.

Fonseca MS, Cahalan JA. (1992). A preliminary evaluation of wave attenuation by four species of seagrass. *Estuarine, Coastal and Shelf Science*, **35**, 565-576.

Greve TM, Borum J, Pedersen O. (2003). Meristematic oxygen variability in eelgrass (*Zostera marina*). *Limnology and Oceanography*, **48**, 210-216.

Glud R.N. (2008). Oxygen dynamics of marine sediments. *Marine Biology Research*, **4**, 243-289.

Glud RN, Kühl M, Kohls O, Ramsing NB. (1999). Heterogeneity of oxygen production and consumption in a photosynthetic microbial mat as studied by planar optodes. *Journal of Phycology* **35:** 270-279.

Glud RN, Ramsing NB, Gundersen JK, Klimat I. (1996). Planar optrodes: a new tool for fine scale measurements of two-dimensional O2 distribution in benthic communities. *Marine Ecology Progress Series* **140:** 217-226.

Hansen JW, Udy JW, Perry CJ, Dennison WC, Lomstein BA. (2000). Effect of the seagrass *Zostera capricorni* on sediment microbial processes. *Marine Ecology Progress Series*, **199**, 83-96.

Hasler-Sheetal H, Holmer M. (2015). Sulfide Intrusion and Detoxification in the Seagrass *Zostera marina*. *PloS one* **10**(6): e0129136.

Hastings K, Hesp P, Kendrick GA. (1995). Seagrass loss associated with boat moorings at Rottnest Island, Western Australia. *Ocean & Coastal Management* **26**(3): 225-246.

Holmer M, Frederiksen MS, Møllegaard H. (2005). Sulfur accumulation in eelgrass (*Zostera marina*) and effect of sulfur on eelgrass growth. *Aquatic Botany* **81:** 367-379.

Holmer M, Pedersen O, Ikejima K. (2006). Sulfur cycling and sulfide intrusion in mixed Southeast Asian tropical seagrass meadows. *Botanica Marina* **49:** 91-102.

Isaksen MF, Finster K. (1996). Sulphate reduction in the root zone of the seagrass *Zostera noltii* on the intertidal flats of a coastal lagoon (Arcachon, France). *Marine Ecology Progress Series*, **137**, 187-194.

Jensen SI, Kühl M, Glud RN, Jørgensen LB, Prieme A. (2005). Oxic microzones and radial oxygen loss from roots of *Zostera marina*. *Marine Ecology Progress Series* **293:** 49-58.

Jensen SI, Kühl M, Prieme A. (2007). Different bacterial communities in the rhizoplane and bulk sediment of the seagrass *Zostera marina*. *FEMS Microbiology Ecology* **62:** 108-117.

Jovanovic Z, Pedersen MØ, Larsen M, Kristensen E, Glud RN. (2015). Rhizosphere O_2 dynamics in young *Zostera marina* and *Ruppia maritima*. *Marine Ecology Progress Series*, **518**, 95-105.

Jørgensen BB. (1982). Mineralization of organic matter in the sea bed-the role of sulphate reduction. *Nature* **296**: 643-645.

Jørgensen BB, Des Marais DJ. (1990). The diffusive boundary layer of sediments: Oxygen microgradients over a microbial mat. *Limnology and Oceanography* **35:** 1343-1355.

Jørgensen BB, Revsbech NP. (1983). Colorless sulfur bacteria, *Beggiatoa* spp. & *Thiovulum* spp., in O_2 and H_2S microgradients. *Applied and Environmental Microbiology*, **45**, 1261-1270.

Jørgensen BB, Revsbech NP. (1985). Diffusive boundary layers and the oxygen uptake of sediments and detritus. *Limnology and Oceanography*, **30**, 111-122.

Lamers LP, Govers LL, Janssen IC, Geurts JJ, Van der Welle ME, Van Katwijk MM, Van der Heide T, Roelofs JG, Smolders AJ. (2013). Sulfide as a soil phytotoxin—a review. *Frontiers in plant science*, **4**.

Larkum AWD, Mccomb AJ, Shepherd SA. (1989). Biology of Seagrass. Elsevier, Amsterdam.

Larkum AWD, Orth RJ, Duarte CM. (2006). Seagrasses: Biology, Ecology, and Conservation. Springer, Berlin.

Lee KS, Park SR, Kim YK. (2007). Effects of irradiance, temperature, and nutrients on growth dynamics of seagrasses: A review. *Journal of Experimental Marine Biology and Ecology* **350:** 144-175.

Les DH, Cleland MA, Waycott M. (1997). Phylogenetic studies in the Alismatidae, II: Evolution of the marine angiosperms (seagrasses) and hydrophily. *Systematic Botany* **22:** 443–463.

Maberly SC. (2014). The fitness of the environments of air and water for photosynthesis, growth, reproduction and dispersal of photoautotrophs: An evolutionary and biogeochemical perspective. *Aquatic Botany*, **118**, 4-13.

Moriarty DJW, Iverson RL, Pollard PC. (1986). Exudation of organic carbon by the seagrass *Halodule wrightii* Aschers. and its effect on bacterial growth in the sediment. *Journal of Experimental Marine Biology and Ecology*, **96**, 115-126.

Nelson DC, Jørgensen BB, Revsbech NP. (1986). Growth pattern and yield of a chemoautotrophic *Beggiatoa sp.* in oxygen-sulfide microgradients. *Applied and Environmental Microbiology*, **52**, 225-233.

Nielsen LB, Finster K, Welsh DT, Donelly A, Herbert RA, De Wit R, Lomstein BA. (2001). Sulphate reduction and nitrogen fixation rates associated with roots, rhizomes and sediments from *Zostera noltii* and *Spartina maritima* meadows. *Environmental Microbiology*, **3**, 63-71.

Orth RJ, Carruthers TJB, Dennison WC, Duarte CM, Fourqurean JW, Heck Jr. KL, Hughes AR, Kendrick GA, Kenworthy WJ, Olyarnik S, et al. (2006). A global crisis for seagrass ecosystems. *BioScience* **56:** 987-996.

Pagès A, Teasdale PR, Robertson D, Bennett WW, Schäfer J, Welsh DT. (2011). Representative measurement of two-dimensional reactive phosphate distributions and co-distributed iron(II) and sulfide in seagrass sediment porewaters. *Chemosphere*, **85**, 1256-1261.

Pedersen O, Binzer T, Borum J. (2004). Sulphide intrusion in eelgrass (*Zostera marina L*). *Plant, Cell and Environment* **27:** 595-602.

Pedersen O, Borum J, Duarte CM, Fortes MD. (1998). Oxygen dynamics in the rhizosphere of *Cymodocea rotundata*. *Marine Ecology Progress Series* **169:** 283-288.

Perez-Perez ME, Lemaire SD, Crespo JL. (2012). Reactive oxygen species and autophagy in plants and algae. *Plant Physiology* **160:** 156-164.

Pollard PC, Moriarty D. (1991). Organic carbon decomposition, primary and bacterial productivity, and sulphate reduction, in tropical seagrass beds of the Gulf of Carpentaria, Australia. *Marine ecology progress series*, **69**, 149-159.

Pulido Pérez C, Borum J. (2010). Eelgrass (*Zostera marina*) tolerance to anoxia. *Journal of Experimental Marine Biology and Ecology* **385:** 8-13.

Ralph PJ, Durako MJ, Enríquez S, Collier CJ, Doblin MA. (2007). Impact of light limitation on seagrasses. *Journal of Experimental Marine Biology and Ecology* **350:** 176-193.

Ralph PJ, Tomasko D, Seddon S, Moore K, Macinnis-Ng C. (2006). Human impact on Seagrasses: Contamination and Eutrophication; in Larkum et al. 2006, *Seagrass: Biology, Ecology and Conservation*. Springer, Berlin**:** 567-593.

Raun AL, Borum J. (2013). Combined impact of water column oxygen and temperature on internal oxygen status and growth of *Zostera marina* seedlings and adult shoots. *Journal of Experimental Marine Biology and Ecology* **441:** 16–22.

Raven JA, Scrimgeour CM. (1997). The influence of anoxia on plants of saline habitates with special reference to the sulfur cycle. *Annals of Botany*, **79**, 79-86.

Ricart AM, York PH, Rasheed MA, Perez M, Romero J, Bryant CV, Macreadie PI. (2015). Variability of sedimentary organic carbon in patchy seagrass landscapes. *Marine Pollution Bulletin*.

Robertson D, Teasdale PR, Welsh DT. (2008). A novel gel-based technique for the high resolution, two-dimensional determination of iron (II) and sulfide in sediment. *Limnology and Oceanography: Methods* **6**: 502-512.

Sand-Jensen K, Pedersen O, Binzer T, Borum J. (2005). Contrasting oxygen dynamics in the freshwater isoetid *Lobelia dortmanna* and the marine seagrass *Zostera marina*. *Annals of Botany* **96**: 613-623.

Truong DH, Eghbal MA, Hindmarsh W, Roth SH, O'brien PJ. (2006). Molecular mechanisms of hydrogen sulfide toxicity. *Drug Metab Rev* **38:** 733-744.

van der Heide T, Govers LL, de Fouw J, Olff H, van der Geest M, van Katwijk MM, Peiersma T, van de Koppel J, Silliman BR, Smolders AJP, et al. (2012). A Three-Stage Symbiosis Forms the Foundation of Seagrass Ecosystems. *Science* **336:** 1432-1434.

Watson RA, Coles RG, Lee Long WJ. (1993). Simulation estimates of annual yield and landed value for commercial penaeid prawns from a tropical seagrass habitat. *Australian Journal of Marine and Freshwater Research* **44:** 211–219.

Waycott M, Duarte CM, Carruthers TJB, Orth RJ, Dennison WC, Olyarnik S, Calladine A, Fourqurean JW, Heck Jr. KL, Hughes AR, et al. (2009). Accelerating loss of seagrasses across the globe threatens coastal ecosystems. *PNAS* **106:** 12377–12381.

Welsh DT. (2000). Nitrogen fixation in seagrass meadows: regulation, plant–bacteria interactions and significance to primary productivity. *Ecology Letters* **3**: 58-71.

York PH, Carter AB, Chartrand K, Sankey T, Wells L, Rasheed MA. (2015). Dynamics of a deep-water seagrass population on the Great Barrier Reef: annual occurrence and response to a major dredging program. *Scientific reports* **5**: 13167.

Publication List

(1) Brodersen KE, Nielsen DA, Ralph PJ, Kühl M (2014). A split flow-chamber with artificial sediment to examine the below-ground microenvironment of aquatic macrophytes.
Marine Biology **161** (12): 2921-2930. doi: 10.1007/s00227-014-2542-3.

(2) Brodersen KE, Nielsen DA, Ralph PJ, Kühl M (2015). Oxic microshield and local pH enhancement protects *Zostera muelleri* from sediment-derived hydrogen sulphide.
New Phytologist **205** (3): 1264-1276. doi: 10.1111/nph.13124.

(3) Koren K*, Brodersen KE*, Jakobsen S, Kühl M (2015). Optical sensor nanoparticles in artificial sediments – a new tool to visualize O_2 dynamics around the rhizome and roots of seagrasses.
Environmental Science and Technology **49**(4): 2286-2292. doi: 10.1021/es505734b.

(4) Brodersen KE*, Koren K*, Lichtenberg M, Kühl M (2016). Nanoparticle-based measurements of pH and O_2 dynamics in the rhizosphere of *Zostera marina* L.: Effects of temperature elevation and light-dark transitions.
Plant, Cell & Environment (*First view*) (Accepted on March 22, 2016)

(5) Brodersen KE, Siboni N, Nielsen DA, Pernice M, Ralph PJ, Seymour JR, Kühl M. Seagrass-altered rhizosphere biogeochemistry controls microbial community compositions at the microscale. (In preparation for *the ISME journal*).

(6) Brodersen KE*, Lichtenberg M*, Paz LC, Kühl M (2015). Epiphyte-cover on seagrass (*Zostera marina* L.) leaves impedes plant performance and radial O_2 loss from the below-ground tissue.
Frontiers in Marine Science **2**:58. doi: 10.3389/fmars.2015.00058

(7) Brodersen KE*, Koren K*, Mosshammer M*, Ralph PJ, Kühl M, Santner J. Seagrass-derived rhizospheric phosphorus and iron mobilization. (In preparation for *Nature*).

(8) Brodersen KE, Hammer KJ, Schrameyer V, Fløytrup A, Rasheed M, Ralph PJ, Kühl M, Pedersen O. Sediment resuspension and deposition on seagrass leaves impedes internal plant aeration and promotes phytotoxic H_2S intrusion. (In review - *New Phytologist*).

(9) Brodersen KE, Kühl M, Nielsen DA, Pedersen O, Larkum AWD. Rhizome, Root/Sediment interactions, Aerenchyma and Internal Pressure Changes in Seagrasses. Chapter 18 in *Seagrasses of Australia*. Eds. AWD Larkum, G Kendrick, PJ Ralph. (In review).

**These authors have contributed equally to this work and share the first authorship.*

All experimental chapters presented in this thesis are my original ideas/hypothesis, I have designed the research and conducted the experiments (some as a result of a joint effort), and the data analysis and interpretations, as well as the written manuscripts are my work (with editorial assistance from my supervisors and co-authors). In the following chapters, people that have contributed to the research in question are acknowledged either as co-authors or in the acknowledgements. For the published manuscripts contained in this PhD thesis, I have the permission of all co-authors to implement this work in my thesis.

Chapter 1

A split flow chamber with artificial sediment to examine the below-ground microenvironment of aquatic macrophytes

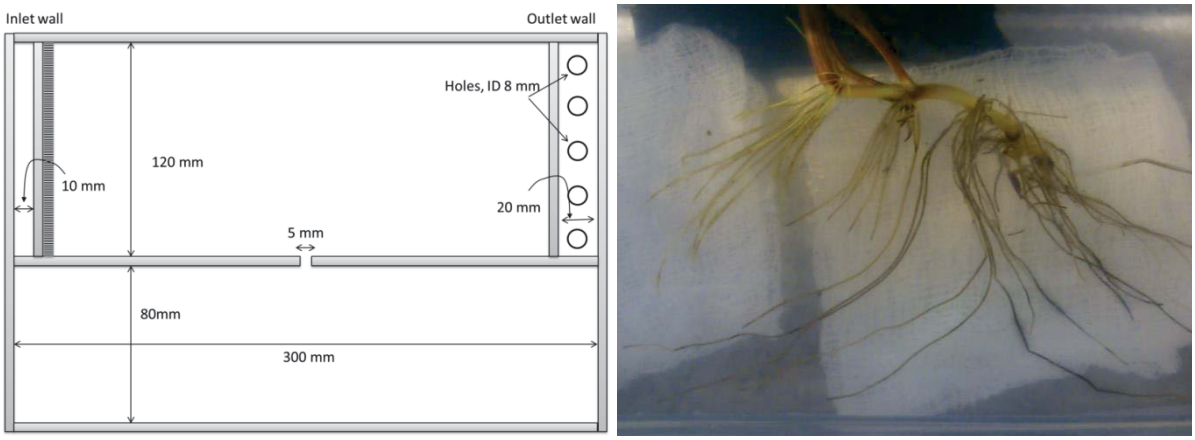

TOC figure. *Left panel shows the design of the custom-made split flow chamber. Right panel shows the below-ground tissue embedded within the reduced, artificial sediment matrix.*

Citation: Brodersen KE, Nielsen DA, Ralph PJ. & Kühl M. (2014). A split flow chamber with artificial sediment to examine the below-ground microenvironment of aquatic macrophytes. *Marine Biology*, **161**: 2921-2930.

Highlights: This chapter describes a new fine-scale experimental approach to analyse how changing environmental conditions affect the below-ground biogeochemical microenvironment of aquatic macrophytes. The applied novel split flow-chamber with artificial sediment was assembled to enable manipulation of the seagrass leaf environment (e.g., flow rate, light intensity, water-column O_2 concentration, temperature, etc.) while observing the impact on the below-ground biogeochemical microenvironment around the rhizome and roots of seagrasses. Seagrass leaves were positioned in free-flowing seawater in the "seawater compartment" and the rhizome and roots supported in a transparent, deoxygenated and reduced seawater/agar matrix in the "artificial sediment compartment". The dynamics of the below-ground chemical microenvironment were analyzed in high spatio-temporal resolution by means of advanced microsensor and planar optode technology.

A split flow-chamber with artificial sediment to examine the below-ground microenvironment of aquatic macrophytes

Kasper Elgetti Brodersen[1,*], Daniel Aagren Nielsen[1], Peter J. Ralph[1], Michael Kühl[1,2,3]

[1]Plant Functional Biology and Climate Change Cluster, University of Technology, Sydney, 15 Broadway, Ultimo, Sydney, NSW 2007, Australia

[2]Marine Biological Section, Department of Biology, University of Copenhagen, Strandpromenaden 5, DK-3000 Helsingør, Denmark

[3]Singapore Centre on Environmental Life Sciences Engineering, School of Biological Sciences, Nanyang Technological University, Singapore.

*Corresponding author, e-mail: kasper.e.brodersen@student.uts.edu.au and phone: +61 414 954 017

ABSTRACT

We present a new experimental setup enabling fine-scale examination of how changing environmental conditions affect the below-ground biogeochemical microenvironment of aquatic macrophytes. By means of microsensor and planar optode technology the influence of plant-mediated radial O_2 release on the below-ground chemical microenvironment of *Zostera muelleri* and *Halophila ovalis* was determined in high spatio-temporal resolution. The seagrass specimens were cultured in a new split flow-chamber with artificial sediment made of a deoxygenated seawater-agar solution with added sulphide. Microelectrode measurements revealed radial O_2 release from the root-shoot junction of both *Z. muelleri* and *H. ovalis* during both light stimulation and darkness, resulting in a rapid decrease in H_2S concentration, and a significant drop in pH was observed within the plant-derived oxic microzone of *Z. muelleri*. No radial O_2 release was detectable from the below-ground tissue of *Z. muelleri* during conditions of combined water-column hypoxia and darkness, leaving the plants more susceptible to sulphide invasion. The spatial O_2 heterogeneity within the immediate rhizosphere of *Z. muelleri* was furthermore determined in two-dimensions by means of planar optodes. O_2 images revealed a decrease in the spatial extent of the plant-derived oxic microzone surrounding the below-ground tissue during darkness, supporting the microelectrode measurements. This new experimental approach can be applied to all rooted aquatic plants, as it allows for direct visual assessment of the below-ground tissue surface during microprofiling, while enabling modification of the above-ground environmental conditions.

Keywords: reduced artificial sediment, microelectrodes, planar optodes, changing environmental conditions, biogeochemical processes, oxygen sink, plant-sediment interactions.

INTRODUCTION

Seagrass meadows provide a diverse range of key ecosystem services such as coastal protection from erosion and enhancement of marine biodiversity (Larkum et al. 2006; Orth et al. 2006; Waycott et al. 2009), and they are ranked 2-4 times higher than mangroves/saltmarshes and coral reefs in ecosystem service value (Costanza, 1997). However, seagrass meadows are currently declining at an alarming rate worldwide, mainly as a result of anthropogenic stressors including eutrophication from land run-off and coastal developments such as harbour dredging and boating activities (Holmer et al. 2009; Orth et al. 2006; Ralph et al. 2006; Waycott et al. 2009). Inadequate internal aeration resulting in low meristematic (below-ground tissue) O_2 content, is considered one of the key factors in seagrass die-off events (Borum et al. 2005; Greve et al. 2003; Pedersen et al. 2004; Raun and Borum, 2013).

As seagrasses typically inhabit organically enriched, sulphidic sediments, they are challenged to provide their below-ground tissue with sufficient O_2 in order to sustain aerobic metabolism in roots and rhizomes and provide protection against sediment-derived phytotoxic compounds (Borum et al. 2006). The internal O_2 supply mainly stems from photosynthesis in the leaves during daytime or from diffusive supply across the leave surface from the surrounding water column during night-time or low light conditions. In the plant, O_2 is transported from the above-ground tissue to the below-ground tissue via low-resistance, intercellular gas-filled spaces (aerenchyma) (Borum et al. 2006; Greve et al. 2003; Jensen et al. 2005; Pedersen et al. 1998; Pedersen et al. 1999). The total amount of O_2 supplied to the root-system is determined by the internal oxygen partial pressure (pO_2) of the shoots relative to the resistance of the below-ground tissue towards cross-tissue gas diffusion, as well as the consumption of O_2 via respiration and leakage along the diffusion path (Borum et al. 2006). The O_2 supply to the below-ground tissue is therefore strongly dependent on the environmental conditions, and may be severely limited during the night when the water-column O_2 concentration is often reduced (Borum et al. 2006; Greve et al. 2003; Pedersen et al. 2004). Unusually calm weather resulting in lowered flow as well as high water-column temperatures have also been shown to impede O_2 diffusion to the below-ground tissue (Binzer et al. 2005; Raun and Borum, 2013).

Apart from directly restricting metabolic processes, inadequate internal aeration can also result in H_2S intrusion, leading to seagrass mortality from chemical asphyxiation (Holmer and Bondgaard, 2001; Perez-Perez et al. 2012; Raven and Scrimgeour, 1997). Previous studies have revealed that seagrasses often leak O_2 from their below-ground tissue to the surrounding rhizosphere, in particular from the area close to the root-apex (Frederiksen and Glud, 2006; Jensen et al. 2005; Pedersen et al. 1998). Such radial O_2 loss (ROL) to the rhizosphere results in an oxidized microenvironment adjacent to the root surface, enabling chemical and/or microbial oxidation of reduced phytotoxic compounds (Jensen et al. 2005; Jensen et al. 2007). In this way, healthy seagrasses may be actively modifying the geochemical microenvironment within the sediment to accommodate their growth (Brodersen et al. submitted).

The current understanding of the chemical microenvironment in the seagrass rhizosphere is largely based on microelectrode and planar optode measurements, which provide excellent means for describing internal and external O_2, H_2S and pH variability with high precision and high temporal and spatial resolution. (Brodersen et al. submitted; Borum et al. 2005; Frederiksen and Glud, 2006; Greve et al. 2003; Jensen et al. 2005; Pedersen et al. 2004; Pedersen et al. 1998). Microelectrodes were introduced to seagrass research in the early 90s (Caffrey and Kemp, 1991) and have since revolutionized the understanding of the internal gas transport in seagrass tissue (Borum et al. 2005; Borum et al. 2006; Pedersen et al. 2004). Later these findings were supported by planar optode measurements (Frederiksen and Glud, 2006; Jensen et al. 2005) enabling non-invasive imaging of the two-dimensional microdistribution of O_2 within the seagrass rhizosphere.

Microsensor techniques are limited by the difficulty of precise positioning of the microelectrode relative to roots and rhizomes. A commonly used method involves uncovering the root for microsensor positioning and subsequent covering with sediment. This limits the number of measuring points and can disturb redox conditions in natural sediment, especially when attempting microsensor measurements on actively growing roots (Jensen et al. 2005; Pedersen et al. 1998). Planar optodes provide a better overview of heterogeneity in the O_2 dynamics around the below-ground tissue but the biomass must be closely associated with the planar optode, which can affect the distribution of solutes in the

sediment by acting as a physical barrier to the diffusion of analyte compounds such as O_2 (Frederiksen and Glud, 2006). Most studies of the below-ground chemical microenvironment of seagrasses have focused on the O_2 microdistribution in the rhizosphere, while knowledge about the microdistribution and dynamics of important chemical species such as H_2S and pH is very limited. Effect of changing environmental conditions on seagrass health are thus largely based on several internal microelectrode measurements in the meristematic region of the rhizome (Binzer et al. 2005; Borum et al. 2005; Borum et al. 2006; Pedersen et al. 2004; Raun and Borum, 2013), while knowledge about the dynamics of the external below-ground biogeochemical microenvironment is still lacking.

In order to address some of the experimental limitations in previous studies, we developed a new methodology employing a split flow-chamber wherein seagrass specimens could be cultured in a transparent, sulphidic medium with properties mimicking those of typical reduced sediment. The setup enables the use of both microsensors and planar optodes for rapid determination of changes in the below-ground tissue chemical microenvironment in response to changing environmental conditions in the leaf region (i.e. light/dark shifts and water-column O_2 content). This experimental approach allows for efficient analyses of the effect of combined environmental stressors, such as those predicted from climate changes or caused by human activity, on the health of seagrasses and other aquatic macrophytes. Hence, the aims of this study were to: i) describe a new experimental approach that allows for measuring the dynamics of the chemical microenvironment around the tissue surface of aquatic macrophytes as a response to experimentally manipulated changing environmental conditions, and ii) investigate whether results obtained with this method are comparable to below-ground chemical microdynamics previously reported in natural sediment.

MATERIALS AND METHODS

Flow-chamber design

The flow-chamber consisted of a “water phase” compartment and an adjoining “sediment” compartment, connected by a small slit (Fig. 1.1).

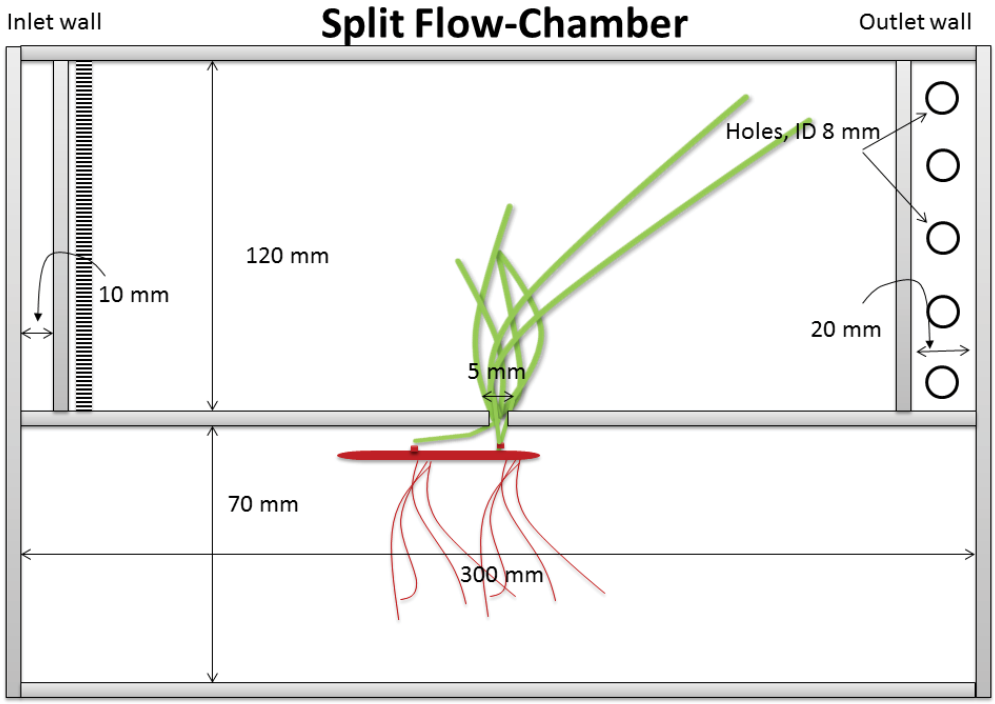

Figure 1.1. Schematic drawing of the applied split flow-chamber (top view) visualising the position of the examined seagrass specimen, with leaves in the "water" compartment and roots/rhizome in the "sediment" compartment (Detailed drawings are available in the supplementary information).

The "water" compartment was designed as a conventional flow cell, in which water flows uniformly from an inlet towards an outlet on the opposite side of the chamber. Water flow was maintained with a submersible pump connected to the chamber via a silicon hose (Fig. 1.2). The "sediment" compartment was fully closed off except for the narrow opening (5 mm) to the "water" compartment, through which the seagrass leaves could reach the water phase. This narrow opening was closed off by a small polystyrene-wedge after positioning of the seagrass specimen. To reduce influx of O_2 to the artificial sediment (described below) a silicon tube with numerous holes was positioned below the waterline in the "sediment" compartment and continuously flushed with humidified N_2. The water phase in the "sediment" compartment was covered with parafilm to reduce evaporation and advection, and lastly, a layer of aluminium foil was applied to further retain the N_2 in the chamber and to prevent roots being exposed to light. Microsensor measurements were performed through a small opening in the aluminium foil which could be closed off between measurements. In order to facilitate planar optode measurements (described below) from

the underside of the sediment chamber, the bottom of the split flow chamber was made from 3 mm thick, highly transparent polycarbonate. Detailed drawings of the flow chamber are provided as supplementary information (Fig. S1.1, S1.2, S1.3, S1.4 and S1.5).

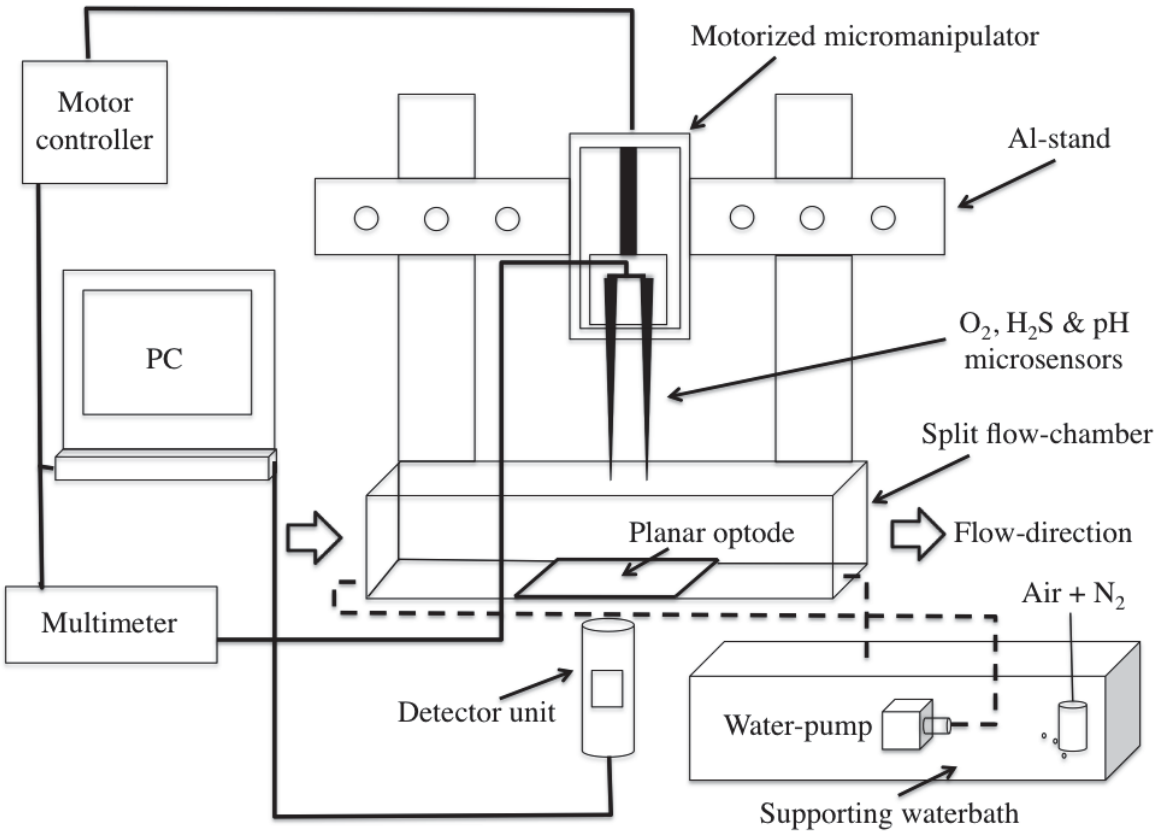

Figure 1.2. Schematic diagram of the experimental setup. Data acquisition and microsensor positioning was done with dedicated PC software (SensorTrace Pro, Unisense A/S, Denmark; VisiSens, PreSense, Germany).

Transparent artificial sediment

Artificial sediment was constructed to mimic chemical conditions in natural sediment while enabling direct visual navigation when performing the below-ground microsensor measurements. The artificial sediment (in the "sediment" compartment) consisted of three functional layers: 1) a bottom layer (~3 mm) of Na_2S enriched gauze (~1 mM H_2S) to ensure a continued diffusive supply of H_2S to the sediment, 2) a viscous, (~40 mm thick) anoxic layer of a ~0.2-0.7% agar-seawater solution deoxygenated via N_2 bubbling, buffered with HEPES buffer (10 mM) and amended with Na_2S to a final concentration of 50-200 µM H_2S,

and 3) a top layer (10-20 mm) of seawater kept hypoxic via continuous bubbling with humidified N_2 and thus functioning as an O_2 sink.

Filtered (0.22 μm) seawater was used throughout the experiment in order to ensure natural ratios of essential nutrients and avoid salinity gradients within the artificial sediment. For experiments involving planar optode measurements (see below), the gauze (layer 1) was excluded from the area above the planar optode to allow for direct visual inspection of the below-ground tissue from below the chamber. The separation of the different layers during casting of the artificial sediment was enabled by carefully pouring the upper medium with a plastic spoon to lower the impact force on the below medium.

Seagrass collection and maintenance

The seagrass specimens (i.e., *Halophila ovalis* and *Zostera muelleri* subsp. *capricorni*) were collected from shallow waters (less than 2 m depth) at Narrabeen Lagoon and Brisbane Waters, NSW, Australia. Specimens were transported to the University of Technology, Sydney within 2h of sampling, where the plants were maintained in a glasshouse under a natural light regime at a temperature of ~22°C and a salinity of ~ 34. The below-ground tissue of the plants selected for measurements was gently washed free of adhering sediment particles and left in the water column attached with loose rubber bands to small glass jars filled with sand. The latter was done to remove any remaining sediment particles from the root surface and root-hairs, without causing any damage to the root tissue. Furthermore, to obtain information on the natural chemical conditions in the sediment at the sampling site, a sediment core was collected at Narrabeen Lagoon adjacent to the seagrass meadow with a plastic tube (inner diameter 6.3 cm) used as corer.

Prior to each experiment, the seagrass plant was positioned horizontally in the split flow-chamber with the leaves in the free-flowing “water” compartment and the rhizome and roots supported in the deoxygenated agar matrix. Each plant was acclimatized in the split flow-chamber for several days prior to measurements and was acclimatized to the experimental conditions for a minimum of 3h before each experiment to ensure steady-state conditions.

Experimental setup

Illumination was provided by a tungsten halogen lamp fitted with a collimating lens (KL-2500, Schott GmbH, Germany). The downwelling photon irradiance (PAR, 400-700 nm) was measured with a scalar irradiance minisensor (US-SQS/L, Walz GmbH, Germany) connected to a calibrated quantum light meter (LI-250A, LI-COR, USA). The seagrass leaf canopy was positioned at the centre of the narrow light beam, thus limiting light exposure to the above-ground tissue. The plants were illuminated with an incident photon irradiance of 350-500 µmol photons m^{-2} s^{-1}. A constant flow (~1 cm s^{-1}) of aerated and thermostated seawater (22°C; salinity of 34) was maintained in the free-flowing seawater compartment by the submerged pump. Hypoxic water-column conditions (see experimental treatments below) were obtained by constantly flushing the supporting water-bath with a mixture of atmospheric air and nitrogen. The oxygen concentration of the water bath was monitored via a Clark-type O_2 microsensor (OX-100, tip diameter of ~100 µm, Unisense A/S, Aarhus, Denmark). Plants were cultured in the flow chamber for more than 2 weeks under constant conditions (22°C; Salinity of 34; 10:14 h light-dark cycle) and Chl *a* fluorometry was used to determine the longevity of seagrass plants held in the split flow-chamber.

Experimental treatments

To demonstrate the potential of the novel experimental approach, we aimed to examine the impact of following treatments: i) the effect of light exposure on the radial O_2 loss (ROL) from the below-ground tissue of *Halophila ovalis*; ii) the effect of light exposure and hypoxic (~50% air saturation) conditions in the water column during darkness on ROL from the below-ground tissue of *Zostera muelleri*; iii) the steady state dynamics of the below-ground chemical microenvironment modified by *Zostera muelleri*; and finally, iv) how the oxic microshield and the spatial O_2 heterogeneity within the rhizosphere of *Zostera muelleri* is affected by a light-dark transition. The *Halophila ovalis* measurements are mainly included in this study to show that the experimental approach can be applied to different aquatic macrophytes with e.g. highly different morphological appearance (i.e., the leaves of the *Zostera muelleri* specimens were ~40 cm in length, as compared to *Halophila ovalis* only ~5 cm), thereby illustrating the high potential of the used methodology.

Microsensor measurements

We used Clark-type O_2 and H_2S microsensors (OX-50 and H2S-50, tip diameter of ~50 µm, Unisense A/S, Aarhus, Denmark; response time <5 and 10 s, respectively; stirring sensitivity <2%) to measure the O_2 and H_2S concentrations of the below-ground microenvironment (Jeroschewski et al. 1996; Revsbech 1989). pH values were measured with pH microelectrodes (PH-50, Unisense A/S, Denmark; Kühl and Revsbech (2001)). All microsensors were mounted on a motorized micromanipulator and connected to a 4-channel multimeter (Unisense A/S, Denmark) both interfaced with a PC running data acquisition and positioning software (SensorTrace PRO, Unisense A/S, Denmark). The microsensors were linearly calibrated at experimental temperature and salinity before microprofiling commenced (further information on the calibration procedures is provided by the manufacture on www.unisense.com). The microsensors were positioned at the seagrass tissue surface (defined as 0 µm distance) by means of the micromanipulator. This was done by manually moving the microsensors while observing the microsensor tip and tissue surface through a stereo-microscope (AmScope, Irvine, CA, USA) equipped with a small observation device in the form of a custom-made polycarbonate plastic tube closed off by a clear window. The device was carefully submerged into the water column of the sediment compartment without disturbing the artificial sediment surface, and enabled a less obstructed/distorted view through the microscope by excluding the air/water interface. Microprofiles around the below-ground tissue were measured in increments of 50-100 µm, whereas microprofiles describing the artificial sediment were measured in vertical step sizes of 1000 µm.

Microsensor measurements within natural sediment

Vertical O_2 and H_2S microprofiles in natural sediment were obtained as described above. The sediment core was submerged into a cylinder-shaped aquarium (~2 L), and stirring was achieved via a constant flow of atmospheric air from an air-pump, applied onto the water surface through a Pasteur pipette (sediment surface at ~3 cm depth; ~22°C; salinity of 34; incident irradiance of ~10 µmol photons m^{-2} s^{-1}).

Planar optode measurements

The spatial O_2 heterogeneity within the immediate rhizosphere of *Zostera muelleri* was mapped with a transparent planar O_2 optode (Glud et al. 1996; Jensen et al. 2005) providing information on the two-dimensional O_2 distribution around the below-ground tissue. The planar optode consisted of an O_2 quenchable platinum(II)octaethylporphyrin luminophore (indicator dye) combined with a light harvesting antenna dye (Macrolex® fluorescence yellow 10GN) immobilized in polystyrene on a 125 µm thick, transparent polyester support foil and covered with a semi-transparent silicon layer containing carbon powder (Larsen et al. 2011). The planar optode was imaged with a compact USB-camera O_2 imaging system (Visisens, Presens, Germany) interfaced to a PC running the manufacturers imaging software system (VisiSens, PreSens, Germany). The detecting unit consisted of a digital camera equipped with a long pass filter and violet-blue LEDs for excitation of the planar optode (VisiSens, PreSens, Germany).

The planar optode system used a colour ratiometric imaging approach (Larsen et al. 2011), where the LED excites both the reference and the O_2 sensitive dye causing dual emission, i.e., red luminescence from the O_2-quenchable indicator dye and green luminescence from the inert reference. The recorded intensity ratio between the recorded luminescence intensity in the red and green channel of the USB camera (i.e., Ratio = (Red – Green) / Green) provides a measure of the O_2 concentration at the surface of the planar optode. The planar optode was calibrated in anoxic (N_2 flushed) and air-saturated seawater before measurements commenced (further information on calibration procedures and image-recordings are provided in Larsen et al. (2011)).

The planar optode was fixed on the bottom wall of the “sediment” compartment of the split flow-chamber, using a thin layer of non-toxic silicone grease to “glue” the optode to the chamber bottom, carefully avoiding formation of air bubbles in between the chamber wall and optode. The sides of the optode were fixed with small pieces of tape. A seagrass plant was then positioned with the below-ground tissue touching the optode, where after the fluid artificial sediment (~36°C) was gently poured into the compartment followed by rapid cooling to air temperature (22°C). Finally, a layer of anoxic seawater was established above

the solidified artificial sediment by gently pouring nitrogen flushed seawater over the sediment as described above.

Flux calculations

A cylindrical version of Fick's first law of diffusion was used to calculate the radial oxygen fluxes from the root-shoot junctions (Steen-Knudsen 2002), assuming a perfect homogeneous and cylinder shaped oxic microzone:

$$J(r)_{below\text{-}ground\ tissue} = \varphi Ds\ (C_1 - C_2) / r \ln (r_1/r_2)$$

where ϕ is the porosity, *Ds* is the apparent oxygen diffusion coefficient within the artificial sediment (here assumed similar to the molecular diffusion coefficient of O_2 in seawater, D_0), *r* is the tissue radius, and C_1 and C_2 are the measured O_2 concentrations at the distances r_1 and r_2, respectively (i.e. the inner and outer distance from the root centre). The porosity of the artificial sediment was calculated to be 0.95 from the weight loss of wet-sediment (known initial volume) after drying in a 105°C oven until a constant weight was reached. The radius of the root-shoot junction was defined under a stereo-microscope. D_0 at the experimental temperature and salinity was obtained from tables available from Unisense A/S (www.unisense.com).

RESULTS

Chemical properties of the artificial sediment

The O_2 concentration of the seawater layer overlying the artificial sediment (i.e., the O_2 sink) was ~15 µmol L^{-1} owing to the continuous flushing with N_2 gas, which kept the artificial sediment anoxic for the duration of the experiments (Fig. 1.3a). In the first few mm of the artificial sediment, O_2 concentrations were low and decreased rapidly with depth as typical for natural marine sediment (Fig. 1.3a, b). The thin oxic zone was followed by an anoxic homogeneous zone, which extended to the bottom of the chamber. The seagrass below-ground tissue (i.e., root-shoot junction, rhizome and roots) was placed >20 mm below the artificial sediment surface to ensure no O_2 from the surface would reach the below-ground tissue, and all microsensor measurements were performed below this depth. In the anoxic part of the artificial sediment, we observed a rapid increase in the H_2S concentration with depth, reaching a maximum concentration of ~65 µmol L^{-1} at 3.6 cm depth (i.e. the deepest measured point within the artificial sediment ~10 mm below the below-ground tissue (Fig. 1.3a)). The pH value of the artificial sediment decreased from ~7.5 at the surface of the sediment to pH 7 at the deepest point measured (~4 cm depth) (Fig. 1.3a). In comparison, the O_2 penetration depth within the natural marine sediment was ~ 1 mm and the H_2S concentration reached ~ 65 µmol L^{-1} at 4.5 cm depth (Fig. 1.3b).

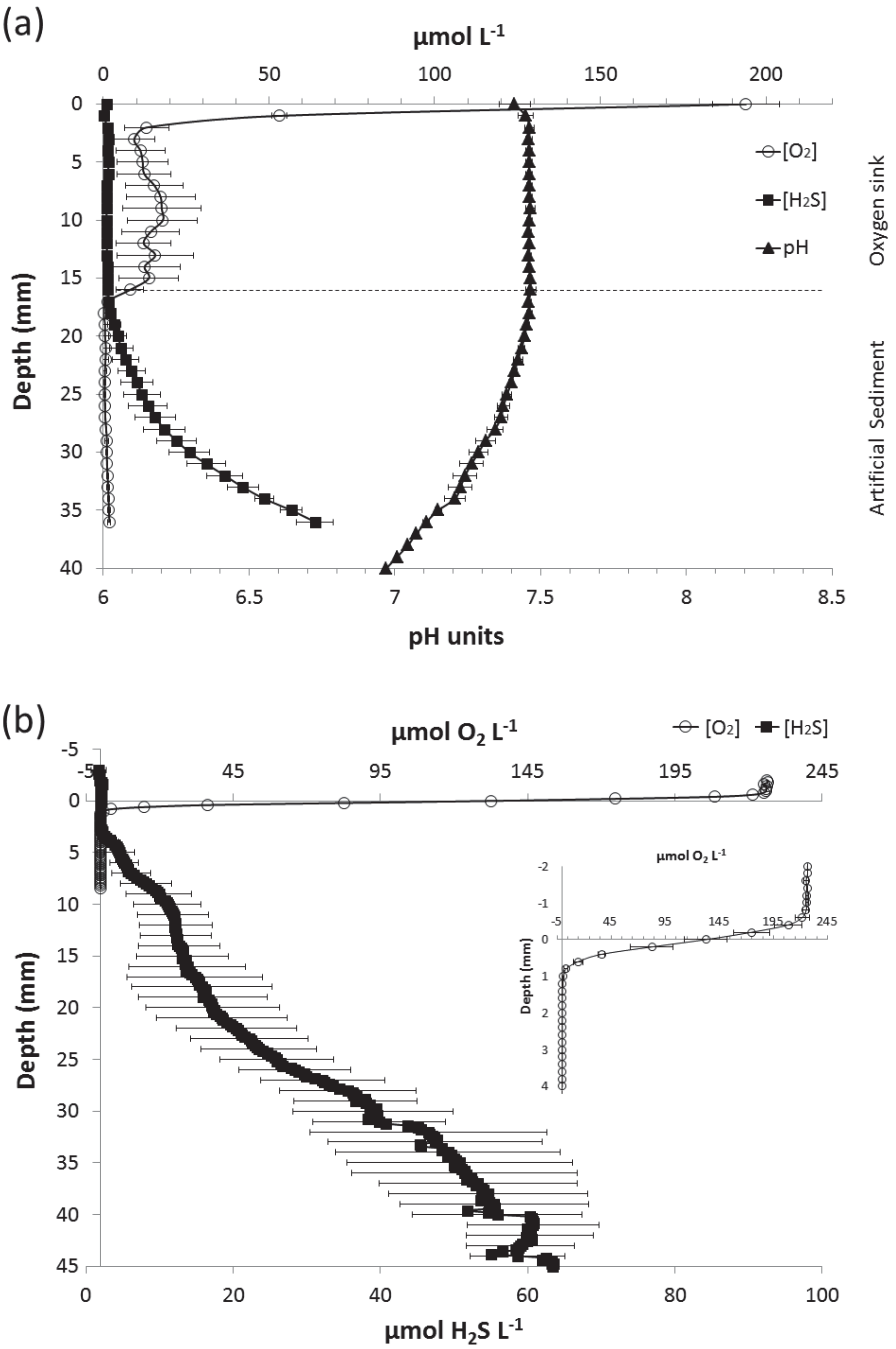

Figure 1.3. (a) Vertical microprofiles of $[O_2]$, $[H_2S]$ and pH in the artificial sediment from the surface of the overlying O_2 sink (N_2 flushed seawater; ~16 mm deep) until ~10 mm below the below-ground tissue at a total vertical depth of ~4 cm. The dotted line represents the surface of the artificial sediment. All microsensor measurements are performed after the acclimatization period of the plants in the chamber, just prior to the experiments. (b) Vertical microprofiles of $[O_2]$ and $[H_2S]$ in natural sediment originating from Narrabeen Lagoon, NSW, Australia. An enlarged plot of the $[O_2]$ microprofile across the water-sediment interface is inserted. Legends depict the different chemical species. Symbols and error bars indicate mean ± SD (n = 3-4).

Seagrass health during cultivation

Pulse amplitude modulated (PAM) fluorometry measurements of photosynthetic performance (Beer et al. 1998; Ralph and Short 2002) confirmed that the plants were still healthy and photosynthetic competent after the two week incubation (Fv/Fm ~0.7; *Z. muelleri*). Furthermore, a complete new root-bundle, internode and new leaves developed over a 7-8 day period in both species, signifying active growth in the flow chamber. Over the duration of the experiment, the new roots reached a length of 3 cm on average, corresponding to a growth rate of 0.4 cm d^{-1}, which is comparable to growth rates found for *Zostera marina* growing in natural sediment (Jensen et al. 2005).

Below-ground O_2 dynamics in the seagrass rhizosphere

Light exposure of the above-ground tissue of *Zostera muelleri* resulted in a ~3-fold increase in the radial O_2 loss from the root-shoot junction, increasing from 1.05 mmol O_2 m^{-2} h^{-1} in darkness to ~3.0 mmol O_2 m^{-2} h^{-1} under an incident irradiance of ~350 µmol photons m^{-2} s^{-1} (Fig. 1.4a). The radial O_2 loss from the root-shoot junction resulted in the establishment of a ~300 µm thick oxic micro-niche in the surrounding sediment. Hypoxic conditions (~50% air saturation) in the water-column of the "water" compartment resulted in a complete disappearance of the oxic microzone surrounding the meristematic region of the rhizome, i.e., around the combined rhizome/basal leaf meristem area at the root-shoot junction (Fig. 1.4a). From the root-shoot junction of *Halophila ovalis* we found a ~6-fold increase in the radial O_2 loss as a response to light stimuli, with O_2 fluxes increasing from 1.06 mmol O_2 m^{-2} h^{-1} in darkness to 6.5 mmol O_2 m^{-2} h^{-1} under an incident irradiance of ~500 µmol photons m^{-2} s^{-1} (Fig. 1.4b).

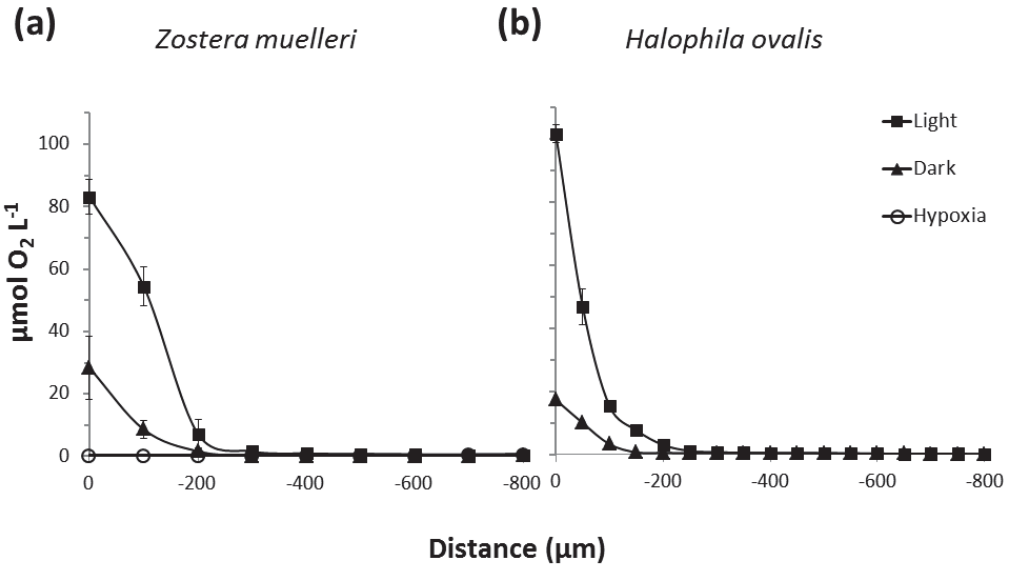

Figure 1.4. (a) Radial O_2 loss from the root-shoot junction of *Zostera muelleri* as measured with O_2 microelectrodes during darkness (triangles), under an incident irradiance of ~350 µmol photons m^{-2} s^{-1} (squares), and in darkness with hypoxic conditions (~50% air saturation) in the water-column surrounding the leaves (empty circles). n=3. (b) Microelectrode measurements of the radial O_2 loss from the root-shoot junction of *Halophila ovalis* measured in darkness (triangles) and under an incident irradiance of ~500 µmol photons m^{-2} s^{-1} (squares). n = 4-5. Plants were investigated at the light intensity they were acclimatized to during cultivation/maintenance. Distance (in µm) refers to the distance from the below-ground tissue, where x-axis = 0 indicate the below-ground tissue surface. Symbols and error bars indicate mean ± SD.

Chemical microenvironment at the below-ground tissue surface

The chemical microenvironment in the immediate rhizosphere of *Zostera muelleri* at the root-shoot junction during darkness is shown in Figure 1.5. Microelectrode measurements revealed a decrease in the H_2S concentration within the oxic microshield, decreasing from ~11.3 to 0 µmol H_2S L^{-1} at the below-ground tissue surface over a distance of ~1 mm, demonstrating complete re-oxidation and removal of phytotoxic H_2S at the tissue surface. The pH value decreased from 6.8 in the immediate rhizosphere to 4.7 at the tissue surface,

likewise with a relatively steep gradient within the ~400µm thick oxic micro-niche (Fig. 1.5). The O_2 concentration at the below-ground tissue surface was ~65 µmol O_2 L^{-1} (Fig. 1.5).

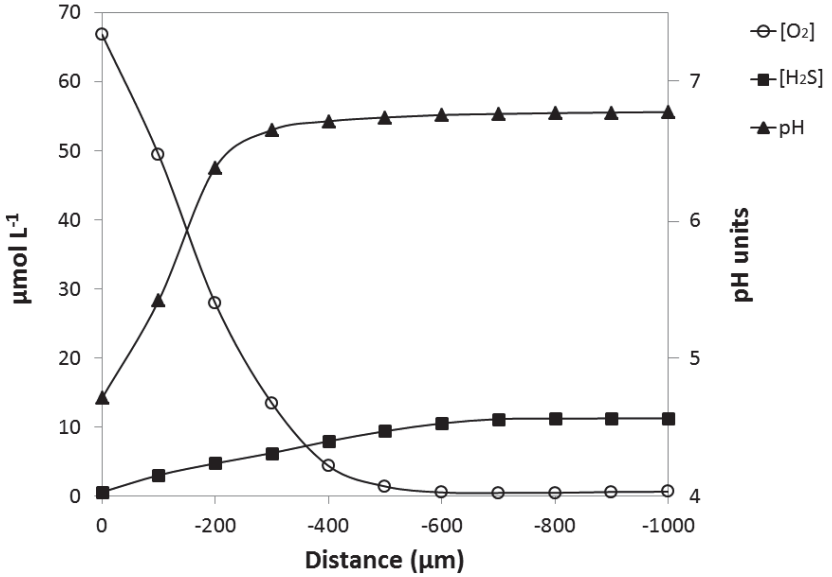

Figure 1.5. The chemical microenvironment at the meristematic region of the rhizome of *Zostera muelleri* measured with O_2, H_2S and pH microelectrodes. Legend depicts the different chemical species: O_2 concentration (empty circles); H_2S concentration (squares); pH values (triangles). Distance (in µm) refers to the distance from the below-ground tissue, where x-axis = 0 indicate the below-ground tissue surface. Average; no error bars. n = 2.

Distribution of O_2 within the rhizosphere of *Zostera muelleri*

The two-dimensional planar optode images, visualising the spatial O_2 microdistribution at the root-shoot junction, revealed O_2 loss from the below-ground tissue of *Zostera muelleri* both from roots of the first actively growing root-bundle and from the root-shoot junction. This lead to the establishment of oxic microzones with O_2 concentrations reaching up to ~60% air saturation in light (~300 µmol photons m^{-2} s^{-1}; Fig. 1.6). Light stimulation of the leaf canopy resulted in an expansion of the oxic microzones and enhanced O_2 leakage into the rhizosphere, as compared to in darkness (Fig. 1.6).

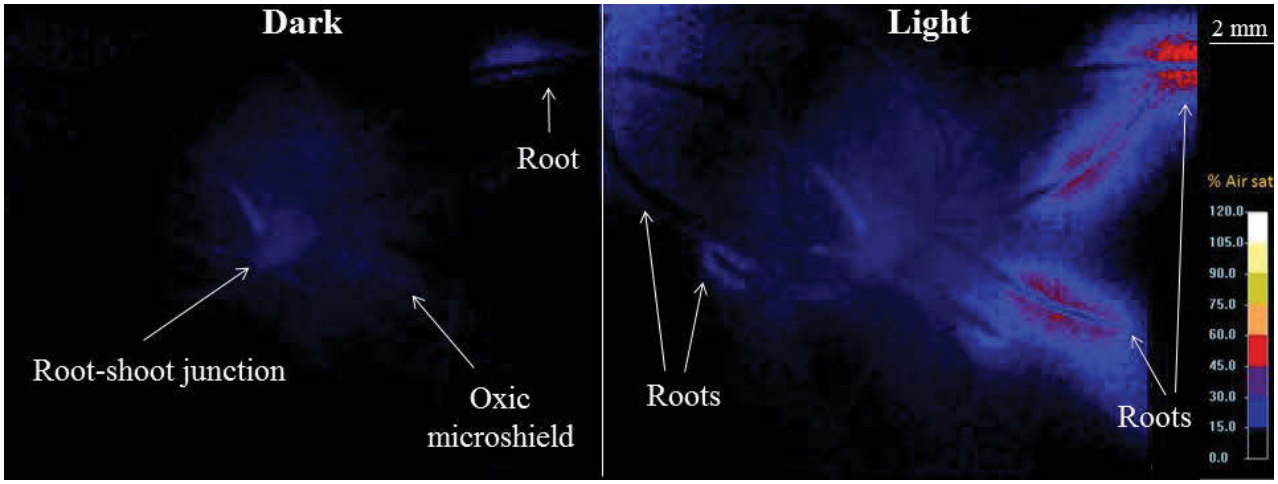

Figure 1.6. The spatial O_2 heterogeneity within the rhizosphere of *Zostera muelleri* mapped via planar optodes during light-dark transitions. Measurements were taken at quasi-steady state at a temperature of 22°C, a salinity of 35 and a water column flow-velocity of 1 cm s^{-1}. The legend shows the O_2 concentration in % air saturation.

DISCUSSION

The new split flow-chamber with transparent, artificial sediment enables investigations with high spatio-temporal resolution and replication to resolve effects of changing environmental conditions on seagrasses and their ability to modify the chemical microenvironment around their below-ground tissue. We examined the effect of light-dark transitions and hypoxic water column conditions on the oxidation capability of the below-ground tissue. The O_2 flux rates measured at the below-ground tissue of both seagrass species were similar to previous reported O_2 flux rates from the roots of *Cymodocea rotundata* in natural sediment (Pedersen et al. (1998); 2.3 and 5.3 mmol O_2 m^{-2} h^{-1} in darkness and light at equivalent incident irradiance, respectively). The radial O_2 loss (ROL) resulted in a 200-400 µm oxic microzone surrounding the root-shoot junction (Fig. 1.4), with a slight enhanced spatial distribution during light stimulation (~50 µm), owing to additional O_2 in the leaf aerenchyma due to photosynthesis (Fig. 1.4). The extent of the oxygenated microzones is defined by the balance between the rate of ROL and the total O_2 consumption rate of the surrounding sediment and were similar in extension to what has been found in previous studies in natural sediment (Jensen et al. 2005). Hence, the artificial sediment in the split flow-chamber setup appeared to mimic basic properties of natural sediment. Furthermore,

seagrass sediments are generally very rich in organic matter and therefore exhibit high microbial activity, which in combination with a low O_2 solubility in water and low diffusion rate, results in very low O_2 penetration depths (often only a few mm; as seen on Figure 1.3b). As such, by far most of the seagrass below-ground biomass resides in anoxic sediment, and therefore, we find that the chosen method to a reasonable extent replicates natural conditions. While the present study focuses on chemical dynamics, the setup could be further modified to include natural sediment pore-water with its abundance of microbes. This would allow for the development and quantification of biogeochemical processes (such as microbial sulphide oxidation) in the setup, which likely would influence the chemical microenvironment around the below ground tissue. Such studies are underway.

When atmospheric O_2 was introduced to the seawater overlying the artificial sediment (O_2 sink) during measurements, the O_2 concentration of this sink depended on the total time that was spent on measuring during an experiment. During prolonged measurements (>4h), the O_2 concentration reached a maximum of ~40 µmol O_2 L^{-1} (data not shown), whereas the O_2 concentration of the sink was ~0 µmol O_2 L^{-1} in between measurements, as a result of the covering of the "sediment" compartment containing the artificial sediment (based on initial measurements in the sink just after removing the cover; data not shown). Importantly, however the increase in O_2 concentration did not extend to the deeper parts of the artificial sediment, where the seagrass rhizome and roots persisted in anoxia. Nevertheless, it is advisable to limit the measuring time and completely cover the "sediment" compartment of the split flow-chamber between measurements to flush out the small amount of O_2 introduced during measurements. To avoid movement (wobbling) of the artificial sediment, the flow rate of N_2 had to be limited, resulting in the less than optimal O_2 removal efficiency during measurements. However, this issue may be alleviated by increasing the agar concentration of the artificial sediment at the cost of a significantly reduced visibility through the sediment.

The planar optode images revealed O_2 leakage from both the root-shoot junction and from the new and actively growing roots of *Zostera muelleri* (Fig. 1.6). The spatial distribution of O_2 expanded during light stimulation of photosynthesis in the leaf canopy, thus supporting the microelectrode findings (Fig. 1.4). Both the microelectrode and planar optode

measurements confirmed decreased oxidation capability of the below-ground tissue during darkness. In addition, hypoxic conditions in the water column resulted in an inability to sustain the external oxic microshield around the meristematic region of the rhizome, likely as a result of inadequate internal aeration (Fig. 1.4). This confirms a dependency of *Z. muelleri* on passive diffusion of O_2 from the water column during night time, as previously reported in other seagrass species (e.g., Pedersen et al. 2004; Borum et al. 2005), particularly during summertime where plant respiration rates may be high, as a result of elevated seawater temperatures (Raun and Borum, 2013).

The presence of the oxic microshield seemed to reduce the concentration of H_2S in the rhizosphere, most likely as a result of chemical oxidation of H_2S with O_2 ($2O_2 + H_2S \rightarrow 2H^+ + SO_4^{2-}$). This process leads to formation of protons and can therefore explain the observed decrease in pH within the oxic microzone (Fig. 1.5). This phenomenon was also observed in a recent study, describing the dynamics of the chemical below-ground microenvironment of *Z. muelleri* under changing environmental conditions (Brodersen et al. submitted). Interestingly, a drop in pH within the oxic microzone towards the tissue surface (as seen on Fig. 1.5), would likely lead to dissolution of carbonates and concomitant release of sediment-bound phosphorus, which is generally a limiting nutrient in carbonate-rich sediments.

Prolonged periods of darkness thus have a significant negative impact on the oxidation capacity of the below-ground tissue, and in combination with decreased water column O_2 content, this could leave seagrasses more sensitive to H_2S in the sediment as a result of inadequate internal aeration (Borum et al. 2005; Pedersen et al. 2004). Anthropogenic activities resulting in poor light conditions in the seagrass canopy, such as in the case of dredging operations where water-column turbidity is greatly increased (Erftemeijer and Lewis 2006), may thus have a substantial negative impact on the health of seagrass meadows, especially if enhanced respiration rates in the water column results in overnight hypoxia.

The presented experimental approach has broad applications within aquatic macrophyte ecophysiology and ecology. In this study, we focussed on the impact of environmental

changes to the below-ground microenvironment, but effects on the above-ground microenvironment can easily be addressed as well. This could include investigations of: i) how the thickness of the diffusive boundary layer around the leaves is affected by decreased water motion due to epiphyte growth on the leaf surface; and ii) how the internal O_2 levels in leaves and rates of photosynthesis and respiration are affected by water turbidity. The main advantage of the presented experimental approach, as compared to previous used methodology (e.g. Jensen et al. 2005; Pedersen et al. 1998) is, however, that it simplifies the use of microsensors for measurements of the chemical microenvironment in the immediate rhizosphere, allowing for more frequent and detailed measurements with minimal risk of breaking the fragile microsensor tip. The artificial sediment allows for exact determination of the position of the microelectrode tip relative to the tissue surface, which is essential when doing quantitative calculations of fluxes and metabolic rates from microgradients. Such measurements can now be combined with planar optode measurements to get a more detailed mapping of the heterogeneity in the chemical microenvironment around the below-ground tissue, which otherwise would be challenging to obtain in natural sediment.

In summary, the experimental approach described in this paper has broad application within all micro-scale studies of aquatic macrophytes including plant-sediment interactions. A detailed understanding of how changing environmental conditions affect the health of aquatic macrophytes such as seagrasses, through its effect on the plants performance and its interaction with the surrounding sediment biogeochemistry, can lead to important new insight enabling better direction of coastal management resources, as well as provide a better understanding of the consequences of anthropogenic-induced stressors such as eutrophication and harbour dredging operations.

ACKNOWLEDGEMENTS

We would like to thank technical officer Paul Brooks (UTS) for fruitful discussions and help during the development of the experimental setup and Frederic Cadera (UTS) for helping with seagrass and sediment sampling. We thank Michael A. Rasheed for his intellectual contribution to the research in question. We acknowledge Ole Pedersen and Jens Borum for thoughtful initial discussions. This research was funded by the Australian Research Council (ARC) (MK, PJR), the Danish Council for Independent Research | Natural Sciences (MK) and through grants from the *Augustinus Foundation* and *Fabrikant P.A. Fiskers Foundation* (KEB).

REFERENCES

Beer S, Vilenkin B, Weil A, Veste M, Susel L, Eshel A. (1998). Measuring photosynthetic rates in seagrasses by pulse amplitude modulated (PAM) fluorometry. *Marine Ecology Progress Series* **174:** 293-300.

Binzer T, Borum J, Pedersen O. (2005). Flow velocity affects internal oxygen conditions in the seagrass *Cymodocea nodosa*. *Aquatic Botany* **83:** 239-247.

Borum J, Pedersen O, Greve TM, Frankovich TA, Zieman JC, Fourqurean JW, Madden CJ. (2005). The potential role of plant oxygen and sulphide dynamics in die-off events of the tropical seagrass, *Thalassia testudinum*. *Journal of Ecology* **93:** 148-158.

Borum J, Sand-Jensen K, Binzer T, Pedersen O, Greve T. (2006). Oxygen movement in seagrasses. In: Larkum AWD, Orth JR & Duarte CM, Eds., Seagrass: Biology, Ecology, and Conservation, Springer, Dordrecht, The Netherlands**:** 255-270.

Caffrey JM, Kemp WM. (1991). Seasonal and spatial patterns of oxygen production, respiration and root-rhizome release in *Potamogeton perfoliatus L*. and *Zostera marina L*. *Aquatic Botany* **40:** 109-128.

Costanza REA. (1997). The value of the world's ecosystem services and natural capital. *Nature* **387:** 253-260.

Erftemeijer PLA, Lewis RRR. (2006). Environmental impacts of dredging on seagrasses: a review. *Marine Pollution Bulletin* **52:** 1553-1572.

Frederiksen MS, Glud RN. (2006). Oxygen dynamics in the rhizosphere of Zostera marina: A two-dimensional planar optode study. *Limnol. Oceanogr* **51:** 1072-1083.

Glud RN, Ramsing NB, Gundersen JK, Klimat I. (1996). Planar optrodes: a new tool for fine scale measurements of two-dimensional O2 distribution in benthic communities. *Marine Ecology Progress Series* **140:** 217-226.

Greve TM, Borum J, Pedersen O. (2003). Meristematic oxygen variability in eelgrass (Zostera marina). *Limnology and Oceanography* **48:** 210-216.

Holmer M, Bondgaard EJ. (2001). Photosynthetic and growth response of eelgrass to low oxygen and high sulfide concentrations during hypoxic events. *Aquatic Botany* **70:** 29-38.

Holmer M, Pedersen O, Krause-Jensen D, Olesen B, Hedegård Petersen M, Schopmeyer S, Koch M, Lomstein BA, Jensen HS. (2009). Sulfide intrusion in the tropical seagrasses *Thalassia testudinum* and *Syringodium filiforme*. *Estuarine, Coastal and Shelf Science* **85:** 319-326.

Jensen SI, Kühl M, Glud RN, Jørgensen LB, Prieme A. (2005). Oxic microzones and radial oxygen loss from roots of *Zostera marina*. *Marine Ecology Progress Series* **293:** 49-58.

Jensen SI, Kühl M, Prieme A. (2007). Different bacterial communities in the rhizoplane and bulk sediment of the seagrass Zostera marina. *FEMS Microbiology Ecology* **62:** 108-117.

Jeroschewski P, Steuckart C, Kühl M. (1996). An amperometric microsensor for the determination of H2S in aquatic environments. *Analytical Chemistry* **68:** 4351-4357.

Kühl M, Revsbech NP. (2001). Biogeochemical microsensors for boundary layer studies, p. 180-210. In: B. P. Boudreau and B. B. Jørgensen [eds.], *The benthic boundary layer*. Oxford University Press, New York.

Larkum AWD, Orth RJ, Duarte CM. (2006). Seagrasses: Biology, Ecology, and Conservation. Springer, Berlin.

Larsen M, Borisov SM, Grunwald B, Klimant I, Glud RN. (2011). A simple and inexpensive high resolution color ratiometric planar optode imaging approach: application to oxygen and pH sensing. *Limnol. Oceanogr.: Methods* **9:** 348-360.

Orth RJ, Carruthers TJB, Dennison WC, Duarte CM, Fourqurean JW, Heck Jr. KL, Hughes AR, Kendrick GA, Kenworthy WJ, Olyarnik S, et al. (2006). A global crisis for seagrass ecosystems. BioScience **56:** 987-996.

Pedersen O, Binzer T, Borum J. (2004). Sulphide intrusion in eelgrass (*Zostera marina L*). *Plant, Cell and Environment* **27:** 595-602.

Pedersen O, Borum J, Duarte CM, Fortes MD. (1998). Oxygen dynamics in the rhizosphere of *Cymodocea rotundata*. *Marine Ecology Progress Series* **169:** 283-288.

Pedersen O, Borum J, Duarte CM, Fortes MD. (1999). ERRATUM: Oxygen dynamics in the rhizosphere of *Cymodocea rotundata*. *Marine Ecology Progress Series* **178:** 310.

Perez-Perez ME, Lemaire SD, Crespo JL. (2012). Reactive oxygen species and autophagy in plants and algae. *Plant Physiology* **160:** 156-164.

Ralph PJ, Short FT. (2002). Impact of the wasting disease pathogen, Labyrinthula zosterae, on photobiology of eelgrass *Zostera marina*. *Marine Ecology Progress Series* **226:** 265-271.

Ralph PJ, Tomasko D, Moore K, Seddon S, Macinnis-Ng C. (2006). Human impact on Seagrasses: Eutrophication, Sedimentation and Eutrophication. In: Larkum AWD, Orth JR & Duarte CM, Eds. *Seagrass Biology, Ecology and Conservation*. Springer, Berlin**:** 567-593.

Raun AL, Borum J. (2013). Combined impact of water column oxygen and temperature on internal oxygen status and growth of Zostera marina seedlings and adult shoots. *Journal of Experimental Marine Biology and Ecology* **441:** 16–22.

Raven JA, Scrimgeour CM. (1997). The influence of anoxia on plants of saline habitates with special reference to the sulfur cycle. *Annals of Botany* **79:** 79-86.

Revsbech NP. (1989). An oxygen microsensor with a guard cathode. *Limnology and Oceanography* **34:** 474-478.

Steen-Knudsen O. (2002). Biological membranes: Theory of Transport, Potentials and Electric Impulses. Cambridge University Press.

Waycott M, Duarte CM, Carruthers TJB, Orth RJ, Dennison WC, Olyarnik S, Calladine A, Fourqurean JW, Heck Jr. KL, Hughes AR, et al. (2009). Accelerating loss of seagrasses across the globe threatens coastal ecosystems. *PNAS* **106:** 12377–12381.

SUPPORTING INFORMATION

A split flow-chamber with artificial sediment to examine the below-ground microenvironment of aquatic macrophytes

Kasper Elgetti Brodersen, Daniel A. Nielsen, Peter J. Ralph & Michael Kühl

University of Technology, Sydney, Australia & University of Copenhagen, Denmark.

SPLIT FLOW-CHAMBER DRAWINGS

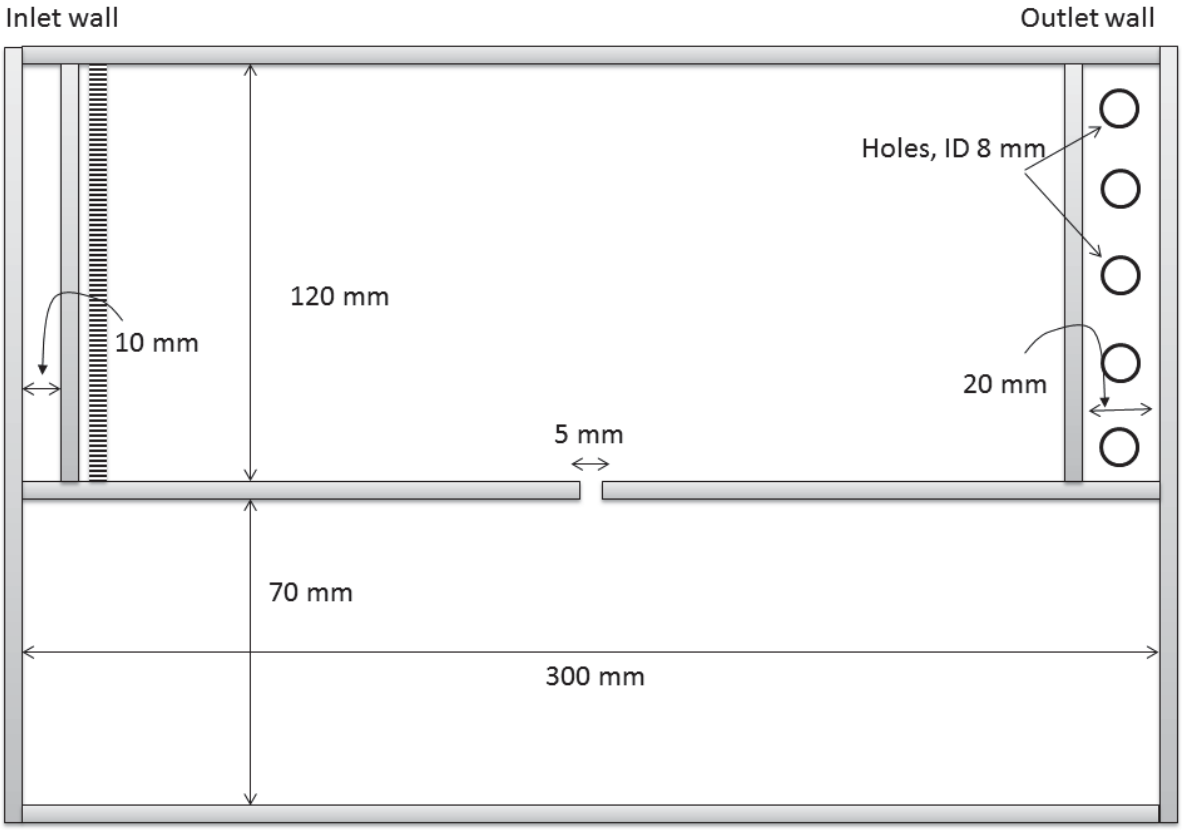

Fig. S1.1: Schematic drawing of the split flow-chamber (top view).

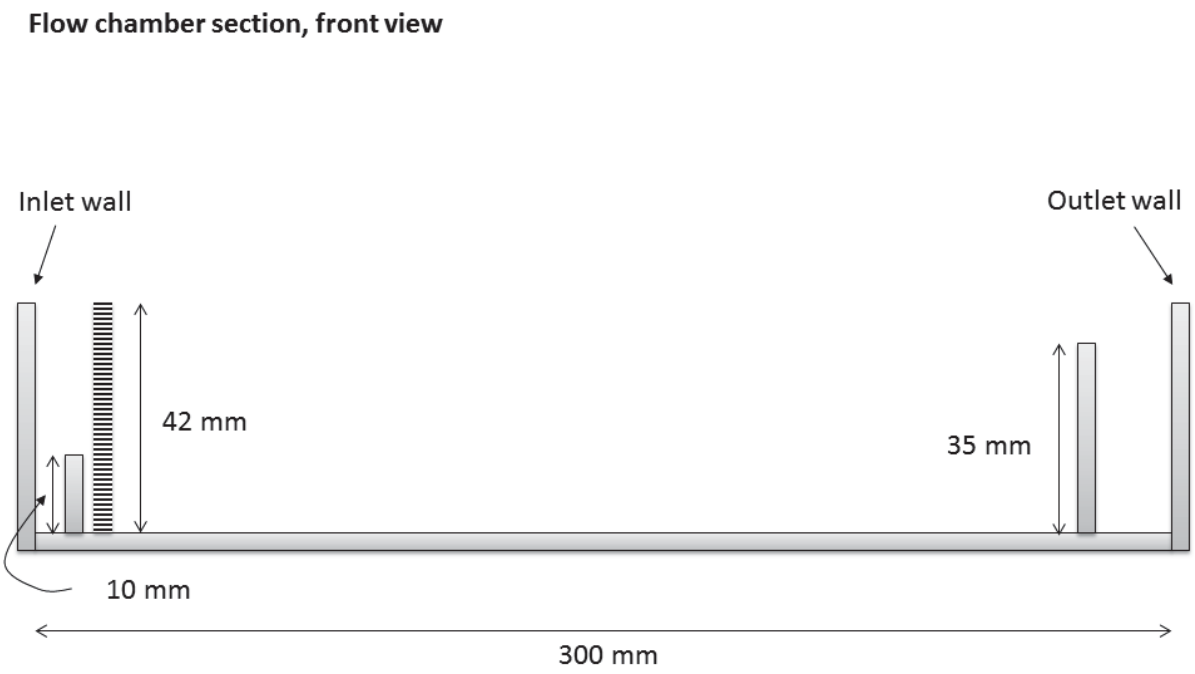

Fig. S1.2: Schematic drawing of the split flow-chamber (front view). Illustrating the upper compartment (flow cell) containing the free-flowing seawater.

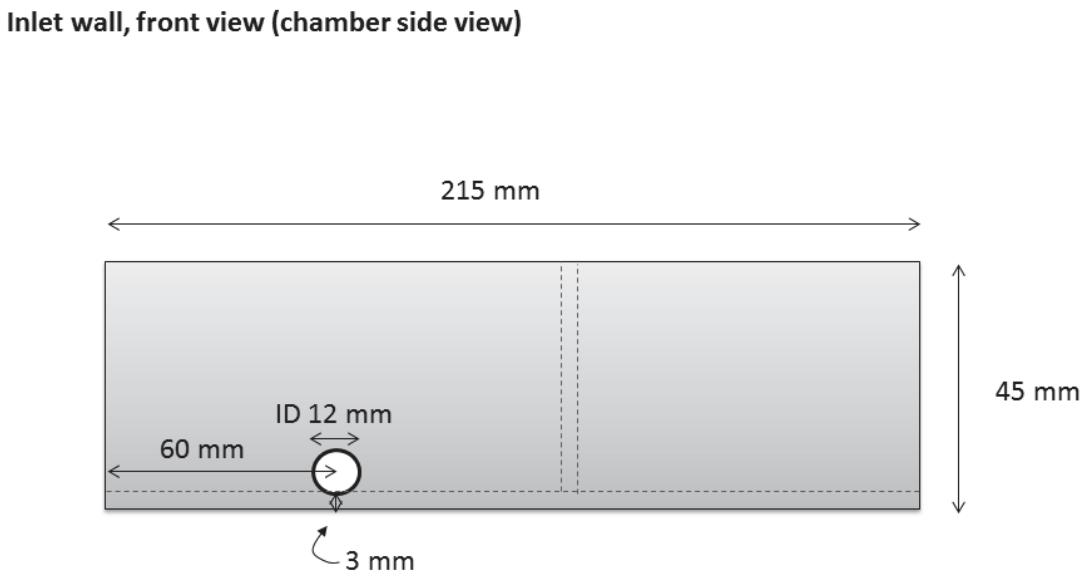

Fig. S1.3: Schematic drawing of the split flow-chamber (side view). Illustrating the inlet wall at the side of the chamber and the division of the chambers.

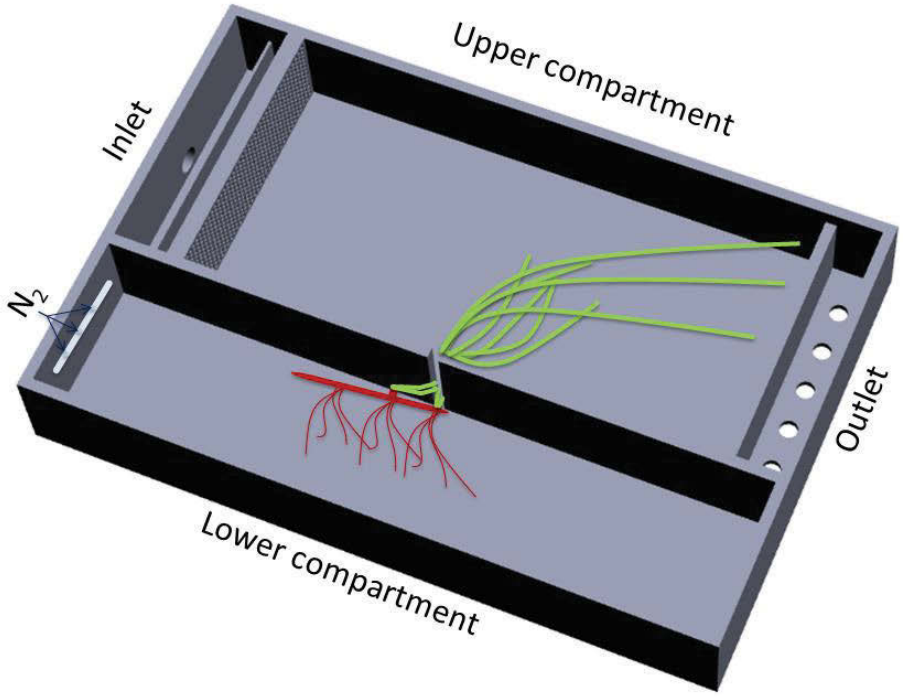

Fig. S1.4: Schematic drawing of the applied split flow-chamber (in 3-D) visualising the position of the examined seagrass specimen. Illustrated by DOTMAR Engineering Plastic Products (DOTMAR EPP) Pty Ltd, NSW, Australia (www.dotmar.com.au).

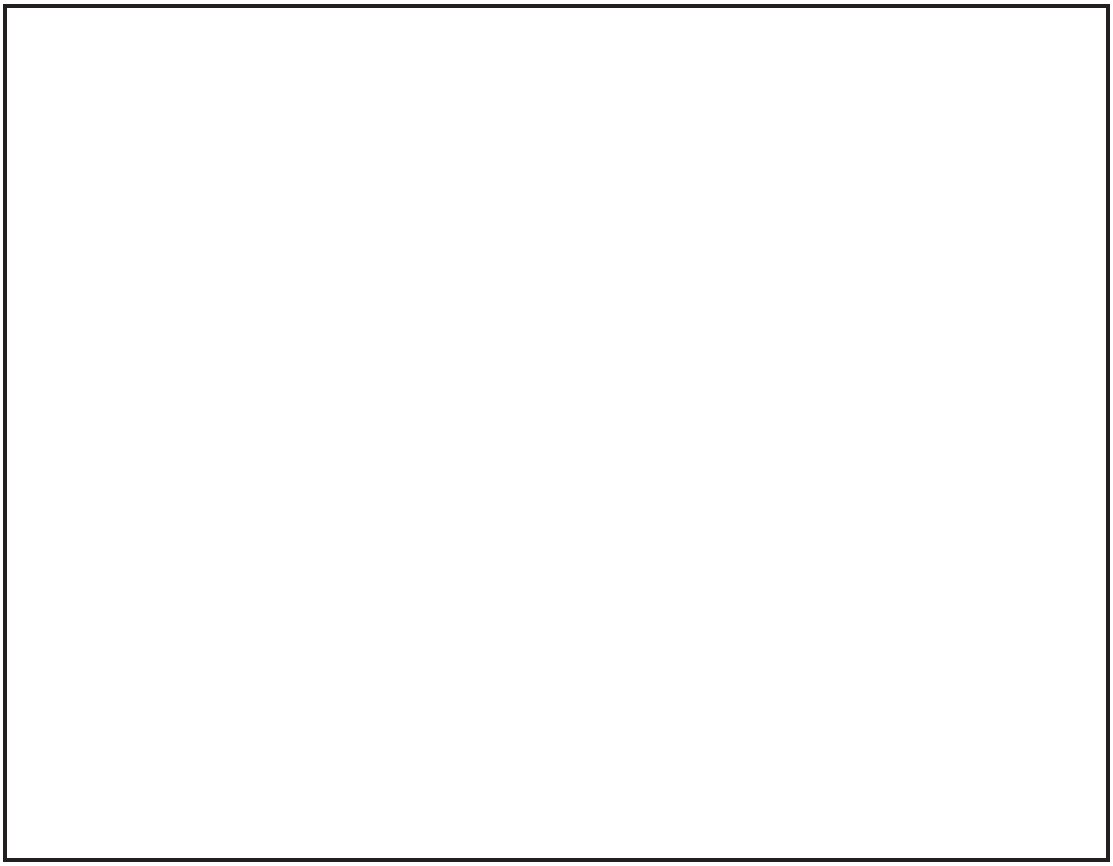

Fig. S1.5: 3-D animation of the applied split flow-chamber. Double-click to open Acrobat document (animation provided by DOTMAR Engineering Plastic Products (DOTMAR EPP) Pty Ltd, NSW, Australia; www.dotmar.com.au).

Chapter 2

Oxic microshield and local pH enhancement protects *Zostera muelleri* from sediment derived hydrogen sulphide

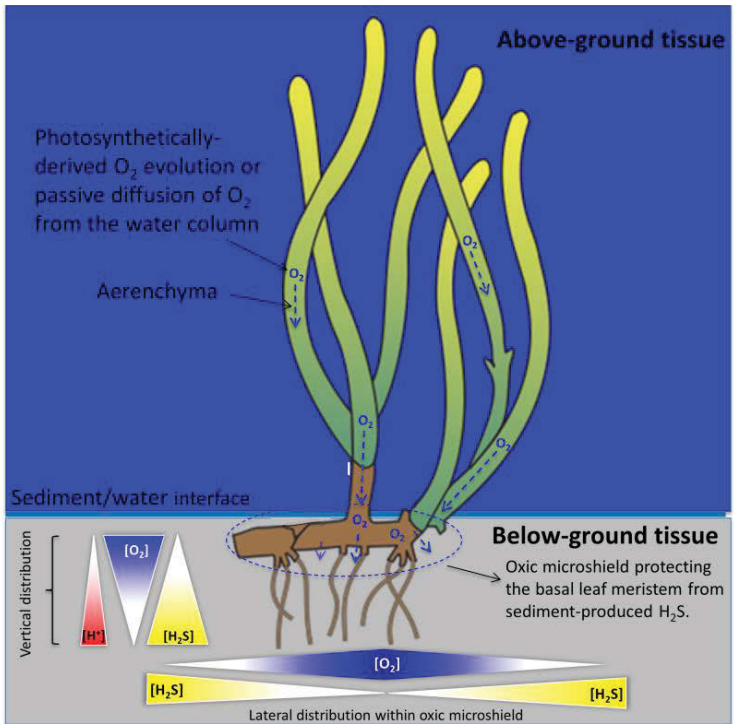

TOC figure. *Plant-derived alterations of the below-ground geochemical microenvironment.*

Citation: Brodersen KE, Nielsen DA, Ralph PJ. & Kühl M. (2015). Oxic microshield and local pH enhancement protects *Zostera muelleri* from sediment-derived hydrogen sulphide. *New Phytologist* **205** (3): 1264-1276.

Highlights: This chapter describes how *Zostera muelleri* ssp. *capricorni* modifies the biogeochemical conditions in its immediate rhizosphere through high radial O_2 loss (ROL) from the below-ground tissue, as well as via a plant-induced local enhancement of rhizosphere pH. O_2 leakage into the immediate rhizosphere, especially from around the root/shoot junctions (including the basal leaf meristem with leaf sheath), resulted in pronounced sediment detoxification within the plant-derived rhizospheric oxic microshields. Moreover, this chapter describes how changing environmental conditions, such as overnight water-column hypoxia, affect the plants performance.

Oxic microshield and local pH enhancement protects *Zostera muelleri* from sediment derived hydrogen sulphide

Kasper Elgetti Brodersen[1,*], Daniel Aagren Nielsen[1], Peter J. Ralph[1], Michael Kühl[1,2,3]

[1]Plant Functional Biology and Climate Change Cluster, University of Technology, Sydney, 15 Broadway, Ultimo, Sydney, NSW 2007, Australia.

[2]Marine Biological Section, Department of Biology, University of Copenhagen, Strandpromenaden 5, DK-3000 Helsingør, Denmark.

[3]Singapore Centre on Environmental Life Sciences Engineering, School of Biological Sciences, Nanyang Technological University, Singapore.

*Corresponding author, e-mail: kasper.e.brodersen@student.uts.edu.au and phone: +61 414 954 017

ABSTRACT

Seagrass is constantly challenged to transport sufficient O_2 from above- to below-ground tissue via aerenchyma to maintain aerobic metabolism and provide protection against phytotoxins.

Electrochemical microsensors were used in combination with a custom-made experimental chamber to analyse the below-ground biogeochemical microenvironment of *Zostera muelleri* under changing environmental conditions.

Measurements revealed high radial O_2 release of up to 500 nmol O_2 cm^{-2} h^{-1} from the base of the leaf sheath, maintaining a ~300 µm wide plant-mediated oxic microzone and thus protecting the vital meristematic regions of the rhizome from reduced phytotoxic metabolites such as H_2S. Hydrogen sulphide intrusion was prevented through passive diffusion of O_2 to below-ground tissue from leaf photosynthesis in light, as well as from the surrounding water-column into the flow-exposed plant parts during darkness.
Under water-column hypoxia, high below-ground H_2S concentrations at the tissue surface correlated with the inability to sustain the protecting oxic microshield around the meristematic regions of the rhizome. We also found increased pH levels in the immediate rhizosphere of *Z. muelleri*, which may contribute to further detoxification of H_2S through shifts in the chemical speciation of sulphide.

Zostera muelleri can modify the geochemical conditions in its immediate rhizosphere thereby reducing its exposure to H_2S.

Keywords: Radial oxygen release, oxic microshield, biogeochemistry, microelectrodes, Zostera muelleri, rhizosphere, plant-sediment interactions

INTRODUCTION

Seagrasses (angiosperms) are considered crucial ecological engineers as they provide important ecosystem services that have a significant positive impact on their physical, chemical and biological surroundings (Costanza, 1997; Larkum et al., 2006; Orth et al., 2006; Waycott et al., 2009). Over the past century, seagrass meadows have faced worldwide decline, mainly as a result of anthropogenic impacts such as eutrophication and coastal development (Orth et al., 2006; Ralph et al., 2006), resulting in an increasing number of seagrass die-off events (Seddon et al., 2000; Plus et al., 2003; Borum et al., 2005), ranging from frequent small scale events (Carlson et al., 1994; Zieman et al., 1999) to isolated episodes of mass mortality (Robblee et al., 1991). The exact causes leading to such die-offs remain largely unknown, but combined stressors such as high temperatures, high salinity, low flow-rates and water-column hypoxia, causing plant tissue anoxia, in combination with H_2S invasion from the surrounding sediment, have been suggested as likely causes (Carlson et al., 1994; Zieman et al., 1999; Borum et al., 2005; Frederiksen et al., 2006b; Holmer et al., 2009; Raun & Borum, 2013).

Because seagrasses mostly grow in highly reduced sediments (Borum et al., 2006), they are constantly challenged to supply sufficient O_2 to their below-ground tissue to sustain aerobic metabolism, as well as to provide protection against invasion of reduced phytotoxic compounds such as H_2S from the surrounding sediment (Armstrong, 1979; Borum et al., 2005; Borum et al., 2006). To facilitate this, seagrasses have well-developed aerenchyma (lacunar system), which enables rapid internal gas-phase diffusion of O_2 to the roots, rhizomes and basal meristems. During daytime, photosynthesis in the seagrass leaves coupled with efficient gas transport in the aerenchyma ensures an adequate O_2 supply to the below-ground tissues. At night time, on the other hand, seagrasses are completely dependent upon passive diffusion of O_2 into leaves from the water column (Pedersen et al., 1998; Borum et al., 2006); a process that is influenced by the O_2 concentration in the surrounding water, the thickness of the seagrass leaf diffusive boundary layer (DBL), and thereby the flow-velocity of the surrounding water, as well as by the plant respiration rate itself (Pedersen et al., 2004; Binzer et al., 2005). This important physiological adaptation enables seagrasses to maintain an oxidized microzone (oxic microshield) around their roots

(Pedersen et al., 1998; Jensen et al., 2005; Borum et al., 2006; Frederiksen & Glud, 2006), typically originating from around the root apex/apical meristem (Jensen et al., 2005; Borum et al., 2006) and resulting in a temporally oxidized microzone 1-2 mm behind the root-tip. The impact of such O_2 release on the biogeochemistry and microbial diversity in the seagrass rhizosphere is, however, still under-explored (e.g., Pedersen et al., 1998; Pedersen et al., 1999; Jensen et al., 2005; Jensen et al., 2007).

The O_2 budget of seagrass determining the sulphide oxidation capability of the below-ground tissue is a complex interaction between several sources and sinks. Sources include photosynthetically-derived O_2 evolution and passive diffusion of O_2 into the seagrass leaves from the ambient water column. The sinks encompass the sediment O_2 demand due to biotic and abiotic chemical reactions, as well as the plants own respiration (Greve et al., 2003; Borum et al., 2005; Borum et al., 2006; Holmer et al., 2006). Plant tissue respiration is strongly influenced by changes in water temperature, and increased respiration as a result of increasing temperature can lead to decreased O_2 supply to below-ground tissue resulting in inadequate internal aeration (Raun & Borum, 2013), which in turn may lead to H_2S intrusion.

Sulphide is produced by sulphate reducing bacteria in anoxic marine sediment, where it exhibits a pH dependent speciation with H_2S as the predominant form at porewater pH <7, whereas HS^- is predominating at higher pH. As dissolved H_2S gas is the only form of sulphide that can freely permeate the cell membrane, the toxicity of sulphide in sediment not only relies on the overall sulphide concentration, but is also strongly affected by the sediment pH. High H_2S levels have a negative effect on the viability of submerged plants by i) reducing photosynthesis, ii) reducing nutrient uptake, and iii) by blocking the mitochondrial respiratory electron transport chain through its strong binding with iron in cytochrome c oxidase (Goodman *et al.*, 1995; Raven & Scrimgeour, 1997; Holmer & Bondgaard, 2001; Perez-Perez et al., 2012). Hydrogen sulphide is thus considered a broad-spectrum toxin that leads to chemical asphyxiation and formation of reactive oxygen species (ROS), which can lead to protein degradation and peroxidation of membrane lipids (Raven & Scrimgeour, 1997; Eghbal et al., 2004; Truong et al., 2006; Perez-Perez et al., 2012).

As H_2S can be chemically oxidised by O_2 (i.e., $2O_2 + H_2S \rightarrow 2H^+ + SO_4^{2-}$), the influx of H_2S into plant tissue seems to correlate with the inability to sustain a protective oxic microzone around the below-ground tissue (Pedersen et al., 2004; Borum et al., 2005). The thickness and efficiency of such an oxic microshield depends on the rate of O_2 leakage to the rhizosphere relative to the O_2 consumption rate in the surrounding sediment. Bacterial sulphide oxidation in the immediate rhizosphere may also dramatically lower the half-life of H_2S in comparison to the spontaneous chemical oxidation alone (Cline & Richards, 1969; Chen & Morris, 1972; Almgren & Hagstrom, 1974; Jorgensen & Revsbech, 1983; Pedersen et al., 2004) further alleviating the H_2S exposure of seagrass roots. Yet another potential chemical defence mechanism could involve a local increase of rhizosphere or root surface pH, shifting the sulphide speciation away from H_2S towards non-permeable and thereby non-phytotoxic HS^- ions. A detailed description of the pH microheterogeneity within the seagrass rhizosphere is, however, still lacking.

Mature seagrass roots also exhibit a range of anatomical adaptations, including casparian band-like structures (Barnabes, 1996) and/or suberized lamellae (e.g., Enstone et al., 2003) that reduce cross tissue gas transport. This is likely to increase the efficiency with which O_2 is carried to the roots, thus facilitating the maintenance of aerobic metabolism and possibly also reducing H_2S intrusion (Armstrong, 1979; Armstrong & Armstrong, 2001; Jensen et al., 2005). The presence of a strong barrier against cross tissue gas transport has been shown to correlate with anaerobic conditions within the sediment, as well as the presence of phytotoxins (Colmer et al., 1998; Armstrong & Armstrong, 2001).

In this study, we elucidate the dynamics of the chemical microenvironment in the rhizosphere of *Zostera muelleri* under changing environmental conditions. We present the first detailed micro-scale mapping of O_2, H_2S and pH gradients around the basal meristems with leaf sheath (BM), rhizome and roots of *Zostera muelleri* and investigate whether local pH enhancement and sulphide oxidation contribute to H_2S detoxification in the rhizosphere.

MATERIALS AND METHODS

Seagrass samples

Zostera muelleri ssp. *capricorni* (Asch.) S.W.L.Jacobs specimens were collected from a sheltered lagoon exposed to low flow rates (Narrabeen Lagoon, NSW, Australia). Specimens were sampled in shallow waters (~1 m depth) and transported in seawater from the sampling site to the laboratory within one hour of sampling. Specimens were kept in a greenhouse under a natural light regime (~11:13h light-dark cycle) for a minimum of 72h before further handling. Three specimens with similar above-ground and below-ground biomass (i.e., two shoots with intact root bundles and more than two internodes) were selected for this study. Rhizome and roots were gently washed, and plants were left free of sediment over night to aerate roots and rhizomes before placing them in the split flow-chamber (see below).

Split flow-chamber and artificial sediment

A seagrass specimen was placed horizontally in a custom-made split flow-chamber (Fig. 2.1), with the above-ground tissue positioned in the upper compartment with free-flowing seawater and the below-ground tissue inserted in viscous, reduced artificial sediment consisting of: 0.19% anoxic seawater-agar (grade J3, Gelita, QLD, Australia) solution amended with Na_2S to a final concentration of 250 µM H_2S and buffered with 10 mM anoxic HEPES buffer (N-2-hydroxyethylpiperazine-N'-2-ethanesulfonic acid; pH range 6.8-8.2). Natural seawater was used to ensure natural levels and ratios of essential nutrients. The artificial sediment was kept anoxic in the chamber by constantly flushing the overlying layer of seawater with humidified nitrogen (Fig. 2.1). To ensure a continuous supply of H_2S to the artificial sediment, pieces of gauze were soaked in anoxic and acidic (pH 4) 1 mM Na_2S solution and placed in the bottom of the lower chamber before adding the artificial sediment. The O_2 demand of the reduced artificial sediment was kept relatively high in order to mimic natural sediment conditions. This was achieved through the combined effect of the added reducing agent (H_2S) constantly diffusing up into the artificial sediment from the bottom layer and the above-lying oxygen sink (further information on the experimental approach is provided in Brodersen et al. (2014)).

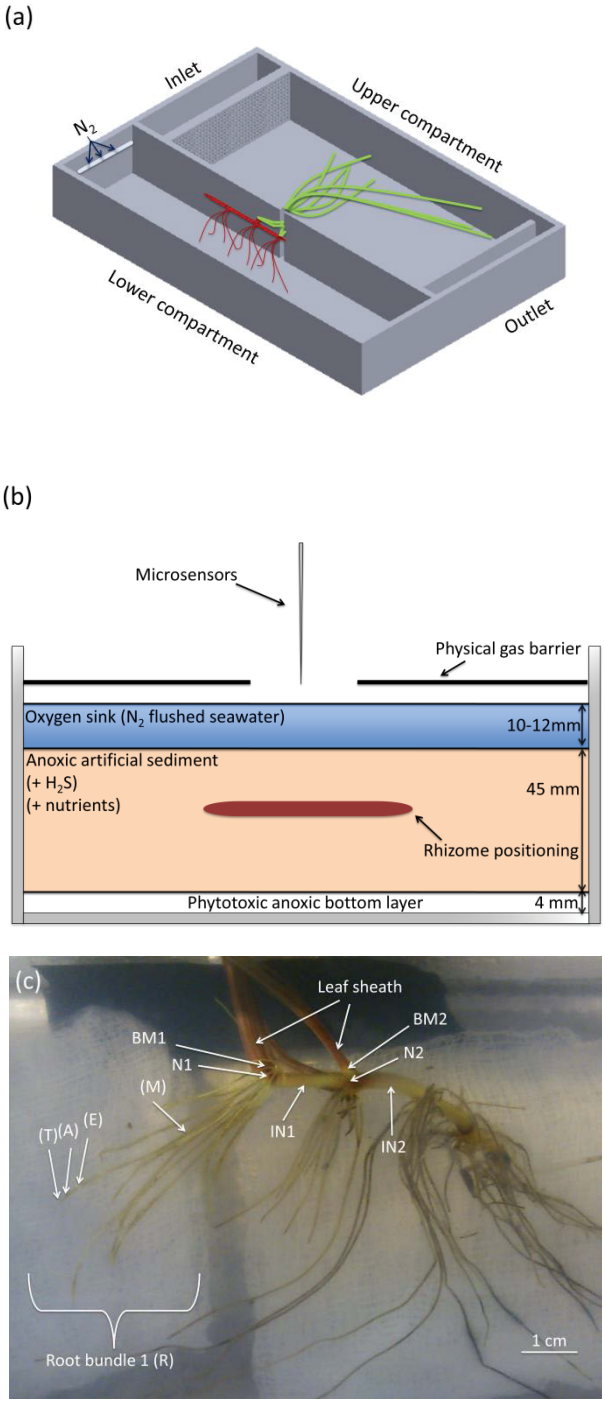

Figure 2.1: (a) Split flow-chamber shown from above, with the free flowing water section (upper chamber) and the anoxic artificial sediment compartment (lower chamber) (Split flow-chamber illustration provided by Dotmar EPP, Australia). (b) Median section of lower part of split flow-chamber illustrating the three layers of the artificial sediment. (c) Schematic illustration of *Zostera muelleri* below-ground tissue, visualizing the spatial distribution of the microsensor measurements within the immediate rhizosphere. Abbreviations: T = Root tip/Root cap; A = Apical meristem region; E = Elongation zone; M = Mature zone (i.e., formation of root hairs); BM = Basal meristem with leaf sheath; N = Node; IN = Internode.

A constant flow-velocity (~1 cm s^{-1}) of aerated and thermostated seawater (21°C; salinity of 34) was maintained in the upper compartment via a pump submerged in an aerated, temperature controlled water bath. Illumination in the upper compartment (with seagrass leaves) was provided by a fibre-optic tungsten halogen lamp (KL-2500, Schott GmbH, Mainz, Germany). The downwelling quantum irradiance (PAR) was measured with a calibrated quantum irradiance meter (Li-250A, LiCor, USA) equipped with an irradiance sensor (Walz GmbH, Effeltrich, Germany) kept at the same distance from the light source as the seagrass leaf canopy.

Plants were acclimatized to the split flow-chamber under standard conditions (~250 µmol photons m^{-2} s^{-1}; 10:14h light-dark cycle) for several days before measurements commenced. The seagrass specimens were then acclimatized to different treatment conditions: (i) dark + air saturated water-column; (ii) 260 µmol photons m^{-2} s^{-1} + air saturated water-column; (iii) 350 µmol photons m^{-2} s^{-1} + air saturated water-column; and (iv) dark + ~50% air saturation in the water-column (hypoxia). Treatments were applied for at least 3h prior to the microelectrode measurements to ensure steady state biogeochemical conditions (as confirmed by repeated microprofile measurements). The hypoxia treatment (i.e., ~50% air saturation in the water column of the upper compartment) was achieved by simultaneously flushing the water in the supporting water bath with a mixture of N_2 and atmospheric air. The O_2 concentration in the water was constantly monitored by a calibrated Clark-type O_2 microsensor (OX-100, tip size ~100 µm, 90% response time <8 s, stirring sensitivity <1.5%, Unisense A/S, Aarhus, Denmark). 36 hours prior to the hypoxia experiment, additional sulphide (5 mL, 10mM Na_2S) was injected to the bottom layer of the artificial sediment in order to re-establish H_2S levels as preliminary experiments had shown that photosynthesis-induced O_2 release during the light treatment completely removed H_2S from the basal meristem microenvironment. The split flow-chamber was left untouched for 36h after the injection to ensure steady-state biogeochemical conditions as confirmed by repetitive vertical microsensor profiles. Before microelectrode measurements commenced, O_2 microprofiles were performed at the cut end of the rhizome to ensure no O_2 release was detectable, indicating intact plants and thereby an enclosed aerenchyma.

Microsensor measurements

Pre-contaminated (i.e., pre-exposed to H_2S) Clark-type O_2 microsensors (OX-50, tip diameter ~50 µm, Unisense A/S, Aarhus, Denmark; Revsbech, 1989), with a fast 90% response time of <5 s and a low stirring sensitivity of <2% were used to measure the radial O_2 release from the below-ground tissue. Oxygen microelectrodes were linearly calibrated from signal readings in 100% air saturated seawater and anoxic seawater (seawater amended with the O_2 scavenger sodium dithionite) at experimental temperature and salinity.

H_2S concentrations were measured with Clark-type H_2S microelectrodes (H_2S-50, tip diameter ~50 µm, 90% response time <10 s, stirring sensitivity <2%, Unisense A/S; Jeroschewski *et al.*, 1996; Kühl *et al.*, 1998) that were linearly calibrated (3-points) in anoxic, acidic Na_2S (pH 4) solutions of known H_2S concentrations (i.e., 0, 50, and 100 µM; at experimental temperature and salinity). The microelectrode is only sensitive to H_2S (Jeroschewski et al., 1996), which is the only sulphide species that is able to penetrate plant tissue by liquid-solution permeation of the plasmalemma (Raven & Scrimgeour, 1997).

pH measurements were done with pH microelectrodes (PH-50, tip diameter ~50 µm, linear range pH 4-9, Unisense A/S; Kühl & Revsbech, 2001) with a 90% response time <10 s and a detection limit of 0.05-0.1 pH units. The pH microelectrodes were used in combination with a reference electrode (REF-RM, tip diameter of ~5 mm, Unisense A/S) immersed in the seawater in the flow-through chamber in which measurements were taken. The pH microelectrode was linearly calibrated from sensor readings in three pH buffers (pH 4, 7 and 9; at experimental temperature and salinity). The pH electrode responded linearly to pH over the calibration range with a signal to pH ratio of ~52 mV/pH unit.

All microsensors were connected to a 4-channel multimeter (Unisense A/S, Aarhus, Denmark) interfaced with a PC running data acquisition software (SensorTrace PRO, Unisense A/S, Aarhus, Denmark). During operation, the microsensors were mounted on a PC-interfaced motorized micromanipulator (MM33-2, MC-232; Unisense A/S, Aarhus, Denmark) controlled by dedicated positioning software (SensorTrace PRO, Unisense A/S, Aarhus, Denmark). All microprofiles were measured in steps of 100 µm (except vertical profiles describing the relative difference between the rhizosphere and the artificial sediment that were performed in 1000 µm step sizes). Before each microprofile

measurement commenced, the microsensors were positioned at the tissue surface (indicated as 0 µm on graphs) by means of the micromanipulator, while observing the plant tissue surface and microsensor tip in the transparent, artificial sediment through a stereo-microscope mounted on an articulating arm (SM-6TZ, Amscope, Irvine, CA, US) equipped with a hand-held lens (further described in Brodersen et al. (2014)).

Mapping the chemical microenvironment

Microelectrode measurements were performed at the basal meristems with leaf sheath (meristematic regions of the rhizome; base of leaf sheath), at the nodes (meristematic regions of the rhizome; root-shoot junctions), on the internodes (3 points/locations along the latitude direction), as well as on the first root-bundle (n = 2-4; where "n" represents numbers of technical replicates). Note that the meristematic region of the rhizome is a combined basal leaf/rhizome meristem area located between the leaf bundle and rhizome (Short & Duarte, 2001); in this study divided up in two regions, namely the nodium and the basal meristem with leaf sheath ~1 mm apart. The first root-bundle was divided into four areas: root mature zone (with completely developed root-hairs; RM), root elongation zone (RE), root apical meristem region (area of root cell division; RA) and root-tip (RT) based on observations under a stereo microscope (see Figure 2.1).

Flux calculations

The radial oxygen flux (*J(r)*; nmol O_2 cm^{-2} h^{-1}) from the below-ground tissue was calculated via a cylindrical version of Fick's first law of diffusion, assuming homogeneous O_2 release from a perfect cylinder (Steen-Knudsen, 2002):

$$J(r)_{root\text{-}system} = \varphi Ds\ (C_1 - C_2) / r\ ln\ (r_1/r_2)$$

where ϕ is the porosity, Ds is the diffusion coefficient for oxygen in the artificial sediment, r is the radius of the given root/rhizome, ΔC is the oxygen concentration gradient through the oxic microzone (i.e., from the tissue surface to the last point of the linear concentration gradient ~300 µm away from the tissue surface), r_1 and r_2 are the distance from the root centre (i.e., radius of inner and outer cylinder shell) equivalent to the measured O_2 concentrations C_1 and C_2, respectively. Radial H_2S consumption rates ($J(r)_{H2S}$; in nmol H_2S cm^{-2} h^{-1}) were calculated in a similar manner only replacing the respective diffusion coefficient (see below).

The porosity, ϕ, of the artificial sediment was calculated to be 0.95, after drying the sediment at 105°C in an oven, until a constant weight was reached (known initial volume and wet-weight). The following equation was used for the calculation; $\varphi(\%) = ((M_w/D_w)\cdot 100)/((M_w/D_w)+(M_a/D_a))$, where M_w is the weight of seawater, D_w is the density of seawater, M_a is the weight of agar and D_a is the density of agar. The respective diffusion coefficients within the sediment were calculated to be $D_{S,H2S} = 1.5251\cdot 10^{-5}$ cm^2 s^{-1} and $D_{S,O2} = 2.0138\cdot 10^{-5}$ cm^2 s^{-1} at experimental temperature and salinity (assuming similar diffusion rates as in seawater). The molecular diffusion coefficient for O_2 in seawater, D_0, and the multiplication factor for calculating the molecular diffusion coefficient of H_2S at experimental temperature and salinity, were taken from tables available at www.unisense.com (Ramsing & Gundersen).

Measurements of seagrass health and photosynthetic capacity during cultivation

Maximum and effective quantum yields of PSII in *Z. muelleri* were measured by pulse amplitude modulated (PAM) fluorometry (PocketPAM equipped with an optical fiber; PAM settings: saturating intensity 6, saturating width 0.6s, F>100). The measurements were used as a general indicator of the seagrasses health. Light energy absorbed by chlorophylls can either be used for photochemistry, re-emitted as fluorescence (i.e., as longer wavelengths) or dissipated as heat (non-photochemical quenching (NPQ)). The relative proportions of energy directed through each of these different pathways define the health of the photosystems, and can be used to determine maximum PSII quantum yield as

$$Fv/Fm = (Fm-Fo)/Fm$$

and the effective quantum yield of PSII as

$$\Delta F/Fm' = (Fm'-F)/Fm'$$

where Fm is the maximal fluorescence yield for dark-acclimated plants; Fo is the minimum fluorescence yield; and Fm' is the light-adapted maximum fluorescence yield. As quantum yields are ratios of fluorescence yield measurements, they have no units (Beer et al., 1998; Ralph & Short, 2002). The maximum quantum yield provides a measure of Photosystem II (PSII) photochemical efficiency (after a dark adaptation period of minimum 10 min) and the effective quantum yield is a measure of PSII photosynthetic activity (measured under experimented irradiance levels, i.e., 260 and 350 µmol photons m^{-2} s^{-1}). Seagrass specimens were maintained in the artificial sediment for >14 days prior to experiments (similar

conditions as used during the microsensor measurements), to verify long-term health of the plants under the experimental conditions. This was confirmed by the observation of active growth in both above- and below-ground biomass during cultivation, as well as by measured effective and maximum quantum yields. A complete new root-bundle, internode and bundle of leaves were developed during cultivation. The rhizome was growing ~0.8 cm and the new root-bundle reached an average root length of 2.6 cm over a 7 days period.

Histology

The base of the leaf sheath of the first shoot and the first internode of each plant were cut into 20 to 40 µm transverse tissue sections by means of a cryotome after pre-fixation in cryo-gel (Tissue-Tek®, ProSciTech, QLD, Australia). The samples were left embedded in the cryo-gel at ~4°C for 24h prior to the cutting process, to ensure efficient tissue penetration. The obtained sections of the below-ground tissue were then transferred to microscope glass slides where they were gently washed to remove any remaining cryo-gel. The cleaned sections were then examined under a stereo microscope and photographed with a digital camera (Nikon, Coolpix 995, Tokyo, Japan).

RESULTS

The detailed mapping of the below-ground chemical microenvironment presented in the following originates from three *Zostera muelleri* plants exposed to similar experimentally manipulated environmental conditions, as well as above- and below-ground microenvironmental conditions. Results are shown from the two plants examined in most detail.

Chemical conditions in the immediate rhizosphere

Photosynthetic O_2 evolution, as well as diffusion of O_2 from the ambient water column into the aerenchyma, resulted in high radial O_2 release to the immediate rhizosphere of *Zostera muelleri* (Figure 2.2; Table 2.1). The O_2 release originating from the base of the leaf sheath, as well as the rhizome (i.e., node and internodes), resulted in the establishment of a ~300 µm thick oxic microshield around the basal meristems with leaf sheath (BM), nodes (during light and dark treatments; Figure 2.2) and internodes (only during light treatments; Figure

2.2). Furthermore, a slightly deeper O_2 penetration depth was observed within the immediate rhizosphere of *Z. muelleri*, here defined as from the oxic microshield-reduced sediment interface to the last measured point in the rhizosphere (i.e., ~0.3-5 mm distance away from the below-ground tissue) as compared to the bulk artificial sediment (Figure S2.1, S2.2 and S2.3; except during hypoxic water-column conditions [further described in Notes S2.1]). H_2S was completely removed from the artificial sediment surrounding the BM, as well as from the first sections of the rhizome (until internode 2), and the H_2S concentration was generally highly reduced (up to 20-fold) within the immediate rhizosphere, as compared to the bulk artificial sediment concentrations measured at a similar depth (Figure 2.2; Figure S2.1 and S2.2; except during hypoxic water-column conditions). Serving as a reference to the measurements at the BM, H_2S microprofiles performed at the same vertical depth but ~5 mm away from the meristematic regions of the rhizome, confirmed that H_2S was present at concentrations up to 23 µmol H_2S L^{-1} just outside the immediate rhizosphere (Figure S2.4).

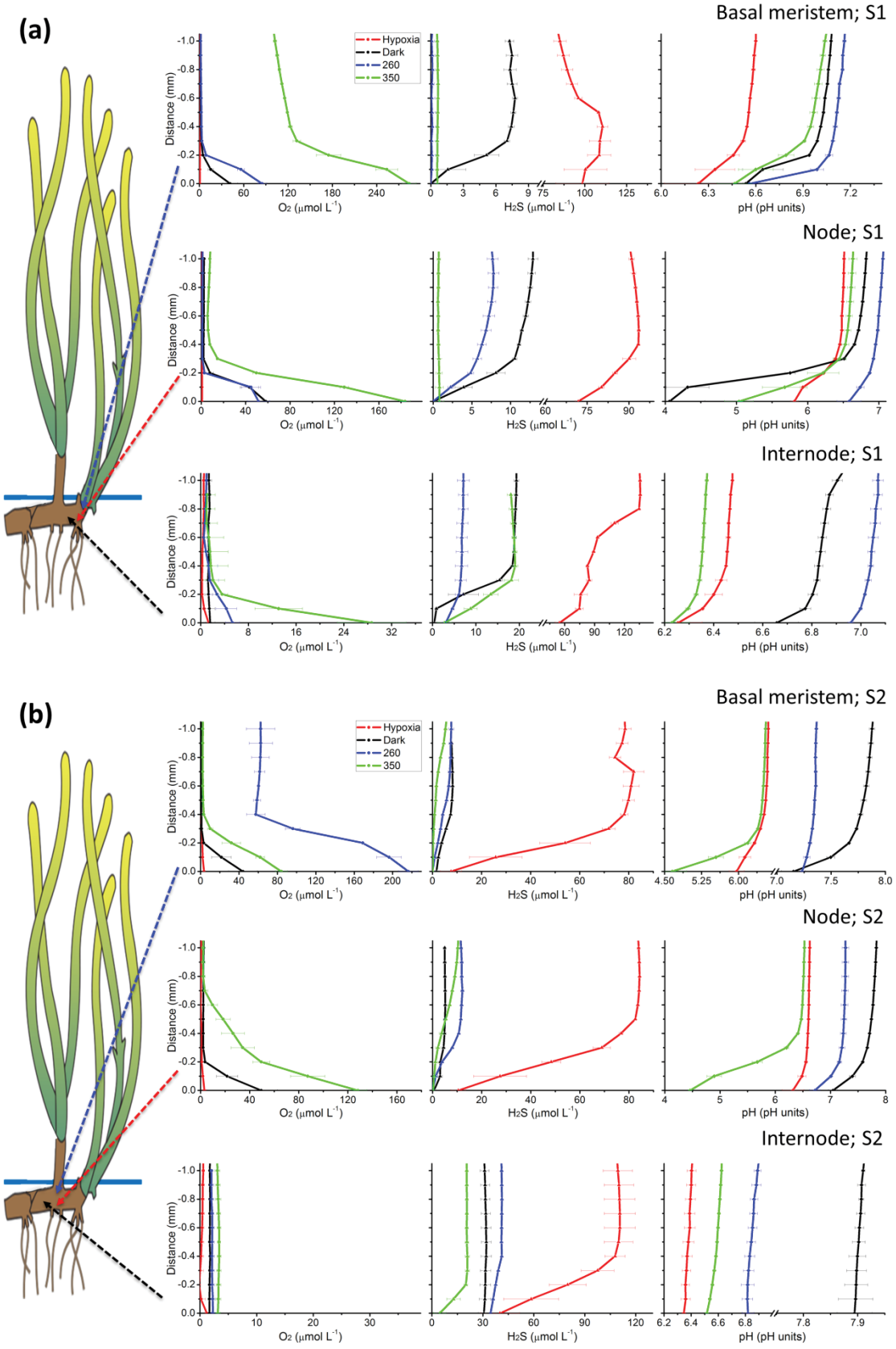

Figure 2.2: The dynamics of the below-ground chemical microenvironment of *Zostera muelleri* under experimentally changed environmental conditions as mapped with microelectrodes, illustrating the rhizome region including basal meristems with leaf sheath:

(a) shoot 1; (b) shoot 2. The x- and y-axis are organized spatially, thus reflecting the actual orientation of the below-ground microsensor measurements. Y=0 indicate the below-ground tissue surface. Error bars are ±SD. n=2-4. The illustration of *Zostera muelleri* originates from the IAN/UMCES symbol and image libraries (Diana Kleine, Integration and Application Network (IAN), University of Maryland Center for Environmental Science (ian.umces.edu/imagelibrary/)).

Table 2.1.

Radial oxygen release (O_2 flux), oxygen concentration at the below-ground tissue surface, H_2S consumption within the oxic microshield, total sulphide concentration at the tissue surface (S) and at the oxic microzone-reduced sediment interface (I), and ΔpH through the oxic microshield. Calculated for each of the four different treatments: dark, 260 µmol photons m^{-2} s^{-1}, 350 µmol photons m^{-2} s^{-1} and hypoxia, at the: Basal meristem with leaf sheath (BM); Node (N); Internode (IN); mature zone of roots (RM); and apical meristem region of roots (RA). Mean values±SE; except internode and root values which are given as mean ±SD; and the total sulphide concentration which is given as a mean (n = 3-15). As flux rates are calculated from mean values only SE are provided. (-) Indicates zero flux rate. Additional statistical information confirming the resemblance between the examined plants is provided in the supporting information (Figure S2.5).

Treatment (µmol photons m^{-2} s^{-1})		**O_2 flux** (nmol O_2 cm^{-2} h^{-1})	**[O_2] at surface** (µmol L^{-1})	**H_2S consumption** (nmol H_2S cm^{-2} h^{-1})	**[Total sulphide] surface & interface (S : I)** (µmol L^{-1})	**ΔpH** (pH units)
0	BM	170.8±34	68.8±21	15.8±1.6	1.2 : 24.8	0.90±0.4
	N	125.4±29	45.5±8.8	16.5±4.3	0.7 : 20.5	1.69±0.4
	IN	0.5±0.5	1.5±0.7	37.3±9	0.5 : 27.8	0.56±0.5
	IN2	0.6±0.5	2.1±0.4	25.2±23	221.3 : 251.9	0.02±0.0
	RM	(-)	2.0±0.3	(-)	(S: 253.5)	0.03
	RA	(-)	0.8±0.1	(-)	(S: 271.0)	0.00
260	BM	355.2±66	150.6±66	3.9±3.9	0.0 : 9.6	0.33±0.2
	N	312.5±123	134.0±82	19.5±5.3	0.0 : 27.5	0.44±0.1
	IN	9.9	5.3±1.2	8.8	7.5 : 18.4	0.08
	IN2	0.4	2.3±0.4	12.1	70.9 : 85.7	0.01
	RM	(-)	1.3±0.1	(-)	(S: 77.2)	0.01
	RA	(-)	0.7±0.0	(-)	(S: 156.1)	0.00
350	BM	304.6±108	184.1±100	5.3±5.3	0.5 : 1.4	1.14±0.7
	N	395.0±102	155.9±28	5.9±5.9	0.5 : 3.1	1.72±0.2
	IN	92.8	28.7±5.8	29.9	3.5 : 25.8	0.12
	IN2	0.0	3.1±0.5	42.7	7.0 : 33.6	0.07
	RM	(-)	1.1±2.3	(-)	(S: 63.7)	0.01
	RA	(-)	1.8±0.4	(-)	(S: 123.9)	0.00
Hypoxia	BM	1.8±1.7	1.4±0.7	86.4±57	67.1 : 145.8	0.29±0.1
	N	2.0±2.0	1.3±0.6	81.2±44	46.6 : 130.0	0.30±0.1
	IN	2.0±2.0	1.0±0.1	59.8	70.4 : 120.2	0.26±0.1
	IN2	2.5±2.5	0.6±0.4	110.6	54.3 : 148.2	0.02±0.0
	RM	(-)	0.7±0.2	8.7	(S: 113.5)	0.01
	RA	(-)	0.7±0.1	(-)	(S: 102.3)	0.00

No or low radial O_2 release was detectable from the root-bundles, as well as further down the rhizome, i.e., away from the growing direction (Figure 2.3; data from root-bundle 2 not shown). This correlated with the relatively high H_2S concentrations found in the surrounding artificial sediment at the root-tips of >200 µmol H_2S L^{-1}(Figure 2.3; dark treatment).

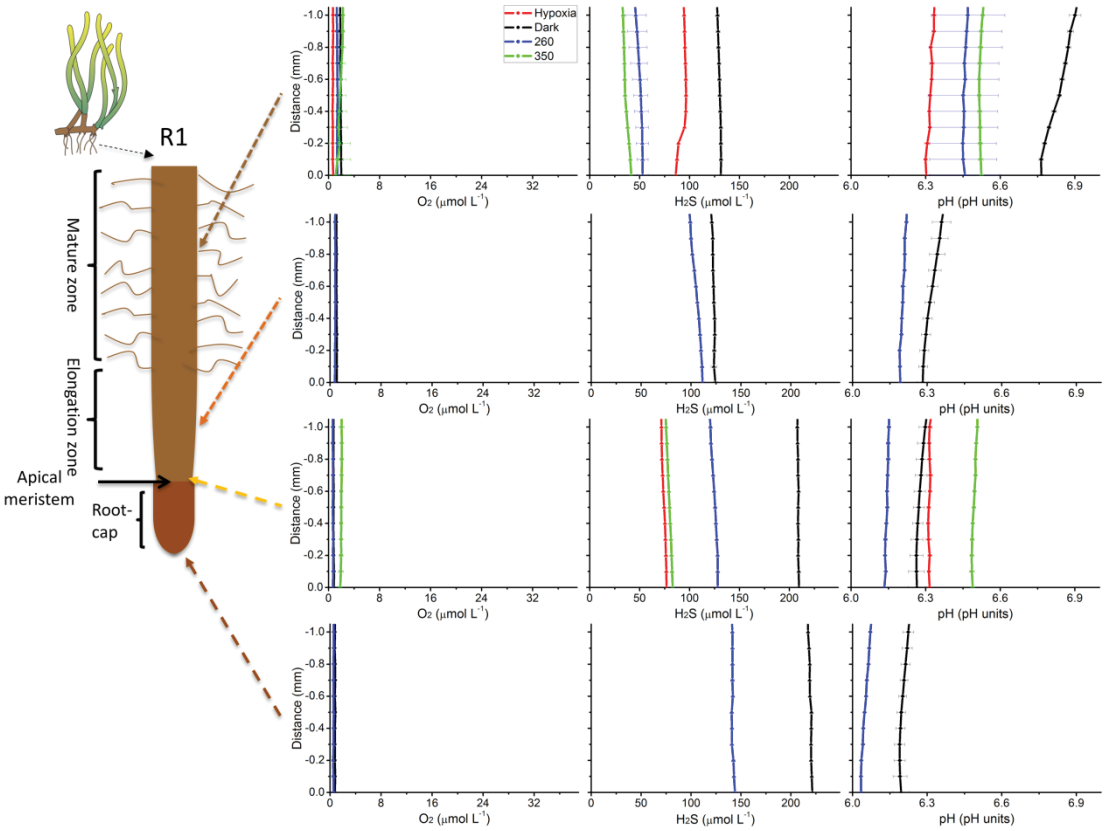

Figure 2.3: Microprofiles showing the below-ground microenvironment surrounding the roots of the first root-bundle. Y=0 indicates the below-ground tissue surface. Error bars are ±SD. n=2-4. Abbreviations are explained in the main text (Seagrass illustration from ian.umces.edu/imagelibrary/).

In the immediate rhizosphere of the meristematic tissue, pH values reached up to ~7.9 as compared to pH ~6.2 in the bulk of the artificial sediment at similar vertical depth (Figure 2.2; Figure S2.1 and S2.2). Within the immediate rhizosphere, pH decreased towards the root-tips (Figure 2.3), reaching pH values of ~6.0 at the root-tip surface. Due to the horizontal orientation of the below-ground tissue in the flow-chamber, these findings could not have been simply a result of the vertical pH microgradient present in the reduced artificial sediment (Figure 2.1; Figure S2.1 and S2.2).

Microgradients and oxic microshield

At an incident irradiance of 350 µmol photons m^{-2} s^{-1}, radial O_2 release rates reached local maxima of ~500 nmol O_2 cm^{-2} h^{-1} at the base of the leaf sheath, located at the meristematic region of the rhizome (Figure 2.2; plant 2, node 1; Table 2.1). This correlated with a complete removal of H_2S in the same region (Figure 2.2). The highest re-oxidation rate of H_2S was measured at the second internode of plant 2 during the dark treatment, reaching approximately 48 nmol H_2S cm^{-2} h^{-1}. This somewhat unexpected region of the rhizome consuming most H_2S per unit time was likely a result of the almost complete re-oxidation and thereby removal of H_2S in the immediate rhizosphere of the meristematic regions of the rhizome (Figure 2.2, Table 2.1). Hence, flux calculation from this region with the highest O_2 leakage was impossible. The highest O_2 release rates were measured at the meristematic regions of the rhizome (i.e., BM and nodes), with >3-fold higher release rates, as compared to any other regions of the below-ground tissue (Table 1; expect during hypoxia conditions). Inside the oxic microshield, pH levels decreased towards the tissue surface with an average of ~1 pH unit (Table 2.1). A close-up of the oxic microshield and the overall dynamics of the chemical microenvironment within the immediate rhizosphere, as well as throughout the oxic microzone is shown in Figure 2.4.

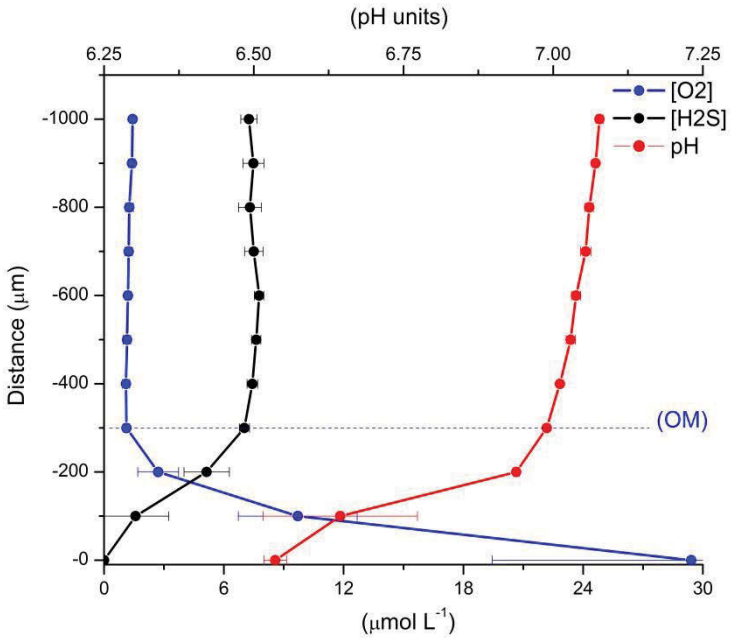

Figure 2.4: Selected microprofiles showing the oxic microshield (OM) at the basal meristem with leaf sheath. [O_2], [H_2S] and pH values measured at increasing distance away from the below-ground tissue (base of the leaf sheath), illustrating the dynamics of the below-ground chemical microenvironment across the oxygen-sulphide interface as well as throughout the oxic microzone. Y=0 indicate the below-ground tissue surface. Error bars are ±SD (n=3). The microprofiles shown are from the dark treatment.

Changing environmental conditions

The main difference between the light and dark treatments was the establishment of an oxic microshield around the first internode during illumination, as a result of radial O_2 release from this section of the plant (Figure 2.2). At the tissue surface of the first internode, an average radial O_2 release rate of 93 nmol O_2 cm^{-2} h^{-1} and an average H_2S consumption rate of 30 nmol H_2S cm^{-2} h^{-1} was found, under an incident irradiance of 350 µmol photons m^{-2} s^{-1} (Table 2.1).

The radial O_2 release from the meristematic regions of the rhizome increased from 2 nmol O_2 cm^{-2} h^{-1} during hypoxia to 395 nmol O_2 cm^{-2} h^{-1} at an incident irradiance of 350 µmol photons m^{-2} s^{-1} in an air saturated water column (Table 2.1).

The H_2S concentration at the surface of this region varied between 0 and ~2 µmol H_2S L^{-1} in darkness, and between 0 and 1 µmol H_2S L^{-1} under the highest experimental incident

irradiance (350 µmol photons m^{-2} s^{-1}; Figure 2.2). During water column hypoxia, the H_2S concentration increased to between 8 and 99 µmol H_2S L^{-1} (Figure 2.2).

The low or lacking radial O_2 release from the below-ground tissue during and after water column hypoxia thus resulted in high average H_2S concentrations at the below-ground tissue surface of 56 µmol H_2S L^{-1} (Figure 2.2 and 2.3; Table 2.1). These findings suggest very limited consumption and removal of H_2S during the hypoxia treatment as a result of the much lower oxidation capability of the below-ground tissue. Furthermore, *Z. muelleri* specimens showed low recovery after the hypoxia treatment, where no below-ground radial O_2 release was detectable for a period of 48h after the exposure (12:12h light-dark cycle; leaf canopy exposed to 100% air saturated water column during the recovery time), and a loss of above-ground biomass was observed (i.e., detachment of leaves; data not shown).

Oxygen source and rhizome histology

Histological studies of the BM and the surrounding leaf sheath revealed extensive internal gas channels (lacunar system) inside the tissue of the leaf sheath at the meristematic region of the rhizome, in addition to the internal gas-channels found in the meristematic tissue (Figure 2.5). The transverse sections of the first internode, i.e., further away from the growth direction, also showed well-developed aerenchyma situated in the cortex in a circular orientation close to the tissue centre (Figure 2.5). Moreover, a central stele was distinct in the cross-tissue section of the internode, as well as the initial formation of a root-bundle, clearly impeding the distribution of the aerenchyma, was visible in the cross-tissue section of the basal meristem area (Figure 2.5).

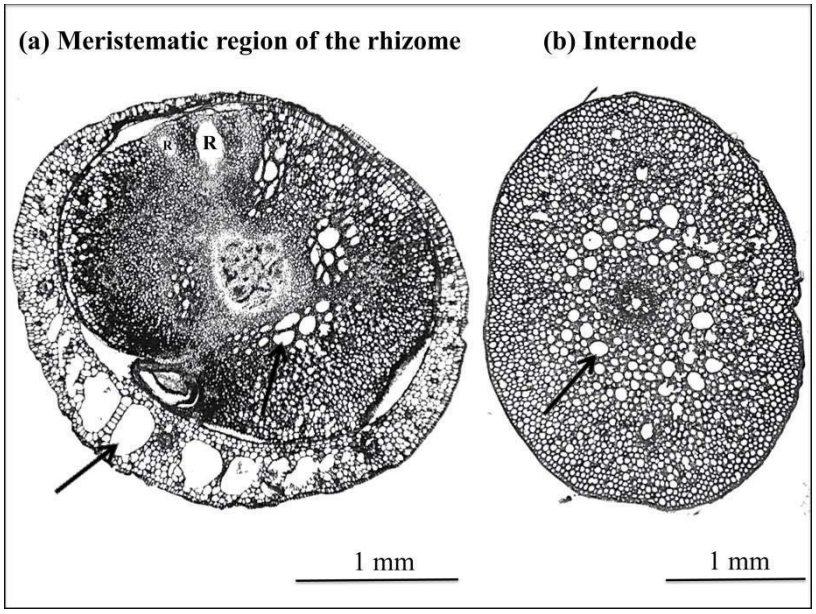

Figure 2.5: Transverse sections of the rhizome. (a) = Meristematic region of the rhizome, including the surrounding leaf sheath; (b) = Internode. Black arrows show aerenchyma, i.e., the extensive internal lacunar system. Note the extensive distribution of the internal gas channels in the leaf sheath. R = initial formation of a root-bundle.

Pulse amplitude modulated (PAM) fluorometry measurements

The maximum quantum yields of PSII measured at the centre of each leaf in the middle of the leaf canopy was about 0.67 for both plants (Table 2.2). After exposure to hypoxic conditions in the water column, the maximum quantum yield decreased 6% to 0.61 (measured on plant 2, n=4; Table 2.2). The effective quantum yield increased 23% (from 0.43 to 0.53) when the light intensity was increased from 260 to 350 µmol photons m^{-2} s^{-1}, but decreased by more than 50% (to 0.27) after exposure to hypoxic conditions under an incident irradiance of 350 µmol photons m^{-2} s^{-1} (Table 2.2). These results verify that the measured microprofiles of the chemical microenvironment represent the dynamics of healthy and photosynthetic competent seagrasses (under the light-dark treatments) and that the seagrass photosynthetic quantum efficiency was affected by the hypoxic conditions (measured after a 24h recovery time; 12:12h light-dark cycle).

Table 2.2. Maximum and effective quantum yields of PSII measured at the center of the leaf in the middle of the leaf canopy of both vertical shoots. The after hypoxia measurements were conducted after a 24h (12:12h) light-dark cycle. Leafs were exposed to a 100% air saturated water column during the 24h recovery time. Means±SD (n = 2-4).

	Fv/Fm max	**ΔF/Fm'** effective	**Incident irradiance** (µmol photons m^{-2} s^{-1})
Plant 1	0.67±0.1	0.43±0.1	260
Plant 2	0.67±0.1	0.53±0.1	350
Plant 2 (after HYPOXIA)	0.61±0.1	0.26±0.1	350

DISCUSSION

Our results show, that the seagrass *Z. muelleri* can modify the biogeochemical conditions of its immediate rhizosphere, via O_2 release from below-ground tissue, resulting in an almost complete re-oxidation of phytotoxic H_2S around the basal meristems with leaf sheath (BM) and rhizome in the growing direction (Figure 2.2 and 2.6). This supports earlier findings in studies of *Thalassia* sp., showing significantly decreased sulphate reduction rates and H_2S pools in seagrass-vegetated sediment as compared to non-vegetated areas (Borum et al., 2005; Holmer et al., 2006). The continuous release of O_2 from the below-ground tissue of *Z. muelleri* likely ensures the maintenance of an oxic microshield around vital and metabolically active parts of the plant (Figure 2.2 and 2.4). The oxic microshield was widest at the base of the leaf sheath (Figure 2.2 and Table 2.1), which likely protects this important but vulnerable part of the plant from H_2S intrusion. The leaf sheath surrounds the meristematic plant tissue, that, owing to its compact anatomy, has poorly developed aerenchyma, wherefore O_2 transport and supply to this sensitive area is impeded (Raun & Borum, 2013). This is supported by our observations of the morphological characteristics of the aerenchyma in the leaf sheath (Figure 2.5), showing a well-developed lacunar system at the basal meristems with large internal gas-channels, thus enabling rapid and extensive O_2 release to the rhizosphere. Furthermore, a slightly deeper O_2 penetration and a downward movement of the H_2S front were found within the immediate rhizosphere as compared to the bulk artificial sediment (Figure S2.1 and S2.2), a result of plant-mediated alterations of the below-ground biogeochemical microenvironment, whereby the plants promote their own growth.

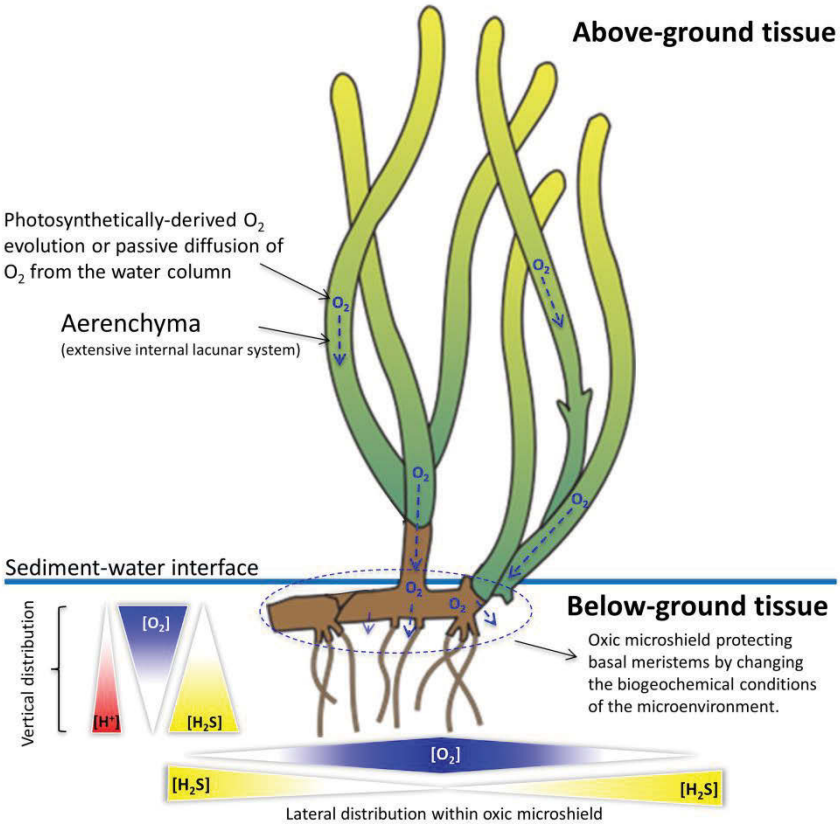

Figure 2.6: Conceptual diagram visualizing the results of the microelectrode measurements performed in the below-ground microenvironment of *Zostera muelleri* and presented here in this study. The colour gradient in the immediate rhizosphere indicates the relative concentration of the chemical species (blue = oxygen; yellow = H_2S; red = pH value [indicated as the relative amount of hydrogen ions]). Seagrass illustration from ian.umces.edu/imagelibrary/.

The calculated radial O_2 fluxes from the meristematic regions of the rhizome (up to ~5 mmol O_2 m^{-2} h^{-1} in light and 3.32 mmol O_2 m^{-2} h^{-1} in darkness; Figure 2.2 and Table 2.1) are similar to previously reported rates measured in the rhizosphere of *Cymodocea rotundata* [5.25 mmol O_2 m^{-2} h^{-1} in light and 2.28 mmol O_2 m^{-2} h^{-1} in darkness (Pedersen et al., 1998)]. Earlier studies have shown, that photosynthetically-derived O_2 evolution during illumination results in an enhanced O_2 partial pressure in the internal gas channels of the plant, as compared to in darkness, where the below-ground tissue is only supported by passive diffusion from the surrounding water column through the leaf tissue and into the lacunar system (Greve et al., 2003; Sand-Jensen et al., 2005; Borum et al., 2006). This is supported by our findings of higher O_2 release during light exposure, as well as the formation of an oxic

microshield around the first internode as a result of O_2 release from the rhizome under an incident irradiance of 350 µmol photons m^{-2} s^{-1} (Figure 2.2). The thickness of the oxic microshield (~300 µm; Figure 2.2 and 2.4) surrounding the rhizome of *Z. muelleri* was similar to previous measurements around *Zostera marina* in natural sediment, where Jensen et al. (2005) found an ~500 µm thick O_2 microzone surrounding the root-tip. The high O_2 demand of the surrounding reduced artificial sediment in our experimental setup was thus of similar magnitude as in natural settings. Previous O_2 microelectrode and planar optode studies of *Z. marina* roots (Jensen et al., 2005; Frederiksen & Glud, 2006) demonstrated a heterogeneous microdistribution of O_2 along the first actively growing root-bundle, with O_2 mainly leaking out from around the apical meristem of the root-tip (i.e., 1-2 mm away from root-apex). Low rates of O_2 release were also observed from the meristematic region of the rhizome of *Z. marina* by Jensen et al. (2005), indicating an analogous protection mechanism provided by the leaf sheath to the diminished gas channels in the compact meristematic tissue in this particular *Zostera* species. This is also supported by findings by Caffrey and Kemp (1991), who detected O_2 release to the rhizosphere from both roots and rhizomes of *Z. marina*.

The observed co-existence of H_2S and O_2 within the oxic microzone (Figure 2.2 and 2.4), suggests that spontaneous chemical re-oxidation was the dominant sulphide oxidizing mechanism in this experiment, as bacteria-mediated oxidation is 10^4 to 10^5 times faster than the chemical oxidation and thus rarely allows for co-existence to such temporal and spatial extent (Jørgensen & Revsbech, 1983; Nelson et al., 1986; Pedersen et al., 2004). However, microbially mediated oxidation of H_2S is likely more important in natural sediments in which the bacterial abundance is much higher than in the artificial sediment employed in this study. As such, the presence of sulphide-oxidizing bacteria would lead to shorter turnover time of H_2S and decrease the likelihood of H_2S to reach the rhizome in the presence of O_2 (Jørgensen & Revsbech, 1983; Nelson et al., 1986).

The decreased pH levels found within the oxic microshield of the meristematic regions of the rhizome may be a result of the formation of sulphuric acid as a by-product of the spontaneous chemical reactions between O_2 and H_2S (Figure 2.2 and 2.4). Interestingly, such locally decreased pH levels could lead to the release of sediment bound phosphorus, which is often considered a limiting nutrient in carbonate-rich marine sediments (Fourqurean & Zieman, 2002; Holmer et al., 2006), thus allowing for these plants to grow in phosphorus-

limited regions (Holmer et al., 2006). The increased pH just outside the oxic microshield, as compared to the bulk artificial sediment (Figure 2.2 and 2.4), indicates that *Z. muelleri* may secrete chemical substances (allelochemicals) to compensate for the generally decreased pH levels in the oxic microzone. An increase in the sediment pH would furthermore lead to a decrease in the H_2S levels in the immediate rhizosphere as a result of a pH-induced change in the sulphide equilibrium towards non-phytotoxic HS^- ions, thus acting as a counterbalance to the supposedly plant-induced formation of sulphuric acid. The enhanced pH level in the rhizosphere could consequently act as an additional chemical defence mechanism against toxic H_2S. This potential importance of pH changes in the rhizosphere of aquatic macrophytes has largely been overlooked in previous studies (Caffrey & Kemp, 1991; Pedersen et al., 1998; Jensen et al., 2005).

The limited O_2 release during water column hypoxia (Figure 2.2), resulted in the deterioration of the oxic microshield and a concomitant increase in the flux of H_2S towards the tissue surface (Table 2.1). This likely enhanced the risk of H_2S intrusion into the plant tissue as H_2S reaches the tissue surface as a consequence of inadequate internal aeration (Table 2.1; Figure 2.2). Particularly interesting is the observation of H_2S intrusion to the mature zone of roots when exposed to hypoxic conditions (Figure 2.3). This was not observed in any of the other treatments (i.e., an influx of H_2S) and thus strongly suggests that this happened as a result of lowered O_2 release from the rhizome and less O_2 support to roots (Figure 2.3). These results are supported by findings of Pedersen et al. (2004), showing H_2S intrusion into seagrass meristem tissue at low-moderate water column O_2 concentrations (~35% of air saturation). In our study, we found a slightly enhanced O_2 compensation point of ~50% of air saturation in the water column, i.e. the O_2 level where the total O_2 demand exceeds the rate of passive O_2 diffusion from the surrounding water column. This can most likely be explained by relatively thicker diffusive boundary layers over the leaves (Binzer et al., 2005), although enhanced plant respiration and a higher O_2 demand of the artificial sediment are also possible explanations.

A recent study by Raun and Borum (2013) showed, that internal meristematic anoxia (or hypoxia) occurred in *Z. marina* at a water column O_2 concentration of ~30% air saturation at 15°C, but already at ~60% air saturation at 25°C. High temperatures can thus have a

substantial negative impact on the O_2 levels of the meristematic tissue as a result of increased plant tissue respiration. The experiments of Raun and Borum (2013) were conducted in water-filled jars, i.e., with the above- and below-ground tissue experiencing exact same conditions, and did not take into account the potential importance of bacterial respiration and spontaneous chemical reactions such as H_2S re-oxidation. Hence, a slight decrease or increase in one of the numerous sinks or sources of O_2 could explain the higher O_2 compensation point seen in our experiment (Figure 2.2, Table 2.1).

No radial O_2 release was found from the roots of *Z. muelleri* (Figure 2.3). A barrier to radial O_2 release from the root-region of seagrasses has previously been shown to be restricted to the mature zone of the roots of *Z. marina*, with O_2 leaking out from around the root-cap (Jensen et al., 2005). Roots growing in reduced environments rely on a continued supply of O_2 to the active apical meristem during elongation. A barrier to O_2 release, such as provided by casparian band-like structures composed of suberin (Barnabes, 1996), can ensure an efficient transport of O_2 to the roots, as well as provide protection against intrusion of phytotoxic compounds such as H_2S. Additionally, the oxic microzone described in this study forms a protective oxidized zone, in which new roots can form and reach maturity with developed barriers to O_2 release and H_2S intrusion (Figure 2.7).

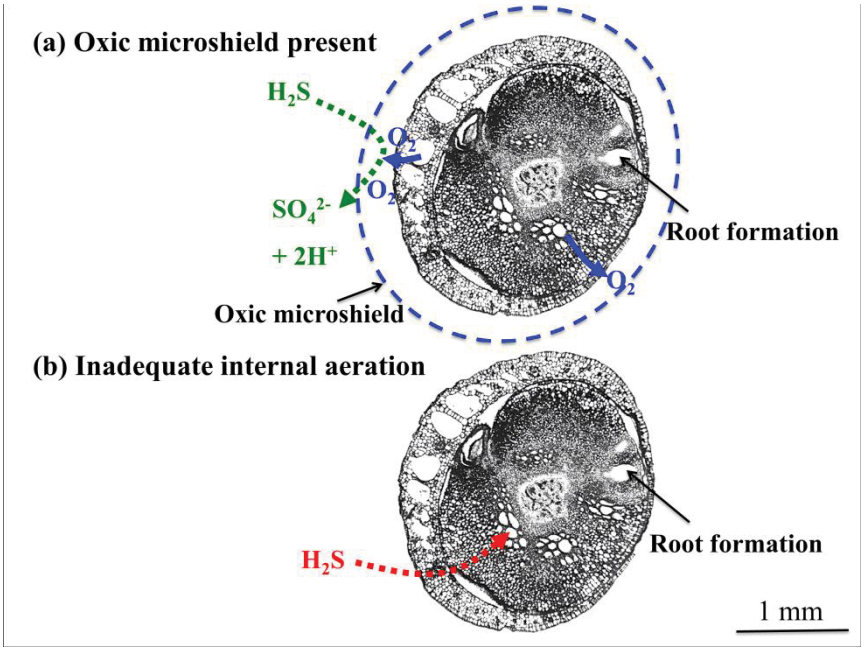

Figure 2.7: Conceptual diagram illustrating the protecting oxic microshield at the meristematic region of the rhizome (cross tissue section of the basal meristem with leaf sheath). The presence of the oxic microshield leads to a plant-derived oxidation of sediment produced H_2S (a). Inadequate internal aeration may result in H_2S intrusion (b).

Loss of seagrass meadows has been related to H_2S poisoning during water column hypoxia (Pedersen et al., 2004; Borum et al., 2005), as the internal O_2 partial pressure of the aerenchyma has been found to be highly correlated with the water column O_2 content (Pedersen et al., 2004; Borum et al., 2005). Water column hypoxia leads to inadequate internal aeration, which in turn may result in H_2S intrusion. Our results strongly support these previous findings showing that seagrass is more sensitive to water column hypoxia during nighttime, where there is no photosynthesis-driven O_2 supply to the rhizosphere. This underlines the importance of the diffusive supply of water column O_2 over the seagrass leaf DBL during the night. Sufficient oxygen support from the water column in darkness ensures the maintenance of a protecting oxic microshield around meristematic regions of the rhizome, and is thus vital for seagrass survival in highly reduced sediments.

In conclusion, we found that *Z. muelleri* is able to modify the chemical conditions of its immediate rhizosphere, resulting from high radial O_2 release from the base of the leaf sheath surrounding the meristematic regions of the rhizome. This enables oxidation of

ambient phytotoxic H_2S, and thereby acts as a chemical defence mechanism, protecting the most vulnerable meristematic tissue. In addition, plant-mediated pH increase in the immediate rhizosphere likely reduces the concentration of phytotoxic H_2S by shifting the speciation of sulphide towards non-phytotoxic HS^- ions, thus leading to further detoxification of the below-ground microenvironment. Water column hypoxia may lead to an inadequate internal O_2 supply to the below-ground tissues, resulting in H_2S intrusion as a consequence of the degradation of the protecting oxic microshield. Prolonged or sudden degradation of the oxic microshield protecting the vital basal meristems may thus be the initial external chemical mechanism behind sudden seagrass die-off events in highly reduced marine sediments.

ACKNOWLEDGEMENTS

We thank Jens Borum and Ole Pedersen (University of Copenhagen) for helpful discussions during the outline and design process of the experimental setup. We thank Dr Milan Szabo and Dr Verena Schrameyer (UTS) for help and discussions during PAM measurements. We acknowledge Dr Ingo Burghardt, Jacqueline Loyola-Echeverria and Dr Mathieu Pernice for fruitful discussions during the preparation of our histology samples. This research was funded by grants from *Augustinus Fonden*, *Fabrikant P.A. Fiskers Fond* (KEB), and the Danish Council for Independent Research | Natural Sciences (MK), the Australian Research Council (PJR, MK) and the University of Technology, Sydney (KEB).

SUPPORTING INFORMATION

Figure S2.1 and S2.2: The vertical distribution of O_2, H_2S and pH in the immediate rhizosphere of *Zostera muelleri* as compared to the reduced, bulk artificial sediment.

Figure S2.3. Conceptual diagram roughly illustrating the approximate position of the microprofile measurements, as well as the in this study defined zones of interest within the artificial sediment.

Figure S2.4. Microprofile of the H_2S concentration in the "bulk" artificial sediment (at a ~5mm horisontal distance away from the basal meristem with leaf sheath of *Zostera muelleri*), thus serving as a reference to the H_2S measurements just at and at increasing distance away from the below-ground tissue surface.

Figure S2.5. The O_2 concentration at the meristematic tissue surface (in µmol L^{-1}) under three different treatments.

REFERENCES

Almgren T, Hagstrom I. (1974). The oxidation rate of sulphide in sea water. *Water research* **8**: 395-400.

Armstrong J, Armstrong W. (2001). Rice and *Phragmites*: effects of organic acids on growth, root permeability, and radial oxygen loss to the rhizosphere. *American Journal of Botany* **88**: 1359-1370.

Armstrong W. (1979). *Aeration in higher plants*. London: Academic Press, London.

Barnabes AD. (1996). Casparian band-like structures in the root hypodermis of some aquatic angiosperms. *Aquatic Botany* **55**: 217-225.

Beer S, Vilenkin B, Weil A, Veste M, Susel L, Eshel A. (1998). Measuring photosynthetic rates in seagrasses by pulse amplitude modulated (PAM) fluorometry. *Marine Ecology Progress Series* **174**: 293-300.

Binzer T, Borum J, Pedersen O. (2005). Flow velocity affects internal oxygen conditions in the seagrass *Cymodocea nodosa*. *Aquatic Botany* **83**: 239-247.

Borum J, Pedersen O, Greve TM, Frankovich TA, Zieman JC, Fourqurean JW, Madden CJ. (2005). The potential role of plant oxygen and sulphide dynamics in die-off events of the tropical seagrass, *Thalassia testudinum*. *Journal of Ecology* **93**: 148-158.

Borum J, Sand-Jensen K, Binzer T, Pedersen O, Greve T. (2006). Oxygen movement in seagrasses. In: Larkum AWD, Orth JR & Duarte CM, eds. *Seagrasses: Biology, Ecology and Conservation.* Dordrecht, The Netherlands: Springer, Berlin, 255-270.

Brodersen KE, Nielsen DA, Ralph PJ, Kühl M. (**2014).** A split flow chamber with artificial sediment to examine the below-ground microenvironment of aquatic macrophytes. *Marine Biology*. doi: 10.1007/s00227-014-2542-3

Caffrey JM, Kemp WM. (1991). Seasonal and spatial patterns of oxygen production, respiration and root-rhizome release in *Potamogeton perfoliatus L*. and *Zostera marina L*. *Aquatic Botany* **40**: 109-128.

Carlson J, Paul R, Yarbro LA, Barber TR. (1994). Relationship of sediment sulfide to mortality of *Thalassia testudinum* in Florida Bay. *Bulletin of marine Science* **54**(3): 733-746.

Chen KY, Morris JC. (1972). Kinetics of oxidation of aqueous sulfide by O_2. *Environ. Sci. Technol.* **6**: 529-537.

Cline JD, Richards RA. (1969). Oxygenation of hydrogen sulfide in seawater at constant salinity, temperature, and pH. *Environ. Sci. Technol.* **3**: 838-843.

Colmer TD, Gibberd MR, Wiengweera A, Thin TK. (1998). The barrier to radial oxygen loss from roots of rice (*Oryza sativa* L.) is induced by growth in stagnant solution. *Journal of Experimental Botany* **49**: 1431-1436.

Costanza REA. (1997). The value of the world's ecosystem services and natural capital. *Nature* **387**: 253-260.

Eghbal MA, Pennefather PS, O'Brien PJ. (2004). H_2S cytotoxicity mechanism involves reactive oxygen species formation and mitochondrial depolarisation. *Toxicology* **203**: 69-76.

Enstone DE, Peterson CA, Ma F. (2003). Root endodermis and exodermis: structure, function, and responses to the environment. *Journal of Plant Growth Regulation* **21**: 335-351.

Fourqurean JW, Zieman JC. (2002). Nutrient content of the seagrass *Thalassia testudinum* reveals regional patterns of relative availability of nitrogen and phosphorus in the Florida Keys USA. *Biogeochemistry* **61**(3): 229-245.

Frederiksen MS, Glud RN. (2006). Oxygen dynamics in the rhizosphere of *Zostera marina*: A two-dimensional planar optode study. *Limnol. Oceanogr* **51**(2): 1072-1083.

Frederiksen MS, Holmer M, Borum J, Kennedy H. (2006b). Temporal and spatial variation of sulfide invasion in eelgrass (*Zostera marina*) as reflected by its sulfur isotopic composition. *Limnology and Oceanography* **51**(5): 2308-2318.

Goodman JL, Moore KA, Dennison WC. (1995). Photosynthetic responses of eelgrass (*Zostera marina* L.) to light and sediment sulfide in a shallow barrier island lagoon. *Aquatic Botany* **50**: 37-47.

Greve TM, Borum J, Pedersen O. (2003). Meristematic oxygen variability in eelgrass (*Zostera marina*). *Limnology and Oceanography* **48**(1): 210-216.

Holmer M, Bondgaard EJ. (2001). Photosynthetic and growth response of eelgrass to low oxygen and high sulfide concentrations during hypoxic events. *Aquatic Botany* **70**: 29-38.

Holmer M, Pedersen O, Ikejima K. (2006). Sulfur cycling and sulfide intrusion in mixed Southeast Asian tropical seagrass meadows. *Botanica Marina* **49**: 91-102.

Holmer M, Pedersen O, Krause-Jensen D, Olesen B, Hedegård Petersen M, Schopmeyer S, Koch M, Lomstein BA, Jensen HS. (2009). Sulfide intrusion in the tropical seagrasses *Thalassia testudinum* and *Syringodium filiforme*. *Estuarine, Coastal and Shelf Science* **85**(2): 319-326.

Jensen SI, Kühl M, Glud RN, Jørgensen LB, Prieme A. (2005). Oxic microzones and radial oxygen loss from roots of *Zostera marina*. *Marine Ecology Progress Series* **293**: 49-58.

Jensen SI, Kühl M, Prieme A. (2007). Different bacterial communities in the rhizoplane and bulk sediment of the seagrass *Zostera marina*. *FEMS Microbiology Ecology* **62**: 108-117.

Jeroschewski P, Steuckart C, Kühl M. (1996). An amperometric microsensor for the determination of H_2S in aquatic environments. *Analytical Chemistry* **68**: 4351-4357.

Jørgensen BB, Revsbech NP. (1983). Colorless sulfur bacteria, *Beggiatoa* spp. & *Thiovulum* spp., in O_2 and H_2S microgradients. *Applied and Environmental Microbiology* **45**: 1261-1270.

Kühl M, Revsbech NP. (2001). Biogeochemical microsensors for boundary layer studies. In: Boudreau BP, Jørgensen BB, eds. *The benthic boundary layer*. New York: Oxford University Press, New York, 180-210.

Kühl M, Steuckart C, Eickert G, Jeroschewski P. (1998). A H_2S microsensor for profiling sediments and biofilms: Application in acidic sediment. *Aquatic Microbial Ecology* **15**: 201-209.

Larkum AWD, Orth RJ, Duarte CM. (2006). *Seagrasses: Biology, Ecology and Conservation*. Berlin, Germany: Springer.

Nelson DC, Jørgensen BB, Revsbech NP. (1986). Growth pattern and yield of a chemoautotrophic *Beggiatoa sp.* in oxygen-sulfide microgradients. *Applied and Environmental Microbiology* **52**(2): 225-233.

Orth RJ, Carruthers TJB, Dennison WC, Duarte CM, Fourqurean JW, Heck Jr. KL, Hughes AR, Kendrick GA, Kenworthy WJ, Olyarnik S, et al. (2006). A global crisis for seagrass ecosystems. *BioScience* **56**(12): 987-996.

Pedersen O, Binzer T, Borum J. (2004). Sulphide intrusion in eelgrass (*Zostera marina* L). *Plant, Cell and Environment* **27**: 595-602.

Pedersen O, Borum J, Duarte CM, Fortes MD. (1998). Oxygen dynamics in the rhizosphere of *Cymodocea rotundata*. *Marine Ecology Progress Series* **169**: 283-288.

Pedersen O, Borum J, Duarte CM, Fortes MD. (1999). ERRATUM: Oxygen dynamics in the rhizosphere of *Cymodocea rotundata*. *Marine Ecology Progress Series* **178**: 310.

Perez-Perez ME, Lemaire SD, Crespo JL. (2012). Reactive oxygen species and autophagy in plants and algae. *Plant Physiology* **160**: 156-164.

Plus M, Deslous-Paoli J-M, Dagault F. (2003). Seagrass (*Zostera marina* L.) bed recolonisation after anoxia-induced full mortality. *Aquatic Botany* **77**(2): 121-134.

Ralph PJ, Short FT. (2002). Impact of the wasting disease pathogen, *Labyrinthula zosterae*, on photobiology of eelgrass *Zostera marina*. *Marine Ecology Progress Series* **226**: 265-271.

Ralph PJ, Tomasko D, Moore K, Seddon S, Macinnis-Ng CMO. (2006). Human impacts on Seagrasses: Eutrophication, Sedimentation and Contamination. In: Larkum AWD, Orth RJ, Duarte CM, eds. *Seagrasses: Biology, Ecology and Conservation*. Springer, Berlin: 567-593.

Ramsing NB, Gundersen JK. (2012). Seawater and Gasses: Tabulated physical parameters of interest to people working with microsensors in marine systems: Unisense data tables. [PDF document] Available from Unisense A/S, Denmark. URL http://www.unisense.com. [accessed 17 September 2014].

Raun AL, Borum J. (2013). Combined impact of water column oxygen and temperature on internal oxygen status and growth of *Zostera marina* seedlings and adult shoots. *Journal of Experimental Marine Biology and Ecology* **441**: 16–22.

Raven JA, Scrimgeour CM. (1997). The influence of anoxia on plants of saline habitates with special reference to the sulfur cycle. *Annals of Botany* **79**: 79-86.

Revsbech NP. (1989). An oxygen microsensor with a guard cathode. *Limnology and Oceanography* **34**(2): 474-478.

Robblee MB, Barber TR, R. CP, Durako MJ, Fourqurean JW, Muehlstein LK, Prorter D, Yarbro LA, Zieman RT, Zieman JC. (1991). Mass mortality of the tropical seagrass *Thalassia testudinum* in Florida Bay (USA). *Marine Ecology Progress Series* **71**: 297-299.

Sand-Jensen K, Pedersen O, Binzer T, Borum J. (2005). Contrasting oxygen dynamics in the freshwater isoetid *Lobelia dortmanna* and the marine seagrass *Zostera marina*. *Annals of Botany* **96**(4): 613-623.

Seddon S, Connolly R, Edyvane KS. (2000). Large-scale seagrass dieback in northern Spencer Gulf, South Australia. *Aquatic Botany* **66**(4): 297-310.

Short FT, Duarte CM. (2001). Methods for the measurement of seagrass growth and production. *In Short, F. T., Coles, R. G., Eds., Global Seagrass Research Methods, Elsevier, Amsterdam, Netherlands.*: 155-182.

Steen-Knudsen O. (2002). *Biological membranes: Theory of Transport, Potentials and Electric Impulses*. Cambridge, UK: Cambridge University Press.

Truong DH, Eghbal MA, Hindmarsh W, Roth SH, O'Brien PJ. (2006). Molecular mechanisms of hydrogen sulfide toxicity. *Drug Metab Rev* **38**(4): 733-744.

Waycott M, Duarte CM, Carruthers TJB, Orth RJ, Dennison WC, Olyarnik S, Calladine A, Fourqurean JW, Heck Jr. KL, Hughes AR, et al. (2009). Accelerating loss of seagrasses across the globe threatens coastal ecosystems. *PNAS* **106**: 12377–12381.

Zieman JC, Fourqurean JW, Frankovich TA. (1999). Seagrass die-off in Florida Bay: Long-term trends in abundance and growth of turtle grass, *Thalassia testudinum*. *Estuaries* **22**(2): 460-470.

SUPPORTING INFORMATION

Oxic microshield and local pH enhancement protects *Zostera muelleri* from sediment derived hydrogen sulphide

Kasper Elgetti Brodersen, Daniel A. Nielsen, Peter J. Ralph, Michael Kuhl

University of Technology, Sydney, Australia & University of Copenhagen, Denmark

Notes S2.1 and Figures S2.1-S2.5

NOTES S2.1

The below-ground microenvironment of *Zostera muelleri* was investigated by means of microelectrodes, enabling mapping of the spatial microdistribution of O_2, H_2S and pH in the seagrass rhizosphere. The seagrass specimens were cultured in reduced, fluid artificial sediment (i.e., a deoxygenated ager-seawater solution with added Na_2S, HEPES buffer and nutrients), wherein we examined how changing environmental conditions affected the chemical microenvironment around below-ground tissue. We applied a novel custom-made split flow-chamber with an added compartment of seawater-agar, in which the leaves of the plant were in the free-flowing water section and the roots supported in the agar matrix. The split flow-chamber enabled us to manipulate the seagrass leaf environment, i.e., light/dark and water-column oxygen concentration, while observing the impact on the chemical microenvironment around the seagrass root-system. The plants were growing in anoxic, reduced artificial sediment containing hydrogen sulfide concentrations of 200-300 µM to mimic natural conditions. The lower compartment of the split flow-chamber containing the artificial sediment consisted of a tripartite-layer in the vertical orientation, that is, a ~10 mm thick layer of nitrogen flushed seawater working as an oxygen sink, followed by a ~45 mm thick layer of artificial sediment (as from above) and finally at the bottom a ~5 mm thin highly phytotoxic (~1000 µM Na_2S) and anoxic bottom layer, continuously supporting the artificial sediment with H_2S. The lower compartment was covered by parafilm and then Aluminium-foil, to minimize the exposure to O_2 and keep the below-ground tissue in darkness.

H_2S levels in the transparent, reduced artificial sediment under different experimental conditions

No bacterial community was added to the artificial sediment in this experimental setup. At time t_0, the H_2S concentration within the sediment was homogenous (with equal amounts of Na_2S added to the initial identical volume of artificial sediment), but was then reduced via chemical re-oxidation throughout the experiment as a result of the radial O_2 loss from the below-ground biomass (especially during light exposure). Slight differences in below-ground and above-ground tissue surface areas and cultivation time could have resulted in different

total oxidation capabilities between plants and lower H_2S concentrations in the artificial sediment as a result of the longer cultivation time, respectively. Furthermore, after light exposure and before the hypoxia treatment, H_2S was injected to layer 3 (the highly phytotoxic bottom layer) of the artificial sediment to re-establish the initial H_2S concentration as preliminary studies had shown total removal of H_2S during light exposure. Hence, the altered background H_2S levels seen under different experimental conditions are most likely due to the above-mentioned methodology and variances in oxidation capacity between the examined plants.

As such this experiment does not examine the response to certain H_2S concentrations within the seagrass rhizosphere. Instead, we investigated whether the plants were able to actively modify the biogeochemical conditions in the immediate rhizosphere to promote their own growth and how such below-ground microenvironments were affected by changing environmental conditions.

SUPPLEMENTARY RESULTS AND FIGURES

Figure S2.1a-i and S2.2a-f shows vertical microsensor measurements of O_2, H_2S and pH in the immediate rhizosphere of *Z. muelleri* (i.e., measured at ~1 mm horizontal distance away from the meristematic region of the rhizome, at the first root bundle; black dots and lines), as compared to the bulk reduced fluid artificial sediment measured at ~3 cm distance away from the below-ground tissue (grey dots and lines). Microprofiles illustrated in Figure S2.1 originate from plant 1, and Figure S2.2 from plant 2. The vertical microprofiles were performed from the surface of the oxygen sink down to below the below-ground tissue (located at ~25 mm depth). The vertical microprofiles were measured under four different treatments: dark + 100% air saturated water-column (leaf region); 260 µmol photons m^{-2} s^{-1} + 100% air saturated water-column; 350 µmol photons m^{-2} s^{-1} + 100% air saturated water-column; and dark + 50% air saturation in the water-column, i.e., hypoxic conditions (n=2); Performed in the above-presented chronological order. The vertical microdistribution of the chemical species elucidates the effect of the experimentally changed environmental conditions as well as differences between plant-vegetated and non-vegetated areas. Y=0 indicate the surface of the oxygen sink (i.e., the nitrogen bubbled seawater). The reduced,

anoxic artificial sediment surface was at ~10 mm depth. The position of the below-ground tissues was at ~25 mm depth. Error bars are ± SD. Figure legends are beneath the last graph of the figures. Notice as fewer measurements were performed on the roots-system of plant 2 the total culture time in the artificial sediment of this plant decreased. Hence, plant 2 had less time to modify the biogeochemical condition in the immediate rhizosphere.

Supporting results and discussion

Our results suggest that O_2 release from the meristematic region of the rhizome, and possible secretion of allelochemicals, leads to higher pH values and lower H_2S concentrations in the immediate rhizosphere (< 5 mm distance from the tissue surface) at the position of the below-ground meristematic tissue (at ~ 25 mm depth) as compared to the bulk artificial sediment (Figure S2.1 and S2.2). Furthermore, such leakage from the below-ground meristematic tissue results in a slightly deeper O_2 penetration depth and a downward movement of the sulphide front in the immediate rhizosphere as compared to the bulk artificial sediment (Figure S2.1 and S2.2). The observed differences between the immediate rhizosphere and the bulk artificial sediment were thus due to plant-mediated alterations of the local chemical microenvironment.

Moreover, a limitation of the constructed artificial sediment used in this experiment, is that, there is no natural microbial community in the sediment (e.g., sulphate reducing bacteria) providing a constant source of H_2S to the immediate rhizosphere. Such studies are underway.

FIGURE S2.1

(a) DARK O_2 concentrations: Vertical microprofiles of the oxygen concentration in the immediate rhizosphere (black) as compared to in the bulk artificial sediment (grey), showing a somewhat similar thickness of the oxygenated zone, but with much higher oxygen concentrations, ~75 µmol O_2 L^{-1} at 1.5 cm depth, within the immediate rhizosphere.

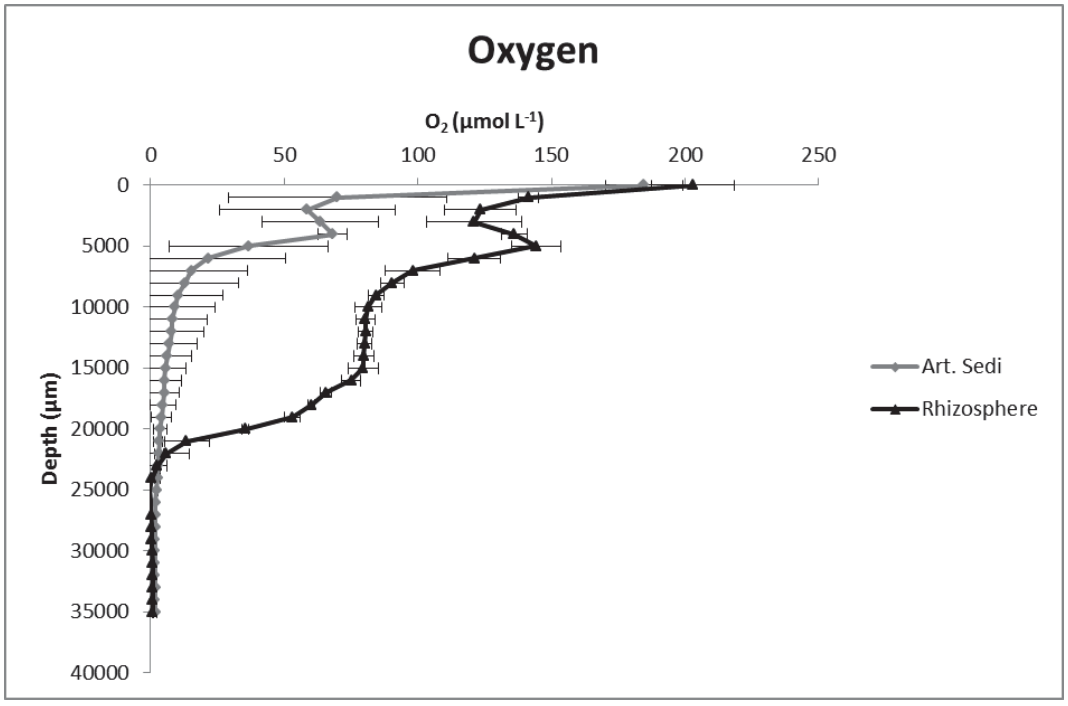

(b) DARK H_2S concentrations: Vertical microprofiles of the hydrogen sulphide concentration in the immediate rhizosphere as compared to in the bulk artificial sediment, showing a downward movement of the initial presence of hydrogen sulphide, ~7 mm, within the immediate rhizosphere.

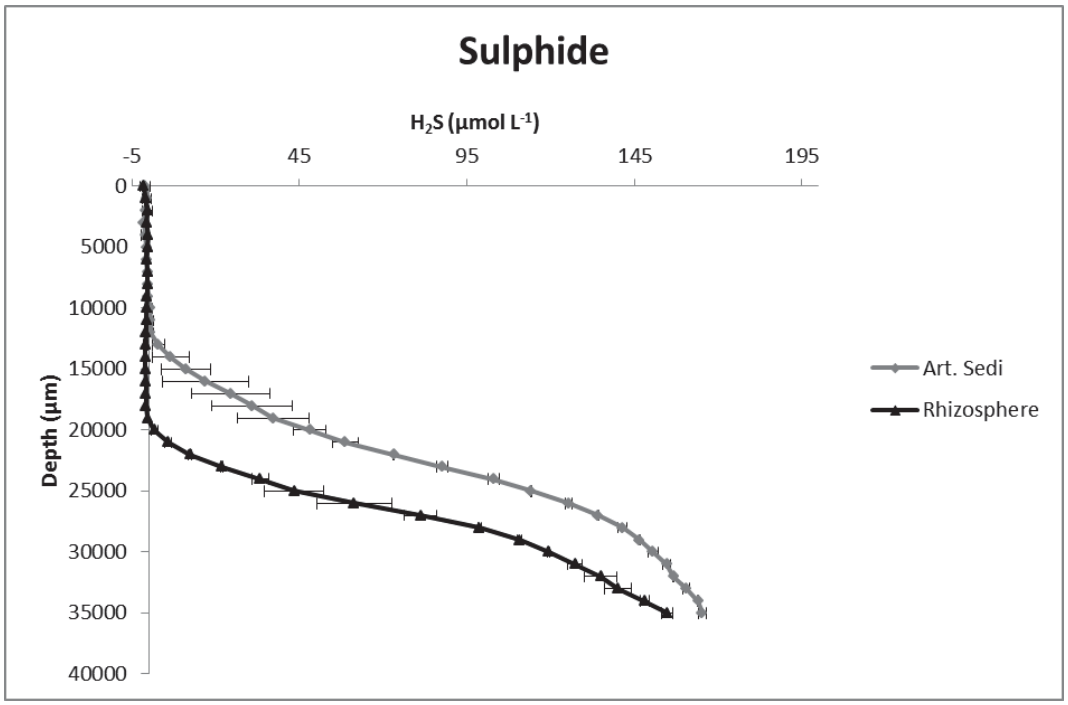

(c) DARK pH values: Vertical microprofiles of the pH value in the immediate rhizosphere as compared to in the bulk artificial sediment, showing much higher pH values, ~1 pH unit, within the immediate rhizosphere at the approximate location of the below-ground tissue.

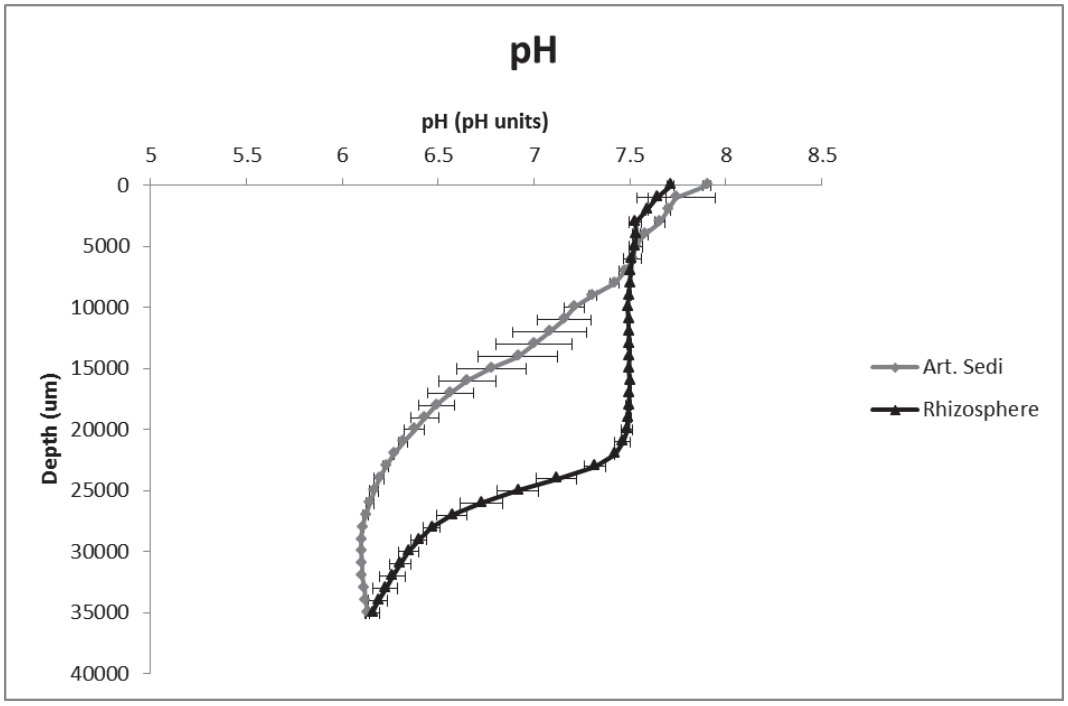

(d) 260 LIGHT O_2 concentrations: Vertical microprofiles of the oxygen concentration in the immediate rhizosphere as compared to in the bulk artificial sediment, showing a thicker oxygenated zone, ~1 cm, within the immediate rhizosphere under an incident irradiance of 260 µmol photons m^{-2} s^{-1}.

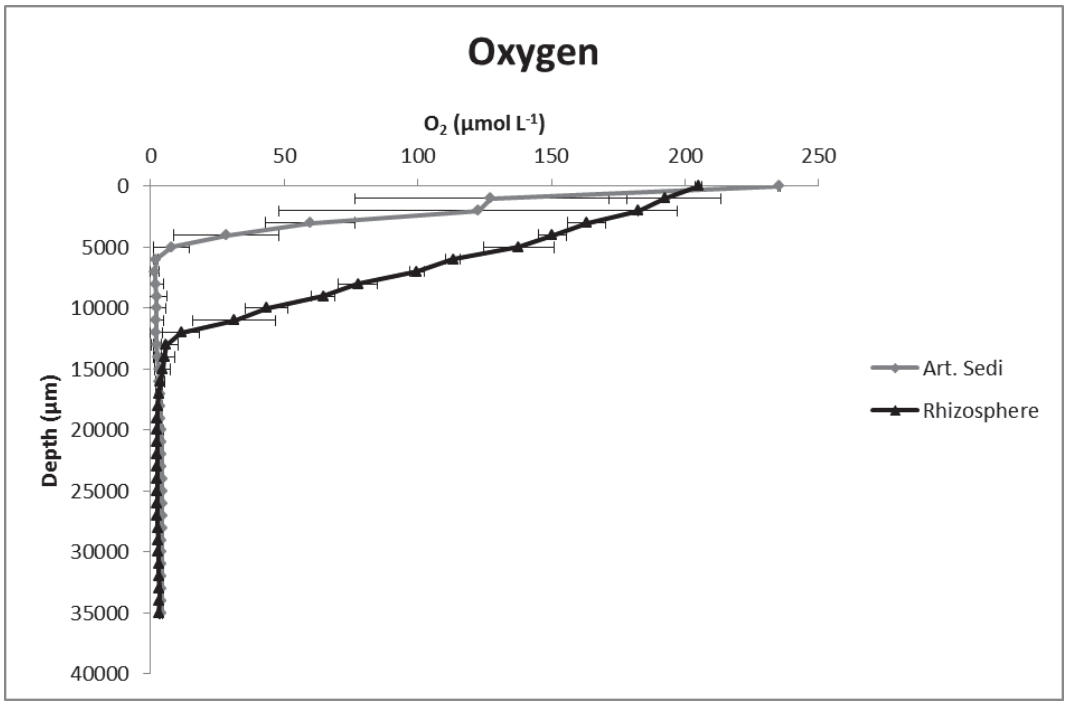

(e) 260 LIGHT H_2S concentrations: Vertical microprofiles of the hydrogen sulphide concentration in the immediate rhizosphere as compared to in the bulk artificial sediment, showing a downward movement of the initial presence of hydrogen sulphide, ~1 cm, within the immediate rhizosphere under an incident irradiance of 260 µmol photons m^{-2} s^{-1}.

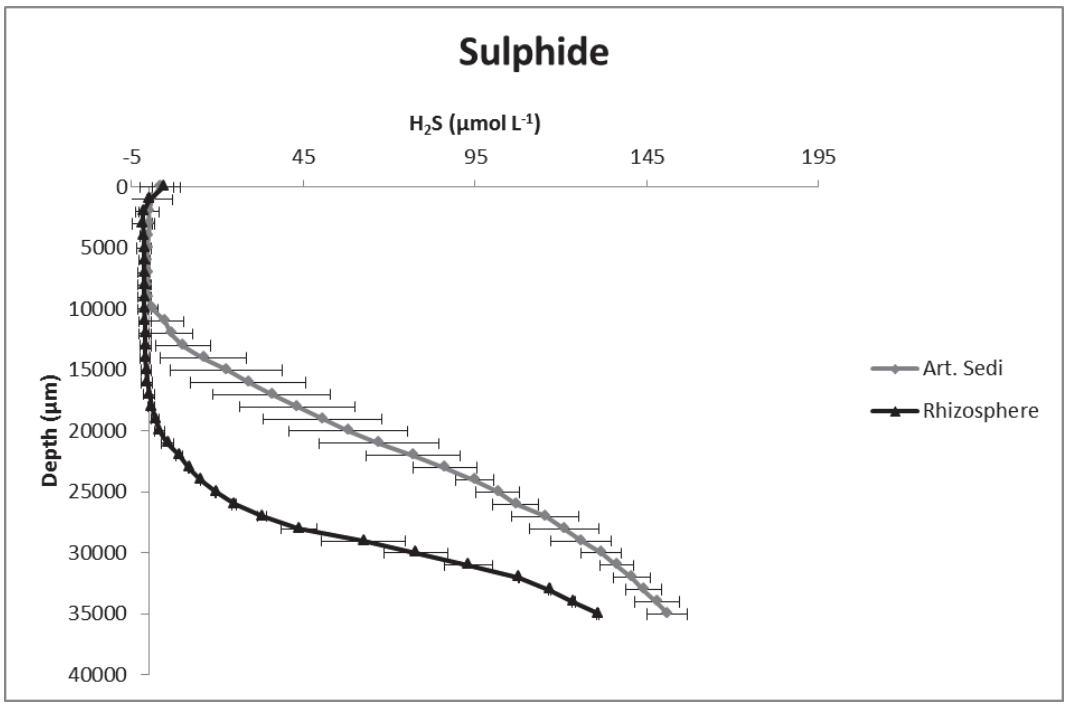

(f) 260 LIGHT pH values: Vertical microprofiles of the pH value in the immediate rhizosphere as compared to in the bulk artificial sediment, showing much higher pH values, ~1 pH unit, within the immediate rhizosphere at the approximate position of the below-ground tissue under an incident irradiance of 260 µmol photons m^{-2} s^{-1}.

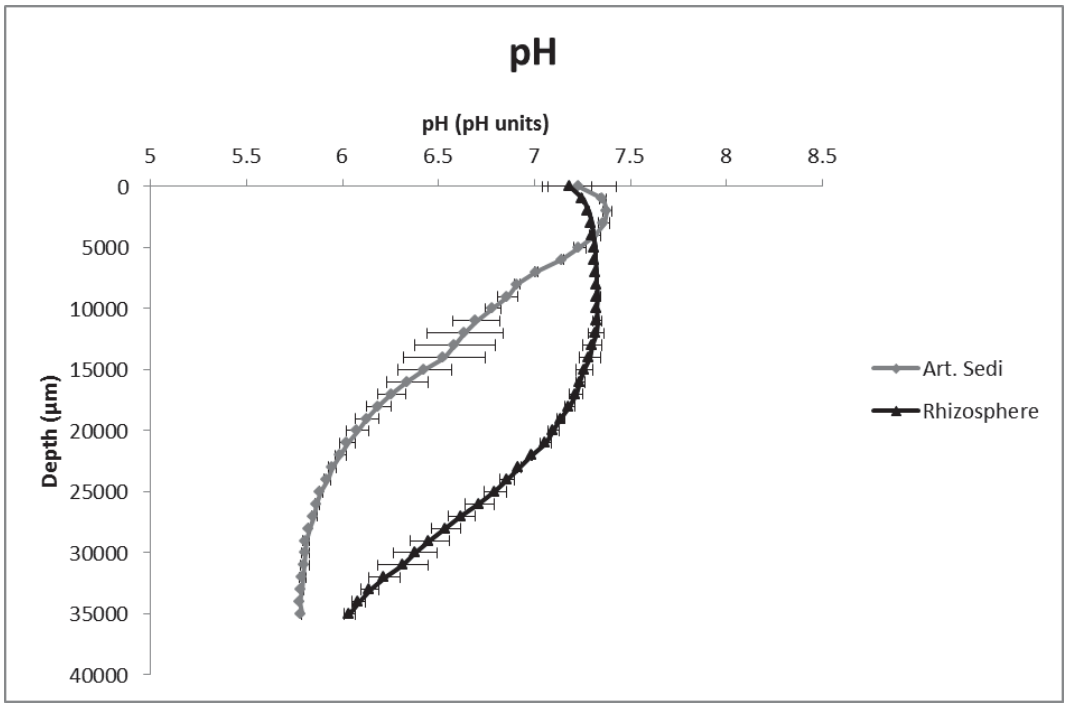

(g) HYPOXIA O_2 concentrations: Vertical microprofiles of the oxygen concentration in the immediate rhizosphere as compared to in the bulk artificial sediment, showing a very similar oxygen penetration depth under hypoxic conditions in the leaf region.

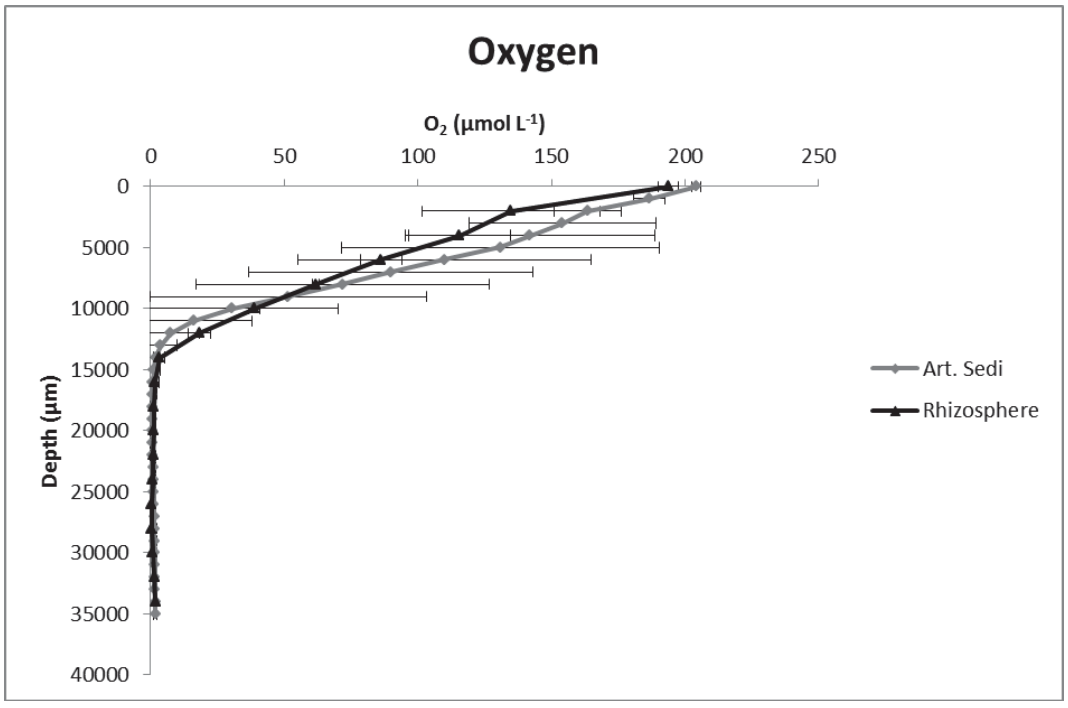

(h) HYPOXIA H_2S concentrations: Vertical microprofiles of the hydrogen sulphide concentration in the immediate rhizosphere as compared to in the bulk artificial sediment, showing a deeper initial presence of hydrogen sulphide, ~1 cm, within the immediate rhizosphere under hypoxia.

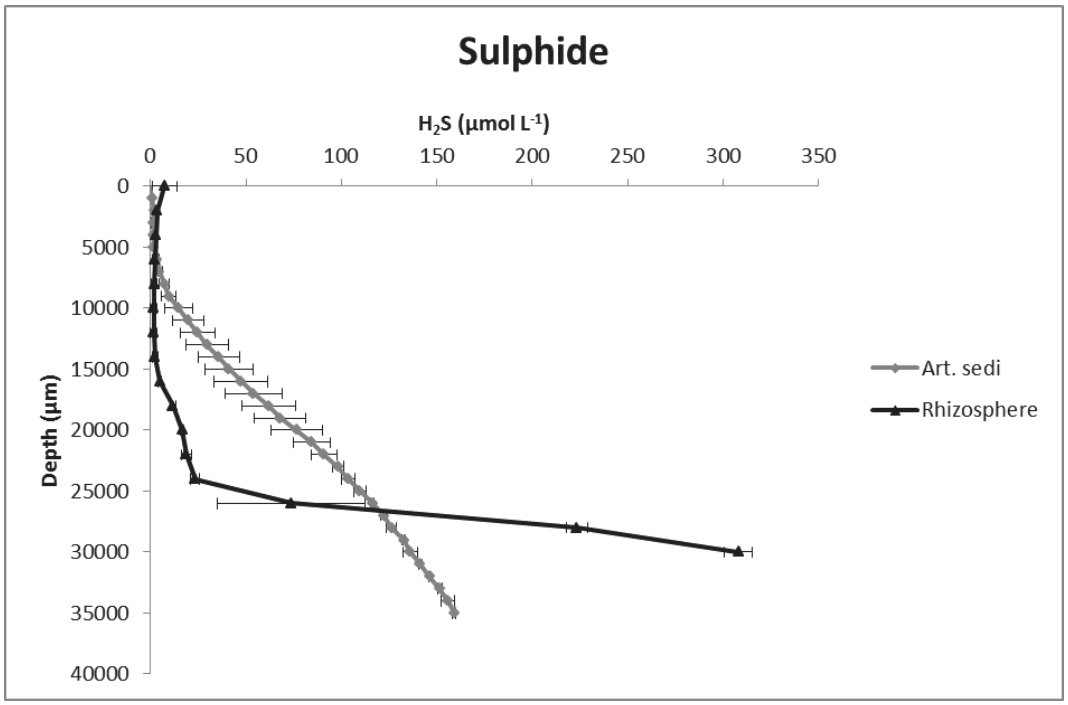

(i) HYPOXIA pH values: Vertical microprofiles of the pH value in the immediate rhizosphere as compared to the bulk artificial sediment, showing much higher pH values, ~1.1 pH units, at the approximate position of the below-ground tissue within the immediate rhizosphere.

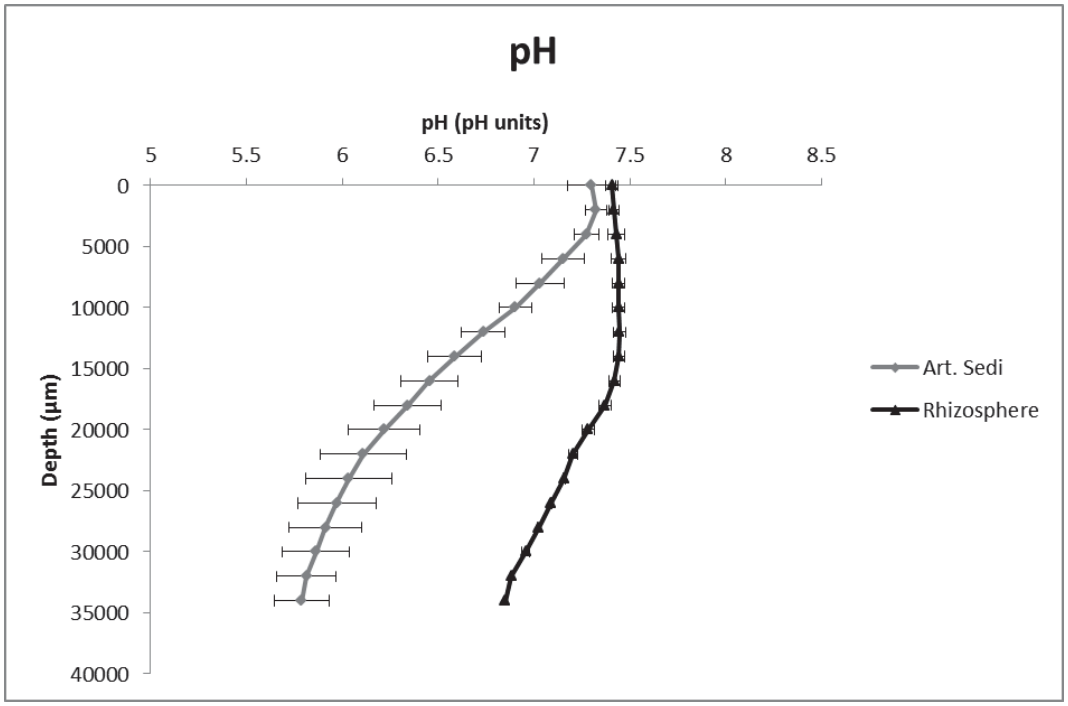

Figure S2.1. The vertical distribution of $[O_2]$, $[H_2S]$ and pH values in the immediate rhizosphere of *Zostera muelleri* (Plant 1) as compared to in the reduced artificial sediment elucidating the effect of the experimentally changed environmental conditions as well as differences between plant-vegetated and non-vegetated areas. Grey lines represent profiles in the bulk artificial sediment; Black lines represent profiles the immediate rhizosphere. Vertical microprofiles in the immediate rhizosphere were performed in the region of the basal meristem. Y=0 indicate the surface of the nitrogen bubbled seawater (oxygen sink). The artificial sediment surface is at ~10 mm depth; the below-ground tissue at ~25 mm depth. Error bars are ± SD. n=2.

FIGURE S2.2

(a) 350 LIGHT O_2 concentrations: Vertical microprofiles of the oxygen concentration in the immediate rhizosphere (black) as compared to in the bulk artificial sediment (grey), showing a thicker oxygenated zone, ~1 cm, within the immediate rhizosphere under an incident irradiance of 350 µmol photons m^{-2} s^{-1}.

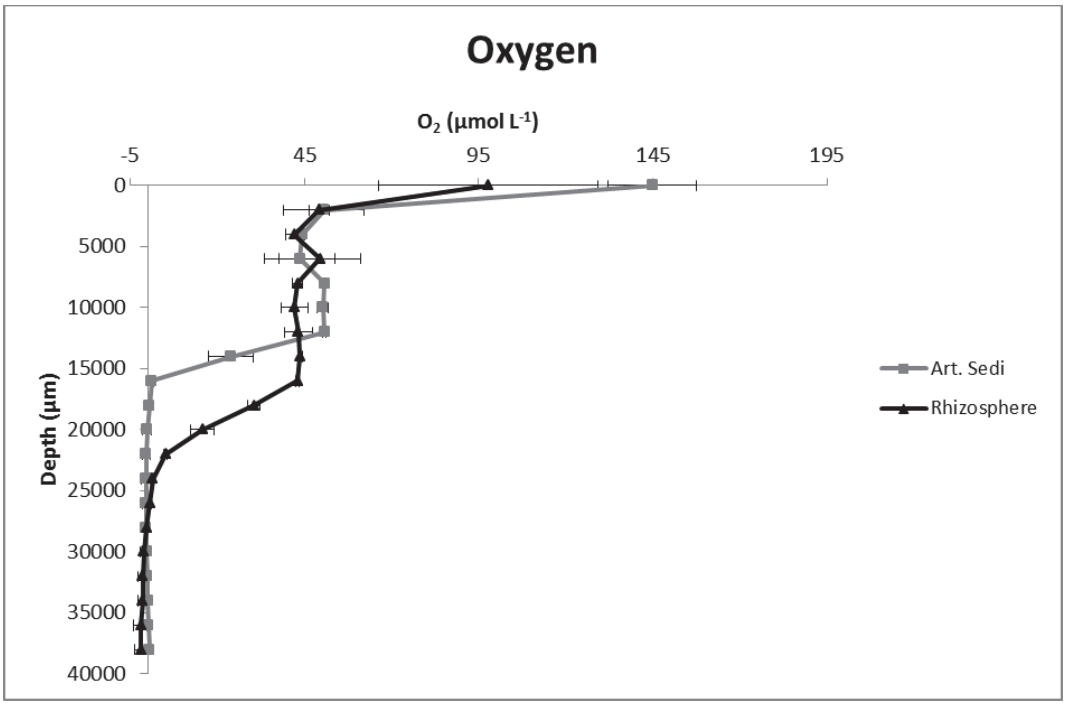

(b) 350 LIGHT H_2S concentrations: Vertical microprofiles of the hydrogen sulphide concentration in the immediate rhizosphere as compared to in the bulk artificial sediment, showing a downward movement of the initial presence of hydrogen sulphide, ~6 mm, within the immediate rhizosphere under an incident irradiance of 350 µmol photons m^{-2} s^{-1}.

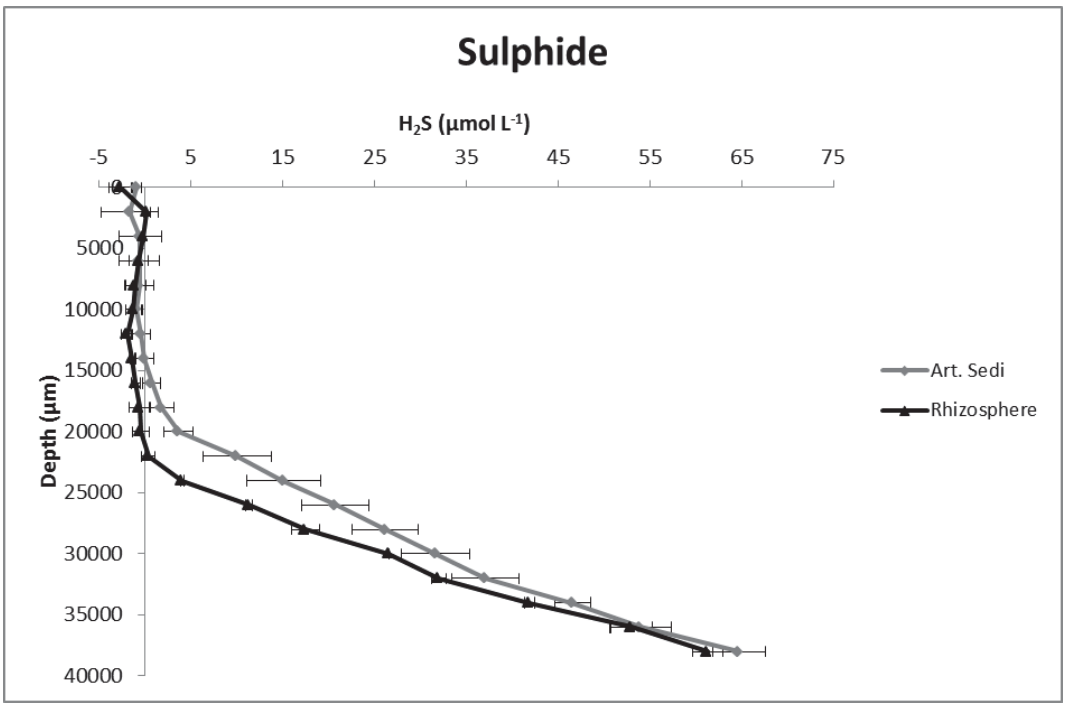

(c) 350 LIGHT pH values: Vertical microprofiles of the pH value in the immediate rhizosphere as compared to in the bulk artificial sediment, showing slight higher pH values just above the approximate position of the below-ground tissue within the immediate rhizosphere under an incident irradiance of 350 µmol photons m^{-2} s^{-1}.

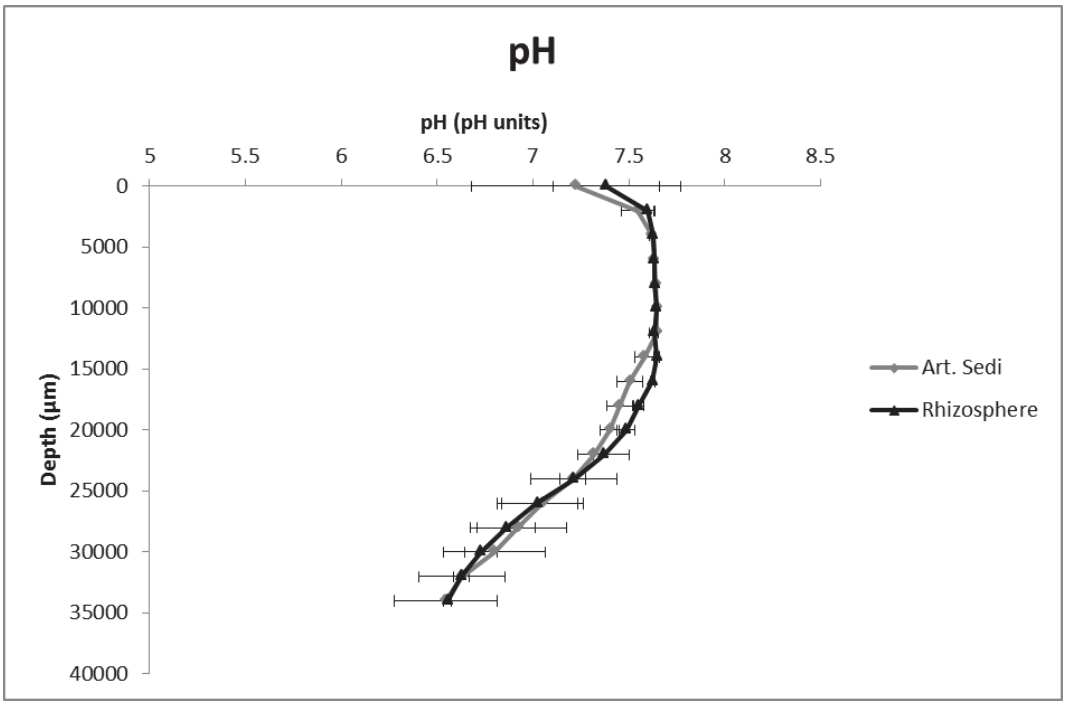

(d) HYPOXIA O_2 concentrations: Vertical microprofiles of the oxygen concentration in the immediate rhizosphere as compared to in the bulk artificial sediment, showing very similar thickness of the oxygenated zone during water-column hypoxia.

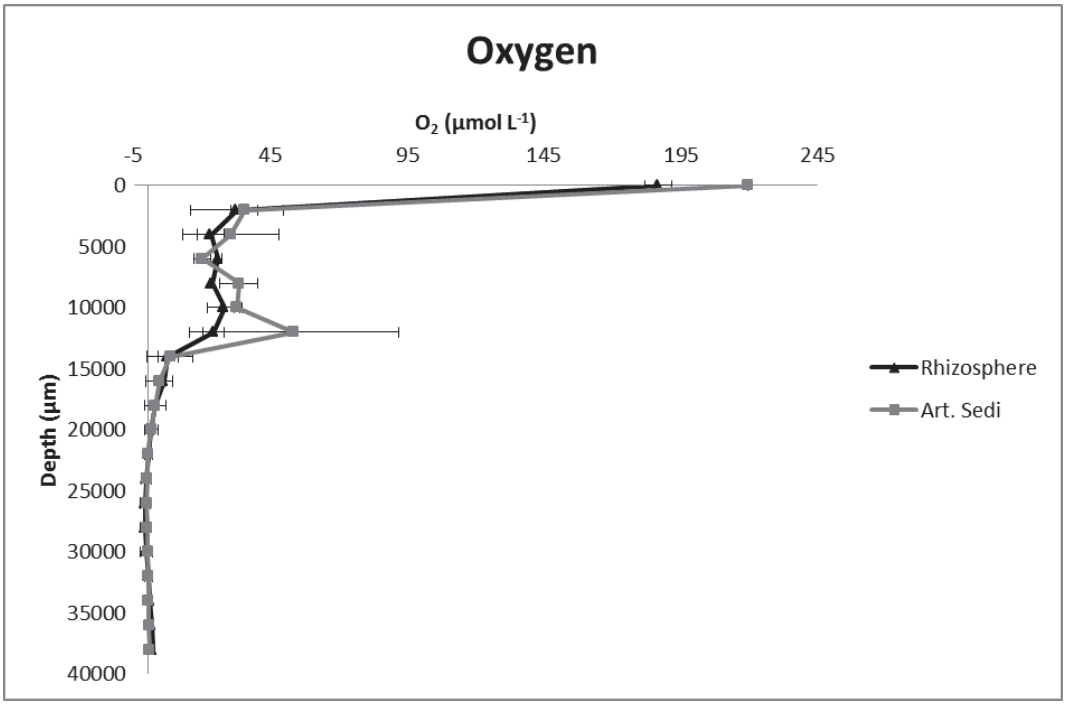

(e) HYPOXIA H_2S concentrations: Vertical microprofiles of the hydrogen sulphide concentration in the immediate rhizosphere as compared to in the bulk artificial sediment, showing slightly higher hydrogen sulphide levels, ~25 µmol H_2S L^{-1}, within the immediate rhizosphere at the approximate location of the below-ground tissue during water-column hypoxia.

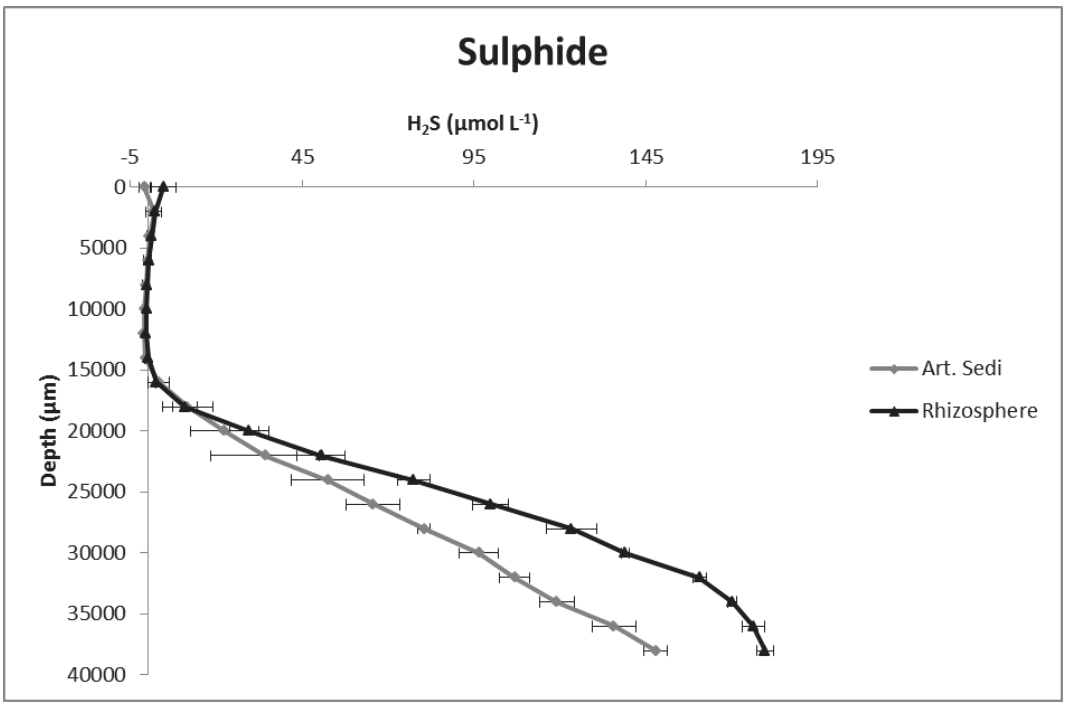

(f) HYPOXIA pH values: Vertical microprofiles of the pH value in the immediate rhizosphere as compared to in the bulk artificial sediment, showing higher pH values, ~0.4 pH units, within the immediate rhizosphere at the approximate position of the below-ground tissue during water-column hypoxia.

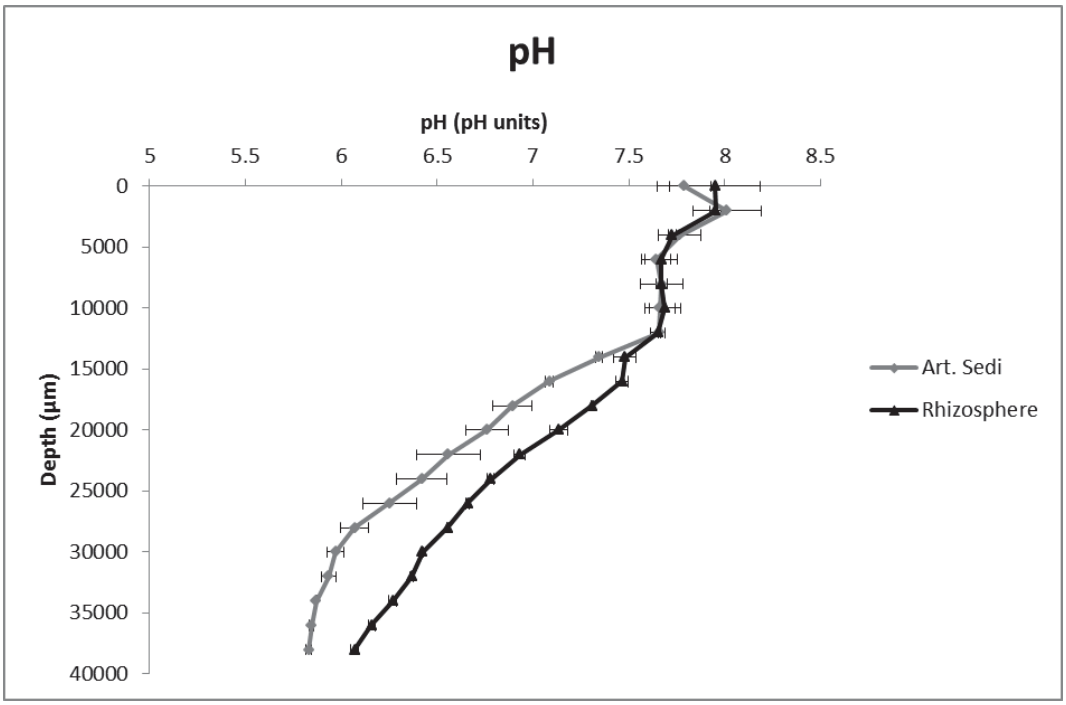

Figure S2.2. The vertical distribution of [O_2], [H_2S] and pH values in the immediate rhizosphere of *Zostera muelleri* (Plant 2) as compared to in the reduced artificial sediment elucidating the effect of the experimentally changed environmental conditions as well as differences between plant-vegetated and non-vegetated areas. Grey lines represent profiles in the bulk artificial sediment; Black lines represent profiles in the immediate rhizosphere. Vertical microprofiles in the immediate rhizosphere were performed at the basal meristem. Y=0 indicate the surface of the nitrogen bubbled seawater (oxygen sink). The artificial sediment surface is at ~10 mm depth; the below-ground tissue at ~25 mm depth. Error bars are ± SD. n=2. Notice as fewer measurements were performed on the roots-system of plant 2 the total culture time in the artificial sediment of this plant decreased. Hence, plant 2 had less time to modify the biogeochemical condition in the immediate rhizosphere.

FIGURE S2.3

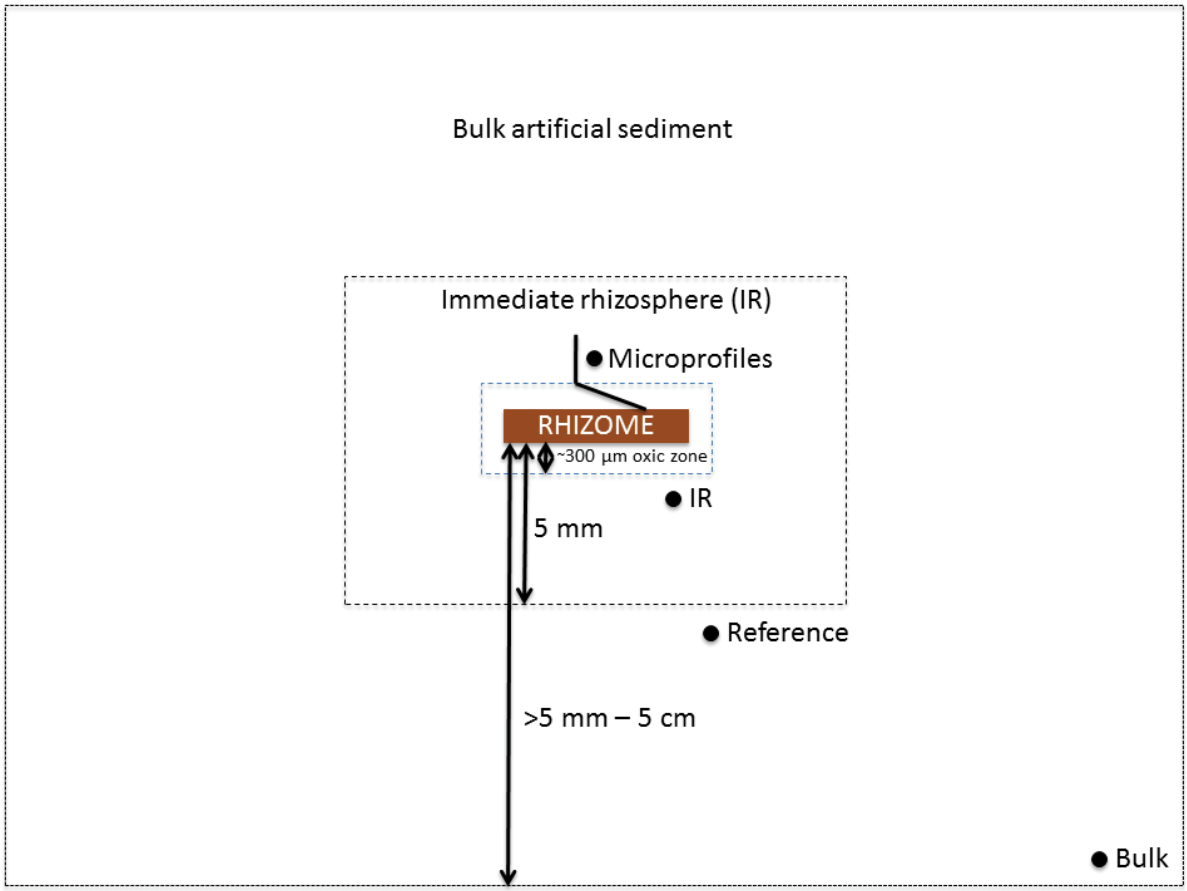

Figure S2.3. Conceptual diagram roughly illustrating the approximate position of the microprofile measurements (black dots), as well as the in this study defined zones of interest within the artificial sediment (area enclosed by dotted lines). Note that the chemical microprofiles of the below-ground tissue, describing the dynamics of the chemical microenvironment of *Z. muelleri* (abbreviated microprofiles in the figure), covers both the oxic microzone and the immediate rhizosphere (solid black line). IR represents the profiles measured within the immediate rhizosphere of *Z. muelleri* (i.e. the plant-vegetated area) as compared to the bulk artificial sediment (Bulk). Reference is the approximate position of the basal meristem H_2S concentration reference. Arrows indicate the respective distances from the below-ground tissue surface.

FIGURE S2.4

The H_2S concentration within the artificial sediment measured at the same vertical depth as the basal meristem tissue of *Z. muelleri* but at a ~ 5mm distance away from the tissue surface was ~23 µmol L^{-1} (Figure S2.4). The measurement serves as a reference to the measurements performed at the tissue surface of the meristematic region of the rhizome (plant 2; under an incident irradiance of ~350 µmol photons $m^{-2}s^{-1}$) and was achieved by using the motorized micromanipulator.

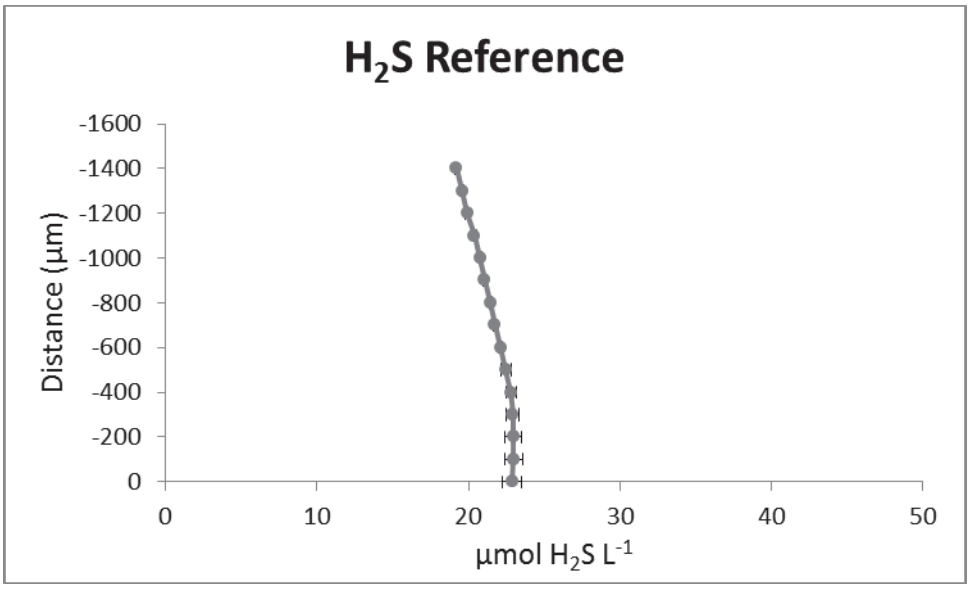

Figure S2.4. The H_2S concentration in the artificial sediment at a ~5mm horisontal distance away from the basal meristem of *Zostera muelleri* (plant 2). The graph serves as a reference to the H_2S measurements just at and at increasing distance away from the below-ground tissue surface. Y = 0 indicate the same vertical depth as the surface of the meristematic tissue. Error bars indicate ± SD. n = 2.

FIGURE S2.5

Statistical analysis confirming the resemblance between plant 1 and 2 based on O_2 concentration measurements at the surface of the meristematic region of the rhizome (Students t-test; $p \geq 0.3$, all treatments; df = 8-9 [dark treatments: p=0.9, light treatments: p=0.4, hypoxia treatments: p=0.3]).

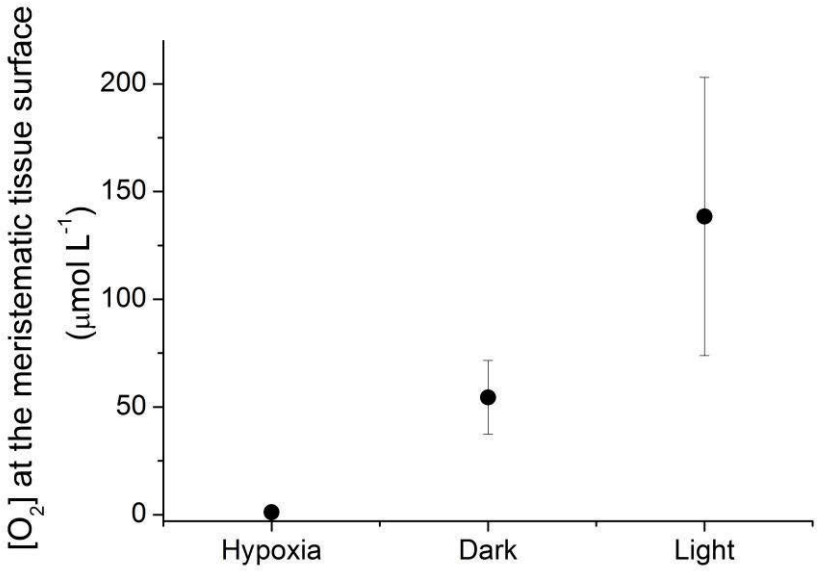

Figure S2.5. The O_2 concentration at the meristematic tissue surface (in µmol L^{-1}) under three different treatments. Values are mean values calculated as an average of both plants. Error bars indicate mean ± SD. n = 10-11.

Chapter 3

Optical sensor nanoparticles in artificial sediments – a new tool to visualize O_2 dynamics around the rhizome and roots of seagrasses

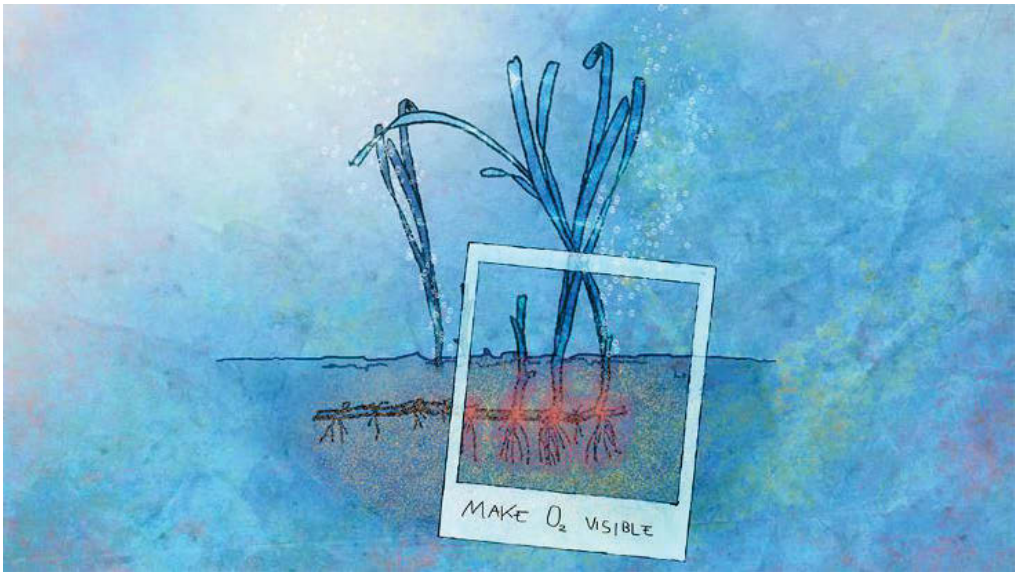

TOC figure. *O_2 distributions in the seagrass rhizosphere as determined with novel optical sensor nanoparticles incorporated into transparent, artificial sediment.*

Shared first authorship with Klaus Koren from the University of Copenhagen.

Citation: Koren K, Brodersen KE, Jakobsen S. & Kühl M. (2015). Optical sensor nanoparticles in artificial sediments – a new tool to visualize O_2 dynamics around the rhizome and roots of seagrasses. *Environmental Science and Technology* **49**(4): 2286-2292.

Highlights: This chapter describes a new methodology to analyse the below-ground chemical microenvironment of aquatic macrophytes, such as seagrasses, in high spatio-temporal resolution by means of advanced optical nanoparticle-based sensor technology. As seagrass beds currently are declining with alarming rates worldwide, new insight into the dynamics of the below-ground biogeochemical microenvironment is crucial for the preservation of this vital marine ecosystem. Our novel microenvironmental approach determined, for the first time, the O_2 dynamics and distribution around the rhizome and roots of *Zostera marina* L. on an entire rhizosphere scale at once.

Optical sensor nanoparticles in artificial sediments – a new tool to visualize O_2 dynamics around the rhizome and roots of seagrasses

Klaus Koren[a‡], Kasper E. Brodersen[b‡], Sofie L. Jakobsen[a], Michael Kühl[a,b,c*]

[a] Marine Biological Section, Department of Biology, University of Copenhagen, Helsingør, Denmark

[b] Plant Functional Biology and Climate Change Cluster, University of Technology Sydney, Australia

[c] Singapore Centre on Environmental Life Sciences Engineering, School of Biological Sciences, Nanyang Technological University, Singapore.

‡These authors contributed equally.

*Corresponding Author, E-mail: mkuhl@bio.ku.dk.

ABSTRACT

Seagrass communities provide important ecosystems services in coastal environments but are threatened by anthropogenic impacts. Especially the ability of seagrasses to aerate their below-ground tissue and immediate rhizosphere to prevent sulfide intrusion from the surrounding sediment is critical for their resilience to environmental disturbance. There is a need for chemical techniques that can map the O_2 distribution and dynamics in the seagrass rhizosphere upon environmental changes and thereby identify critical stress thresholds of e.g. water flow, turbidity and O_2 conditions in the water phase. In a novel experimental approach, we incorporated optical O_2 sensor nanoparticles into a transparent artificial sediment matrix consisting of pH-buffered deoxygenated sulfidic agar. Seagrass growth and photosynthesis was not inhibited in the experimental setup when the below-ground biomass was immobilized in the artificial sulfidic sediment with nanoparticles and showed root growth rates (~5 mm day^{-1}) and photosynthetic quantum yields (~0.7) comparable to healthy seagrasses in their natural habitat. We mapped the real-time below ground O_2 distribution and dynamics in the whole seagrass rhizosphere during experimental manipulation of light exposure and O_2 content in the overlaying water. Those manipulations showed that oxygen release from the belowground tissue is much higher in light as compared to darkness and that water column hypoxia leads to diminished oxygen levels around the rhizome/roots. Oxygen release was visualized and analyzed on a whole rhizosphere level, which is a substantial improvement to existing methods relying on point measurements with O_2 microsensors or partial mapping of the rhizosphere in close contact with a planar O_2 optode. The combined use of optical nanoparticle-based sensors with artificial sediments enables imaging of chemical microenvironments in the rhizosphere of aquatic plants at high spatio-temporal resolution with a relatively simple experimental setup and thus represents a significant methodological advancement for studies of environmental impacts on aquatic plant ecophysiology.

INTRODUCTION

Seagrasses are marine flowering plants that provide a range of essential eco-engineering services, such as facilitating carbon sequestration, improving water clarity and protecting coastal areas against erosion (Orth et al. 2006). Despite being considered as a high-value ecosystem, providing nursery areas and feeding grounds to numerous important commercial marine fish and crustacean species, seagrass meadows are currently declining with alarming rate mainly due to human activity (Larkum et al. 2006; Waycott et al. 2009). Seagrass plants mostly inhabit shallow coastal sediments, where they form an important coastal ecosystem with high productivity and biodiversity (Larkum et al. 2006; Orth et al. 2006). However, the below-ground biomass of seagrasses is anchored and grows in organic rich, reduced and often sulphidic sediments, which present a challenge to the plants and can potentially be involved in die-off events (Holmer & Bondgaard, 2001; Holmer et al. 2005). Sulfide, and especially dissolved H_2S is highly toxic for seagrasses (Pérez-Pérez et al. 2012; Lamers et al. 2013) that have developed a variety of structural defense mechanisms such as the presence of an intracellular gas-filled lacunar system (aerenchyma) enabling rapid and low-resistance exchange of gasses between the above- and below-ground tissue and rhizosphere (Borum et al. 2006). However our understanding of the function of this system and its role for the survival of seagrasses under environmental stress is still incomplete. The chemical microenvironment in the seagrass rhizosphere exhibits a high spatio-temporal heterogeneity that remains to be studied in detail. Especially the O_2 dynamics in the rhizosphere is of importance as radial O_2 loss from the below-ground biomass can act as a microshield against toxic H_2S from the surrounding sediment (Connell et al. 1999; Jensen et al. 2005; Brodersen et al. 2015). Inadequate O_2 transport from seagrass leaves to the below-ground tissue is regarded a key mechanism in seagrass die-off events (Pedersen et al. 2005; Borum et al. 2005) upon anthropogenic impacts such as dredging and eutrophication affecting the transparency and/or O_2 level in the overlaying water (Erftemeijer & Lewis, 2006).

It has recently been shown that O_2 released from the meristematic region of the rhizome of the seagrass species *Zostera muelleri* subsp. *capricorni* alters the local below-ground chemical microenvironment by chemically re-oxidizing H_2S and thereby detoxifying the surrounding sediment (Brodersen et al. 2015). This chemical defense mechanism is highly affected by hypoxic water-column conditions during darkness, as the oxidation capacity of

the below-ground tissue of seagrasses is completely dependent on the passive diffusion of O_2 from the surrounding water-column, across diffusive boundary layers and into the aerenchyma when no O_2 is evolved via photosynthesis (Pedersen et al. 2004; Borum et al. 2005; Brodersen et al. 2015).

Most studies of the O_2 dynamics in the seagrass rhizosphere have used electrochemical or optical microsensors (Pedersen et al. 1998; Connell et al. 1999; Jensen et al. 2005; Brodersen et al. 2015) that enable measurements with a very high spatio-temporal resolution but only at a limited set of measuring points. Therefore studying different regions of the rhizome is very tedious and it is impossible to account for the complete O_2 distribution around the below-ground biomass. There is thus a need for techniques that can map the heterogeneous O_2 microdistribution and dynamics around the rhizome and roots of seagrasses over larger spatial scales.

Imaging of chemical parameters using planar optical sensor foils, i.e., planar optodes, is a powerful alternative to microsensor measurements (Schäferling, 2012). While planar optodes are excellent tools for visualizing dynamic processes in sediments (Glud et al. 2001; Polerecky et al. 2006; Kühl & Polerecky, 2008), this approach is not as straight forward for investigations of the rhizosphere, where a good contact between the sensor foil and the plant tissue is needed. Achieving such a good contact is not easy and obviously only possible for selected parts of the roots at once (Frederiksen & Glud, 2006; Jovanovic et al. 2015). Depending on the root geometry and the planar sensor layer thickness, diffusive smearing of the true O_2 distribution can also be induced due to the presence of the O_2-impermeable sensor foil up against the biomass (Meysman et al. 2010).

In the present study we used O_2 sensitive optical nanosensors (Borisov et al. 2009) in combination with an artificial, semi-transparent sulphidic sediment matrix to simultaneously map the O_2 dynamics in the whole rhizosphere of the seagrass *Zostera muelleri*. We present the new methodology and show its application for mapping responses in the rhizosphere O_2 microenvironment due to changes in irradiance and O_2 content in the overlaying water.

MATERIALS AND METHODS

Materials for the nanosensors:

Platinum(II) meso(2,3,4,5,6-pentafluoro)phenyl porphyrin (PtTFPP) was bought from Frontier Scientific (www.frontiersci.com), Macrolex® fluorescence yellow 10GN (MY) was obtained from Kremer Pigments (http://kremerpigments.com). The styrene maleic anhydride copolymer (PSMA with 8% MA, Mw: 250000 $g*mol^{-1}$) XIRAN® was generously provided by Polyscope (http://www.polyscope.eu). Tetrahydrofuran (THF) was obtained by Sigma-Aldrich.

Materials for the transparent, artificial sediment:

Agar powder for microbiology (gel point ~35°C; gel strength >300 g cm^{-2}), HEPES buffer (N-(2-Hydroxyethyl)piperazine-N'-(2-ethanesulfonic acid; pKa (at 25°C) = 7.48; useful pH range=6.8-8.2) and sodium sulfide nonahydrate (Na_2S*9H_2O) were purchased from Sigma-Aldrich (www.sigmaaldrich.com).

Nanosensor preparation:

The sensor nanoparticles were prepared according to the previously described method by Mistlberger et al. (2010). Briefly, 200 mg of PSMA, 3 mg of MY (reference dye) and 3 mg of PtTFPP (O_2 indicator) were dissolved in 20 g of THF. This mixture was quickly poured into 200 ml of vigorously stirred distilled water. After evaporating the THF under an air stream, the particle suspension was concentrated at elevated temperature (60°C) until a concentration of 5 mg per ml was reached. The concentration was checked by drying and subsequent weighing of 1 ml of the particle suspension. The obtained particles have a size of several hundred nm and a strongly negative zeta potential of around -30 mV as shown elsewhere (Mistlberger et al. 2010). The particle suspension could be stored over several weeks without any signs of sedimentation, color change or change in the calibration characteristics.

Seagrass Collection:

Seagrass specimens of *Zostera muelleri subsp. capricorni* (Asch.) S.W.L.Jacobs were collected from a shallow (<1 m deep) coastal site at Brisbane Waters, NSW, Australia. The plants were transported (in water from the sampling site) to a greenhouse facility at the University of

Technology Sydney, where they were kept under natural light at a salinity of ~34 ppt and a temperature of ~22°C. Prior to the experiments, specimens were gently washed free of any adhering sediment particles before transferring them to the experimental chamber.

Experimental setup

The experimental chamber (inner dimensions 10x130x120 mm) consisted of a custom-made narrow, transparent acrylic chamber with a removable front window made of polycarbonate for ease of access when casting the sediment and improved optical properties during imaging, respectively (See Fig. 3.1 and supplementary video). Illumination of the plant leaves was provided by a tungsten halogen lamp equipped with a collimating lens (KL-2500, Schott GmbH, Germany). Stirring and aeration of the water-column was obtained via a submerged Pasteur pipette connected to an air pump or a gas mixer (Sensorsense, The Netherlands).

Preparation of the Artificial Sediment

The transparent, artificial sediment consisted of a de-oxygenated ~0.5% (w/w) agar-seawater solution (100 mL), buffered with HEPES (final concentration of 10 mM), amended with O_2-sensitive nanoparticles (2% w/w) and Na_2S to a final H_2S concentration of 250 µM (at pH 7). Prior to casting the sediment, the agar powder had been pre-washed over night in cold seawater to improve clarity. The reduced, artificial sediment was thus constructed to mimic chemical settings in natural sediment while allowing for direct visual investigation of the below-ground tissue during measurements.

The sensor nanoparticles were added to the heated artificial sediment mixture during the preparation. Oxygen sensor nanoparticles could be homogeneously incorporated into the artificial sediment matrix with no visible formation of larger sensor particle aggregates in the agar. To ensure this, the timing of the nanoparticle addition to the agar is important and this should be done shortly before the artificial sediment is poured into the chamber (i.e., at ~38°C). The concentration of nanoparticles in the agar ensured a good measuring signal, while preserving a good visual transparency. To further avoid potential limitations of transparency, we placed the seagrass rhizome close to (without touching) the polycarbonate plate of the experimental chamber when pouring the agar with nanoparticles (at an agar matrix temperature of ~ 36°C that rapidly cooled to room temperature upon contact with

the experimental chamber). The chamber could then be sealed and positioned in front of the imaging system. Gas supply from a gas mixer was ensured and a fiber-optic optode (Pyro-Science GmbH, Germany) was introduced to continuously monitor the O_2 concentration in the water column. The leaf canopy was kept in the upper stirred water-phase. A schematic of the setup can be seen in Fig. 3.1. A detailed video documentation of these preparation steps can be found in the supplemental information.

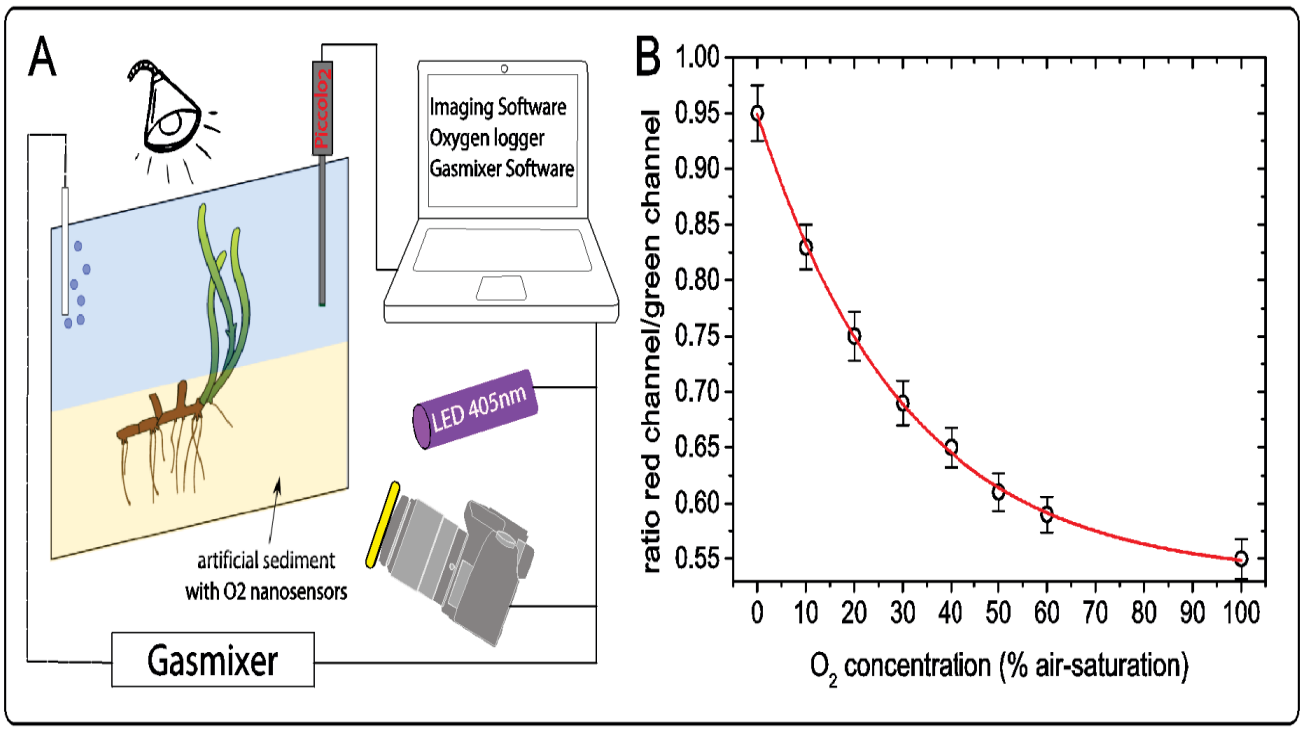

Figure 3.1: A: Experimental setup. The below-ground tissue of the seagrass is embedded in the artificial sediment containing the O_2 sensitive nanoparticles. A SLR camera and LED are mounted perpendicular to the transparent chamber wall. Gas supply and reference optode are immersed in the overlaying water. B: Calibration curve of the sensor nanoparticles in the artificial sediment. Symbols and error bars represent means ± SD (n=3). The red curve shows a fit of an exponential decay function to the calibration data (R^2>0.999).

Imaging setup:

We used a ratiometric RGB camera setup for O_2 imaging (Larsen et al. 2011). The system consisted of a SLR camera (EOS 1000D, Canon, Japan) combined with a macro objective (Macro 100 f2,8 D, Tokina, Japan) equipped with a 455 nm long pass filter (Uqgoptics.com). Excitation of sensor particles was achieved with a 405nm multichip LED equipped with a bandpass filter (NT43-156, Edmundoptics.com). The LED was powered by a USB-controlled

LED driver unit for fluorescence imaging applications (available from http://imaging.fish-n-chips.de). Image acquisition control of the SLR and LED were done with the software look@RGB (http://imaging.fish-n-chips.de).

Image analysis and calibration:

Acquired images were split into red, green, and blue channels and analyzed using the freely available software ImageJ (http://rsbweb.nih.gov/ij/). In order to obtain O_2 concentration images the following steps were performed: First the red channel (O_2 sensitive emission of PtTFPP) and green channel (emission of the reference dye MY) images were divided using the ImageJ plugin Ratio Plus (http://rsb.info.nih.gov/ij/plugins/ratio-plus.html). Afterwards, the obtained ratio-image was fitted with the previously obtained calibration curve using the Curve Fitting tool of ImageJ (exponential decay). The calibration curve was generated to follows. A small piece of nanosensor-containing non-sulfidic agar was immobilized in the chamber. Oxygen levels of the water on top of the agar were altered with the help of compressed air and nitrogen, which were mixed by a PC- controlled gas mixer (SensorSense, The Netherlands). Simultaneously, the O_2 level in the water column was monitored by means of a calibrated O_2 optode system (Oxygen dipping probe connected to Piccolo2 meter; PyroScience GmbH, Aachen, Germany). To ensure that equilibrium was reached, each calibration step was held for 60 min. The calibration was obtained by linking the measured image ratios to the measured O_2 level (Fig. 3.1). A visualization of the calibration process can be found in the supporting information.

Seagrass photosynthetic performance:

We assessed the photosynthetic competence of various parts of the seagrasses using a fiber-optic pulse amplitude modulated (PAM) fluorometer (PocketPAM, Walz GmbH, Germany) measuring the quantum yield of the PSII photosynthetic electron transport in the dark adapted state (F_v/F_m=the maximal quantum yield) and in the presence of actinic light (YII=the effective quantum yield) (Ralph & Short, 2002).

Experimental treatments:

We monitored the O_2 distribution around the seagrass roots under 2 experimental manipulations:

i) During a light-dark transition, where the plant leaves were first illuminated with an incident photon irradiance of ~500 µmol photons m^{-2} s^{-1} for 90 min to ensure that equilibrium conditions were reached in the light. Thereafter, the external illumination was switched off and the plant was left in the dark for 3 hours. During the dark incubation, the image acquisition could be automated, while measurements in light required switching the external light source off for a brief period just before and during image acquisition.

ii) During decreasing O_2 contents in the water-column, from 100% air saturation down to ~0% air saturation. The plant was first kept at an irradiance of ~500 µmol photons m^{-2} s^{-1} for 90 min in air saturated water to ensure that equilibrium conditions was reached. Then the external illumination was switched off and the overlaying water was flushed with N_2 gas for 2.5 hours to simulate water column hypoxia. Finally the water-column was again bubbled with air and the plant was still kept in the dark for another 4.5 hours. The O_2 concentration in the water-column was monitored simultaneously by the above-mentioned fiber-optic O_2 optode. Image acquisition was performed as described above.

RESULTS AND DISCUSSION

Introduction of optical sensor nanoparticles into the artificial sediment did not affect the sensor performance. The calibration curve of the agar-immobilized O_2 nanoparticles showed the expected exponential decay typical for optical O_2 sensors based on luminescence quenching (Meier et al. 2013) (Fig. 3.1).

Obviously, it is important to assess potential effects of the artificial sediment with nanosensors on the seagrass health. In this study, we evaluated two plants of the species *Z. muelleri*. Both plant specimens tolerated the artificial sediment with nanoparticles well and new root growth (at a rate of ~5 mm d^{-1}) was actually observed in both plants after a few days. Good plant health was also confirmed by measurements of photosynthetic performance of the two plants (Table 3.1). PAM fluorometry measurements in both plants revealed a high quantum efficiency of photosynthesis in the leaf canopy (shoot 1); i.e., maximum and effective quantum yields of PSII ~0.7 and ~0.6 (at a light intensity of 500 µmol photons m^{-2} s^{-1}), respectively. As seagrasses are considered healthy when maximum PSII

quantum yields of the shoot are around 0.7 (Macinnis-Ng & Ralph, 2003), we concluded that the two studied plants cultivated in the artificial sediment were healthy. Besides the shoot, the photosynthetic performance of the prophyllum, i.e., single leaves originating from the horizontal rhizome, was also evaluated. Whereas plant 1 had photosynthetically active prophyllums, albeit with a lower photosynthetic quantum efficiency than the fresh leaves, plant 2's prophyllums showed no photosynthetic activity (Table 3.1); these observations were also supported by the respective images of O_2 concentration around these structures (see Fig. 3.2). The presence of photosynthetically active prophyllums was a surprising finding, as these older plant structures are typically considered inactive. A more detailed investigation of this finding was, however, beyond the scope of this study and will be examined in future work.

Table 3.1: Maximum (F_v/F_m) and effective (Y(II)) quantum yields of PSII-related photosynthestic electron transport in seagrass leaves of plants mounted in the experimental setup with artificial sediment + O_2 nanoparticles (mean ± SD; n = 4-6). (-) indicates no photosynthetic activity.

Plant 1	Shoot Nodium 1	Prophyllum Nodium 5	Prophyllum Nodium 8
Fv/Fm	0.74±0.01	0.61±0.02	0.59±0.02
Y(II)	0.60±0.01	0.48±0.02	0.39±0.01

Plant 2	Shoot Nodium 1	Prophyllum Nodium 2	Prophyllum Nodium 5
Fv/Fm	0.73±0.01	(-)	(-)
Y(II)	0.58±0.02	(-)	(-)

While the presented O_2 nansosensor methodology is not applicable to natural non-transparent sediments, it is well suited to investigate the below-ground chemical microenvironment of seagrasses embedded in artificial transparent sediment matrices that mimic key aspects of the sediment biogeochemistry such as high sulfide contents (Brodersen et al. 2015). With the experimental setup, both structural images of the two plants as well as images of O_2 concentration surrounding their below-ground biomass could be recorded (Fig. 3.2). Both images were taken after exposing the plants to an irradiance of 500 µmol photons m^{-2} s^{-1} for 90 minutes. The O_2 distribution in the belowground environment was evidently

very different between the two investigated specimens. In plant 1, photosynthetically active prophyllums (one marked as P in each picture) oxidized the sediment, while plant 2 mainly showed O_2 leakage around the nodiums (marked as N), the basal meristem (B) and at the root tips. One of the benefits of the method presented here is that aligned structural and chemical (O_2 concentration) images can easily be obtained. While the chamber is illuminated by an external light source a structural image can be taken and by switching off the external light source and triggering the LED illumination, a luminescence image can be acquired that leads to an O_2 concentration image. In this way the position of structural elements (e.g. roots, rhizome) can be precisely aligned with the chemical information. A slight drawback is that due to the emission filter in front of the SLR camera, the structural picture appears slightly yellow.

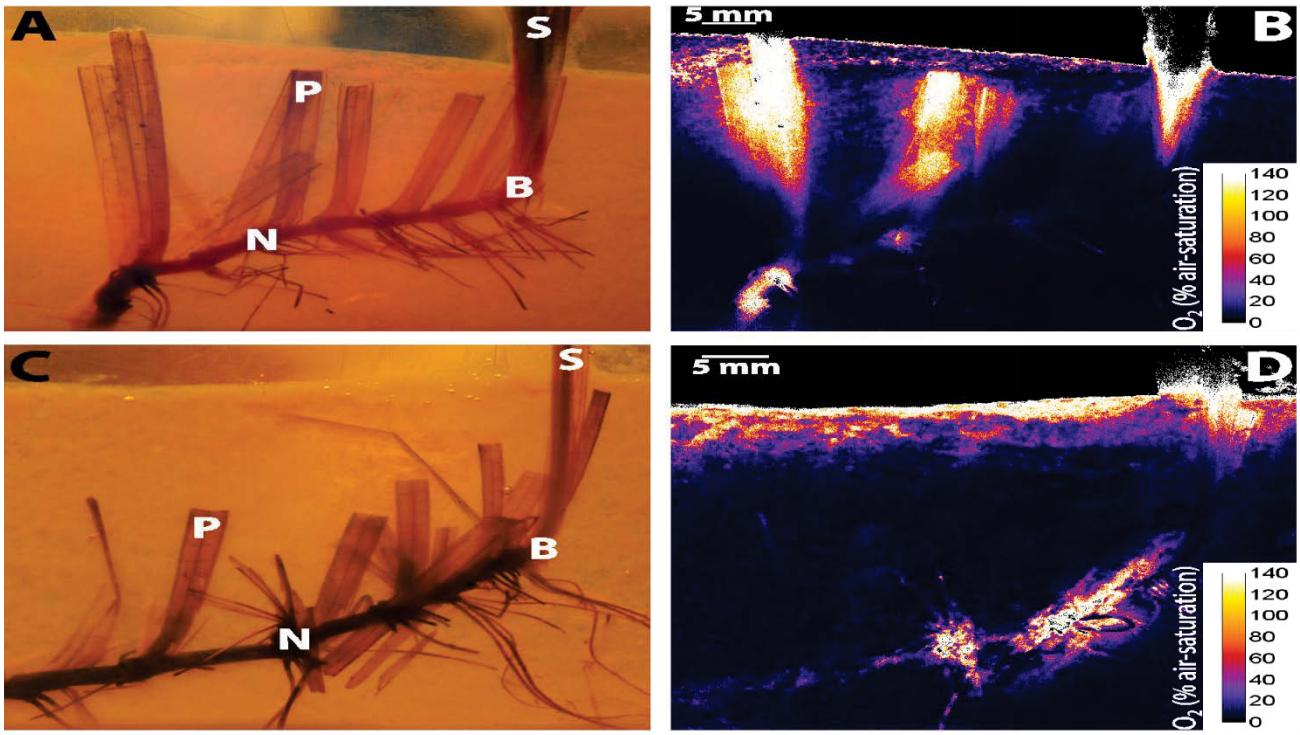

Figure 3.2: Structural images of the seagrass *Z. muelleri* mounted in the artificial sediment (A, C) and the respective false color images of the O_2 concentration distribution (B, D) around plant 1 (top) and plant 2 (bottom) recorded after 90 min illumination of the leaves with 500 µmol photons m^{-2} s^{-1}. Several plant structural elements are pointed out: S – shoot, N - nodium, P – prophyllum, B - basal meristem.

The O_2 imaging showed that it is possible to simultaneously map the O_2 distribution within the entire seagrass rhizosphere (Fig. 3.2, 3.3), and the method is well suited to observe changes in sediment oxygenation under different environmental conditions. Light exposure of the leaf canopy thus dramatically changed the O_2 status around the roots and rhizome (Fig. 3.3). Under high irradiance, seagrass leaf photosynthesis produced O_2 that was transported to the below-ground biomass of the plant, where it supported aerobic metabolism and leaked into the immediate rhizosphere leading to locally increasing O_2 levels during illumination (Fig. 3.3A, 3.3C; region of interest (ROI), 1-3). During illumination, leakage of O_2 was also observed at the node region (ROI 2) and the basal meristem (ROI 3). In contrast to the area on top of one of the prophyllums (ROI 1), this leakage did not originate from photosynthesis at the spot, but was due to diffusive transport through the aerenchyma.

In darkness, O_2 diffuses into the leaves from the surrounding water, across the diffusive boundary layer (DBL) and is then transported to the below-ground tissue. This caused less oxygenation of the rhizosphere, due to a relatively lower O_2 supply from the above-ground tissue and owing to O_2 consumption along the diffusive transport path (Fig. 3.3; ROI 1-3 and line profile). To visualize the changes between high light and dark conditions, we calculated an O_2 concentration difference picture by subtracting the dark O_2 image (time point 240 min) from the high light O_2 image (time point 90) (Fig. 3.3B). This showed that the O_2 production in the prophyllum had a high local impact, but clear differences were also evident at the root tips, close to the nodium and the basal meristem. Such O_2 leakage into the rhizosphere can protect the seagrass from H_2S intrusion through development of an oxic microshield around the below-ground tissue that prevents H_2S from reaching the tissue surface, via chemical oxidation with O_2 (i.e. $2O_2 + H_2S \rightarrow 2H^+ + SO_4^{2-}$) (Brodersen et al. 2015). Furthermore, the line profile in Fig. 3.3D showed significant O_2 leakage around the root tips. This leakage may have a particular important defense role for the plant as this may enable intermittent root growth through relatively oxidized microzones.

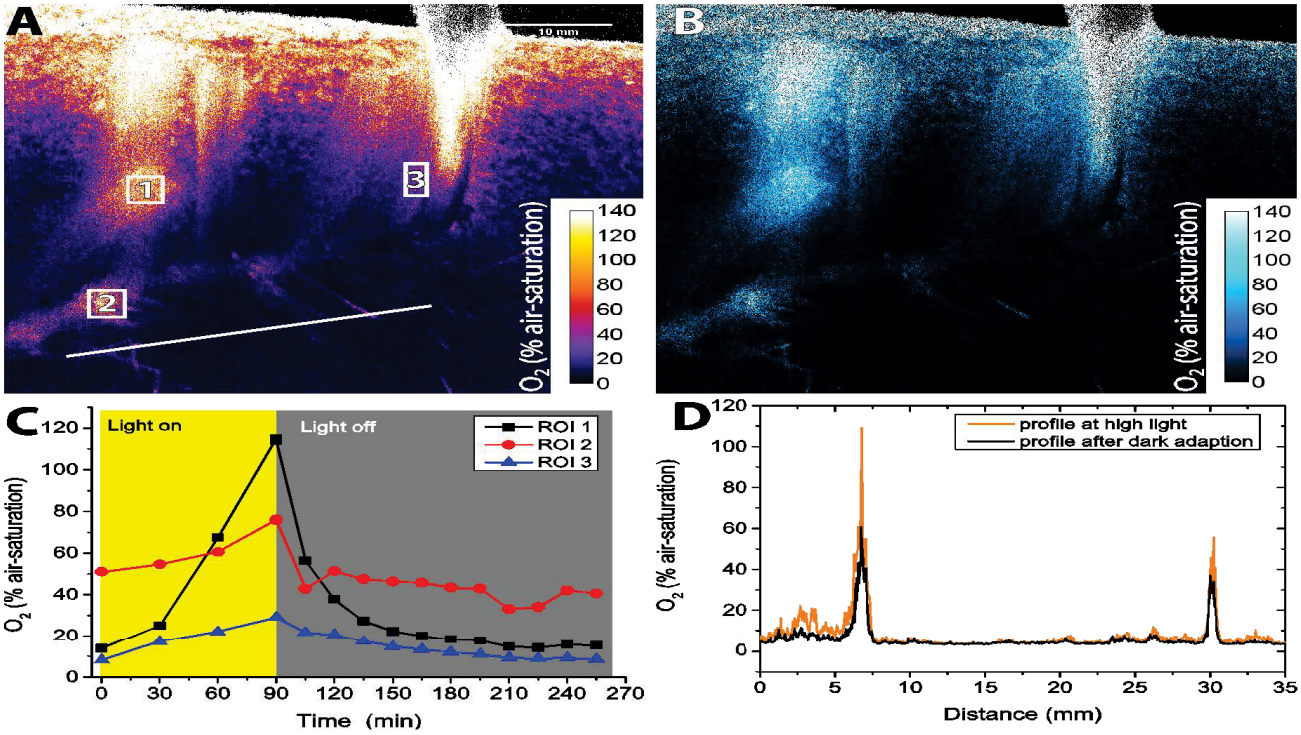

Figure 3.3: A: False color image of the O_2 concentration around the seagrass roots taken after 90 min illumination of the leaves with 500 µmol photons m^{-2} s^{-1}. B: An O_2 depletion image visualizing the change in O_2 concentration between the end of the light period (i.e. onset of darkening) and 130 min later. C: time profile of the 3 regions of interest (ROIs) over the light-dark exposure experiment. D: line profile (line shown in A) across some small roots at the time points 90 min and 240 min.

While light-dark shifts appear on a diel basis, other environmental changes such as O_2 depletion in the water column appear more rarely in the natural environment. Hypoxic water-column conditions may be caused by anthropogenic impacts such as eutrophication (e.g. due to land run-off and nutrient loadings) and/or by dredging operations in areas close to the seagrass meadows. During the latter, re-suspended anoxic sediment attenuates light and consumes O_2 in the water column leading to hypoxia (or even anoxia) (Erftemeijer & Lewis, 2006). This is especially critical for seagrasses during night-time, where photosynthetic O_2 supply in the leaves is absent. To investigate such effects, we monitored how defined changes in the O_2 content of the water column affected the rhizosphere O_2 microenvironment of the seagrass (Fig. 3.4). In 5 of the selected ROIs, O_2 was rapidly depleted in the seagrass rhizosphere under dark anoxic conditions in the overlaying water. After re-establishing full atmospheric saturation in the water column, O_2 diffusion from the

water column into above-ground tissue resulted in increased below-ground O_2 levels in the rhizosphere that approached steady state (Fig. 3.4; ROI 2, 3, 5 and 6). This was further confirmed by measuring line profiles of the O_2 concentration across some smaller roots (Fig. 3.4F). Notably, ROI 1 in Fig. 3.4 showed no increase in O_2 concentration indicating that the prophyllums were not supplied with O_2 via the aerenchyma. The presented experimental setup thus provides important information about the oxidation capability of the below-ground tissue of seagrasses under various environmental scenarios. Spatially explicit investigations are important, especially seen in the light of recent studies linking seagrass die-backs with hypoxic water-column conditions, leading to internal anoxia, and thereby making the plants more susceptible to sulfide intrusion (Pedersen et al. 2004; Borum et al. 2005; Brodersen et al. 2015).

In Fig. 3.4, ROI 4 was chosen to follow the O_2 dynamics in the artificial sediment in close proximity to the artificial sediment surface. This area showed efficient O_2 diffusion into the uppermost few mm's within the time frame of the experiments. The sulfide in the top layer of the artificial sediment thus gets depleted over time, when O_2 is present in the overlaying water and such depletion has to be considered as this limits the long-term applicability of the experimental setup. Possible ways to avoid such oxygenation over longer incubation times are presented elsewhere (Brodersen et al. 2014). The O_2 concentration difference images comparing high light and darkness (under water column anoxia) showed pronounced changes around the photosynthetic prophyllum (Fig 3.4B), while O_2 leakage was predominantly observed at the root tips and the nodiums when diffusion from the water column was the only supply mechanism (Fig. 3.4C).

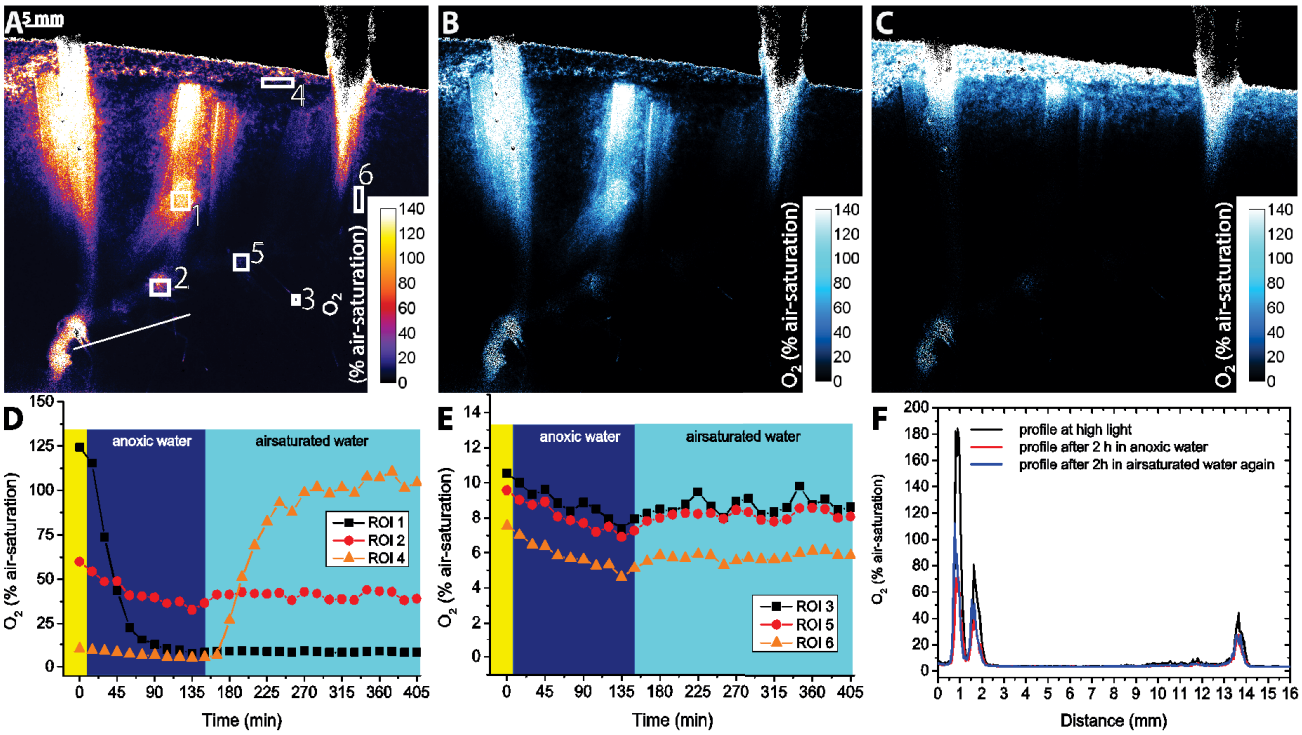

Figure 3.4: A: False color image of the O_2 concentration around the seagrass roots taken after 90 min illumination of the leaves at 500 µmol photons m^{-2} s^{-1}. Oxygen dynamics pictures visualizing the change in oxygenation between the time points 0 min (light) and 135 min (anoxic water) (B) and between the time points 135 min (anoxic water) and 405 min (airsaturated water) (C). D-E: time profile of the 6 ROIs. F: line profile across some small roots at the time points 0, 120 and 240 min.

While planar optrodes only generate luminescence images when the focal plane of the camera matches with the plane of the optrode, the method presented here enables imaging at different focal planes. As the entire artificial sediment is stained with optical sensor nanoparticles it is in principle possible to image at different focal planes. In the supplemental information O_2 distribution images at six different focal plains within the artificial sediment are shown. Only in one of the pictures is the rhizome in focus the others present focal planes in front and in the back of the rhizome. The further away from the actual roots the picture is taken the lower the O_2 concentration. This explains why close contact to the roots is required when working with planar optrodes. When the sensor film is further away from the roots only a blurry image can be observed.

In conclusion, the use of O_2 sensitive nanoparticles in artificial transparent sediment represents a powerful new tool to analyze the microenvironment of the below-ground

biomass of seagrasses and to quantify O_2 dynamics at high spatio-temporal resolution in the whole rhizosphere upon environmental changes. The possibility of mapping the whole below-ground O_2 distribution and dynamics in the seagrass rhizosphere enables identification of particular hot spots with different O_2 supply mechanisms. In contrast to microsensor measurements, this method can thus generate data for multiple parts of the plant simultaneously significantly accelerating studies of the chemical dynamics in the rhizosphere of aquatic plants. In future studies, O_2 mapping can be easily supplemented with detailed spot measurements with microsensors for O_2 and other chemical parameters such as pH and H_2S (Brodersen et al. 2014, 2015), where the selection of specific measuring sites can be guided by O_2 sensitive nanoparticle maps. The application of this new experimental approach is not limited to seagrasses and can easily be adapted to studies of other waterlogged plants and environments. For example, studies of O_2 dynamics in rice with the new approach presented here could easily be combined with other techniques for monitoring metal concentrations around the roots (Williams et al. 2014).

ACKNOWLEDGMENT

We thank Dr. Daniel A. Nielsen for help with the experimental setup and for fruitful discussions, Josua Hösch for help with video editing and Sabrina Kapus for providing the TOC picture. This study was funded by research grants from the Australian Research Council (MK), the Danish Council for Independent Research | Natural Sciences (MK), the Villum Foundation (MK, KK), the Augustinus Foundation (KEB) and PA Fiskers Fund (KEB).

AUTHOR INFORMATION

Corresponding Author

* E-mail: mkuhl@bio.ku.dk

Author Contributions

KK, KEB and MK designed the research. KK, KEB, MK and SLJ conducted experiments. KK, KEB and MK analyzed the data. KK wrote the manuscript with editorial help from KEB and MK. All authors have given approval to the final version of the manuscript.

‡These authors contributed equally.

ASSOCIATED CONTENT

Supplementary Information

Visualization of the image analysis and O_2 concentration images obtained in different focal planes; A detailed video documentation of the O_2 sensitive sediment preparation and mounting of seagrass in the experimental chamber.

REFERENCES

Borisov SM, Mayr T, Mistlberger G, Waich K, Koren K, Chojnacki P, Klimant I. (2009). Precipitation as a simple and versatile method for preparation of optical nanochemosensors. *Talanta*, **79**, 1322–1330.

Borum J, Pedersen O, Greve TM, Frankovich TA, Zieman JC, Fourqurean JW, Madden CJ. (2005). The potential role of plant oxygen and sulphide dynamics in die-off events of the tropical seagrass, *Thalassia testudinum*. *J. Ecol.*, **93**, 148–158.

Borum J, Sand-Jensen K, Binzer T, Pedersen O, Greve TM. (2006). Oxygen Movement in Seagrasses. In *Seagrasses: Biology, Ecology and Conservation*; Springer Netherlands: Dordrecht; pp. 255–270.

Brodersen KE, Nielsen DA, Ralph PJ, Kühl M. (2014). A split flow chamber with artificial sediment to examine the below-ground microenvironment of aquatic macrophytes. *Mar. Biol.*.

Brodersen KE, Nielsen DA, Ralph PJ, Kühl M. (2015). Oxic microshield and local pH enhancement protects *Zostera muelleri* from sediment derived hydrogen sulphide. *New Phytol.*, **205**, 1264–1276.

Connell EL, Colmer TD, Walker DI. (1999). Radial oxygen loss from intact roots of *Halophila ovalis* as a function of distance behind the root tip and shoot illumination. *Aquat. Bot.*, **63**, 219–228.

Erftemeijer PLA, Lewis RRR. (2006). Environmental impacts of dredging on seagrasses: a review. *Mar. Pollut. Bull.*, **52**, 1553–1572.

Frederiksen MS, Glud RN. (2006). Oxygen dynamics in the rhizosphere of *Zostera marina*: A two-dimensional planar optode study. *Limnol. Oceanogr.*, **51**, 1072–1083.

Glud RN, Tengberg A, Kühl M, Hall P, Klimant I, H. G. (2001). An in situ instrument for planar O 2 optode measurements at benthic interfaces. *Limnol. Oceanogr.*, **46**, 2073–2080.

Holmer M, Bondgaard EJ. (2001). Photosynthetic and growth response of eelgrass to low oxygen and high sulfide concentrations during hypoxic events. *Aquat. Bot.*, **70**, 29–38.

Holmer M, Frederiksen MS, Møllegaard H. (2005). Sulfur accumulation in eelgrass (*Zostera marina*) and effect of sulfur on eelgrass growth. *Aquat. Bot.*, **81**, 367–379.

Jensen S, Kühl M, Glud RN, Jørgensen L, Priemé A. (2005). Oxic microzones and radial oxygen loss from roots of *Zostera marina*. *Mar. Ecol. Prog. Ser.*, **293**, 49–58.

Jovanovic Z, Pedersen M, Larsen M, Kristensen E, Glud RN. (2015). Rhizosphere O2 dynamics in young *Zostera marina* and *Ruppia maritima*. *Mar. Ecol. Prog. Ser.*, **518**, 95–105.

Kühl M, Polerecky L. (2008). Functional and structural imaging of phototrophic microbial communities and symbioses. *Aquat. Microb. Ecol.*, **53**, 99–118.

Lamers LPM, Govers LL, Janssen ICJM, Geurts JJM, Van der Welle MEW, Van Katwijk MM, Van der Heide T, Roelofs JGM, Smolders AJP. (2013). Sulfide as a soil phytotoxin-a review. *Front. Plant Sci.*, **4**, 268.

Larkum AWD, Orth RJ, Duarte CM. (2006). *Seagrasses: biology, ecology and conservation*; Springer Netherlands: Dordrecht.

Larsen M, Borisov SM, Grunwald B, Klimant I, Glud RN. (2011). A simple and inexpensive high resolution color ratiometric planar optode imaging approach: application to oxygen and pH sensing. *Limnol. Oceanogr. Methods*, **9**, 348–360.

Macinnis-Ng CM, Ralph PJ. (2003). Short-term response and recovery of *Zostera capricorni* photosynthesis after herbicide exposure. *Aquat. Bot.*, **76**, 1–15.

Meier RJ, Fischer LH, Wolfbeis OS, Schäferling M. (2013). Referenced luminescent sensing and imaging with digital color cameras: A comparative study. *Sensors Actuators B Chem.*, **177**, 500–506.

Meysman FJR, Galaktionov OS, Glud RN, Middelburg JJ. (2010). Oxygen penetration around burrows and roots in aquatic sediments. *J. Mar. Res.*, **68**, 309–336.

Mistlberger G, Koren K, Scheucher E, Aigner D, Borisov SM, Zankel A, Pölt P, Klimant I. (2010). Multifunctional Magnetic Optical Sensor Particles with Tunable Sizes for Monitoring Metabolic Parameters and as a Basis for Nanotherapeutics. *Adv. Funct. Mater.*, **20**, 1842–1851.

Orth RJ, Carruthers T. I. M. J. B, Dennison WC, Duarte CM, James W, Jr, K. L. H, Hughes AR, Kendrick GA, Kenworthy WJ, Olyarnik S et al. (2006). A Global Crisis for Seagrass Ecosystems. *BiosSience*, **56**, 987–996.

Pedersen O, Binzer T, Borum J. (2004). Sulphide intrusion in eelgrass (*Zostera marina* L.). *Plant, Cell Environ.*, **27**, 595–602.

Pedersen O, Borum J, Duarte CM. (1998). Oxygen dynamics in the rhizosphere of *Cymodocea rotundata* . *Mar. Ecol. Prog. Ser.*, **169**, 283–288.

Pérez-Pérez ME, Lemaire SD, Crespo JL. (2012). Reactive oxygen species and autophagy in plants and algae. *Plant Physiol.*, **160**, 156–164.

Polerecky L, Volkenborn N, Stief P. (2006). High Temporal Resolution Oxygen Imaging in Bioirrigated Sediments. *Environ. Sci. Technol.*, **40**, 5763–5769.

Ralph PJ, Short FT. (2002). Impact of the wasting disease pathogen , *Labyrinthula zosterae* , on the photobiology of eelgrass *Zostera marina*. *Mar. Ecol. Prog. Ser.*, **226**, 265–271.

Schäferling M. (2012). The art of fluorescence imaging with chemical sensors. *Angew. Chem. Int. Ed. Engl.*, **51**, 3532–3554.

Waycott M, Duarte CM, Carruthers TJB, Orth RJ, Dennison WC, Olyarnik S, Calladine A, Fourqurean JW, Heck KL, Hughes AR et al. (2009). Accelerating loss of seagrasses across the globe threatens coastal ecosystems. *Proc. Natl. Acad. Sci. U. S. A.*, **106**, 12377–12381.

Williams PN, Santner J, Larsen M, Lehto NJ, Oburger E, Wenzel W, Glud RN, Davison W, Zhang H. (2014). Localized Flux Maxima of Arsenic, Lead, and Iron around Root Apices in Flooded Lowland Rice. *Environ. Sci. Technol.*, **48**, 8498–8506.

SUPPORTING INFORMATION

Optical sensor nanoparticles in artificial sediments – a new tool to visualize O_2 dynamics around the rhizome and roots of seagrasses

Klaus Koren[a‡*], Kasper E. Brodersen[b‡], Sofie L. Jakobsen[a], Michael Kühl[a,b,c*]

[a] Marine Biological Section, Department of Biology, University of Copenhagen, Helsingør, Denmark

[b] Plant Functional Biology and Climate Change Cluster, University of Technology Sydney, Australia

[c] Singapore Centre on Environmental Life Sciences Engineering, School of Biological Sciences, Nanyang Technological University, Singapore

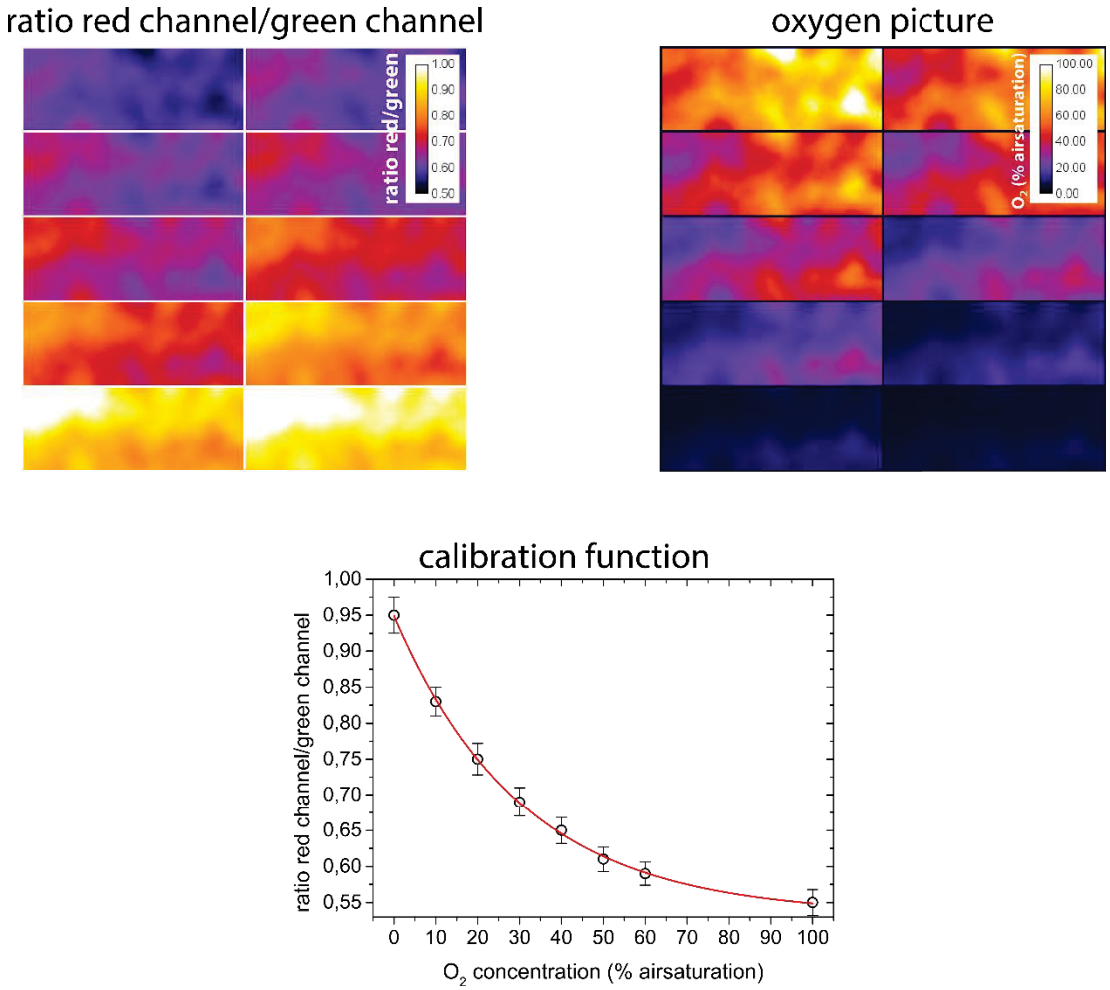

Figure S3.1: Visualization of the calibration process.

Acquired images were split into red, green, and blue channels and analyzed using the freely available software ImageJ (http://rsbweb.nih.gov/ij/). In order to obtain O_2 concentration images the following steps were performed: First the red channel (oxygen sensitive emission of PtTFPP) and green channel (emission of the reference dye MY) images were divided using the ImageJ plugin Ratio Plus (http://rsb.info.nih.gov/ij/plugins/ratio-plus.html). This gave pictures as shown in the top left. For the calibration the obtained pictures were correlated to the measured O_2 levels in the water column. There different regions were measured and used to generate the calibration plot. This calibration cure could then be used to transfer an ratio image to an O_2 image (top right)

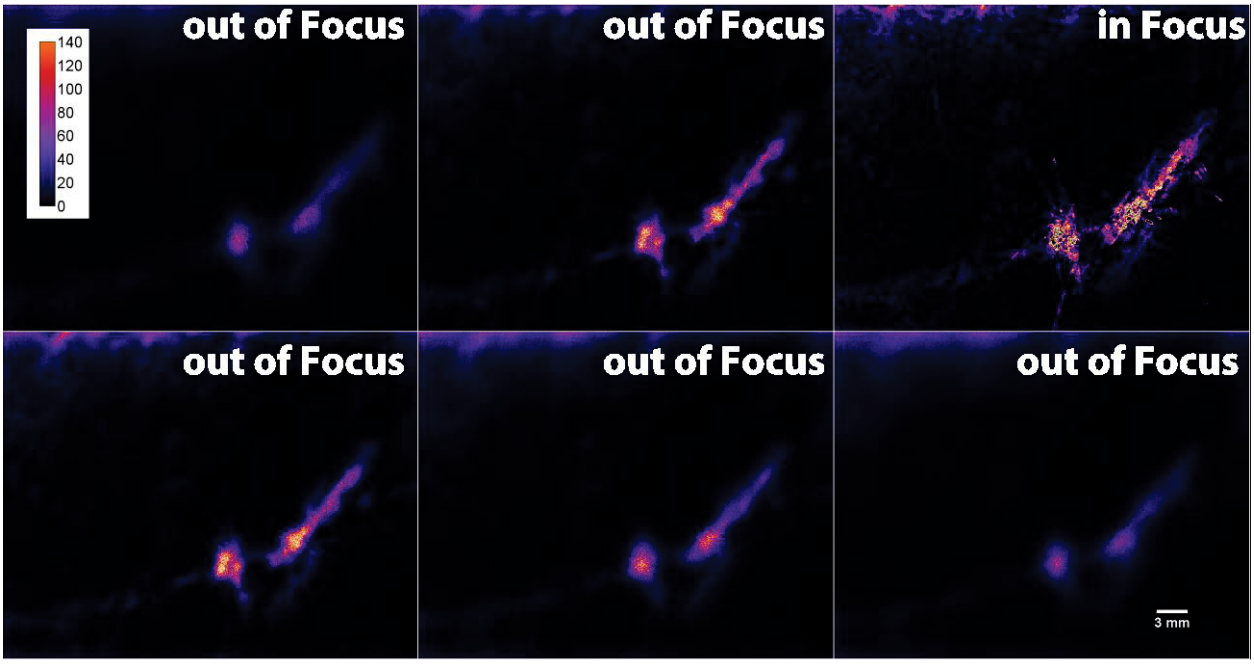

Figure S3.2: Oxygen pictures (scale in % air saturation) in focus and out of focus. It can be seen that in the focal plane of the rhizome the greatest level of detail can be obtained. Out of focus the picture gets blurry and only parts of the structures can be visualized.

For planar optrodes this can be a resolution limiting factor as close contact of the rhizome to the optrode is needed.

Chapter 4

Nanoparticle-based measurements of pH and O_2 dynamics in the rhizosphere of *Zostera marina* L.: Effects of temperature elevation and light-dark transitions

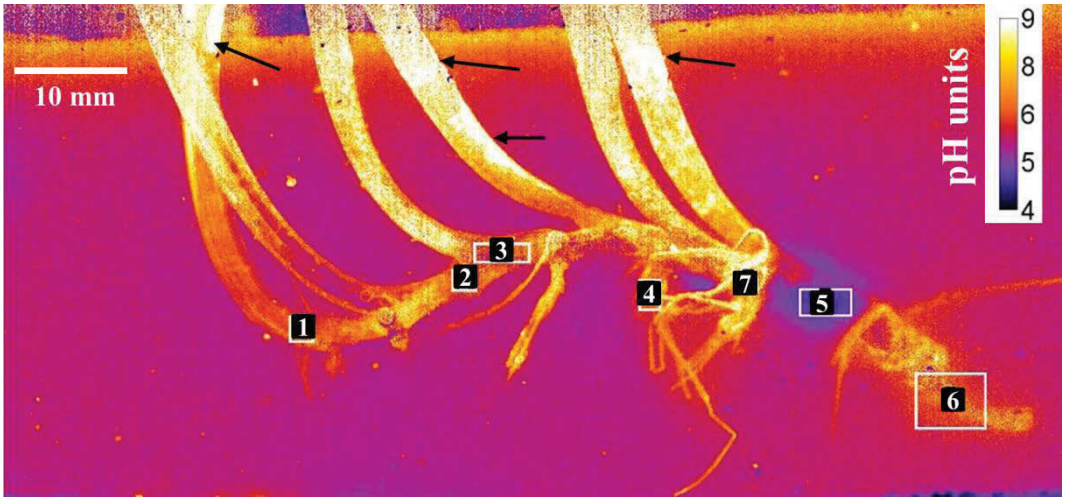

TOC figure. *pH heterogeneity in the seagrass rhizosphere as determined with novel optical sensor nanoparticles incorporated into reduced, artificial sediment.*

Citation: Brodersen KE, Koren K, Lichtenberg M. & Kühl M. (2016). Nanoparticle-based measurements of pH and O_2 dynamics in the rhizosphere of *Zostera marina* L.: Effects of temperature elevation and light-dark transitions. *Plant, Cell & Environment* (*In Press*). (Accepted on March 22, 2016)

Highlights: By means of novel optical nanoparticle-based O_2 and pH sensors, this chapter describes how seagrasses (*Zostera marina* L.) alter the biogeochemical conditions in their immediate rhizosphere through plant-derived changes in the rhizosphere pH microenvironment and via radial O_2 loss from the below-ground tissue. Local pH enhancements protect the plants from sediment-derived H_2S via chemical sulphide speciation shifts towards non-tissue-permeable HS^- ions, thereby further detoxifying the surrounding sediment. Plant-derived microniches of low-pH may lead to nutrient mobilization especially in carbonate-rich sediments. Moreover, this study gives novel insight into the microdynamics and heterogeneity of the rhizosphere pH microenvironment of seagrasses on a whole rhizosphere level (which is an improvement to existing methods such as via microsensors and planar optodes), and how the rhizosphere oxidation capacity of seagrasses changes during light/dark transitions and experimentally elevated temperatures.

Nanoparticle-based measurements of pH and O_2 dynamics in the rhizosphere of *Zostera marina* L.: Effects of temperature elevation and light-dark transitions

Kasper Elgetti Brodersen[1,a,b], Klaus Koren[2,a], Mads Lichtenberg[2], Michael Kühl[1,2,b]

[1]Plant Functional Biology and Climate Change Cluster, University of Technology, Sydney, 15 Broadway, Ultimo, Sydney, NSW 2007, Australia

[2]Marine Biological Section, Department of Biology, University of Copenhagen, Strandpromenaden 5, DK-3000 Helsingør, Denmark

[a] These authors contributed equally to this work.

[b] Corresponding authors, e-mail: mkuhl@bio.ku.dk and kasper.e.brodersen@student.uts.edu.au; phone: +45 4047 6304 and +61 414 954 017

ABSTRACT

Seagrasses can modulate the geochemical conditions in their immediate rhizosphere through the release of chemical compounds from their below-ground tissue. This is a vital chemical defence mechanism, whereby the plants detoxify the surrounding sediment.

Using novel nanoparticle-based optical O_2 and pH sensors incorporated in reduced and transparent artificial sediment, we investigated the spatio-temporal dynamics of pH and O_2 within the entire rhizosphere of *Zostera marina* L. during experimental manipulations of light and temperature. We combined such measurements with O_2 microsensor measurements of the photosynthetic productivity and respiration of seagrass leaves.

We found pronounced pH and O_2 microheterogeneity within the immediate rhizosphere of *Z. marina*, with higher below-ground tissue oxidation capability and rhizoplane pH levels during both light exposure of the leaf canopy and elevated temperature, where the temperature-mediated stimuli of biogeochemical processes seemed to predominate. Low rhizosphere pH microenvironments appeared to correlate with plant-derived oxic microzones stimulating local sulphide oxidation and thus driving local proton generation, although the rhizoplane pH levels generally where much higher than the bulk sediment pH.

Our data show that *Z. marina* can actively alter its rhizosphere pH microenvironment alleviating the local H_2S toxicity and enhancing nutrient availability in the adjacent sediment via geochemical speciation shift.

Keywords: microbial metabolism, nanoparticles, O_2, pH, plant-sediment interactions, seagrass, temperature elevation

INTRODUCTION

To accommodate growth in often highly reduced, sulphidic sediment environments, seagrasses possess aerenchymal tissue composed of a system of interconnected gas channels facilitating rapid transport of O_2 from the seagrass leaves to the below-ground tissue (Larkum et al. 1989; McComb et al. 1999). Aerenchymal O_2 supply supports aerobic metabolism at the root apical meristems, and also facilitates radial O_2 loss (ROL) to the immediate rhizosphere from the basal meristems with leaf sheath, rhizome and the root apical meristems (Pedersen et al. 1998 and 1999; Jensen et al. 2005; Frederiksen & Glud, 2006; Brodersen et al. 2014, 2015a; Koren et al. 2015). The below-ground ROL drives local chemical oxidation of the surrounding sediment in plant-derived oxic microniches, wherein new actively growing roots can form and reach maturity with protective barriers to ROL and sulphide intrusion (Barnabas, 1996; Enstone et al. 2003; Brodersen et al. 2014, 2015a). Most of these barriers to ROL are induced by anoxic, sulphidic conditions (Armstrong & Armstrong, 2001 and 2005) and inhibit gas-exchange over most of the root surface area ensuring an efficient internal gas transport to the apical parts of growing roots (Colmer, 2003).

Seagrasses can thus actively alter their rhizosphere microenvironment through the release of O_2 from their below-ground tissue, thereby enhancing the redox potential of the immediate rhizosphere and stimulating re-oxidation of sediment-produced reduced phytotoxins, such as H_2S (Lamers et al. 2013; Brodersen et al. 2014, 2015a). The oxidation capacity of the below-ground tissue is determined by numerous O_2 sources and sinks (Borum et al. 2006), where the most important regulating parameters include the O_2 conditions in the water column during night-time as the plants are completely dependent on passive diffusion of O_2 into their leaves when photosynthesis ceases (O_2 source) (Greve et al. 2003; Pedersen et al. 2004; Borum et al. 2005; Frederiksen & Glud, 2006; Brodersen et al. 2015a), the light availability and quality during day-time strongly regulating rates of shoot photosynthesis (O_2 source) (Brodersen et al. 2015a,b), ambient water temperature affecting plant and sediment respiratory needs and reaction kinetics (mainly regulating the O_2 sinks, but also affects rates of leaf photosynthesis) (Raun & Borum, 2013), as well as the thickness of the seagrass leaf diffusive boundary layer impeding gas and nutrient exchange with the

surrounding water-column and thereby the water flow (thus negatively affecting the O_2 source) (Binzer et al. 2005; Brodersen et al. 2015b).

Recently, Brodersen et al. (2015a) showed that the seagrass *Zostera muelleri* subsp. *capricorni* can modulate the pH microenvironment in its immediate rhizosphere, further alleviating the risk of H_2S intrusion through local sediment pH enhancements. This chemical defence mechanism, whereby pH enhancement changes the sulphide speciation in the rhizoplane towards non-permeable HS^- ions, is still poorly understood and there is therefore a need to elucidate the sediment pH microheterogeneity on a whole rhizosphere-scale.

Possible mechanisms behind such pH changes in the immediate rhizosphere are plant-derived allelochemicals. Rhizome/root exudation of organic carbon to the rhizosphere, as a result of internal carbon translocation, leads to enhanced bacterial productivity and growth in the seagrass rhizosphere (Moriarty et al. 1986). Rates of sulphate reduction have been coupled to plant photosynthesis and below-ground biomass (Pollard & Moriarty, 1991; Blaabjerg et al. 1998; Blaabjerg & Finster, 1998; Hansen et al. 2000; Nielsen et al. 2001) and young seagrass roots have also been found to stimulate the growth of *epsilon*- and *gamma-proteobacteria* that can utilize O_2 and nitrate as electron acceptors to re-oxidize sulphide (Jensen et al. 2007). Interestingly, the younger plant structures often leak O_2 from around the root-cap, where the presence of sulphide oxidizers overlaps with the plant-derived oxygenated microniches (Jensen et al. 2005; Frederiksen & Glud, 2006; Brodersen et al. 2014).

The root-shoot junctions (including the basal leaf meristem) and the root apical meristems (Moriarty et al. 1986) have been suggested as sites of exudation, with rhizome/root organic carbon exudation amounting up to 18% of the total carbon fixed by the seagrass host (Hansen et al. 2000). The highest sulphate reduction rates in the seagrass rhizosphere have correspondingly been observed at the seagrasses rhizomes and roots, where, for example, Pollard and Moriarty (1991) found 6 times higher sulphate reduction rates in seagrass-vegetated sediment as compared to non-vegetated areas. Sulphate reducing bacteria associated with the below-ground tissue of seagrasses show high O_2 tolerance (Blaabjerg & Finster, 1998), and several studies have shown that increasing temperature and light exposure of the seagrass leaf canopy has a pronounced positive impact on the rhizosphere

sulphate reduction rate (Isaksen & Jørgensen, 1994; Isaksen & Finster, 1996; Blaabjerg et al. 1998). Sulphate reduction can have a positive impact on the availability of phosphate in marine sediment owing to its reducing properties (Pollard & Moriarty, 1991), adding to the growing evidence of a specific relationship between the seagrass host and sulphate reducing bacteria based on a reciprocal exchange of nutrients (Moriarty et al. 1986; Blaabjerg et al. 1998; Hansen et al. 2000; Nielsen et al. 2001).

The consumption or production of protons as a result of microbial metabolisms and/or plant-derived allelochemicals plays an important role in the determination of sediment pH (Srinivasan & Mahadevan, 2010; Brodersen et al. 2015a). Such sediment pH alterations can influence the chemical speciation and availability of vital nutrients (e.g. ammonium and phosphate) at the plant/sediment interfaces (Pollard & Moriarty, 1991; Pagès et al. 2011, 2012; Brodersen et al. 2015a). Yet the understanding of rhizosphere pH dynamics in seagrasses is underexplored and data on pH microheterogeneity at plant/sediment interfaces are lacking.

In present study, we used novel O_2 and pH sensitive optical nanosensors incorporated in artificial, transparent sediment to investigate the pH and O_2 microdynamics in the rhizosphere of *Zostera marina* L. during light/dark transitions and temperature elevations. Our results provide new insights into the pH microheterogeneity and O_2 distribution in the *Zostera marina* L. rhizosphere during changing environmental conditions. We discuss how such pH and O_2 microgradients may alter the geochemical speciation of vital chemical species at plant/sediment- and oxic/anoxic interfaces.

MATERIALS AND METHODS

Seagrass sampling

Zostera marina L. specimens were collected in shallow waters (less than 2 m depth) near Rungsted Harbour, Denmark and were transported in seawater from the sampling site to the laboratory within 1h of sampling. The collected seagrass specimens were transplanted into sieved sediment from the sampling site to exclude burrowing animals from the holding tank. Specimens were held in a 30 L aquarium continuously flushed with aerated seawater (5 L h^{-1}; salinity of 34‰; temperature of ~12°C) under a 14:10 h light/dark cycle. Illumination with a photon irradiance (400-700 nm) of ~200 µmol photons m^{-2} s^{-1} was provided by a combination of fluorescent and halogen lamps. Prior to experiments, selected plants were gently washed free of any adhering sediment particles and rhizome ends were carefully sealed with petroleum jelly to avoid gas leakage from damaged older rhizome parts, before placement in the custom-made, narrow split flow chamber (described below; Fig. 4.1). Relative small *Z. marina* specimens were used owing to the chamber dimension restrictions.

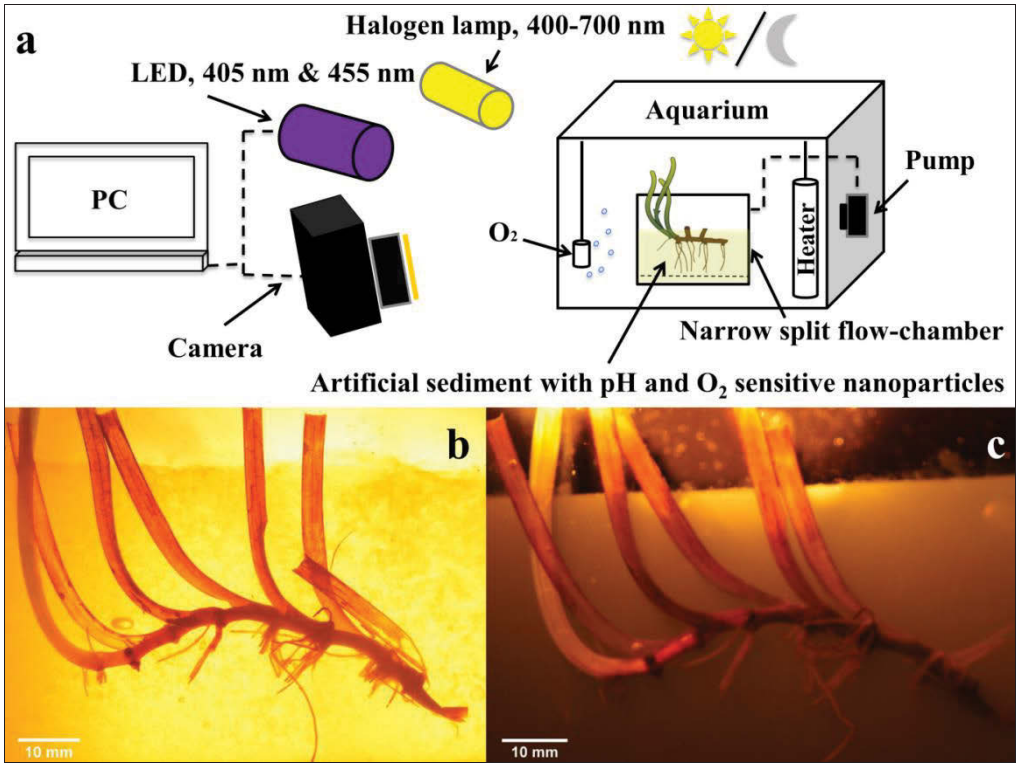

Figure 4.1. Schematic diagram of the experimental setup, showing the custom-made aquarium equipped with the narrow split flow-chamber and the ratiometric bio-imaging camera system (a). Image of the below-ground plant tissue structure during O_2 measurements (b). Image visualising the below-ground plant tissue structure during pH measurements (c). Note that the difference in brightness seen on the structural images (b, c) is due to the specific long pass filters used for luminescence imaging.

Experimental setup and artificial, transparent sediment

The applied experimental chamber consisted of a custom-made narrow, transparent acrylic split flow chamber attached to the side of a 30 L aquarium (inner dimensions 1×13×12 cm; Fig. 4.1). The split flow chamber was divided into an upper and lower compartment by means of an acrylic wall with numerous holes (inner diameter of ~1mm) and was equipped with a removable front window for ease of access when casting the sediment and positioning the seagrass. A seagrass specimen was positioned in the upper compartment with the above-ground tissue in the free-flowing seawater phase and the below-ground tissue embedded in reduced, artificial sediment (Fig. 4.1). The artificial, transparent sediment with embedded nanosensors was designed to mimic chemical settings in natural marine sediment (Brodersen et al. 2014), while enabling direct visual assessment of the

below-ground tissue during measurements (Fig. 4.1; further described in Koren et al. 2015). The transparent artificial sediment consisted of a deoxygenated ~0.5% (w/v) agar-seawater gel, buffered with HEPES (final concentration of 10 mM; pH ~7), amended with O_2 or pH sensitive nanoparticles (~3 and 7 % v/v, respectively) and Na_2S*9H_2O to a final H_2S concentration of 500 µM (at pH 7). The agar powder was pre-washed in continuously stirred cold seawater to improve clarity. The lower compartment of the split flow chamber contained a highly sulphidic (final H_2S concentration of 2500 µM) deoxygenated ~0.5% (w/v) agar-seawater solution buffered with HEPES (10 mM), ensuring a continuous supply of H_2S to the above artificial sediment with nanosensors during experiments, thereby maintaining a constantly high O_2 demand in the sediment (Brodersen et al. 2014, 2015a). After positioning of the plant and casting the sediments, the chamber was sealed and placed in front of the imaging system (described below).

Illumination of the leaf canopy was provided by a fibre-optic tungsten halogen lamp (KL-2500; Schott GmbH, Mainz, Germany) equipped with a collimating lens. The incident photon irradiance (PAR, 400-700 nm) at the level of the seagrass leaf canopy was measured with a calibrated irradiance sensor (Walz GmbH, Effeltrich, Germany) connected to a quantum irradiance meter (LI-250; LiCor, Lincon, NE, USA). A constant flow of seawater (salinity of 34‰) was maintained in the water-column of the upper flow chamber compartment via a connected pump submerged in an aerated and temperature-controlled seawater tank. The below-ground pH and O_2 microenvironment within the *Zostera marina* L. rhizosphere was investigated during light/dark transitions (incident photon irradiance of 500 µmol photons m^{-2} s^{-1}) and at two different experimental temperatures (~16 and 24°C). Plants were acclimatized to the experimental conditions for a minimum of 4h prior to start of measurements to ensure steady-state biogeochemical conditions in the rhizosphere (as confirmed from repetitive image recordings). Temperature changes were induced by slowly increasing the temperature of the seawater reservoir for ~3h until the desired temperature was reached and the plants were then allowed to acclimatize to the experimental temperature and irradiance for another 4h before image recordings commenced.

Optical nanoparticle-based sensors

The optical nanoparticle-based pH sensors were prepared based on a modified literature method (Xie et al. 2013; Wang et al. 2012). Briefly, 1 mg of perylene (Sigma-Aldrich), 1 mg of lipophilic indicator1-hydroxypyrene-3,6,8-tris-bis(2-ethylhexyl)sulfonamide (lipo-HPTS) (generously provided by Dr. Sergey Borisov TU Graz; Borisov et al. 2009) and 100 mg of the triblock copolymer Pluronic® F-127 (Sigma-Aldrich) were dissolved in 15 mL of tetrahydrofuran (THF). The mixture was poured into 100 mL of continuously stirred distilled water, the THF was evaporated under an air stream, and the particle suspension was concentrated to a final concentration of 5 mg mL^{-1} at 60 °C. The obtained pH sensor nano particles had an average size of <100nm as shown in the literature (Xie et al. 2013). The pH sensor nanoparticles were added to the pre-heated and previously deoxygenated artificial sediment in the last stage of the casting procedure, i.e., during cooling at ~38 °C to obtain a final concentration of ~7 % (v/v) in the agar matrix.

A detailed description of the optical nanoparticle-based pH sensors, including optical properties and calibration procedures is provided in the supporting information (Fig. S4.1-4.4 and S4.6; Notes S4.1).

Artificial sediment with optical O_2 sensor nanoparticles was prepared according to Koren *et al*. (2015). Briefly, 3 mg of platinum(II) meso-(2,3,4,5,6-pentafluoro)phenyl porphyrin (PtTFPP; indicator dye), 3 mg of Macrolex fluorescence yellow 10GN (MY; reference dye) and 200 mg of the styrene maleic anhydride copolymer (PSMA with 8% MA) XIRAN were dissolved in 20 g of Tetrahydrofuran (THF). This mixture was then poured into 200 mL of continuously stirred distilled water. THF was evaporated under an air stream, and the particle suspension was concentrated to a final concentration of 5 mg mL^{-1} at 60°C. The optical O_2 sensor nanoparticles were added to the pre-heated and previously deoxygenated artificial sediment in the last stage of the casting procedure at an agar temperature of ~38°C to obtain a final concentration of ~ 3% (v/v) in the agar matrix.

Calibration curves of the optical O_2 sensor nano particles at the two different experimental temperatures are provided in the supporting information (Fig. S4.5).

Imaging setup and data acquisition

A RGB camera setup (Larsen et al. 2011) was used for ratiometric pH and O_2 imaging (Fig. 4.1). The imaging system consisted of a SLR camera (EOS 1000D, Canon, Japan) mounted on a tripod and equipped with a macro objective lens (Macro 100 f2,8 D, Tokina, Japan) and a long pass filter (pH imaging, 455 nm; O_2 imaging, 530 nm; Uqgoptics.com). Excitation of the luminescent sensor nano particles was achieved by means of a multichip LED (LedEngin Inc, RS Components Ltd, Corby, UK) combined with a bandpass filter (pH imaging, 405 nm; O_2 imaging, 455 nm). The applied LEDs were powered by a USB-controlled LED driver unit designed for luminescence imaging applications (imaging.fish-n-chips.de). Data acquisition and control of the SLR exposure and LED light were achieved with a PC running custom software "look@RGB" (imaging.fish-n-chips.de).

Image calibration and analysis

The obtained SLR images were first split into red, green and blue channels and were then analysed via the Java-based image processing software ImageJ (rsbweb.nih.gov/ij/). In order to achieve images of pH and O_2 dependent ratios, raw images were divided using the ImageJ plugin Ratio Plus (rsb.info.nih.gov/ij/plugins/ratio-plus.html). For O_2 imaging, this implied dividing the red channel (emission of the O_2 sensitive dye) with the green channel (emission of the reference dye). For pH imaging, the red channel (indicator dye) was divided with the blue channel (reference dye). The obtained ratio images were fitted with previously obtained calibration curves (Fig. S4.4 and S4.5) using the Curve Fitting function in ImageJ, by means of linking the ratio images to the respective O_2 concentrations or pH units (see further details in Larsen et al. 2011; Koren et al. 2015).

Net photosynthesis and plant respiration rates

A seagrass leaf was positioned in a custom-made sample holder consisting of two 2 mm plexiglass plates to ensure a steady sample during microsensor measurements. Profiles were made through a hole in the plates (ø = 3 mm) towards the seagrass leaf surface. The

sample holder was positioned in a flow chamber (25×8×5 cm), which was connected to an aquarium pump ensuring a steady flow of ~3 cm s^{-1} of aerated seawater (salinity = 34) from a 25 L aquarium, wherein the temperature was kept constant at either ~16 or 24°C by a thermostate (F25-HD, Julabo GmbH, Germany). Light was provided with a fiber-optic tungsten halogen lamp (KL-2500 LCD, Schott GmbH, Germany) positioned at a 45° angle above the sample. The experimental photon irradiance (PAR) was 500 µmol photons m^{-2} s^{-1}, measured at the position of the sample, i.e., the leaf canopy, with a calibrated quantum irradiance meter (ULM-500, Walz GmbH, Germany) connected to an submersible spherical micro-quantum-sensor (US-SQS/L, Walz Gmbh, Germany).

Vertical profiles of O_2 concentration were measured in 50 µm increments from 0.5 mm above the leaf towards the tissue surface, using a Clark-type O_2 microsensor with a tip diameter of <25 µm (OX-25, Unisense, Denmark; Revsbech, 1989), with a fast response time (t_{90}<0.5 s) and a low stirring sensitivity (1-2%). The microsensor was mounted on a motorized micromanipulator (MU-1, PyroScience GmbH, Germany) and connected to a pA-meter (OXY-meter, Unisense, Denmark) that was interfaced to a PC via an A/D converter (DCR-16, PyroScience GmbH, Germany). Microsensor positioning and data acquisition were controlled by dedicated software (Profix, PyroScience GmbH, Germany).

Net photosynthesis and dark respiration rates were calculated from Fick's 1st law of diffusion:

$$J_{O_2} = -D_0 \frac{\partial C}{\partial z}$$

where D_0 is the salinity and temperature dependent diffusion coefficient of O_2 in seawater (www.unisense.com) and dC/dz is the linear concentration gradient of O_2 in the diffusive boundary layer.

RESULTS

Rates of photosynthesis and respiration

The net photosynthesis and respiration rates of *Zostera marina* L. at the two experimental temperatures were determined via O_2 concentration microprofiles measured towards the

leaf tissue surface (Fig. 4.2). Measurements revealed a 2.2 times higher net photosynthesis rate at 24°C as compared to 16°C, amounting to an increase in O_2 efflux from 0.117 to 0.252 nmol O_2 cm^{-2} s^{-1}; and a 1.4 times higher respiration rate at 24°C as compared to 16°C, which amounted to an increase in O_2 influx from -0.116 to -0.159 nmol O_2 cm^{-2} s^{-1}. The measured temperature-induced enhancement in the rate of net photosynthesis and respiration corresponded to Q_{10} temperature coefficients of 2.6 and 1.5, respectively.

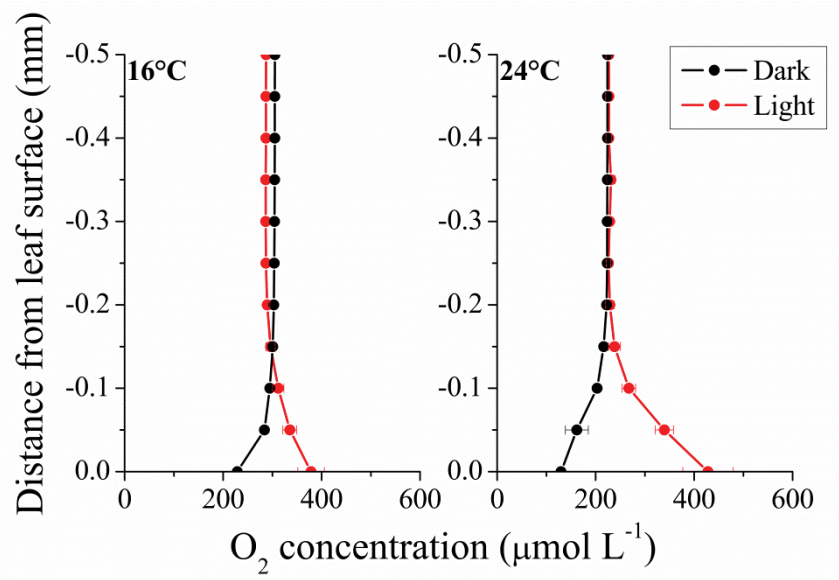

Figure 4.2. Vertical O_2 concentration microprofiles measured towards the leaf tissue surface of *Z. marina* during light-dark transitions (incident irradiance (PAR) of 500 µmol photons m^{-2} s^{-1}) at the two experimental temperatures (~16 and 24 °C). Y = 0 indicate the leaf tissue surface. Symbols with error bars represent the mean ±SD. n = 3; leaf level replicates.

O_2 distribution and microdynamics

The two-dimensional O_2 distribution in the *Z. marina* L. rhizosphere at 16 and 24°C during light-dark transitions is shown in Figure 4.3. The O_2 images showed an O_2 release, i.e., radial oxygen loss, especially from the root-shoot junctions (nodiums) and the rhizome, leading to several oxic microniches in the immediate rhizosphere of *Z. marina* L. The seagrass was able to maintain oxic conditions around the rhizome even without photosynthetic activity (Fig. 4.3).

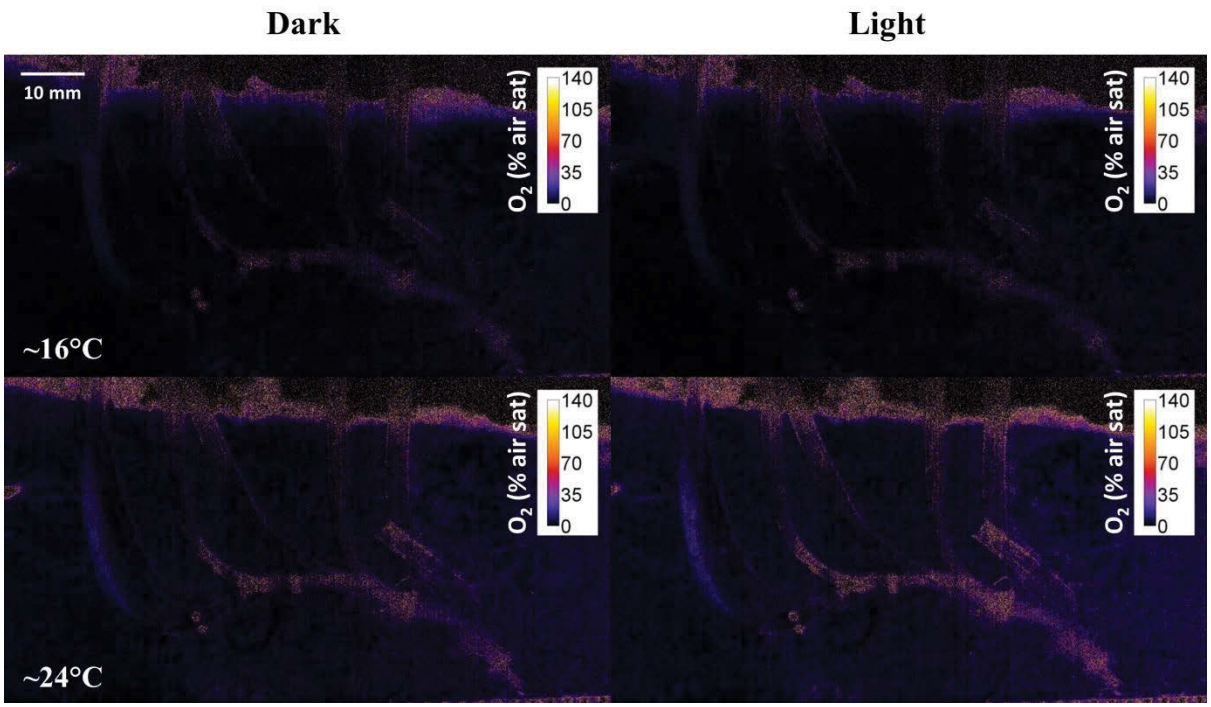

Figure 4.3. O_2 distribution and microdynamics within the rhizosphere of *Zostera marina* L. determined via optical nanoparticle-based O_2 sensors (O_2 colour coded image). The steady-state O_2 images were obtained at two different temperatures (16 and 24 °C) during light-dark transitions (photon irradiance (PAR) of 500 µmol photons m^{-2} s^{-1}). Legends depict the O_2 concentration in % air saturation. The presented images represent an average of 2 images.

The O_2 concentration images revealed a distinct increase in the belowground tissue oxidation capacity at 24°C as compared to 16°C; this temperature effect predominated over light stimulation of the plants photosystems (Fig. 4.3). The extent of oxygenated regions and the below-ground tissue surface O_2 concentration did only increase slightly during light exposure of the leaf canopy (incident irradiance of 500 µmol photons m^{-2} s^{-1}; Fig. 4.3). Some of the prophyllums (single leaves originating from the rhizome at the nodiums), as well as the leaf sheath at the base of the shoot also released O_2 to the rhizosphere. The maximal width of the oxic microniches around the rhizomes was ~5.0 mm at nodium 7 during light exposure at a temperature of 24°C, corresponding to an oxic microshield thickness of ~0.75 mm surrounding the respective root-shoot junction (data obtained by subtracting the diameter of the rhizome), which is similar to previous findings in natural sediment (e.g. Pedersen et al. 1998; Jensen et al. 2005). The O_2 concentrations determined within selected

regions of interest (ROIs) in the *Z. marina* rhizoplane confirmed these observations (Fig. 4.4; Table 4.1). Based on O_2 concentration measurements in ROI 1-7, we calculated a mean of a 1.1-fold increase in the oxidation capability of the belowground tissue as a result of the dark/light transitions as compared to a 1.3-fold increase in response to the 8°C temperature elevation. The highest rhizome surface O_2 levels were found at the root-shoot junctions (nodium 4, 5 and 7) corresponding to O_2 concentrations reaching up to 122 µmol L^{-1} (ROI 3, 4 and 5 in Fig. 4.4; Table 4.1). The O_2 imaging thus documented pronounced spatial microheterogeneity and high spatio-temporal microdynamics of the belowground oxic microzones around the rhizome of *Z. marina* that was modulated by changes in light and temperature.

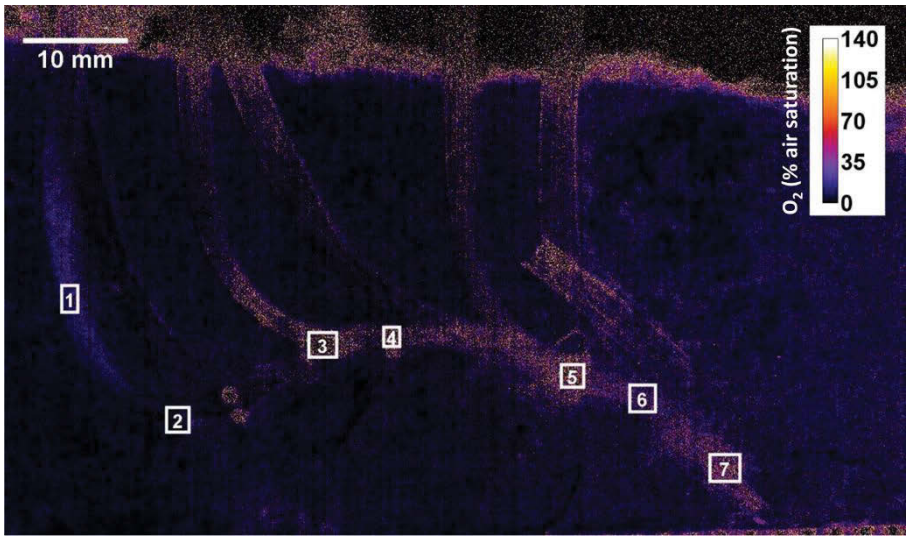

Figure 4.4. Selected regions of interest (ROI) within the immediate rhizosphere of *Zostera marina* L. used to determine the O_2 distribution during light/dark transitions (incident irradiance (PAR) of 500 µmol photons m^{-2} s^{-1}) at the experimental temperatures (~16 and 24 °C). Boxes and numbers indicate the measured ROI. Mean O_2 concentration values representing the entire ROI are presented in Table 4.1.

Table 4.1. O_2 concentrations at selected regions of interest (ROI) within the immediate rhizosphere of *Zostera marina* L. Boxes and numbers indicate the measured ROI. O_2 concentrations are given in both % air saturation and µmol L^{-1} at ~16 and 24 °C during light-dark transitions.

	~16°C				~24°C			
$[O_2]$	**Dark**		**Light**		**Dark**		**Light**	
	% air sat.	µmol L^{-1}	% air sat.	µmol L^{-1}	% air sat.	µmol L^{-1}	% air sat.	µmol L^{-1}
ROI 1	5.8	(14.6)	6.2	(15.4)	11.8	(25.5)	14.2	(30.6)
ROI 2	8.9	(22.3)	9.0	(22.5)	10.7	(23.1)	13.2	(28.6)
ROI 3	37.2	(93.2)	37.5	(94.0)	49.3	(106.6)	54.9	(118.6)
ROI 4	32.3	(81.0)	36.1	(90.6)	50.3	(108.7)	52.7	(113.9)
ROI 5	34.6	(86.7)	35.1	(88.0)	47.3	(102.3)	56.3	(121.8)
ROI 6	12.2	(30.6)	12.5	(31.3)	18.2	(39.3)	23.2	(50.3)
ROI 7	24.0	(60.2)	25.6	(64.3)	35.2	(76.0)	42.3	(91.5)

ROI 1 represents measurements at the non-illuminated part of the shoot; ROI 2 = at the root-shoot junction (nodium 2); ROI 3 = at the base of the prophyllum close to the root-shoot junction (nodium 4); ROI 4 = at the root-shoot junction (nodium 5); ROI 5 = at the root-shoot junction (nodium 7); ROI 6 = internode 7 with prophyllum; ROI 7 = at the rhizome-end.

pH heterogeneity and dynamics

We found a high degree of pH heterogeneity within the seagrass rhizosphere, with distinct microzones of very low pH (down to ~pH 4), as well as rhizome/rhizoplane pH levels well above the pH of the surrounding bulk sediment (up to pH > 8; Fig. 4.5).

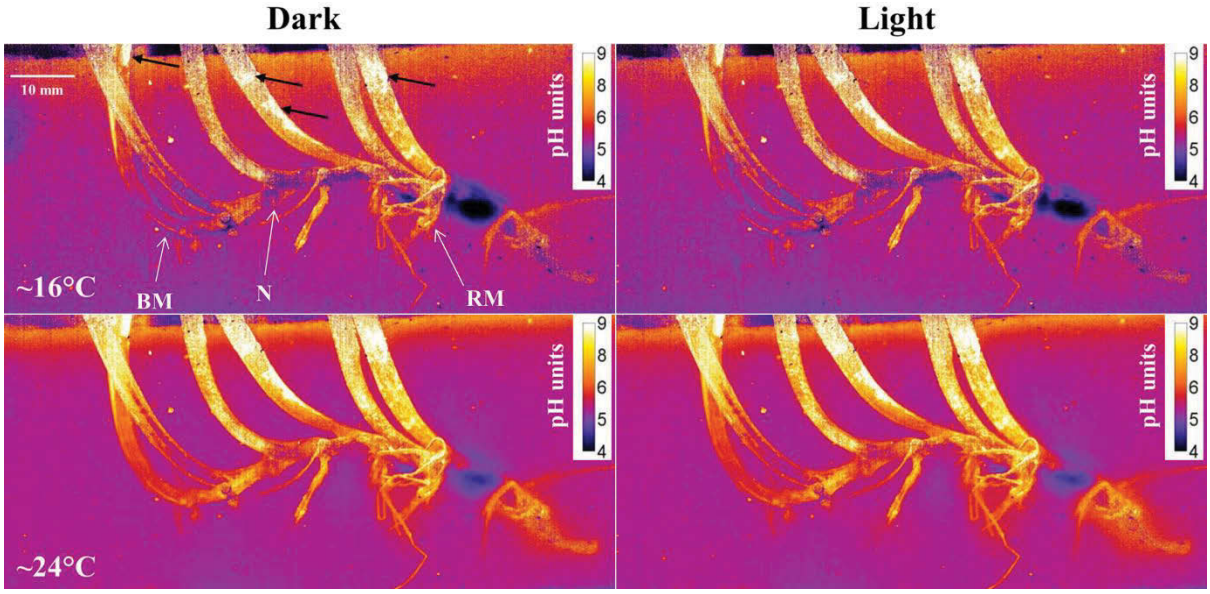

Figure 4.5. pH heterogeneity and microdynamics within the rhizosphere of *Zostera marina* L. determined via optical nanoparticle-based pH sensors (pH colour coded image). The steady-state pH images were obtained at two different temperatures (i.e. ~16 and 24 °C) during light-dark transitions (incident light intensity (PAR) of 500 µmol photons m^{-2} s^{-1}). Legends depict the pH value. BM indicates the basal leaf meristem; N indicates nodium 4; RM indicates the mature zone of roots in root-bundle 7. Images represent the average of 3 measurements. Note that white areas on leaves/prophyllums (marked with black arrows on the figure) should be interpreted with caution as some of these high pH microniches (pH of ≥9) seemed to be caused by epiphyte-derived red background luminescence (for further information see Notes S4.1; Figure S4.6).

Comparison of O_2 and pH images revealed that areas of low pH overlapped with oxic microniches in the seagrass rhizosphere, whereas the high pH levels predominantly were measured on the surface of the mature part of the roots, the prophyllums and at the end of the rhizome, although patchy distributions of relatively high pH levels (as compared to bulk sediment pH levels) were observed on the surface of the entire belowground tissue. Selected regions of interest (ROIs) within the immediate rhizosphere of *Z. marina* exhibited higher pH levels (ΔpH of 0.02 - 0.31) in the rhizoplane during light exposure of the leaf canopy as compared to dark conditions at both experimental temperatures (ROI 1-7; Fig. 4.6; Table 4.2). The light-driven pH microdynamics was surpassed by the effect of the 8°C temperature elevation showing much higher pH levels (ΔpH of 0.46 - 0.88) in the rhizoplane of *Zostera marina* L. at 24°C as compared to 16°C during both light exposure and darkness

(ROI 1-3 and 5-7; Fig. 4.6; Table 4.2). A distinct hotspot of low pH was measured in the region of nodium 7, internode 7 and nodium 8 with an up to 5.2 mm wide zone of pH <5. The lowest rhizosphere pH levels were measured within this distinct zone with pH levels reaching the lower detection limit (pH 4) of the pH indicator (Fig. 4.5 and 4.6). The region of the belowground tissue with the highest pH levels was also found adjacent to nodium 7, corresponding to ROI 7 in Figure 4.6 (Table 4.2).

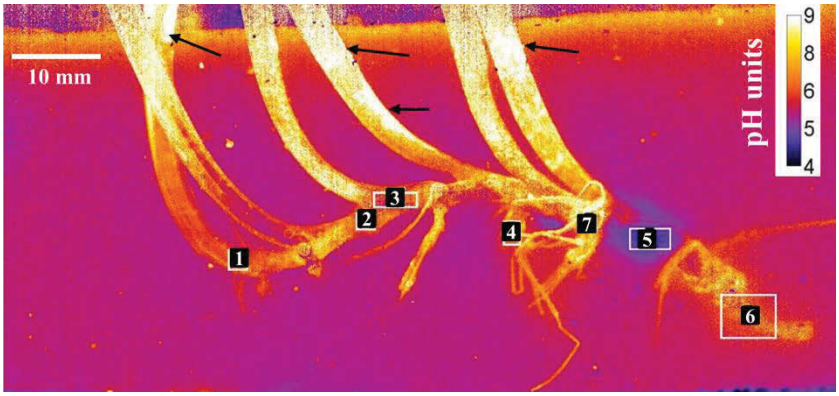

Figure 4.6. Selected regions of interest (ROI) within the immediate rhizosphere of *Zostera marina* L. used to determine the pH heterogeneity and dynamics during light-dark transitions (incident irradiance (PAR) of 500 µmol photons m^{-2} s^{-1}) at the two experimental temperatures (~16 and 24 °C). Boxes and numbers indicate the measured ROI. Mean pH values representing the entire ROI are presented in Table 4.2. Note that the white areas on leaves/prophyllums (marked with black arrows on the figure) should be interpreted with caution as some of these high pH microniches (pH of ≥9) seemed to be caused by epiphyte-derived red background luminescence (Notes S4.1; Figure S4.6).

Table 4.2. pH values in selected regions of interest (ROI) within the immediate rhizosphere of *Zostera marina* L. Values are given as a mean of the entire ROI ± S.E; and as the relative difference in pH between the experimentally changed environmental conditions (ΔpH). n = 5-18. The average pH of the bulk, artificial sediment at similar vertical depth as the below-ground biomass was ~ 5.7±0.0 (includes all treatments).

	16°C		24°C		16°C	24°C	dark	light
	dark	light	dark	light	dark/light	dark/light	16/24°C	16/24°C
	pH	pH	pH	pH	ΔpH	ΔpH	ΔpH	ΔpH
ROI 1	5.8±0.0	5.8±0.0	6.4±0.0	6.4±0.0	0.0	0.1	0.6	0.6
ROI 2	5.6±0.0	5.7±0.1	6.3±0.0	6.5±0.1	0.1	0.2	0.7	0.8
ROI 3	5.6±0.0	5.7±0.1	6.3±0.0	6.4±0.1	0.1	0.2	0.7	0.7
ROI 4	6.7±0.0	6.7±0.1	6.6±0.0	6.8±0.0	0.0	0.2	-0.1	0.1
ROI 5	3.9±0.0	4.2±0.1	4.8±0.0	4.9±0.0	0.3	0.1	0.9	0.7
ROI 6	5.9±0.0	6.0±0.1	6.3±0.0	6.6±0.1	0.1	0.3	0.5	0.7
ROI 7	6.6±0.1	6.9±0.2	7.1±0.0	7.4±0.1	0.2	0.2	0.5	0.5

ROI 1 represents measurements at the basal leaf meristem (nodium 1); ROI 2 = the root-shoot junction (nodium 4); ROI 3 = at the base of the prophyllum close to the root-shoot junction (nodium 4); ROI 4 = root-bundle at nodium 6; ROI 5 = internode 7 with prophyllum; ROI 6 = at the rhizome-end; ROI 7 = root-shoot junction (nodium 7).

pH microheterogeneity at interfaces

Extraction of cross-tissue pH values along line profiles in the pH images revealed pronounced pH microheterogeneity at interfaces (Fig. 4.7). The pH increased relative to the ambient sediment across internode 3 with the surrounding prophyllum, reaching pH levels of up to 8.3 on the rhizome surface and correlating with rapidly increasing pH levels at the rhizome/sediment interface (Fig. 4.7b; CTS 1). Interestingly, the cross tissue pH profile across internode 4 with prophyllum close to nodium 4 showed increasing pH levels at the approximate position of the oxic/anoxic interface with pH levels reaching up to 8.0 during light exposure of the leaf canopy (Fig. 4.7c; CTS2). This was contrary to the rhizome/sediment interface where decreasing pH levels down to 4.1 were observed on the rhizome surface (measured during light exposure at 16 °C), thus indicative of proton consuming and producing biogeochemical processes altering the geochemical microenvironment at this specific belowground oxic microniche (Fig. 4.7c; CTS2).

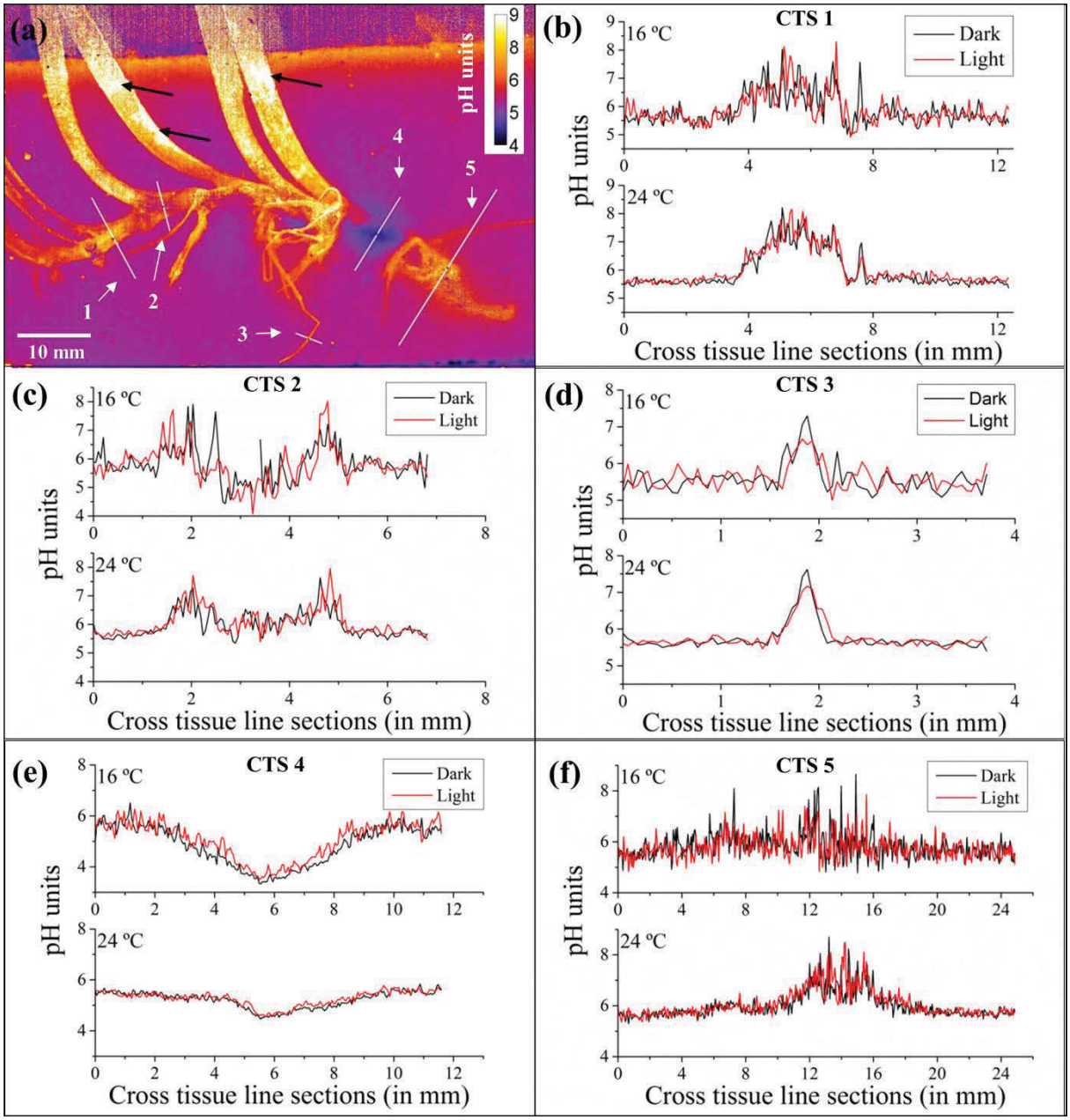

Figure 4.7. Cross tissue line sections (CTS) determining the pH microdynamics at the plant/rhizosphere interface and on the plant tissue surface. The steady-state cross tissue line sections were determined at the two experimental temperatures (i.e. ~16 and 24 °C) during light-dark transitions (under an incident photon irradiance (PAR) of 500 µmol photons m^{-2} s^{-1}). (a) Structural image of the seagrass *Z. marina* L. embedded in the artificial, transparent sediment with pH sensitive nanoparticles (pH colour coded image), illustrating the positions of the respective cross tissue line sections (CTS1-5). (b) Line microprofile across internode 3 with attached prophyllum (CTS1). (c) Line microprofile across internode 4 with prophyllum close to nodium 4 (CTS2). (d) Line microprofile across root from root-bundle 6 (CTS3). (e) Line microprofile across internode 7 with propyllum at the base of the prophyllum (CTS4). (f) Line microprofile across nodium 9 at the end of the rhizome with degraded prophyllum (CTS5). n = 3. Note that the white areas on leaves/prophyllums

(marked with black arrows on the figure) should be interpreted with caution, as some of these high pH microniches (pH of ≥9) seemed to be caused by epiphyte-derived red background luminescence (Notes S4.1; Figure S4.6).

A line microprofile across a root from root-bundle 6 showed similar microheterogeneity as found at internode 3, with increasing pH levels at the root/sediment interface, and root surface pH levels of up to 7.6 (Fig. 4.7d; CTS 3). Cross tissue microprofile 4 across internode 7 with prophyllum showed a pronounced decrease in pH at the approximate position of the oxic/anoxic interface with pH levels within the low pH hotspot approaching the lower detection limit of the pH indicator (Fig. 4.7e; CTS 4). Across nodium 9 at the end of the rhizome with a degraded prophyllum, pH increased at the approximate position of the rhizome up to pH 8.7 (Fig. 4.7f; CTS5). These observations were supported by vertical pH microprofiles measured from the seawater/sediment interface down to the bottom of the pH sensitive sediment (Fig. 4.8). A rapid decrease in pH was observed within the uppermost 5 mm as typically observed in natural marine sediments (Stahl et al. 2006; Zhu et al. 2006), with pH levels decreasing from about ~ 7 at the water/sediment interface down to pH ~6 at 5 mm depth where after it stabilised.

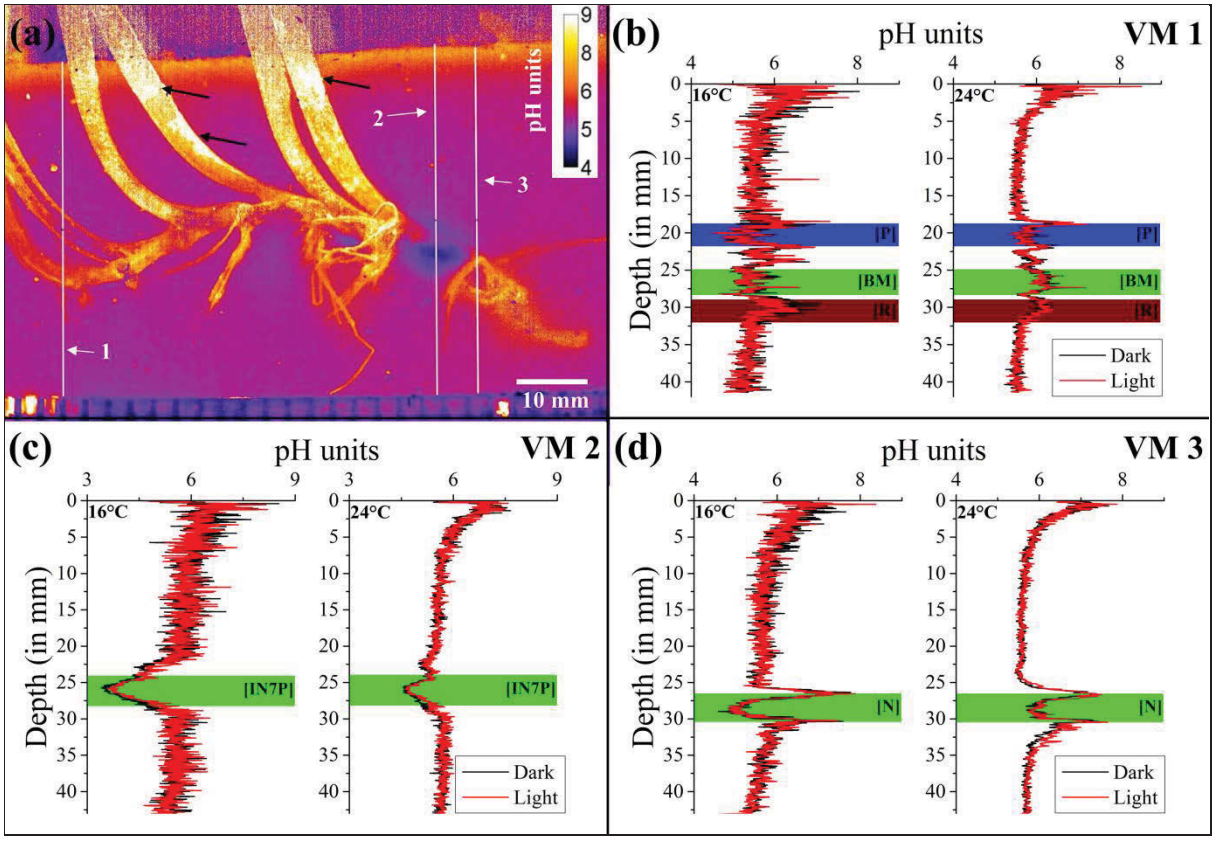

Figure 4.8. Vertical pH microprofiles (VM) illustrating the pH heterogeneity and microdynamics in the rhizosphere of *Z. marina* L. The vertical pH microprofiles were determined at steady-state conditions during light-dark transitions (photon irradiance (PAR) of 500 µmol photons m^{-2} s^{-1}) at ~16 and 24 °C. (a) Structural image of the *Z. marina* L. plant illustrating the spatial positions of the vertical pH microprofiles (colour coded image). (b) Vertical pH microprofile from the water/sediment interface across the first prophyllum and the basal meristem with leaf sheath to the bottom of the artificial sediment (VM1). (c) Vertical pH microprofile from the water/sediment interface across the base of the fifth prophyllum and the rhizome (internode 7) to the bottom of the artificial sediment (VM2). (d) Vertical pH microprofile from the water/sediment interface across the root-shoot junction at nodium 8 to the bottom of the artificial sediment (VM3). Y-axis = 0 indicate the artificial sediment surface. The approximate position of the below-ground tissue is indicated on the graphs by means of colour coded boxes (i.e. P = Prophyllum (blue), BM = Basal meristem with leaf sheath (green), R = Roots (brown); IN7P = Internode 7 at the base of the prophyllum (green); N = Nodium 8 (green)). n = 3. Note that the white areas on leaves/prophyllums (marked with black arrows on the figure) should be interpreted with caution, as some of these high pH microniches (pH of ≥9) seemed to be caused by epiphyte-derived red background luminescence (Notes S4.1; Figure S4.6).

A vertical pH microprofile extracted from pH images (VM1; Fig. 4.8b) showed the pH microdynamics and microheterogeneity at the interfaces between the sediment and the first prophyllum, as well as between the sediment and the basal meristem with leaf sheath. An increase in pH was measured at the position of the basal meristem with leaf sheath, i.e., the meristematic region of the rhizome, and along roots of the first root bundle (Fig. 4.8b). This was in contrast to pH conditions at the prophyllum/sediment interface, where we observed a rapid increase in pH towards the leaf tissue surface followed by a rapid decrease across the prophyllum, possibly due to oxic conditions and/or biological re-oxidation of H_2S (Fig. 4.8b; VM1). Another vertical pH microprofile (Fig. 4.8c; VM2) showed a rapid pH decrease at the interface between the sediment and the base of the fifth prophyllum/internode 7. At nodium 8 (root-shoot junction), a rapid increase in pH was seen at the approximate position of the oxic/anoxic interface with pH levels up to 8.4, followed by a strong decrease in pH across the rhizome tissue with pH levels decreasing to ~4.6 (Fig. 4.8d; VM3). A root from root-bundle 8 may have interfered with the interpretation of the pH microdynamics at nodium 8 (see Fig. 4.8d; VM3; ~26 mm depth). Nevertheless, our results clearly showed that plant-derived alterations of the belowground chemical microenvironment caused pH changes in the rhizoplane with a high degree of spatial microheterogeneity.

DISCUSSION

Our results showed a high spatio-temporal pH and O_2 microheterogeneity in the rhizosphere of *Z. marina*, where the chemical conditions in the immediate rhizosphere were highly affected by the plant host (Fig. 4.3 and 4.5). Radial O_2 loss (ROL) from the below-ground tissue of *Z. marina* resulted in oxic microniches around the root-shoot junctions and the rhizome (Fig. 4.3 and 4.4). Such oxic microniches have recently been shown to facilitate chemical re-oxidation of sediment-produced H_2S, and ROL is therefore an important chemical defence mechanism whereby the plants can actively detoxify phytotoxins in the surrounding sediment (Brodersen et al. 2014, 2015a).

Oxidation capacity of the below-ground tissue

The higher oxidation capacity of the below-ground tissue observed at 24°C as compared to 16°C (Fig. 4.4; Table 4.1) was due to a relatively higher rate of shoot photosynthesis (Fig. 4.2). The light-independent reactions, i.e., the enzyme-controlled reactions in the photosystems, are highly temperature dependent and the rate of photosynthesis, therefore, increases in direct proportion to temperature until it reaches a temperature optimum for the given plant, where after it rapidly decreases e.g. due to enzyme denaturation (Staehr & Borum, 2011). The optimum temperature for oxygenic photosynthesis in summer acclimated *Z. marina* plants is ~24°C (Staehr & Borum, 2011). The higher ROL from the rhizome in darkness at 24°C as compared to 16°C (Fig. 4.3 and 4.4) may be explained by a significantly higher O_2 diffusion coefficient in the temperature elevated water. As a water column temperature elevation of 8°C results in a ~ 25% increase in the rate of O_2 diffusion across the diffusive boundary layer (DBL) and into the above-ground tissue from the surrounding aerated water column (Ramsing & Gundersen, 2015), thus allowing enhanced internal O_2 supply through the aerenchyma (low-resistance internal gas channels) to the belowground tissue during darkness. This enhancement of the internal O_2 concentration gradient may be supported by a simultaneous temperature-induced increase in ROL owing to (i) the relatively increased lateral molecular O_2 diffusion rate across the epidermal layer of the belowground tissue at higher temperatures (although this might be counter-balanced by the higher tissue respiration), and (ii) the high leaf surface-to-volume ratio of the small *Z. marina* specimens used in this study leading to a relatively high efflux of O_2 from the leaves into the water column in light and a relatively high influx of O_2 from the water column into leaves in darkness.

Most prophyllums seemed to release O_2 into the rhizosphere (Fig. 4.3), and where prophyllum 1-5 potentially could be fueled by O_2 from the water-column, the fully buried prophyllum 6 at nodium 9 must be supplied with O_2 from the rhizome. Only a minor O_2 leakage was detected from the roots of the 2nd root-bundle close to the basal meristem during light exposure and a temperature of 24°C (Fig. 4.3). Structural tissue barriers to ROL (e.g. suberin; Barnabas, 1996) minimize cross tissue gas permeability of mature roots (e.g. Colmer, 2003; Jensen et al. 2005; Frederiksen & Glud, 2006; Brodersen et al. 2015a). Frederiksen and Glud (2006) found that the root oxygenated zones diminished with root age

and suggested that O_2 leakage from *Z. marina* roots eventually ceased. Our results further support such anatomical root adaptation of *Z. marina* to a life in a hostile reduced sediment environment. Barriers to ROL protect the plants against exposure to sediment-derived reduced phytotoxins such as H_2S and increase the amount of internal O_2 transported to the apical root meristems ensuring aerobic metabolism in distal parts of the plants.

pH microheterogeneity in the rhizosphere

The novel pH sensitive nanosensors incorporated in the transparent sediment matrix enabled the first detailed mapping of the spatio-temporal pH microheterogeneity in the whole rhizosphere of *Z. marina* (Fig. 4.5). A similar pattern was recently observed in the rhizosphere of *Zostera muelleri spp. capricorni* by means of point measurements using electrochemical microsensors (Brodersen et al. 2015a). Regions in the immediate rhizosphere of *Z. marina* with very low pH levels (pH <5) seemed to correlate with the plant-derived oxic microniches. Such acidification could be due to proton formation as a byproduct of the spontaneous chemical reactions between plant-released O_2 and sediment H_2S within the oxic microzone (Fig. 4.5 and 4.6). We also measured slightly lower pH values in the immediate rhizosphere during darkness as compared to in light (Fig. 4.5 and 4.6), owing to plant and sediment respiration processes in addition to the aforementioned plant-derived spontaneous chemical re-oxidation of H_2S.

At the end of the rhizome around nodium 9, the pH imaging revealed high pH levels in the adjacent sediment (Fig. 4.7f). We speculate that such local pH enhancement may be due to high levels of accessible organic carbon in this specific region of the rhizoplane, as a result of tissue degradation and rhizome exudates, leading to proton consumption through microbial metabolisms such as sulphate reduction (Isaksen & Finster, 1996; Blaabjerg et al. 1998; Hansen et al. 2000; Nielsen et al. 2001). These plant-microbial mediated local changes in the rhizosphere pH microenvironment are potentially very important for seagrasses as enhanced pH levels in the immediate rhizosphere lead to a shift in the sulphide speciation away from H_2S and towards non-permeable and thus non-phytotoxic HS^- ions. Besides formation of oxic microniches due to ROL (see above), rhizosphere pH changes represent another chemical defense mechanism, whereby the plants further detoxify the surrounding

sediment to accommodate their own growth in the often reduced, anoxic environments (Brodersen et al. 2015a).

Biogeochemical processes

The enhanced photosynthetic activity of *Z. marina* L. at its photosynthetic temperature optimum (~24°C) (Fig. 4.2), positively affects the production of photosynthates and thereby lead to diurnal increases in the secretion of root/rhizome exudates and ROL (Moriarty et al. 1986; Blaabjerg et al. 1998; Nielsen et al. 2001) that may stimulate the microbial activity (such as sulphate reduction and sulphide oxidation, respectively) on the root/rhizome surface and in the immediate rhizosphere. The overall higher pH levels measured in the immediate rhizosphere at 24°C as compared to 16°C (Fig. 4.5 and 4.6), may thus be a result of a temperature-induced enhancement in the plants photosynthetic activity leading to increased rhizome/root exudation of organic carbon to the rhizosphere (Moriarty et al. 1986; Blaabjerg et al. 1998). Such exudation could either directly increase the pH levels in the immediate rhizosphere and on the below-ground tissue surface through secreted allelochemicals like amines (although this would be an expensive chemical defence mechanism for the plants) and other alkaline substances, and/or indirectly via stimulation of microbial processes such as sulphate reduction (as indicated at the plant-derived oxic/anoxic interfaces (Fig. 4.7c and 4.8d)), in combination with the generally temperature-mediated increase of the sulphate reduction rates owing to reaction kinetics (Isaksen & Finster, 1996; Blaabjerg et al. 1998). Sulphate reduction rates associated with rinsed *Zostera muelleri* spp. *capricorni* roots/rhizomes have been found to be up to 11 times higher than in the bulk sediment (Hansen et al. 2000), and both rhizome and roots have been shown to be important habitats for sulphate-reducing and N_2-fixing bacteria (Blaabjerg & Finster, 1998; Nielsen et al. 2001). Sulphate-reducing bacteria associated with rhizomes/roots possess a high N_2-fixing activity that can cover up to 65% of the nitrogen needed by the seagrass plants (Hansen et al. 2000; Nielsen et al. 2001).

Notably, high sulphate reduction rates in the seagrass rhizosphere, furthermore, leads to a sulphide-induced release of sediment-bound phosphorus, as the reduction of Fe(III)(oxyhydroxides) to Fe(II) results in phosphate release to the pore water, which then becomes available for plant growth (Pollard & Moriarty, 1991; Pagès et al. 2011; Pagès et al. 2012). A mutual beneficial relationship between the *Zostera marina* L. plant host and

sulphate reducing bacteria in the rhizoplane seems therefore likely during non-stressed environmental conditions, where the sulphate reducing bacteria provides nutrients in the form of nitrogen and phosphate to the plant host as a response to plant-mediated rhizome/root exudates. However, we note that this hypothesis remains speculative and needs further experimental support. Our study did not aim to investigate the role of sulphate reducing bacteria in the *Z. marina* rhizosphere, and as we have used a sterile artificial sediment any sulphate reducing bacteria in the immediate rhizosphere must have originated from the non-sterile plant tissue. Future studies could e.g. involve artificial sediment based on extracted pore water or even cultures of sulphate reducing bacteria in combination with quantification of bacteria around the root biomass, e.g. using FISH with group-specific probes.

In other microniches associated with the formation of oxic microzones (Fig. 4.7c and 4.8d) biological and/or spontaneous chemical sulphide re-oxidation processes reduced the rhizoplane pH levels (Fig. 4.5). Such hotspots of low pH may well be due to a relatively higher abundance of sulphide oxidizing bacteria at that specific region, as microbes associated with the below-ground tissue of seagrass show a patchy distribution (Nielsen et al. 2001).

Optical nanoparticle-based sensors incorporated into transparent artificial sediment

The combined use of O_2 and pH sensitive nanoparticles with transparent artificial sediments enabled combined chemical and structural imaging on the whole rhizosphere level. This novel application of optical nanoparticle-based sensors represents an important supplement to existing methods, such as planar optodes and microsensors, when elucidating the rhizosphere of aquatic macrophytes, as the former rarely allows close contact to the entire belowground tissue at once and the latter rely on precise point measurements, which makes mapping the entire rhizosphere extremely tedious if not impossible. In addition, the optical nanoparticle-based sensors enable close spatial alignment of pH and O_2 concentration mapping thus facilitating co-localization of these important chemical parameters relative to particular plant/sediment and oxic/anoxic interfaces within the rhizosphere. However, at the current state, the present nanoparticle methodology only allows for O_2 and pH imaging in artificial sediments.

The strengths of employing such reduced artificial sediment, as compared to natural sediment, encompass: (i) significantly improved visual assessment within the investigated rhizosphere, thus allowing for determination of the exact position of the entire below-ground tissue during imaging, which is a necessity when determining the effects of plant/sediment interactions on the rhizosphere biogeochemistry, and (ii) changes observed within the homogenous artificial sediment can be assigned to plant-mediated alterations, which can be difficult to conclude in highly heterogeneous natural sediment. Weaknesses of using an artificial sediment matrix, as compared to natural sediment, include: (i) a significantly reduced microbial abundance in the bulk sediment, and (ii) a potential lower sediment pH buffering capacity, which may lead to slightly overestimated responses. Moreover, a minor limitation of current ratiometric pH imaging is that high energy excitation light has to be used when exciting the pH sensitive indicator dyes, potentially causing artefacts in the pH images owing to, for example, chlorophyll-derived red background luminescence. Further information on how to avoid/limit such potential artefacts in the pH images is available in the supporting information (Notes S4.1; Fig. S4.6). Nevertheless, nanoparticle-based imaging provides detailed information about the geochemical conditions and dynamics in the rhizosphere of aquatic macrophytes at high spatio-temporal resolution without the potential smearing effects seen with planar optodes and allows the first investigations of pH and O_2 dynamics in the entire seagrass rhizosphere in real-time and at all below-ground tissue/sediment interfaces. Nanoparticle-based imaging thus has the potential to further resolve important plant-sediment interactions, such as, for example, plant-derived sediment detoxification processes, in addition to, simply directing precise microsensor measurements to biogeochemical hotspots within natural sediment.

In conclusion, novel optical nanoparticle-based imaging revealed a pronounced spatio-temporal pH and O_2 microheterogeneity in the immediate rhizosphere of *Z. marina* L. Light stimulation of the leaf canopy and temperature elevation to the plants photosynthetically temperature optimum, i.e., from ~16 to 24°C, lead to higher oxidation capacity of the belowground tissue and higher pH levels in the immediate rhizoplane, where the temperature-induced stimulation seemed to predominate. Low rhizosphere pH levels correlated with the plant-derived oxic microniches. Patchy distributions of high rhizosphere

pH levels were found on the tissue surface, and cross tissue pH microprofiles revealed enhanced pH levels at selected oxic/anoxic interfaces. We speculate that the higher pH levels on the tissue surface and at the oxic/anoxic interface may be due to a plant-derived stimulation of proton consuming microbial metabolisms such as sulfate reduction and excretion of alkaline substances. Protons produced or consumed during microbial metabolisms, in addition to plant-mediated allelochemicals and chemical re-oxidation of H_2S, thus seemed responsible for the photosynthesis/temperature-driven alterations of the geochemical microenvironment determined in the *Zostera marina* L. rhizosphere.

SUPPLEMENTARY DATA

Supplementary material is available online.

Figure S4.1. Luminescence spectra of the optical pH nanosensors.

Figure S4.2. Calibration of pH nanosensor luminescence.

Figure S4.3. Calibration curves for optical pH nanoparticle-based sensors.

Figure S4.4. pH microprofiles in the bulk, artificial sediment containing pH sensitive nanoparticles measured with both a calibrated pH microelectrode and the optical nanoparticle-based pH sensors.

Figure S4.5. Calibration curves of optical O_2 nanoparticle-based sensors.

Figure S4.6. Potential artefacts in pH images.

Notes S4.1. Luminescence imaging.

ACKNOWLEDGEMENTS

We would like to thank Egil Nielsen, University of Copenhagen (KU) for manufacturing the applied aquarium and experimental split flow chamber. We thank Sofie Lindegaard Jakobsen (KU) for technical assistance and Dr. Sergey Borisov (Graz University of Technology) for generously providing the used pH indicator. The study was funded by research grants from the Augustinus Foundation (KEB); Fab. P.A. Fiskers Fund (KEB); the Danish Council for Independent Research | Natural Sciences (MK); the Villum Foundation (MK, KK); and the Australian Research Council [ARC Linkage, LP 110200454] (MK).

Conflict of Interest

The authors declare no conflict of interest and no competing financial interest.

REFERENCE LIST

Armstrong J, Armstrong W. (2001). Rice and *Phragmites*: effects of organic acids on growth, root permeability, and radial oxygen loss to the rhizosphere. *American Journal of Botany* **88**: 1359-1370.

Armstrong J, Armstrong W. (2005). Rice: Sulfide-induced Barriers to Root Radial Oxygen Loss, Fe^{2+} and Water Uptake, and Lateral Root Emergence. *Annals of Botany* **96**(4): 625-638.

Barnabas AD. (1996). Casparian band-like structures in the root hypodermis of some aquatic angiosperms. *Aquatic Botany* **55**: 217-225.

Binzer T, Borum J, Pedersen O. (2005). Flow velocity affects internal oxygen conditions in the seagrass *Cymodocea nodosa*. *Aquatic Botany* **83**: 239-247.

Blaabjerg V, Finster K. (1998). Sulphate reduction associated with roots and rhizomes of the marine macrophyte *Zostera marina*. *Aquatic Microbial Ecology* **15**(3): 311-314.

Blaabjerg V, Mouritsen KN, Finster K. (1998). Diel cycles of sulphate reduction rates in sediments of a *Zostera marina* bed (Denmark). *Aquatic Microbial Ecology* **15**(1): 97-102.

Borisov SM, Herrod DL, Klimant I. (2009). Fluorescent poly(styrene-block-vinylpyrrolidone) nanobeads for optical sensing of pH. *Sensors Actuators B Chem.* **139**: 52–58.

Borum J, Pedersen O, Greve TM, Frankovich TA, Zieman JC, Fourqurean JW, Madden CJ. (2005). The potential role of plant oxygen and sulphide dynamics in die-off events of the tropical seagrass, *Thalassia testudinum*. *Journal of Ecology* **93**: 148-158.

Borum J, Sand-Jensen K, Binzer T, Pedersen O, Greve TM. (2006). Oxygen movement in seagrasses. In: Larkum AWD, Orth JR & Duarte CM, Eds., *Seagrasses: Biology, Ecology and Conservation,* Dordrecht, The Netherlands: Springer, Berlin: 255-270.

Brodersen KE, Lichtenberg M, Paz L-C, Kühl M. (2015b). Epiphyte-cover on seagrass (*Zostera marina* L.) leaves impedes plant performance and radial O_2 loss from the below-ground tissue. *Frontiers in Marine Science* **2**: 58. DOI: 10.3389/fmars.2015.00058.

Brodersen KE, Nielsen DA, Ralph PJ, Kühl M. (2014). A split flow chamber with artificial sediment to examine the below-ground microenvironment of aquatic macrophytes. *Marine Biology* **161** (12): 2921-2930. DOI: 10.1007/s00227-014-2542-3.

Brodersen KE, Nielsen DA, Ralph PJ, Kühl M. (2015a). Oxic microshield and local pH enhancement protects *Zostera muelleri* from sediment derived hydrogen sulphide. *New Phytologist* **205** (3): 1264-1276. DOI: 10.1111/nph.13124.

Colmer TD. (2003). Long-distance transport of gases in plants: a perspective on internal aeration and radial oxygen loss from roots. *Plant, Cell & Environment* **26**: 17-36.

Enstone DE, Peterson CA, Ma F. (2003). Root endodermis and exodermis: structure, function, and responses to the environment. *Journal of Plant Growth Regulation* **21**: 335-351.

Frederiksen MS, Glud RN. (2006). Oxygen dynamics in the rhizosphere of *Zostera marina*: A two-dimensional planar optode study. *Limnol. Oceanogr* **51**(2): 1072-1083.

Greve TM, Borum J, Pedersen O. (2003). Meristematic oxygen variability in eelgrass (*Zostera marina*). *Limnology and Oceanography* **48**(1): 210-216.

Hansen JW, Udy JW, Perry CJ, Dennison WC, Lomstein BA. (2000). Effect of the seagrass *Zostera capricorni* on sediment microbial processes. *Marine Ecology Progress Series* **199**: 83-96.

Isaksen MF, Finster K. (1996). Sulphate reduction in the root zone of the seagrass *Zostera noltii* on the intertidal flats of a coastal lagoon (Arcachon, France). *Marine Ecology Progress Series* **137**(1): 187-194.

Isaksen MF, Jørgensen BB. (1994). Thermophilic sulfate-reducing bacteria in cold marine sediment. *FEMS Microbiology Ecology* **14**: 1-8.

Jensen SI, Kühl M, Glud RN, Jørgensen LB, Prieme A. (2005). Oxic microzones and radial oxygen loss from roots of *Zostera marina*. *Marine Ecology Progress Series* **293**: 49-58.

Jensen SI, Kühl M, Prieme A. (2007). Different bacterial communities in the rhizoplane and bulk sediment of the seagrass *Zostera marina*. *FEMS Microbiology Ecology* **62**: 108-117.

Koren K, Brodersen KE, Jakobsen SL, Kühl M. (2015). Optical sensor nanoparticles in artificial sediments – a new tool to visualize O_2 dynamics around the rhizome and roots of seagrasses. *Environmental Science and Technology* **49**: 2286-2292. DOI: 10.1021/es505734b

Lamers LP, Govers LL, Janssen IC, Geurts JJ, Van der Welle ME, Van Katwijk MM, Van der Heide T, Roelofs JG, Smolders AJ. (2013). Sulfide as a soil phytotoxin—a review. *Frontiers in plant science* **4**.

Larkum AWD, McComb AJ, Shepherd SA. (1989). *Biology of Seagrass*. Elsevier, Amsterdam.

Larsen M, Borisov SM, Grunwald B, Klimant I, Glud RN. (2011). A simple and inexpensive high resolution color ratiometric planar optode imaging approach: application to oxygen and pH sensing. *Limnol. Oceanogr.: Methods* **9**: 348-360.

McComb AJ, Dennison WC, Atwell B. (1999). Seagrasses: angiosperms adapted to sea floors. In: Kriedemann P.E., Atwell B.J., Turnbull C.G.N., eds. *Plants in action: Adaptation in nature, performance in cultivation*.

Moriarty DJW, Iverson RL, Pollard PC. (1986). Exudation of organic carbon by the seagrass *Halodule wrightii* Aschers. and its effect on bacterial growth in the sediment. *Journal of*

Experimental Marine Biology and Ecology **96**(2): 115-126.

Nielsen LB, Finster K, Welsh DT, Donelly A, Herbert RA, De Wit R, Lomstein BA. (2001). Sulphate reduction and nitrogen fixation rates associated with roots, rhizomes and sediments from *Zostera noltii* and *Spartina maritima* meadows. *Environmental Microbiology* **3**(1): 63-71.

Pagès A, Teasdale PR, Robertson D, Bennett WW, Schäfer J, Welsh DT. (2011). Representative measurement of two-dimensional reactive phosphate distributions and co-distributed iron(II) and sulfide in seagrass sediment porewaters. *Chemosphere* **85**(8): 1256-1261.

Pagès A, Welsh DT, Robertson D, Panther JG, Schäfer J, Tomlinson RB, Teasdale PR. (2012). Diurnal shifts in co-distributions of sulfide and iron(II) and profiles of phosphate and ammonium in the rhizosphere of *Zostera capricorni*. *Estuarine, Coastal and Shelf Science* **115**: 282-290.

Pedersen O, Binzer T, Borum J. (2004). Sulphide intrusion in eelgrass (*Zostera marina* L.). *Plant, Cell and Environment* **27**, 595-602.

Pedersen O, Borum J, Duarte CM, Fortes MD. (1998). Oxygen dynamics in the rhizosphere of *Cymodocea rotundata*. *Marine Ecology Progress Series* **169**: 283-288.

Pedersen O, Borum J, Duarte CM, Fortes MD. (1999). ERRATUM: Oxygen dynamics in the rhizosphere of *Cymodocea rotundata*. *Marine Ecology Progress Series* **178**: 310.

Pollard PC, Moriarty D. (1991). Organic carbon decomposition, primary and bacterial productivity, and sulphate reduction, in tropical seagrass beds of the Gulf of Carpentaria, Australia. *Marine Ecology Progress Series* **69**(1): 149-159.

Ramsing NB, Gundersen JK. (2015). Seawater and Gasses: Tabulated physical parameters of interest to people working with microsensors in marine systems: Unisense data tables. Available at: www.unisense.dk.

Raun AL, Borum J. (2013). Combined impact of water column oxygen and temperature on internal oxygen status and growth of *Zostera marina* seedlings and adult shoots. *Journal of Experimental Marine Biology and Ecology* **441**: 16–22.

Revsbech NP. (1989). An oxygen microsensor with a guard cathode. *Limnology and Oceanography* **34**(2): 474-478.

Staehr P, Borum J. (2011). Seasonal acclimation in metabolism reduces light requirements of eelgrass (*Zostera marina*). *Journal of Experimental Marine Biology and Ecology* **407**(2): 139-146.

Stahl H, Glud A, Schröder CR, Klimant I, Tengberg A, Glud RN. (2006). Time-resolved pH imaging in marine sediments with a luminescent planar optode. *Limnol. Oceanogr.: Methods* **4**: 336-345.

Srinivasan K, Mahadevan R. (2010). Characterization of proton production and consumption associated with microbial metabolism. *BMC Biotechnology* **10**: 2. Doi: 10.1186/1472-6750-10-2

Wang X, Stolwijk JA, Lang T, Sperber M, Meier RJ, Wegener J, Wolfbeis OS. (2012). Ultra-small, highly stable, and sensitive dual nanosensors for imaging intracellular oxygen and pH in cytosol. *J. Am. Chem. Soc.* **134**: 17011–17014.

Xie X, Mistlberger G, Bakker E. (2013). Ultrasmall fluorescent ion-exchanging nanospheres containing selective ionophores. *Analytical Chemistry* **85**: 9932–9938.

Zhu Q, Aller RC, Fan Y. (2006). Two-dimensional pH distributions and dynamics in bioturbated marine sediments. *Geochimica et Cosmochimica Acta* **70**(19): 4933-4949.

SUPPORTING INFORMATION

Nanoparticle-based measurements of pH and O_2 dynamics in the rhizosphere of *Zostera marina* L.: Effects of temperature elevation and light-dark transitions

Kasper Elgetti Brodersen[1,a,*], Klaus Koren[2,a], Mads Lichtenberg[2], Michael Kühl[1,2,*]

[1]Plant Functional Biology and Climate Change Cluster, University of Technology, Sydney, 15 Broadway, Ultimo, Sydney, NSW 2007, Australia

[2]Marine Biological Section, Department of Biology, University of Copenhagen, Strandpromenaden 5, DK-3000 Helsingør, Denmark

[a] These authors contributed equally to this work.

[*] Corresponding author, e-mail: mkuhl@bio.ku.dk and phone: +45 4047 6304

SUPPORTING FIGURES AND NOTES

Figure S4.1.

Luminescence spectra of the optical pH nanosensors in alkaline (pH 10; green) and acidic (pH 3; orange) solutions, showing a marked drop in luminescence in the yellow-orange-red wavelength interval (~550-675 nm) combined with an increase in the violet-blue-green wavelength interval (~430-530 nm) under acidic conditions. The nanoparticles were excited by a 405 nm LED and the spectra were recorded with a fiber-optic spectrometer (QE65000; oceanoptics.com).

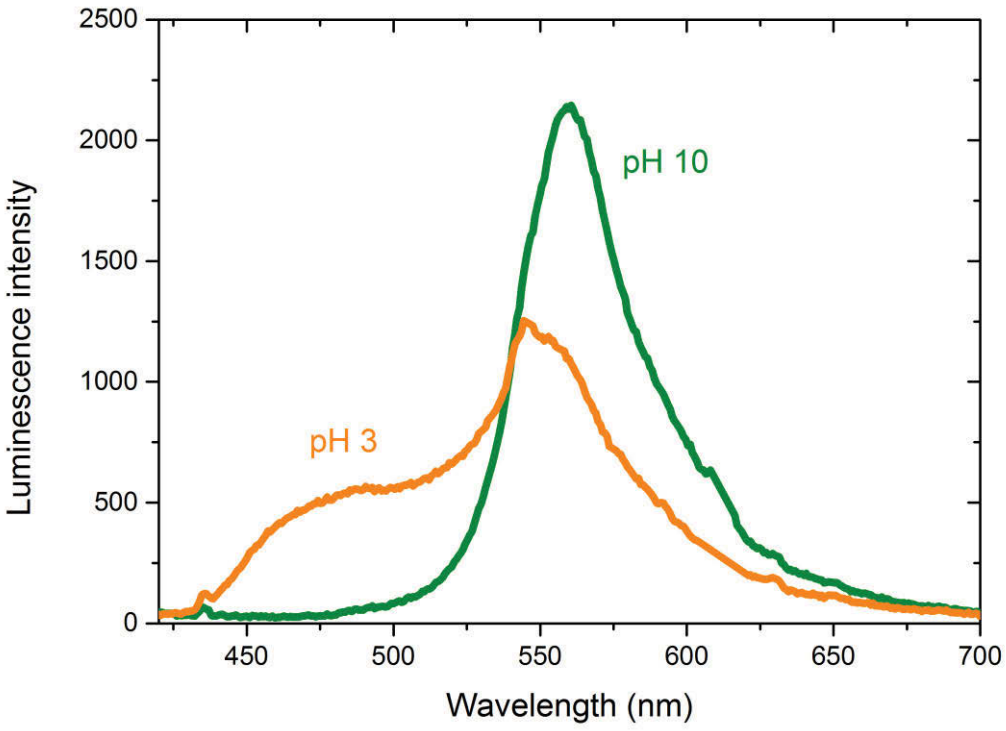

Figure S4.2

Calibration of pH nanosensor luminescence. Ratio images, i.e., the ratio of red and blue channels extracted from the recorded RGB image, were quantified in small transparent glass vials with pH nanoparticle-containing agar buffered to defined pH levels spanning pH 4-10.

The pH sensor nanoparticles were calibrated as follows. A solution of ~0.5% (w/w) agar-NaCl water (with a salinity of 34) was poured into small glass vials (3 mL volume). To adjust the pH value, 300 µL of a 100 mM buffer solution (citrate, phosphate or TRIS) were added. At a temperature of ~40°C, a small volume of the pH sensitive nanoparticles was added to a final concentration as used in the artificial sediment. After a short mixing step the agar was left to solidify. The glass vials were kept at constant temperature (16°C or 24°C) in a thermostated water bath and were then imaged with the ratiometric camera system using identical settings as for the seagrass sample. The ratio (red/blue channel) images were then correlated to the known pH values.

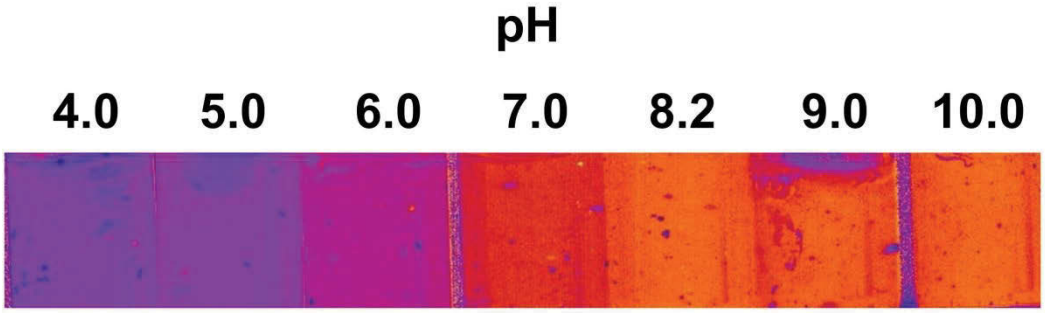

Ratio (red/blue channel)							
16°C:	2.47	2.58	3.25	4.50	5.16	5.27	5.31
24°C:	1.59	1.63	1.87	2.67	3.99	4.53	4.82

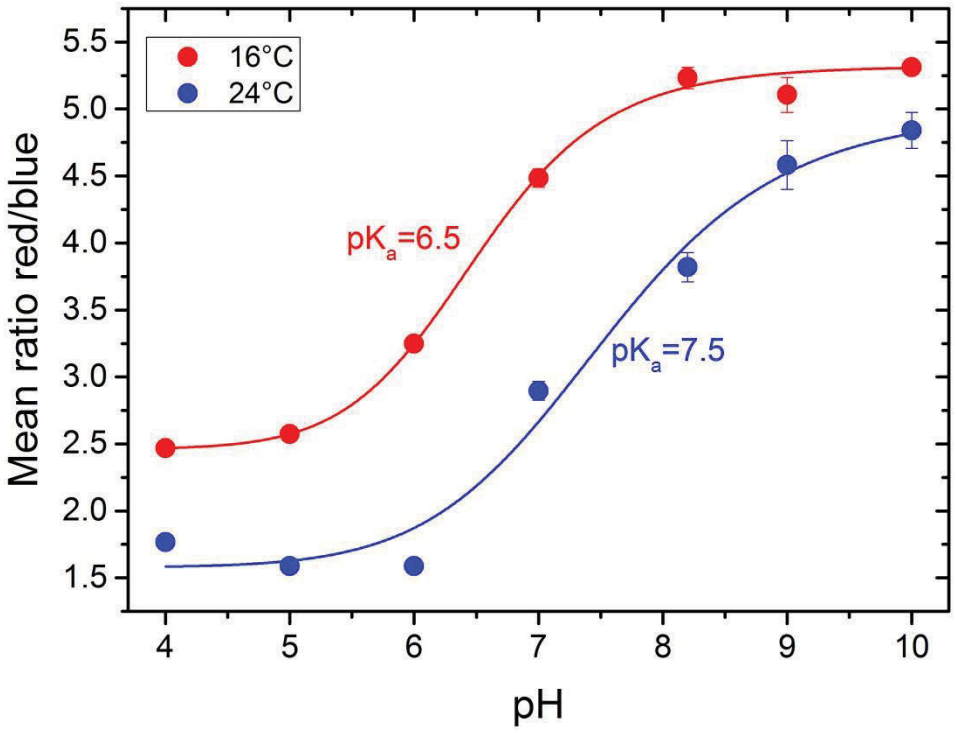

Figure S4.3. Calibration curves for optical pH nanoparticle-based sensors at the two experimental temperatures 16 and 24 °C. Mean ratio values were fitted with a sigmoidal function (r^2 = 0.99 and 0.97, respectively). Error bars are ± SD (n=3).

Figure S4.4.

Vertical pH microprofiles in the bulk, artificial sediment containing pH sensitive nanoparticles measured with both a calibrated pH microelectrode (pH-50, tip diameter of ~50 µm; Unisense A/S, Aarhus, Denmark; Kühl & Revsbech, 2001) and the optical nanoparticle-based pH sensors. There was a high resemblance between pH microprofiles (and thereby the sediment pH levels) determined with the two different sensor types. The pH levels of the bulk, artificial sediment dropped rather rapidly in the first 0-5 mm depth from ~pH 7.5 at the seawater/sediment interface to ~pH 6 at the approximate position of the below-ground biomass, thus mimicking chemical settings in natural sediment (Burdige and Zimmerman, 2002; Stahl et al. 2006; Zhu et al. 2006) (further information about the casting procedure of the reduced, artificial sediment is provided in Brodersen et al. (2014)).

pH microelectrode measurements. The pH microelectrode was mounted on a micromanipulator (Unisense A/S, Denmark) and used in combination with a reference electrode (tip diameter of ~5 mm; Unisense A/S) immersed in the supporting water reservoir; both connected to a pH/mV-Meter (Unisense A/S). Before measurements commenced, the pH microelectrode was linearly calibrated from sensor readings in three pre-known pH buffers (pH 4, 7 and 9; linearly responding over the pH calibration range with a signal to pH ratio of 51 mV/pH unit) at experimental temperature and salinity. The microelectrode measurements were performed in the custom-made narrow split-flow chamber (Fig. 4.1), in the same area as the extracted vertical pH microprofiles obtained via the pH sensitive nanosensors, by manually handling the micromanipulator (increments of 1 mm). The artificial sediment surface was determined by manually moving the microsensor towards the seawater/sediment interface, while observing the microsensor tip and the sediment surface through a magnifying glass, as well as from signal readings.

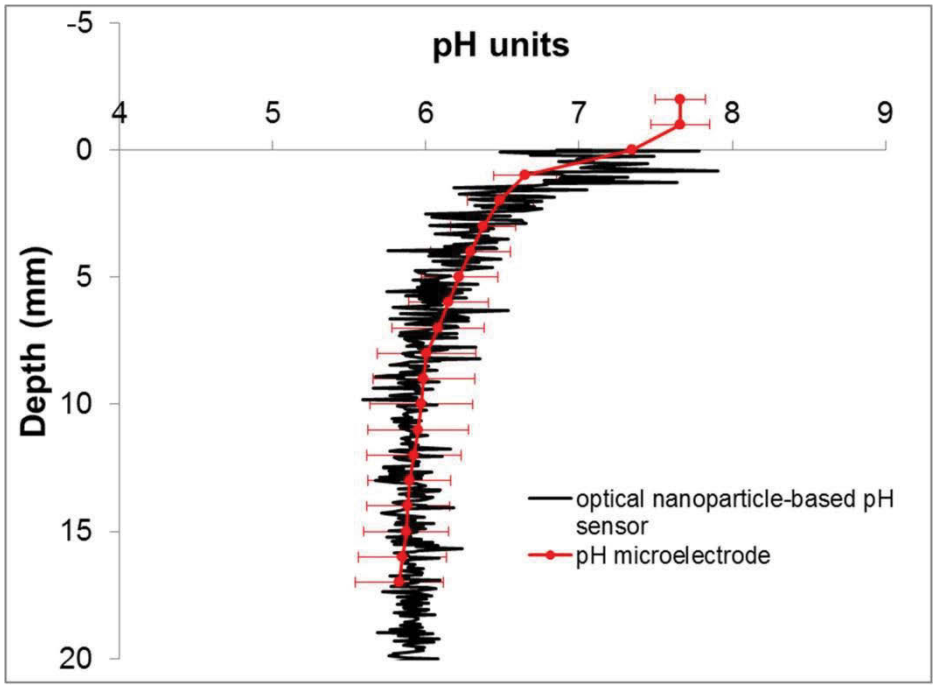

Figure S4.4. pH microprofiles measured in the bulk, artificial sediment containing pH sensitive nanoparticles with a pH microelectrode (red symbols; mean ± SD; n=3) and with the optical nanoparticle-based sensors (black line). Y = 0 indicates the artificial sediment surface.

Figure S4.5.

Calibration curves of optical O_2 nanosensors measured at the two experimental temperatures (Blue = 16°C; Red = 24°C; mean red/green ratio values were fitted with an exponential decay function, r^2 = 0.99). The optical O_2 nanoparticle-based sensors incorporated in the artificial, transparent sediment were calibrated as described in Koren et al. (2015).

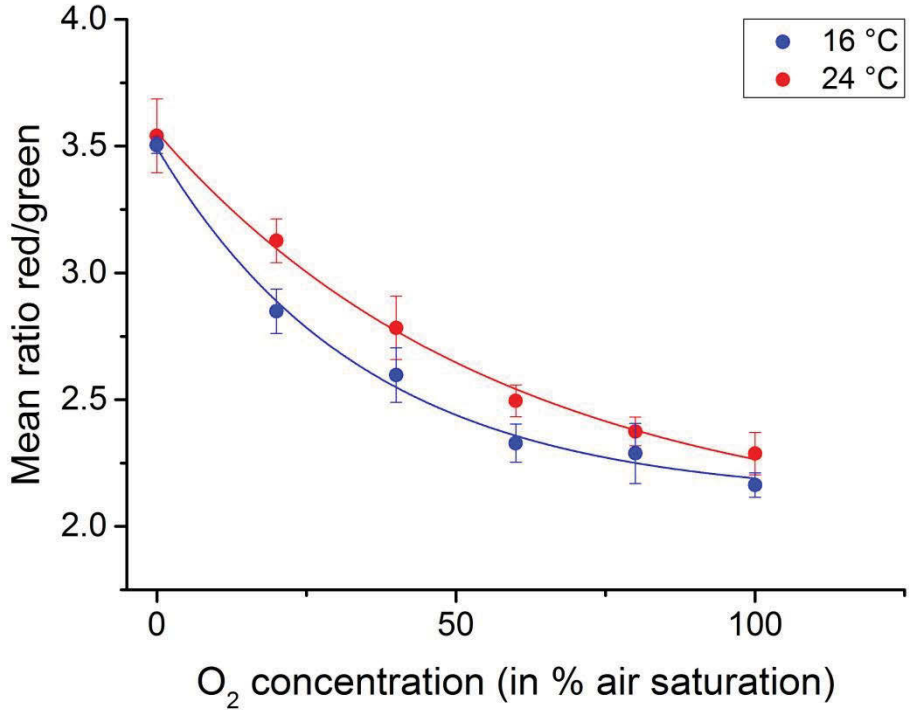

Figure S4.5. Calibration curves of optical O_2 nanoparticle-based sensors measured at the two experimental temperatures (16°C and 24°C). Mean ratio values were fitted with an exponential decay function (r^2 = 0.99 for both curves). Legend depicts the different temperatures. Error bars are ± SD. n=3.

Notes S4.1.

When working with optical (luminescence-based) sensors several factors can lead to artefacts and consequently misinterpretation of the results. The following paragraph intends to create awareness of potential problems and gives direction for possible solutions.

Intensity, ratiometric and lifetime based imaging:

In general, three different types of luminescence imaging are used for readout of optical chemical sensors. The most error prone is simple luminescence intensity-based imaging, where the intensity of a pixel or region is correlated to the analyte concentration. This approach is affected by numerous potential artefacts such as fluctuations in the illumination source, uneven illumination and/or distribution of the luminescent indicator, interference from background illumination and bleaching of the sensor material. In order to overcome some of these potential artefacts, a ratiometric imaging approach (where the ratio between the luminescence intensity of an analyte-sensitive indicator dye and the luminescence intensity of an inert reference dye is correlated to the analyte concentration) can be used to correct for uneven illumination or sensor distribution, and fluctuations in the illumination source. In terms of bleaching effects, a similar bleaching rate of the indicator and reference dyes is favourable; if one of them bleaches more easily than the other, this will lead to erroneous analyte concentrations. Background light and autofluorescence remains a problem in ratiometric imaging. Ratiometric imaging can be realized with relatively simple camera systems, like the SLR camera system used in this study (Larsen et al. 2011). Lifetime-based imaging, where the analyte-dependent change in the indicator luminescence decay time is monitored, is a very good and reliable alternative method but involves complicated and expensive instrumentation. Further details on this topic can be found in Meier et al. (2013).

Planar optodes vs. nanoparticle-stained artificial sediments

As this study utilizes nanoparticle-based sensors incorporated into transparent, artificial sediment we want to briefly discuss the benefits, but also potential artefacts, of this novel methodology in particular in comparison to the more commonly used planar sensor optode methods. Further details about the planar sensor optode method can be found in Santner et

al. (2015). In brief, the use of planar optodes enables chemical imaging in the plane of an optical sensor foil. Analysis of complex structures like the below-ground tissue of seagrasses requires a close proximity of the planar optode to the tissue surface. This is often difficult, if not impossible, to achieve and can limit the part of the belowground tissue that can actually can be analysed. In contrast, the nanoparticle method applied in this study enables simultaneous imaging of the entire below-ground tissue of seagrasses on a whole rhizosphere level (Koren et al. 2015).

An advantage of planar optodes is that an optical isolation can be applied on top of the sensor film. This protects the sensor from external light and protects the structure to be analyzed from the sensor excitation light (Glud et al (1996)). The latter is particularly important when high energy light (e.g. UV light) is used for excitation as this can easily cause background fluorescence from biological samples. An optical isolation layer can obviously not be applied in case of the nanoparticle stained transparent, artificial sediment. This means that things like background fluorescence from the sample have to been taken into account when interpreting the images.

Avoiding artefacts when working with intensity or ratiometric based imaging

In general the following rules apply when trying to avoid potential artefacts

- Use an excitation light that will not cause autofluorescence in the biological sample.
    - If this is not possible, as the indicator requires a certain excitation wavelength, try to image the sample without the sensor particles to see how high the background is and subtract this if needed in the subsequent image analysis.
- Be aware of color-dependent scattering
    - Use as thin a layer of artificial sediment as possible, to reduce the light path, and use color-corrected optics
- Avoid background light
    - If not possible, e.g. if darkening of the room is not entirely possible; take an image with the excitation light source off. This “dark” picture can then be subtracted from the images with the excitation light on. Nevertheless, it is advisable to get the surroundings as dark as possible.

- Bleaching: In case long-term light exposure is planned, it is recommended to test photostability prior to the measurements and account for potential photobleaching.
- Calibration: It is recommended to calibrate the sensor with the exact same conditions/settings as planned for the later measurements.

In the present study, all of the above-mentioned precautions were followed/secured during imaging. As UV light had to be used for pH imaging (e.g. Larsen et al. 2011), a few potential artefacts associated with the high energy excitation light were observed and are discussed below. All other above mentioned sources of potential artefacts could be excluded from the images.

Artefacts seen in the pH images

Artefacts are often easier to discover in the raw images of the different colour channels of the recorded RGB images. As seen in Figure S4.6, the blue colour channel appears to have a homogeneous intensity distribution (A), while the red channel shows some spots of high light (B). Especially in biological samples, this can e.g. be due to background fluorescence induced by the sensor excitation light. As the ratio of the two colour channels is used to calculate the pH image, such artefacts results in locally false pH readings. For example, Figure S4.6 depicts 4 small areas with very high red luminescence (white arrows, B) associated with leaves and prophyllums, that are probably partly covered by epiphytes, where the blue excitation light induced chlorophyll-derived red background luminescence. In contrast to other regions that show dynamics in response to altered environmental conditions (such as at the rhizome; Fig. S4.6, A), the 4 high red luminescence areas remain unchanged.

All images were therefore interpreted with caution. Potential artefacts were thoughtfully analysed, as demonstrated in Figure S4.6. Signals from regions potentially affected by artefacts (such as epiphyte-derived red background luminescence) were excluded from further analysis and marked on presented images by arrows, to ensure sufficient precaution was/are taken into account when interpreting the images. This is, as previously mentioned,

a minor limitation of current pH imaging, as high energy excitation light has to be used when exciting the pH sensitive indicator/reference dyes.

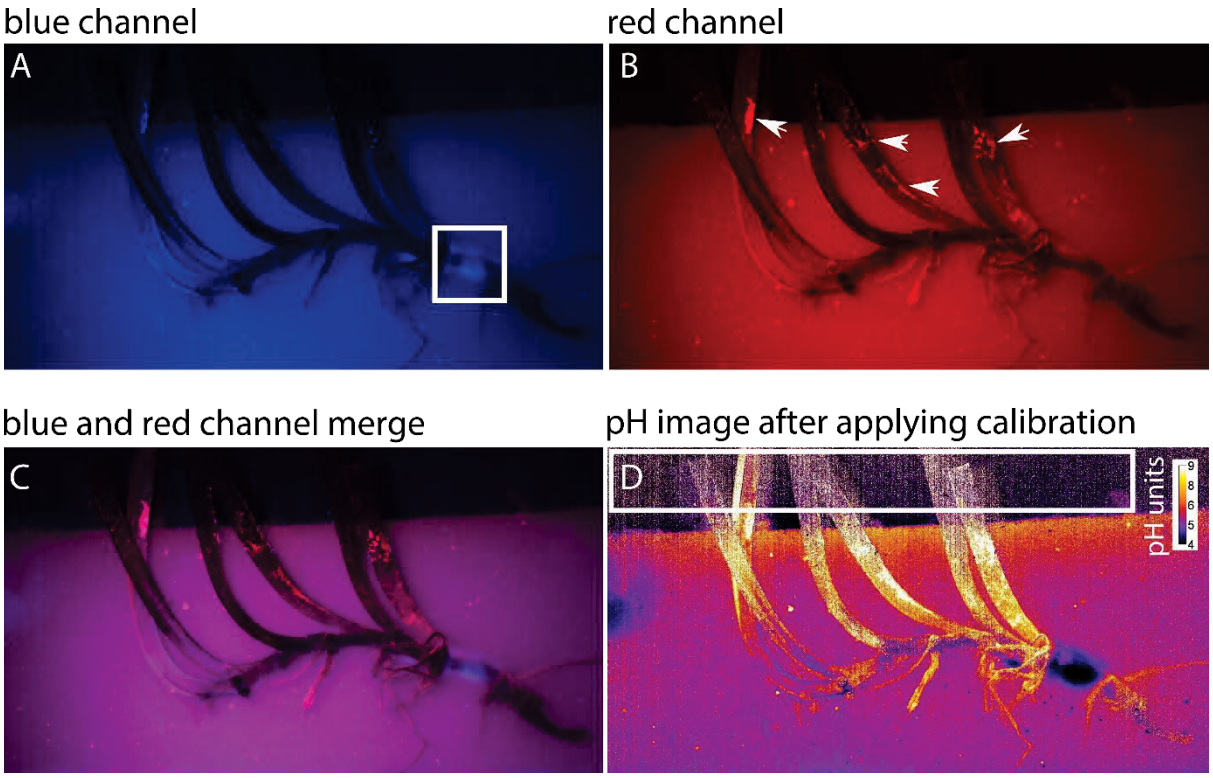

Figure S4.6. Visualization of potential artefacts in the obtained pH images (images are from the 16°C treatment). The blue and red channel images are obtained by splitting the original RGB picture into its respective colour channels. The blue channel image (A) appears quite homogeneous in terms of intensity, while the red channel image (B) shows several high intensity regions. When merging the two channels (C) it can be seen that most of the picture appears in a homogeneous pink colour, while the hotspots in the red picture remain. This subsequently leads to very high apparent pH values at those spots as the ratio of red and blue channel leads to the final pH image (D). In contrast to other regions (e.g. low pH hotspot at the rhizome; A) those spots do not change over time and in response to the altered light levels and/or temperature. An additional artefact is presented by the region on top of the artificial sediment (e.g. square in the pH image; D). In this region the measured intensities are not due to the optical nanoparticle based sensors and only represent noise such as scattered light, wherefore this region has been excluded.

REFERENCE LIST

Brodersen KE, Nielsen DA, Ralph PJ, Kühl M. (2014). A split flow chamber with artificial sediment to examine the below-ground microenvironment of aquatic macrophytes. *Marine Biology* **161**(12): 2921-2930. DOI: 10.1007/s00227-014-2542-3.

Burdige DJ, Zimmerman RC. (2002). Impact of sea grass density on carbonate dissolution in Bahamian sediments. *Limnol. Oceanogr.* **47**(6): 1751-1763

Glud RN, Ramsing NB, Gundersen JK, Klimant I. (1996). Planar optrodes: a new tool for fine scale measurements of two- dimensional O2 distribution in benthic communities. *Mar Ecol Prog Ser* **140**: 217–226

Kühl M, Revsbech NP. (2001). Biogeochemical microsensors for boundary layer studies. In: Boudreau BP, Jorgensen BB eds. *The benthic boundary layer*. New York: Oxford University Press, New York, 180-210.

Koren K, Brodersen KE, Jakobsen SL, Kühl M. (2015). Optical sensor nanoparticles in artificial sediments – a new tool to visualize O_2 dynamics around the rhizome and roots of seagrasses. *Environmental Science and Technology* **49**(4): 2286-2292. doi: 10.1021/es505734b

Meier RJ, Fischer LH, Wolfbeis OS, Schäferling M. (**2013).** Referenced luminescent sensing and imaging with digital color cameras: A comparative study. *Sensors Actuators B Chem.* **177:** 500–506.

Santner J, Larsen M, Kreuzeder A, Glud RN. (**2015).** Two decades of chemical imaging of solutes in sediments and soils – a review. *Anal. Chim. Acta*. doi:10.1016/j.aca.2015.02.006

Stahl H, Glud A, Schröder CR, Klimant I, Tengberg A, Glud RN. (2006). Time-resolved pH imaging in marine sediments with a luminescent planar optode. *Limnol. Oceanogr.: Methods* **4**: 336-345.

Zhu Q, Aller RC, Fan Y. (2006). Two-dimensional pH distributions and dynamics in bioturbated marine sediments. *Geochimica et Cosmochimica Acta* **70**(19): 4933-4949.

Chapter 5

Seagrass-altered rhizosphere biogeochemistry controls microbial community compositions at the microscale

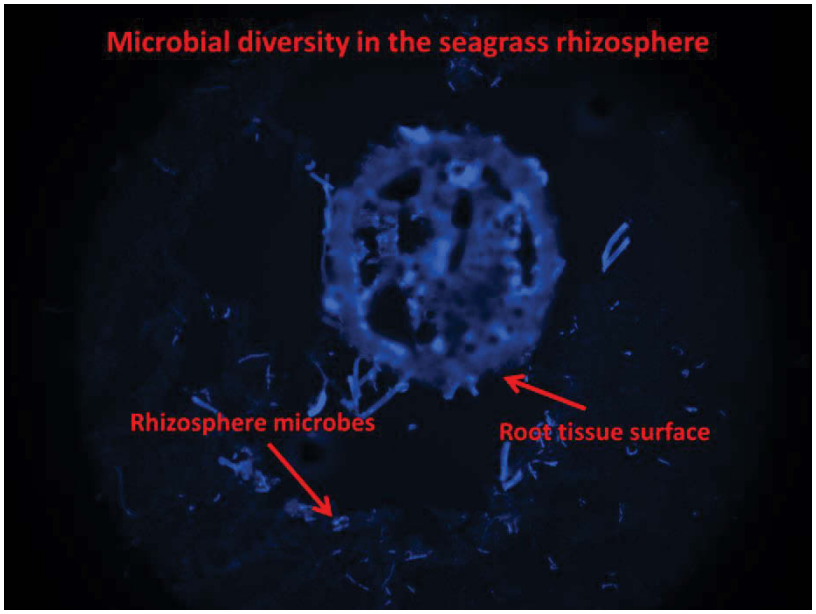

TOC figure. *Distribution of rhizosphere microbes in artificial sediment with added pore-water microbes as determined via epifluorescence microscope imaging of DAPI-stained bacteria.*

Citation: Brodersen KE, Siboni N, Nielsen DA, Pernice M, Ralph PJ, Seymour JR. & Kühl M. Seagrass-altered rhizosphere biogeochemistry controls microbial community compositions at the microscale. (In prep.).

Highlights: Potential mutual beneficial relationships between seagrass hosts and their rhizosphere microbes were analysed via high-resolution 16S rRNA amplicon sequencing and detailed rhizospheric microsensor measurements. This was enabled through a novel experimental approach, where the investigated seagrasses were cultured in a reduced, artificial sediment matrix that was either enriched with pore-water microbes or sterilized (including the below-ground biomass surface). Applying such artificial sediment matrix allowed the combined use of molecular and microsensor techniques, without disturbing the below-ground biogeochemical microenvironment during detailed microsensor measurements. The specific aim was to elucidate if seagrass hosts stimulate the growth and activity of sulphide-oxidizing bacteria within seagrass-driven oxic microniches to enhance sediment H_2S detoxification rates in the seagrass rhizosphere.

Seagrass-altered rhizosphere biogeochemistry controls microbial community compositions at the microscale

Kasper Elgetti Brodersen[1,*], Nachshon Siboni[1], Daniel A. Nielsen[1], Mathieu Pernice[1], Peter J. Ralph[1], Justin Seymour[1], Michael Kühl[1,2]

[1]Plant Functional Biology and Climate Change Cluster, Faculty of Science, University of Technology Sydney (UTS), Sydney, NSW, Australia.

[2]Marine Biological Section, Department of Biology, University of Copenhagen, Helsingør, Denmark.

Running title: "Seagrass rhizosphere microbes".

Subject Category: "Microbe-microbe and microbe-host interactions".

*Corresponding author: Kasper Elgetti Brodersen, email: kasper.e.brodersen@uts.edu.au.

ABSTRACT

The seagrass rhizosphere harbors dynamic microenvironments where plant-driven gradients of O_2 and dissolved organic carbon form microhabitats that select for distinct microbial communities. To examine how seagrass-mediated alterations of rhizosphere biogeochemistry affect microbial communities at the microscale level, we applied 16S rRNA amplicon sequencing of artificial sediments surrounding the meristematic tissues of the seagrass *Zostera muelleri* together with microsensor measurements of the biogeochemical conditions at the basal leaf meristem. Higher relative abundances of the sulphate reducing bacterial class *Clostridia* were observed around the meristematic tissues compared to the bulk sediment, with particular high abundance of sulphate reducers around the root apical meristems. Within plant-driven oxic microniches located at the basal leaf meristem, higher abundance of sulphide oxidizing bacteria was observed, but this did not seem to initiate beneficial effects in terms of H_2S detoxification suggesting a limited symbiotic relationship between *Z. muelleri* and rhizospheric, sulphide oxidizing bacteria.

MAIN BODY

Seagrasses grow in largely anoxic marine sediments (Borum et al. 2005) that are often enriched in the potent phytotoxin H_2S (Lamers et al. 2013). To accommodate growth in such hostile environments, seagrasses release O_2 into the rhizosphere from their basal leaf meristem and root apical meristems leading to the formation of localised oxic microniches (Jensen et al. 2005; Koren et al. 2015). These plant-driven oxic microzones support local H_2S re-oxidation protecting the most vulnerable parts of the plants against the H_2S produced by sulphate-reducing bacteria in the surrounding anoxic sediments (Brodersen et al. 2015). Significant amounts of labile dissolved organic carbon (DOC) are also exuded from the rhizome/roots, especially around the root cap (Moriarty et al. 1986; Pollard & Moriarty, 1991) stimulating microbial activity, including sulphate reduction, in the rhizosphere (Blaabjerg et al. 1998; Nielsen et al. 2001).

Seagrass-driven modulation of the rhizosphere microbial community has been suggested to initiate mutualistic relationships between seagrasses and often diazotrophic sulphate-reducing bacteria based on reciprocal nutrient exchange (Hansen et al. 2000; Welsh et al. 2000; Nielsen et al. 2001). Sulphide oxidizing bacteria within oxic microenvironments in the rhizosphere have also been proposed to play an important role in sediment detoxification (Jensen et al. 2007; Cúcio et al. 2016). Bacterial H_2S oxidation is 10^4-10^5 times faster than spontaneous chemical oxidation (Jørgensen & Revsbech, 1983; Nelson et al. 1986) and given ample O_2 supply, sulphide oxidizing bacteria may thus efficiently remove toxic H_2S facilitating seagrasses to colonize sulfidic sediments. However, technical constraints in examining the distribution and activity of sulphide oxidizing bacteria at the appropriate microscale resolution have prevented confirmation of the existence of a beneficial role of these bacteria within the seagrass rhizosphere. Here we present a detailed description of the microbial diversity surrounding the meristematic tissues of *Z. muelleri* in combination with measurements of plant-modulated micro habitats in the seagrass rhizosphere. The aim was (i) to elucidate the potential importance of sulphide oxidizing bacteria in detoxifying sediments for seagrasses, relative to plant-derived spontaneous chemical re-oxidation with O_2, and (ii) to reveal other beneficial and detrimental roles of seagrass rhizosphere microbes.

Z. muelleri specimens were cultured in a custom-made split flow-chamber (Brodersen et al. 2014) with the leaf canopy positioned in aerated, free-flowing seawater and the below-ground biomass embedded in a reduced, deoxygenated artificial sediment matrix (Supplementary Materials and Methods). To enable identification of potential mutual beneficial relationships, two treatments were applied, whereby the artificial sediment matrix was either (i) sterilized, including the below-ground biomass surface, or (ii) enriched with native pore water microbes. The transparent, artificial sediment matrix applied here permitted the precise and combined application of microsensor measurements and molecular characterisation of microbial communities within specific microzones of interest. These included investigations around the root apical meristems (the root-caps), the basal leaf meristem (the root/shoot junction) and within the bulk sediment. This approach permitted sampling at the desired spatial scales (~1mm radial distance from the below-ground tissue surface; Supplementary Materials and Methods). The rhizosphere microbial community composition was analysed via 16S rRNA amplicon sequencing (Supplementary Methods and Materials), while the chemical microenvironment was determined at high spatio-temporal resolution with O_2, H_2S and pH microsensor measurements (Kühl & Revsbech, 2001) (Supplementary Methods and Materials).

We observed higher mean relative abundance of sulphate-reducing bacteria (SRB), including Operational Taxonomic Units (OTUs) matching *Desulfovibrio* sp., around the below-ground biomass of *Z. muelleri* as compared to the bulk sediment, with particularly high levels of SRB occurring around the root apical meristems (Fig. 5.1). At the root apical meristems, members of the N_2 fixing SRB class *Clostridia* (Devereux, 2005; Sallam & Steinbüchel, 2009) dominated, comprising ~57% of sequences affiliated with this bacterial class ($p<0.05$; Fig. 5.1). Such elevated abundance of heterotrophic, diazotrophic bacteria around the below-ground biomass (e.g. *Lachnospiraceae* & *Desulfovibrio* sp.) supports beneficial relationships between seagrasses and N_2 fixing bacteria (e.g. Welsh, 2000), where the seagrass plant provides rhizosphere microbes with DOC and sulphate reducing diazotrophs provide fixed nitrogen to the seagrass. In addition, we speculate that high rhizosphere sulphide

production may lead to increased phosphorus solubilisation owing to reduction of Fe(III) oxyhydroxides (Pagès et al. 2011).

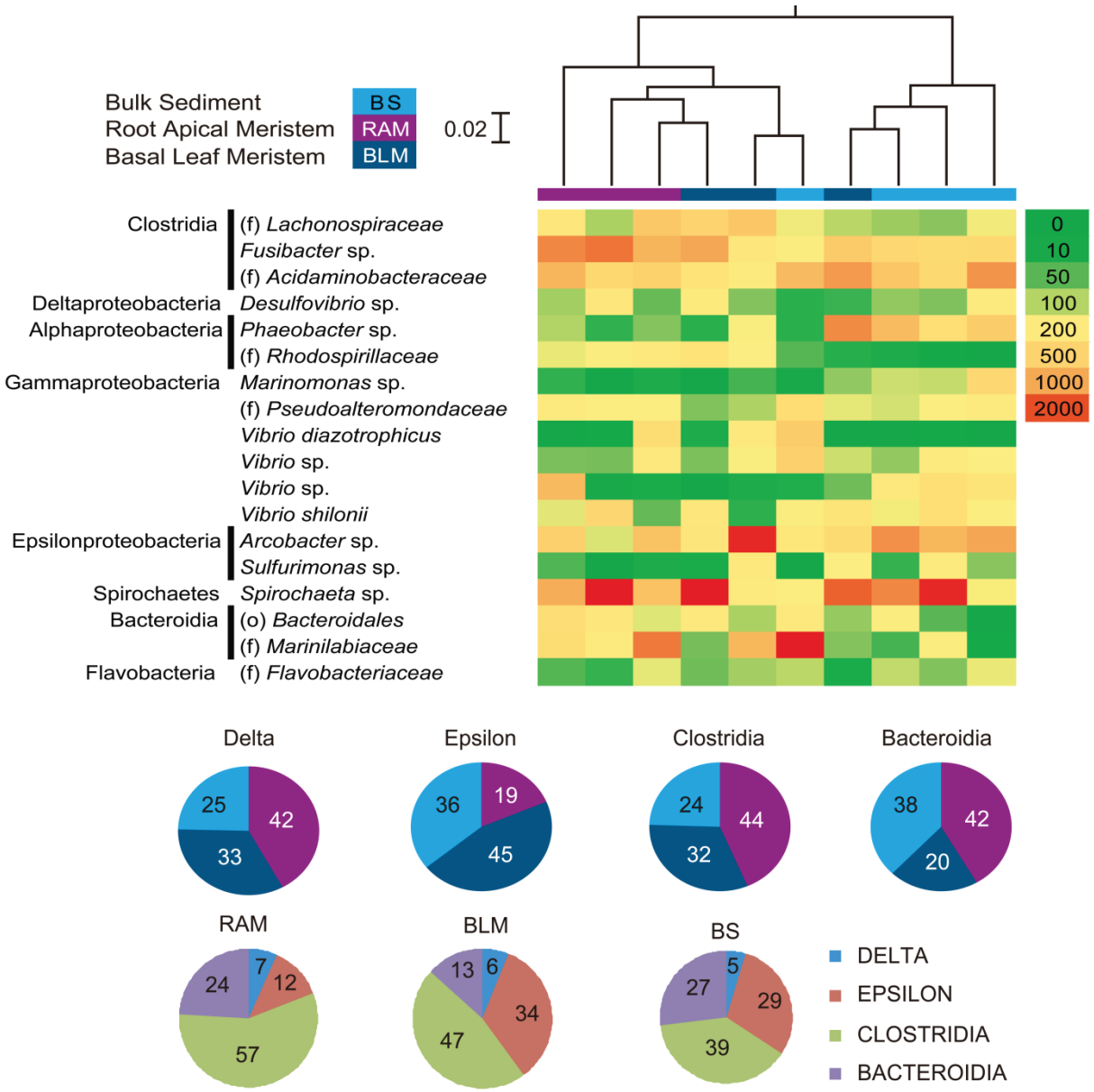

Figure 5.1. Microbial diversity in the rhizosphere of the seagrass *Zostera muelleri* determined via 16S rRNA amplicon sequencing. The phylogenetic tree denotes the spatial separation of the microbial consortia as determined via beta diversity analysis by Jackknife comparison of the weighted sequences data. The heat-map shows the abundance of the respective bacterial class/genus within the selected regions of interest, where (o) and (f) denote order and family classification, respectively. The heat-map includes taxonomic groups within each sample that represent >1% of the total sequences, which cumulatively represents >85% of the total sequenced data. Diagrams (in %) show the mean relative abundance of designated bacterial classes present within the selected regions of interest of the artificial sediment matrix. All data originate from reduced, artificial sediment with added

native pore water microbes (described in the Supplementary Materials and Methods; Notes S5.1). n = 2-3.

Radial O_2 loss (ROL) from the basal leaf meristem led to a ~300 µm thick oxic microshield, protecting seagrasses from intrusion of phytotoxic H_2S through chemical sulphide re-oxidation at the oxic/anoxic interface (Fig. 5.2; Table S5.2). Within this oxic microzone, slightly higher relative abundances of sulphide-oxidizing *Epsilonproteobacteria* (~45%), for example *Arcobacter* sp. and *Sulfurimonas* sp., were observed compared to the bulk sediment (~36%) and around the root apical meristem (~19%) ($p>0.05$; Fig. 5.1). This corresponded to a mean relative *Epsilonproteobacteria* abundance of ~34% at the basal leaf meristem compared to other designated bacterial classes, and thus an increase of ~22% as compared to around the root apical meristems (Fig. 5.1).

The higher relative abundance of sulphide oxidizing bacteria within plant-derived oxic microniches did not enhance sulphide detoxification, as we observed similar H_2S re-oxidation rates within the sterilized and microbe-enriched treatments (Fig. 5.2; Table S5.2). This may indicate that spontaneous chemical H_2S re-oxidation via ROL was the dominant sulphide oxidation mechanism in the immediate rhizosphere with only a minor influence of sulphide-oxidizing bacteria suggesting that their mutualistic relationship with *Z. muelleri* may be weaker than previously thought (Fig. 5.2; Supplementary Results). It is notable; however, that some sulphide-oxidizing *Arcobacter* sp. are capable of N_2 fixation, and such *Epsilonproteobacteria* may also contribute to the observation of high N_2 fixation rates within the seagrass rhizosphere (Jensen et al. 2007).

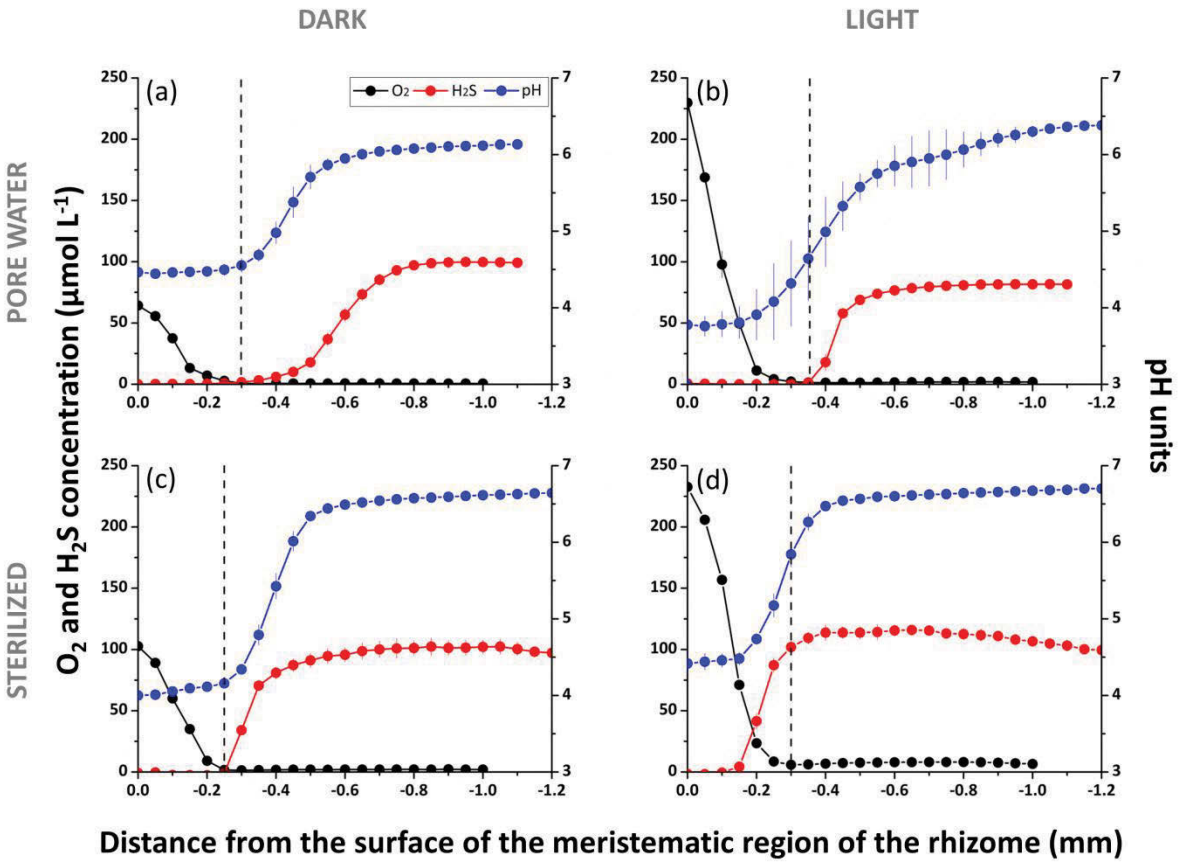

Figure 5.2. The below-ground chemical microenvironment at the basal leaf meristem, i.e., the meristematic region of the rhizome of the seagrass *Zostera muelleri*. (a) and (b) represent microsensor measurements in an artificial sediment matrix with added pore water microbes. (c) and (d) represent microsensor measurements in a sterilized environment, i.e., sterilized artificial sediment matrix and below-ground tissue surface. (a) and (c) show measurements in darkness. (b) and (d) show measurements in light (photon irradiance of ~150 µmol photons m^{-2} s^{-1}). Black line and symbols show the O_2 concentration; Red line and symbols show the H_2S concentration; Blue line and symbols show pH. The dotted lines indicate the thickness of the plant-derived oxic microzone, and X = 0 indicates the surface of the basal leaf meristem. Symbols with error bars represent means ± S.D (n = 3-4 technical replicates; biological replication of the below-ground chemical microenvironment dynamics is shown in the Supplementary Results; Fig. S5.1 and S5.2).

Our new approach of measuring microscale patterns in microbial diversity and sediment chemical characteristics within an artificial sediment matrix has allowed us to directly confirm that seagrass-mediated alterations of rhizosphere biogeochemistry result in pronounced shifts of the rhizosphere microbial community composition. Specifically, we observed significantly elevated abundances of sulphate-reducing bacteria in the seagrass

rhizosphere, and slightly higher abundances of sulphide-oxidizing bacteria within oxic microniches. Coupling these observations with high resolution characterisation of rhizosphere chemistry, our results indicate a limited beneficial relationship between seagrasses and rhizospheric sulphide-oxidizing bacteria in terms of H_2S detoxification. On the other hand our observations provide further evidence of a potential mutualistic relationship between seagrasses and heterotrophic, diazotrophic bacteria based on reciprocal nutrient exchange.

ACKNOWLEDGEMENTS

We thank Jessica Tout and Jean-Baptiste Raina from the University of Technology Sydney for fruitful discussions and support during experiments. The research project was funded by grants from the *Australian Research Council* (LP 110200454 to MK, JS, PR, and FT130100218 to JS) and the *Danish Council for Independent Research*|*Natural Sciences* (MK).

SUPPLEMENTARY INFORMATION

Supplementary Information accompanies the paper on The ISME Journal website (http://www.nature.com/ismej).

REFERENCE LIST

Blaabjerg V, Mouritsen KN, Finster K. (1998). Diel cycles of sulphate reduction rates in sediments of a *Zostera marina* bed (Denmark). *Aquatic Microbial Ecology* **15**(1): 97-102.

Borum J, Pedersen O, Greve TM, Frankovich TA, Zieman JC, Fourqurean JW, Madden CJ. (2005). The potential role of plant oxygen and sulphide dynamics in die-off events of the tropical seagrass, *Thalassia testudinum*. *Journal of Ecology* **93**: 148-158.

Brodersen KE, Nielsen DA, Ralph PJ, Kühl M. (2014). A split flow chamber with artificial sediment to examine the below-ground microenvironment of aquatic macrophytes. *Marine Biology* **161**(12): 2921-2930.

Brodersen KE, Nielsen DA, Ralph PJ, Kühl M. (2015). Oxic microshield and local pH enhancement protects *Zostera muelleri* from sediment derived hydrogen sulphide. *New Phytologist* **205**: 1264-1276.

Cúcio C, Engelen AH, Costa R, Muyzer G. (2016). Rhizosphere microbiomes of European seagrasses are selected by the plant, but are not species specific. *Frontiers in microbiology* **7**: 440.

Devereux R. (2005). Seagrass rhizosphere microbial communities. In *Coastal and estuarine studies: Interactions between macro- and microorganisms in marine sediments*, editors: Erik Kristensen, Ralf R. Haese & Joel E. Kostka. American Geophysical Union. Washington, USA.

Hansen JW, Udy JW, Perry CJ, Dennison WC, Lomstein BA. (2000). Effect of the seagrass *Zostera capricorni* on sediment microbial processes. *Marine Ecology Progress Series* **199**: 83-96.

Jensen SI, Kühl M, Glud RN, Jorgensen LB, Prieme A. (2005). Oxic microzones and radial oxygen loss from roots of *Zostera marina*. *Marine Ecology Progress Series* **293**: 49-58.

Jensen SI, Kühl M, Prieme A. (2007). Different bacterial communities in the rhizoplane and bulk sediment of the seagrass *Zostera marina*. *FEMS Microbiology Ecology* **62**: 108-117.

Jørgensen BB, Revsbech NP. (1983). Colorless sulfur bacteria, *Beggiatoa* spp. and *Thiovulum* spp., in O_2 and H_2S microgradients. *Applied and Environmental Microbiology* **45**: 1261-1270.

Koren K, Brodersen KE, Jakobsen SL, Kühl M. (2015). Optical sensor nanoparticles in artificial sediments – a new tool to visualize O_2 dynamics around the rhizome and roots of seagrasses. *Environmental Science and Technology* **49**(4): 2286-2292.

Kühl M, Revsbech NP. (2001). Biogeochemical microsensors for boundary layer studies. In Boudreau BP, Jorgensen BB, eds. *The Benthic Boundary Layer*. Oxford University Press, New York, 180-210.

Lamers LP, Govers LL, Janssen IC, Geurts JJ, Van der Welle ME, Van Katwijk MM, Van der Heide T, Roelofs JG, Smolders AJ. (2013). Sulfide as a soil phytotoxin—a review. *Frontiers in Plant Science* **4**: 268.

Moriarty DJW, Iverson RL, Pollard PC. (1986). Exudation of organic carbon by the seagrass *Halodule wrightii* Aschers. and its effect on bacterial growth in the sediment. *Journal of Experimental Marine Biology and Ecology* **96**(2): 115-126.

Nelson DC, Jørgensen BB, Revsbech NP. (1986). Growth pattern and yield of a chemoautotrophic *Beggiatoa sp.* in oxygen-sulfide microgradients. *Applied and Environmental Microbiology* **52**(2): 225-233.

Nielsen LB, Finster K, Welsh DT, Donelly A, Herbert RA, De Wit R, Lomstein BA. (2001). Sulphate reduction and nitrogen fixation rates associated with roots, rhizomes and sediments from *Zostera noltii* and *Spartina maritima* meadows. *Environmental Microbiology* **3**(1): 63-71.

Pagès A, Teasdale PR, Robertson D, Bennett WW, Schäfer J, Welsh DT. (2011). Representative measurement of two-dimensional reactive phosphate distributions and co-distributed iron(II) and sulfide in seagrass sediment porewaters. *Chemosphere* **85**(8): 1256-1261.

Pollard PC, Moriarty D. (1991). Organic carbon decomposition, primary and bacterial productivity, and sulphate reduction, in tropical seagrass beds of the Gulf of Carpentaria, Australia. *Marine Ecology Progress Series* **69**(1): 149-159.

Sallam A, Steinbüchel A. (2009). *Clostridium sulfidigenes* sp. nov., a mesophilic, proteolytic, thiosulfate- and sulfur-reducing bacterium isolated from pond sediment. *International Journal of Systematic and Evolutionary Microbiology* **59**(7): 1661-1665.

Welsh DT. (2000). Nitrogen fixation in seagrass meadows: regulation, plant–bacteria interactions and significance to primary productivity. *Ecology Letters* **3**(1): 58-71.

SUPPORTING INFORMATION

Seagrass-altered rhizosphere biogeochemistry controls microbial community compositions at the microscale

Kasper Elgetti Brodersen[1,*], Nachshon Siboni[1], Daniel A. Nielsen[1], Mathieu Pernice[1], Peter J. Ralph[1], Justin Seymour[1], Michael Kühl[1,2]

[1]Plant Functional Biology and Climate Change Cluster, University of Technology Sydney (UTS), Sydney, NSW, Australia.

[2]Marine Biological Section, Department of Biology, University of Copenhagen, Helsingør, Denmark.

Running title: "Seagrasses alter their rhizosphere microbial community".

Subject Category: "Microbe-microbe and microbe-host interactions".

*Corresponding author: Kasper Elgetti Brodersen, email: elgetti@hotmail.com.

SUPPORTING DATA

SUPPLEMENTARY MATERIALS AND METHODS

Notes S5.1. Detailed description of applied materials and methods.

SUPPLEMENTARY RESULTS

Figure S5.1. Chemical microenvironment as measured with microsensors at the surface of the basal leaf meristem of *Zostera muelleri* maintained in (i) a sterilized environment and (ii) with added native pore water microbes – plant 2.

Figure S5.2. Chemical microenvironment as measured with microsensors at the surface of the basal leaf meristem of *Zostera muelleri* maintained in reduced, artificial sediment with added native pore water microbes – plant 3.

Figure S5.3. Principle component analysis plot of the rhizosphere microbial community composition, illustrating the separation of the microbial consortia within selected rhizospheric regions of interest.

Figure S5.4. Spatial distribution of rhizosphere microbes around the root apical meristem (RAM) as determined via fluorescence microscopy after DAPI-staining.

Figure S5.5. Conceptual diagram visualizing sampling areas (i.e. region of interests) within the reduced, artificial sediment.

Table S5.1. Photosynthetic parameters as measured by variable chlorophyll fluorescence and measures of the above-ground:below-ground biomass ratios.

Table S5.2. Radial O_2 loss (ROL), plant-derived H_2S re-oxidation and rhizosphere ΔpH at the basal leaf meristem of *Zostera muelleri* as determined via detailed microsensor measurements.

SUPPLEMENTARY MATERIALS AND METHODS

Notes S5.1

Seagrass specimens and sediment sampling

Specimens of *Zostera muelleri subsp. capricorni* (Asch.) S.W.L. Jacobs and marine sediment were collected from shallow waters (<2 m depth) in a dense seagrass meadow at Narrabeen Lagoon, NSW, Australia. After sampling, the sediment and seagrass samples were transported to a greenhouse facility at the University of Technology Sydney, where they were kept under natural sunlight in large, aerated and thermostated seawater reservoirs (temperature of 22°C; salinity of 34) before further treatments. Prior to experiments, selected seagrass specimens were gently uprooted and washed free of any adhering sediment particles.

Experimental setup

Selected seagrass specimens (one seagrass at a time) were maintained in a custom-made split flow chamber (Brodersen et al. 2014) with the leaf canopy positioned in the free-flowing seawater compartment and the roots/rhizome in the adjoining sediment compartment (see further details below). Light was provided as a 12h:12h light/dark cycle with a fiber-optic tungsten halogen lamp (KL-2500; Schott GmbH, Mainz, Germany) connected to a timer and equipped with a collimating lens to restrict the illumination to the leaf canopy only. The incident photon scalar irradiance (PAR, 400-700 nm) at the leaf canopy during cultivation was ~150 µmol photons m^{-2} s^{-1}. Scalar irradiance was measured with a spherical quantum irradiance sensor (Walz GmbH, Effeltrich, Germany) connected to a calibrated quantum irradiance meter (Li-250A, LiCor, Lincoln, NE, USA).

A pump submerged into an aerated and thermostated seawater bath (temperature of ~22°C; Salinity of ~34) provided a constant flow (~0.5 cm s^{-1}) of aerated seawater to the water compartment of the flow chamber. Within the sediment compartment, a ~3 cm-thick anoxic and HEPES buffered (10 mM) water layer, residing above the artificial sediment matrix (described below), functioned as a liquid-phase diffusional barrier to O_2 invasion into

the artificial sediment (Brodersen et al. 2014). The anoxic water layer was constantly flushed with humidified N_2 throughout the seagrass cultivation period. Below the artificial sediment matrix, pieces of gauze pre-soaked in an acidic (pH 4) and anoxic 1 mM Na_2S solution were deployed to ensure a continuous supply of H_2S to the overlaying artificial sediment matrix. Finally, the sediment compartment was covered with aluminium (AL) foil to avoid incoming stray light, retain N_2 and thus limit O_2 intrusion into the anoxic water layer.

Artificial sediment matrix in the sediment compartment

Amended with pore water microbes

The transparent, reduced artificial sediment consisted of a ~0.7% (w/v) deoxygenated agar/seawater solution, buffered with anoxic HEPES (final concentration of 10 mM; pH ~7), and amended with Na_2S (final H_2S concentration of 500 µM; pH 7) and pore-water microbes (~50% pore-water in the final 0.7% w/v solution). During casting of the artificial sediment with pore-water microbes, the pore-water was homogenously incorporated into the pre-heated agar/seawater solution (~1.4% w/v) shortly before the artificial sediment matrix was poured into the sediment compartment of the split flow chamber at a matrix temperature of ~38°C. Thereafter, the artificial sediment with microbes was rapidly cooled down to room temperature in the sediment compartment embedding the below-ground tissue of the investigated seagrass specimen. The applied pore water was extracted from 50 mL Falcon tubes containing sediment from the sampling site by means of (i) mild ultrasonication (30 s) to dissociate microorganisms from the sediment grain surfaces and release microbes entrapped within sediment aggregates (Ramsay, 1984; Lindahl & Bakken, 1995), (ii) centrifugation (2 x 3500g for 5 min at 20°C), and (iii) filtration of supernatants (continuously flushed with N_2 to avoid oxygenation)(Millipore®, Polycarbonate membrane filters, 10 µm, USA) to exclude the remaining fine sediment particles.

Sterilized below-ground environment

The below-ground biomass of the investigated seagrasses was surface-sterilized by submerging sediment-free roots/rhizomes in a saline, anoxic ~1.05% (w/v) hypochlorite solution for 30 s (Blaabjerg & Finster, 1998) followed by 3 x 1 min rinses in anoxic, filter-sterilized (0.2 µm) seawater. Prior to casting the sterilized artificial sediment, all added solutions/seawater were filter-sterilized (0.2 µm) and the subsequently used agar was heated to 120°C in an oven for 30 min. The sterilized artificial sediment matrix consisted of a ~0.7% (w/v) deoxygenated agar/seawater solution, buffered with sterilized, anoxic HEPES (final concentration of 10 mM: pH ~7) and amended with Na_2S to a final H_2S concentration of 500 µM (at pH 7); thereby mimicking the chemical properties of the artificial sediment with added pore water microbes (described above).

Specimen characteristics and performance

Seagrass specimens with similar above- to below-ground biomass ratio (aiming at a ratio of ~1) were selected for this study, to ensure comparable below-ground tissue oxidation capabilities of the investigated specimens (e.g. Frederiksen et al. 2006; Frederiksen & Glud, 2006) (Table S5.1). Following cultivation and the experiments, the g DW biomass ratio of the above- to below-ground tissues was obtained after drying each seagrass specimen in an oven at 60°C until a constant weight was reached. The photosynthetic performance of the investigated seagrasses during cultivation was determined as the maximum PSII quantum yield in dark-adapted samples and the effective PSII quantum yield in illuminated samples by means of pulse amplitude modulated (PAM) variable chlorophyll fluorometry (Beer et al. 1998; PocketPAM, equipped with an optical fiber; Gademann Messtechnik GmbH, Germany) (Table S5.1) to confirm that the seagrasses were generally healthy and photosynthetically active under the experimental conditions.

DNA extraction and PCR sequencing

Phenol:chloroform DNA extraction

A standard phenol:chloroform protocol with modifications was used for DNA extractions (Zhou et al. 1996). Briefly, artificial sediment samples were obtained from selected regions of interest, i.e., around the basal leaf meristem (BLM), around the root apical meristem (RAM), and from the bulk sediment (BS) via a sterilized surgical knife and spatula. Samples around the below-ground tissues were carefully collected at a radial distance of up to ~1 mm from the tissue surface (final volume of ~100 µL). After sampling, the sediment samples were stored in 2 mL Eppendorf tubes in a -80°C freezer until further analysis. Prior to the phenol:chloroform DNA extractions, four rounds of washing were performed in order to remove the agarose. The artificial sediment samples were first liquefied in a dry bath at ~50°C and were then subsequently diluted via centrifugation with 1 mL of 3x PBS (2x 7500g at room temperature for 10 min, followed by 2x 4000g at 40°C for 10 min; all after re-heating the sample/PBS mixture to ~45°C). This additional cleaning step was implemented to separate bacterial cells from the agarose medium and thus avoid problems for downstream applications. DNA was extracted from the artificial sediment pellets by addition of 600 µL lysis buffer (TE buffer pH 8, 0.5% SDS, 0.1 mg mL^{-1}) and incubated at 37°C for 1 h. Then 100 µL of 5 M NaCl, and 80 µL of 10% CTAB were added and the mixture was incubated at 65°C for 10 min. Lysates were transferred to sterile tubes and DNA was extracted following standard phenol:chloroform procedures. The obtained DNA was air-dried, resuspended in 20 µL of dH_2O and stored at -20°C until further analysis. DNA quantity and purity was evaluated using a Nanodrop-1000 Spectrophotometer (NanoDrop 1000; Thermo Scientific, USA), as well as tested for PCR amplification using bacterial primers (27F, 1492R).

PCR amplification and sequencing

Microbial diversity and phylogenetic analysis:

To track shifts in the overall composition of the bacterial community, we sent DNA samples for amplicon sequencing using PCR amplicons of variable regions V1-V3 of the 16S rRNA gene with 27F (5'-AGAGTTTGATCMTGGCTCAG-3') (Weinbauer et al. 2002) and 519R (5'-GWATTACCGCGGCKGCTG-3') (Lane, 1991; Turner et al., 1999) on the Illumina MiSeq platform (at Molecular Research LP; Shallowater, TX, USA) following the manufacturer's guidelines. Raw data files in FASTQ format were deposited in the NCBI Sequence Read Archive (SRA) with the study accession number SRP073850 under Bioproject number PRJNA315465. Bacterial 16S rRNA gene sequences were analysed using the QIIME pipeline (Caporaso et al., 2010; Kuczynski et al., 2012). Briefly, paired-end DNA sequences were joined, *de novo* Operational Taxonomic Units (OTUs) were defined at 97% of sequences, identity was assigned against the Greengenes database (version 13/8/2013) using BLAST (Altschul et al., 1990). Chimeric sequences were detected using ChimeraSlayer (Haas et al., 2011) and filtered out from the dataset. Sequences were then rarefied to the same depth (7265 sequences per sample) to remove the effect of sampling effort upon analysis. A table which represented taxonomic groups within each sample was used to build a heat map in Excel. The QIIME pipeline was also used to analyse beta diversity by Jackknife comparison of the weighted data and to build a Principal Component Analysis (PCA) plot, in order to view the relationships between samples.

Microsensor measurements and flux calculations

We used Clark-type O_2 microsensors (OX-50, Unisense A/S, Aarhus, Denmark; Revsbech, 1989) to measure the radial O_2 loss (ROL) from the below-ground tissue of *Zostera muelleri*. The O_2 microsensors were linearly calibrated from signal readings in 100% air saturated seawater and anoxic seawater (obtained by flushing with N_2 and adding the O_2 scavenger sodium sulphite) at experimental temperature and salinity. To avoid drifting calibrations during measurements, the O_2 microsensors were pre-contaminated with H_2S before calibrations (Brodersen et al. 2015a). Clark-type H_2S microsensors (H_2S-50, Unisense A/S,

Aarhus, Denmark; Kühl et al. 1998) were used to measure the H_2S concentration at and around the below-ground tissue of *Zostera muelleri*. The H_2S microsensors were linearly calibrated in acidic (pH 4), anoxic Na_2S solutions of defined H_2S concentrations (0, 50 and 100 µM) at experimental temperature and salinity. pH measurements were performed by means of pH microelectrodes (pH-50, Unisense A/S, Aarhus, Denmark; Kühl & Revsbech, 2001) that were used in combination with a reference electrode (REF-RM, Unisense A/S, Aarhus, Denmark) submerged in the split flow chamber to allow the pH microelectrode to develop an electric potential relative to the reference electrode. The pH microelectrodes were linearly calibrated from signal readings in pH buffers (pH 5, 8 and 9) at experimental temperature and salinity. Microsensors were mounted on a motorized micromanipulator (MM33-2 & MC-232, Unisense A/S, Aarhus, Denmark) and connected to a microsensor multimeter (Unisense A/S, Aarhus, Denmark) that was interfaced with a PC running dedicated microsensor positioning and data acquisition software (SensorTrace PRO, Unisense A/S, Aarhus, Denmark). The microsensors were carefully positioned at the surface of the basal leaf meristem (defined as 0 mm distance from the below-ground tissue on the figures) by manually operating the micromanipulator while observing the tip of the microsensor relative to the surface of the below-ground tissue through a submerged hand-held lens (described in Brodersen et al. 2014) with a stereo microscope mounted on an articulating arm (SM-6TZ, Amscope, Irvine, CA, USA). All microprofiles were measured in distance increments of 50 µm. Plants were allowed to acclimatize to the experimental conditions for ~72 h before microsensor measurements commenced to ensure steady state geochemical conditions. Moreover, during microsensor profiling an additional source of N_2 was immersed into the anoxic seawater layer of the sediment compartment (described above) to avoid O_2 intrusion into the layer and H_2S loss from the artificial sediment when removing the covering alu-foil (Brodersen et al. 2014; 2015a).

Flux calculations

The radial O_2 loss (ROL) from the below-ground tissue (nmol O_2 cm^{-2} h^{-1}) was calculated via a cylindrical version of Fick's first law of diffusion (Steen-Knudsen, 2002) assuming a homogenous, cylinder-shaped O_2 flux from the surface:

$$J(r)_{BLM} = \varphi D_0(C_1 - C_2)/rln(\frac{r_1}{r_2})$$

where φ is the porosity of the artificial sediment (here assumed to be similar to seawater); D_0 is the apparent diffusion coefficient of O_2 in seawater at experimental temperature and salinity; r is the radius of the basal leaf meristem; and C_1 and C_2 are the O_2 concentrations measured at the radial distances r_1 and r_2 from the tissue surface, respectively. The H_2S oxidation rates in the immediate rhizosphere (nmol H_2S cm^{-2} h^{-1}) were calculated in a similar manner by correcting D_0 to the molecular diffusion coefficient for H_2S at experimental temperature and salinity (factor 0.7573; tabulated values are accessible on www.unisense.com).

Fluorescence microscopy

A standard microscopy protocol with minor modifications was used for DAPI staining and imaging using an epifluorescence microscope (Amann et al. 1990). Briefly, small samples (~4 x 4 x 4 mm) of artificial sediment embedding a root-tip were obtained by cutting out the region of interest with a surgical knife. The achieved root-cap tissue and surrounding artificial sediment sample were then fixed in 4% paraformaldehyde (PFA), washed by immersing the sample in a 1x phosphate-buffered saline (PBS) solution (2 times), and were then structurally preserved in 50% EtOH until further analysis. To ensure optimal cutting temperature, the investigated samples were embedded in cryo-gel (OCT, Tissue-Tek®; ProSciTech, Kirwan, Qld, Australia) at 4°C for 24h before snap-freezing in a cryobath at -60°C. The frozen samples were sectioned on a cryomicrotome (Shandon cryotome E, Thermo Scientific, Australia) into 20-30 µm-thick transverse tissue/sediment sections at -36°C, before immobilization on Teflon coated microscope slides (www.proscitech.com). Tissue/sediment samples were then dehydrated by immersing the slides in ascending ethanol series (50-80-96% EtOH), stained by an anti-bleaching/DAPI mixture (using Citifluor as the anti-bleaching agent; Citifluor AF1, Citifluor Ltd, London) and imaged on an inversed epifluorescence microscope (Nikon Eclipse Ti; Nikon Instruments Inc, Tokyo, Japan).

Statistical analysis

Data were tested for equal variance prior to statistical analysis. Student's *t*-tests were used to compare relative microbial abundances between the different regions of interest (i.e. RAM, BLM and BS) on data that met the above-mentioned assumptions. The significance level was set to $p < 0.05$. All statistical tests were performed in Excel.

SUPPLEMENTARY RESULTS

FIGURE S5.1.

The below-ground chemical microenvironment measured with microsensors at the basal leaf meristem of *Zostera muelleri* (investigated plant #2). Blue symbols and lines indicate pH, red symbols and lines indicate H_2S concentration, and black symbols and lines indicate O_2 concentration. The dotted lines denote the thickness of the plant-derived oxic microzone. Left panels represent measurements in the dark, right panels represent measurements in the light (at an incident photon irradiance of ~150 µmol photons m^{-2} s^{-1}). Upper panels are measurements in artificial sediment with added pore water microbes. Lower panels are measurements in a sterilized environment (i.e. below-ground tissue surface and sediment). X = 0 indicate the below-ground tissue surface. Symbols with error bars indicate means ± S.D; n = 3-5, technical replicates.

The minor co-existence of O_2 and H_2S within the oxic microzones in both treatments suggests that spontaneous chemical H_2S re-oxidation is the dominant sulphide oxidation mechanism in the seagrass rhizosphere.

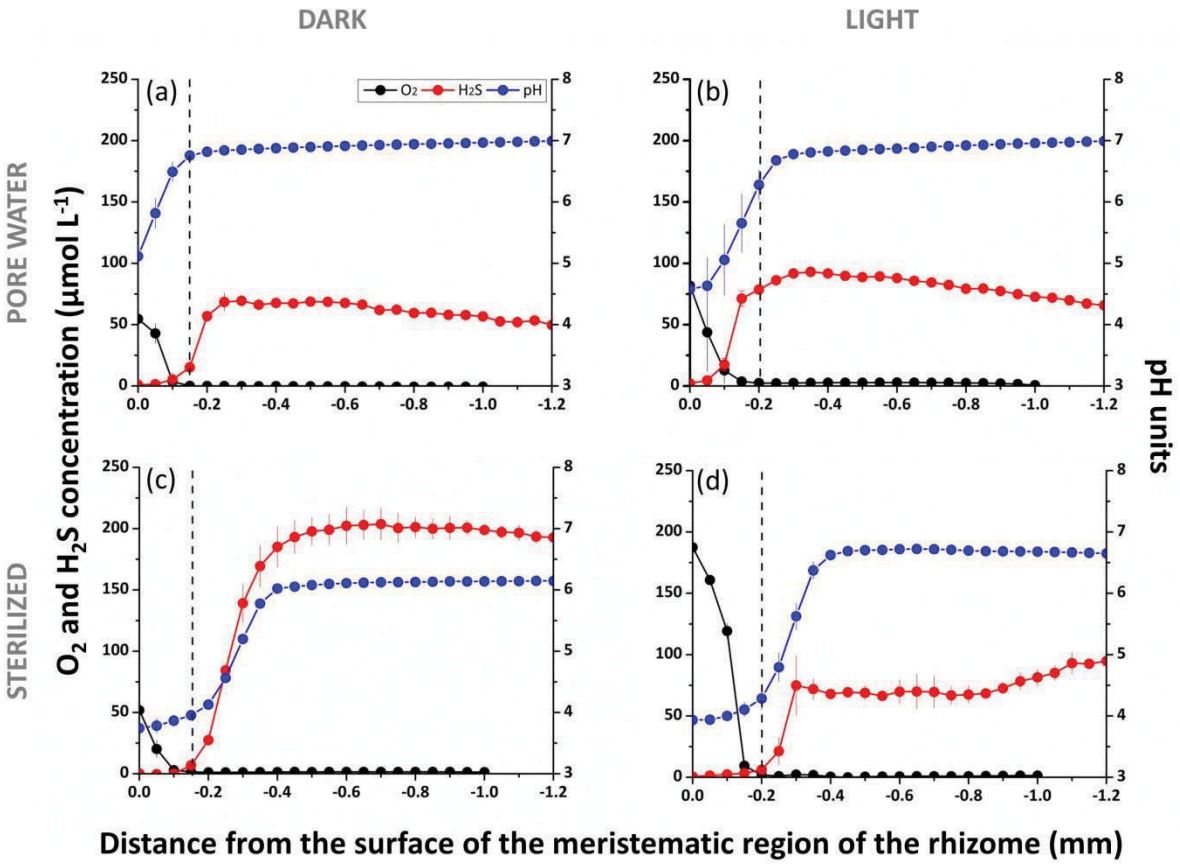

Figure S5.1. Chemical microenvironment at the interface between the surface of the meristematic region of the rhizome and the immediate rhizosphere. Biological replication #2.

FIGURE S5.2.

The below-ground chemical microenvironment measured with microsensors at the basal leaf meristem of *Zostera muelleri* (investigated plant #3). Blue symbols and lines indicate pH, red symbols and lines indicate H_2S concentration, and black symbols and lines indicate O_2 concentration. The dotted lines denote the thickness of the plant-derived oxic microzone. Left panels represent measurements in the dark, right panels represent measurements in the light (at an incident photon irradiance of ~150 µmol photons m^{-2} s^{-1}). Graphs show measurements in artificial sediment with added pore water microbes. X = 0 indicate the below-ground tissue surface. Symbols with error bars indicate means ± S.E.M; n = 3-5, technical replicates.

Microsensor measurements from plant 3 kept in a sterilized environment were excluded as we could not convincingly determine the surface of the below-ground tissue during measurements. This was unfortunately a potential limitation of the experimental setup/methodology, as we had to use a relatively high agar concentration (0.7% w/v) to enable artificial sediment sampling around the selected plant structures in the desired spatial scale (i.e. radial distance of < 2mm from the tissue surface) for downstream applications, such as DNA extraction, PCR sequencing and fluorescence imaging. This, unfortunately, reduced the visual assessment of the below-ground tissue during measurements. Further information on limitations of the methodology is provided in Brodersen et al. 2014.

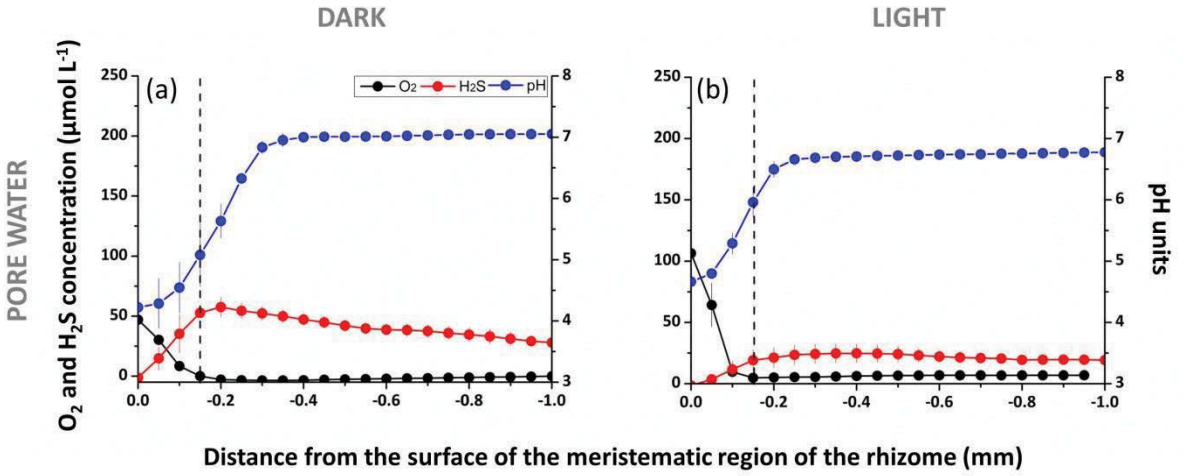

Figure S5.2. Chemical microenvironment at the interface between the surface of the meristematic region of the rhizome and the immediate rhizosphere. Biological replication #3.

FIGURE S5.3.

Principal component analysis (PCA) among bulk sediment (BS), root apical meristem (RAM) and basal leaf meristem (BLM) samples in the artificial sediment with added native pore water microbes. The PCA explains more than 75% of the variances in our samples. The PCA plot represents the mean relative abundance of microbes within selected areas of the *Zostera muelleri* rhizosphere, and includes all data acquired via PCR sequencing excluding non-sense, i.e., ~99.9% of all bacterial sequences.

Our results suggest that the rhizosphere microbial community composition within the sediment surrounding the root apical meristems were mostly affected by the plant host (Figure S5.3). Root exudates could be the driver of these microbial community modifications. The microbial community composition at the basal leaf meristem and within the bulk sediment was less differentiated/separated according to the PCA.

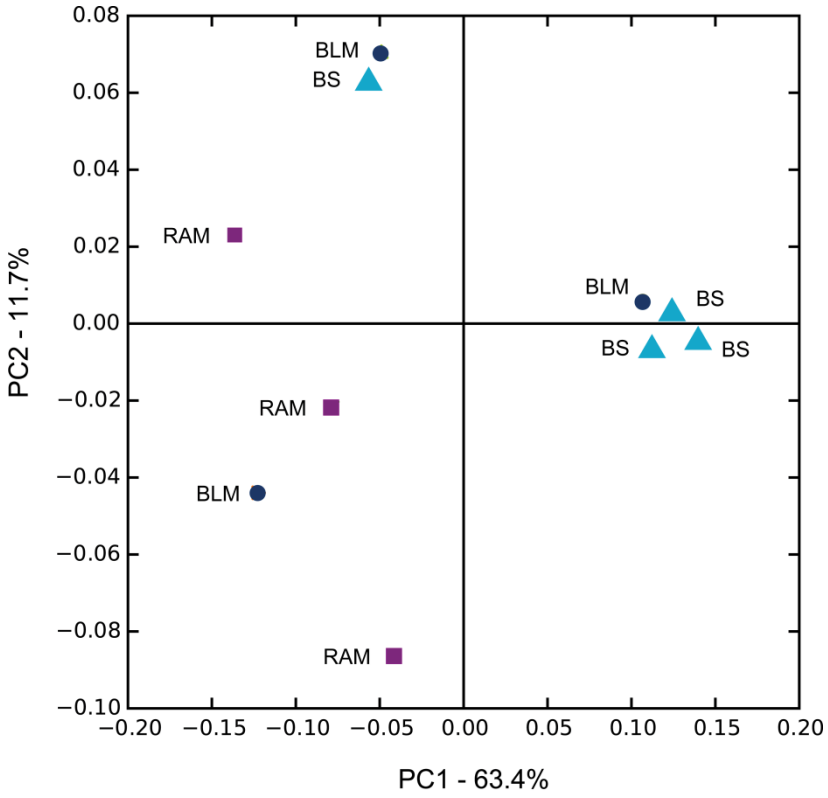

Figure S5.3. Principal component analysis (PCA) of the bacterial community composition within the seagrass rhizosphere and the bulk sediment. RAM = root apical meristem area; BLM = basal leaf meristem area; BS = bulk sediment. This PCA explained more than 75% of the variances of our samples.

FIGURE S5.4

Spatial distribution of rhizosphere microbes at the root apical meristem (RAM) of *Zostera muelleri* as determined via epifluorescence microscopy of DAPI stained bacteria. The transverse root-cap and artificial sediment sample originated from the artificial sediment matrix with added native pore water microbes. Image (b) is a close-up image of the root/sediment interface as shown in image (a), illustrating the root-cap tissue surface and the bacterial distribution within the immediate rhizosphere. Unfortunately, it seemed like the cutting/immobilization procedure (described in the Supplementary Materials and Methods) caused the formation of a small cavity between the root-cap tissue surface and the surrounding artificial sediment, wherefore additional identifications of the microbial community composition and diversity using group-specific probes for fluorescence *in situ* hybridization (FISH) determinations were excluded. Further investigations of the rhizospheric spatial distribution of important bacterial functional-groups, such as sulphide-oxidizing and sulphate-reducing bacteria are underway.

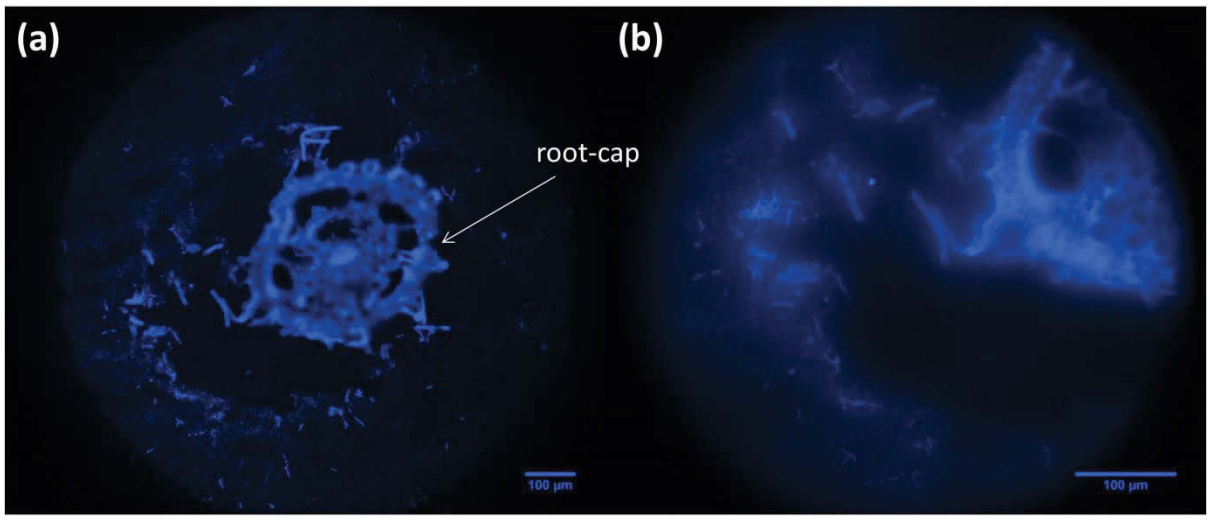

Figure S5.4. Spatial distribution of rhizosphere microbes around the root apical meristem (RAM) of the seagrass *Zostera muelleri* as determined via epifluorescence microscopy of DAPI-stained bacteria.

FIGURE S5.5

Selected regions of interest within the seagrass vegetated artificial sediment. BLM refers to the basal leaf meristem (i.e. at the base of the shoot), RAM refers to the root apical meristems (i.e. at the apex of the roots) and BS refers to the bulk sediment, several centimetres away from the below-ground tissue.

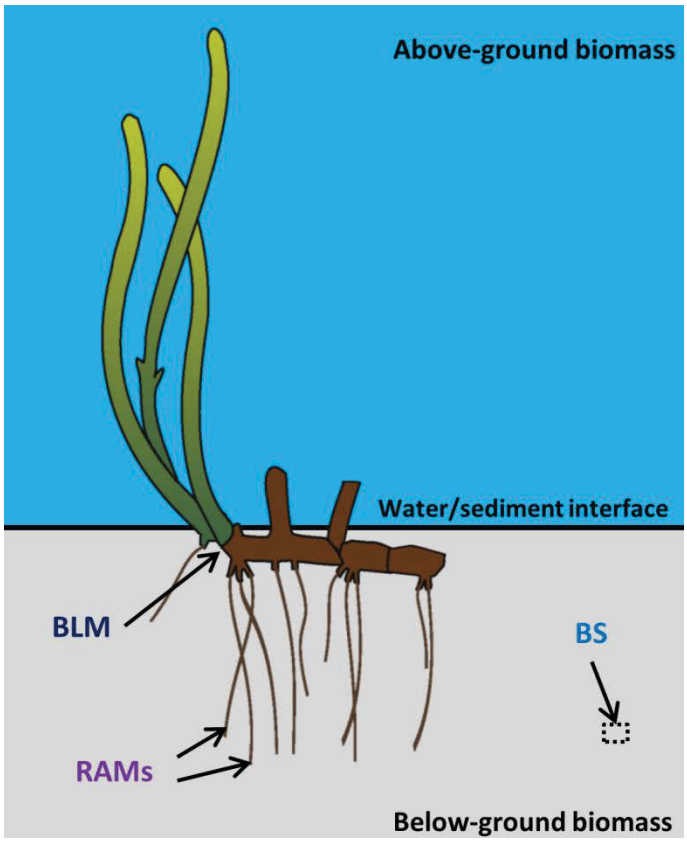

Figure S5.5. Conceptual diagram visualizing sampling areas within the reduced, artificial sediment.

TABLE S5.1.

Pulse Amplitude Modulated (PAM) variable chlorophyll fluorescence measurements determining the maximum quantum yield of photosystem II (PSII) (F_v/F_m) and the effective quantum yield of PSII ($\Delta F/F_m'$) were recorded after ~72h and ~168h, to ensure that the investigated seagrass (*Zostera muelleri*) specimens were photosynthetic compatible and healthy during cultivation. Measurements were performed with a hand-held PocketPAM equipped with an optical fiber (PAM settings: saturating intensity 8, saturation width 0.6 s, F>100) to ensure no damage was caused to the leave surfaces during measurements, at the expense of slightly lower signal recordings. The PSII effective quantum yield gives an estimate of the photosynthetic activity at the given incident photon irradiance (~150 µmol photons m^{-2} s^{-1}) and thus can be used as a general indicator of the health status of the seagrasses in question (e.g. Beer et al. 1998).

Table S5.1. Photosynthetic capability and below-ground tissue oxidation capacity based on PAM measurements and above- to below-ground biomass ratio, respectively, of all investigated *Zostera muelleri* specimens.

	PAM measurements		**Above-ground:Below-ground biomass ratio**
	Max. QY	**Eff. QY**	
Pore-water			
plant 1	0.70±0.02	0.47±0.02	0.99
plant 2	0.66±0.01	0.54±0.02	0.59
plant 3	0.76±0.04	0.59±0.05	1.77
Sterilized			
plant 1	0.65±0.01	0.53±0.03	0.88
plant 2	0.70±0.01	0.56±0.02	1.13

n=3-7; Incident photon irradiance = 150 µmol photons m^{-2} s^{-1}; Temp = 22 °C; Sal = 34 ppt; Flow velocity = 0.5 cm s^{-1}; Maximum quantum yield of PSII (max) = F_v/F_m; Effective quantum yield of PSII (eff) = $\Delta F/F_m'$; f > 100.

TABLE S5.2.

Calculated O_2 and H_2S fluxes within the immediate rhizosphere of *Zostera muelleri* to elucidate potential symbiotic relationships between the plant host and sulphide oxidizing bacteria (SOB). Bacteria-mediated H_2S oxidation is 10.000-100.000 times faster than spontaneous chemical oxidation (e.g. via plant-derived radial O_2 loss) (Jørgensen & Revsbech, 1983; Nelson et al. 1986) and would therefore have pronounced positive effects on the H_2S re-oxidation rates, which was not the case in the present study. This suggests that plant-derived spontaneous chemical H_2S re-oxidation is the predominant H_2S oxidation mechanism in the immediate rhizosphere of seagrasses.

The ratio between the O_2 and total sulphide fluxes, i.e., the amount of O_2 molecules released from the below-ground tissue compared to the total amount of sulphide (H_2S, HS^- and S^{2-}) oxidized at the basal leaf meristem in the artificial sediment, were 0.6 in darkness and 1.7 in light in both treatments. Thus indicating incomplete H_2S oxidation to elemental sulphur (S) in the dark and complete H_2S re-oxidation to sulphuric acid (H_2SO_4) in the light; and/or higher microbial O_2 consumptions rates and chemical oxidation of other reduced compounds, such as Fe^{2+}, within the rhizosphere in the light.

Table S5.2. Radial O_2 loss (ROL), plant-derived H_2S re-oxidation/sediment detoxification and ΔpH in the immediate rhizosphere of *Z. muelleri*.

	ROL nmol O_2 cm^{-2} h^{-1}	H_2S re-oxidation nmol H_2S cm^{-2} h^{-1}	ΔpH pH units
pore water			
dark	-322 ± 39	334 ± 1	2.1 ± 0.4[a]
light	-745 ± 118	418 ± 4	2.4 ± 0.2
sterilized			
dark	-378 ± 3	636 ± 136[a]	2.5 ± 0.1
light	-891 ± 52	508 ± 33	2.5 ± 0.2

n = 2-3, biological replication. Values are mean ± S.E.M. *Pore water* indicate artificial sediment matrix with added pore water microbes. *Sterilized* indicate a sterilized below-ground environment, i.e., sterilized sediment and below-ground biomass.
[a]Note relative high standard error of the mean (S.E.M.).

REFERENCE LIST

Altschul SF, Gish W, Miller W, Myers EW, Lipman DJ. (1990). Basic local alignment search tool. *Journal of molecular biology* **215**: 403-410.

Amann RI, Krumholz L, Stahl DA. (1990). Fluorescent-oligonucleotide probing of whole cells for determinative, phylogenetic, and environmental studies in microbiology. *Journal of bacteriology* **172**: 762-770.

Beer S, Vilenkin B, Weil A, Veste M, Susel L, Eshel A. (1998). Measuring photosynthetic rates in seagrasses by pulse amplitude modulated (PAM) fluorometry. *Marine Ecology Progress Series* **174**: 293-300.

Blaabjerg V, Finster K. (1998). Sulphate reduction associated with roots and rhizomes of the marine macrophyte *Zostera marina*. *Aquatic Microbial Ecology* **15**(3): 311-314.

Brodersen KE, Nielsen DA, Ralph PJ, Kühl M. (2014). A split flow chamber with artificial sediment to examine the below-ground microenvironment of aquatic macrophytes. *Marine Biology* **161**(12): 2921-2930.

Brodersen KE, Lichtenberg M, Paz L-C, Kühl M. (2015a). Epiphyte-cover on seagrass (*Zostera marina* L.) leaves impedes plant performance and radial O_2 loss from the below-ground tissue. *Frontiers in Marine Science* **2**: 58.

Caporaso JG, Kuczynski J, Stombaugh J, Bittinger K, Bushman FD, Costello EK, Fierer N, Pena AG, Goodrich JK, Gordon JI, Huttley GA, Kelley ST, Knights D, Koenig JE, Ley RE, Lozupone CA, McDonald D, Muegge BD, Pirrung M, Reeder J, Sevinsky JR, Turnbaugh PJ, Walters WA, Widmann J, Yatsunenko T, Zaneveld J, Knight R. (2010). QIIME allows analysis of high-throughput community sequencing data. *Nature Methods* **7:** 335-336.

Frederiksen MS, Glud RN. (2006). Oxygen dynamics in the rhizosphere of *Zostera marina*: A two-dimensional planar optode study. *Limnology and Oceanography* **51**(2): 1072-1083.

Frederiksen MS, Holmer M, Borum J, Kennedy H. (2006). Temporal and spatial variation of sulfide invasion in eelgrass (*Zostera marina*) as reflected by its sulfur isotopic composition. *Limnology and Oceanography* **51**(5): 2308-2318.

Haas BJ, Gevers D, Earl AM, Feldgarden M, Ward DV, Giannoukos G, Ciulla D, Tabbaa D, Highlander SK, Sodergren E. (2011). Chimeric 16S rRNA sequence formation and detection in Sanger and 454-pyrosequenced PCR amplicons. *Genome research* **21**: 494-504.

Jørgensen BB, Revsbech NP. (1983). Colorless sulfur bacteria, *Beggiatoa* spp. & *Thiovulum* spp., in O_2 and H_2S microgradients. *Applied and Environmental Microbiology* **45**: 1261-1270.

Kuczynski J, Stombaugh J, Walters WA, González A, Caporaso JG, Knight R. (2012). Using QIIME to analyze 16S rRNA gene sequences from microbial communities. *Current protocols in microbiology***,** 1E. 5.1-1E. 5.20.

Kühl M, Revsbech NP. (2001). Biogeochemical microsensors for boundary layer studies. In: Boudreau BP, Jorgensen BB eds. *The benthic boundary layer*. New York: Oxford University Press, New York, 180-210.

Kühl M, Steuckart C, Eickert G, Jeroschewski P. (1998). A H_2S microsensor for profiling sediments and biofilms: Application in acidic sediment. *Aquatic Microbial Ecology* **15**: 201-209.

Lane D. (1991). 16S/23S rRNA sequencing. In: Stackebrandt E & Goodfellow M., eds. *Nucleic acid techniques in bacterial systematics*. New York, NY: John Wiley and Sons: 125-175.

Lindahl V, Bakken LR. (1995). Evaluation of methods for extraction of bacteria from soil. *FEMS Microbiology Ecology* **16**(2): 135-142.

Nelson DC, Jørgensen BB, Revsbech NP. (1986). Growth pattern and yield of a chemoautotrophic *Beggiatoa sp.* in oxygen-sulfide microgradients. *Applied and Environmental Microbiology* **52**(2): 225-233.

Ramsay AJ. (1984). Extraction of bacteria from soil: efficiency of shaking or ultrasonication as indicated by direct counts and autoradiography. *Soil biology and biochemistry* **16**(5): 475-481.

Revsbech NP. (1989). An oxygen microsensor with a guard cathode. *Limnology and Oceanography* **34**(2): 474-478.

Steen-Knudsen O. (2002). *Biological membranes: Theory of Transport, Potentials and Electric Impulses*. Cambridge: Cambridge University Press.

Turner S, Pryer K, Miao V, Palmer J. (1999). Investigating deep phylogenetic relationships among cyanobacteria and plastids by small subunit rRNA sequence analysis. *Journal of Eukaryotic Microbiology* **46**: 327-338.

Weinbauer MG, Fritz I, Wenderoth DF, Höfle MG. (2002). Simultaneous extraction from bacterioplankton of total RNA and DNA suitable for quantitative structure and function analyses. *Applied and Environmental Microbiology* **68**(3): 1082-1087.

Zhou J, Bruns MA, Tiedje JM. (1996). DNA recovery from soils of diverse composition. *Applied and Environmental Microbiology* **62**: 316-322.

Chapter 6

Epiphyte-cover on seagrass (*Zostera marina* L.) leaves impedes plant performance and radial O_2 loss from the below-ground tissue.

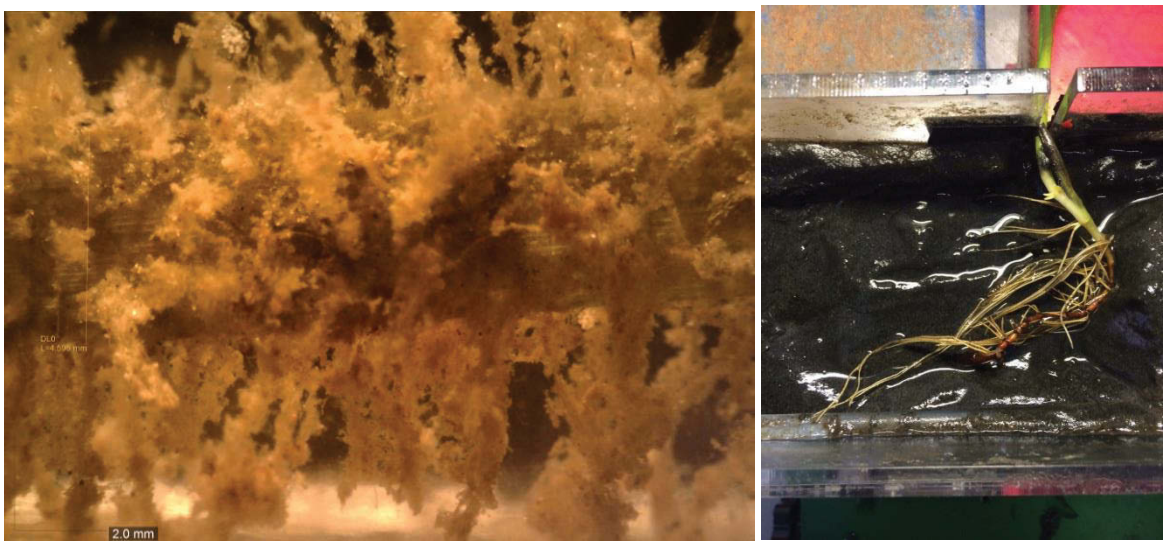

TOC figure. *Left panel show a seagrass leaf with filamentous algal epiphyte overgrowth. Right panel shows the below-ground tissue of one of the investigated seagrass specimens cultured in natural, homogenized sediment from the sampling site. The roots have been exposed to allow positioning of the O_2 sensitive microsensor at the root tissue surface.*

Citation: Brodersen KE, Lichtenberg M, Paz LC. & Kühl M. (2015). Epiphyte-cover on seagrass (*Zostera marina* L.) leaves impedes plant performance and radial O_2 loss from the below-ground tissue. *Frontiers in Marine Science* **2**:58.

Highlights: This study investigated the effects of epiphyte overgrowth on seagrass leaves on (i) the overall plant performance, (ii) the light availability and quality at the leaf surface and (iii) how this affects the rhizosphere oxidation capacity of the below-ground tissue in the temperate seagrass *Zostera marina* L. Our study gives novel insight into the negative effects of leaf epiphyte overgrowth on the fitness and resistance capabilities of seagrasses to environmental disturbance/anthropogenic stressors.

Epiphyte-cover on seagrass (*Zostera marina L.*) leaves impedes plant performance and radial O_2 loss from the below-ground tissue

Kasper Elgetti Brodersen[1,a,b], Mads Lichtenberg[2,a], Laura-Carlota Paz[3], Michael Kühl[1,2]

[1]Plant Functional Biology and Climate Change Cluster, University of Technology, Sydney, 15 Broadway, Ultimo, Sydney, NSW 2007, Australia

[2]Marine Biological Section, Department of Biology, University of Copenhagen, Strandpromenaden 5, DK-3000 Helsingør, Denmark

[3]Department of Bioscience - Microbiology, Aarhus University, Ny Munkegade 116, DK-8000 Aarhus C, Denmark

[a] These authors contributed equally to this work.

[b] Corresponding author, e-mail: kasper.e.brodersen@student.uts.edu.au and phone: +61 414 954 017

ABSTRACT

The O_2 budget of seagrasses is regulated by a complex interaction between several sources and sinks, which is strongly regulated by light availability and mass transfer over the diffusive boundary layer (DBL) surrounding the plant. Epiphyte growth on leaves may thus strongly affect the O_2 availability of the seagrass plant and its capability to aerate its rhizosphere as a defence against plant toxins.

We used electrochemical and fiber-optic microsensors to quantify the O_2 flux, DBL and light microclimate around leaves with and without filamentous algal epiphytes. We also quantified the below-ground radial O_2 loss from roots (~1 mm from the root-apex) to elucidate how this below-ground oxic microzone was affected by the presence of epiphytes.

Epiphyte-cover on seagrass leaves (~21% areal cover) resulted in reduced light quality and quantity for photosynthesis, thus leading to reduced plant fitness. A ~4 times thicker diffusive boundary layer around leaves with epiphyte-cover impeded gas (and nutrient) exchange with the surrounding water-column and thus the amount of O_2 passively diffusing down to the below-ground tissue through the aerenchyma in darkness. During light exposure of the leaves, radial oxygen loss from the below-ground tissue was ~2 times higher from plants without epiphyte-cover. In contrast, no O_2 was detectable at the surface of the root-cap tissue of plants with epiphyte-cover during darkness, leaving the plants more susceptible to sulphide intrusion.

Epiphyte growth on seagrass leaves thus has a negative effect on the light climate during daytime and O_2 supply in darkness, hampering the plants performance and thereby reducing the oxidation capability of its below-ground tissue.

Keywords: epiphyte-cover, light, diffusive boundary layer, radial O_2 loss, oxic microshield, microenvironment

INTRODUCTION

Seagrasses are angiosperms that form coastal habitats of prime importance for marine biodiversity and carbon sequestration (Duarte, 2001; Duarte et al., 2005). Over the past century, seagrasses have faced an alarming global decline, owing to both direct and indirect human interference (Robblee et al., 1991; Zieman et al., 1999; Seddon et al., 2000; Plus et al., 2003; Orth et al., 2006). Seagrasses inhabit organic rich, reduced sediments and the exposure of their below-ground biomass to sediment-derived hydrogen sulphide (H_2S), as a result of inadequate internal aeration due to low water-column O_2 levels during darkness, has been identified as a key factor in seagrass die-back events (Greve et al., 2003; Borum et al., 2005; Brodersen et al., 2015). Hydrogen sulphide is produced in reduced sediment through bacterial sulphate reduction, which is considered the quantitatively most important anaerobic degradation process in coastal marine sediment (Jørgensen, 1982). H_2S is a phytotoxin that leads to chemical asphyxiation, due to a strong chemical binding with cytochrome *c* in the mitochondrial electron transport chain (Eghbal et al., 2004; Perez-Perez et al., 2012; Lamers et al., 2013). If H_2S reaches the root tissue surface it may enter the lacunar system of the seagrass plant via lipid-solution permeation of the plasmalemma (Raven and Scrimgeour, 1997). Such H_2S intrusion into the below-ground tissue of seagrasses has mainly been related to inadequate internal aeration during night-time, as a result of a low water-column O_2 content and thus a decrease in the diffusive O_2 supply from the surrounding water-column (Pedersen et al., 2004; Borum et al., 2005). The amount of O_2 passively diffusing into the leaves from the water-column during darkness, is thus highly dependent on the water-column O_2 content, but is also strongly affected by other factors such as the diffusive boundary layer (DBL) thickness (Binzer et al., 2005; Borum et al., 2006) and the leaf surface area. The DBL surrounds all aquatic surfaces, such as seagrass leaves, and functions as a diffusive barrier to the exchange of gasses and nutrients with the surrounding water-column by impeding water motions towards the leaf tissue surface (Jørgensen and Revsbech, 1985). The width and thus the mass transfer impedance of the DBL depends on factors such as the surface topography and the flow velocity, where e.g. relative low flow rates and uneven surfaces increases the thickness of the DBL (Jørgensen and Des Marais, 1990); both parameters are highly affected by epiphyte growth on the leaf surface.

Light availability is the key environmental factor regulating photosynthesis and thus the O_2 supply during day-time, and small decreases in irradiance can cause significant declines in the growth and distribution of seagrasses (Burkholder et al., 2007; Ralph et al., 2007). In eutrophic coastal waters, light can be attenuated up to 100-fold in the upper 1-4 m of the water column, often with dramatic changes in the spectral composition (Sand-Jensen & Borum, 1991). Therefore, rooted macrophytes are often spatially limited to biotopes with sufficient light exposure, i.e., water depths experiencing a minimum of 10% of surface irradiance for temperate seagrasses (Borum, 1983; Duarte, 1991). Eutrophication can stimulate epiphyte colonization on seagrass leaves (Richardson, 2006) potentially affecting the light availability for the plant. Epiphytes may thus have a major impact on the photosynthetic O_2 evolution of rooted macrophytes, such as seagrasses (Sand-Jensen, 1977).

The O_2 budget of seagrass plants is regulated by a complex interaction between several sources and sinks. Sources encompass photosynthetic O_2 evolution in leaves during day-time and passive diffusion of O_2 into the leaves from the water-column in darkness. Sinks encompass the total O_2 demand of the surrounding sediment, including bacterial respiration and chemical reactions with reduced compounds, as well as the plants own respiratory needs. The amount of O_2 produced or passively diffusing into the leaves is affected by external physical factors such as the light availability for underwater photosynthesis, the flow-dependent thickness of the DBL and the water-column O_2 content, whereas the sinks are highly affected by elevated seawater temperatures and the quantity of accessible organic matter in the rhizosphere (Pedersen et al., 2004; Binzer et al., 2005; Borum et al., 2006; Raun and Borum, 2013).

The O_2 is transported from the above-ground tissue to the below-ground tissue through the aerenchyma, i.e., an internal gas-filled lacunar system, whereby the plants supports aerobic metabolism in their root-system and provide protection against reduced toxic compounds such as H_2S and Fe^{2+} (Armstrong, 1979; Borum et al., 2006). Some of the transported O_2 is leaked to the rhizosphere as the so-called radial oxygen loss (ROL), especially at the basal meristems, root-shoot junctions and root-caps (Koren et al., 2015). During non-stressful environmental conditions, ROL maintains a ~0.5 mm wide oxic microzone around the leaking areas that continuously oxidizes the surrounding sediment and thus alters the immediate sediment biogeochemistry in the seagrass rhizosphere (Pedersen et al., 1998;

Jensen et al., 2005; Brodersen et al., 2015). This chemical defence mechanism is, however, negatively affected by over-night water-column hypoxia (Brodersen et al., 2015).

Seagrass morphology is an important controlling factor affecting the likelihood of H_2S intrusion into seagrasses, where a higher above- to below-ground biomass ratio positively affects the seagrasses oxidation capacity and reduces the risk of H_2S intrusion (Frederiksen et al., 2006). Seagrass roots possess structural barriers to ROL in mature root tissue regions such as Casparian band-like structures of suberin in the hypodermis (Barnabas, 1996). Such barriers to ROL in the basal-parts of seagrass roots increases the intra-plant O_2 transport to the active apical root meristem and therefore are very important for seagrass root metabolism.

In this study we used electrochemical and fiber-optic microsensors to investigate effects of epiphyte-cover on seagrass leaves on the below-ground aeration of the rhizosphere of the seagrass *Zostera marina* kept in a custom-made split flow-chamber with natural sediment. This microenvironmental approach allowed us to i) analyse the DBL and light microclimate around seagrass leaves with- and without epiphytes, and ii) correlate changes in these above-ground microenvironmental parameters with changes in the ROL from the root-caps, and thereby, the oxidation capacity of the below-ground tissue.

MATERIALS AND METHODS

Seagrass and sediment sampling

Marine sediment and *Zostera marina* specimens with and without leaf epiphyte-cover were collected from shallow coastal waters (<2 m depth) at Aggersund, Limfjorden, Denmark. After sampling, plants and sediment were transported to a nearby field station (Rønbjerg Marine Biological Station, Aarhus University, Denmark), where they were kept in constantly aerated and water flushed water reservoirs prior to experiments. Seagrass specimens with similar above- and below-ground biomass ratios were selected from the reservoirs and gently washed free of adhering sediment before transferred to the experimental split flow-chamber (see below; Brodersen et al., 2014). In the following, seagrasses with epiphyte-cover refer to plants with ~21% areal cover with filamentous algal epiphytes on leaves in

contrast to seagrasses without visible leaf epiphyte-cover. The above- to below-ground biomass ratio was 1.0 and 0.8 of selected plants with and without leaf epiphyte-cover, respectively, based on g DW values obtained after drying the plants in an oven at 60ºC until a constant weight was reached.

Experimental setup

Plants were horizontally positioned in the flow-chamber (one plant at a time) with the leaf canopy in the free flowing water phase compartment and the below-ground biomass transplanted in homogenized sediment from the sampling site in the adjoining "sediment" compartment (Figure 6.1). An anoxic water column (~2 cm depth) functioned as a liquid-phase diffusion barrier to O_2 intrusion over the sediment compartment of the flow chamber, as preliminary studies had shown a constant loss/efflux of reduced compounds such as H_2S from the sediment during cultivation. Illumination of the leaf canopy was provided by a fiber-optic tungsten halogen lamp (KL-2500LCD, Schott GmbH, Germany). The downwelling photon irradiance (PAR, 400-700 nm) at the leaf surface was measured with a spherical quantum sensor (US-SQS/L, Walz GmbH, Germany) connected to a calibrated quantum irradiance meter (ULM-500, Walz GmbH, Germany). A constant flow-rate (~0.5 cm s^{-1}) of aerated seawater (~22°C, Salinity=30) was maintained in the seawater compartment of the flow chamber by means of a pump submersed in an aerated seawater reservoir (Figure 6.1).

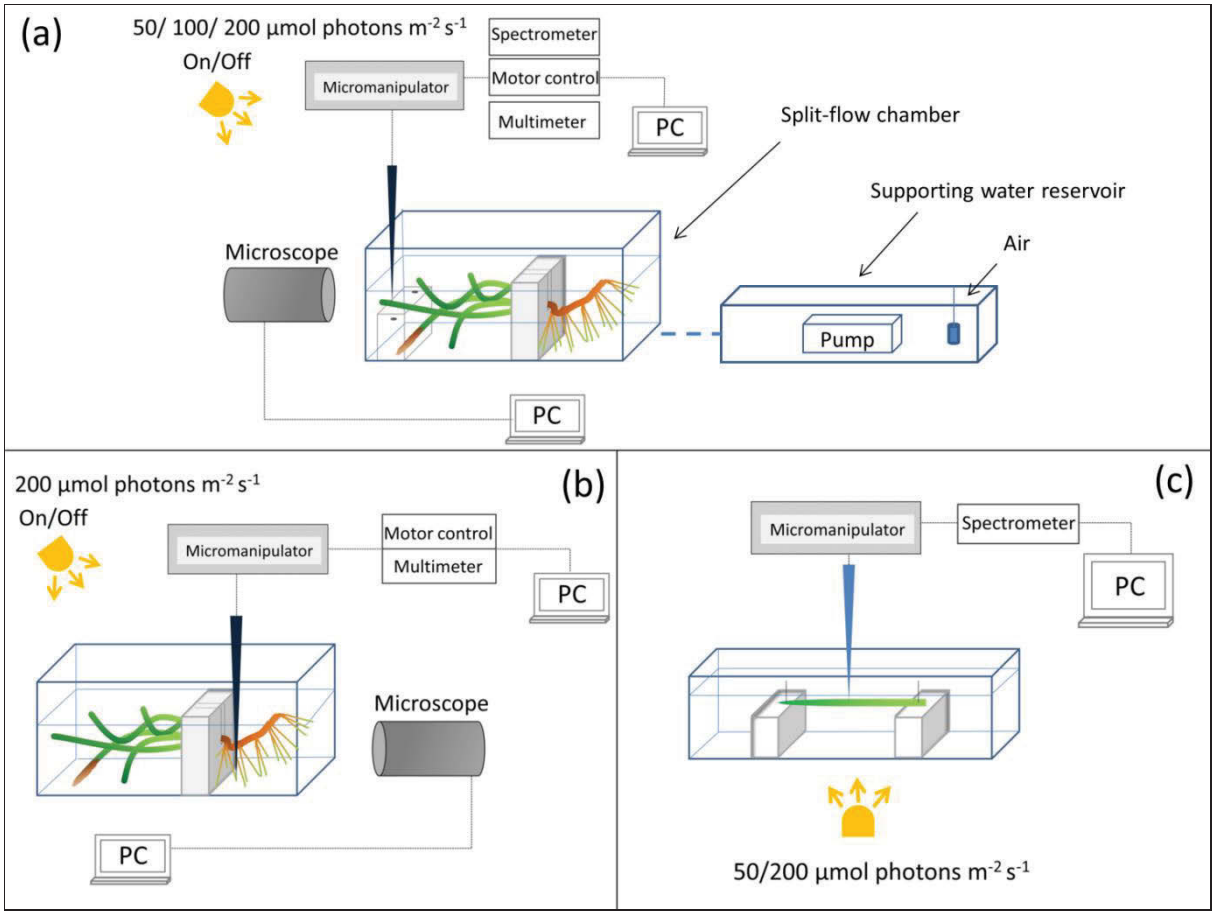

Figure 6.1. Schematic diagram of the experimental setups. (a) Above-ground light and O_2 microsensor measurements. (b) Measurements on the below-ground chemical microenvironment with Clark-type O_2 microsensors. (c) Measuring light transmission spectra at the seagrass leaf surface.

Light and O_2 measurements

We used scalar irradiance microprobes (sphere diameter 50 µm; manufactured by a modified procedure of Lassen et al., 1992; Rickelt et al., submitted) to quantify the light microenvironment around leaves of *Z. marina* with- and without epiphyte cover under two different irradiance levels (50 and 200 µmol photons m^{-2} s^{-1}; Figure 6.1a). The scalar irradiance microprobe was connected to a fiber-optic spectrometer (USB 2000+, Ocean Optics, USA), interfaced to a PC running spectral acquisition software (SpectraSuite, Ocean Optics, USA). We measured vertical profiles of spectral scalar irradiance in 0.1 mm steps from the leaf surface to 1 mm above the leaf surface, and in 1 mm steps from 1-10 mm from the leaf surface. To quantify the downwelling irradiance, we recorded spectra of the

vertically incident light with the scalar irradiance microprobe tip positioned over a black non-reflective light well at the same position and distance in the light beam as the seagrass tissue surface; in a collimated light field the downwelling- and scalar irradiance are identical (Kühl and Jørgensen, 1994).

Clark-type O_2 microsensors (OX-10 and OX-50, Unisense A/S, Aarhus, Denmark; Revsbech, 1989) with a fast response time (<0.5 s) and low stirring sensitivity (<2-3 %) were used to measure i) the radial O_2 loss from the below-ground biomass of *Z. marina* (~1 mm from the root-apex; Figure 6.1b), and ii) the O_2 concentration at and towards the leaf surface (Figure 6.1a). The O_2 microsensors were linearly calibrated from signal readings in 100% air saturated seawater and anoxic seawater (by addition of ascorbate) at experimental temperature and salinity; prior to calibrations and measurements in natural sediment, the microsensors were pre-contaminated with sulphide, i.e., they were pre-polarized in a Na_2S solution, to avoid drifting calibrations during experiments.

Microsensors were mounted on a motorized micromanipulator (Unisense A/S, Denmark) and connected to a PC-interfaced microsensor multimeter (Unisense A/S, Denmark); both were controlled by dedicated data acquisition and positioning software (SensorTrace Pro, Unisense A/S, Denmark). Microsensors and microprobes were carefully positioned at the tissue surface (defined as 0 µm) by manual operation of the micromanipulator, while observing the microsensor tip and tissue surface through a USB microscope (AD7013MZT, DinoLite, AnMo Electronics Corp., Taiwan). When positioning the O_2 microsensors at the below-ground tissue surface, a root from the first root-bundle was first gently un-covered from sediment before manually moving the microsensor to the surface of the root-cap, where after the root was gently covered again with sediment. Steady state O_2 levels at the below-ground tissue surface were re-established after ~3h (data not shown). Microprofiles of O_2 concentration were measured in depth increments of 50 µm.

Light calculations

To quantify PAR, we integrated the measured scalar irradiance spectra over 400-700 nm and calculated the fractions of incident PAR irradiance for each measured depth position. By

multiplying with the known incident quantum irradiance (in µmol photons m^{-2} s^{-1}), measured with a calibrated quantum irradiance meter (ULM-500, Walz GmbH, Germany) equipped with a spherical quantum sensor (US-SQS/L, Walz GmbH, Germany), absolute levels of light in each depth could be calculated as:

$$E(PAR)_z = \left(\frac{A_z}{A_D}\right) E_d$$

where $E(PAR)_z$ is the PAR photon irradiance in depth z, A_z is the wavelength integrated signal in depth z, A_D is the wavelength integrated downwelling irradiance, and E_d is the downwelling photon irradiance (in µmol photons m^{-2} s^{-1}).

Since the leaves of *Z. marina* were ~50 µm thick, it was not possible to measure internal light gradients in the leaves with microprobes. Instead we measured the spectral attenuation of light through leaves with and without epiphyte cover. A leaf, with- or without epiphytes, was positioned in a transparent acrylate chamber illuminated from below and with the incident irradiance determined as above (Figure 6.1c). Concomitantly, the microprobe was positioned at the abaxial surface of the leaf and the transmitted spectra were recorded on leaves with- and without epiphytes.

Flux calculations

The O_2 flux between the leaf surface and the surrounding seawater was calculated using Fick's first law of diffusion:

$$J_{O_2} = -D_0 \frac{\partial C}{\partial z}$$

where D_0 is the molecular diffusion coefficient of O_2 in seawater at experimental temperature and salinity ($2.0845 \cdot 10^{-5}$ cm^{-2} s^{-1}; tabulated values available at www.unisense.com), and $\frac{\partial C}{\partial z}$ is the slope of the linear O_2 concentration gradient within the diffusive boundary layer.

A cylindrical version of Fick's first law of diffusion, described by Steen-Knudsen (2002), was used to calculate the radial O_2 loss from the below-ground tissue surface (assuming a homogenous and cylinder-shaped O_2 loss from the roots):

$$J(r)_{root-cap} = \varphi D_0(C_1 - C_2)/rln(\frac{r_1}{r_2})$$

where ϕ is the porosity of the sediment and ϕD_0 estimates the diffusivity of O_2 within the sediment at experimental temperature and salinity, *r* is the radius of the root, and C_1 and C_2 are the O_2 concentrations measured at the radial distances r_1 and r_2, respectively. Porosity was determined from the weight loss of wet sediment from the sampling site (known initial volume and weight) after drying at 60°C until a constant weight was reached (Porosity=0.51).

Statistical procedures

Data were tested for normality (Shapiro-Wilk) and equal variance prior to statistical analysis. Student's *t*-tests were used to compare treatments (with- or without leaf epiphytes) on data that met the above-mentioned assumptions. Mann-Whitney Rank Sum tests were used on data lacking normality and/or equal variance. A two-way ANOVA was performed to examine the influence of leaf epiphyte-cover and incident irradiance on O_2 fluxes across the leaf tissue surface (Table S6.1). Analysis of covariance (ANCOVA) was used to examine the effect of leaf epiphytes on scalar irradiance with distance from the leaf surface as a covariant. The significance level was set to $p < 0.05$. Statistical tests were performed in SigmaPlot and SPSS.

RESULTS

Light climate

Our observations on the light microclimate around the leaves of *Z. marina* revealed that epiphyte cover affect the quantity and quality of light reaching the seagrass leaf. In the presence of epiphytes, scalar irradiance (PAR, 400-700 nm) on the surface of seagrass leaves was reduced by 54% and 92% under a downwelling irradiance of 50 and 200 µmol photons m^{-2} s^{-1} respectively (Figure 6.2). Without epiphytes, we observed a 3% and 4% increase in

scalar irradiance at incident irradiance levels of 50 and 200 µmol photons m^{-2} s^{-1}, respectively. Analysis of covariance (ANCOVA) confirmed significant difference in the scalar irradiance at the leaf tissue surface of plants with leaf epiphyte cover as compared to plants without leaf epiphyte cover ($p < 0.01$), as well as between scalar irradiance measured at z = 10 mm and z = 0 mm for plants with leaf epiphyte cover ($p < 0.01$). No significant difference was found between scalar irradiance measured at z = 10 mm and z = 0 mm for plants without leaf epiphyte cover ($p > 0.05$).

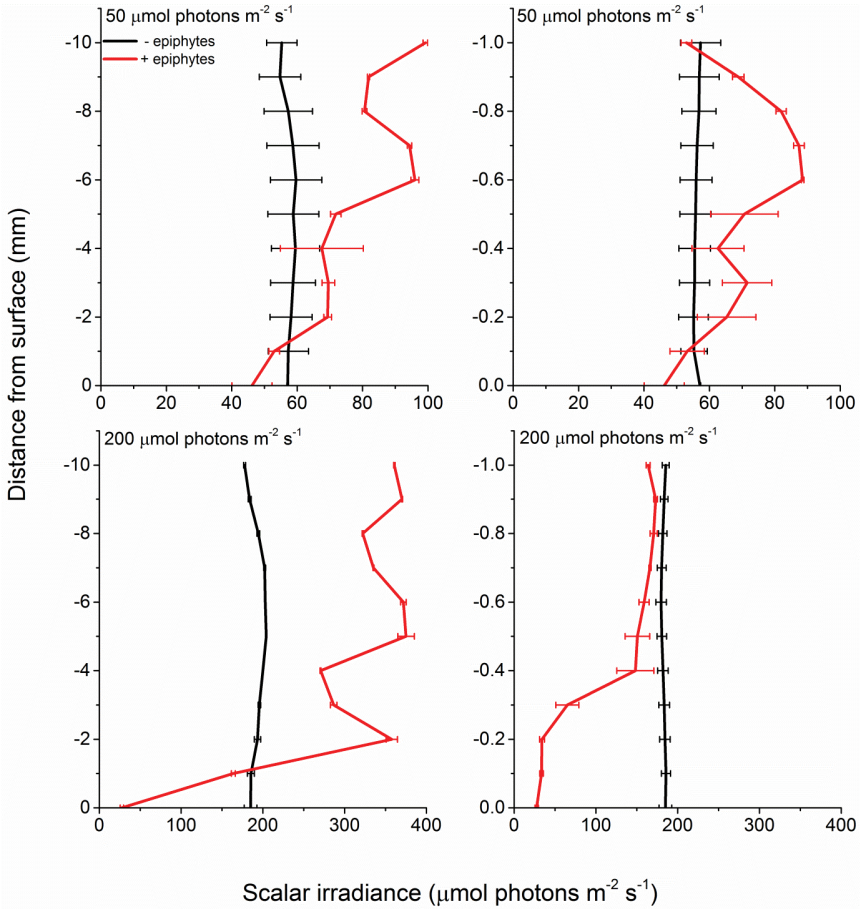

Figure 6.2. Profiles of photon scalar irradiance measured at two different downwelling photon irradiances (50- and 200 µmol photons m^{-2} s^{-1}) on *Z. marina* leaves with- and without epiphyte cover. Left panels show the scalar irradiance 0-10 mm from the leaf surface measured in 1 mm steps. Right panels show the scalar irradiance 0-1 mm from the leaf surface measured in 0.1 mm steps (enlarged plots of the scalar irradiance showed in the left panels). Data points represents means ± S.D. n=3; leaf level replicates.

The decrease in scalar irradiance in the upper canopy (1-10 mm above the leaf surface) was uniform across wavelengths in the PAR region while a spectral shift became evident in the lower canopy (0-1 mm above the leaf surface) with blue light and light around 675 nm being absorbed preferentially (Figure 6.3). However, approaching the surface of the seagrass leaf we also observed an enhanced absorption around 625 nm indicative of phycocyanin found in cyanobacteria.

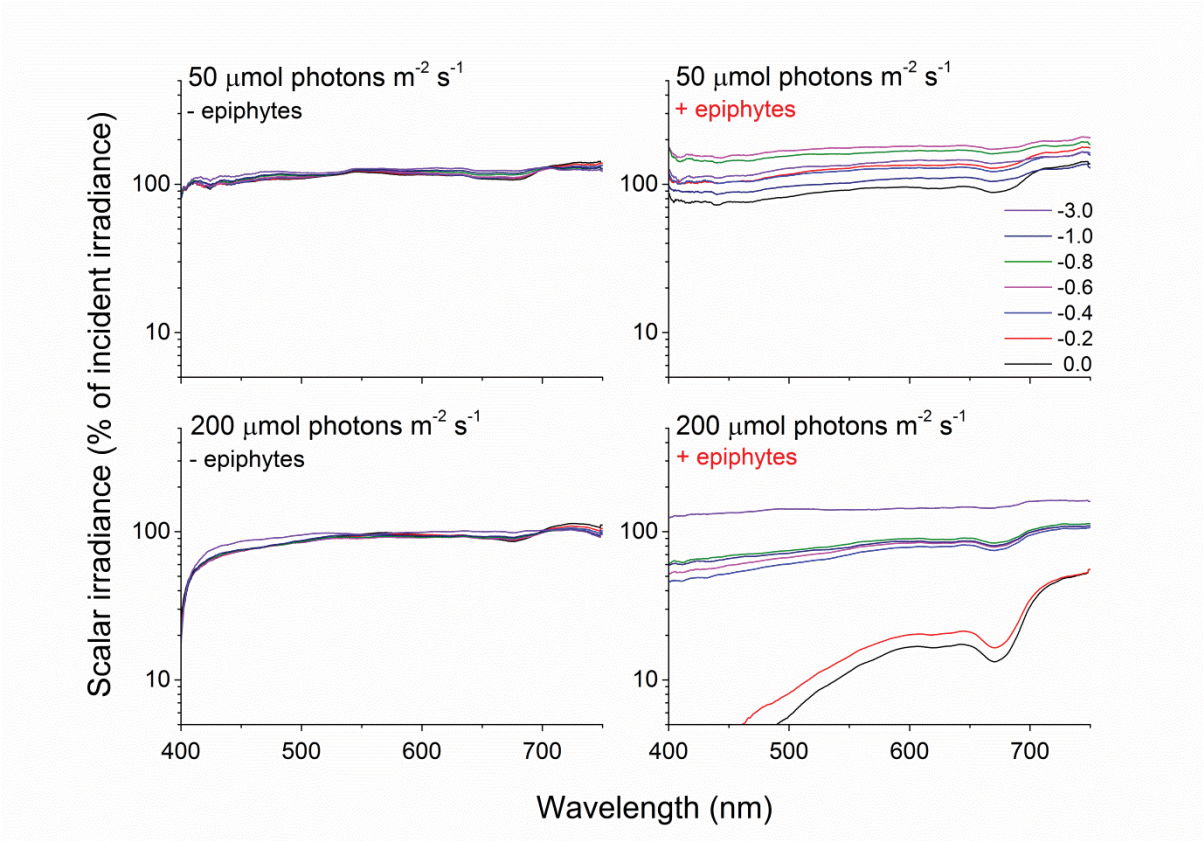

Figure 6.3. Spectral scalar irradiance measured over *Z. marina* leaves under an incident irradiance of 50 and 200 μmol photons m^{-2} s^{-1} with- (right panels) and without epiphytes (left panels). Coloured lines represents spectra collected at the given depths in mm above the leaf surface expressed as % of incident irradiance on a log-scale. n=3; leaf level replicates.

This was further clarified in the seagrass light transmission spectra (Figure 6.4) where, in the absence of epiphytes, mainly actinic light and light around 675 nm were absorbed, corresponding to the absorption spectrum of Chl *a*. In the presence of epiphytes there was a profound decrease in all wavelengths in the PAR region leading to a reduction in the

transmitted light with 71 and 88% (downwelling irradiance of 50 and 200 µmol photons m^{-2} s^{-1} respectively). Students t-tests performed at 425nm, 560nm and 675nm (except at 425nm under an incident irradiance of 50 µmol photons m^{-2} s^{-1}, where a Mann-Whitney test was preformed due to data lacking normality; $p < 0.05$) confirmed significant difference in the transmitted light spectra between plants with leaf epiphyte cover and plants without leaf epiphyte cover ($p < 0.01$). In addition there was a relatively larger absorption of green light in the presence of epiphytes, evident from a change in the ratio of wavelengths 560nm:675nm from 6 without epiphytes to 3 with epiphytes suggesting absorption from accessory epiphyte pigments.

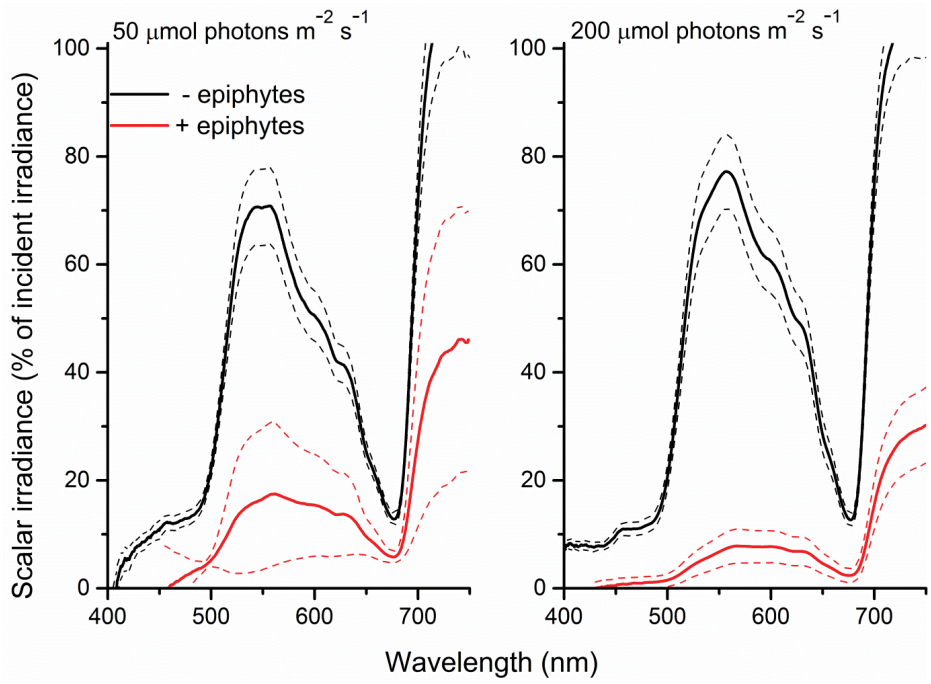

Figure 6.4. Spectra of photon scalar irradiance transmitted through *Z. marina* leaves with- (red line) and without (black line) epiphyte cover and at two different downwelling irradiances (50- and 200 µmol photons m^{-2} s^{-1}). Dashed lines represents ± S.D. n=4; leaf level replicates.

Diffusive boundary layer and photosynthesis

The O_2 concentration microprofiles at the *Z. marina* leaf tissue surface revealed a ~4 times thicker diffusive boundary layer (DBL) around leaves with epiphyte-cover as compared to leaves without epiphyte-cover, i.e., an increase in the DBL thickness from ~350 to 1400 µm (Figure 6.5). During darkness, passive diffusion of O_2 from the surrounding water-column

resulted in a constant influx of O_2 into leaves both with and without epiphyte-cover, supporting the below-ground tissue with O_2 (Figure 6.5; Table 6.1). However, the thick DBL around leaves with epiphyte-cover impeded the diffusive O_2 supply in darkness as compared to plants without epiphyte-cover (seen as a reduction in the seagrass leaf surface O_2 concentration from ~198 to 51 µmol L^{-1} (Student's t-test, $p < 0.001$); Figure 6.5), leaving these plants more vulnerable to low water-column O_2 contents at night-time.

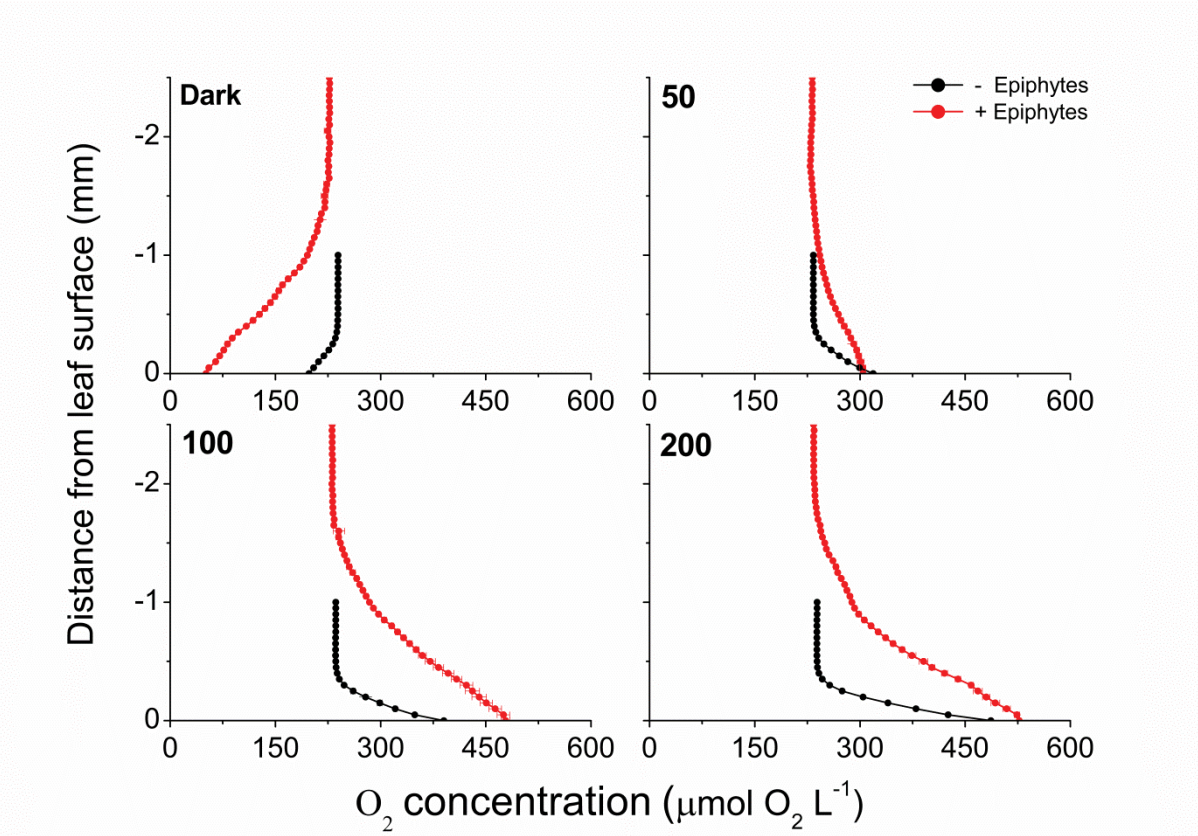

Figure 6.5. Vertical microprofiles of the O_2 concentration measured towards the leaf surface under 4 different incident irradiances (0, 50, 100 and 200 µmol photons m^{-2} s^{-1}). Red symbols and lines represent leaves with 21% epiphyte-cover, Black symbols and lines represent leaves without epiphyte-cover. y = 0 indicates the leaf surface. Symbols and errors bars represent means ± SD. n = 3-4; leaf level replicates.

Net O_2 production increased with increasing irradiance, as a result of enhanced shoot photosynthesis (Figure 6.5). The lower light availability for plants with epiphyte-cover resulted in relatively lower net photosynthesis rates, and the compensation irradiance increased from ~12 to 27 µmol photons m^{-2} s^{-1} for plants with epiphyte-cover (Figure 6.6;

Table 6.1). Despite the lower net photosynthesis in plants with leaf epiphyte-cover, there was a higher build-up of O_2 on the tissue surface under moderate irradiances (100 µmol photons m^{-2} s^{-1}) as compared to plants without leaf epiphyte-cover, owing to limited gas exchange with the surrounding water-column as a result of the enhanced DBL thickness.

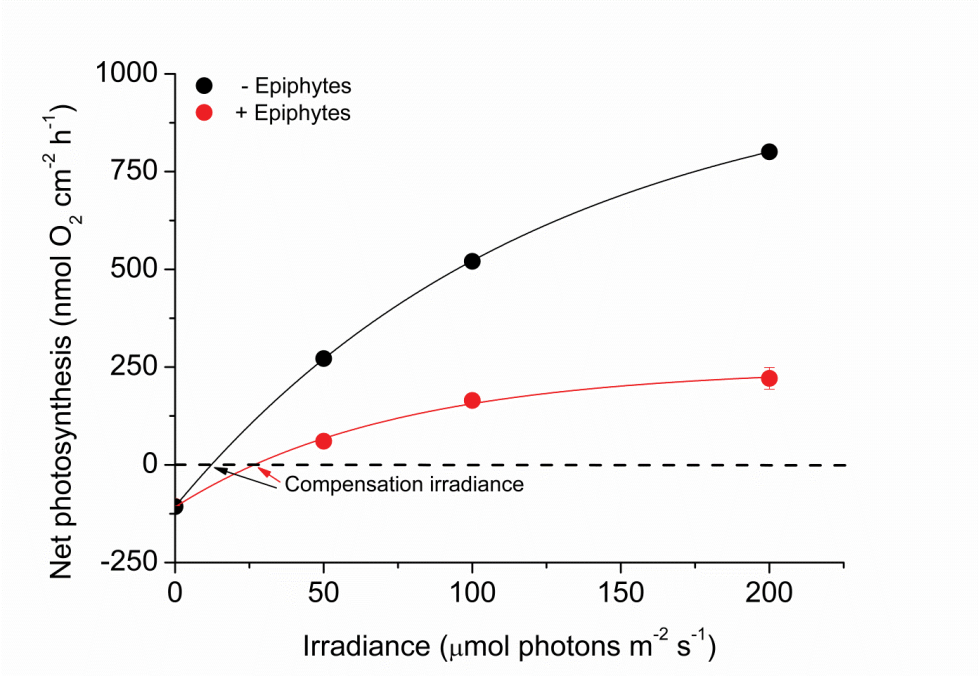

Figure 6.6. Net photosynthesis rates as a function of downwelling photon irradiance. Rates were calculated for the 4 different incident irradiances (0, 50, 100 and 200 µmol photons m^{-2} s^{-1}) and were fitted with a hyperbolic tangent function (Webb *et al.,* 1974) with an added term to account for respiration (Spilling *et al.,* 2010) (R^2 = 0.99). Red symbols and line represent leaves with ~21% epiphyte-cover. Black symbols and line represent leaves without epiphyte-cover. Error bars are ±SD. n = 3-4; leaf level replicates.

Table 6.1. O_2 fluxes across the leaf surface and radial O_2 loss from the root-cap (~1 mm from the root-apex). (-) indicate no data points. Negative values denote net O_2 uptake. Rates are mean±S.D. n = 3-5; leaf/root level replicates. [a,b]indicates significant difference between seagrasses with leaf epiphyte cover as compared to seagrasses without leaf epiphyte cover (control plants) ([a] Two-way ANOVA, $F_{3,3\ (PAR)} = 2931.2$, $F_{1,3\ (epiphytes)} = 3555.1$, $p < 0.01$; [b] Mann-Whitney test, $p < 0.05$).

Downwelling irradiance µmol photons m^{-2} s^{-1}	**Leaves (+ Epiphytes)** nmol O_2 cm^{-2} h^{-1}	**Leaves (- Epiphytes)** nmol O_2 cm^{-2} h^{-1}	**Root-cap (+ Epiphytes)** nmol O_2 cm^{-2} h^{-1}	**Root-cap (- Epiphytes)** nmol O_2 cm^{-2} h^{-1}
0	-106.4±1.8	-107.1±1.0	0	0.8±0.1
50	60.6±4.0 [a]	271.9±3.3	(-)	(-)
100	164.7±4.9 [a]	520.7±12.8	(-)	(-)
200	221.2±27.8 [a]	800.9±14.7	65.7±21.0 [b]	152.7±7.5

Radial O_2 loss

We used the measured steady state O_2 microprofiles around the root-cap of *Z. marina* with and without leaf epiphyte-cover (Figure 6.7), to calculate the radial O_2 flux into the surrounding sediment. In light, we calculated the radial O_2 loss (ROL) from the root-cap to be 65.7 nmol O_2 cm^{-2} h^{-1} from plants with leaf epiphyte-cover as compared to 152.7 nmol O_2 cm^{-2} h^{-1} from plants without leaf epiphyte-cover (Table 6.1). The ROL maintained a ~300 µm thick oxic microzone around the root-cap of *Z. marina* (Figure 6.7). In darkness, the ROL from the root-cap dramatically decreased to 0 nmol O_2 cm^{-2} h^{-1} in plants with leaf epiphyte-cover (i.e. no O_2 was detectable at the root surface during darkness; Figure 6.7), and 0.8 nmol O_2 cm^{-2} h^{-1} in plants without leaf epiphyte-cover (Table 6.1). Epiphyte-covered plants did thus lose their oxic microshield against H_2S intrusion in darkness.

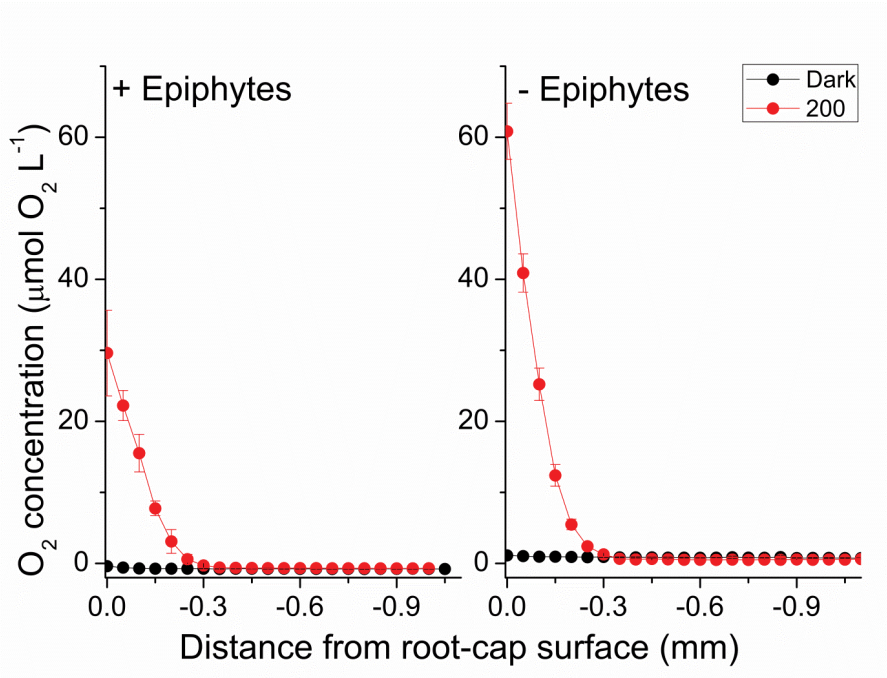

Figure 6.7. Radial O_2 loss from the root-cap of *Z. marina* (~1 mm from the root-apex) to the immediate rhizosphere measured at two different irradiances (0 and 200 µmol photons m^{-2} s^{-1}). Left panel show radial O_2 loss from seagrass with leaf epiphyte-cover, right panel show radial O_2 loss from seagrass without leaf epiphyte-cover. X = 0 indicates the root surface. Error bars are ±SD. n = 3-5; root level replicates.

DISCUSSION

Our results provide clear experimental evidence that epiphyte growth on *Z. marina* leaves reduces both light quantity and quality reaching the seagrass leaf, thereby impeding the overall plant performance during day-time. Furthermore, leaf epiphyte-cover lead to an enhanced thickness of the diffusive boundary layers (DBL) surrounding the leaves, thus impeding the exchange of gasses and essential nutrients with the ambient water-column. In darkness, this resulted in a negative effect on the intra-plant O_2 status that subsequently reduced the oxidation capability of the below-ground tissue, thereby rendering plants more vulnerable to sediment-produced reduced phytotoxic compounds, such as H_2S.

Light microenvironment and shoot photosynthesis

Light availability on the surface of the leaves of *Z. marina* covered by epiphytes was dramatically decreased compared to leaves without epiphytes in agreement with previous studies (Drake et al., 2003; Pedersen et al., 2014). Effectively, this means that higher

downwelling irradiance is needed to meet the compensation irradiance for the epiphyte covered leaf (Figure 6.6). We expected a larger change in the spectral quality of light reaching the leaf surface through the epiphyte canopy, but as the generation time of unicellular and filamentous algae colonizing the seagrass are short relative to the seagrass leaves, there might have been a large proportion of dead epiphytes thus acting as particulate organic matter with a more uniform light attenuation (Figure 6.3, upper right). However, in the lower canopy (0-1mm above the seagrass surface) there was a non-uniform attenuation of light leading to a strong reduction in blue light reaching the seagrass surface (Figure 6.3, lower right). In the transmittance spectra, we saw a disproportionate large amount of green light being attenuated in the presence of epiphytes indicating the presence of a community possessing accessory pigments able to utilize green light, such as red algal or cyanobacterial phycobiliproteins.

Although a large proportion of the green light was attenuated by epiphytes, blue and red light were almost completely removed, leaving the plant in a light environment with predominately green light which is less effectively absorbed by Chl *a*. Thus, both quality and especially the quantity of light were diminished in the presence of epiphytes thereby leaving the plant for longer periods near the minimal light requirement for growth, which is high in *Z. marina* (~20% of surface irradiance; Dennison et al., 1993). A recent study showed ~90% reduction in biomass under prolonged diminished light conditions, comparable to the decrease in light shown here (Kim et al., 2015). It has been speculated that the high minimum light requirement for growth reflects that seagrasses often grow in anoxic, sulphide-rich sediments (Ralph et al., 2007). The presence of sulphide results in decreased photosynthesis and increased O_2 consumption in the dark (Goodman et al., 1995; Holmer and Bondgaard, 2001), which means that more light is needed to drive a sufficient photosynthetic O_2 supply to maintain positive growth. Diminished light conditions due to epiphyte cover can thus reduce the fitness of the plant.

The ~4 times enhanced DBL thickness around leaves with epiphyte-cover adversely affected the internal O_2 supply to the below-ground tissue at night-time. In addition, it lead to a build-up of O_2 at the leaves surface under high incident photon irradiance (≥100 µmol photons m^{-2} s^{-1}; Figure 6.5), which potentially could lead to enhanced photorespiration (as surplus internal O_2 molecules may bind competitively to RuBisCO instead of CO_2 resulting in

decreased CO_2 fixation and reduced photosynthetic efficiency) and/or internal oxidative stress (Maberly, 2014). At low photon irradiance (50 µmol photons m^{-2} s^{-1}), the reduced light availability and lower photosynthetic activity, seemed to counter-balance this internal O_2 build-up caused by the insulating DBL (Figure 6.5). Furthermore, the epiphytes themselves, i.e., filamentous algal epiphytes and most probably leaf- and filamentous algal epiphyte-associated bacterial communities, contribute with oxygenic photosynthesis and respiration, thereby further enhancing the O_2 consumption at the leaf surface during night-time. Correspondingly, we found a ~2 times higher compensation irradiance of plants with leaf epiphyte-cover, as compared to plants without epiphyte-cover (Figure 6.6). This may be a very important factor during prolonged events of poor light conditions, such as during dredging operations and eutrophication, making plants with leaf epiphyte-cover more prone to sulphide invasion as a result of inadequate internal aeration (Pedersen et al., 2004; Borum et al., 2005). The generally reduced net photosynthesis rates of plants with epiphyte-cover (Figure 6.6), was most likely a combined result of the poor light conditions and a limited influx of CO_2 from the surrounding water-column. Such DBL-induced limited gas exchange with the ambient water-column can lead to inorganic carbon limitation enhancing photorespiration (e.g. Maberly, 2014) thereby impeding shoot photosynthesis.

Light-driven O_2 microdynamics in the rhizosphere

Photosynthetic O_2 evolution resulted in the establishment of a ~300 µm wide oxic microzone around the root-cap of *Zostera marina* at the approximate position of the apical root meristem (Figure 6.7). Plants with epiphyte-cover exhibited a negative effect on the below-ground tissue oxidation capacity with ~2 times lower radial O_2 loss (ROL) from the root-apex during light stimulation of the leaf canopy, as compared to plants without leaf epiphyte-cover. Although the ROL in light from the root-cap of plants with and without epiphyte-cover were of similar magnitude to fluxes previously reported by Jensen *et al*. (2005; Table 6.1), a lower oxidation capability of the below-ground tissue will almost certainly have a negative effect on the overall plants performance. ROL has been shown to improve the chemical conditions in the immediate rhizosphere of seagrasses due to enhanced sulphide reoxidation (Brodersen et al., 2015). The oxic microshield at the root-cap surface can thus protect the apical root meristem from reduced phytotoxic compounds, such as H_2S, through chemical re-oxidation with O_2.

Dark O_2 microdynamics in the rhizosphere

During darkness, no O_2 was detected at the root-cap surface of plants with leaf epiphyte-cover, indicative of inadequate internal aeration in contrast to plants without leaf epiphyte-cover, where low levels of O_2 were detectable at the root-cap surface during darkness (Figure 6.7; Table 6.1). Such breakdown of the oxic microshield in presence of epiphytes on seagrass leaves can be of great importance, as a shift to anaerobic metabolism in the root-system results in a much less efficient energy utilization than with aerobic metabolism, as anaerobic conditions inhibit the translocation of carbohydrates supporting plant metabolism (Greve et al., 2003; Zimmerman and Alberte, 1996). Previous studies of *Z. marina* have shown that the ROL from the root-apex persists during darkness at a much higher flux rate (up to 16.2 nmol O_2 cm^{-2} h^{-1} measured 2 mm behind the root-apex) than reported in this study (Jensen et al., 2005; Frederiksen and Glud, 2006). This apparent discrepancy may be explained by bacterial colonisation of the root-cap surface consuming the small amounts of leaked O_2 through microbial respiration and/or by ferrous sulphide (FeS) and iron plaques. Sulphate reducing bacteria have thus previously been isolated from surface-sterilised roots of *Zostera marina* (Nielsen et al., 1999; Finster et al., 2001).

Interestingly, the root-cap mediated O_2 leakage to the rhizosphere may also be important for plant-beneficial root-associated microbial processes, such as H_2S re-oxidation, in addition to simply detoxifying reduced substances in the immediate rhizosphere through spontaneous chemical reactions. Bacterially-mediated H_2S oxidation is about 10.000-100.000 times faster than the chemical reaction alone (Jørgensen and Postgate, 1982) and therefore has potential to be of high value for the plants. It has been suggested that H_2S oxidation also takes place inside the plant (Holmer et al., 2005; Holmer and Hasler-Sheetal, 2014), as seagrass exposed to high sediment H_2S levels showed internal accumulation of elemental sulphur that is an intermediate in the sulphide oxidation. This process is, however, driven by simple chemical reactions between H_2S and O_2 and is not mediated by intra-plant enzymes or bacteria (Pedersen et al., 2004) as seen in some marine invertebrates (Grieshaber and Völkel, 1998).

The lower light availability for photosynthesis of plants with filamentous algal epiphyte-cover seemed to be the key factor behind the lower ROL from the root-cap (Figure 6.7), as a result of the relative lower net photosynthesis rates and thereby lower O_2 production in

leaves, as compared to plants without epiphyte-cover (Figure 6.6). This might seem obvious, but the DBL-induced impedance of O_2 exchange with the water-column of plants with epiphyte-cover, could also have resulted in an enhancement in the aerenchymal O_2 level (seen as the build-up in the surface O_2 concentration on Figure 6.5) and thereby a concomitant higher ROL from the root-apex, but this effect was apparently overruled by lower seagrass photosynthesis due to epiphyte shading and/or inorganic carbon limitation due to increased DBL thickness.

Burnell et al. (2014) recently demonstrated that high incident irradiance (~200 µmol photons m^{-2} s^{-1}) in combination with elevated water-column CO_2 concentrations (up to 900 µl L^{-1}, representing high future predictions of water-column CO_2 levels) had a negative effect on seagrass biomass and leaf growth, as compared to low light conditions. The observed negative growth response to combined high CO_2 and light conditions appeared to be closely related to overgrowth of seagrass leaves with filamentous algal epiphytes. This finding supports our microsensor measurements demonstrating the negative effects of leaf epiphyte-cover on the intra-plant O_2 status and the below-ground tissue oxidation capacity. Epiphyte-induced low O_2 evolution in seagrass leaves causing reduced internal aeration and increased H_2S intrusion may result in enhanced seagrass mortality if unfavourable light conditions persist for longer periods of time. This emphasizes the importance of minimizing nutrient loading into seagrass inhabited marine coastal waters, as eutrophication often leads to poor light conditions, low water quality, algal blooms and enhanced night-time O_2 consumption in the water column.

In conclusion, the present study shows that epiphyte-cover of seagrass leaves leads to reduced oxidation capability of the below-ground tissue, due to a combined result of lower light availability and thicker diffusive boundary layers around leaves, impeding seagrass photosynthesis. This synergetic negative effect on the plants performance, resulted in a ~2 times higher compensation irradiance in *Z. marina* leaving epiphyte-covered seagrasses more vulnerable to H_2S invasion during prolonged events of poor light conditions in the surrounding water-column. Seagrasses with leaf epiphyte-cover are thus more prone to anthropogenic impacts and activity in coastal environments, as leaf epiphytes reduce their resilience towards environmental disturbances.

ACKNOWLEDGEMENTS

We thank Unisense A/S, the microbiology group at Aarhus University and Johan F. Kraft for providing the microsensor equipment used in this study. We thank Lars F. Rickelt for manufacturing the scalar irradiance microsensors and Peter Ralph (UTS) for financial support of KEB. The research was funded by grants from the *Augustinus Foundation*, *P. A. Fiskers Fund* and *Jorck and Wife's Fund* (KEB), the *Danish Council for Independent Research | Natural Sciences* (MK), and the *Australian Research Council* (ARC LP 110200454) (MK).

AUTHOR CONTRIBUTIONS

KEB, ML, LCP and MK designed the research. KEB, ML and LCP conducted the experiments. KEB, ML, LCP and MK analysed the data. KEB and ML wrote the manuscript with editorial help from MK. All authors have given approval to the final version of the manuscript. The authors declare no competing financial interest.

REFERENCES

Armstrong W. (1979). *Aeration in higher plants*. London: Academic Press, London.

Barnabes AD. (1996). Casparian band-like structures in the root hypodermis of some aquatic angiosperms. *Aquatic Botany* **55**: 217-225.

Binzer T, Borum J, Pedersen O. (2005). Flow velocity affects internal oxygen conditions in the seagrass *Cymodocea nodosa*. *Aquatic Botany* **83**: 239-247.

Borum J. (1983). The quantitative role of macrophytes, epiphytes, and phytoplankton under different nutrient conditions in Roskilde Fjord, Denmark. *Proceedings of the International Symposium on Aquatic Macrophytes, Nijmegen, 18-23 September 1983*, pp. 35-40.

Borum J, Pedersen O, Greve TM, Frankovich TA, Zieman JC, Fourqurean JW. *et al.* (2005). The potential role of plant oxygen and sulphide dynamics in die-off events of the tropical seagrass, *Thalassia testudinum*. *Journal of Ecology* **93**: 148-158.

Borum J, Sand-Jensen K, Binzer T, Pedersen O, Greve TM. (2006). Oxygen movement in seagrasses. In: Larkum AWD, Orth JR & Duarte CM, Eds., *Seagrasses: Biology, Ecology and Conservation.* Dordrecht, The Netherlands, Springer, Berlin: 255-270.

Brodersen KE, Nielsen DA, Ralph PJ, Kühl M. (2014). A split flow chamber with artificial sediment to examine the below-ground microenvironment of aquatic macrophytes. *Marine Biology* **161**: 2921-2930.

Brodersen KE, Nielsen DA, Ralph PJ, Kühl M. (2015). Oxic microshield and local pH enhancement protects *Zostera muelleri* from sediment derived hydrogen sulphide. *New Phytologist*. **205**: 1264–1276.

Burkholder JM, Tomasko DA, Touchette BW. (2007). Seagrasses and eutrophication. *Journal of Experimental Marine Biology and Ecology.* **350**(1-2):46-72.

Burnell OW, Russell BD, Irving AD, Connell SD. (2014). Seagrass response to CO_2 contingent on epiphytic algae: indirect effects can overwhelm direct effects. *Oecologia* **176**(3):871-82. doi: 10.1007/s00442-014-3054-z

Dennison WJ, Orth RJ, Moore KA, Stevenson JC, Carter V, Kollar S. *et al.*(1993). Assessing water quality with submerged aquatic vegetation. *BioScience* **43** (2), 86–94.

Drake LA, Dobbs FC, Zimmerman RC. (2003). Effects of epiphyte load on optical properties and photosynthetic potential of the seagrasses *Thalassia testudinum* Banks ex König and *Zostera marina* L. *Limnology and Ocenography* **48**: 456-463.

Duarte CM. (1991). Seagrass depth limits. *Aquatic Botany* **40**: 363-377.

Duarte CM. (2001). Seagrass Ecosystems. In: Leven SL, Ed., *Encyclopedia of biodiversity.*

Academic Press, San Diego **5**: 254-268.

Duarte CM, Middelburg JJ, Caraco N. (2005). Major role of marine vegetation on the oceanic carbon cycle. *Biogeosciences* **2**: 1-8.

Eghbal MA, Pennefather PS, O'Brien PJ. (2004). H_2S cytotoxicity mechanism involves reactive oxygen species formation and mitochondrial depolarisation. *Toxicology* **203**: 69-76.

Finster K, Thomsen TR, Ramsing NB. (2001). *Desulfomusa hansenii gen. nov., sp. nov.,* a novel marine propionate-degrading, sulfate-reducing bacterium isolated from *Zostera marina* roots. *International Journal of Systematic and Evolutionary Microbiology* **51**: 2055-2061.

Frederiksen MS, Glud RN. (2006). Oxygen dynamics in the rhizosphere of *Zostera marina*: A two-dimensional planar optode study. *Limnology and Oceanography* **51**(2): 1072-1083.

Frederiksen MS, Holmer M, Borum J, Kennedy H. (2006). Temporal and spatial variation of sulfide invasion in eelgrass (*Zostera marina*) as reflected by its sulfur isotopic composition. *Limnology and Oceanography* **51**(5): 2308-2318.

Greve TM, Borum J, Pedersen O. (2003). Meristematic oxygen variability in eelgrass (*Zostera marina*). *Limnology and Oceanography* **48**(1): 210-216.

Grieshaber MK, Völkel S. (1998). Animal adaptations for tolerance and exploitation of poisonous sulfide. *Annual Review of Physiology* **60**: 33-53.

Goodman JL, Moore KA, Dennison WC. (1995). Photosynthetic responses of eelgrass (*Zostera marina* L.) to light and sediment sulfide in a shallow barrier island lagoon. *Aquatic Botany* **50**: 37-47.

Holmer M, Bondgaard EJ. (2001). Photosynthetic and growth response of eelgrass to low oxygen and high sulfide concentrations during hypoxic events. *Aquatic Botany* **70**: 29-38.

Holmer M, Frederiksen M, Møllegaard H. (2005). Sulfur accumulation in eelgrass (*Zostera marina*) and effect of sulfur on eelgrass growth. *Aquatic Botany* **81**: 367-379.

Holmer M, Hasler-Sheetal H. (2014). Sulfide intrusion in seagrasses assessed by stable sulfur isotopes – a synthesis of current results. *Frontiers in Marine Science* **1**: 64. doi: 10.3389/fmars.2014.00064

Jensen SI, Kühl M, Glud RN, Jørgensen LB, Prieme A. (2005). Oxic microzones and radial oxygen loss from roots of *Zostera marina*. *Marine Ecology Progress Series* **293**: 49-58.

Jørgensen BB. (1982). Mineralization of organic matter in the sea bed - the role of sulfate reduction. *Nature* **296**: 643-645.

Jørgensen BB, Des Marias DJ. (1990). The diffusive boundary layer of sediments: Oxygen microgradients over a microbial mat. *Limnology and Oceanography* **35**(6): 1343-1355.

Jørgensen BB, Postgate JR. (1982). Ecology of the bacteria of the Sulfur cycle with special reference to anoxic oxic interface environments. *Philosophical Transactions of the Royal Society of London Series B-Biological Sciences* **298**: 543-561.

Jørgensen BB, Revsbech NP. (1985). Diffusive boundary layers and the oxygen uptake of sediments and detritus. *Limnology and Oceanography* **30**(1): 111-122.

Kim YK, Kim SH, Lee KS. (2015). Seasonal growth responses of the seagrass *Zostera marina* under severely diminished light conditions. *Estuaries and Coasts* **38**: 558-568.

Koren K, Brodersen KE, Jakobsen S, Kühl M. (2015). Optical sensor nanoparticles in artificial sediments – a new tool to visualize O_2 dynamics around the rhizome and roots of seagrasses. *Environmental Science and Technology*. doi: 10.1021/es505734b

Kühl M, Jørgensen BB. (1994). The Light-Field of Microbenthic Communities - Radiance Distribution and Microscale Optics of Sandy Coastal Sediments. *Limnology and Oceanography* **39**(6): 1368-1398.

Kühl M, Revsbech NP. (2001). Biogeochemical microsensors for boundary layer studies. *In Boudreau BP and Jørgensen BB, Eds., The Benthic Boundary Layer*. *Oxford University Press, Oxford*: 180-210.

Lamers LP, Govers LL, Janssen IC, Geurts JJ, Van der Welle ME, Van Katwijk MM, *et al.* (2013). Sulfide as a soil phytotoxin—a review. *Frontiers in plant science* **4**: 268. doi: 10.3389/fpls.2013.00268

Lassen C, Ploug H, Jørgensen BB. (1992). "A Fiberoptic Scalar Irradiance Microsensor - Application for Spectral Light Measurements in Sediments." *FEMS Microbiology Ecology* **86**(3): 247-254.

Maberly SC. (2014). The fitness of the environments of air and water for photosynthesis, growth, reproduction and dispersal of photoautotrophs: An evolutionary and biogeochemical perspective. *Aquatic Botany* **118:** 4-13.

Nielsen JT, Liesack W, Finster K. (1999). *Desulfovibrio zosterae sp. nov.,* a new sulphate reducer isolated from surface-sterilized roots of the seagrass *Zostera marina. International Journal of Systematic and Evolutionary Microbiology* **49**: 859-865.

Orth RJ, Carruthers TJ, Dennison WC, Duarte CM, Fourqurean JW, Heck KL, *et al.* (2006). A global crisis for seagrass ecosystems. *Bioscience* **56**(12): 987-996.

Pedersen MF, Nejrup LB, Pedersen TM, Frederiksen S. (2014). Sub canopy light conditions only allow low annual net productivity of epiphytic algae on kelp *Laminaria hyperborea. Marine Ecology Progress Series* **516**: 163-176.

Pedersen O, Binzer T, Borum J. (2004). Sulphide intrusion in eelgrass (*Zostera marina* L.). *Plant, Cell and Environment* **27**: 595-602.

Pedersen O, Borum J, Duarte CM, Fortes MD. (1998). Oxygen dynamics in the rhizosphere of *Cymodocea rotundata*. *Marine Ecology Progress Series* **169**: 283-288.

Perez-Perez ME, Lemaire SD, Crespo JL. (2012). Reactive oxygen species and autophagy in plants and algae. *Plant Physiology* **160**: 156-164.

Plus M, Deslous-Paoli J-M, Dagault F. (2003). Seagrass (*Zostera marina* L.) bed recolonisation after anoxia-induced full mortality. *Aquatic Botany* **77**(2): 121-134.

Ralph PJ, Durako MJ, Enriquez S, Collier CJ, Doblin MA. (2007). Impact of light limitation on seagrasses. *Journal of Experimental Marine Biology and Ecology.* **350** (1-2):176-93.

Raun AL, Borum J. (2013). Combined impact of water column oxygen and temperature on internal oxygen status and growth of *Zostera marina* seedlings and adult shoots. *Journal of Experimental Marine Biology and Ecology* **441**: 16–22.

Raven JA, Scrimgeour CM. (1997). The influence of anoxia on plants of saline habitats with special reference to the Sulfur cycle. *Annals of Botany* **79**: 79-86.

Revsbech NP. (1989). An oxygen microsensor with a guard cathode. *Limnology and Oceanography* **34**(2): 474-478.

Richardson SL. (2006). Response of epiphytic foraminiferal communities to natural eutrophication in seagrass habitats off Man O'War Cay, Belize. *Marine Ecology.* **27**(4):404-16.

Robblee MB, Barber TR, Carlson jr. PR, Durako MJ, Fourqurean JW, Muehlstein, *et al.* (1991). Mass mortality of the tropical seagrass *Thalassia testudinum* in Florida Bay (USA). *Marine Ecology Progress Series* **71**: 297-299.

Sand-Jensen K. (1977). Effect of epiphytes on eelgrass photosynthesis. *Aquatic Botany* **3**: 55-63.

Sand-Jensen K, Borum J. (1991). Interactions among phytoplankton, periphyton, and macrophytes in temperate freshwaters and estuaries. *Aquatic Botany*. **41**:137-75.

Seddon S, Connolly R, Edyvane KS. (2000). Large-scale seagrass dieback in northern Spencer Gulf, South Australia. *Aquatic Botany* **66**(4): 297-310.

Spilling K, Titelman J, Greve TM, Kühl M. (2010). Microsensor measurements of the external and internal microenvironment of *Fucus vesiculosus* (Phaeophyceae). *Journal of Phycology* **46**: 1350-1355.

Webb WL, Newton M, Starr D. (1974). Carbon-dioxide exchange of *Alnus-rubra* - mathematical-model. *Oecologia* **17**: 281-291.

Zieman JC, Fourqurean JW, Frankovich TA. (1999). Seagrass die-off in Florida Bay: Long-term trends in abundance and growth of turtle grass, *Thalassia testudinum*. *Estuaries* **22**(2): 460-470.

Zimmerman RC, Alberte RS. (1996). Effect of light/dark transition on carbon translocation in eelgrass *Zostera marina* seedlings. *Marine Ecology Progress Series* **136**: 305-309.

SUPPORTING INFORMATION

Epiphyte-cover on seagrass (*Zostera marina L.*) leaves impedes plant performance and radial O_2 loss from the below-ground tissue

Kasper Elgetti Brodersen[1,a,b], Mads Lichtenberg[2,a], Laura-Carlota Paz[3], Michael Kühl[1,2]

[1]Plant Functional Biology and Climate Change Cluster, University of Technology, Sydney, 15 Broadway, Ultimo, Sydney, NSW 2007, Australia

[2]Marine Biological Section, Department of Biology, University of Copenhagen, Strandpromenaden 5, DK-3000 Helsingør, Denmark

[3]Department of Bioscience - Microbiology, Aarhus University, Ny Munkegade 116, DK-8000 Aarhus C, Denmark

[a] These authors contributed equally to this work.

[b] Corresponding author, e-mail: kasper.e.brodersen@student.uts.edu.au and phone: +61 414 954 017

RESULTS OF STATISTICAL ANALYSIS

Table S6.1: Two-way ANOVA for O_2 evolution (nmol O_2 cm^{-2} h^{-1}). TMT = Experimental treatments, i.e., with or without leaf epiphytes; PAR = incident irradiance (0, 50, 100 and 200 µmol photons m^{-2} s^{-1}).

Dependent Variable: Oxygen evolution							
Source	Sum of Squares	df	Mean Square	F	Sig. (P-Value)	Noncent. Parameter	Observed Power[b]
Corrected Model	2043159.8[a]	7	291880.0	2040.1	.000	14280.5	1.000
Intercept	1291479.2	1	1291479.2	9026.7	.000	9026.7	1.000
TMT	508645.6	1	508645.6	3555.1	.000	3555.1	1.000
PAR	1258149.6	3	419383.2	2931.2	.000	8793.7	1.000
TMT * PAR	269624.4	3	89874.8	628.2	.000	1884.5	1.000

[a]. R^2 = .999 (Adjusted R^2 = .998)
[b]. Computed using alpha = .01

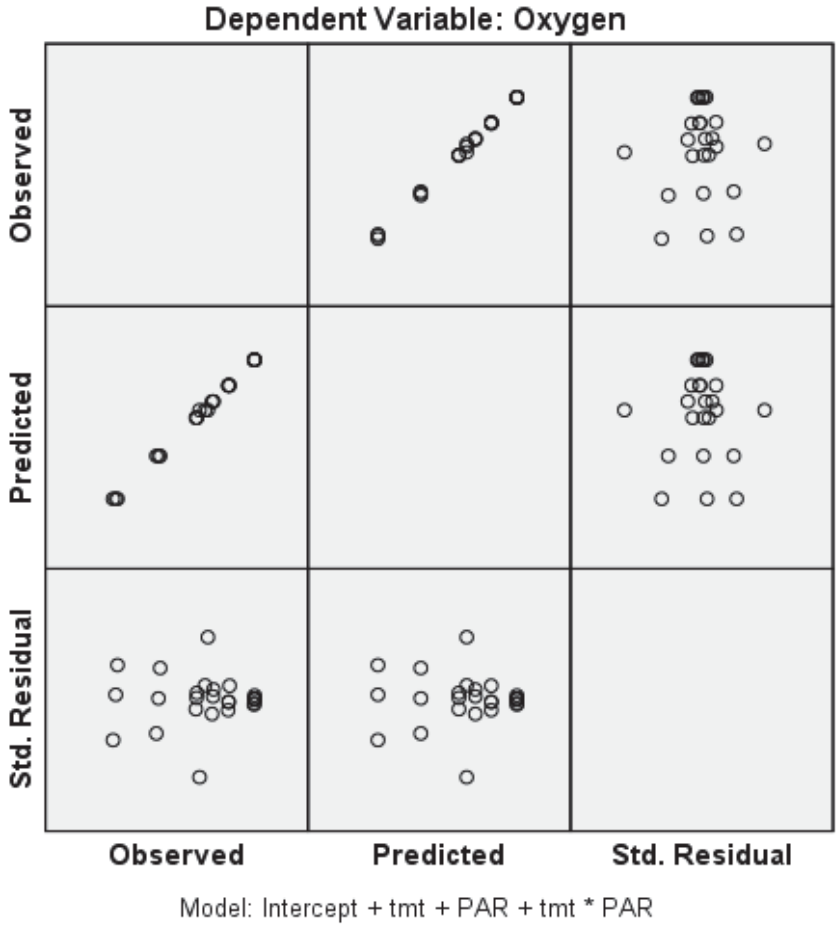

Chapter 7

Seagrass-derived rhizospheric phosphorus and iron mobilization

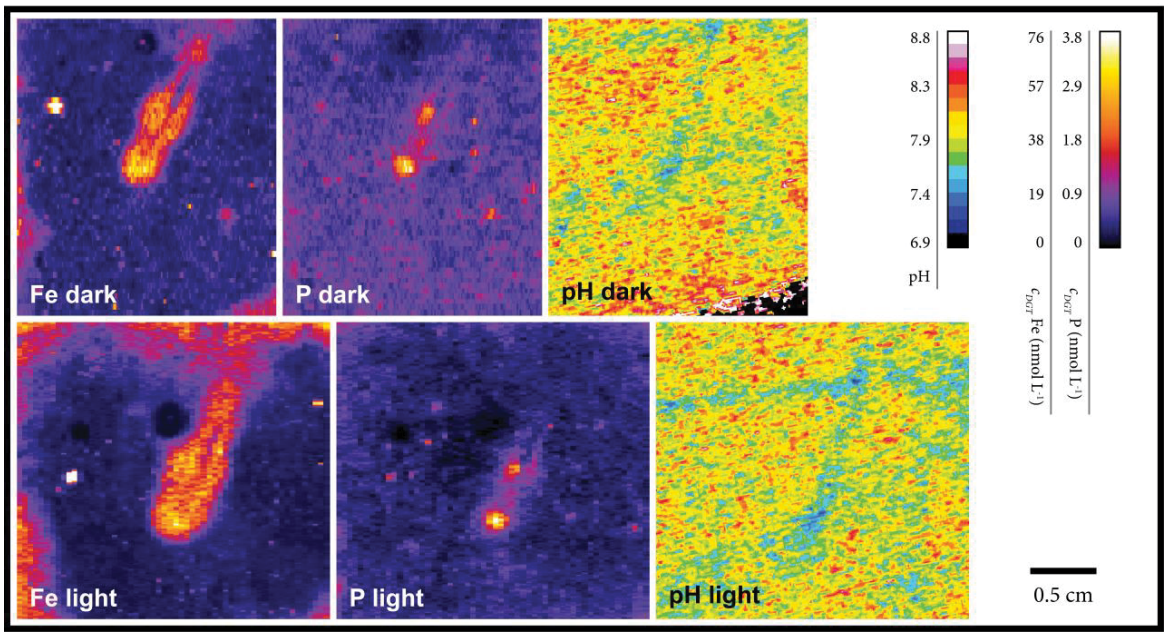

TOC figure. *Colour coded images illustrating plant-derived nutrient mobilization around roots of the tropical seagrass species Cymodocea serrulata growing in carbonate-rich sediments.*

Citation: Brodersen KE, Koren K, Mosshammer M, Ralph PJ, Kühl M. & Santner J. Seagrass-derived rhizospheric phosphorus and iron mobilization. (In prep).

Highlights: This chapter describes how tropical seagrasses, such as *Cymodocea serrulata*, can solubilize nutrients around their below-ground tissue to accommodate growth in phosphorous- and iron-limited carbonate-rich tropical marine sediments. Using high-resolution two-dimensional chemical imaging of O_2, pH, iron, sulphide, calcium and phosphorus, we found that tropical seagrasses are able to mobilize the essential nutrients iron and phosphorus in their rhizosphere via multiple biogeochemical pathways. This now explains the immense success of seagrass ecosystems in oligotrophic, tropical waters.

Seagrass-derived rhizospheric phosphorus and iron mobilization

Kasper Elgetti Brodersen[1,*], Klaus Koren[2,*], Maria Mosshammer[2,*], Peter J. Ralph[1], Michael Kühl[1,2,#], Jakob Santner[3,4,#]

[1]Plant Functional Biology and Climate Change Cluster, Faculty of Science, University of Technology Sydney (UTS), Sydney, Australia.

[2]Marine Biological Section, Department of Biology, University of Copenhagen, Helsingør, Denmark.

[3]Division of Agronomy, Department of Crop Sciences, University of Natural Resources and Life Sciences, Vienna, Austria.

[4]Rhizosphere Ecology and Biogeochemistry Group, Institute of Soil Research, Department of Forest and Soil Sciences, University of Natural Resources and Life Sciences, Vienna, Austria.

[*]These authors contributed equally to this work and share the first authorship of this paper

[#]Corresponding authors: mkuhl@bio.ku.dk (Michael Kühl) and jakob.santner.boku.ac.at (Jakob Santner)

ABSTRACT

Tropical seagrass meadows are largely phosphorus limited owing to the strong phosphorus fixation capacity of carbonate-rich sediments (Short et al. 1990; Fourqurean et al. 1992; Jensen et al. 1998), yet seagrasses thrive in often densely-vegetated, multi-species meadows in oligotrophic tropical waters (Larkum et al. 2006). Here we show how tropical seagrasses, such as *Cymodocea serrulata*, solubilize phosphorus and iron in carbonate-rich sediments. Seagrass-derived rhizospheric phosphorus and iron mobilization was the combined result of a low pH-induced phosphorus release leading to dissolution of carbonates within microenvironments in the seagrass rhizosphere, and a sulphide-induced phosphorus release, owing to reduction of insoluble Fe(III) oxyhydroxides to dissolved Fe(II). These mobilization mechanisms were strongly coupled to seagrass-derived radial O_2 loss and secretion of other allelochemicals, such as organic acids and dissolved organic carbon from the below-ground tissue into the immediate rhizosphere, directly affecting the pore-water phosphorus and iron availability through localized acidification of the rhizosphere, or indirectly via root-associated microbes, such as sulphate reducers, generating reduced sediment microniches of high sulfide concentrations in the seagrass rhizosphere. Our demonstration of seagrass-derived rhizospheric phosphorus and iron mobilization explains the long-lasting conundrum why seagrasses are widespread in oligotrophic tropical waters.

Keywords: carbonate, *in situ*, iron, pH, phosphorus, seagrass, sediment, solubilisation, sulphide

MAIN BODY

Seagrass meadows are important high-value ecosystems (Costanza et al. 1997; Waycott et al. 2009) providing numerous ecological services to marine environments in terms of high biodiversity (Harborne et al. 2006), enhanced sediment carbon sequestration (Duarte et al. 2005), and coastal zone protection against erosion (Koch et al. 2009). Seagrasses grow in coastal waters worldwide except from Antarctica. In tropical environments, seagrass growth is largely phosphorus limited owing to strong fixation of phosphorus in the prevailing carbonate sediments (Short et al. 1990; Fourqurean et al. 1992; Jensen et al. 1998) and the adsorption of phosphorus to insoluble iron(Fe)(III) oxyhydroxides (Pagès et al. 2012). Phosphorus is mainly absorbed through the rhizome and roots of seagrasses (McRoy et al. 1972), and despite very low (nM) phosphorus levels in porewaters of oligotrophic, carbonate-rich sediments, seagrasses thrive and sustain high primary production. Tropical seagrass species such as *Cymodocea* sp., *Halodule* sp., *Halophila* sp., and *Thalassia* sp., thus seem to have evolved phosphorus, and possibly iron acquisition mechanisms to support their nutrient requirements.

Seagrass-generated rhizospheric phosphorus solubilisation has been suggested to be initiated by the release of organic acids from roots (Long et al. 2008), as well as due to plant-derived reductions in rhizosphere pH as a result of root/rhizome-released acidic substances and/or radial O_2 loss (ROL) leading to sulphuric acid production through chemical reactions with sediment-produced hydrogen sulphide (H_2S) (Brodersen et al. 2015, 2016). Such rhizosphere acidification may result in carbonate dissolution and concomitant phosphate release to the pore-water.

Seagrasses also secrete dissolved organic carbon (DOC) to their rhizosphere as root/rhizome exudates (Moriarty et al. 1986) that can fuel the rhizospheric microbial community (Badri & Vivanco, 2009). Sulphate-reducing bacteria (SRB) are highly abundant in the seagrass rhizosphere and rhizoplane (Welsh, 2000), and sediment sulphate reduction rates have been shown to increase during photosynthesis (Blaabjerg et al. 1998; Nielsen et al. 2001). High rhizospheric H_2S concentrations can reduce insoluble Fe(III) oxyhydroxides to dissolved Fe(II), which has been proposed to mobilize the Fe(III) oxyhydroxide-bound phosphate to the pore-water (Pagès et al. 2012). However, the mentioned plant-mediated rhizospheric

phosphorus mobilization mechanisms remain speculative and have hitherto never been demonstrated directly. Using a combination of high resolution chemical imaging methods, we present the first experimental demonstration of seagrass-derived rhizospheric phosphorus and iron mobilization, thus resolving the long-standing debate on how tropical seagrasses thrive in nutrient-poor carbonate sediments.

In situ sulfide measurements within tropical seagrass (including *Cymodocea serrulata*, *Halophila ovalis*, *Halodule uninervis* and *Thalassia hemprichii*) vegetated carbonate-rich sediments revealed an overall downward movement of the sulphide front during day-time and a concomitant general reduction in phytotoxic sulfide concentrations within the upper ~10 cm of the sediments (Fig. 7.1a). Enhanced re-oxidation of sediment-produced sulfide during day-time is caused by higher ROL from the below-ground seagrass tissue due to high O_2 partial pressure (pO_2) in the photosynthetic leaves causing an increased internal O_2 gradient and thus O_2 transport to the rhizosphere (Pedersen et al. 2004; Koren et al. 2015; Brodersen et al. 2015). During night-time, when seagrasses are completely dependent on passive O_2 influx into the leaves from the surrounding water-column (Borum et al. 2005; Brodersen et al. 2015), the sulphide front migrated towards the water/sediment interface increasing the tissue exposure to phytotoxic H_2S (Fig. 7.1a). However, microniches at the below-ground tissue/sediment interface exhibited distinct low-sulfide microzones around the root/shoot junctions of the seagrasses in the uppermost part of the rhizosphere, as well as around some of the deeper-laying root-tips (Fig. 7.1c). Other microniches around mature parts of the roots exhibited high sulfide concentrations indicative of high sulphate reduction rates within these plant regions probably owing to root/rhizome exudation of DOC during photosynthesis (Pollard & Moriarty, 1991; Blaabjerg et al. 1998; Nielsen et al. 2001) stimulating the activity of root-associated sulphate-reducing bacteria (Fig. 7.1c). Such distinct microheterogeneity in the rhizospheric sulfide concentration and distribution can be explained by the higher ROL from the root/shoot junctions and apical root meristems (i.e. meristematic region of the root-tips) of the investigated tropical seagrass *Cymodocea serrulata* as compared to the remainder of the below-ground tissue (Extended Data Fig. 7.1; demonstrating seagrass-generated rhizospheric O_2 distributions during light and dark conditions), which is similar to other seagrass species (Jensen et al. 2005; Koren et al. 2015; Brodersen et al. 2015). Seagrass-derived sediment detoxification furthermore resulted in

rhizospheric proton formation and thus localized acidification of the immediate rhizosphere (Fig. 7.2), as previously shown for the temperate seagrass species *Zostera muelleri* and *Zostera marina* (Brodersen et al. 2015, 2016).

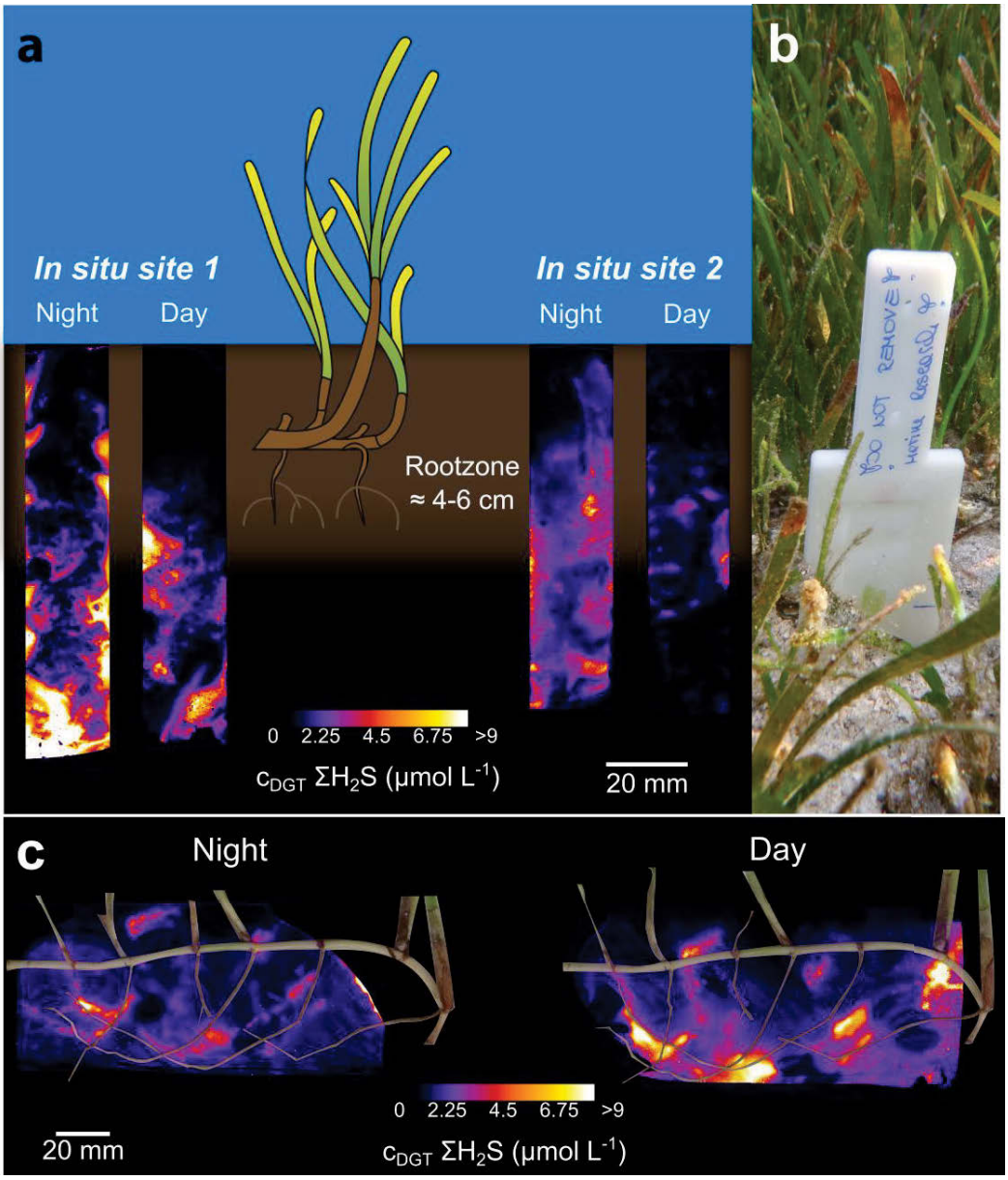

Figure 7.1. *In situ* distribution of phytotoxic sulfide during light (photon irradiance of 500 µmol photons m^{-2} s^{-1}) and dark conditions in a sediment colonised by the tropical seagrass species *Cymodocea rotundata*, *Cymodocea serrulata*, *Halophila ovalis*, *Halodule uninervis*, *Syringodium isoetifolium* and *Thalassia hemprichii* as determined with sulfide sensitive AgI DGT probes (a). The width of all deployed DGT gels was 18 mm (b). Distribution of sulfide concentrations in the rhizosphere of *Cymodocea serrulata* during light and dark conditions (c). All images are color coded, where the color scale depicts the sediment sulfide concentration.

Distinct seagrass-generated rhizospheric pH heterogeneity was demonstrated, with low-pH microniches (as compared to the bulk sediment) at the meristematic region of the rhizome (i.e. the basal leaf meristem), and around the roots and older parts of the rhizome, which all seemed to be further acidified during light exposure of the leaf canopy (Fig. 7.2a; Extended Data Fig. 7.2). Microniches of high pH were also observed around the first internode of the rhizome adjacent to the basal leaf meristem, as well as around the prophyllums (i.e. single leaves originating from the root/shoot junctions) (Fig. 7.2a). Such rhizospheric pH microheterogeneity was driven by ROL, resulting in sulphuric acid formation owing to localised H_2S re-oxidation via plant-released O_2, and potentially also by DOC leakage which may stimulate proton-consuming sulphate reduction in line with previous findings in the temperate seagrass species *Zostera marina* (Brodersen et al. 2016). At the roots, seagrass-derived rhizospheric microniches of low pH may have been further supported by secretion of organic acids from the roots (Long et al. 2008), although this can lead to both a direct reduction in rhizosphere pH and an indirect increase in pH via stimulation of the sulphate-reducing microbial community.

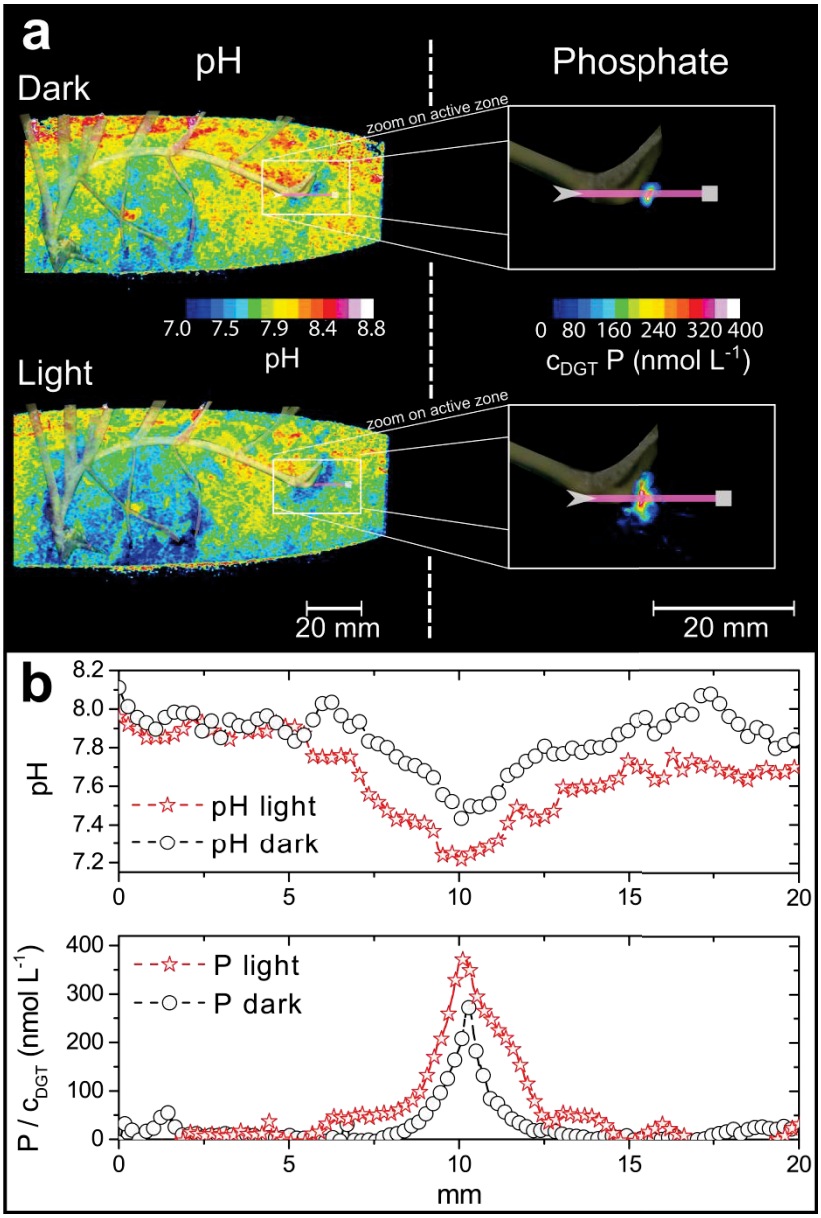

Figure 7.2. (a) Rhizospheric pH heterogeneity and phosphorus distributions in carbonate-rich sediment with the tropical seagrass *Cymodocea serrulata* during light (photon irradiance of 500 µmol photons m^{-2} s^{-1}) and dark conditions. The enlarged plot focusses on the basal leaf meristem area, i.e., the meristematic region of the rhizome. (b) Rhizospheric pH and phosphate concentrations during light and dark conditions as obtained from the extracted cross tissue line profiles shown in (a). All images are color coded, where the color scales depict the sediment pH and phosphate concentrations.

Seagrass-derived local reductions in rhizosphere pH resulted in pronounced phosphorus solubilisation at the basal leaf meristem as a response to acidification-induced calcium carbonate dissolution (Fig. 7.2a). High-resolution cross tissue line profiles confirmed these

observations showing a localised, seagrass-mediated reduction in rhizosphere pH of ~0.8 pH units at the basal leaf meristem, which correlated with a localised ~100-fold increase in pore-water phosphorus availability (Fig. 7.2b). Such high phosphorus mobilization at the plant/sediment interface of tropical seagrasses colonizing carbonate-rich sediments could potentially be further supported by Fe(III)-reducing and/or phosphorus-solubilizing bacteria if present in the adjacent sediment (Pagès et al. 2012).

Spatial co-distributions of rhizospheric dissolved Fe(II) and phosphorus during light and dark conditions demonstrated combined sulphide- and acidification-induced phosphorus and iron solubilisation in the carbonate-rich sediments around seagrass roots; especially around the root-tips (Fig. 7.3). At the root-tip of the root originating from the 4th root/shoot junction (Extended Data Fig. 7.3b), the seagrass-mediated phosphorus solubilisation was dominated by low pH-induced dissolution of calcium carbonates and thus the release of calcium-bound phosphorus to the pore-water (Fig. 7.3a,b). Around the root originating from the 3rd root/shoot junction (Extended Data Fig. 7.3b), the seagrass-driven phosphorus solubilisation was due to combined sulphide- and low pH-induced phosphorus release owing to reduction of insoluble Fe(III) oxyhydroxides releasing adsorbed phosphorus to the pore-water as well as carbonate dissolution, respectively (Fig. 7.3a-c). Seagrass-generated phosphorus mobilization around roots resulted in an up to ~10-fold increase in the rhizospheric phosphorus availability (Fig. 7.3a,b). Such high phosphorus mobilization capacity by tropical seagrasses in carbonate-rich sediments inevitably leads to beneficial effects on primary production, plant fitness and growth rates. In addition, the enhanced Fe(II) availability around roots (~10-fold increase) may alleviate Fe deficiency in leaves positively affecting photo-pigment concentrations such as Chl *a* (Duarte et al. 1995) (Fig. 7.3a,b). The slightly lower phosphate concentration around roots revealed in light as compared to darkness (Fig. 7.3), was probably due to higher phosphate absorption rate of seagrass rhizome and roots in the light (McRoy and Barsdate 1970). In general, our results show that the below-ground tissue nutrient mobilization capacity increased in the light owing to enhanced ROL and potentially also due to root/rhizome exudation of DOC and organic acids (Fig. 7.2; Extended Data Fig. 7.1 & 7.3).

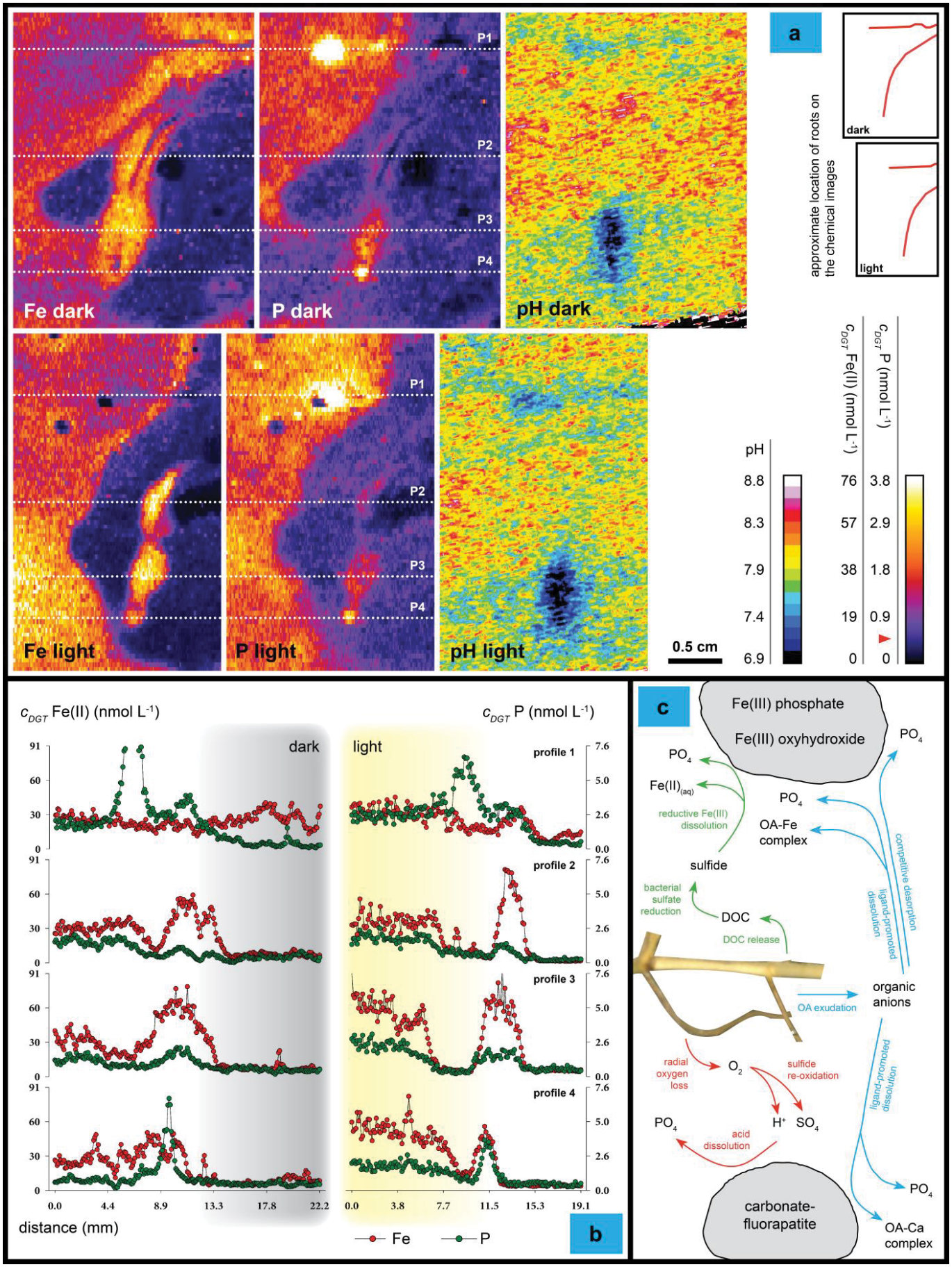
a
Fe dark
P dark
pH dark
P1
P2
P3
P4
approximate location of roots on the chemical images
dark
light
Fe light
P light
pH light
pH
8.8
8.3
7.9
7.4
6.9
c_{DGT} Fe(II) (nmol L^{-1})
76
57
38
19
0
c_{DGT} P (nmol L^{-1})
3.8
2.9
1.8
0.9
0
0.5 cm
c_{DGT} Fe(II) (nmol L^{-1})
c_{DGT} P (nmol L^{-1})
profile 1
profile 2
profile 3
profile 4
distance (mm)
Fe
P
b
c
Fe(III) phosphate
Fe(III) oxyhydroxide
PO_4
$Fe(II)_{(aq)}$
reductive Fe(III) dissolution
OA-Fe complex
sulfide
bacterial sulfate reduction
DOC
DOC release
competitive desorption
ligand-promoted dissolution
organic anions
OA exudation
radial oxygen loss
O_2
sulfide re-oxidation
H^+
SO_4
acid dissolution
carbonate-fluorapatite
OA-Ca complex

Figure 7.3. Co-distributions of seagrass-mediated rhizospheric phosphorus and Fe(II) solubilisation coupled to the plant-generated pH microheterogeneity at the root/sediment interface during light (photon irradiance of 500 µmol photons m^{-2} s^{-1}) and dark conditions in carbonate-rich marine sediment inhabited by the tropical seagrass *Cymodocea serrulata*. Panel (a) show the rhizospheric pH, Fe(II) and phosphorus concentrations within the selected region of interest, as shown on the provided illustration of the below-ground plant tissue structure (a; Extended Data Fig. 7.3). Panel (b) represent the line profiles (P1-4) as indicated on the two-dimensional chemical images (a), showing the cross tissue Fe(II) and phosphorus concentrations during light and dark conditions. All images are color coded, where the color scales depict the sediment pH, Fe(II) and phosphorus concentrations, respectively (a). The red arrow on the phosphorus scale bar indicates the detection limit for the applied phosphorus sensitive multi-ion gel (Zr-oxide - SPR-IDA) probe (a). Note the different scales on the y-axes in panel (b). Panel (c) shows a conceptual diagram of the seagrass-derived rhizospheric phosphorus and iron mobilization mechanisms in carbonate-rich sediments.

We have demonstrated that seagrasses can solubilize phosphorus and iron around their below-ground biomass in carbonate-rich sediments. Seagrass-derived rhizospheric phosphorus mobilization was mainly the result of a low pH-induced dissolution of sediment calcium carbonates combined with a sulphide-induced reduction of Fe(III) oxyhydroxides leading to local enhancement of dissolved Fe(II) and release of Fe(III)-bound phosphate in the rhizosphere pore-water (Fig. 7.3c). Phosphorus and iron are key limiting nutrients in tropical environments, including tropical seagrass meadows, owing to their high insolubility in the sediment. The revealed seagrass-driven phosphorus and iron mobilization mechanisms in carbonate-rich sediments thus explain how seagrasses can thrive in oligotrophic, tropical waters and sustain important ecosystem services, such as sequestration of carbon, i.e., blue carbon, coastal protection and marine biodiversity refugia.

MATERIALS AND METHODS

Experimental setup and study site

Seagrass specimens of *Cymodocea serrulata* (R.Br.) Asch. & Magnus, and carbonate-rich, tropical marine sediment were collected at Green Island, Cairns, Australia. Prior to experiments, the sediment was sieved down to <1mm sediment fraction to exclude any borrowing animals and bivalves, while maintaining essential nutrients, buffering salts and microbes. Seagrass specimens were gently uprooted and transplanted into the sieved sediment within narrow experimental chambers submerged in 20L aquariums (temperature of 28°C, salinity = 30) (supplementary materials and methods; Figure S7.1). Illumination was provided by halogen lamps (Philips Incandescent 230V PAR38 80W) illuminating the leaf canopy with a photon irradiance (PAR, 400-700nm) of ~500 µmol photons m^{-2} s^{-1} (resembling natural mid-day conditions at the study site), as measured with a spherical quantum sensor (US-SQD/L, Walz GmbH, Germany) connected to a calibrated quantum irradiance meter (ULM-500, Walz GmbH, Germany). Water movement and aeration were ensured via a submerged water- and air-pump, respectively.

Diffusive gradient thin film (DGT) gel foils for quantification of sulfide and phosphate were positioned at the back-wall of the experimental chambers and were separated from the sediment/below-ground seagrass biomass by a fine mesh (plankton mesh DIN 100-60, mesh size 60 µm, thickness of 50 µm), to allow for gel deployment and sampling without disturbing the sediment. Multi-ion gel foils were covered with a Whatman Nuclepore membrane and positioned in direct contact with the sediment. Planar optical sensor foils for pH and O_2 imaging were fixed onto the transparent aquarium wall (supplementary materials and methods).

Seagrass specimens were positioned in the experimental chamber ensuring good contact between the below-ground biomass and the optodes or the DGT gel foils on the opposite site of the investigated roots, before addition of pre-sieved natural marine sediment from the sampling site (supplementary materials and methods).

In situ measurements of the natural dynamics and concentrations of sulfide within the investigated seagrass meadow were obtained by deploying sulfide sensitive gels mounted in

commercial DGT samplers (DGT Research Ltd., www.dgtresearch.com) in the sediment over diurnal cycles (supplementary materials and methods; Figure S7.2). For day-time sulfide measurements, the gel probes were deployed in the seagrass meadow at sunrise and retrieved at sunset, and vice versa for the night-time sulfide measurements.

Luminescence imaging

A ratiometric RGB camera setup was used for O_2 imaging (Larsen et al. 2011) with a SLR camera (EOS 1000D, Canon, Japan) combined with a macro objective lens (Macro 100 f2,8 D, Tokina, Japan), a 530 nm long-pass filter (Uqgoptics.com), and an additional plastic filter (#10 medium yellow; leefilters.com) positioned in front of the long-pass filter to reduce the background fluorescence. A 455nm multichip LED (LedEngin Inc, RS Components Ltd, Corby, UK) combined with a bandpass filter was used for excitation of the O_2 planar optode; the LED was powered by a USB-controlled LED driver unit (imaging.fish-n-chips.de). Image acquisition and control of the SLR and LED were achieved with the software look@RGB (imaging.fish-n-chips.de).

A similar ratiometric approach was chosen for pH imaging (Mosshammer et al. 2016), with a 2CCD multispectral camera (JAI AD-080 GE; jai.com) equipped with a video objective lens (1.4/23 CCTV-LENS 400 - 1000 nm; schneiderkreuznach.com) mounted with a 460nm long-pass filter (Schneider KREUZNACH) and an additional plastic filter (#10 medium yellow; leefilters.com). The pH planar optode was excited with a high-power 405nm LED (LedEngin; rs-online.com) with a custom-built LED trigger (National instruments USB 6008). Image acquisition and triggering of the LED was done via custom-made software (bioras.com).

Acquired luminescence color images were split into red, green, and blue channels and analyzed using the software ImageJ (rsbweb.nih.gov/ij/). For O_2 concentration images, the red channel (O_2 sensitive emission of the indicator dye) and green channel (emission of the inert reference dye) of the color images were divided using the ImageJ plugin Ratio Plus. Afterwards, the obtained ratio image was fitted with the previously obtained calibration curve (described in the supplementary results) using the Curve Fitting tool of ImageJ (exponential decay function). For pH images, the red channel (pH sensitive emission of the

indicator dye) and the blue channel (emission of the reference dye) of the images were divided using the ImageJ plugin Ratio Plus. Subsequently, the obtained ratio image was fitted with the previously obtained calibration (described in supplementary results) using a linear fit within the boundaries (pKa ± 1 pH units). Calibrated O_2 concentration and pH images were further analyzed in ImageJ.

DGT gel based rhizospheric sulfide and phosphate determinations

Preparation details for the applied diffusive (polyacrylamide) gels, precipitated Zr-oxide binding gel for densitometric phosphate mapping and AgI binding gels for densitometric sulfide mapping can be found in the Supplementary Materials and Methods. After gel deployment, precipitated Zr-oxide gels were immersed in water and incubated at 85°C for 12h in order to irreversibly immobilize the phosphate bound to the Zr-oxide gel. This is necessary, as otherwise some phosphate dissolves from the binding gel in the acidic staining solution. After the heat treatment, the precipitated Zr-oxide gels were immersed in a molybdate blue staining reagent containing 11.3 mmol L^{-1} MoO_4, 0.16 mmol L^{-1} SbO_4, 8.50 mmol L^{-1} ascorbic acid and 0.38 mol L^{-1} H_2SO_4 for 45 min. This procedure leads to blue color formation at gel locations where phosphate is bound. Subsequently, the stained Zr-oxide gels were subjected to computer imaging densitometric (CID) analysis. No staining step is necessary for the sulfide bound to the AgI gels, as the Ag_2S formed as a result of sulphide binding is black, while the AgI background is pale white (Teasdale et al. 1999).

Computer imaging densitometry of the AgI and precipitated Zr-oxide gels.

CID analysis was conducted using a simple, commercially available Canon MG2460 printer with incorporated flatbed scanner. After retrieval of the sulfide and phosphate sensitive gels, the protective mesh was removed. The gels were then fixed flat between two PET sheets for avoiding direct contact with the scanner, scanned at a resolution of 600 dpi and saved as color and greyscale .tiff files. For calibration, standard gels with known analyte concentrations were scanned using the exact same scanner settings. Acquired images were calibrated and analyzed using ImageJ and Origin Pro.

High-resolution LA-ICPMS analysis of pore-water Fe(II) and P concentrations

Zr-oxide - SPR-IDA gels for simultaneous anion and cation mapping using laser ablation inductively coupled plasma mass spectrometry (LA-ICPMS) were prepared and analyzed according to Kreuzeder et al. (2013). After the deployment to the microcosms, the retrieved gels were immediately transferred onto a polyethersulfone (SUPOR, Pall corporation) membrane and dried using a gel dryer (Unigeldryer 3545, Laborgeräte and Vertriebs GmbH), resulting in an inseparable composite of the membrane and the dried gel. This composite was then mounted on glass slides using double-sided adhesive tape and subjected to LA-ICPMS analysis on a UP 193-FX (ESI, NWR division) laser ablation instrument coupled to a Nexion 350D ICPMS (Perkin Elmer) in line-scanning mode using the following parameters: inter-line distance: 400 µm, laser spot size diameter: 150 µm, line scanning speed: 250 µm s^{-1}, laser pulse frequency: 20 Hz, irradiance: 1-2 J cm^{-2}. Argon was used as the carrier gas. Count rates were recorded for several isotopes including ^{13}C, ^{31}P and ^{57}Fe. ^{13}C was used as internal normalisation standard. Total ICPMS measurement cycle times were 0.383 and 0.453 s for two individual measurement days. These settings resulted in a spatial resolution of 96 µm (Fig. 7.3, dark; Extended Data Fig. 7.3, light) and 113 µm (Fig. 7.3 light; Extended Data Fig. 7.3, dark) in the x direction and 400 µm in the y direction. For calibration, standard gels with known analyte concentrations were scanned using the same procedure. Chemical images were generated and arranged using Microsoft Excel, ImageJ, Systat SigmaPlot, Adobe Photoshop and Adobe InDesign.

ACKNOWLEDGEMENTS

We thank Paul York (James Cook University (JCU), Cairns) for field guidance and assistance during seagrass sampling, Michael Rasheed (JCU, Cairns) for help with seagrass identification, Egil Nielsen (University of Copenhagen) for manufacturing experimental chambers, Joey Crosswell (University of Technology Sydney) for manufacturing LED lamps, Christoph Hoefer (University of Natural Resources and Life Science, Vienna) for help with DGT gel preparation and analysis, and Sergey M. Borisov (Graz University of Technology) for help with optical sensor development. The study was funded by research grants from the Danish Council for Independent Research|Natural Sciences (*Sapere-Aude Advanced* grant, MK); the Villum Foundation (MK, KK); the Australian Research Council (ARC Linkage, LP110200454) (MK, PJR); and the Austrian Science Fund (FWF): P23798-B16, P27571-BBL (JS).

AUTHOR CONTRIBUTIONS

KEB, KK, JS, MM, PJR and MK planned and designed the study. KEB, KK, MM and JS performed the experiments. KEB, KK, MM and JS processed the data with inputs from MK. KEB, KK, JS, MM and MK analysed the data. KEB wrote the manuscript with editorial inputs from KK, JS, MM, PJR and MK. KK, MM, JS and KEB prepared the supporting material with editorial inputs from MK and PJR.

SUPPORTING INFORMATION

Supplementary Information accompanies the paper on the Nature journal website (http://www.nature.com).

CONFLICT OF INTEREST STATEMENT

The authors declare that the research was conducted in the absence of any commercial or financial relationships that could be construed as a potential conflict of interest.

REFERENCE LIST

Badri DV, Vivanco JM. (2009). Regulation and function of root exudates. *Plant, Cell & Environment* **32**: 666–681.

Blaabjerg V, Mouritsen KN, Finster K. (1998). Diel cycles of sulphate reduction rates in sediments of a *Zostera marina* bed (Denmark). *Aquatic Microbial Ecology* **15**: 97-102.

Borum J, Pedersen O, Greve TM, Frankovich TA, Zieman JC, Fourqurean JW, Madden CJ. (2005). The potential role of plant oxygen and sulphide dynamics in die-off events of the tropical seagrass, *Thalassia testudinum*. *Journal of Ecology* **93**: 148-158.

Brodersen KE, Koren K, Lichtenberg M, Kühl M. (2016). Nanoparticle-based measurements of pH and O_2 dynamics in the rhizosphere of *Zostera marina* L.: Effects of temperature elevation and light/dark transitions. *Plant, Cell & Environment* (Accepted on March 22, 2016).

Brodersen KE, Nielsen DA, Ralph PJ, Kühl M. (2015). Oxic microshield and local pH enhancement protects *Zostera muelleri* from sediment derived hydrogen sulphide. *New Phytologist* **205**: 1264-1276.

Costanza R, d'Arge R, de Groot R, Farber S, Grasso M, Hannon B, Limburg K, Naeem S, O'Neill RV, Paruelo J, et al. (1997). The value of the world's ecosystem services and natural capital. *Nature* **387**: 253-260.

Duarte CM, Merino M, Gallegos M. (1995). Evidence of iron deficiency in seagrasses growing above carbonate sediments. *Limnology and Oceanography* **40**: 1153-1158.

Duarte CM, Middelburg J, Caraco N. (2005). Major role of marine vegetation on the oceanic carbon cycle. *Biogeosciences* **2**: 1–8.

Fourqurean JW, Zieman JC, Powell GVN. (1992). Phosphorus limitation of primary production in Florida Bay: evidence from C:N:P ratios of the dominant seagrass *Thalassia testudinum*. *Limnology and Oceanography* **37**: 162–171.

Harborne AR, Mumby PJ, Micheli F, Perry CT, Dahlgren CP, Holmes KE, Brumbaugh DR. (2006). The functional value of Caribbean coral reef, seagrass and mangrove habitats to ecosystem processes. *Advances in marine biology* **50**: 57-189.

Jensen HS, McGlathery KJ, Marino R, Howarth RW. (1998). Forms and availability of sediment phosphorus in carbonate sand of Bermuda seagrass beds. *Limnology and Oceanography* **43**: 799–810.

Jensen SI, Kühl M, Glud RN, Jørgensen LB, Prieme, A. (2005). Oxic microzones and radial oxygen loss from roots of *Zostera marina*. *Marine Ecology Progress Series* **293**: 49-58.

Koch EW, Barbier EB, Silliman BR, Reed DJ, Perillo GM, Hacker SD, Granek EF, Primavera JH, Muthiga N, Polasky S. (2009). Non-linearity in ecosystem services: temporal and spatial variability in coastal protection. *Frontiers in Ecology and the Environment* **7**: 29-37.

Koren K, Brodersen KE, Jakobsen SL, Kühl M. (2015). Optical sensor nanoparticles in artificial sediments – a new tool to visualize O_2 dynamics around the rhizome and roots of seagrasses. *Environmental Science and Technology* **49**: 2286-2292.

Kreuzeder A, Santner J, Prohaska T, Wenzel WW. (2013). Gel for simultaneous chemical imaging of anionic and cationic solutes using diffusive gradients in thin films. *Analytical Chemistry* **85**: 12028-12036.

Larkum AWD, Orth RJ, Duarte CM. (2006). *Seagrasses: Biology, Ecology and Conservation*. Springer, Berlin.

Larsen M, Borisov SM, Grunwald B, Klimant I, Glud RN. (2011). A simple and inexpensive high resolution color ratiometric planar optode imaging approach: application to oxygen and pH sensing. *Limnology and Oceanography: Methods* **9**: 348-360.

Long MH, McGlathery KJ, Zieman JC, Berg P. (2008). The role of organic acid exudates in liberating phosphorus from seagrass-vegetated carbonate sediments. *Limnology and Oceanography* **53**: 2616-2626.

McRoy CP, Barsdate RJ. (1970). Phosphate absorption in eelgrass. *Limnology and Oceanography* **15**: 6-13.

McRoy CP, Barsdate RJ, Nebert M. (1972). Phosphorus cycling in an eelgrass (*Zostera marina* L.) ecosystem. *Limnology and Oceanography* **17**: 58-67.

Moriarty DJW, Iverson RL, Pollard PC. (1986). Exudation of organic carbon by the seagrass *Halodule wrightii* Aschers. and its effect on bacterial growth in the sediment. *Journal of Experimental Marine Biology and Ecology* **96**: 115-126.

Mosshammer M, Strobl M, Kühl M, Klimant I, Borisov SM, Koren K. (2016). Design and application of an optical sensor for simultaneous imaging of pH and dissolved O_2 with low cross-talk. *ACS Sensors*.

Nielsen LB, Finster K, Welsh DT, Donelly A, Herbert RA, De Wit R, Lomstein BA. (2001). Sulphate reduction and nitrogen fixation rates associated with roots, rhizomes and sediments from *Zostera noltii* and *Spartina maritima* meadows. *Environmental Microbiology* **3**: 63-71.

Pagès A, Welsh DT, Robertson D, Panther JG, Schäfer J, Tomlinson RB, Teasdale PR. (2012). Diurnal shifts in co-distributions of sulfide and iron(II) and profiles of phosphate and ammonium in the rhizosphere of *Zostera capricorni*. *Estuarine, Coastal and Shelf Science* **115**: 282-290.

Pedersen O, Binzer, T, Borum J. (2004). Sulphide intrusion in eelgrass (*Zostera marina* L.). *Plant, Cell and Environment* **27**: 595-602.

Pollard PC, Moriarty D. (1991). Organic carbon decomposition, primary and bacterial productivity, and sulphate reduction, in tropical seagrass beds of the Gulf of Carpentaria, Australia. *Marine Ecology Progress Series* **69**: 149-159.

Short FT, Dennison WC, Capone DG. (1990). Phosphorus-limited growth of the tropical seagrass *Syringodium filiforme* in carbonate sediments. *Marine Ecology Progress Series* **62**: 169-174.

Teasdale PR, Hayward S, Davison W. (1999). In situ, high-resolution measurement of dissolved sulfide using diffusive gradients in thin films with computer-imaging densitometry. *Analytical Chemistry* **71**: 2186–2191.

Waycott M, Duarte CM, Carruthers TJB, Orth RJ, Dennison WC, Olyarnik S, Calladine A, Fourqurean JW, Heck Jr. KL, Hughes AR, et al. (2009). Accelerating loss of seagrasses across the globe threatens coastal ecosystems. *PNAS* **106**: 12377–12381.

Welsh DT. (2000). Nitrogen fixation in seagrass meadows: regulation, plant–bacteria interactions and significance to primary productivity. *Ecology Letters* **3**: 58-71.

EXTENDED DATA

Seagrass-derived rhizospheric phosphorus and iron mobilization

Kasper Elgetti Brodersen[1,*], Klaus Koren[2,*], Maria Moßhammer[2,*], Peter J. Ralph[1], Michael Kühl[1,2,#], Jakob Santner[3,4,#]

[1]Plant Functional Biology and Climate Change Cluster (C_3), Aquatic Processes Group, Faculty of Science, University of Technology Sydney (UTS), Sydney, Australia.

[2]Marine Biological section (MBL), Microenvironmental Ecology Group, Department of Biology, University of Copenhagen, Helsingør, Denmark.

[3]Division of Agronomy, Department of Crop Sciences, University of Natural Resources and Life Sciences, Vienna, Austria.

[4]Rhizosphere Ecology and Biogeochemistry Group, Institute of Soil Research, Department of Forest and Soil Sciences, University of Natural Resources and Life Sciences, Vienna, Austria.

[*]These authors contributed equally to this work and share the first authorship of this paper.

[#]Corresponding authors: mkuhl@bio.ku.dk (Michael Kühl) and jakob.santner@boku.ac.at (Jakob Santner)

Extended Data Fig. 7.1.

O_2 distribution and dynamics in the seagrass rhizosphere

The seagrasses were leaking O_2 from the basal leaf meristem (upper arrow) and the root apical meristems (two lower arrows) into the immediate rhizosphere, with profoundly higher rates of radial O_2 loss (ROL) during light stimulation of the leaf canopy. These seagrass-derived oxic microzones alter the sediment biogeochemistry and thus provide micro-habitats for distinct microbial communities, such as sulfide-oxidizing bacteria, within the oxic microniches and sulfate-reducing bacteria at the plant/sediment- and oxic/anoxic interface (Brodersen et al. *in review*; Jensen et al. 2007). Furthermore, the oxic microzones lead to sediment detoxification through chemical H_2S re-oxidation via O_2 within the seagrass-derived oxic microniches (Brodersen et al. 2015).

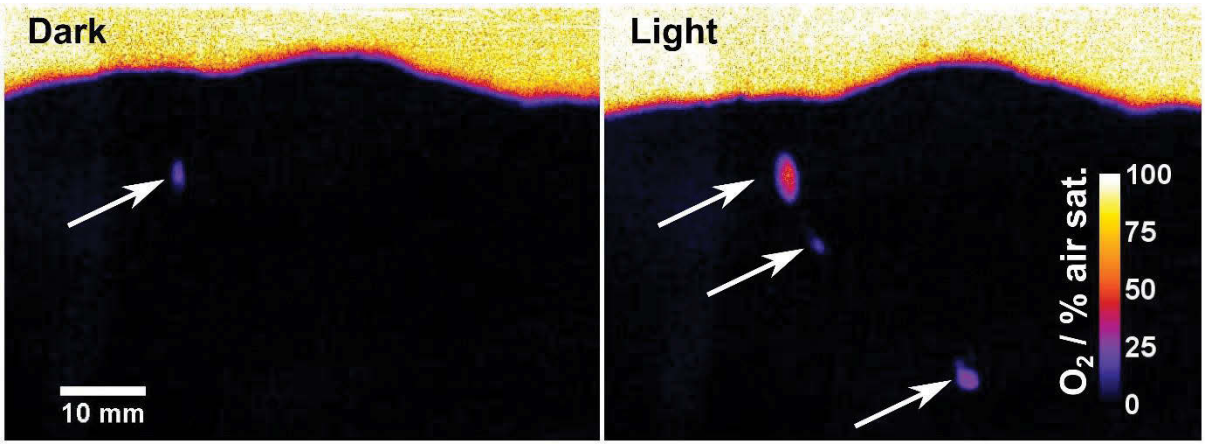

Extended Data Fig. 7.1. Distribution and dynamics of O_2 concentration within the rhizosphere of the tropical seagrass *Cymodocea serrulata*. Seagrasses were exposed to dark and light conditions (incident photon irradiance of ~500 µmol photons m^{-2} s^{-1}). Arrows indicate seagrass-derived oxic microzones. The color bar depicts the O_2 concentration in % air saturation. The seagrasses were transplanted into sieved (<1mm sediment fraction) natural sediment from the sampling site to exclude any larger animals and bivalves, as well as to ensure natural ratios of essential nutrients and rhizosphere microbes.

Extended Data Fig. 7.2

pH heterogeneity and dynamics within the seagrass rhizosphere

Pronounced spatio-temporal pH heterogeneity and dynamics was observed in the seagrass rhizosphere, with several microniches of low pH especially around the root apical meristems (i.e. the root-caps), the root/shoot junctions and the basal leaf meristem (i.e. the meristematic region of the rhizome). These observations correlated well with the O_2 images revealing radial O_2 loss (ROL) from these specific regions of the plant (Extended Data Fig. 7.1). Light stimulation of the leaf canopy leading to photosynthetic O_2 evolution in the seagrass leaves, and thus an enhanced internal O_2 concentration gradient and thereby ROL to the rhizosphere, resulted in lower rhizosphere pH levels around roots and root/shoot junctions.

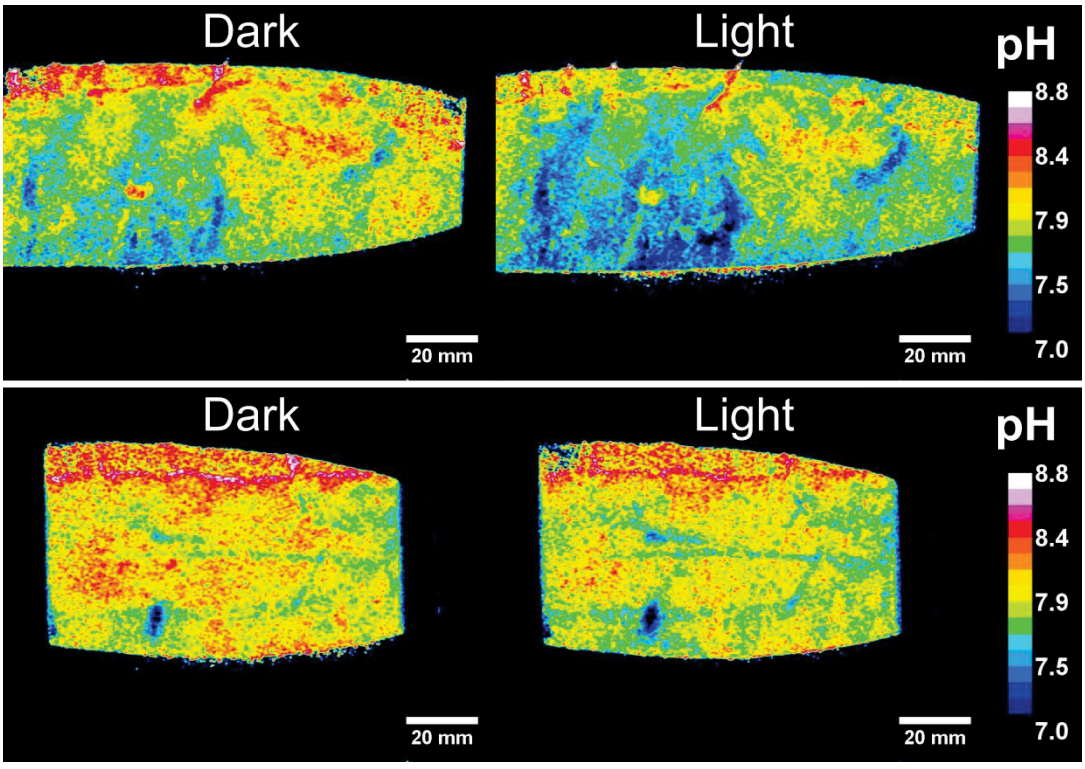

Extended Data Fig. 7.2. pH heterogeneity and dynamics within the seagrass rhizosphere of two specimens of the tropical seagrass *Cymodocea serrulata* during dark and light conditions (incident photon irradiance of ~500 µmol photons m^{-2} s^{-1}). The color coding depicts the pH value. The seagrasses were transplanted into sieved (<1mm sediment fraction) natural sediment from the sampling site to exclude larger animals and bivalves, as well as to ensure natural ratios of essential nutrients, buffering salts and microbes, respectively.

Extended Data Fig. 7.3

Concomitant chemical imaging of Fe(II), phosphate and pH

Extended Data Figure 7.3 shows the Fe(II), phosphorus and pH conditions at the root/sediment interface during light and dark conditions. Relative high concentrations of soluble Fe(II) and phosphorus were revealed around the roots of the seagrass *Cymodocea serrulata* (Extended Data Fig. 7.3a,c). All data originates from carbonate-rich sediments, which is known to have high phosphorus fixation capacities leading to insoluble calcium phosphate minerals that are not available to the plants. Seagrass-generated rhizospheric low-pH microniches owing to radial O_2 loss (ROL) and organic acid release led to carbonate dissolution and subsequent phosphate release to the pore water around the root-tip of the 4^{th} root (Extended Data Fig. 7.1-7.3). Our results also show that plant-released dissolved inorganic carbon (DOC) that has been shown to stimulate rhizospheric microbes, such as sulfate-reducing bacteria in the rhizosphere, leads to increased local sulfide production and thus reduction of Fe(III)-oxyhydroxides to dissolved Fe(II) (Extended Data Fig. 7.3a,c). Concomitantly, phosphate precipitated as Fe(III)phosphate and adsorbed by Fe(III)oxyhydroxides is released to the porewater. Rhizospheric Fe(II) and phosphorus concentrations along cross tissue line profiles (Profile 1-2 on chemical images; Extended Data Fig. 7.3a) are shown in panel c, which indicated that the phosphorus solubilization around the 4^{th} root was mainly induced by stimulation of sulfate reducers, and thus sulfide production, within the seagrass rhizosphere (Extended Data Fig. 7.3c).

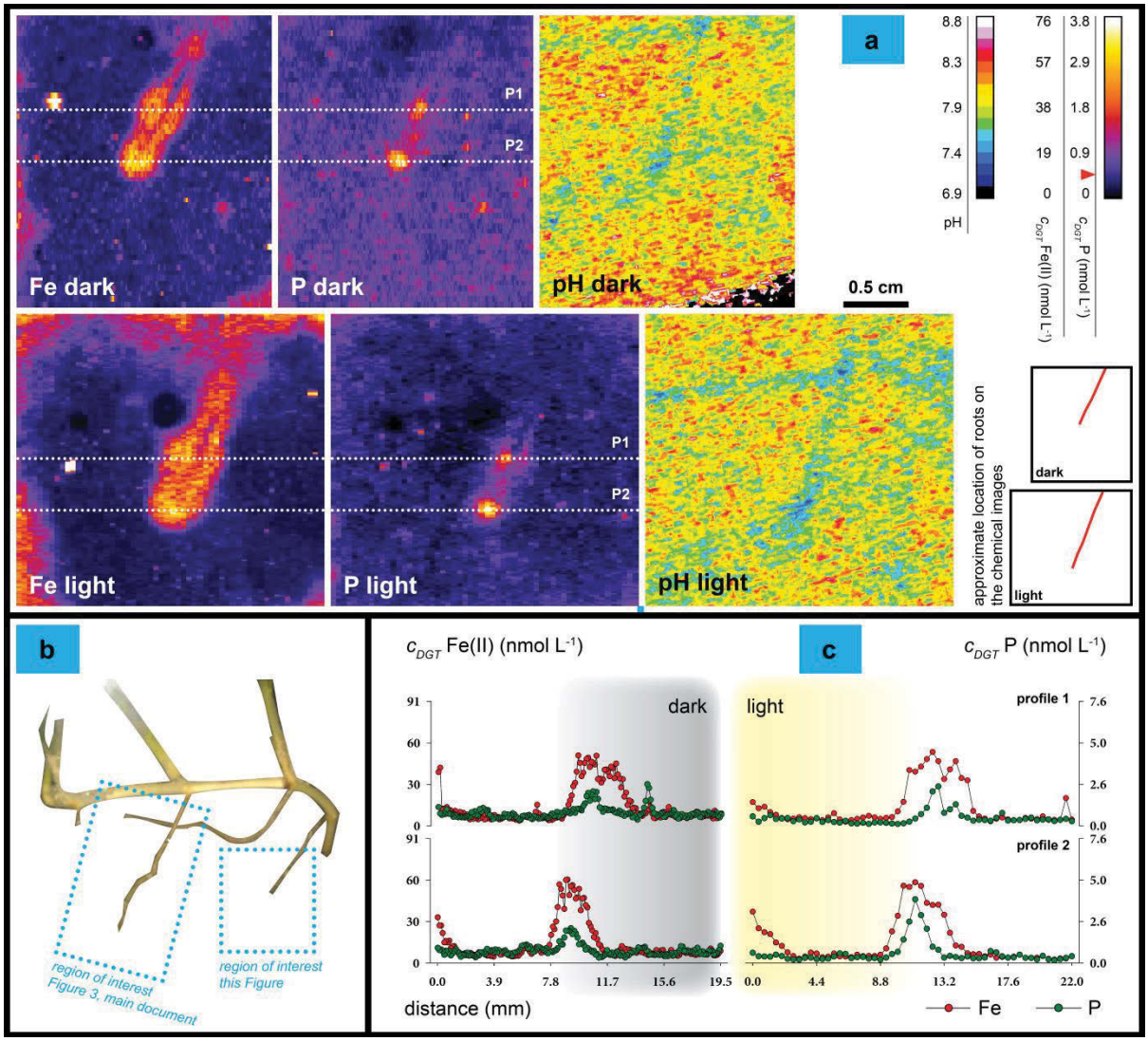

Extended Data Fig. 7.3. Rhizospheric Fe(II), phosphorus and pH conditions during dark and light conditions (incident photon irradiance of ~500 µmol photons m^{-2} s^{-1}) (a,c). Data is shown from the tropical seagrass species *Cymodocea serrulata*. Images are colour coded. Legends depict the analyte concentration (a). The red arrow on the phosphate calibration bar denotes the method detection limit (MDL) of the LA-ICPMS measurement (a). No such arrow is shown for Fe as the MDL was negligibly small in this case. Marked areas depict the selected regions of interest (b), as shown on the chemical images (panel a; and on figure 7.3 in the main text). Note the different scale on the y-axis.

Extended Data Fig. 7.4

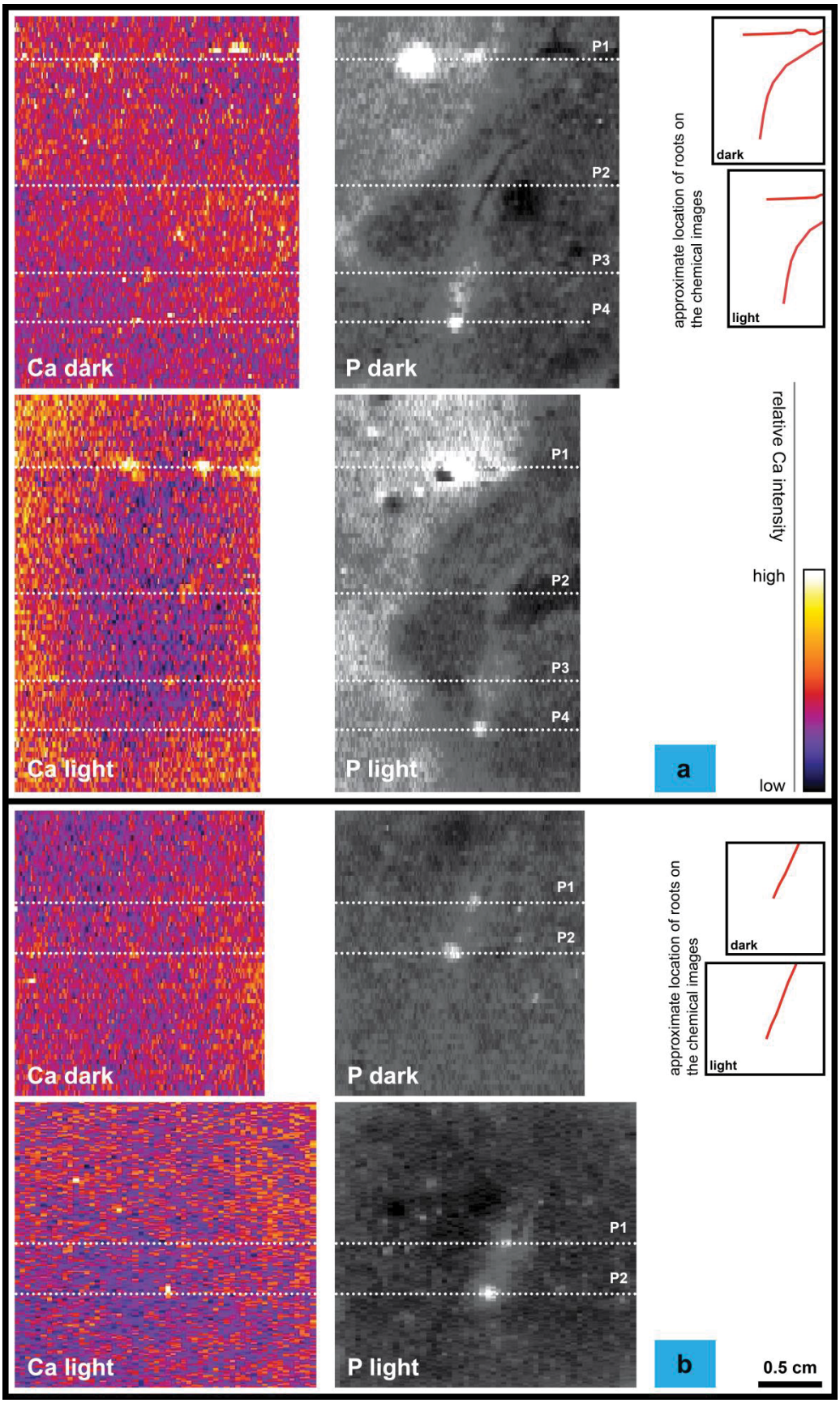

Extended Data Fig. 7.4. Distribution and dynamics of Ca concentration within the rhizosphere of the tropical seagrass *Cymodocea serrulata*. Seagrasses were exposed to dark and light conditions (incident photon irradiance of ~500 µmol photons m^{-2} s^{-1}). The color bar depicts the relative Ca concentration. The seagrasses were transplanted into sieved (<1mm sediment fraction) natural sediment from the sampling site to exclude any larger animals and bivalves, as well as to ensure natural ratios of essential nutrients and rhizosphere microbes.

SUPPORTING INFORMATION

Seagrass-derived rhizospheric phosphorus and iron mobilization

Kasper Elgetti Brodersen[1,*], Klaus Koren[2,*], Maria Moßhammer[2,*], Peter J. Ralph[1], Michael Kühl[1,2,#], Jakob Santner[3,4,#]

[1]Plant Functional Biology and Climate Change Cluster (C_3), Aquatic Processes Group, Faculty of Science, University of Technology Sydney (UTS), Sydney, Australia.

[2]Marine Biological section (MBL), Microenvironmental Ecology Group, Department of Biology, University of Copenhagen, Helsingør, Denmark.

[3]Division of Agronomy, Department of Crop Sciences, University of Natural Resources and Life Sciences, Vienna, Austria.

[4]Rhizosphere Ecology and Biogeochemistry Group, Institute of Soil Research, Department of Forest and Soil Sciences, University of Natural Resources and Life Sciences, Vienna, Austria.

[*]These authors contributed equally to this work and share the first authorship of this paper.

[#]Corresponding authors: mkuhl@bio.ku.dk (Michael Kühl) and jakob.santner@boku.ac.at (Jakob Santner)

Table of Contents

SUPPLEMENTARY MATERIALS AND METHODS

Notes S7.1.

In the following sections, we provide detailed information about techniques, methods and materials used to obtain the chemical images and results presented in the main document.

(a) List of used chemicals

Chemicals for optical sensor preparation:

Platinum(II)-meso(2,3,4,5,6-pentafluoro)phenyl-porphyrin (PtTFPP) was bought from Frontier Scientific (frontiersci.com). Macrolex® fluorescence yellow 10GN (MY) and carbon black were obtained from KREMER (kremer-pigmente.de). The lipophilic pH indicator 1-hydroxypyrene-3,6,8-tris-bis(2-ethylhexyl)sulfonamide (lipo-HPTS) was generously provided by Dr. Sergey Borisov (Graz University of Technology, Austria) who prepared it according to the literature (Borisov et al. 2009). Perylene and all organic solvents were obtained from Sigma-Aldrich (sigmaaldrich.com). The Polyethylene terephthalate (PET) support foil was obtained from Goodfellow (goodfellow.com). Polyurethane hydrogel (Hydromed D4) was obtained from AdvanSource biomaterials (advbiomaterials.com). Polystyrene (PS, MW 250,000 g mol^{-1}) was bought from ACROS Organics (acros.com).

Chemicals for diffusive gradients in thin films (DGT) gel preparation:

Acrylamide, $AgNO_3$, ferrozine, KI, NaCl, MES buffer, $NaNO_3$, ascorbic acid, KH_2PO_4, H_2SO_4, potassium antimony tartrate, CH_3COOH and CH_3COONa were obtained from Sigma-Aldrich (sigmaaldrich.com). HNO_3 · HCl, NaOH, $FeSO_4$, and ammonium molybdate tetrahydrate were purchased from Merck (merck.de). High-purity NaOH, $ZrOCl_2$ · xH_2O and AgI were bought from Alfa Aesar (alfa.com). HNO_3 was purchased from Roth and $(NH_4)_2S_2O_8$ (APS) as well as tetramethylethylenediamine (TEMED) were obtained from VWR (vwr.com). Membranes for the calibration were purchased from Whatman (whatman.com). The DGT gel cross-linker was bought from DGT research (dgtresearch.com). The suspended particle reagent iminodiacetic acid (SPR-IDA), a resin mainly selective for transition metal cations, was

purchased from Cetac (cetac.com). All chemicals were of highest available purity and were, if not stated differently, used as received.

(b) Experimental setup and sampling site

Seagrasses and carbonate-rich sediment sampling

Seagrass specimens, *Cymodocea serrulata* (R.Br.) Asch. & Magnus, and tropical carbonate-rich marine sediment were collected from shallow coastal waters (<2m depth) at Green Island, Cairns, Australia. After sampling, the seagrasses and the sediment were kept in constantly aerated seawater reservoirs at the Green Island Field Research Station (The Monkman Reef Research Station, Green Island, Cairns, Australia) before further analysis. Prior to experiments, the sediment was sieved down to <1 mm sediment fraction to exclude larger animals and bivalves. The investigated seagrasses were gently uprooted and transplanted into the pre-sieved/homogenized sediment within narrow experimental chambers (described below; Figure S7.1) and submerged in 20 L aquariums. Natural seawater from the sampling site was used throughout the experiments (temperature of ~28 °C; salinity of 30).

Experimental chambers

The experimental chambers (inner dimensions 10 × 130 × 120 mm) consisted of custom-made, narrow, transparent acrylic chambers with a removable back window made of polycarbonate for ease of access when transplanting the seagrasses and positioning the sensors/gels (described below). The experimental chambers were glued onto the side of aquaria in the upright position. The aquaria were made of thin glass walls (~3mm) to improve the optical properties during imaging. Illumination was provided by halogen lamps (Philips Incandescent 230V PAR38 80W). The downwelling photon irradiance (PAR, 400-700nm) at the leaf canopy level within the aquarium was ~500 µmol photons m^{-2} s^{-1}, as measured with a spherical quantum sensor (US-SQD/L, Walz GmbH, Germany) connected to a calibrated quantum irradiance meter (ULM-500, Walz GmbH, Germany). The light level was mimicking natural mid-day photon irradiances at leaf canopy height of the seagrass meadow. Water-column movement and aeration were ensured via a submerged water

pump and an air stone connected to an air pump, respectively. AgI and precipitated Zr-oxide diffusive gradients in thin films (DGT) gels sensitive to sulfide and phosphate, respectively, were positioned at the back-wall of the experimental chambers and were separated from the sediment/below-ground seagrass biomass by a fine mesh (plankton mesh DIN 100-60; mesh opening 60 µm, thickness 50 µm; obtained from www.tanaka-sanjiro.com), to allow for gel deployment and sampling without disturbing the sediment. Zr-oxide - SPR-IDA gels (multi-ion gels) were exposed to the sediment by a Whatman Nuclepore membrane, which furthermore was used to structurally preserve the gels during deployment and sampling. The planar optodes (described below) were fixed onto the aquarium wall using a thin layer of seawater, carefully avoiding air bubble formation in between the optode and the aquarium wall. Investigated seagrass specimens were positioned in the experimental chamber ensuring good contact between the below-ground biomass and the optode, before addition of natural marine sediment from the sampling site. When positioning the below-ground biomass at the optode or DGT gel, respectively, several camera pictures were recorded while marking the position of the below-ground biomass on either the non-sensitive site of the DGTs or on the chamber walls. This procedure enabled subsequent superimpose of the plant tissue structures on the chemical images. To precisely align the below-ground tissue with the chemical images, all obtained camera pictures included a ruler for guidance, which along with detailed root structure observations on the chemical images allowed us to precisely position the seagrass tissue on the colour coded chemical images as shown in the main text. The plant tissue structures were positioned on the chemical images using the software inkscape (version 0.48; inkscape.org).

The transplanted seagrass specimens and sediment were left undisturbed for a minimum of 12 h prior to experiments to ensure steady state redox conditions. This did not account for the multi-ion gels as they were covered with a Whatman Nuclepore membrane and then positioned in direct contact with the sediment, in a chamber not containing the fine plankton mesh, for 24h to ensure good signal readings. This procedure was chosen as the restricted spatial dimensions of the multi-ion gels (~4x5cm) did not allow for retrieving the gels without opening the experimental chamber.

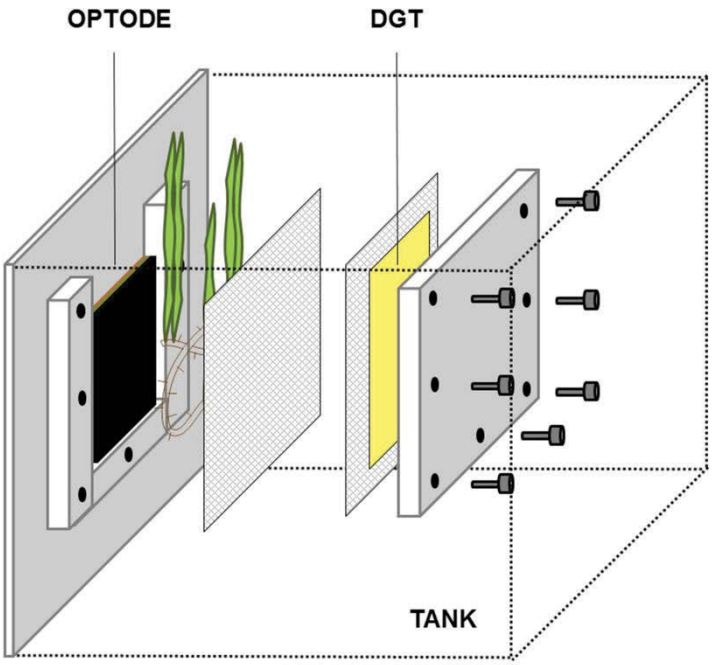

Figure S7.1. Schematic drawing of the custom-made, narrow experimental chambers positioned within the 20 L seawater reservoirs. Note the position of the optode and DGT gels on opposite sides of the investigated roots. During measurements we carefully ensured good contact between the below-ground biomass and the optode or the DGT gels, respectively.

Seagrass photosynthetic performance during cultivation

To monitor seagrasses health and photosynthesis during cultivation, we assessed the photosynthetic competence of the investigated seagrasses using fiber-optic pulse amplitude modulated (PAM) fluorometry (JuniorPAM, Walz GmbH, Germany) measuring the maximum quantum yield of photosystem II (PSII) activity in the dark adapted state (F_v/F_m= the maximal quantum yield of PSII) (Ralph & Short, 2007). The F_v/F_m, of all investigated seagrasses remained >0.7 throughout experiments confirming that the seagrasses were photosynthetically competent during cultivation (data not shown).

In situ measurements

To investigate the natural *in situ* dynamics and concentrations of the potent phytotoxin H_2S within the investigated seagrass meadow over a diel cycle, we deployed sulfide sensitive AgI DGT gels mounted within DGT samplers (DGT Research Ltd., www.dgtresearch.com) (Figure S7.2). DGT probes monitoring day-time sulfide concentrations within the meadow were

deployed at sunrise and retrieved at sunset. DGT probes monitoring night-time sulfide concentrations within the meadow were deployed at sunset and retrieved at sunrise.

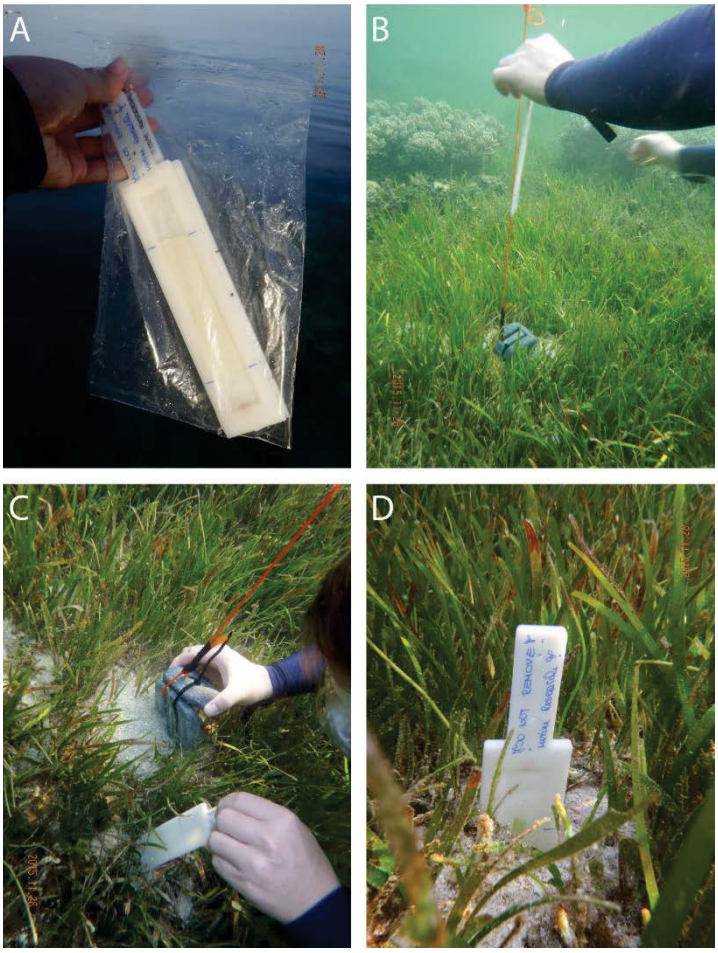

Figure S7.2. Deployment of sulfide sensitive AgI DGT gels *in situ*. (A) The sulfide sensitive DGT gels were mounted in DGT samplers, (B) the study site within the seagrass meadow (Green Island, Carins, Australia), (C) DGT gel deployment, and (D) gel sampler position within the seagrass meadow. To enable DGT deployment, a less densely vegetated spot was selected within the dense multi-species seagrass meadow. The DGTs were deployed at sunrise and retrieved at sunset for the daytime measurements and *vice versa* for the night measurements. Two deployments were performed in the investigated seagrass meadow.

(c) Optode preparation

Optical sensor films (i.e. planar optodes) where prepared via knife coating a sensor cocktail onto a transparent PET foil as follows. The cocktail used for the O_2 optode consisted of 1.5 mg of MY, 1.5 mg of PtTFPP, 100 mg of PS and 1 g of $CHCl_3$. After all components were

dissolved in $CHCl_3$, the solution was spread on a dust free PET foil using a film applicator (byk.com) to yield a ~10 µm thick sensor film after solvent evaporation. In order to exclude background light and to achieve highest possible resolution, an optical isolation layer was coated on top of the sensor film. This layer consisted of 1 % w/w (10 mg) of carbon black dispersed in 1 g 10 % w/w solution of D4 (EtOH: water, 9:1 w/w) and was knife coated on top of the sensor film (final thickness of the isolation layer ~7.5 µm).

The applied pH optode was prepared by knife coating a sensor cocktail consisting of 1 mg lipo-HPTS, 1 mg perylene and 100 mg D4 dissolved in 1 g of THF on a dust-free PET support foil. After solvent evaporation, the sensor layer had a thickness of ~10 µm. For the pH optode we decided not to use an isolation layer as migration of the indicator dye into this layer is more likely than in case of the O_2 optode, at the expense of a slightly reduced spatial resolution owing to light scattering from the sediment.

(d) Planar optode calibration

The calibration curve for the planar O_2 optode was generated to follows. A small piece of O_2 optode was taped into the experimental chamber. Oxygen levels of the seawater within the chamber were altered by means of compressed air and nitrogen, which were mixed by a PC-controlled gas mixer (SensorSense, The Netherlands). Simultaneously, the O_2 level in the water column was monitored via a calibrated O_2 optode system, i.e., an oxygen dipping probe connected to a Piccolo2 meter (PyroScience GmbH, Aachen, Germany). To ensure that equilibrium was reached, each calibration step was held for a minimum of 20 min. The final calibration was obtained by relating the measured red/green ratios to the measured O_2 levels. The calibration curve for the planar pH optode was generated by exposing the pH optode to buffer solutions with known pH (pH of 5.3, 6.7, 7.2, 7.6, 8.1, 9.1 and 12) measured using a calibrated pH microelectrode (Unisense A/S, Aarhus, Denmark). The salinity was adjusted to 30 ‰ using NaCl and was checked using a calibrated refractometer.

(e) DGT gel preparation

Diffusive gel (plain polyacrylamide) preparation. The polyacrylamide gels were prepared from a stock gel solution, according to standard procedures (Zhang and Davison 1999). This stock was produced by adding 15 mL DGT gel cross-linker to 47.5 mL MilliQ water (i.e. ultra-pure laboratory water; resistivity: >14.1 MΩ cm^{-1}), then adding 37.5 mL acrylamide solution (40% w/w). The mixture was stirred and afterwards stored at 4°C. Acid washed glass plates were separated by a spacer (either 0.25 mm or 0.5 mm) and clipped together. The gel solution (2 mL) was mixed with 14 µL APS solution (10% w/w) and 5 µL TEMED and quickly pipetted between the glass plates. The plates were placed in an oven at 42°C for 40 minutes for polymerization. The polyacrylamide hydrogels were soaked in MilliQ water for 24 hours (the water was exchanged at least three times) and stored in a 0.03 M $NaNO_3$ solution.

Precipitated Zr-oxide binding gel for densitometric phosphate mapping. The phosphate binding gel was prepared by soaking a 0.4 mm thick diffusive gel in a $ZrOCl_2$ solution according to Guan et al. (2015). For this, 1.78 g $ZrOCl_2$ x H_2O were dissolved in 40 mL MilliQ water, a diffusive gel was added and the volume topped up to 100 mL. The gel was soaked for at least 2 hours, retrieved, rinsed with MilliQ water, put into 100 mL MES buffer (0.05 M, pH 6.7) and placed for 40 minutes on a shaker. Zirconium oxide precipitation started immediately, resulting in a gel densely impregnated with Zr-oxide. The gel was retrieved, rinsed with MilliQ water and stored in a 0.01 M $NaNO_3$ solution. After phosphate sampling, this gel was subjected to the densitometric phosphate mapping method described by Ding et al. (2013). However, due to time restrictions on the field station, the temperature treatment steps were reduced for the deployed gels from 5 days at 85°C to 12 h, which accounts for by far the most of the heat effect (Ding et al. 2013), and the color development step was conducted at room temperature (30°C instead of 35 °C). As the calibrations of the Zr-oxide gels were performed in the exact same manner, this should counter-balance the potential minor dissolution (reduction) of phosphate from the binding gels in the acidic staining solution.

AgI binding gels for densitometric sulfide mapping. For densitometric sulfide analysis, we modified the sulfide binding gels described in Teasdale et al. (1999) by replacing the polyacrylamide gel matrix with Hydromed D4. The novel sulfide gels were produced by

dispersing 1.25 g of the AgI slurry in 7.5 g 10% w/w D4 (ethanol : water, 9:1 w/w) solution using an Ultra-Turrax disperser. This cocktail was then knife-coated onto a dust-free Mylar PET foil using a 0.25 mm spacer. This novel procedure avoided handling of carcinogenic acrylamide and resulted in a more homogeneous AgI distribution than in the older method (Teasdale et al. 1999).

Zr-oxide - SPR-IDA gels for anion-cation mapping using LA-ICPMS. Gels for simultaneous anion and cation binding were prepared according to Kreuzeder et al. (2013). Briefly, Zr-oxide was precipitated by slowly titrating a 30 g L^{-1} $ZrOCl_2 \times xH_2O$ solution with 0.1 mol L^{-1} NaOH until the pH stabilized at pH 7.0. The precipitate was washed and the water removed using a Buechner funnel. A D4 solution was prepared by dissolving 10 g of D4 in 100 mL of a 9:1 v/v ethanol-water solution. Fifteen grams of the Zr-oxide slurry were put into a vial and topped up to 100 mL with the D4 solution. The mixture was homogenized using an Ultra-Turrax disperser. Afterwards, 1 mL of SPR-IDA suspension was added to 9 mL of the Zr-oxide solution and mixed vigorously by hand. Air bubbles were removed by rotating the vial slowly in an overhead shaker overnight. Subsequently, three layers of this solution were knife-coated onto a glass plate on top of each other, with evaporating the solvent in an oven between coating the individual layers. The glass plate was immersed in MilliQ for at least 4 h for gel hydration. After this period, the gel detached easily from the glass. The gel was fully hydrated for another 24 h and stored in a 10 mmol L^{-1} $NaNO_3$ solution at 6°C.

(f) DGT gel analysis and image generation

Computer imaging densitometry of AgI and precipitated Zr-oxide gels.

Molybdate-blue staining of the precipitated Zr-oxide gels. Analysis of precipitated Zr-oxide gels was performed according to Ding et al. (2013) with some modifications due to limitations on the field station (described above). After the heat treatment, applied to irreversibly immobilize the phosphate bound to the Zr-oxide gel, the precipitated Zr-oxide gels were immersed in a molybdate blue staining reagent for 45 min (Ding et al. 2013). This procedure leads to blue color formation at gel locations where phosphate was bound.

Subsequently, the stained Zr-oxide gels were subjected to computer imaging densitometric (CID) analysis.

No staining step was necessary for the sulfide bound to the AgI gels (Teasdale et al. 1999).

Computer imaging densitometry of the AgI and precipitated Zr-oxide gels. This analysis was conducted using a simple, commercially available Canon MG2460 printer with incorporated flatbed scanner according to published procedures (Ding et al. 2013, Teasdale et al. 1999). After retrieval of the gels, the protective mesh was removed. The precipitated Zr-oxide gels were stained as described above, and the AgI gels were left untreated. The gels were then fixed flat between two PET sheets in order to avoid direct contact with the scanner, scanned at a resolution of 600 dpi and saved as color and greyscale .tiff files. For calibration, standard gels were exposed to known analyte concentrations, subsequently stained (only accounts for the phosphorous sensitive gels) and scanned using the same scanner settings. From the obtained grayscale values and the known analyte concentrations, calibrations functions were determined using ImageJ (readout of grayscale values) and Origin Pro (data analysis and fitting). Applied calibration curves are provided below (Fig. S7.5 & S7.6). Based on the acquired calibrations functions the sample gels were analyzed.

Laser ablation inductively coupled plasma mass spectrometric (LA-ICPMS) analysis

LA-ICPMS analysis was performed following Kreuzeder et al. (2013). After deployment to the microcosms, Zr-oxide - SPR-IDA gels were transferred to a piece of polyethersulfone (SUPOR, Pall corporation) membrane and dried using a gel dryer (Unigeldryer 3545, Laborgeräte and Vertriebs GmbH), resulting in an inseparable composite of the membran and the dried gel (Kreuzder et al. 2013). This composite was then mounted on glass slides using double-sided adhesive tape and subjected to LA-ICPMS analysis on a UP 193-FX (ESI, NWR division) laser ablation instrument coupled to a Nexion 350D ICPMS (Perkin Elmer) in line-scanning mode using the following parameters: inter-line distance: 400 µm, laser spot size diameter: 150 µm, line scanning speed: 250 µm s^{-1}, laser pulse frequency: 20 Hz, irradiance: 1-2 J cm^{-2}. Argon was used as the carrier gas. Count rates were recorded for several isotopes including ^{13}C, ^{31}P and ^{57}Fe. ^{13}C was used as internal normalisation standard. Total ICPMS measurement cycle times were 0.383 and 0.453 s for two individual

measurement days. These settings resulted in a spatial resolution of 96 - 113 µm in the x direction and 400 µm in the y direction, which is essential when determining biogeochemical process at interfaces (Brodersen et al. 2016). For calibration, standard gels with known analyte concentrations were scanned using the same procedure. Chemical images were generated and arranged using Microsoft Excel, ImageJ, Systat SigmaPlot, Adobe Photoshop and Adobe Indesign.

(g) DGT interpretation

While planar optodes provide a direct concentration measurement, the DGT measurement cannot be directly interpreted as an actual porewater concentration. DGT gels continuously bind analytes from the exterior solution during deployment. After gel retrieval, LA-ICPMS and CID measure the mass of analyte taken up by the gel as a surface concentration c_S, e.g. in µg cm^{-2}. Due to the well-defined sampling geometry, this parameter can be converted to the concentration at the sampler-exterior solution interface, c_{DGT}, using (Davison and Zhang 1994)

$$c_{DGT} = c_S \frac{\Delta g}{Dt}$$

where Δg is the thickness of the diffusion layer overlying the binding gel, in this case the protective mesh, D is the analyte diffusion coefficient inside the diffusion layer and t is the deployment time. As c_{DGT} is calculated from the mass of analyte accumulated during the total gel deployment time, it represents the time-averaged analyte concentration at the sampler-solution interface.

In simple, synthetic aqueous solutions, where only fully labile analyte species are present, c_{DGT} provides a direct measure of the exterior solution concentration, as the flux of analyte to the DGT gel is constant throughout the deployment time. In sediments, the porewater concentration of many solutes is governed by sorption/desorption and dissolution/precipitation equilibria, so solutes are usually not fully labile (Davison et al. 2007). Moreover, sediment tortuosity further restricts solute diffusivity. Therefore, DGT analytes are depleted in sediment adjacent to the sampler as a consequence of being

sequestered on the binding gel. The actual porewater concentration at the sampler-sediment interface is thus decreasing progressively during sampling, as is the flux into the DGT sampler. The c_{DGT} concentration obtained under these circumstances is therefore smaller than the porewater concentration without perturbation by DGT sampling (Davison et al. 2007, Santner et al. 2015).

(h) Calibration plots

Planar optode calibrations:

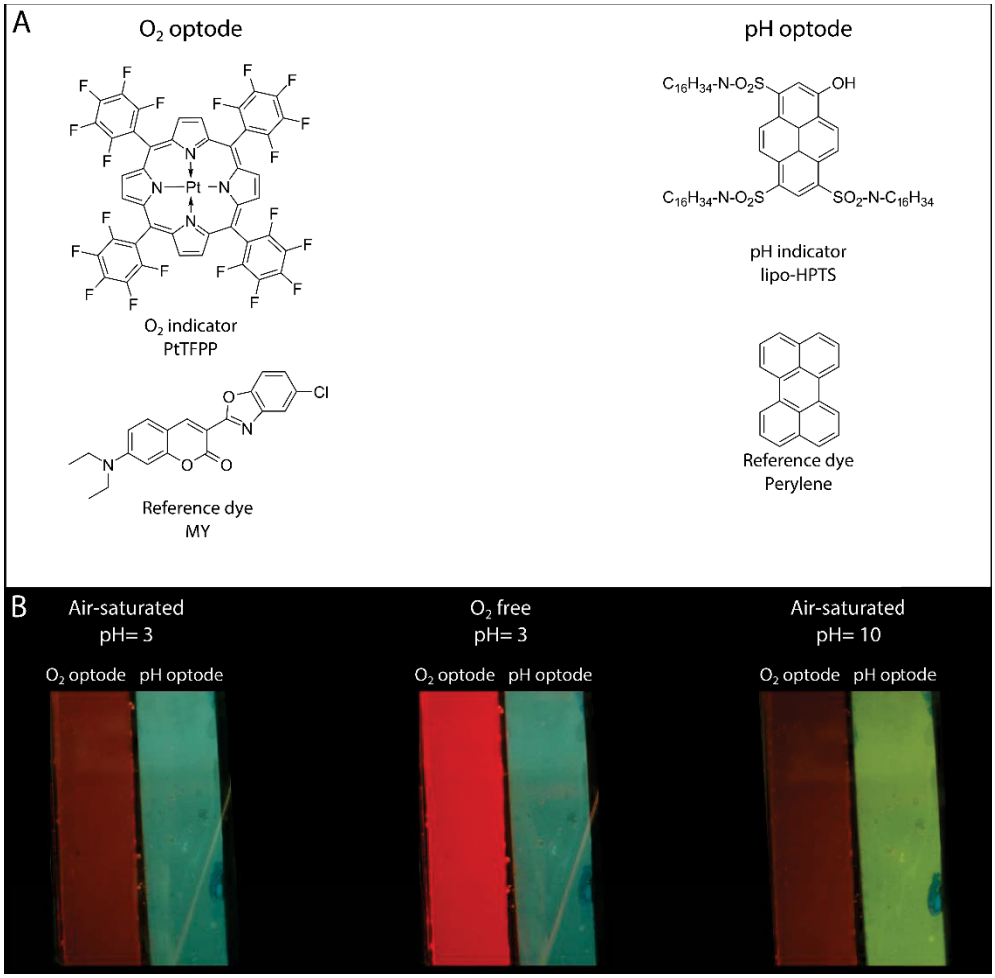

Figure S7.3. (A) Chemical structures of the indicators and references dyes used in the O_2 and pH optodes, respectively. (B) Images of an O_2 and pH optode positioned next to each other and exposed to different analyte concentrations (i.e. O_2 and pH levels). The images were obtained with a SLR camera (EOS 1000D, Canon, Japan) and the optodes were excited using a hand-held UV lamp. In this setup, the O_2 sensor had no additional optical isolation layer.

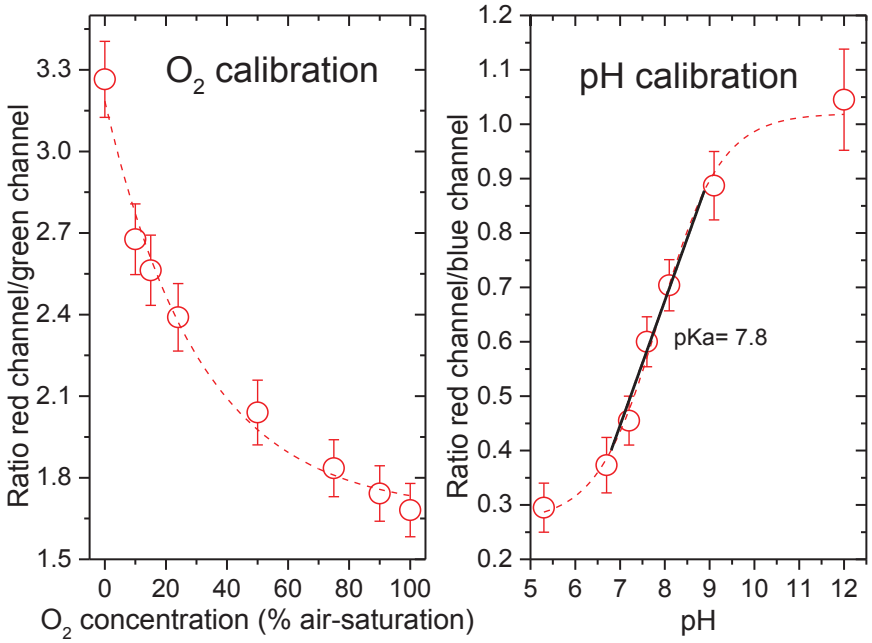

Figure S7.4. Calibration plots of the O_2 and pH optodes used in the study. All data points with erro bars represent mean values with the corresponding standard deviation (n=3-6). For the O_2 optode a single exponential decay function was fitted (dashed line; R^2> 0.98) and this fit was used for calibrating the experimental O_2 images. The pH optode response was fitted using a sigmoidal function (dashed line; R^2> 0.98). For practical reasons (i.e. the applied software ImageJ does not support this type of fit) a linear fit in the range pK_a±1 was used. The used linear fit is depicted as the black line in the calibration plot above (pH range 7-9). Within the chosen pH range this type of linear fit describes the sensor response to changing pH values very well (R^2>0.98), without notable experimental errors.

DGT calibrations:

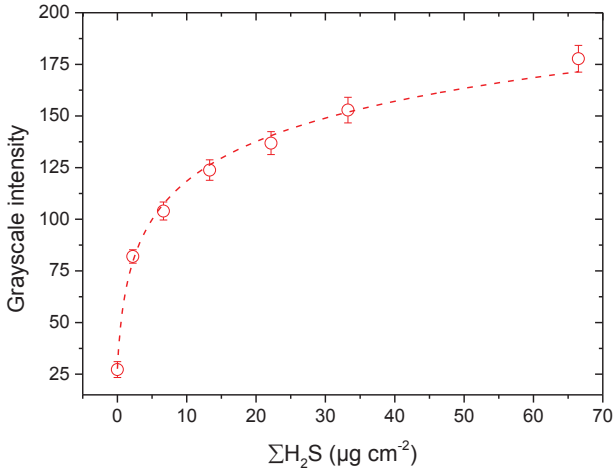

Figure S7.5. Calibration plot of the sulfide binding AgI gel used in this study. All data points represent mean values ± S.D. (n=3-6) and were fitted using the following function: y=b*ln(x-a); (R^2 > 0.99).

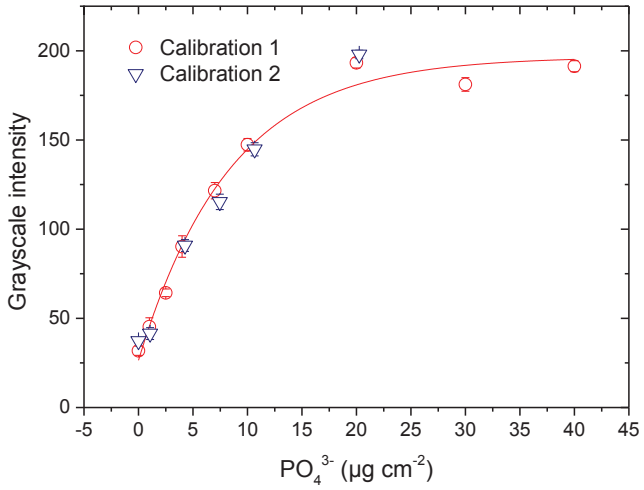

Figure S7.6. Calibration plot of the PO_4^{3-} binding precipitated Zr-oxide gel used in this study. The curve shows a calibration of gels made in Denmark and shipped to Australia (Calibration 1) and one of gels made at the actual remote study site (Green Island, Cairns, Australia; Calibration 2). Data points with error bars represent mean values ± S.D. (n=3-6) and were fitted using the following function: $y=y_0 + A*e^{R0*x}$; (R^2 > 0.98).

REFERENCE LIST

Borisov SM, Herrod DL, Klimant I. (2009). Fluorescent poly(styrene-block-vinylpyrrolidone) nanobeads for optical sensing of pH. *Sensors Actuators B Chem.* **139** (1): 52–58.

Davison W, Zhang H. (1994). In situ speciation measurements of trace components in natural waters using thin-film gels. *Nature* **367**: 546-548.

Davison W, Zhang H, Warnken KW. (2007). Chapter 16 - Theory and applications of DGT measurements in soils and sediments. In: G R., M G., V B. (eds) Comprehensive Analytical Chemistry Passive Sampling Techniques in Environmental Monitoring. Elsevier.

Ding S, Wang Y, Xu D, Zhu C, Zhang C. (2013). Gel-based coloration technique for the submillimeter-scale imaging of labile phosphorus in sediments and soils with diffusive gradients in thin films. *Environ Sci Technol*. **47**: 7821-7829.

Guan D-X, Williams PN, Luo J, Zheng J-L, Xu H-C, Cai C, Ma LQ. (2015). Novel Precipitated Zirconia-Based DGT Technique for High-Resolution Imaging of Oxyanions in Waters and Sediments. *Environ Sci Technol.* **49**: 3653-3661. doi: 10.1021/es505424m.

Ralph PJ, Short FT. (2002). Impact of the wasting disease pathogen , Labyrinthula zosterae , on the photobiology of eelgrass Zostera marina. *Mar. Ecol. Prog. Ser.* **226** (1936): 265–271.

Kreuzeder A, Santner J, Prohaska T, Wenzel WW. (2013). Gel for simultaneous chemical imaging of anionic and cationic solutes using diffusive gradients in thin films. *Anal Chem*. **85**: 12028-12036. doi: 10.1021/ac403050f.

Santner J, Larsen M, Kreuzeder A, Glud RN. (2015). Two decades of chemical imaging of solutes in sediments and soils - a review. *Anal Chim Acta* **878**: 9-42. doi: 10.1016/j.aca.2015.02.006.

Teasdale PR, Hayward S, Davison W. (1999). In situ, High-Resolution Measurement of Dissolved Sulfide Using Diffusive Gradients in Thin Films with Computer-Imaging Densitometry. *Anal. Chem.* **71** (11): 2186–2191.

Brodersen KE, Koren K, Lichtenberg M, Kühl M. (2016). Nanoparticle-based measurements of pH and O_2 dynamics in the rhizosphere of *Zostera marina* L.: Effects of temperature elevation and light/dark transitions. *Plant, Cell & Environment***.** (accpeted on March 22, 2016)

Zhang H, Davison W. (1999). Diffusional characteristics of hydrogels used in DGT and DET techniques. *Anal Chim Acta* **398**: 329-340.

Chapter 8

Sediment resuspension and deposition on seagrass leaves impedes internal plant aeration and promotes phytotoxic H_2S intrusion

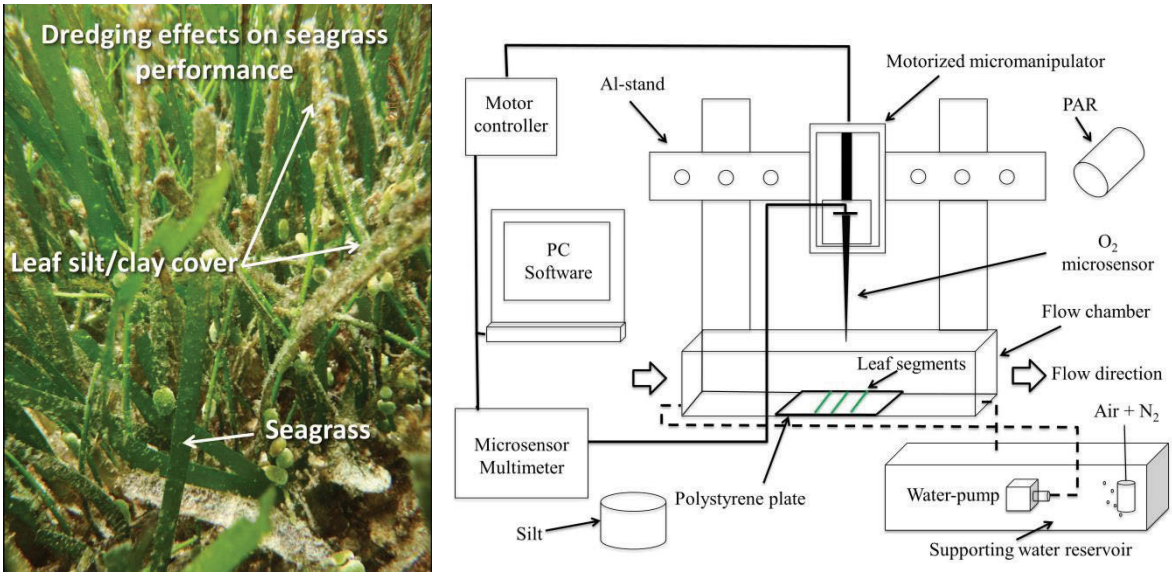

TOC figure. *Left panel show thin silt/clay covers on seagrass leaves. Right panel illustrates the experimental setup. Effects of leaf silt/clay covers were determined both in situ and under controlled conditions in the laboratory.*

Citation: Brodersen KE, Hammer KJ, Schrameyer V, Fløytrup A, Rasheed M, Ralph PJ, Kühl M. & Pedersen O. Sediment resuspension and deposition on seagrass leaves impedes internal plant aeration and promotes phytotoxic H_2S intrusion. (In review).

Highlights: The aim of this study was to investigate effects of sediment re-suspension, caused by e.g. coastal development and Harbour dredging activities, on plants performance, internal tissue aeration and susceptibility to phytotoxic H_2S intrusion in the common temperate seagrass species *Zostera muelleri*. To address this aim, we performed detailed microsensor measurements of O_2 fluxes across the leaf-tissue surface of plants with or without silt/clay-covered leaves measured under controlled conditions in the laboratory, as well as *in situ* measurements of simultaneous meristematic O_2 and H_2S concentrations in seagrasses exposed to experimentally manipulated sediment re-suspension. We found phytotoxic H_2S intrusion into seagrasses exposed to sediment re-suspension and our experiments clearly demonstrated that silt/clay covers on seagrass leaves hamper plant performance reducing the internal tissue aeration and thus enhancing the risk of night-time H_2S intrusion.

Sediment resuspension and deposition on seagrass leaves impedes internal plant aeration and promotes phytotoxic H_2S intrusion

Kasper Elgetti Brodersen[1,*], Kathrine Jul Hammer[2], Verena Schrameyer[1], Anja Fløytrup[2], Michael Rasheed[3], Peter J. Ralph[1], Michael Kühl[1,4], Ole Pedersen[2,5,*]

Running title: "Dredging effects on seagrass performance".

[1] Plant Functional Biology and Climate Change Cluster, Aquatic Process Group, Faculty of Science, University of Technology Sydney, 15 Broadway, Sydney, NSW 2007, Australia

[2]Freshwater Biological Laboratory, Department of Biology, University of Copenhagen, Universitetsparken 4, DK-2100, Copenhagen, Denmark

[3]Centre for Tropical Water & Aquatic Ecosystem Research (TropWater), James Cook University, 14-88 McGregor Rd, Cairns, QLD 4870, Australia

[4]Marine Biological Section, Department of Biology, University of Copenhagen, Strandpromenaden 5, DK-3000, Helsingør, Denmark

[5]School of Plant Biology, The University of Western Australia, 35 Stirling Highway, Crawley, WA 6007, Australia

[*]Corresponding authors: Kasper Elgetti Brodersen, elgetti@hotmail.com and Ole Pedersen, opedersen@bio.ku.dk.

BRIEF SUMMARY

Fine sediment particles on seagrass leaves severely hampers the plants performance in both light and darkness, leading to inadequate internal aeration and intrusion of phytotoxic H_2S.

ABSTRACT

Anthropogenic activities leading to sediment re-suspension have adverse effects on adjacent seagrass meadows, owing to reduced light availability. Moreover, suspended particles settling onto seagrass leaves potentially impede gas exchange with the surrounding water.

We used microsensors to determine O_2 fluxes and diffusive boundary layer (DBL) thickness on leaves of the seagrass *Zostera muelleri* with and without fine sediment particles, and combined these laboratory measurements with *in situ* microsensor measurements of tissue O_2 and H_2S concentrations.

Net photosynthesis rates in leaves with fine sediment particles were down to ~20% of controls without particles, and the compensation irradiance increased from 20-53 to 109-145 µmol photons m^{-2} s^{-1}. An ~2.5-fold thicker DBL around leaves with fine sediment particles impeded O_2 influx into the leaves during darkness. *In situ* leaf meristematic O_2 concentrations of plants exposed to sediment re-suspension were lower than in control plants and exhibited long time periods of complete meristematic anoxia during night-time. Insufficient internal aeration resulted in H_2S intrusion into the leaf meristematic tissues when exposed to sediment resuspension even at relatively high night-time water-column O_2 concentrations.

Re-suspended sediment particles that settle on seagrass leaves thus negatively affect internal tissue aeration and thereby resilience against H_2S intrusion.

Keywords: Diffusive boundary layer, dredging, H_2S, in situ, microsensors, O_2, photosynthesis, seagrass, sediment

INTRODUCTION

Anthropogenic activities that result in the addition and re-suspension of fine materials such as dredging, point source outfall discharges and runoff from agricultural and urban catchments can have substantial negative impacts on the health and fitness of seagrasses (Erftemeijer & Lewis, 2006). Dredging operations e.g. during harbour expansion or construction work can result in direct removal of plant material and plant burial by suspended sediment. The indirect effects associated with turbid sediment plumes, have largely been attributed to reduced light availability impeding seagrass photosynthesis (e.g., Erftemeijer & Lewis, 2006; York et al., 2015). Dredging-induced seagrass mortality depends on the nature of the dredging operations including the duration and intensity (Erftemeijer & Lewis, 2006; York et al., 2015), but some larger dredging activities result in widespread sediment plumes that can significantly reduce light transmission through the water-column (Cutroneo et al., 2013). Even small reductions in light availability can cause pronounced declines in the distribution and growth of seagrass meadows (Ralph et al., 2007). Seagrasses generally have high light requirements, as they are typically found in waters, where at least 10% of incident solar irradiance reaches the seagrass leaf canopy (Duarte, 1991) and sediment resuspension for prolonged time periods can thus strongly affect plant fitness.

Apart from light attenuation, sediment plumes can also result in the settling of fine sediment particles on seagrass leaves, especially if the plants are already covered by epiphytes that have high potential to trap the sediment e.g. due to their excretion of exopolymers. The effects of such sediment coverage on the performance of seagrasses remain largely unexplored although such sediment layers may result in a further substantial reduction in light availability for the underlying leaves, analogous to the adverse shading effects of leaf epiphytes (Brodersen et al., 2015a). Epiphytic microalgae on seagrass leaves have also been shown to significantly increase the thickness of the diffusive boundary layer (DBL) (Brodersen et al., 2015a), that is a thin unstirred layer of water, wherein solute and gas exchange between tissues and the surrounding water occurs by molecular diffusion, which is a slow process compared to bulk exchange (e.g., Jørgensen & Revsbech, 1985; Hurd, 2000). The transport time of O_2 across the DBL increases with the square of the distance and increasing DBL thickness can thus affect the O_2 exchange of the seagrass leaf

substantially (Jørgensen & Des Marais, 1990; Hurd, 2000; Binzer et al., 2005). During the day, thick DBLs may result in increased photorespiration due to tissue accumulation of O_2 (e.g. Maberly, 2014), but thick DBLs can be particularly problematic during darkness, where seagrasses completely rely on the diffusive supply of O_2 from the surrounding water-column to fuel aerobic respiration of their leaves and below-ground tissues (Borum et al., 2006; Pedersen et al., 2016).

Sediment resuspension may also inflict decreased water-column O_2 concentrations due to chemical oxidation of reduced metabolites and metals (Erftemeijer & Lewis, 2006) or increased aerobic mineralization of labile organic matter accumulated in the sediment under anoxic conditions. The chemical and biological O_2 demand of suspended particles adds to the substantial O_2 consumption by the dense seagrass meadows during night-time, potentially resulting in water-column hypoxia (Greve et al., 2003; Borum et al., 2005; 2006). Night-time water-column hypoxia can result in inadequate internal aeration of belowground seagrass tissues resulting in shrinking or disappearance of the oxic micro-shield generated by radial O_2 loss (ROL) in the rhizosphere (Brodersen et al., 2015b; Koren et al., 2015). Decreased or absent ROL, can result in intrusion of phytotoxic H_2S from the surrounding anoxic sediment inhibiting seagrass metabolism due to H_2S strong binding capacity with iron in cytochrome *c* oxidase in the mitochondrial respiratory electron transport chain (Raven & Scrimgeour, 1997; Holmer & Bondgaard, 2001; Perez-Perez et al., 2012; Lamers et al., 2013). Such H_2S intrusion into seagrasses has been demonstrated both under controlled conditions in the laboratory (Pedersen et al., 2004) and in a die-off patch in the field (Borum et al., 2005). Interestingly, seagrasses possess internal detoxification mechanisms, whereby some tissue H_2S is oxidized to elemental sulphur within the aerenchyma (Holmer & Hasler-Sheetal, 2014; Hasler-Sheetal & Holmer, 2015). Adequate internal aeration is thus a perquisite for healthy seagrass meadows.

The O_2 partial pressure (pO_2) of seagrass tissues is determined by four main factors: (i) the diffusive O_2 flux from the water-column into the leaves during darkness (Pedersen et al., 2004), (ii) photosynthetic O_2 production during the day (Dennison, 1987; Fourqurean & Zieman, 1991), (iii) the respiratory demand of the plant that is strongly affected by the ambient temperature (Raun & Borum, 2013), and (iv) the combined sediment O_2 demand

affecting the ROL in the rhizosphere (Pedersen et al., 1998; Jensen et al., 2005; Borum et al., 2006; Frederiksen & Glud, 2006).

In the present study, we combined experimental sediment resuspension experiments with microsensor measurements to investigate (i) the rates of photosynthesis and respiration, (ii) the potential role of settled sediment particles on DBL-impedance of O_2 exchange with the water-column, (iii) the internal O_2 status of the meristematic tissue, and (iv) the meristematic H_2S concentrations in the seagrass *Zostera muelleri* spp*. capricorni*. Detailed microsensor measurements were performed both under controlled laboratory conditions and *in situ*, and were coupled to the light, temperature and O_2 conditions in the surrounding water-column. We thus tested the hypotheses that sediment deposits on seagrass leaves leads to (i) reduced photosynthetic efficiency, owing to reduced light availability, as well as reduced gas exchange with the surrounding water column, (ii) reduced internal aeration of below-ground seagrass tissue, and (iii) intrusion of H_2S into the seagrass. Our data add important ecophysiological information on the resilience/sensitivity of seagrasses to environmental disturbances linked to anthropogenic activities that lead to increases in suspended sediments.

MATERIALS AND METHODS

Seagrass and sediment collection

Specimens of *Zostera muelleri* spp. *capricorni* (Asch.) S.W.L. Jacobs and marine sediment were collected from shallow waters (<2 m depth) in Narrabeen Lagoon, NSW, Australia in April 22, 2015. A plastic corer with an inner diameter of 6.3 cm was used to sample bulk sediment cores adjacent to the investigated seagrass meadow. After sampling, seagrasses and sediment were transported to the laboratory, where they were kept in constantly aerated seawater reservoirs (23°C; salinity = 29) prior to further investigations.

Sediment sieving

Multiple sieves were used to obtain the fine sediment particle fraction with <63 µm grain size, henceforth referred to as silt/clay, from a sheltered area of the lagoon. After sieving,

the obtained silt/clay particles and water were left undisturbed over-night in enclosed 10 L containers to allow the suspended particles to resettle. On the following day, the supernatant was carefully drained off avoiding resuspension, and the silt/clay fraction was stored in 1 L sample jars for up to 7 days until used in subsequent experiments. Furthermore, to enable differentiation between physical effects caused by the grains themselves and effects mainly driven by microbial activity within the silt/clay, some of the obtained silt/clay was sterilized by heating it to 120°C in an oven for 2 h within sealed containers to minimize evaporation.

Laboratory measurements

Experimental setup

Leaf segments from 3 randomly selected *Z. muelleri* plants were positioned horizontally in a custom-made flow chamber (Brodersen et al., 2014). Within the chamber, leaf segments were fixed onto a polystyrene plate by needles. The cut ends of the investigated leaf segments were sealed with petroleum jelly prior to experiments to seal the aerenchyma from the surrounding water. A constant flow (~1 cm s^{-1}) of aerated seawater (23°C, salinity = 29) was maintained in the flow chamber via a pump submerged into a seawater reservoir. Illumination was provided by a fiber-optic tungsten halogen lamp fitted with a collimating lens (KL-2500LCD, Schott GmbH, Germany). The downwelling photon irradiance (PAR, 400-700 nm) at the leaf surface was measured with a scalar irradiance minisensor (US-SQS/L, Walz GmbH, Germany) connected to a calibrated photon irradiance meter (LI-250A, LI-COR, USA). The leaf segments were illuminated with an incident photon irradiance of 0, 75, 200 and 500 µmol photons m^{-2} s^{-1}. Water-column hypoxia was obtained by continuously flushing the seawater in the supporting water reservoir with a mixture of atmospheric air and humidified nitrogen. The O_2 concentration of the water reservoir was simultaneously monitored by a submerged Clark-type O_2 microsensor (OX-10, tip diameter of 10 µm, Unisense A/S, Aarhus, Denmark; Revsbech, 1989).

O_2 microelectrode measurements

We used Clark-type O_2 microsensors (OX-50, tip diameter of ~50 µm, detection limit ~0.3 µM, Unisense A/S, Aarhus, Denmark; Revsbech, 1989) with a fast response time (t_{90} <0.5 s) and a low stirring sensitivity (<2-3%) to measure the O_2 concentration at and towards the leaf surface. The O_2 microsensors were mounted on a motorized micromanipulator (Unisense A/S, Aarhus, Denmark) and connected to a microsensor multimeter (Unisense A/S, Aarhus, Denmark) both interfaced with a PC running dedicated data acquisition and positioning software (SensorTrace Pro, Unisense A/S, Aarhus, Denmark). The O_2 microsensors were linearly calibrated from signal readings in 100% air saturated seawater and anoxic seawater (by N_2 flushing and addition of the O_2 scavenger Na_2SO_3) at experimental temperature and salinity. Prior to measurements and calibrations, the microsensors were pre-conditioned with H_2S to prevent drifting calibrations when exposed to H_2S during experiments (Brodersen et al., 2015a). Microsensors were carefully positioned at the leaf tissue surface (defined as 0 µm distance on figures) by manually operating the micromanipulator, while observing the leaf tissue surface and microsensor tip with a boom-stand dissection microscope (AmScope, Irvine, CA, USA). When changing the downwelling photon irradiance, steady state O_2 conditions at the leaf surface re-occurred after ~60 min (data not shown). Microprofiles of O_2 concentration were measured in vertical increments of 100 µm, from the leaf tissue surface to 2 mm distance away.

Photosynthesis and respiration calculations

O_2 fluxes across the leaf tissue surfaces were calculated using Fick's first law of diffusion:

$$J_{O_2} = -D_0 \frac{\partial C}{\partial z} \quad (1)$$

where D_0 is the molecular diffusion coefficient of O_2 in seawater at experimental temperature and salinity ($2.14 \cdot 10^{-5}$ cm^{-2} s^{-1}; cf. tabulated physical parameters for marine systems available at www.unisense.com), and $\partial C/\partial z$ is the linear O_2 concentration gradient in the diffusive boundary layer (DBL). As we introduced a physical barrier to O_2 diffusion at the abaxial surface by fixing the leaf onto polystyrene with a low O_2 permeability, we take the flux estimated at the adaxial side of the seagrass leaf as representative for the net flux

of O_2 across the leaf surface, i.e., $J_{O2,tot} = J_{O2,upper\text{-}surface}$ in dark (=respiration) and light (=net photosynthesis), respectively.

The calculated net photosynthesis rates (nmol O_2 m^{-2} s^{-1}) as a function of the incident photon irradiance (E; µmol photons m^{-2} s^{-1}) were fitted with an exponential saturation model (Webb et al., 1974) with an added term, *R*, to account for respiration (Spilling et al., 2010):

$$P_n(E) = P_{max}\left(1 - exp^{\frac{-\alpha E}{Pmax}}\right) + R \qquad (2)$$

This equation enables estimation of the irradiance at the onset of photosynthesis saturation as $E_k = P_{max}/\alpha$, where P_{max} is the maximal net photosynthesis rate and α is the initial slope of the P_n *vs* E curve. The compensation irradiance, E_C, was determined as the incident irradiance at which the leaf tissue shifted from a net O_2 consumption to a net O_2 production, i.e., the irradiance where $P_n(E) = 0$.

Bulk sediment O_2 uptake

Depth profiles of O_2 concentration in the bulk sediment were obtained as follows. The sediment core was submerged into a ~2 L aquarium, wherein stirring and aeration of the water column was achieved via a Pasteur pipette connected to an air-pump. The surface of the sediment was determined with a boom-stand dissection microscope (AmScope, Irvine, CA, USA) and the O_2 microsensors were carefully positioned at the sediment surface as described above. Microprofiles were performed in vertical increments of 200 µm down to 2 cm depth, i.e., below the O_2 penetration depth. The volume specific O_2 consumption rate of the bulk sediment, R_{sed} (µmol O_2 m^{-3} s^{-1}), was calculated as:

$$R_{sed} = \frac{J_{O_2}}{d_{O_2}} \qquad (3)$$

where J_{O2} is the O_2 flux at the seawater/sediment interface (µmol O_2 m^{-2} s^{-1}), i.e., the diffusive oxygen uptake (DOU) of the sediment as calculated from Eq. (1), and d_{O2} is the O_2 penetration depth in the sediment (cm).

Potential and biological O_2 consumption of sieved sediment

The O_2 consumption of the fine sediment particles used in the laboratory as well as *in situ* was determined using a slightly modified approach of Pedersen et al. (2011). The O_2 consumption was separated into total (OX_{tot}) or biological (OX_{bio}) O_2 demand in order to determine the chemical O_2 demand as $OX_{chem.} = OX_{tot} - OX_{bio}$.

The total O_2 consumption of the sediment fraction was determined by mixing 50 mL suspended sediment (<63 µm) with 950 mL seawater with a salinity of 28. The solution was immediately transferred into 25 mL glass vials fitted with 2 glass beads to provide mixing and mounted on a rotating wheel (8 rpm) in a constant temperature bath (20.0 ± 0.5°C) (Pedersen et al., 2013). The sediment suspension was incubated for about 1 h (exact times recorded) before the O_2 concentration was measured in each vial using a calibrated sturdy O_2 microsensor (OX500; Unisense A/S, Denmark). Vials with seawater but without suspended sediment served as blanks enabling calculation of the O_2 consumption as nmol O_2 mL^{-1} sediment s^{-1}.

The biological O_2 consumption was measured on a sediment suspension, which was initially purged with atmospheric air for 15 min to oxidize reduced metals and sulphides (Raun et al., 2010). After oxidation, the sediment suspension was transferred into 25 mL glass vials and treated as described above.

In situ measurements

Experimental setup

Two patches (~1 m in diameter) of *Z. muelleri* were enclosed by custom-made transparent, floating curtains with mixing provided by submerged pumps to simulate water motion outside the enclosures (Narrabeen Lagoon, Australia). One enclosure functioned as a *control* treatment and the other enclosure as a *silt/clay* treatment. In the silt/clay treatment, 3 pulses of 375 mL silt/clay particles (see above) were added to the water column to mimic a dredging operation. Sediment resuspension was initiated at the beginning of the experiments (afternoon) (pulse 1), just before sunrise (pulse 2) and at midday (pulse 3).

Measurements were performed on April 17, 2015 (Day #1) and repeated on April 19, 2015 (Day #2).

Internal pO_2 and [H_2S] measurements

Similar data acquisition equipment and microsensor as described above were used for the field measurements of internal O_2 partial pressure (pO_2) and H_2S concentrations ([H_2S]) in the meristematic tissue of *Z. muelleri* over diel cycles. Internal H_2S concentrations were measured with Clark-type H_2S microsensors (H2S-25, tip diameter of ~25 µm, 90% response time <10 s, detection limit ~0.3 µm, Unisense A/S, Aarhus, Denmark; Jeroschewski et al., 1996; Kühl et al., 1998) that were linearly calibrated in anoxic, acidic (pH 4) Na_2S solutions of known H_2S concentrations (0, 50 and 100 µM). Within the enclosures, the microsensors were mounted on micromanipulators that were supported by stabilized aluminium spears at a water depth of ~1 m. The O_2 and H_2S microelectrodes were simultaneously inserted into the briefly exposed shoot base of the target plants close to the basal leaf meristem, which was then re-buried ~2 cm into the sediment to re-establish the biogeochemical gradients (Pedersen et al., 2004). Positioning of the O_2 microsensors was done by observing the sensor signals during insertion until a constant signal was recorded (Borum et al., 2005). The H_2S microsensors were inserted via a similar approach, using a combination of sensor signal responses to light exposure and positioning the electrodes at approximately the same depth into the leaf meristem tissue as the O_2 microsensors.

Physical and chemical parameters of the water-column

Diel changes in ambient incident photon irradiance (continuously measured via Odyssey light loggers; Dataflow Systems, Christchurch, NZ), water-column pO_2 (via O_2 micro-optodes; OXF500PT, Pyroscience, Aachen, Germany; connected to a 4-channel Firesting meter, PyroScience, Germany), and water-column temperature (via HOBO temperature data loggers; UA-002-08, Onset Computer Corporation, Bourne, MA, USA) were recorded over ~24 h within the enclosures. All sensors were calibrated according to the manufactures instructions, mounted on a metal spear and positioned at leaf canopy height. Logging (1 Hz)

by all data loggers was synchronized with the logging of microsensors used for the intra-tissue measurements.

In situ calculations

All microsensors are temperature sensitive (e.g. Kühl & Revsbech, 2001) and thus the measurements of internal pO_2 and [H_2S] obtained by the calibrated O_2 and H_2S microelectrodes were temperature corrected using the following equations (available at www.unisense.com):

$$pO_2 = \frac{S_{amb} - Z}{S_{air} - Z} P_0 \, exp^{k(T_{cal} - T_{amb})} \qquad (4)$$

where S_{amb} is the sensor signal measured *in situ* (mV), S_{air} is the calibration signal of the sensor determined at known partial pressure and temperature (e.g. 100% air saturation; in mV), Z is the zero current of the sensor measured at known partial pressure and temperature (i.e. 0% air saturation; in mV), P_0 is the known partial pressure used to define S_{air} (kPa), k is the temperature coefficient of the respective sensor (~0.02°C^{-1}; exact values for individual sensors can be provided by the manufacturer, www.unisense.com), T_{cal} is the known calibration temperature (°C), and T_{amb} is the ambient temperature (°C) continuously measured *in situ*.

$$[H_2S] = (GS + S_0) \, exp^{k(T_{cal} - T_{amb})} \qquad (5)$$

where G is the slope of the calibration curve that represents the sensitivity of the sensor (µmol L^{-1} mV^{-1}), S is the signal of the sensor (mV), S_0 is a constant that describes the zero current (µmol L^{-1}), k is the temperature coefficient of the respective sensor (~0.02°C^{-1}), T_{cal} is the known calibration temperature (°C), and T_{amb} is the ambient temperature (°C) continuously determined *in situ*.

These final sensor calibrations were done after the *in situ* experiments using the temperature data obtained in the respective enclosures by the submerged HOBO temperature data loggers (HOBO, Onset Computer Corporation, Bourne, MA, USA).

Finally, the internal meristematic pO_2 as a function of the ambient downwelling photon irradiance (PAR, 400-700 nm) were fitted with an exponential saturation model (Webb et al., 1974):

$$P(E) = P_{max}\,(1 - exp^{\frac{-\alpha E}{Pmax}}) \qquad (6)$$

where α is the initial slope of the P_n *vs* E curve and P_{max} is the maximal rate of net photosynthesis.

Data analysis

In the following, O_2 is quantified as µmol L^{-1} when in solution and as kPa when in gas phase. Data obtained under controlled conditions in the laboratory, i.e., O_2 fluxes across the leaf tissue surface, are thus presented in molar concentrations and data obtained *in situ,* i.e., meristematic O_2 concentrations and water-column O_2 conditions are given as partial pressures. Non-linear curve fitting was used to estimate the relationship among variables. All data fitting and analyses were performed in OriginPro (OriginPro 8, OriginLab Corporation, Northampton, MA, USA).

RESULTS

Laboratory measurements

Sediment and silt O_2 consumption rates

To enable comparison of sediment activity, we determined the O_2 demand and characteristics of the added silt/clay particles (<63 µm) and the bulk sediment without seagrass biomass. The O_2 was depleted within the upper 1.2 mm of the bulk sediment and the sediment remained anoxic with depth (Fig. S8.1). The volume-specific O_2 consumption rate of the bulk sediment was estimated to 374±33 µmol O_2 m^{-3} s^{-1} (Table 8.1). In contrast, the re-suspended silt/clay particles consumed 1319±6 µmol O_2 m^{-3} s^{-1} when taking both the biological and chemical O_2 demand into account. The biological O_2 demand of the silt/clay

particles was 1254±29 µmol O_2 m^{-3} s^{-1} resulting in a chemical O_2 demand of 65 µmol O_2 m^{-3} s^{-1} (Table 8.1).

Table 8.1. Volume specific O_2 consumption rates of fine sediment particles (i.e. silt/clay) and bulk sediment.

Sediment type	**O_2 consumption** ($\mu mol\ m^{-3}\ s^{-1}$)
Bulk, sediment (R_{sed})	374 ± 33
Fine sediment particles (Biological O_2 demand, OX_{bio})	1254 ± 29
Fine sediment particles (Biological and chemical O_2 demand, OX_{tot})	1319 ± 6

Rates are mean values ± SE; n = 4. *Biological O_2 demand* refers to the O_2 consumption of fine sediment particles oxygenated via 15 min air flushing prior to measurements. *Biological and chemical O_2 demand* of fine sediment particles refers to the O_2 consumption rate of untreated, i.e. not purged with air prior to incubation, fine sediment particles. 50 mL fine sediment particles were added to 950 mL seawater.

Net photosynthesis and respiration rates

Net photosynthesis rates increased with increasing incident photon irradiance for both plants with and without leaf silt/clay-cover (Fig. 8.1). Moreover, net photosynthesis rates were higher in control leaf segments (no silt/clay added) exposed to hypoxic water conditions, resembling water-column O_2 levels at sunrise, as compared to leaf segments kept in water at 100% air equilibrium (Table 8.2). Plants with leaf silt/clay-cover exhibited net O_2 consumption already at an incident photon irradiance of ~75 µmol photons m^{-2} s^{-1} owing to reduced light availability for leaf photosynthesis (Fig. 8.1; Table 8.2). Net photosynthesis rates of the control plants were 3 to 5-fold higher under moderate photon irradiance (200 µmol photons m^{-2} s^{-1}) as compared to plants with leaf silt/clay-cover (Table 8.2). During darkness, a constant diffusive O_2 influx across the leaf surfaces of both plants with and without leaf silt/clay-cover was observed (Fig. 8.1). However, we found a reduction in the O_2 flux into the silt/clay-covered leaves of 28-35% as compared to leaves without silt/clay-cover (Table 8.2).

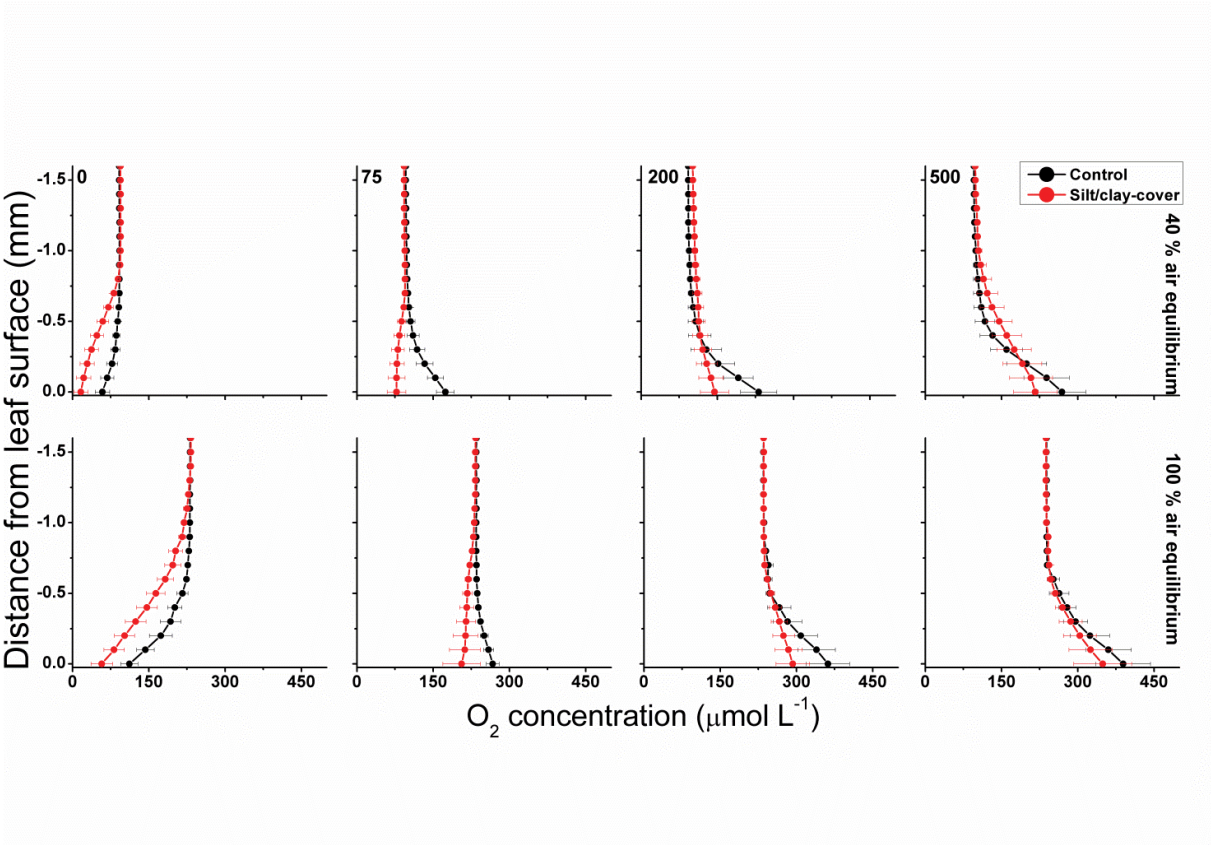

Figure 8.1. Vertical O_2 concentration profiles measured towards the leaf surface under incident photon irradiances of 0, 75, 200 and 500 µmol photons m^{-2} s^{-1}. Red symbols and lines represent leaves with silt/clay-cover; black symbols and lines represent control plants, i.e., leaves without silt/clay-cover. Upper panels are measurements in water with a reduced O_2 level of ~40% of air equilibrium (mimicking night-time water-column O_2 conditions, approximately 8.2 kPa); Lower panels are measurements in water at 100% air equilibrium (mimicking day-time water-column O_2 conditions, 20.6 kPa). y = 0 indicates the leaf surface. Symbols and error bars represent means ± SE; n = 3-4.

Table 8.2. Gas exchange measured as the O_2 flux across leaf surfaces of plants without (control)- and with fine sediment particles (<63 µm) as a function of photon irradiance.

Downwelling photon irradiance (µmol photons m^{-2} s^{-1})	**Control** 40 % air equillibrium (nmol O_2 m^{-2} s^{-1})	**With fine sediment particles** 40 % air equilibrium (nmol O_2 m^{-2} s^{-1})	**Control** 100 % air equilibrium (nmol O_2 m^{-2} s^{-1})	**With fine sediment particles** 100 % air equilibrium (nmol O_2 m^{-2} s^{-1})
0	-205 ± 57	-132 ± 3	-663 ± 223	-479 ± 44
75	435 ± 148	-18 ± 47	179 ± 61	-84 ± 143
200	854 ± 342	164 ± 110	571 ± 274	195 ± 129
500	746 ± 143	270 ± 74	701 ± 217	481 ± 266

Positive values denote O_2 efflux across the seagrass leaf surface. Rates are mean ± SE; n = 3-4. Note that the relative high standard errors in the silt treatment at 75 µmol photons m^{-2} s^{-1} was due to one of the leaf segments producing O_2 via photosynthesis (for further information, please see Fig. S8.2).

During water-column hypoxia, the leaf silt/clay-layer impeded the diffusive O_2 supply resulting in almost anoxic conditions at the leaf tissue surface (~16 µmol O_2 L^{-1}) of plants with leaf silt/clay-cover. This substantially increased the risk of H_2S intrusion into the below-ground tissues during night-time as a result of inadequate internal aeration (Fig. 8.1). The thickness of the DBL surrounding the leaves increased from ~200 µm to ~500 µm in the presence of the leaf silt/clay layer (Fig. 8.2). This resulted in a reduction in the O_2 influx to the leaves from 484±133 nmol O_2 m^{-2} s^{-1} in plants without leaf silt/clay-cover to 419±145 nmol O_2 m^{-2} s^{-1} in plants with an inactivated leaf silt/clay-layer. When coated with a biologically active silt/clay layer, leaves experienced a further reduction of the O_2 influx to 395±102 nmol O_2 m^{-2} s^{-1} (Fig. 8.2).

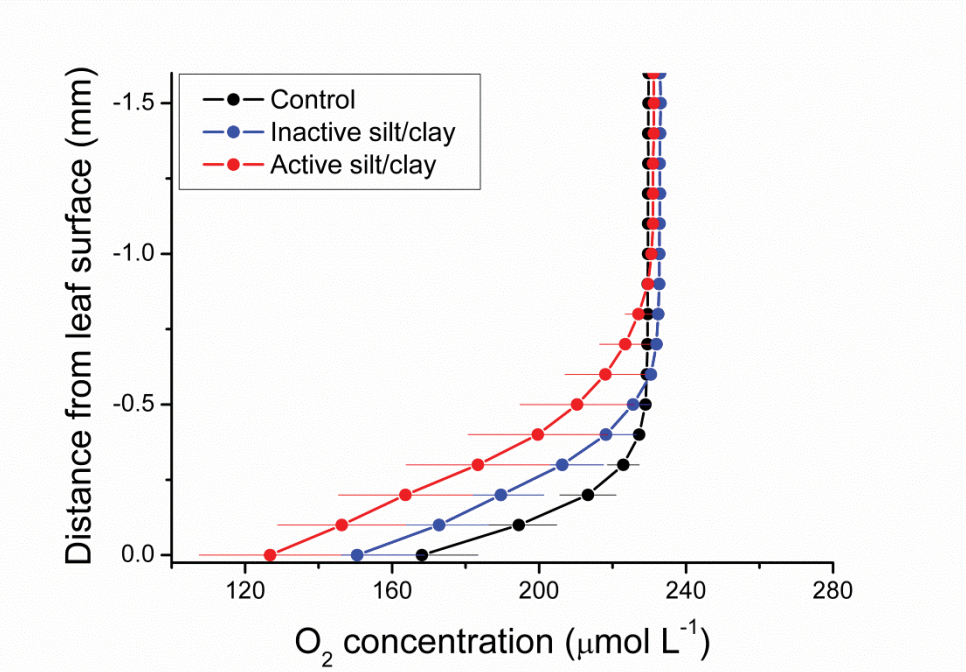

Figure 8.2. Vertical depth profiles of the O_2 concentration measured towards the leaf surface of plants with a microbially active silt/clay-cover (red symbols and lines), with an inactivated silt/clay-cover (obtained by pre-heating the added silt/clay to 120°C in an oven for 2 h; blue symbols and lines), and without silt/clay-cover (control plants; black symbols and lines). All measurements were performed in darkness. y = 0 indicates the leaf surface. Symbols and error bars represent means ± SE; n = 4.

The silt/clay-cover on seagrass leaves resulted in a pronounced increase of the plants' compensation irradiance from 53 µmol photons m^{-2} s^{-1} for control leaf segments to 145 µmol photons m^{-2} s^{-1} for leaf segments with silt/clay cover, both kept in a water column at 100% air equilibrium (Fig. 8.3; Table 8.3). In a water column with O_2 kept at 40% atmospheric equilibrium, the compensation irradiance increased from 20 µmol photons m^{-2} s^{-1} for control leaf segments to 109 µmol photons m^{-2} s^{-1} for leaf segments with silt/clay cover (Fig. 8.3; Table 8.3). The leaf silt/clay-layer effects on plant photosynthesis and respiration lead to a ~2.4-fold increase in the irradiance causing onset of net photosynthesis saturation for plants with leaf silt/clay-cover as compared to plants without leaf silt/clay-cover (Table 8.3), and to a 49-72% reduction of the leaf surface O_2 concentration in darkness for plants with a leaf silt/clay-cover as compared to plants without a leaf silt/clay-cover (Table 8.3).

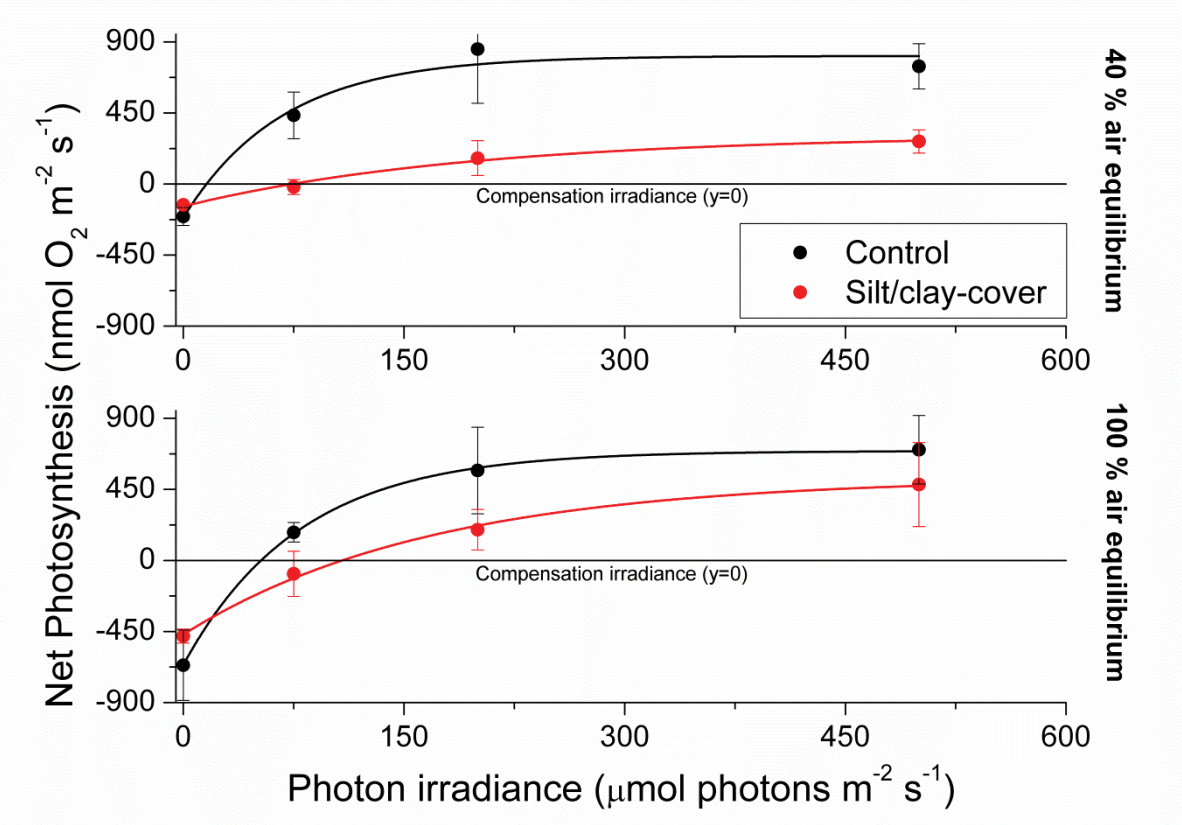

Figure 8.3. Apparent net photosynthesis rates as a function of downwelling photon irradiance (PAR, 400-700 nm) of plants with leaf silt/clay-cover (red symbols and lines) and without leaf silt/clay-cover (control plants; black symbols and lines). Rates were calculated for incident photon irradiances of 0, 75, 200 and 500 µmol photons m^{-2} s^{-1} and were fitted with an exponential function (Webb *et al.*, 1974) with an added term to account for respiration (Spilling et al. 2010) ($R^2_{40\%AS,control}$=0.93; $R^2_{40\%AS,silt\text{-}cover}$=0.98; $R^2_{100\%AS,control}$=0.99; $R^2_{100\%AS,silt\text{-}cover}$=0.99). The upper panel represents measurements in water kept at 40% air equilibrium, while the lower panel represents measurements in water kept at 100% air equilibrium. Error bars are ± SE; n = 3-4.

Table 8.3. Photosynthetic parameters derived from the light response curves in Fig. 8.3. Including photosynthetic activity, compensation irradiance, onset of photosynthesis saturation and respiration rates of investigated *Zostera muelleri* spp. *capricorni* plants with- and without (i.e. control plants) fine sediment particles on leaves. All photosynthetic related parameters were determined at both 40 % of air equilibrium and in air equilibrium. n = 3.

	40 % of air equilibrium		**In air equilibrium**	
	control	**fine sediment particles**	**control**	**fine sediment particles**
α	15 ± 4	3 ± 1	17 ± 6	6 ± 2
P_{max}	1028 ± 176	503 ± 91	1354 ± 478	1010 ± 273
R	-211 ± 48	-141 ± 4	-662 ± 232	-468 ± 28
E_C	20 ± 8	109 ± 47	53 ± 7	145 ± 46
E_k	72 ± 5	174 ± 46	77 ± 2	180 ± 36
$[O_2]$, *dark*	59 ± 14	16 ± 14	112 ± 17	57 ± 21

Values are mean ± SE. α = initial slope of the net photosynthesis rate vs incident photon irradiance; P_{max} = maximum rate of net photosynthesis (in nmol O_2 m^{-2} s^{-1}); R = the respiration rate (in nmol O_2 m^{-2} s^{-1}); E_C = compensation irradiance (i.e. incident photon irradiance where the oxygen produced by photosynthesis meets the respiratory demands) (in µmol photons m^{-2} s^{-1}); E_k = onset of photosynthesis saturation (in µmol photons m^{-2} s^{-1}); $[O_2]$, *dark* = the leaf surface O_2 concentration measured in darkness (in µmol L^{-1}), which can be used as an estimate for the internal O_2 concentration in the aerenchymal tissue of the thin seagrass leaves. 40 % of air equilibrium mimics natural conditions in the seagrass meadow during night-time and at sunrise as seen on Figure 8.4. Air equilibrium mimics natural conditions during most of the day-time (Fig. 8.4). Values are calculated/extracted from the fitted exponential saturation function (Webb et al. 1974) with an added term to account for respiration (Spelling et al. 2010) in Figure 8.3 (apply to: α, P_{max}, R, E_c and E_k) and from the O_2 concentration microprofiles in Figure 8.1 ($[O_2]$, *dark*); and thus all originates from the laboratory experiments.

In situ measurements and effects of sediment re-suspension

Diel changes in the physical/chemical parameters of the surrounding water-column

The pO_2 dynamics in the water-column of the control and silt/clay treatment showed similar patterns on a diel basis, with steadily declining pO_2 during night-time reaching minimal water-column O_2 conditions around sunrise, followed by a rapid increase in the water-column pO_2 shortly after sunrise approaching atmospheric saturation (20.6 kPa) or even leading to water-column supersaturation relative to atmospheric pO_2 around midday (Fig. 8.4a,b). Water-column O_2 levels within the enclosures fluctuated substantially during night-time owing to water bodies with varying O_2 content being introduced to the seagrass meadow from non-vegetated areas within the lagoon and/or from the ocean due to tidal

water movement. In contrast, water-column temperature remained relatively constant on a diel basis but generally decreased from ~22°C on measuring day #1 to ~20°C at the end of measuring day #2. Minor fluctuations in the water-column temperature during night-time correlated with the passing of aerated water bodies as observed in the water-column pO_2 measurements (Fig. 8.4a,b). The incident photon irradiance measured at leaf canopy height followed a typical bell-shaped diel curve, with minor fluctuations in the control treatment due to passing cloud cover. This was in strong contrast to the silt/clay treatment, where we measured substantially reduced light conditions as compared to the control treatment, especially in the hours following experimentally manipulated silt/clay re-suspension (Fig. 8.4a,b). Moreover, a pronounced difference in the light availability was observed between measuring days #1 and #2, where day #1 represented sunny conditions and day #2 represented a cloudy late autumn day at Narrabeen Lagoon (Fig. 8.4a,b).

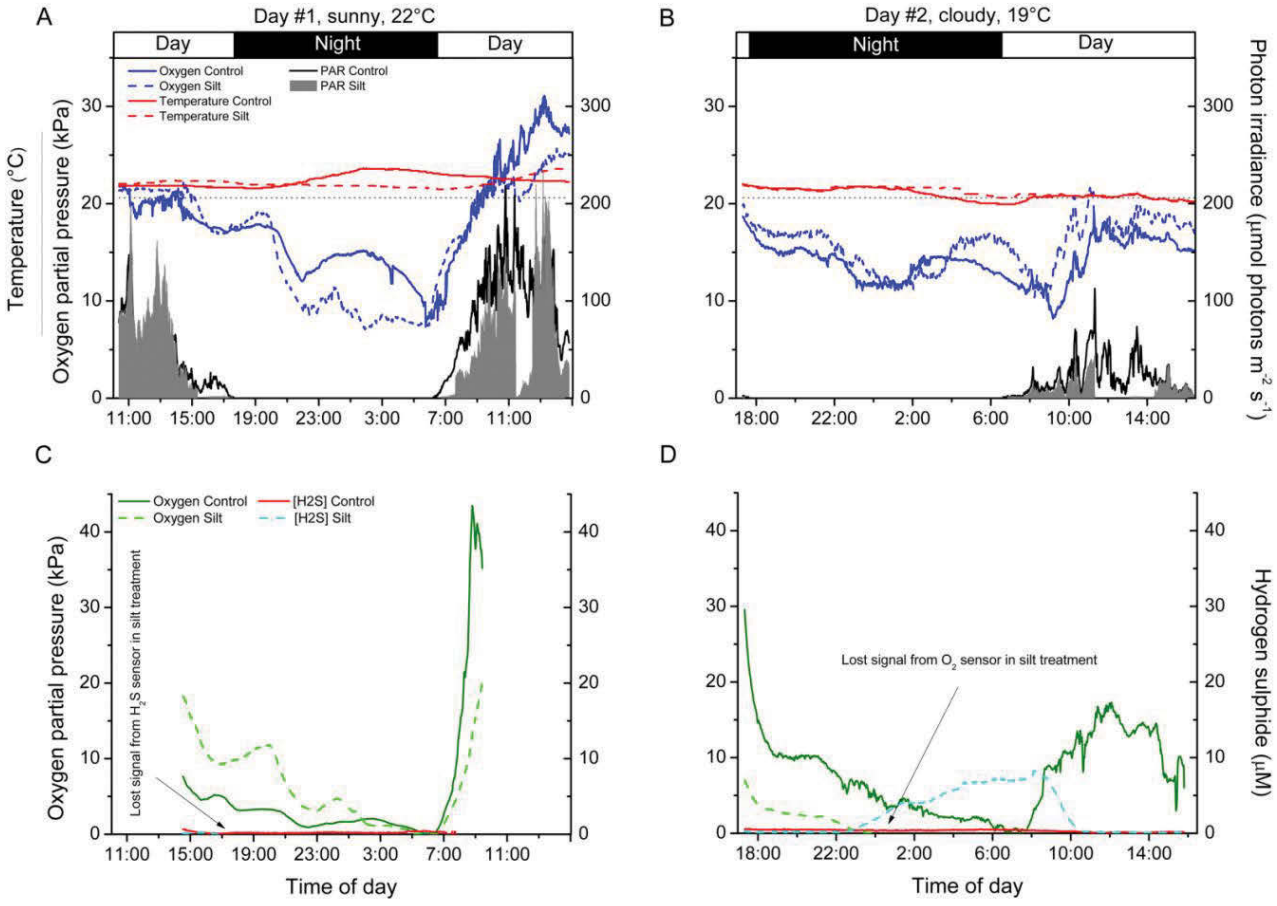

Figure 8.4. *In situ* measurements of diel changes in the O_2 concentration and temperature of the water-column (A, B), the light availability at leaf canopy height (A, B), and of the O_2 partial pressure and H_2S concentration in the meristematic tissue of *Zostera muelleri* plants with and without leaf silt/clay-cover, respectively (C, D) from Narrabeen Lagoon, NSW, Australia. The O_2 and H_2S microsensors were inserted into the shoot base close to the basal leaf meristem, which was buried ~2 cm into the sediment. The horizontal, dashed line in panels A and B corresponds to 100% atmospheric O_2 partial pressure. Legends depict the physical/chemical water-column parameters (A, B) and the chemical species (C, D). Panels A and C are from measuring day #1 (representing a sunny day), while panels B and D are from measuring day #2 (representing a cloudy day). Note the lost signal from the inserted microsensors in the silt/clay treatment (C, D).

In situ measurements of O_2 and H_2S in seagrass meristems

The internal, meristematic pO_2 of both control plants and plants experimentally exposed to suspended silt/clay decreased steadily from early in the afternoon throughout the night. A minimum internal, meristematic pO_2 was reached shortly after sunrise. Thereafter, a rapid

increase in meristematic pO_2 occurred as a response to increasing solar irradiance resulting in photosynthetic O_2 production (Fig. 8.4c,d). Control plants as well as silt/clay-treated plants exhibited lower pO_2 relative to the water-column during night-time with tissue pO_2 fluctuations correlating with changes in water-column pO_2 (Fig. 8.4a-d). A clear discrepancy in the meristematic pO_2 between control plants and leaf silt/clay-treated plants was measured during light-limitation in the early morning hours (06:30-09:00) (Fig. 8.4c) with relatively lower pO_2 in silt/clay-treated plants indicating a silt/clay-induced reduction in light availability.

The meristematic below-ground tissues of both control and silt/clay-treated plants turned anoxic, or severely hypoxic, late at night. Meristematic pO_2 of silt/clay-treated plants reached anoxia from around 05:00-06:30 on Day #1 and already from 23:30 on Day #2, while the control plants only experienced anoxic conditions in the meristematic tissue for short time periods (<1 h; Fig. 8.4c,d). Interestingly, simultaneous measurements of internal, meristematic H_2S concentrations revealed phytotoxic H_2S intrusion into silt/clay-treated plants during night-time on Day #2 from around 23:30 correlating with the recorded period of meristematic tissue anoxia (Fig. 8.4c,d). Internal H_2S levels reached a maximum of 8.3 µmol H_2S L^{-1} around 08:00 in the morning and then started to decrease shortly after sunrise in response to photosynthetic O_2 production leading to disappearance of H_2S in the meristem by 10:30. No H_2S intrusion was detected into the control plants.

Effects of water column O_2 levels and silt/clay on internal O_2 status

During night-time, tissue pO_2 was derived from O_2 in the surrounding water diffusing into the leaves and spreading via aerenchyma to below-ground tissues (Pedersen et al., 1998; Colmer, 2003; Brodersen et al., 2015a). The critical water column O_2 level was defined as the water column pO_2 below which oxic conditions in the meristematic tissue could no longer be sustained, and this critical O_2 level was estimated by plotting the internal pO_2 determined *in situ* against water-column pO_2 (Fig. 8.5). The meristematic tissue of silt/clay-treated plants became anoxic at a higher water-column pO_2 (~9.3 kPa) during night-time as compared to ~7.6 kPa in control plants (based on averaged values from Fig. 8.5); a tendency that became more evident during prolonged exposure to suspended silt/clay particles (Fig.

8.5d). These *in situ* findings aligned well with the lower O_2 influx into leaves with silt/clay-cover, as compared to control leaves, determined in the controlled laboratory experiments during darkness (Fig. 8.1-8.3: Table 8.2 and 8.3).

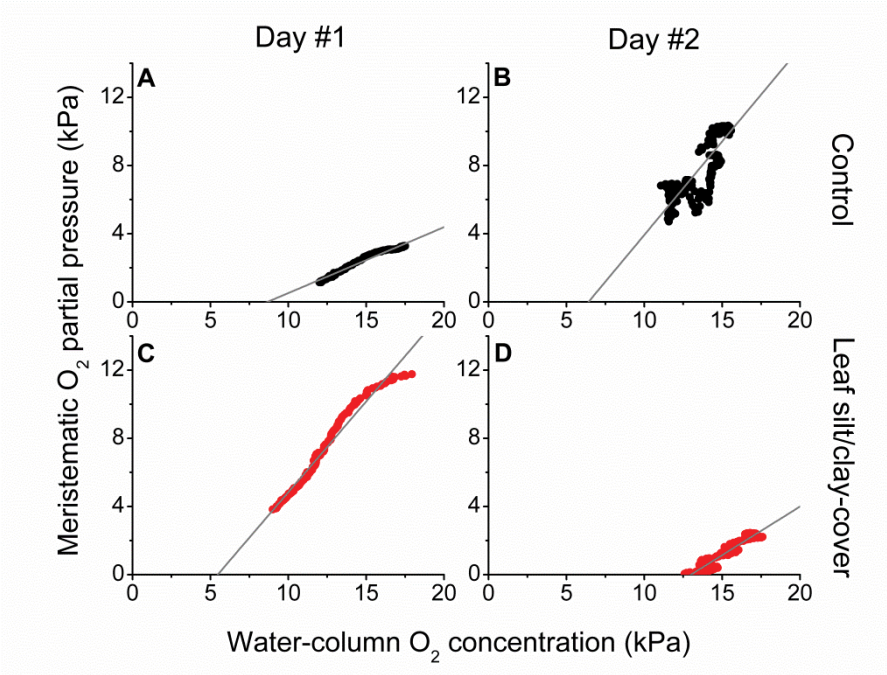

Figure 8.5. *In situ* intra-plant O_2 status as a function of the O_2 partial pressure in the surrounding water-column during night-time. The data were extracted from Figure 8.4 approximately 2h after sunset. The grey lines represent a linear regression and are extrapolated to interception with the horizontal x-axis, to provide an estimate of the water-column O_2 level where the meristematic tissue at the shoot base becomes anoxic ($R^2_{control,day\#1}$ = 0.97; $R^2_{control,day\#2}$ = 0.70; $R^2_{silt\text{-}cover,day\#1}$ = 0.97; $R^2_{silt\text{-}cover,day\#2}$ = 0.94). Upper panels (A, B) are measurements from control plants (black symbols), while lower panels (C, D) are measurements from plants with a silt/clay-cover on the leaves (red symbols).

The silt/clay-induced shading effects on the intra-plant pO_2 during natural light exposure of the seagrass leaf canopy was evaluated by plotting the *in situ* meristematic pO_2 as a function of incident photon irradiance (Fig. 8.6) revealing an ~35% reduction in meristematic pO_2 in plants exposed to suspended silt/clay as compared to control plants, seen as a decrease in α, i.e., the slope describing the internal O_2 evolution as a function of photon irradiance, from 0.15 to 0.10 (Fig. 8.6).

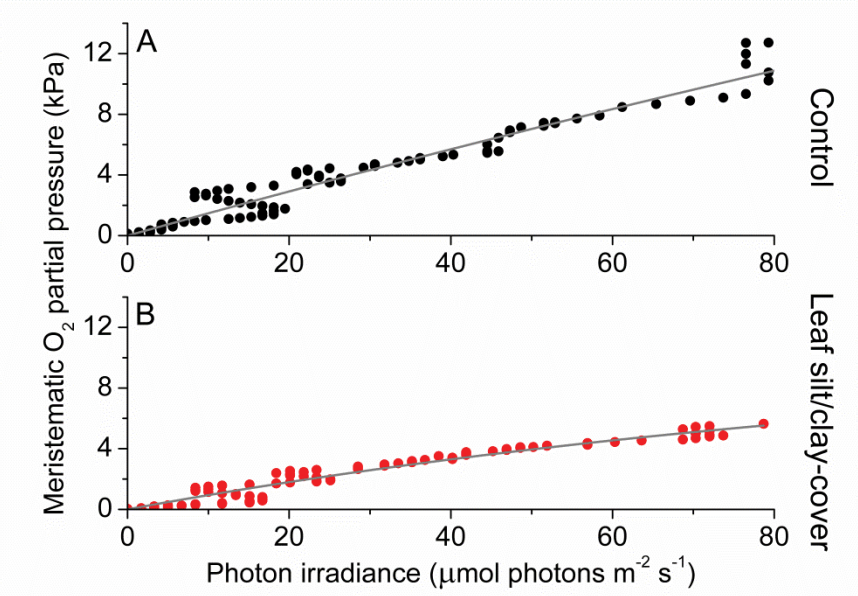

Figure 8.6. *In situ* intra-plant O_2 status as a function of incident photon irradiance (PAR) during daytime. The data were extracted from Figure 8.4 at sunrise (measuring day #1). The intra-plant O_2 evolution during the light-limiting phase of PAR were fitted with an exponential model (Grey lines; Webb *et al*., 1974) ($R^2_{control}$ = 0.95, $\alpha_{control}$ = 0.149; $R^2_{silt\text{-}cover}$ = 0.95, $\alpha_{silt\text{-}cover}$ = 0.098). Upper panel (A) shows measurements from control plants (Black symbols), while the lower panel (B) shows measurements from plants with a silt/clay-cover on the leaves (red symbols).

DISCUSSION

Our results provide strong evidence that silt/clay-cover on seagrass leaves can have substantial negative effects on the plants' photosynthetic activity and efficiency, as well as on the night-time O_2 exchange between leaf tissue and the surrounding water. Reduced internal aeration, and thus decreased below-ground tissue oxidation capacity, rendered plants with leaf silt/clay-cover more prone to H_2S intrusion even at relatively high water-column pO_2 during night-time. Below, we discuss in detail the implications of reduced light availability for photosynthesis owing to silt/clay shading, thicker DBLs, and the introduction of O_2 consumption within the DBL itself, on internal aeration and whole plant performance of seagrasses.

Sediment and silt/clay characteristics

We measured an ~3.4-fold higher volumetric O_2 consumption rate of the re-suspended silt/clay particles (<63 µm), as compared to the bulk sediment, indicative of high microbial activity within the thin silt/clay layer covering the leaf (Table 8.1). Microbial O_2 respiration was the quantitatively most important O_2 consuming process of the re-suspended silt/clay particles, while chemical oxidation only accounted for ~5% of the total O_2 demand (Table 8.1). Hence, the leaf silt/clay-cover not only impeded gas and nutrient exchange with the surrounding water-column owing to the enhanced thickness of the diffusive boundary layer (DBL) around the leaves (Fig. 8.2), it also reduced the passive O_2 influx across the silt/clay layer during night-time owing to high microbial O_2 consumption within the silt/clay layer.

Sediment-cover effects on seagrass photosynthesis and O_2 uptake

In light, the apparent net photosynthesis rates of *Z. muelleri* leaves with silt/clay-cover were dramatically reduced as compared to control leaves, and the reduction was most pronounced at low to moderate photon irradiances (Fig. 8.3; Table 8.2). The reduced leaf photosynthesis was, most likely, a combined negative result of lower light availability at the tissue surface and a DBL-impeded uptake of CO_2 from the surrounding water-column, potentially leading to enhanced photorespiration and thereby reduced photosynthetic efficiency owing to inorganic carbon limitation (e.g. Maberly, 2014) (Fig. 8.1 and 8.3; Table 8.2). Consequently, the compensation irradiance of photosynthesis for plants with leaf silt/clay-cover increased to ~109 and 145 µmol photons m^{-2} s^{-1}, as compared to ~20 and 53 µmol photons m^{-2} s^{-1} for control plants kept in water with O_2 at 40% air equilibrium and 100% air equilibrium, respectively (Table 8.3). Silt/clay-cover can thus keep seagrass plants close to their minimum light requirements on days with poor light conditions. However, in the present experimental set-up we were unable to clearly separate the effect of reduced net photosynthesis caused by reduced light (shading by particles) or increased resistance to CO_2 influx (thicker DBL) from that of O_2 consumption by bacteria within the silt/clay layer.

In darkness, the passive O_2 influx was also strongly affected by the leaf silt/clay-cover, causing a reduction of up to 35% in the O_2 supply (Table 8.2), which resulted in reduced

internal aeration (Table 8.3) especially under hypoxic water-column conditions and thus markedly increased the risk of over-night tissue anoxia. The lower O_2 influx was a combined negative result of an increased DBL thickness impeding the exchange of O_2 with the surrounding water-column (Fig. 8.2) and high microbial O_2 consumption rates within the leaf silt/clay-cover (Table 8.1; Fig. 8.2). Such reduction in the meristematic pO_2 lead to a reduced capability of the silt/clay-covered seagrass plant to aerate its below-ground tissue during night-time increasing the risk for phytotoxic H_2S intrusion (Pedersen et al., 2004; Borum et al., 2005; Brodersen et al., 2015b).

Sediment re-suspension effects on plant meristematic O_2 and H_2S levels

Diel changes in the meristematic O_2 content of seagrasses were mainly driven by irradiance (Fig. 8.4). Experimentally manipulated silt/clay re-suspension within the enclosure of the silt/clay treatment, resulted in a pronounced decrease of light availability for seagrass photosynthesis with up to 3 h of darkening measured around midday on measuring day #2 (Fig. 8.4b). The diminished light conditions resulted in reduced photosynthetic O_2 evolution and thereby reduced meristematic pO_2 in *Z. muelleri* as seen at sunrise on measuring day #1 (Fig. 8.4c), thus correlating with previous findings by Borum et al. (2005). The photosynthetic efficiency of *Z. muelleri* measured *in situ* was also strongly affected by the silt/clay exposure, with an almost 2-fold decrease in the net photosynthetic O_2 evolution of plants exposed to silt/clay re-suspension, as compared to control plants at equivalent incident photon irradiances (Fig. 8.6), leading to reduced internal aeration and below-ground tissue oxidation capacity. This was a result of impeded gas exchange with the surrounding water-column due to a thicker DBL in the presence of a sediment cover of leaves leading to lower photosynthetic efficiencies. The *in situ* measurements thus strongly correlated with findings of a 3-5-fold higher compensation irradiance and an ~2.4-fold increase in the irradiance at onset of photosynthesis saturation in the laboratory experiments for *Z. muelleri* leaves with silt/clay-cover as compared to control leaves (Fig. 8.3; Table 8.3).

Critically low meristematic pO_2 and/or tissue anoxia were only measured during night-time and occurred for longer periods of time, and at higher water-column O_2 levels, for *Z.*

muelleri in the silt/clay treatment as compared to the control treatment (Fig. 8.4 and 8.5). This suggests reduced O_2 supply from the leaves to the below-ground tissue of *Z. muelleri* plants exposed to silt/clay re-suspension. The reduced meristematic pO_2 was caused by (i) the leaf silt/clay-cover induced enhanced DBL thickness impeding the passive O_2 influx into the leaves, and (ii) high rates of microbial O_2 consumption within the leaf silt/clay layer in line with observations in the laboratory experiments (Fig. 8.1 and 8.2). Lowest meristematic pO_2 levels were recorded around sunrise, followed by a rapid increase in the meristematic O_2 content when sunlight supported leaf photosynthesis (Fig. 8.4c,d). Moreover, our results clearly showed that sediment re-suspension did not have substantial negative effects on the overall O_2 conditions within the water-column (Fig. 8.4a,b) as previously suggested (Erftemeijer & Lewis, 2006), thus underpinning the critical importance of silt/clay leaf covers.

Plants with leaf silt/clay-cover experienced internal meristematic tissue anoxia at higher water-column pO_2 levels (~45% of air equilibrium) than plants without leaf silt/clay-cover (~37% of air equilibrium), thus correlating with the lower passive O_2 influx into leaves with silt/clay-cover during night-time determined in the laboratory experiments (Fig. 8.1 and 8.3). The silt/clay-induced negative effect on the intra-plant O_2 status was aggravated during prolonged exposure to re-suspended silt/clay particles in the water-column (Fig. 8.5), where the critical water-column O_2 level for *Z. muelleri* increased to ~63% air saturation after ~54 h of exposure to experimentally manipulated silt/clay re-suspension (Fig. 8.5). Seagrass plants with leaf silt/clay-cover were thus more vulnerable to low water-column pO_2 at night-time and experience an increased risk for H_2S intrusion.

Proof of H_2S intrusion in seagrasses has only been demonstrated *in situ* once (Borum et al., 2005) and never under conditions of such high water column pO_2 as in the silt/clay-treated plants of this study, which was in strong contrast to the control treatment, where no H_2S intrusion was detected (Fig. 8.4c,d). Anoxic conditions in the roots, rhizome and basal leaf meristem of seagrasses lead to ceased radial O_2 loss (ROL) from the below-ground tissue into the immediate rhizosphere and thus resulted in sediment-produced H_2S reaching the below-ground tissue surface (Pedersen et al., 2005; Brodersen et al., 2015b). If H_2S enters the plant e.g. via, the root apical meristems, the transport of H_2S to the basal leaf meristem is relatively fast as it occurs via gas-phase diffusion in the aerenchyma (Pedersen *et al*.,

2004) and this may lead to chemical asphyxiation and thereby enhanced seagrass mortality (Lamers et al., 2013). Normally, H_2S intrusion is prevented by plant-derived ROL creating oxic sediment microniches that are sustained as long as the below-ground tissue is supported with sufficient O_2 from the leaf canopy (Pedersen *et al*., 2004; Brodersen *et al*., 2015b, 2016). Mature regions of seagrass roots do not leak O_2, but instead possess barriers to ROL, and thereby most likely to H_2S intrusion, composed by Casparian-band like structures in the root endodermis (Barnabas, 1996: Enstone et al., 2003). This important anatomical cell-wall modification significantly reduces the consumption of O_2 along the internal diffusion path and thereby ensures an effective O_2 transport to the most distal parts of the seagrass plant (Colmer, 2003). At sunrise, photosynthetic O_2 evolution in the leaves of the silt/clay-treated plants lead to enhanced internal meristematic pO_2 and thereby re-oxidation of intruded H_2S around 08:00-10:00 in the morning (Fig. 8.4d), where after the H_2S concentration remained below the detection limit.

The present study emphasises the importance for seagrasses to maintain protective plant-derived oxic microshields within their rhizosphere, as sediment detoxification via ROL prevents H_2S from accumulating to very high toxic levels in the sediment and thus prevents H_2S from reaching the tissue surface at the most vulnerable regions of the plants (Carlson et al., 1994; Brodersen et al., 2015b). Silt/clay-induced H_2S intrusion into *Z. muelleri* seemed tightly coupled to prolonged exposure to sediment re-suspension, such as typically found during harbour dredging activities (York et al., 2015) and resulting from river plumes (Petus et al., 2014). Leaf silt/clay-covers thus impeded the plants performance and thereby their resilience towards H_2S intrusion. This was as a result of a combined negative plant response to the reduced light availability for photosynthesis, thicker DBLs around leaves and enhanced leaf surface microbial respiration rates, all leading to inadequate internal aeration and reduced below-ground tissue oxidation capacity (Fig. 8.4). Turbidity generating activities such as dredging operations in close proximity to seagrass meadows can thus have strong negative effects on the fitness level and health of seagrasses through multiple pathways and may lead to increased seagrass mortality especially in severely exposed areas.

ACKNOWLEDGEMENTS

We thank all volunteers from University of Technology Sydney (UTS) who kindly helped with setting up the platform in Narrabeen Lagoon and supervised all our equipment during night-time. We acknowledge the workshop at UTS for constructing the platform and enclosures. The research was funded by grants from the Australian Research Council (ARC; LP 110200454) (PR, MR, MK), the Augustinus Foundation (KB, KH), P.A. Fiskers Fund (KB), Jorck and Wife's Fund (KB), the Oticon Foundation (KH), and the Danish Council for Independent Research I Natural Sciences (MK, OP). The research was conducted under the scientific collection and field-work permit (P12/0020-1.2).

SUPPLEMENTARY MATERIAL

The supplementary material for this article is available online.

Figure S8.1. Depth microprofiles of O_2 concentration across the water/sediment interface of sediment from Narrabeen Lagoon, NSW, Australia.

Figure S8.2. Rates of net photosynthesis as a function of incident photon irradiance for all investigated *Zostera muelleri* plants.

AUTHOR CONTRIBUTIONS

KB, OP, MK, PR and MR designed the research. KB, OP, KH, VS and AF conducted the experiments. KB processed the data with help from OP and KH. KB, OP, MK analysed the data. KB wrote the manuscript with editorial help from OP, MK, PR and MR. All authors have given approval to the final version of the manuscript. The authors declare no competing financial interest.

REFERENCE LIST

Barnabas AD. (1996). Casparian band-like structures in the root hypodermis of some aquatic angiosperms. *Aquatic Botany* **55**: 217-225.

Binzer T, Borum J, Pedersen O. (2005). Flow velocity affects internal oxygen conditions in the seagrass *Cymodocea nodosa*. *Aquatic Botany* **83:** 239-247.

Borum J, Pedersen O, Greve TM, Frankovich TA, Zieman JC, Fourqurean JW, Madden CJ. (2005). The potential role of plant oxygen and sulphide dynamics in die-off events of the tropical seagrass, *Thalassia testudinum*. *Journal of Ecology* **93**: 148-158.

Borum J, Sand-Jensen K, Binzer T, Pedersen O, Greve T. (2006). Oxygen movement in seagrasses. In: Larkum AWD, Orth JR & Duarte CM, eds. *Seagrasses: Biology, Ecology and Conservation,* Dordrecht, The Netherlands: Springer, Berlin: 255-270.

Brodersen KE, Koren K, Lichtenberg M, Kühl M. (2016). Nanoparticle-based measurements of pH and O_2 dynamics in the rhizosphere of *Zostera marina* L.: Effects of temperature elevation and light-dark transitions. *Plant, Cell & Environment*. (accepted on March 22, 2016)

Brodersen KE, Lichtenberg M, Paz L-C, Kühl M. (2015a). Epiphyte-cover on seagrass (*Zostera marina* L.) leaves impedes plant performance and radial O_2 loss from the below-ground tissue. *Frontiers in Marine Science* **2**: 58. doi: 10.3389/fmars.2015.00058.

Brodersen KE, Nielsen DA, Ralph PJ, Kühl M. (2014). A split flow chamber with artificial sediment to examine the below-ground microenvironment of aquatic macrophytes. *Marine Biology* **161**: 2921-2930. doi: 10.1007/s00227-014-2542-3.

Brodersen KE, Nielsen DA, Ralph PJ, Kühl M. (2015b). Oxic microshield and local pH enhancement protects *Zostera muelleri* from sediment derived hydrogen sulphide. *New Phytologist* **205**: 1264-1276.

Carlson J, Paul R, Yarbro LA, Barber TR. (1994). Relationship of sediment sulfide to mortality of *Thalassia testudinum* in Florida Bay. *Bulletin of marine Science* **54**(3): 733-746.

Colmer TD. (2003). Long-distance transport of gases in plants: a perspective on internal aeration and radial oxygen loss from roots. *Plant, Cell & Environment* **26**: 17-36.

Cutroneo L, Castellano M, Ferranti MP, Povero P, Tucci S, Capello M. (2013). Use of optical and acoustic instruments to study the turbid plumes generated by three different types of dredges during dredging activities inside and outside of a port. *Journal of Soils and Sediments* **13**(9): 1645-1654.

Dennison WC. (1987). Effects of light on seagrass photosynthesis, growth and depth distribution. *Aquatic Botany* **27**(1): 15-26.

Duarte CM. (1991). Seagrass depth limits. *Aquatic Botany* **40**: 363-377.

Enstone DE, Peterson CA, Ma F. (2003). Root endodermis and exodermis: structure, function, and responses to the environment. *Journal of Plant Growth Regulation* **21**: 335-351.

Erftemeijer PLA, Lewis RRR. (2006). Environmental impacts of dredging on seagrasses: a review. *Marine Pollution Bulletin* **52**(12): 1553-1572.

Fourqurean JW, Zieman JC. (1991). Photosynthesis, respiration and whole plant carbon budget of the seagrass *Thalassia testudinum*. *Marine Ecology Progress Series* **69**:161-170.

Frederiksen MS, Glud RN. (2006). Oxygen dynamics in the rhizosphere of *Zostera marina*: A two-dimensional planar optode study. *Limnology and Oceanography* **51**(2): 1072-1083.

Greve TM, Borum J, Pedersen O. (2003). Meristematic oxygen variability in eelgrass (*Zostera marina*). *Limnology and Oceanography* **48**(1): 210-216.

Hasler-Sheetal H, Holmer M. (2015). Sulfide Intrusion and Detoxification in the Seagrass *Zostera marina*. *PloS one* **10**(6): e0129136.

Holmer M, Bondgaard EJ. (2001). Photosynthetic and growth response of eelgrass to low oxygen and high sulfide concentrations during hypoxic events. *Aquatic Botany* **70**: 29-38.

Holmer M, Hasler-Sheetal H. (2014). Sulfide intrusion in seagrasses assessed by stable sulfur isotopes—a synthesis of current results. *Frontiers in Marine Science* **1**: 64.

Hurd CL. (2000). Water motion, marine macroalgal physiology, and production. *Journal of Phycology* **36**(3): 453-472.

Jensen SI, Kuhl M, Glud RN, Jørgensen LB, Prieme A. (2005). Oxic microzones and radial oxygen loss from roots of *Zostera marina*. *Marine Ecology Progress Series* **293**: 49-58.

Jeroschewski P, Steuckart C, Kühl M. (1996). An amperometric microsensor for the determination of H_2S in aquatic environments. *Analytical Chemistry* **68**: 4351-4357.

Jørgensen BB, Revsbech NP. (1985). Diffusive boundary layers and the oxygen uptake of sediments and detritus. *Limnology and Oceanography* **30**(1): 111-122.

Koren K, Brodersen KE, Jakobsen SL, Kühl M. (2015). Optical sensor nanoparticles in artificial sediments – a new tool to visualize O_2 dynamics around the rhizome and roots of seagrasses. *Environmental Science and Technology* **49**(4): 2286-2292.

Kühl M, Revsbech NP. (2001). Biogeochemical microsensors for boundary layer studies. In: Boudreau BP, Jørgensen BB, eds. *The benthic boundary layer*. New York: Oxford University Press, New York, 180-210.

Kühl M, Steuckart C, Eickert G, Jeroschewski P. (1998). A H_2S microsensor for profiling sediments and biofilms: Application in acidic sediment. *Aquatic Microbial Ecology* **15**: 201-209.

Lamers LP, Govers LL, Janssen IC, Geurts JJ, Van der Welle ME, Van Katwijk MM, Van der Heide T, Roelofs JG, Smolders AJ. (2013). Sulfide as a soil phytotoxin—a review. *Frontiers in plant science* **4**: 268.

Maberly SC. (2014). The fitness of the environments of air and water for photosynthesis, growth, reproduction and dispersal of photoautotrophs: An evolutionary and biogeochemical perspective. *Aquatic Botany* **118**: 4-13.

Pedersen O, Binzer T, Borum J. (2004). Sulphide intrusion in eelgrass (*Zostera marina* L.). *Plant, Cell and Environment* **27**: 595-602.

Pedersen O, Borum J, Duarte CM, Fortes MD. (1998). Oxygen dynamics in the rhizosphere of *Cymodocea rotundata*. *Marine Ecology Progress Series* **169**: 283-288.

Pedersen O, Colmer TD, Sand-Jensen K. **(2013).** Underwater photosynthesis of submerged plants – recent advances and methods. *Frontiers in Plant Science* **4**.

Pedersen O, Pulido C, Rich SM, Colmer TD. (2011). *In situ* O_2 dynamics in submerged *Isoetes australis*: varied leaf gas permeability influences underwater photosynthesis and internal O_2. *Journal of Experimental Botany* **62**: 4691-4700.

Pedersen O, Colmer TD, Borum J, Zavala-Perez A, Kendrick GA. (2016). Heat stress of two tropical seagrass species during low tides – impact on underwater net photosynthesis, dark respiration and diel in situ internal aeration. *New Phytologist* **210**: 1207-1218.

Perez-Perez ME, Lemaire SD, Crespo JL. (2012). Reactive oxygen species and autophagy in plants and algae. *Plant Physiology* **160**: 156-164.

Petus CC, Collier CJ, Devlin M, Rasheed MA and McKenna S. (2014). Using MODIS data for understanding changes in seagrass meadow health: a case study in the Great Barrier Reef (Australia). *Marine Environmental Research* **98**: 68- 85.

Ralph PJ, Durako MJ, Enríquez S, Collier CJ, Doblin MA. (2007). Impact of light limitation on seagrasses. *Journal of Experimental Marine Biology and Ecology* **350**: 176-193.

Raun AL, Borum J. (2013). Combined impact of water column oxygen and temperature on internal oxygen status and growth of *Zostera marina* seedlings and adult shoots. *Journal of Experimental Marine Biology and Ecology* **441**: 16–22.

Raun AL, Borum J, Sand-Jensen K. (2010). Influence of sediment organic enrichment and water alkalinity on growth of aquatic isoetid and elodeid plants. *Freshwater Biology* **55**: 1891-1904.

Raven JA, Scrimgeour CM. (1997). The influence of anoxia on plants of saline habitates with special reference to the sulfur cycle. *Annals of Botany* **79**: 79-86.

Revsbech NP. (1989). An oxygen microsensor with a guard cathode. *Limnology and Oceanography* **34**(2): 474-478.

Spilling K, Titelman J, Greve TM, Kühl M. (2010). Microsensor measurements of the external and internal microenvironment of *Fucus vesiculosus* (Phaeophyceae). *Journal of Phycology* **46**: 1350-1355.

Webb WL, Newton M, Starr D. (1974). Carbon-dioxide exchange of *Alnus-rubra* - mathematical-model. *Oecologia* **17**: 281-291.

York PH, Carter AB, Chartrand K, Sankey T, Wells L, Rasheed MA. (2015). Dynamics of a deep-water seagrass population on the Great Barrier Reef: annual occurrence and response to a major dredging program. *Scientific reports* **5**: 13167.

SUPPORTING INFORMATION

Sediment resuspension and deposition on seagrass leaves impedes internal plant aeration and promotes phytotoxic H_2S intrusion

Kasper Elgetti Brodersen[1,*], Kathrine Jul Hammer[2], Verena Schrameyer[1], Anja Fløytrup[2], Michael Rasheed[3], Peter J. Ralph[1], Michael Kühl[1,4], Ole Pedersen[2,*]

Running title: "Effects of sediment deposits on seagrass performance".

[1]Plant Functional Biology and Climate Change Cluster, Aquatic Process Group, University of Technology Sydney, Sydney, Australia

[2]Freshwater Biological Section, Department of Biology, University of Copenhagen, Copenhagen, Denmark

[3]Centre for Tropical Water & Aquatic Ecosystem Research (TropWater), James Cook University, Cairns, Australia

[4]Marine Biological Section, Department of Biology, University of Copenhagen, Helsingør, Denmark

[5]School of Plant Biology, The University of Western Australia, Crawley, Australia

[*]Corresponding authors: Kasper Elgetti Brodersen, elgetti@hotmail.com and Ole Pedersen, opedersen@bio.ku.dk

FIGURE S8.1. Depth microprofiles of O_2 concentration across the water/sediment interface. Y = 0 indicate the sediment surface. All microsensor measurements were performed in darkness. The investigated marine sediment originated from Narrabeen Lagoon, NSW, Australia. Symbols and error bars are mean ± SEM. n = 4.

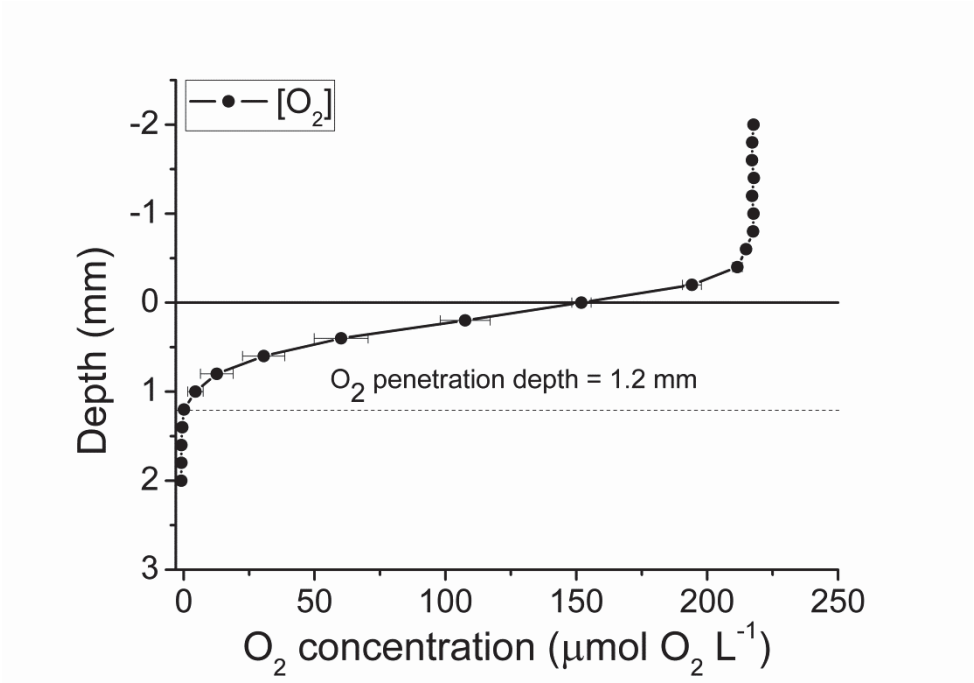

FIGURE S8.2. Net photosynthesis rates of the three investigated *Zostera muelleri* spp. *capricorni* plants as a function of incident photon irradiance. Black symbols and lines represent measurements on control plants; red symbols and lines represent measurements on plants with fine sediment particles (i.e. leaf silt/clay-cover). Left panels are measurements at 40% air saturation in the water-column (mimicking water-column O_2 conditions during darkness and at sunrise). Right panels are measurements in a 100% air saturated water-column (mimicking water-column O_2 conditions at mid-day). The O_2 fluxes are fitted with a saturated exponential function (Webb *et al*., 1974) amended with a term, R, to account for the respiration (Spilling *et al*., 2010).

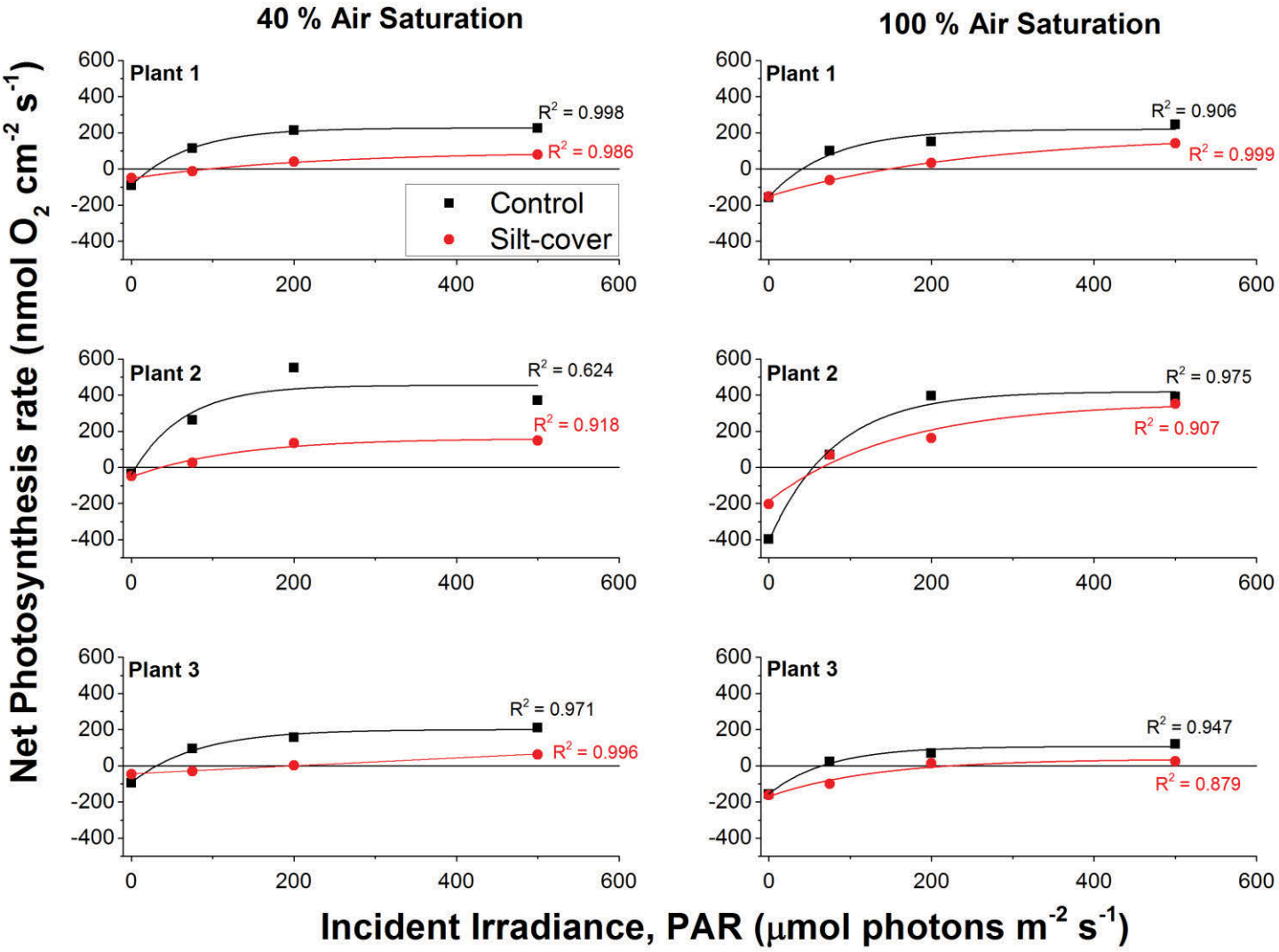

Chapter 9

Rhizome, Root/Sediment interactions, Aerenchyma and Internal Pressure Changes in Seagrasses

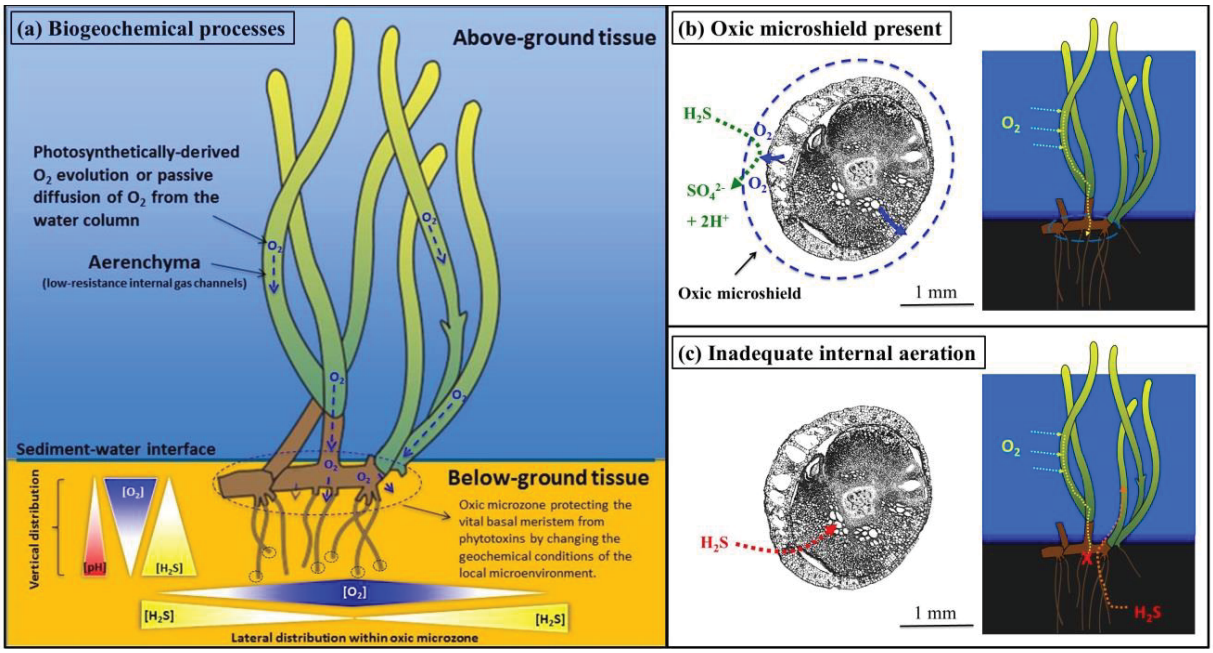

TOC figure. *Conceptual diagram describing important plant-sediment interactions. Radial O_2 loss from the below-ground tissue leads to the formation of an oxic microshield that protects the vital meristematic tissues from sulphide intrusion. Unfavorable environmental conditions, leading to e.g. water-column hypoxia, can result in inadequate internal plant aeration that may lead to sulphide intrusion.*

Citation: Brodersen KE, Kühl M, Nielsen DA, Pedersen O. & Larkum AWD. Rhizome, Root/Sediment interactions, Aerenchyma and Internal Pressure Changes in Seagrasses. Chapter 18 in *Seagrasses of Australia*. Eds. AWD Larkum, G Kendrick, PJ Ralph. (In review).

Highlights: A review (invited by E/Prof Anthony W. D. Larkum) describing (i) diffusive boundary layers around seagrass leaves, (ii) O_2 fluxes across the leaf tissue surface, (iii) aerenchymal tissue, (iv) internal O_2 movement in seagrasses, (v) radial O_2 loss (ROL) from the below-ground tissue, (vi) barriers to ROL, (vii) H_2S intrusion, (viii) the rhizospheric pH microenvironment, (ix) important seagrass/sediment interactions and (x) seagrass-derived sediment detoxification.

Rhizome, Root/Sediment interactions, Aerenchyma and Internal Pressure Changes in Seagrasses

Kasper Elgetti Brodersen[1], Michael Kühl[1,2], Daniel A. Nielsen[1], Ole Pedersen[3,4], Anthony W. D. Larkum[1]

[1]Plant Functional Biology and Climate Change Cluster, University of Technology Sydney, 15 Broadway, Ultimo, Sydney, NSW 2007, Australia.

[2]Marine Biological Section, Department of Biology, University of Copenhagen, Strandpromenaden 5, DK-3000, Helsingør, Denmark.

[3]Freshwater Biological Laboratory, Department of Biology, University of Copenhagen, Universitetsparken 4, DK-2100, Copenhagen, Denmark.

[4]School of Plant Biology, The University of Western Australia, 35 Stirling Highway, Crawley, WA 6007, Australia

Introduction

When higher (seed) plants evolved about 400 million years ago, the challenge was to maintain an adequate water balance through the development of a leaf cuticle, stomata, intercellular spaces and xylem, i.e., to become homiohydric (Raven, 1977). Once this was achieved, life in air enabled higher growth rates due to much faster rates of gaseous exchange, since diffusion coefficients for CO_2 and O_2 are approximately 10,000 times higher in air than in water (Armstrong, 1979). However, some angiosperms returned to an aqueous environment and these plants, i.e., freshwater hydrophytes and marine seagrasses, had to overcome the constraints on gas exchange imposed by the slower gas diffusion in water. Additionally, seagrasses had to contend with mechanical stress such as wave action and other difficulties of living in seawater, for example, ion regulation and sediment-related potential phytotoxins, especially sulphide that occurs in large quantities in marine sediments due to high sulphate levels (~25 mM) in seawater and the prevalence of sulphate reducing bacteria as a major component in anoxic carbon mineralization (Jørgensen, 1982). Seagrasses show many adaptations found in hydrophytes such as aerenchyma, i.e., airspaces in their tissues providing low-resistance internal gas pathways in both roots and shoots, as well as i) a photosynthetic leaf epidermis, ii) loss of stomata, and iii) reinforced structures to withstand wave-action, such as thick shoot bases and tough strap-shaped leaves (with the major exception of the genus *Halophila* and to some extent *Amphibolis*) (e.g. Armstrong, 1979; Larkum et al. 2006).

Gas exchange in seagrasses.

Molecular oxygen (O_2) and carbon dioxide (CO_2) are substrates and products in respiration and photosynthesis; thus transport processes affecting these gases are of vital importance for seagrasses. The dissolution of O_2 in seawater is straightforward, obeying Henry's law, but the dissolution of CO_2 is more complex as it is part of the pH-dependent speciation of dissolved inorganic carbon (DIC) in seawater:

$$\begin{array}{ccccccc} & K_{+1} & & K_{+2} & & K_{+3} & \\ CO_2 + H_20 & \leftrightarrow & H_2CO_3 & \leftrightarrow HCO_3^- + H^+ & \leftrightarrow & CO_3^{2-} + 2H^+ & \text{(Eq. 1)} \\ & K_{-1} & & K_{-2} & & K_{-3} & \end{array}$$

According to Eq.1, CO_2 dissolves in water to form carbonic acid, which is a relatively slow reaction that can be increased by the enzyme carbonic anhydrase (CA) in many biological systems. H_2CO_3 at normal pH of seawater (7.5-8.4) disproportionates rapidly into bicarbonate and a proton. At more alkaline pH, bicarbonate disproportionates into carbonate and another proton. The rate constants in the carbonate system are shown in Table 9.1. The action site of CA is indicated in Eq.1 by a grey box. CA can be located both intra- and extra-cellularly (e.g. Badger and Price, 1994) and there is good evidence in many photosynthetic systems for the secretion of extracellular CA into the cell wall facilitating an enhanced uptake of CO_2 via HCO_3^- conversion (e.g. Badger and Price, 1994). The presence of CAs in seagrasses has been much debated but their presence had until recently only been inferred by inhibitor studies (e.g. Larkum et al. 1996; Beer et al. 2002). However, CA coding genes have now been found to be expressed in the transcriptome of *Zostera muelleri spp. capricorni* (Golicz et al. 2015). Although the precise location of CA in the seagrass tissue has not been resolved, previous evidence indicated their presence in the outer cell wall of the leaf epidermal layers of many seagrasses (Larkum et al. 1996; Beer et al. 2002; Borum et al. 2015).

Table 9.1. Concentration and diffusion coefficients of O_2, CO_2 and bicarbonate ion in air and air-saturated seawater (35 ‰ salinity) at a temperature of 25°C (Larkum et al. 1989).

	Concentration (mmol m^{-3})			Diffusion coefficients (m^2 s^{-1})		
	CO_2	HCO_3^-	O_2	CO_2	HCO_3^-	O_2
Air	17	0	9375	$1.56 \cdot 10^{-5}$	NR	$1.97 \cdot 10^{-5}$
Seawater	11.5	2000	206	$1.55 \cdot 10^{-9}$	$1.00 \cdot 10^{-9}$	$2.26 \cdot 10^{-9}$

Data is calculated based upon an atmospheric CO_2 concentration of 401 ppm.

It appears that seagrasses have developed mechanisms to enhance the uptake of DIC (Beer, 2002; Larkum et al. 2006) and such mechanisms are discussed in detail in Chapter 16. For the present purpose, it is enough to know that photosynthetic carbon fixation is facilitated by several mechanisms that either passively or actively transports DIC from the

surrounding seawater into the cytoplasm and chloroplasts of the epidermal cells, where CO_2 fixation takes place and O_2 is produced. Photosynthesis-generated O_2 moves via diffusion to either the surrounding seawater or inwards from the epidermal cells into the surrounding tissue and the aerenchymal spaces depending on the actual concentration gradient and the resistance to diffusion (Fig. 9.1; e.g. Colmer, 2003).

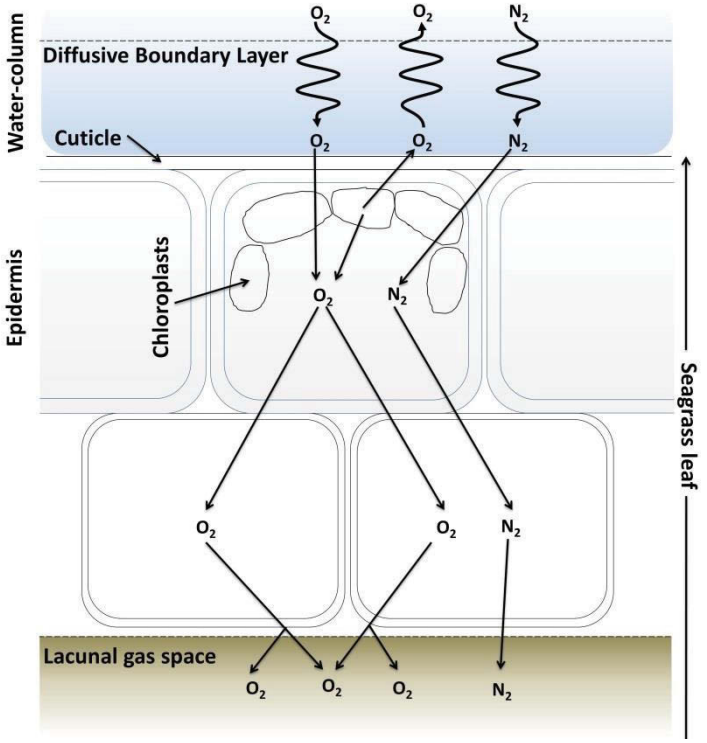

Figure 9.1. Conceptual diagram showing the major diffusional transport routes for O_2 and N_2 from the ambient medium to the lacunal space (under non-pressurised conditions) in a seagrass leaf. Data modified from Larkum et al. (1989).

An important consideration for the movement of gases in seagrasses is the diffusional constraints on the movement of CO_2 and O_2 both in solution and in the gas phase (Larkum et al. 1989; Larkum et al. 2006). The diffusive gas transport is described by Fick's first law:

$$J_j = D_j (C_a – C_s)/l \qquad \text{(Eq. 2)}$$

where J_j is the flux of gas j (mol m^{-2} s^{-1}), D_j is the diffusion coefficient of the gas j (m^2 s^{-1}) (in water or in air; at a given temperature and salinity), l is the distance over which diffusion occurs (m), c_a and c_s are the concentrations of the gas j (mol m^{-3}) at the source and sink,

respectively. In this formulation it is assumed that there is i) unidirectional movement of the gas from source to sink, ii) no net consumption or production of the diffusing species underway, and iii) that c_a and c_s are constant - see Nobel (1990). In the following sections, O_2 will mainly be expressed as a concentration (in µmol L^{-1}) when in solution and as a partial pressure (in kPa) when in the gas phase; where ~240 µmol L^{-1} (depending on salinity and temperature) and ~20.6 kPa represents 100% air saturation in a marine environment.

The diffusive transport of a gas across a given plant tissue compartment can be conceptualized as a set of electrical resistances in series (and parallel) (Van den Honert, 1948; Raven, 1977; Armstrong, 1979; Nobel, 1990):

$$J_j = D_j (C_a - C_s)/l = DF/R_{jT} \qquad \text{(Eq. 3)}$$

where $D_j/l = 1/R_{jT}$ and R_{jT} is the total resistance of the gas transport pathway to species j, having the units, s m^{-1}. DF is the driving force or the concentration gradient ($C_a - C_s$). And each component of the pathway (catenary) can be assigned as previously described in Larkum et al. (1989):

$$J_j = DF/R_{jT} = DF_a/R_{ja} = DF_b/R_{jb} = DF_c/R_{jc}, \text{ etc.} \quad \text{(Eq. 4)}$$

and therefore

$$R_{jT} = R_{ja} = R_{jb} = R_{jc}, \text{ etc.} \qquad \text{(Eq. 5)}$$

where the subscripts T, a, b, c, etc. refer to the total sequence of diffusional steps (T = total) and to the individual steps (a, b, c, etc.).

Using this formulation, it is possible to set out a resistance circuit for the movement of CO_2 and O_2 across the epidermal cell and hypodermal cell of a seagrass, respectively. Such a formulation can then be used to calculate the flux of O_2 either outwards from the epidermal cell or inwards into the aerenchymal spaces (see Larkum et al. 2006) and as we shall in the next section this has important implications for our understanding of the aeration of seagrasses.

Diffusive boundary layers and water motion around seagrass leaves

Gas exchange between aquatic macrophytes and the surrounding water is impeded by the presence of a diffusive boundary layer (DBL) (e.g. Jørgensen and Revsbech, 1985; Hurd, 2000; Brodersen et al. 2015a). As flow declines towards the plant surface, the viscosity of water dampens out turbulences, forming the DBL as a thin layer of water just above the tissue surface where molecular diffusion governs solute exchange between tissue and water. The thickness of the DBL is affected by water flow and surface rugosity (e.g. Jørgensen and Des Marais 1990, Larkum et al. 2003), where low flow and/or more coarse topography lead to a thicker DBL than fast flow and/or a smoother surface. The DBL thickness is an important factor controlling solute exchange as diffusion time increases with the square of the DBL thickness. Therefore, the DBL can present a major barrier to plant solute exchange, especially under low flow conditions or e.g. in the presence of epiphytes on seagrass leaves that increase rugosity (Brodersen et al. 2015a). Larkum et al. (1989) reported a DBL thickness on seagrass leaves ranging from ~50 μm under maximal flow to 200 – 1000 μm under medium to low flow conditions, and this range was later confirmed by microsensor measurements (e.g. Binzer et al. 2005; Borum et al. 2006; Brodersen et al. 2015a). For seagrasses, this means that under natural conditions there will be a strong diffusion resistance to movement of solutes into the leaves from the surrounding seawater (Fig. 9.1).

With respect to O_2, the DBL at the outer surface of the leaves means that, despite the proximity of the epidermal cell layer to the surrounding seawater, the diffusion resistance for molecules moving out of the epidermis or into the airspace system of the aerenchyma can be similar. Thus, during medium to high light exposure, when photosynthesis is active and O_2 is being produced at high rates, accumulating O_2 pressurizes the aerenchyma (Table 9.2; Larkum et al. 1989; Bodensteiner, 2006). This can be seen in many seagrass species where, around midday, the leaves become more erect, and gas bubbles can often be seen escaping from wounds in the leaf surface. The pressurisation of the leaf during active photosynthesis leads to increased O_2 partial pressure (pO_2) which may increase O_2 supply to the roots and rhizome, however, the longitudinal transport to the below-ground tissues is greatly restricted by the diminished aerenchymal spaces in the shoot base manifold (further described below).

Table 9.2. Gaseous composition of the lacunal system of several seagrasses (Larkum et al. 1989).

Species	O_2 (%)	N_2 (%)	CO_2 (%)	% of O_2 flux to lacunae	Max. lacunal pressure (kPa)
Zostera muelleri subsp. *capricorni*	32.3	67.6	-	13	-
Cymodocea serrulata	34.3	65.4	0.0095	16	22.0
Syringodium isoetifolium	32.2	64.4	0.140	17	8.18
Halophila ovalis	34.1	66.1	-	-	10.0
Enhalus acoroides	33.5	67.0	0.1017	12.6	-
Amphibolis antarctica	31.7	67.8	-	8	-
Halodule uninervis	-	-	0.0037	-	-

Internal aeration

The leaves of seagrasses are generated at the base of the shoot, i.e., the basal leaf meristem that in mono-meristematic leaf-replacing species such as *Zostera* and *Posidonia* is a combined rhizome/basal leaf meristem area at the root-shoot junction (Fig. 9.2). Three other forms exists, i.e., di-meristematic leaf-replacing species (such as *Thalassia* and *Cymodocea*), mono-meristematic non-leaf-replacing species (mostly *Halophila*), and di-meristematic non-leaf-replacing species (few species of *Halophila*) (e.g. Short and Duarte, 2001), but in the following we will mainly focus on the mono-meristematic leaf-replacing species. The meristematic region of the rhizome has poorly developed aerenchyma owing to the compact anatomy of the tissue, and thereby O_2 diffusion to this area is impeded. To alleviate this structural limitation to O_2 movement, the surrounding leaf sheath has an extensive distribution of large, internal gas channels (Fig. 9.2). The shoot base also produces fiber-rich tissue that provide a biomechanical strengthening of the root/shoot base against wave action, and many seagrasses also have adventitious roots that anchor the shoot base into the sediment. As a consequence, the aerenchyma system, which consists of long gas channels or lacunae that stretch through the leaves and roots, peter out in the shoot base, where it is replaced by a much more tenuous intercellular pathway for gas transport (Fig. 9.2). The net result of this extended and reinforced gas pathway in the shoot base manifold causes O_2 to diffuse laterally into the surrounding sediment and tissues, especially to the

young developing leaves in addition to the downwards diffusion to the rhizome and roots (e.g. Pedersen et al. 1998, 1999; Jensen et al. 2005; Frederiksen and Glud, 2006; Brodersen et al. 2014; Koren et al. 2015; Brodersen et al. 2015a,b). Hence, while the root/shoot manifold forms a hindrance to the passage of O_2 from shoot to root, it alleviates mechanical stress from wave action and secures the O_2 supply to the young meristematic tissues, thereby enabling a protection against intrusion of sediment-produced H_2S.

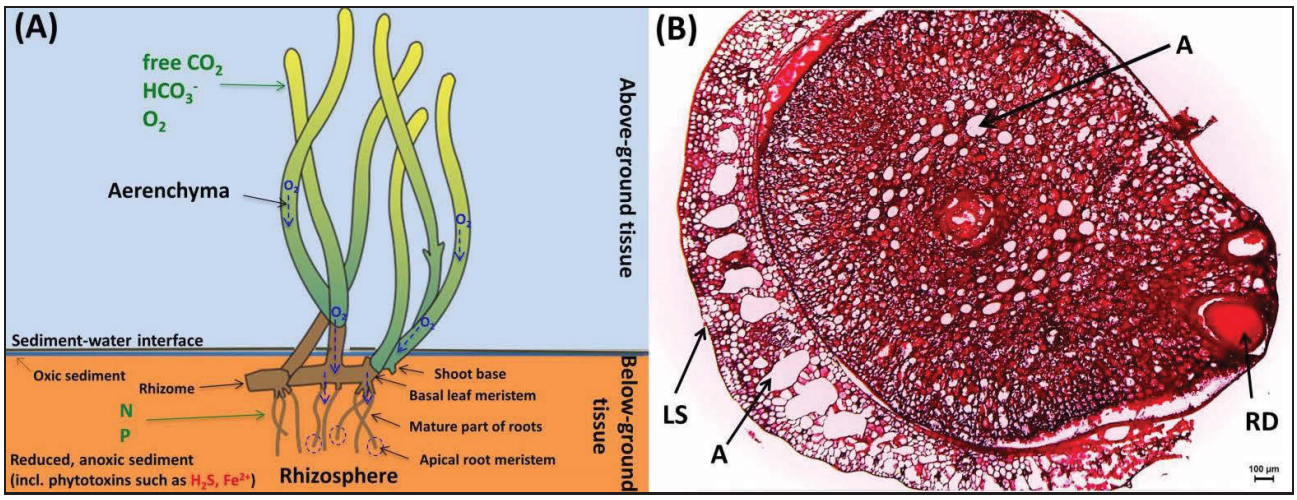

Figure 9.2. (A) Conceptual diagram of the aerenchymal system in seagrass. (B) Cross-sectional image of a shoot base with leaf sheath of *Zostera muelleri spp. capricorni* showing the extended air lacunal system at the meristematic region of the rhizome. Scale bar = 100 µm. LS = indicate the leaf sheath; A = aerenchyma; RD = initial root development. Data modified from Brodersen et al. (2015b). Copyright 2015 John Wiley & Sons Ltd.

Internal O_2 concentration gradients

The seagrass rhizosphere is largely anoxic and thus roots and rhizomes are unable to take up O_2 from the sediment environment. Instead, O_2 moves along a concentration gradient from the above-ground shoot to the rhizome and root-tips by means of molecular gaseous diffusion. As described above, diffusion in liquid phase is slow and not effective over distances larger than a few mm. As a consequence, seagrasses have evolved a network of porous gas-filled spaces (aerenchyma) in all tissues where gas phase diffusion enables sufficient O_2 transport to the below-ground tissues.

The motive force of O_2 transport is the strong internal gradient in O_2 partial pressure (pO_2) from shoot to root tip. The gradient develops as a result of *i*) O_2 consumption of the tissues,

and *ii*) radial O_2 loss (ROL) from the aerenchyma to the environment. In the mature zones of rhizomes and roots, tissue respiration is moderate since the metabolic processes primarily serve to support maintenance respiration, and barriers to ROL exists that reduce the loss of O_2 along the diffusion pathway (Colmer, 2003). In the apical zones of rhizomes and in the root-tips, on the other hand, cell division requires additional energy and thus increased O_2 consumption, resulting in a steep decline in tissue pO_2. The root-tips are highly permeable to O_2 so ROL is extensive (Jensen et al. 2005; Pedersen et al. 1998), resulting in a steep gradient in pO_2 inside the aerenchyma from shoot to root-tip. This gradient drives a steady flux of O_2 to the O_2 demanding tissues. Figure 9.3 demonstrates the point that tissue pO_2 systematically declines with distance to the shoot that acts as entry point of O_2 in the dark and site of production in the light.

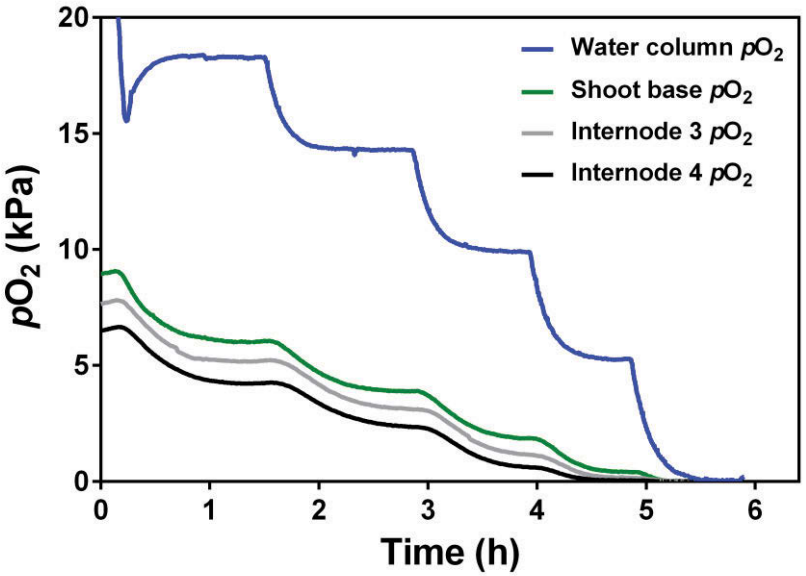

Figure 9.3. Below-ground tissue pO_2 as a function of water-column pO_2 in darkness measured in *Zostera marina*. The O_2 microelectrodes were inserted into the shoot base close to the leaf meristem, which was buried approximately 5 mm into the sediment, and in the 3rd and the 4th internode of the rhizome. The pO_2 of the water-column was successively reduced in steps of 4-5 kPa over a timeframe of 6 h and kept at 20 °C. Data modified from Pedersen et al. (2004).

In the dark, pO_2 of roots and rhizomes is strongly correlated to water-column pO_2 (e.g. Greve et al. 2003), which is reflected by decreasing tissue pO_2 following a decline in water-column pO_2 (Fig. 9.3). A strong dependence of water-column O_2 on the night-time tissue

respiration has also been demonstrated *in situ* (Sand-Jensen et al. 2005; Borum et al. 2005). Sand-Jensen et al. (2005) reported that at dusk, when photosynthesis ceased (~8 p.m., Fig. 9.4), tissue pO_2 declined rapidly to a point where the decline followed water-column pO_2 (Fig. 9.4), and the shoot base became anoxic at a water-column pO_2 of approximately 9-10 kPa (~50% air saturation; Fig. 9.5). The water-column pO_2 required to prevent shoot base anoxia depends on the above-ground:below-ground tissue ratio since the shoot acts as site of O_2 uptake, whereas roots and rhizomes are sinks due to respiration and ROL. At a relatively low ratio, the critical water-column pO_2 for shoot base anoxia would be higher compared to a situation, where the ratio is higher. Implications of tissue anoxia encompass low energy yield when anaerobic fermentation takes over from respiration, reduced nutrient uptake by the roots, impeded translocation of carbohydrates and nutrients between leaves and roots, as well as anoxic rhizosphere conditions near the root-tips potentially leading to sulphide intrusion (see below; e.g. Zimmerman and Alberte, 1996; Pedersen et al. 2004; Borum et al. 2006; Brodersen et al. 2015b).

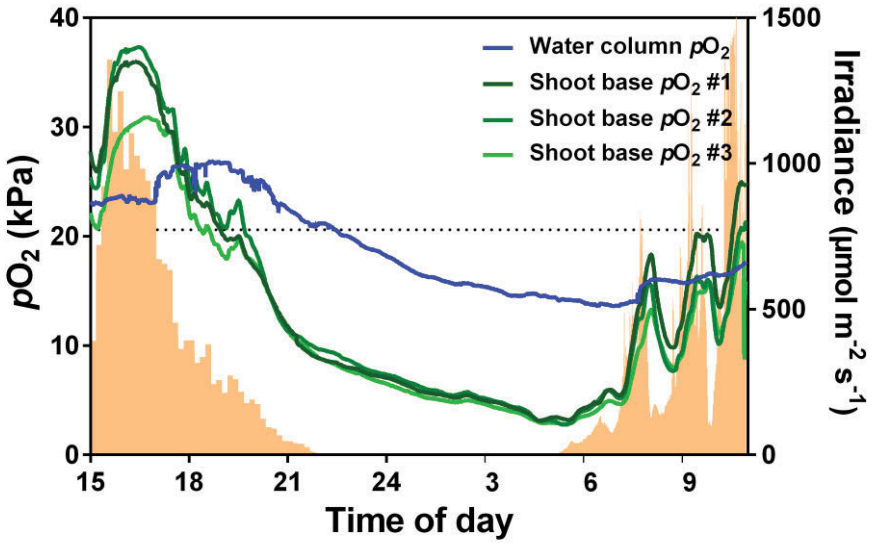

Figure 9.4. *In situ* pO_2 of the shoot base of 3 replicate plants of *Zostera marina* and the water-column over a diurnal cycle measured in Roskilde Fjord, Denmark. The O_2 microelectrodes were inserted into the shoot base close to the leaf meristem, which was buried approximately 5 mm into the sediment. The dotted line indicates air equilibrium of dissolved O_2. Irradiance of the PAR spectrum measured at the canopy surface is shown in orange colour. Data modified from Sand-Jensen et al. (2005).

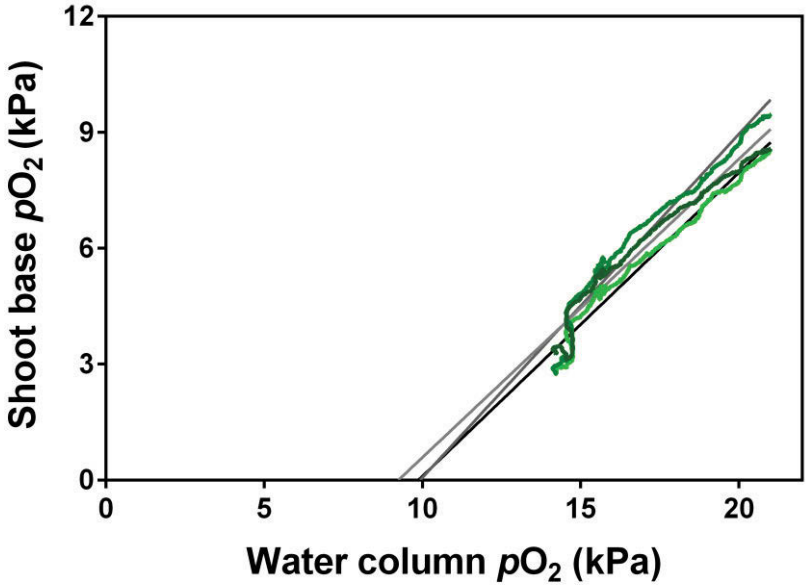

Figure 9.5. Water-column pO_2 versus shoot base pO_2 during night-time of 3 replicate plants of *Zostera marina*. The data are extracted from Figure 9.4 in the time period of 10 p.m. to 5 a.m. The grey lines represent linear regression of each replicate plant and are extrapolated to interception with the horizontal axis (as this gives an estimate of at which water-column pO_2 the vulnerable shoot base tissue becomes anoxic). Data modified from Borum et al. (2006).

The aerenchyma has been suggested to function as an important reservoir of O_2 for respiration in the dark. However, in the case of *Z. marina*, the pool of O_2 initially captured in the aerenchyma would only be able to support respiratory demands for 8-13 min, assuming an initial pO_2 near atmospheric equilibrium (i.e. 20.6 kPa) (Sand-Jensen et al. 2005). Moreover, shoot and apical root tissues are highly gas permeable and the pool of O_2 quickly equilibrates with the environment (e.g. Fig. 9.3) further shortening the time that stored O_2 can meet respiratory demands. Thus, seagrasses primarily rely on a reservoir of O_2 in the water-column surrounding the leaves to support their night-time respiration in their tissues, and this makes them vulnerable to O_2 depletion in the water-column during night-time or periods of low irradiance, e.g. due to low water transparency.

Photosynthetically produced O_2 supports daytime respiration in both above- and below-ground seagrass tissues. In the light, shoot base tissue pO_2 can reach 40 kPa or more (Fig. 9.4) and thereby significantly exceed water-column pO_2. As previously mentioned, the high tissue pO_2 in the leaves in the light results in a steep O_2 gradient to the surrounding water-

column and also internally from shoot to root-tips facilitating that even the most distant root-tips can experience daytime pO_2 of close to air equilibrium as shown for *e.g.*, *Cymodocea rotundata* and *Zostera marina* (Jensen et al. 2005; Pedersen et al. 1998).

The strong relationship between below-ground tissue pO_2 and photosynthesis during the day is illustrated in Figure showing a saturation of shoot base pO_2 with increasing irradiance at leaf canopy height with a shape resembling typical photosynthesis *versus* irradiance curves. The data for Figure 9.6 are extracted from the light period between 6 and 11 a.m. in Figure 9.4, and shows that with a photon irradiance of approximately 250-300 µmol photons m^{-2} s^{-1} and above, shoot base pO_2 exceeds the atmospheric equilibrium of 20.6 kPa. Thus in shallow transparent waters governing good light conditions, the below-ground tissues of seagrasses exhibit a beneficial intra-plant O_2 status due to photosynthetic O_2 production during the day.

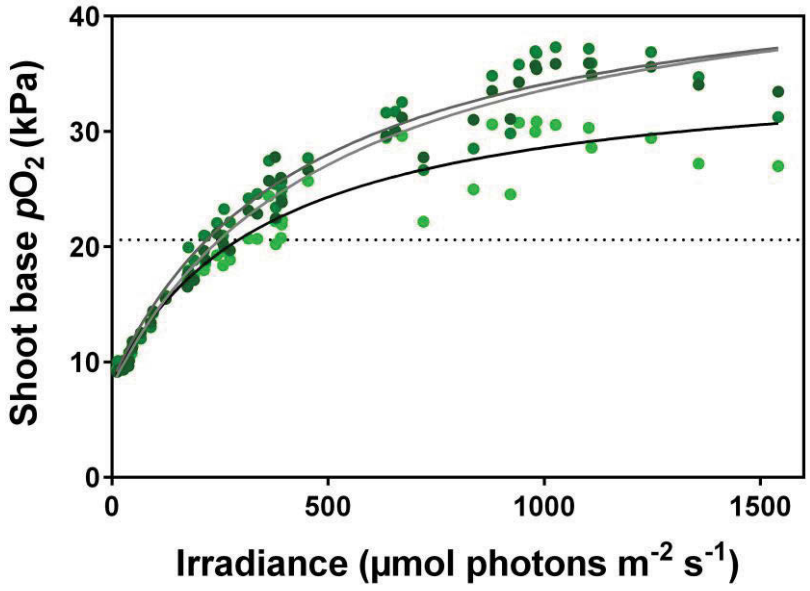

Figure 9.6. Irradiance versus shoot base pO_2 during day-time of 3 replicate plants of *Zostera marina*. The data are extracted from Figure 9.4 in the time period of 6 p.m. to 11 a.m. on day 2. The grey lines represent non-linear regression of each replicate plant applying a Jassby and Platt (1976) model. The dotted line represents air saturation of dissolved O_2. Data modified from Borum et al. (2006).

Seagrass/sediment interactions

Seagrasses are generally found in highly reduced sediments enriched with organic matter (Borum et al. 2006), where such enrichment to a large extent is due to the presence of the seagrass plants and their detritus. The high productivity of seagrass meadows and the resulting continuous contribution of organic matter to the sediment, both from seagrass debris and exudates from roots and rhizomes (Moriarty et al. 1986; Pollard and Moriarty, 1991), as well as from enhanced sedimentation due to diminished flow in dense seagrass beds (Ward et al. 1984; Madsen et al. 2001), supports high rates of microbial carbon mineralization in the sediment. As O_2 solubility in seawater is limited (typically 283.9-195.7 µM in air-saturated seawater at 10-30°C; at a salinity of 34) as compared to terrestrial systems, and the O_2 supply to the sediment from the seawater is impeded by a diffusive boundary layer (DBL) (e.g. Jørgensen and Revsbech, 1985; Jørgensen and Des Marais, 1990; Kühl and Revsbech, 2001), aerobic respiration and re-oxidation of reduced chemical species diffusing towards the sediment-water interface rapidly deplete O_2 in the upper mm's of the sediment. In anoxic marine sediments, microbial sulphate reduction is the dominant anaerobic respiratory process (Jørgensen, 1982), whereby sulphate is reduced to sulphides that shows a pH dependent speciation (with a pK_a value of ~pH 7) into dissolved hydrogen sulphide gas (H_2S) and hydrogen sulphide ions (HS^-) at typical sediment pH values. Sulphides reacts efficiently with oxidized molecules such as Fe(III), causing a further reduction of the sediment. Due to its high toxicity to aerobic organisms, high H_2S concentrations are generally detrimental to plants and animals living in sulphidic sediments (Lamers et al. 2013). It has therefore long been speculated that seagrasses must have a capacity to alleviate H_2S exposure in order to sustain their own growth.

H_2S intrusion at low water-column O_2 concentrations

Water-column hypoxia during night-time can lead to sulphide intrusion into below-ground tissues if the O_2 flux across the DBL is insufficient to maintain ROL at the basal leaf meristem and root-tips. The fast growing root-tips are highly gas permeable because they lack a structural barrier to ROL (Connell et al. 1999), but during conditions with normal water-column pO_2 the ROL results in the formation of a so called "oxic microshield" in the

rhizosphere around the basal leaf meristem and root-tips (Jensen et al. 2005; Frederiksen and Glud, 2006; Brodersen et al. 2015b). The released O_2 can oxidize sulphide and thereby prevent H_2S from diffusing into the young, structurally unprotected tissue (further described below; Brodersen et al. 2015b). During water-column hypoxia, however, the ROL may become insufficient to maintain these oxic shields in the rhizosphere, increasing the risk of H_2S exposure and intrusion (Fig. 9.7).

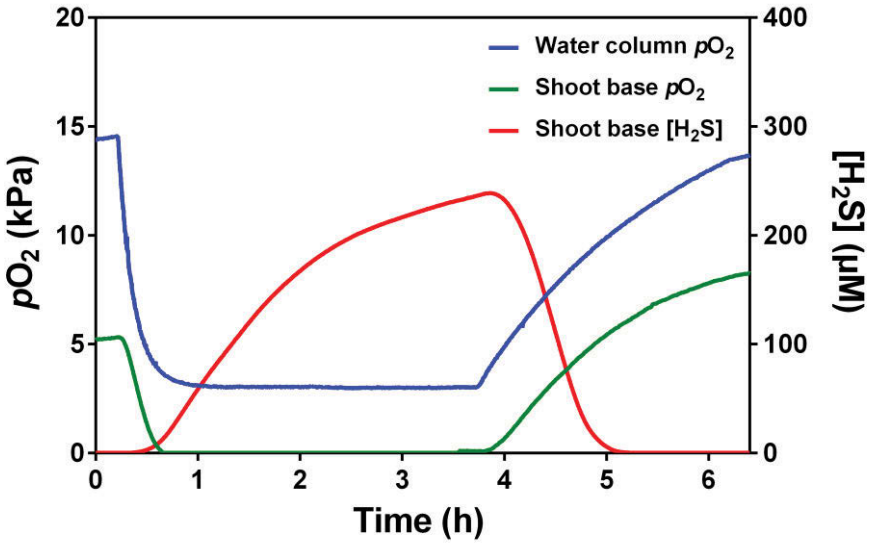

Figure 9.7. Shoot base pO_2 and shoot base H_2S as a function of water-column pO_2 in *Zostera marina*. The O_2 and H_2S microelectrodes were inserted into the shoot base close to the leaf meristem, which was buried approximately 5 mm into the sediment. Water-column pO_2 was manipulated in steps of about 10 kPa and kept at 20 °C. Data modified from Pedersen et al. (2004).

Gaseous H_2S spreads by molecular diffusion inside the aerenchyma from areas of high concentration near the root-tips towards the shoot. In the gas phase, oxidation of H_2S with O_2 is a relatively slow spontaneous chemical reaction, and both O_2 and H_2S can thus coexist for some time in the same tissues (Borum et al. 2005; Pedersen et al. 2004). Figure 9.7 demonstrates an example where water-column pO_2 was experimentally manipulated, and where a decline from 15 to 3 kPa O_2 resulted in H_2S intrusion. At the shoot base, H_2S was detected in the tissue before complete O_2 depletion, where after H_2S continued to rise up to ~250 µM. When the surrounding water-column was brought back to atmospheric equilibrium, pO_2 in the shoot base increased, while H_2S was depleted. However, O_2 and H_2S

co-existed in the same tissue for >1 h until O_2 reached the root-tips and H_2S intrusion was once again restricted by the oxic sediment microshield. Recent studies also suggest an internal H_2S detoxification mechanism, whereby H_2S is oxidized to elemental sulphur (an intermediate in sulphide oxidation) precipitating on the inner walls of the aerenchyma (e.g. Holmer and Hasler-Sheetal, 2014; Hasler-Sheetal and Holmer, 2015).

Sulphide intrusion into seagrass tissue has also been demonstrated *in situ*, where sulphide poisoning has been suggested to result in localised die-off events (e.g. Borum et al. 2005; Carlson Jr et al. 1994). Florida Bay in the U.S. has been severely affected by such die-off events, and Borum et al. (2005) showed that gaseous H_2S started penetrating the below-ground tissues and spread to the shoot base of seagrasses at a water-column pO_2 of approximately half air equilibrium (10 kPa) (Fig. 9.8). As the water-column experienced further hypoxia during the night, H_2S reached a tissue concentration of more than 750 µM in the shoot base. In line with the observations from laboratory experiments (Fig. 9.7), the shoot base never became anoxic and H_2S and molecular O_2 coexisted throughout the night (Fig. 9.8). Tissue H_2S then started declining following sunrise as photosynthetically produced O_2 resulted in higher pO_2 in the below-ground tissues but H_2S persisted in the shoot base tissue until 10 a.m., i.e., >4 h after sunrise. Sulphide intrusion into the below-ground tissue of seagrasses is thus strongly linked to the O_2 status of the plants.

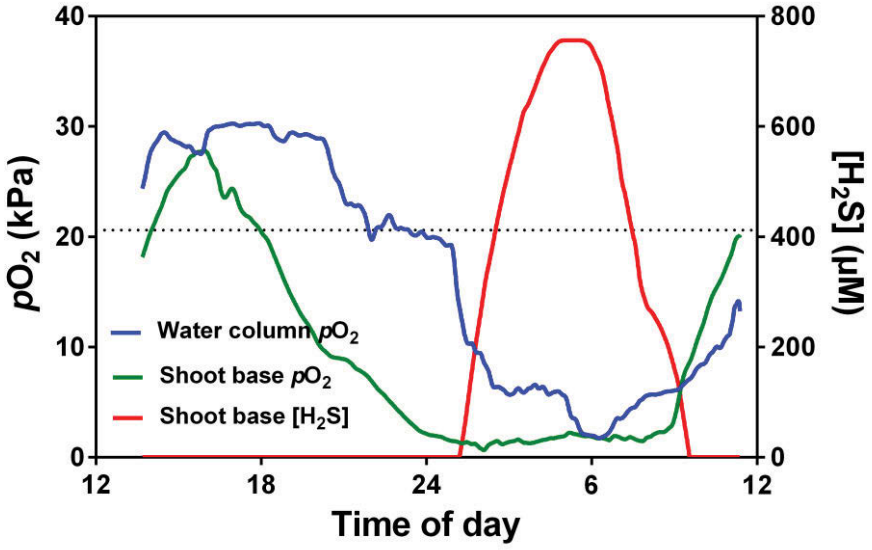

Figure 9.8. In situ pO2 and H2S of the shoot base of Thalassia testudinum and the water-column pO2 over a diurnal cycle measured in a die-off patch at Barnes Key, Florida Bay, USA. The O2 and H2S microelectrodes were inserted into the shoot base close to the leaf meristem, which was buried approximately 20 mm into the sediment. The dotted line indicates air equilibrium of dissolved O2. Data modified from Borum et al. (2005).

Koren et al. (2015) found that the oxygenated region around the seagrass rhizome of *Z. muelleri* was diminished during night-time (Fig. 9.9), likely in response to lowering of the internal pO_2 and thereby a reduction in the O_2 gradient from the rhizome to the anoxic sediment. A combination of darkness and low water-column pO_2 (~50% air equilibrium) has previously been shown to enable H_2S to reach the root and rhizome of the plant, thus exposing the plant to potential poisoning (Fig. 9.10). Seagrasses may thus be sensitive to diminished water flow, light and/or pollution that can affect the O_2 transport to the lower tissue regions of the plant. Pollution effects include sediment re-suspension from dredging, which lowers the photosynthetically active radiation (PAR) reaching the leaves (Erftemeijer and Lewis, 2006), and eutrophication, which causes algal blooms lowering light availability and water-column O_2 concentrations through increased night-time respiration and degradation of settled algal biomass in the sediment. Growth of epiphytic algae on the seagrass leaf can also reduce PAR and increase the DBL thickness and thus impede O_2 transport into the leaf (Drake et al. 2003; Brodersen et al. 2015a).

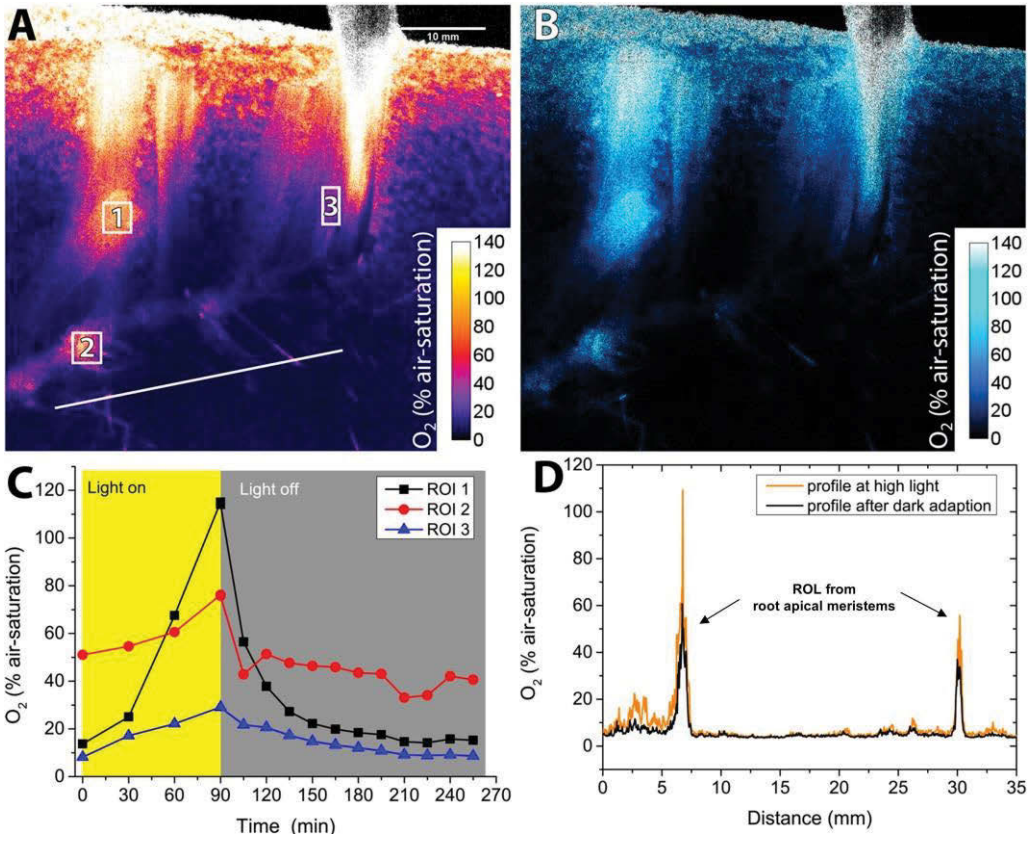

Figure 9.9. (a): Colour coded O_2 image acquired via novel optical nanoparticle-based O_2 sensors, visualising the O_2 distribution in the seagrass rhizosphere under an incident photon irradiance of 500 µmol photons m^{-2} s^{-1}. (b): The relative difference in the below-ground tissue oxidation capacity between measurements in light and darkness. (c): Real-time O_2 concentrations within selected regions of interest (ROIs, as shown in panel A) during a light/dark transition. Black symbols and profile represents measurements at the prophyllum (ROI 1), red symbols and profile represent measurements at the root-shoot junction (ROI 2), blue symbols and profile represent measurements at the basal leaf meristem (ROI 3). (d): The extracted line profile from the O_2 image (shown in panel A) across 2 roots, visualising radial O_2 loss (ROL) from the root apical meristems during a light/dark transition. Partly redrawn with permission from Koren et al. (2015). Copyright 2015 American Chemical Society.

Oxic microshields and below-ground tissue oxidation capacity

The passive, internal aeration system of the seagrass plant thus not only serves to aerate various tissue parts including the below-ground portions (described above). Aerenchymatic gas transport to the below-ground tissue and ROL to the surrounding sediment enables oxidation of the immediate rhizosphere microenvironment and alleviates

exposure to phytotoxins such as H_2S (Brodersen et al. 2015b). The release of O_2 from roots and rhizomes has been demonstrated on multiple occasions over the last three decades (Pedersen et al. 1998, 1999; Jensen et al. 2005; Frederiksen and Glud, 2006; Brodersen et al. 2015a,b; Koren et al. 2015) (Fig. 9.9), but only recently has the direct connection between O_2 release and removal of H_2S around the below-ground tissue been confirmed (Brodersen et al. 2014, Brodersen et al. 2015b). By applying a split flow chamber with artificial, transparent sediment, Brodersen and co-workers used microsensors to measure the O_2 release from the below-ground tissue from *Z. muelleri spp. capricorni* and could align such oxic microzones with the concomitant detection of H_2S depletion towards the roots and rhizomes resulting from chemical oxidation (Fig. 9.10). While the leakage of O_2 varied across the rhizome, a several hundred µm thick oxic microshield was detected at the point of O_2 loss (Fig. 9.11), which was sufficient to oxidize most of the H_2S before it reached the tissue surface (Fig. 9.10 and 9.11).

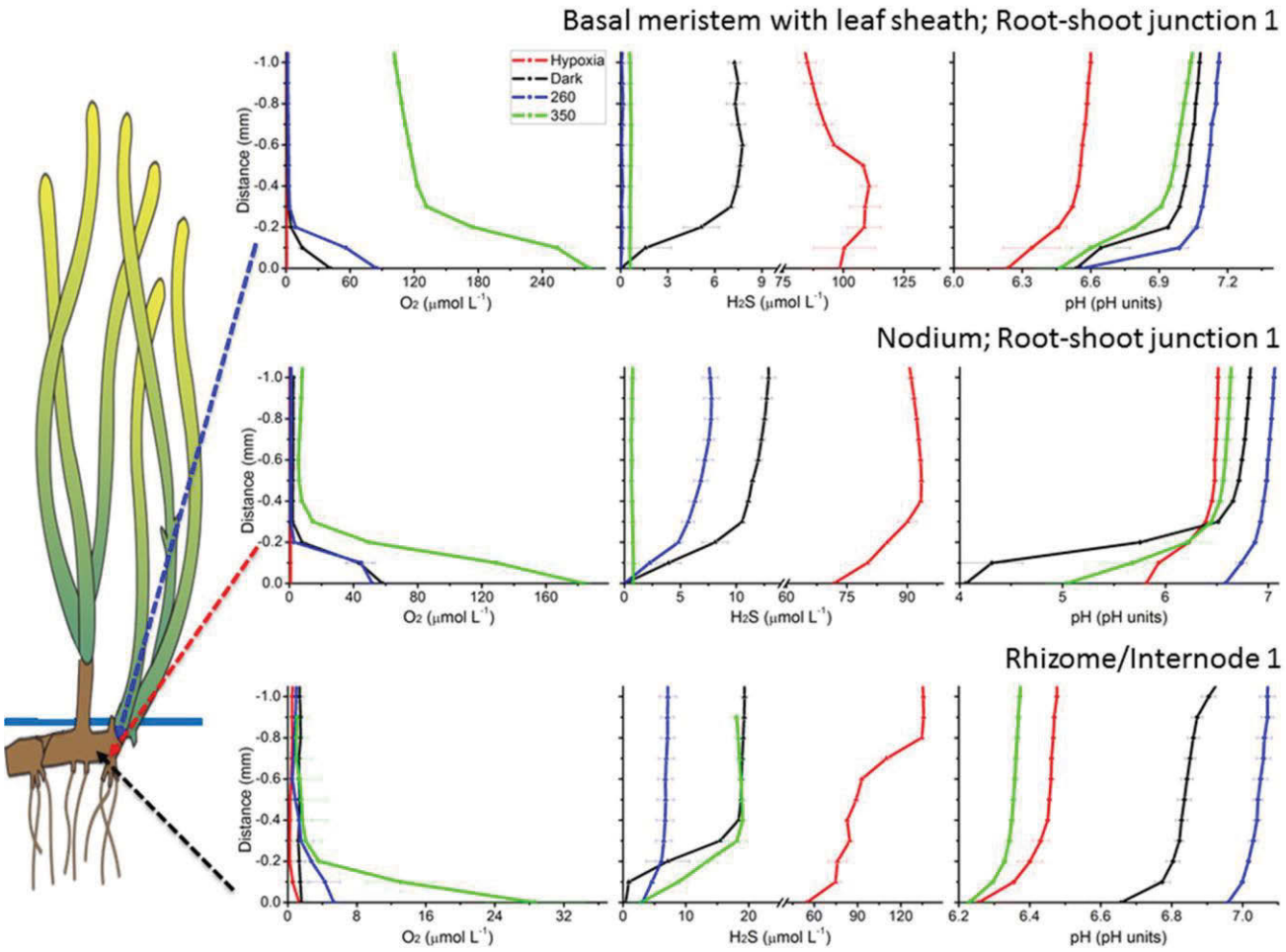

Figure 9.10. Seagrass-derived sediment detoxification as a result of below-ground tissue radial O_2 loss into the immediate rhizosphere. Concentration profiles of O_2, H_2S and pH were measured with microelectrodes in darkness (black profiles), at an incident photon irradiance of 260 (blue profiles) and 350 (green profiles) µmol photons m^{-2} s^{-1}, and in darkness with hypoxic conditions in the water-column (red profiles). *Upper panels* represents measurements at the basal leaf meristem with leaf sheath, *intermediate panels* (horizontally) at the root-shoot junction and *lower panels* at the rhizome. *Left panels* represent the immediate rhizosphere O_2 concentration, *intermediate panels* (vertically) represents the immediate rhizosphere H_2S concentration and *right panels* represents the immediate rhizosphere pH. Y = 0 indicate the below-ground tissue surface. Error bars are ±SD. n = 2–4. Note the break on the x-axis of panels illustrating the immediate rhizosphere H_2S concentration. The illustration of *Z. muelleri spp. capricorni* originates from the IAN/UMCES symbol and image libraries (Diana Kleine, Integration and Application Network (IAN), University of Maryland Center for Environmental Science (ian.umces.edu/imagelibrary/)). Data modified from Brodersen et al. (2015b). Copyright 2015 John Wiley & Sons Ltd.

In contrast to previous observations in temperate *Z. marina* plants (Jensen et al. 2005); *Z. muelleri* which extends into subtropical regions, showed no or very little ROL from the root-tips, and the highest ROL was found around the basal leaf meristem with leaf sheaths, where new leaves are generated (Brodersen et al. 2014, 2015b; Koren et al. 2015). While mature seagrass tissue has a high resistance to radial O_2 transport (Jensen et al. 2005; Frederiksen and Glud, 2006), partly due to the presence of Casparian-band like structures (Barnabas, 1996), the new tissue being formed in the meristem has a poorly developed lacunal system and little resistance to radial gas transport. As such, the concomitant higher lateral movement of O_2 to the meristematic tissue of *Z. muelleri* is likely an adaptation to protect this crucial but vulnerable tissue of the plant against exposure to H_2S, both internally and externally. However, to what extent this is a general feature of seagrasses needs further evaluation.

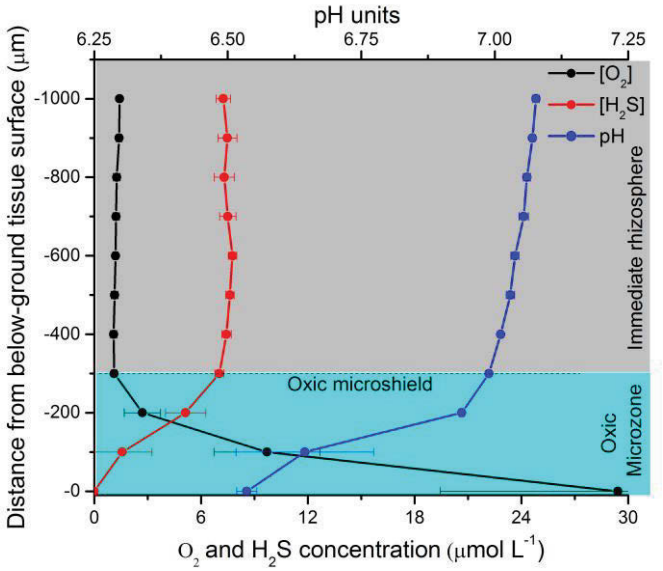

Figure 9.11. Oxic microshields surrounding the root/shoot junctions (including the basal leaf meristem with leaf sheath), the rhizome and the apical root meristems of seagrasses. Black symbols and profile represents [O_2]; red symbols and profile represents [H_2S]; and blue symbols and profile represents pH. The shown microelectrode microprofiles are from the meristematic region of the rhizome. Y=0 indicate the below-ground tissue surface. Error bars are ±SD. n = 3. Data modified from Brodersen et al. (2015b). Copyright 2015 John Wiley & Sons Ltd.

Anoxic, reduced sediment conditions have also been shown to induce development of below-ground tissue gas barriers owing to accumulation of suberin lamellae in the hypodermal tissue of seagrasses (Enstone et al. 2003; Armstrong and Armstrong, 2001; 2005). Adequate internal aeration is thus a key prerequisite for healthy seagrass communities, as the intra-plant O_2 status and thereby the below-ground tissue oxidation capacity to a large extent determines the resilience of the plants towards sediment-produced H_2S and environmental disturbance, such as nutrient loadings and dredging operations leading to markedly reduced light availability and O_2 conditions in the water-column (Brodersen et al. 2015a,b).

Apart from its protective function, ROL into the rhizosphere may also stimulate aerobic heterotrophic bacteria leading to increased local remineralisation and mobilization of nutrients of potential benefit to the seagrasses (Blaabjerg et al. 1998; Hansen et al. 2000; Nielsen et al. 2001) (see also chapter 17). Nutrient mobilization may also happen through a change in the rhizosphere pH as a result of ROL. Brodersen et al. (2015b) showed that the pH micro-environment around the below-ground tissue was affected by ROL with pH decreasing by 1-2 pH units inside the oxic microshield relative to the surrounding buffered, artificial sediment (Fig. 9.10). This drop in pH is likely a result of the release of protons (H^+) from re-oxidation of H_2S, and this mechanism has been proposed to be of significance for the mobilization of phosphate in carbonate-rich sediments (Fourqurean and Zieman, 2002; Holmer et al. 2006; Brodersen et al. 2015b).

Rhizosphere pH heterogeneity and pH-mediated sulphide detoxification

While seagrass O_2 dynamics has been investigated in several studies, much less is known about spatio-temporal pH dynamics in the seagrass rhizosphere. By means of novel nanoparticle-based optical pH imaging, Brodersen et al. (2016) recently documented pronounced spatio-temporal pH heterogeneity and microdynamics in the immediate rhizosphere of the seagrass *Z. marina* L. Imaging of the sediment pH distributions in 2D revealed several distinct micro-niches of low and high pH within the seagrass rhizosphere as compared to the bulk sediment pH (Fig. 9.12). Light exposure of the canopy and an experimental temperature increase from 16 to 24°C, i.e., to the temperature optimum for

oxygenic photosynthesis in summer acclimated *Z. marina* L. plants (Staehr and Borum, 2011), lead to elevated pH levels in the seagrass rhizosphere with rhizome/root surface pH increasing by up to 0.9 pH units relative to the sediment pH. This photosynthesis/temperature-dependent pH effect may be due to: i) secretion of allelochemicals like amines by the plant, ii) CO_2 uptake by the below-ground tissue changing the carbonate equilibrium in the rhizosphere (Colmer, 2003; A.W.D. Larkum unpublished data), and/or iii) enhanced root/rhizome exudates stimulating sulphate reducing bacteria in the rhizoplane consuming protons through their microbial metabolism (Pollard and Moriarty, 1991). Previous studies have shown an increase in sulphate reduction rates (SRR) within seagrass-vegetated sediment and on the below-ground tissue surface of seagrass during photosynthesis, and such stimulation of SRR was attributed to increased exudation of carbohydrates and amino acids (Isaksen and Finster, 1996; Moriarty et al. 1986; Blaabjerg et al. 1998; Hansen et al. 2000; Nielsen et al. 2001). The dissolved organic carbon (DOC) exudation from the seagrass rhizome and roots has been estimated to account for 0.7-18 % of the total carbon fixed via photosynthesis (e.g. Wetzel and Penhale, 1979; Moriarty et al. 1986; Blaabjerg et al. 1998; Hansen et al. 2000).

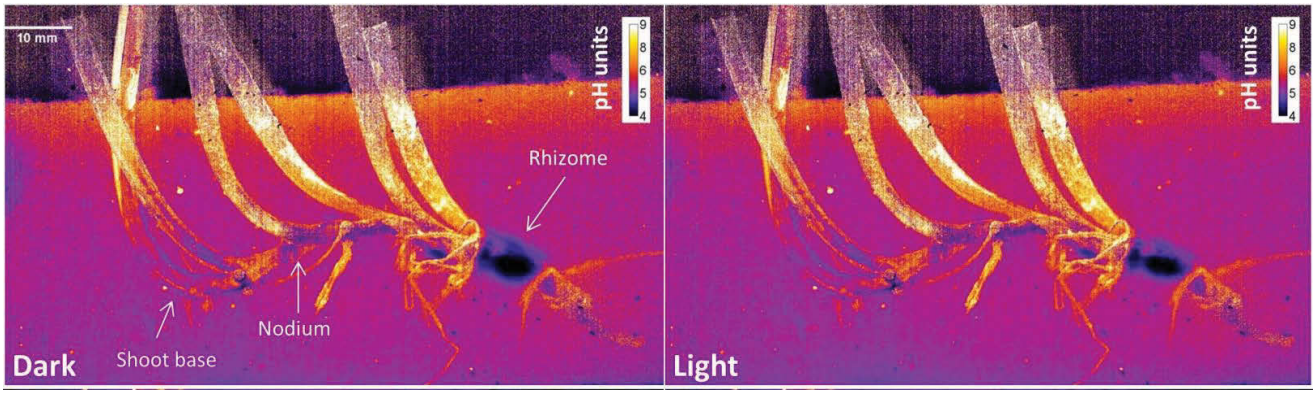

Figure 9.12. pH heterogeneity and dynamics in the seagrass rhizosphere determined via novel optical nanoparticle-based pH sensors during a light/dark transition (incident irradiance of 500 µmol photons m^{-2} s^{-1}). Colour coded pH image; Legend depicts the pH units. *Left panel* represents measurements in darkness; *right panel* represents measurements in light. The colour coded pH images are the average of three measurements. Data modified from Brodersen et al. (2016). Copyright 2015 John Wiley & Sons Ltd.

The chemical speciation of sulphide is pH-dependent, where H_2S predominates at pore-water pH <7 and HS^- ions at pH >7. A plant-induced increase in rhizosphere pH can thus shift the chemical speciation towards the non-tissue-permeable HS^- ion, thereby reducing H_2S exposure of the below-ground tissues (Brodersen et al. 2015b; Brodersen et al. 2016). Brodersen and co-workers (2015b; 2016) showed that regions of the rhizosphere with low pH (down to pH 4) correlated with the presence of plant-mediated oxic microniches (Fig. 9.11 and 9.12), while the tissue surface pH generally was higher than in the bulk sediment. A pH drop within the oxic microshield of the rhizosphere, as a result of the formation of sulphuric acid (i.e. $2O_2 + H_2S \rightarrow 2H^+ + SO_4^{2-}$), could potentially lead to dissolution of carbonates and a concomitant release of sediment-bound phosphorus (Fourqurean and Zieman, 2002; Holmer et al. 2006; Lambers et al. 2009), which would then become available for plant assimilation. However, the exact mechanisms and significance of such a nutrient mobilisation mechanism of seagrasses remain to be demonstrated.

An overview of the effect of plant activity on the rhizosphere pH microenvironment at plant/sediment- and oxic/anoxic interfaces is given in Figure 9.13. Interestingly, at or close to selected root/shoot junctions (Fig. 9.13c, e) either a pronounced decrease in pH towards the tissue surface was observed (Fig. 9.13e), indicating chemical re-oxidation of H_2S via ROL and thereby sediment detoxification in these regions, or an increase in pH towards the approximate oxic/anoxic interface, followed by a rapid decrease in pH towards and on the below-ground tissue surface (Fig. 9.13c). The latter is indicative of proton consuming processes, such as sulphate reduction, at the oxic/anoxic interface followed by chemical re-oxidation of H_2S at the plant/sediment interface (Brodersen et al. 2016). High sediment SRR may lead to a sulphide-induced release of sediment-bound phosphor, from the reduction of Fe(III)oxyhydroxides to Fe(II), as this results in the release of previously sequestered phosphate into the surrounding pore-water (Pollard and Moriarty, 1991; Pagès et al. 2011; Pagès et al. 2012). It is therefore intriguing to speculate that a mutual beneficial relationship may exist between the plant hosts and sulphate reducing bacteria based on a reciprocal exchange of nutrients.

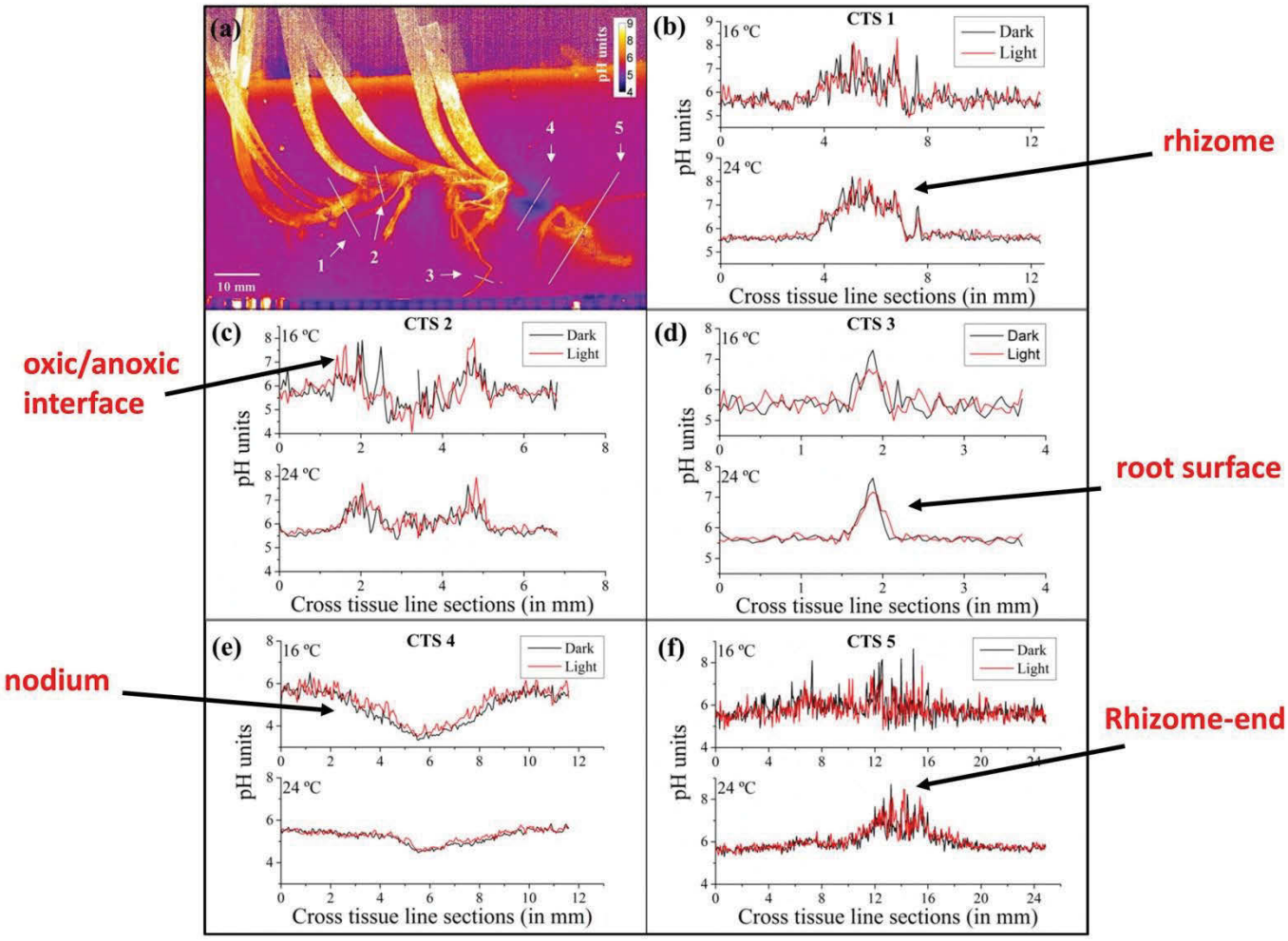

Figure 9.13. pH microdynamics in the seagrass rhizosphere at plant/sediment- and oxic/anoxic interfaces measured via novel optical nanoparticle-based pH sensors during light/dark transitions and at temperatures of 16°C and 24°C (where 24°C represents the temperature optimum for oxygenic photosynthesis in *Zostera marina* L.). (a) Colour coded pH image visualising the extracted cross tissue line profiles in the seagrass rhizosphere. (b-f) Cross tissue line section 1-5 as shown in panel a, determining pH microdynamics at plant/sediment- and oxic/anoxic interfaces. Data modified from Brodersen et al. (2016). Copyright 2015 John Wiley & Sons Ltd.

Thus there is first experimental evidence that seagrasses can modulate their rhizosphere pH microenvironment. Such changes in pH potentially present an important additional chemical defence mechanism, whereby seagrass plants can further alleviate H_2S toxicity by shifting the sulphide speciation towards non-tissue-permeable HS^- ions.

Effects of anthropogenic impacts on seagrass habitats and the rhizosphere microenvironment

Human activity in coastal marine areas such as boating activities, coastal and harbour development, dredging-induced sediment re-suspension and nutrient loadings, can have profound and adverse effects on the health of adjacent seagrass meadows (Erftemeijer and Lewis, 2006; Orth et al. 2006; Waycott et al. 2009). In fact, seagrass meadows are declining worldwide at a rate of ~7% p.a. (Waycott et al. 2009). This is often a result of synergetic negative impacts/effects on the surrounding environment and thereby the plants performance, such as i) lower light availabilities in the water-column caused by, for example, nutrient-driven algal blooms and/or increased water turbidity from anthropogenic-induced land run-off, adversely regulating rates of leaf photosynthesis during day-time (e.g. Dennison, 1987; Short & Burdick, 1995; Erftemeijer and Lewis, 2006), ii) enhanced water-column respiration rates during night-time, reducing the water-column O_2 conditions and thus the passive O_2 influx into the aerenchyma (e.g. Borum et al. 2006), iii) impeded gas exchange with the surrounding water, owing to, for example, nutrient-driven enhanced leaf epiphyte growth further reducing the passive O_2 in-/efflux and the leaves CO_2 uptake thereby potentially leading to inadequate internal aeration and photorespiration (e.g. Maberly, 2014; Brodersen et al. 2015a), as well as iv) high sediment H_2S concentrations, as a response to high sediment SRR fuelled by nutrient inputs, leading to enhanced rhizosphere O_2 demands and sediment toxicity (Borum et al. 2005). Enhanced seagrass mortality has thus often been linked to low light availability (e.g. Kim et al. 2015; York et al. 2015) and low night-time water-column O_2 conditions (Greve et al. 2003; Pedersen et al. 2004; Borum et al. 2005; Brodersen et al. 2015b) coupled with high sediment O_2 demands and H_2S production/concentrations (e.g. Carlson et al. 1994; Borum et al. 2005). These factors can strongly reduce the intra-plant O_2 status owing to a reduction in the O_2 source and/or an increase in the O_2 sink, as the plant-derived rhizosphere oxic microshields, described above, generally ensures protection against phytotoxic H_2S intrusion (Brodersen et al. 2015b). These effects highlight the importance of minimizing environmental disturbance activities in close proximity to seagrass meadows, and pose a challenge for making the increasing exploration of natural resources, e.g. causing increased harbour developments in Australia, environmentally sustainable.

Conclusions

The aerenchyma system of seagrasses ensures aeration of the shoots, rhizomes, roots and, in many cases, the rhizosphere. The shoot and shoot-base manifold are important aspects of this aeration system and have to be understood to fully understand the aeration of the roots and rhizomes. In particular the shoot-base manifold seems to ensure that O_2 is supplied to the young leaf meristem, and this may be particularly important when H_2S penetrates the roots and rhizomes. However, perhaps the major conclusion in this chapter is that seagrasses can actively alter their rhizosphere microenvironment via release of O_2 and allelochemicals into the sediment surrounding their below-ground tissue. This exudation provides a chemical defence mechanism, whereby seagrasses can detoxify their immediate rhizosphere through i) chemical oxidation of sediment-derived H_2S via plant-released O_2, or ii) shifting the chemical sulphide speciation towards non-tissue-permeable and thus non-phytotoxic HS^- ions by local increase of the rhizosphere pH (Fig. 9.14). Radial O_2 loss mainly occurs at the meristematic regions of the rhizome and roots forming oxygenated microzones around the most essential and vulnerable parts of the plants in the otherwise reduced, anoxic sediment environment. The capacity of seagrass below-ground tissue to oxidize the rhizosphere is predominantly regulated by light availability during day-time and by water-column O_2 levels during night-time. Overnight water-column hypoxia may lead to inadequate internal aeration of the seagrass, which in turn may result in sulphide intrusion and thereby increased seagrass mortality owing to chemical asphyxiation. Seagrass plants are thus most vulnerable to phytotoxin intrusion at night-time, where O_2 supply to the below-ground tissue to sustain aerobic metabolism and maintain protective oxic microniches in the immediate rhizosphere is completely dependent on passive diffusion of O_2 from the surrounding water-column into the aerenchymal tissue of the leaves. The most important structural adaptation of seagrasses to life in sulphidic sediment habitats is therefore, most likely, the formation of suberin tissue barriers to ROL, where the low cross tissue gas permeability ensures efficient transport of O_2 to distal parts of the plants and at the same time impedes H_2S intrusion.

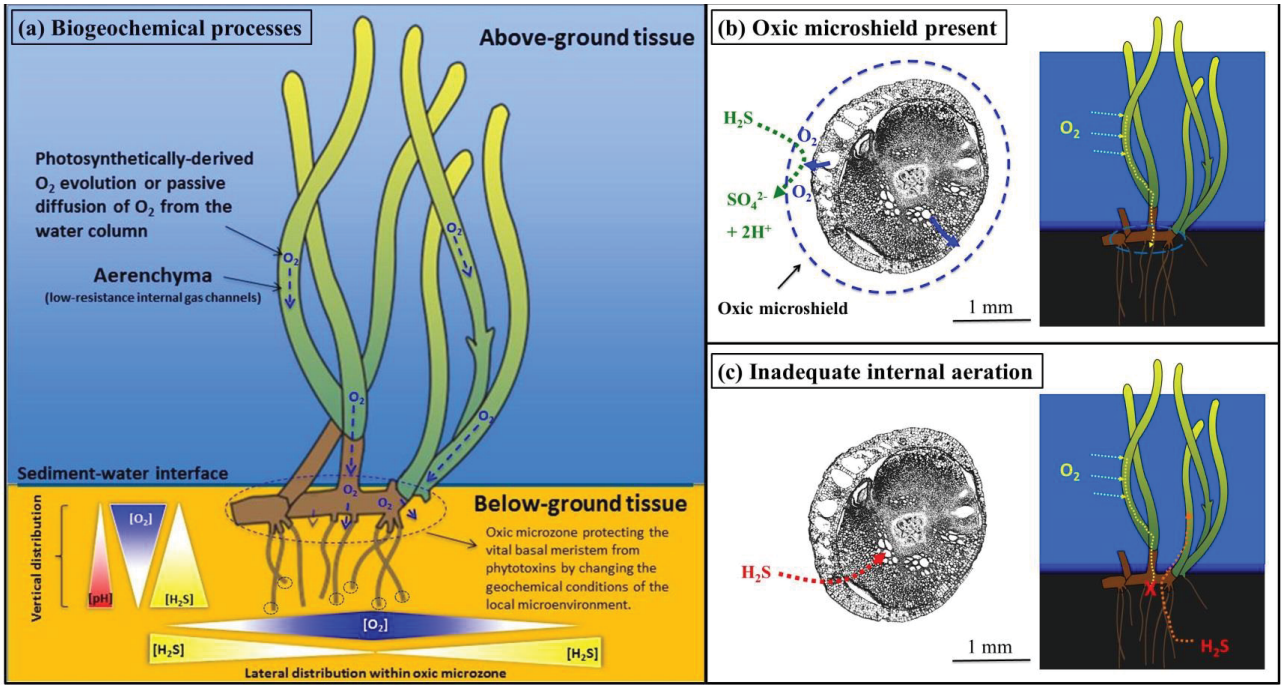

Figure 9.14. Conceptual diagram visualising seagrass-derived sediment detoxification. (a) O_2 transported down to the below-ground tissue via the aerenchyma is released from the meristematic region of the rhizome (basal leaf meristem), the rhizome and from root apical meristems into the immediate rhizosphere. Radial O_2 loss from the below-ground tissue maintaining protective oxic microniches in the immediate rhizosphere, and plant-derived sediment pH changes, chemically detoxifies the surrounding sediment by re-oxidizing sediment-produced H_2S and shifting the geochemical sulphide speciation towards non-tissue-permeable HS^- ions, respectively. (b) Oxic microshield protecting the vulnerable basal leaf meristem. O_2 released from the below-ground tissue drives chemical re-oxidation of sediment-produced H_2S within the oxic microniches. (c) Inadequate internal aeration may lead to H_2S intrusion which in turn may kill the plants as a result of chemical asphyxiation. Data modified from Brodersen et al. (2015b). Copyright 2015 John Wiley & Sons Ltd.

Plant-mediated low pH hotspots in the rhizosphere may lead to a concomitant release of sediment-bound phosphorus, which is often the limiting nutrient in carbonate-rich sediments. Modification of rhizosphere pH may thus be important for nutrient mobilization allowing seagrasses to grow in nutrient-limited marine environments. The relatively higher pH levels on below-ground tissue surfaces also indicate secretion of allelochemicals and/or plant-derived stimulation of proton consuming microbial metabolisms, such as sulphate reduction. However, such mechanisms remain speculative and call for direct experimental confirmation.

The chemical defence systems of seagrasses, described in this chapter, are of great importance for the plants. They ensure protection against sediment-produced phytotoxins and provide oxygenated microniches for the growing seagrass roots. Overnight water-column hypoxia and DBL-impeded O_2 transport/evolution in the leaves may result in the degradation of the below-ground oxic microshields and H_2S exposure of the below-ground tissue surface. Anthropogenic-induced environmental disturbances causing O_2 depletion in coastal marine environments thus represents a major threat to seagrass meadows, as low intra-plant O_2 conditions during night-time is a key factor causing events of seagrass die-backs.

REFERENCES

Armstrong W. (1979). Aeration in higher plants. In *Advances in Botanical Research*, **7**, pp. 225-332. Academic Press, London.

Armstrong J, Armstrong W. (2001). Rice and *Phragmites*: effects of organic acids on growth, root permeability, and radial oxygen loss to the rhizosphere. *American Journal of Botany* **88**: 1359-1370.

Armstrong J, Armstrong W. (2005). Rice: Sulfide-induced Barriers to Root Radial Oxygen Loss, Fe^{2+} and Water Uptake, and Lateral Root Emergence. *Annals of Botany* **96**(4): 625-638.

Badger MR, Price GD. (1994). The role of carbonic anhydrase in photosynthesis. *Annu Rev Plant Physiol Plant Mol Biol.* **45**: 369-392.

Barnabas AD. (1996). Casparian band-like structures in the root hypodermis of some aquatic angiosperms. *Aquatic Botany* **55**: 217-225.

Beer S, Björk M, Hellblom F, Axelson L. (2002). Inorganic carbon utilization in marine angiosperms (seagrasses). *Funct. Plant Biol.* **29**: 349-454.

Binzer T, Borum J, Pedersen O. (2005). Flow velocity affects internal oxygen conditions in the seagrass *Cymodocea nodosa*. *Aquatic Botany* **83**: 239-247.

Bodensteiner LE. (2006). The impact of light availability on benthic oxygen release by the seagrasses *Thalassia testudinum* (Banks ex König) and *Zostera marina*. MS thesis, San Jose State Univ.

Borum J, Pedersen O, Greve TM, Frankovich TA, Zieman JC, Fourqurean JW, Madden CJ. (2005). The potential role of plant oxygen and sulphide dynamics in die-off events of the tropical seagrass, *Thalassia testudinum*. *Journal of Ecology* **93**: 148-158.

Borum J, Pedersen O, Kotula L, Fraser MW, Statton J Colmer TD, Kendrick GA. (2015). Photosynthetic response to globally increasing CO_2 of co-occurring temperate seagrass species. *Plant, Cell & Environment*. doi:10.1111/pce.12658.

Borum J, Sand-Jensen K, Binzer T, Pedersen O, Greve T. (2006). Oxygen movement in seagrasses. In: Larkum AWD, Orth JR & Duarte CM, Eds., *Seagrasses: Biology, Ecology and Conservation,* Dordrecht, The Netherlands: Springer, Berlin: 255-270.

Brodersen KE, Koren K, Lichtenberg M, Kühl M. (2016). Nanoparticle-based measurements of pH and O_2 dynamics in the rhizosphere of *Zostera marina* L.: Effects of temperature elevation and light/dark transitions. *Plant, Cell & Environment*. (accepted on March 22, 2016)

Brodersen KE, Lichtenberg M, Paz LC, Kühl M. (2015a). Epiphyte-cover on seagrass (*Zostera marina* L.) leaves impedes plant performance and radial O_2 loss from the below-ground tissue. *Frontiers in Marine Science* **2**: 58. doi: 10.3389/fmars.2015.00058.

Brodersen KE, Nielsen DA, Ralph PJ, Kühl M. (2014). A split flow chamber with artificial sediment to examine the below-ground microenvironment of aquatic macrophytes. *Marine Biology* **161**(12): 2921-2930. Doi: 10.1007/s00227-014-2542-3.

Brodersen KE, Nielsen DA, Ralph PJ, Kühl M. (2015b). Oxic microshield and local pH enhancement protects *Zostera muelleri* from sediment derived hydrogen sulphide. *New Phytologist* **205** (3): 1264-1276. DOI: 10.1111/nph.13124.

Blaabjerg V, Mouritsen KN, Finster K. (1998). Diel cycles of sulphate reduction rates in sediments of a *Zostera marina* bed (Denmark). *Aquatic Microbial Ecology* **15**(1): 97-102.

Carlson Jr P.R., Yarbro L.A. & Barber T.R. (1994). Relationship of sediment sulfide to mortality of *Thalassia testudinum* in Florida Bay. *Bulletin of Marine Science* **54**: 733-746.

Colmer T.D. (2003). Long-distance transport of gases in plants: a perspective on internal aeration and radial oxygen loss from roots. *Plant, Cell & Environment* **26**: 17-36.

Connell E.L., Colmer T.D. & Walker D.I. (1999). Radial oxygen loss from intact roots of *Halophila ovalis* as a function of distance behind the root tip and shoot illumination. *Aquatic Botany* **63**: 219-228.

Dennison WC. (1987). Effects of light on seagrass photosynthesis, growth and depth distribution. *Aquatic Botany* **27**(1): 15-26.

Drake LA, Dobbs FC, Zimmerman RC. (2003). Effects of epiphyte load on optical properties and photosynthetic potential of the seagrasses *Thalassia testudinum* Banks ex König and *Zostera marina* L. *Limnology and Oceanography* **48**(1, part 2): 456-463.

Enstone DE, Peterson CA, Ma F. (2003). Root endodermis and exodermis: structure, function, and responses to the environment. *Journal of Plant Growth Regulation* **21**: 335-351.

Erftemeijer PLA, Lewis RRR. (2006). Environmental impacts of dredging on seagrasses: a review. *Marine Pollution Bulletin* **52**(12): 1553-1572.

Fourqurean JW, Zieman JC. (2002). Nutrient content of the seagrass Thalassia testudinum reveals regional patterns of relative availability of nitrogen and phosphorus in the Florida Keys USA. *Biogeochemistry* **61**(3): 229-245.

Frederiksen MS, Glud RN. (2006). Oxygen dynamics in the rhizosphere of *Zostera marina*: A two-dimensional planar optode study. *Limnol. Oceanogr* **51**(2): 1072-1083.

Golicz AA, Schliep M, Lee HT, Larkum AWD, Dolferus R, et al. (2015). Genome-wide survey of the seagrass *Zostera muelleri* suggests modification of the ethylene signalling network.

Journal of Experimental Botany **66**: 1489-1498.

Greve TM, Borum J, Pedersen O. (2003). Meristematic oxygen variability in eelgrass (*Zostera marina*). *Limnology and Oceanography* **48**(1): 210-216.

Hansen JW, Udy JW, Perry CJ, Dennison WC, Lomstein BA. (2000). Effect of the seagrass *Zostera capricorni* on sediment microbial processes. *Marine Ecology Progress Series* **199**: 83-96.

Hasler-Sheetal H, Holmer M. (2015). Sulfide Intrusion and Detoxification in the Seagrass *Zostera marina*. *PloS one* **10**(6): e0129136.

Holmer M, Hasler-Sheetal H. (2014). Sulfide intrusion in seagrasses assessed by stable sulfur isotopes—a synthesis of current results. *Frontiers in Marine Science* **1**: 64.

Holmer M, Pedersen O, Ikejima K. (2006). Sulfur cycling and sulfide intrusion in mixed Southeast Asian tropical seagrass meadows. *Botanica Marina* **49**: 91-102.

Hurd CL. (2000). Water motion, marine macroalgal physiology, and production. *Journal of Phycology* **36**(3): 453-472.

Isaksen MF, Finster K. (1996). Sulphate reduction in the root zone of the seagrass *Zostera noltii* on the intertidal flats of a coastal lagoon (Arcachon, France). *Marine Ecology Progress Series* **137**(1): 187-194.

Jassby AD, Platt T. (1976). Mathematical formulation of the relationship between photosynthesis and light for phytoplankton. *Limnology and Oceanography* **21**: 540-547.

Jensen SI, Kühl M, Glud RN, Jorgensen LB, Prieme A. (2005). Oxic microzones and radial oxygen loss from roots of *Zostera marina*. *Marine Ecology Progress Series* **293**: 49-58.

Jørgensen BB. (1982). Mineralization of organic matter in the sea bed - the role of sulfate reduction. *Nature* **296**: 643-645.

Jørgensen BB, Des Marais DJ. (1990). The diffusive boundary layer of sediments: Oxygen microgradients over a microbial mat. *Limnology and Oceanography* **35**(6): 1343-1355.

Jørgensen BB, Revsbech NP. (1985). Diffusive Boundary Layers and the Oxygen Uptake of Sediments and Detritus. *Limnology and Oceanography* **30**(1): 111-122.

Kim YK, Kim SH, Lee K-S. (2015). Seasonal Growth Responses of the Seagrass *Zostera marina* under Severely Diminished Light Conditions. *Estuaries and Coasts* **38**: 558-568.

Koren K, Brodersen KE, Jakobsen SL, Kühl M. (**2015).** Optical sensor nanoparticles in artificial sediments – a new tool to visualize O_2 dynamics around the rhizome and roots of seagrasses. *Environmental Science and Technology* **49** (4): 2286-2292. DOI: 10.1021/es505734b

Kühl M, Revsbech NP. (2001). Biogeochemical microsensors for boundary layer studies. In: Boudreau BP, Jørgensen BB eds. *The benthic boundary layer*. New York: Oxford University Press, New York, 180-210.

Lambers H, Mougel C, Jaillard B, Hinsinger P. (2009). Plant-microbe-soil interactions in the rhizosphere: an evolutionary perspective. *Plant and Soil* **321**: 83-115.

Lamers LP, Govers LL, Janssen IC, Geurts JJ, Van der Welle ME, Van Katwijk MM, Van der Heide T, Roelofs JG, Smolders AJ. (2013). Sulfide as a soil phytotoxin—a review. *Frontiers in plant science* **4**: 268. doi: 10.3389/fpls.2013.00268.

Larkum AWD, McComb AJ, Shepherd SA. (1989). *Biology of seagrass*. Amsterdam: Elsevier, Amsterdam.

Larkum AWD, Orth RJ, Duarte CM. (2006). *Seagrasses: Biology, Ecology and Conservation*. Printed in Dordrecht, The Netherlands: Springer, Berlin.

Larkum AWD, Drew EA, Ralph PJ. (2006b). Photosynthesis and metabolism at the cellular level. In: Larkum AWD, Orth RJ, Duarte, CM, Eds. *Seagrasses: Biology, Ecology and Conservation*. Springer Verlag, Berlin.

Maberly SC. (2014). The fitness of the environments of air and water for photosynthesis, growth, reproduction and dispersal of photoautotrophs: An evolutionary and biogeochemical perspective. *Aquatic Botany* **118**: 4-13.

Madsen JD, Chambers PA, James WF, Koch EW, Westlake DF. (2001). The interaction between water movement, sediment dynamics and submersed macrophytes. *Hydrobiologia* **444**(1-3): 71-84.

Moriarty DJW, Iverson RL, Pollard PC. (1986). Exudation of organic carbon by the seagrass *Halodule wrightii* Aschers. and its effect on bacterial growth in the sediment. *Journal of Experimental Marine Biology and Ecology* **96**(2): 115-126.

Nielsen LB, Finster K, Welsh DT, Donelly A, Herbert RA, De Wit R, Lomstein BA. (2001). Sulphate reduction and nitrogen fixation rates associated with roots, rhizomes and sediments from *Zostera noltii* and *Spartina maritima* meadows. *Environmental Microbiology* **3**(1): 63-71.

Nobel PS. (1983). 'Biophysical Plant Physiology and Ecology'. W. H. Freeman and Co., San Francisco, 608 pp.

Nobel PS. (1990). Physicochemical and Environmental Plant Physiology. Academic Press. San Diego, USA.

Orth RJ, Carruthers TJB, Dennison WC, Duarte CM, Fourqurean JW, Heck Jr. KL, Hughes AR, Kendrick GA, Kenworthy WJ, Olyarnik S, et al. (2006). A global crisis for seagrass ecosystems. *BioScience* **56**(12): 987-996.

Pagès A, Teasdale PR, Robertson D, Bennett WW, Schäfer J, Welsh DT. 2011. Representative measurement of two-dimensional reactive phosphate distributions and co-distributed iron(II) and sulfide in seagrass sediment porewaters. *Chemosphere* **85**(8): 1256-1261.

Pagès A, Welsh DT, Robertson D, Panther JG, Schäfer J, Tomlinson RB, Teasdale PR. 2012. Diurnal shifts in co-distributions of sulfide and iron(II) and profiles of phosphate and ammonium in the rhizosphere of *Zostera capricorni*. *Estuarine, Coastal and Shelf Science* **115**: 282-290.

Pedersen O, Binzer T, Borum J. (2004). Sulphide intrusion in eelgrass (*Zostera marina* L.). *Plant, Cell and Environment* **27**: 595-602.

Pedersen O, Borum J, Duarte CM, Fortes MD. (1998). Oxygen dynamics in the rhizosphere of *Cymodocea rotundata*. *Marine Ecology Progress Series* **169**: 283-288.

Pedersen O, Borum J, Duarte CM, Fortes MD. (1999). ERRATUM: Oxygen dynamics in the rhizosphere of *Cymodocea rotundata*. *Marine Ecology Progress Series* **178**: 310.

Pollard PC, Moriarty DJW. (1991). Organic carbon decomposition, primary and bacterial productivity, and sulphate reduction, in tropical seagrass beds of the Gulf of Carpentaria, Australia. *Marine Ecology Progress Series* **69**(1): 149-159.

Raven JA. (1977). The evolution of vascular land plants in relation to supracellular transport processes. *Adv. Bot. Res.* **5**: 153-219.

Sand-Jensen K., Pedersen O., Binzer T. & Borum J. (2005). Contrasting oxygen dynamics in the freshwater isoetid *Lobelia dortmanna* and the marine seagrass *Zostera marina*. *Annals of Botany* **96**: 613-623.

Short FT, Burdick DM. (1995). Mesocosm experiments quantify the effects of eutrophication on eelgrass, *Zostera marina*. *Limnology and Oceanography* **40**: 740-749.

Short FT, Duarte CM. (2001). Methods for the measurement of seagrass growth and production. In: Short FT, Coles RG, Eds, *Global Seagrass Research Methods,* Elsevier, Amsterdam: 155-182.

Staehr P, Borum J. (2011). Seasonal acclimation in metabolism reduces light requirements of eelgrass (*Zostera marina*). *Journal of Experimental Marine Biology and Ecology* **407**(2): 139-146.

Van den Honert TH. (1948). Water transport in plants as a catenary process. *Discuss. Faraday Soc.* **3**: 146-153.

Ward LG, Kemp WM, Boynton WR. (1984). The influence of waves and seagrass communities on suspended particulates in an estuarine embayment. *Marine Geology* **59**(1):

85-103.

Waycott M, Duarte CM, Carruthers TJB, Orth RJ, Dennison WC, Olyarnik S, Calladine A, Fourqurean JW, Heck Jr. KL, Hughes AR, et al. (2009). Accelerating loss of seagrasses across the globe threatens coastal ecosystems. *PNAS* **106**: 12377–12381.

Wetzel RG, Penhale PA. (1979). Transport of carbon and excretion of dissolved organic carbon by leaves and roots/rhizomes in seagrasses and their epiphytes. *Aquatic Botany* **6**:149-158.

York PH, Carter AB, Chartrand K, Sankey T, Wells L, Rasheed MA. (2015). Dynamics of a deep-water seagrass population on the Great Barrier Reef: annual occurrence and response to a major dredging program. *Scientific reports* **5**: 13167.

Zimmerman RC, Alberte RS. (1996). Effect of light/dark transition on carbon translocation in eelgrass *Zostera marina* seedlings. *Marine Ecology Progress Series* **136**: 305-309.

GENERAL DISCUSSION

The seagrass rhizosphere: a mosaic of chemical microgradients that controls biogeochemical processes at the plant/sediment interface

GENERAL DISCUSSION

Key findings

The overall aim of the research presented in this PhD thesis was to extend our knowledge on the complex seagrass rhizosphere, with special attention on potential seagrass-driven rhizospheric sediment detoxification and nutrient mobilization processes. We investigated the dynamics of the below-ground biogeochemical microenvironment of seagrasses through a wide range of novel chemical imaging techniques and developed methodologies to better understand how seagrasses interact with and directly influence their surrounding environment. This work resulted in 9 manuscripts, most of which have already been published in high-rank scientific journals. From the following major findings, the work presented in this thesis has advanced our knowledge of how seagrasses can alter their below-ground biogeochemical microenvironment to improve their own fitness and health in changing oceans:

(i) Radial O_2 loss (ROL) from the below-ground tissue, especially from the root/shoot junctions and the root apical meristems, leads to oxidized below-ground environments that protect seagrasses against reduced phytotoxic compounds, such as hydrogen sulphide (H_2S) produced in the adjacent anoxic sediment (*Chapters 1, 2, 5 & 7*). Our results suggests, that chemical re-oxidation of phytotoxic H_2S with plant-released O_2 is the most important sediment detoxification process within the seagrass rhizosphere (*Chapter 5*). However, this may depend on the seagrass species and needs to be confirmed within natural sediments. During night time, ROL and sediment oxidation is purely driven by the water-column O_2 content, and hypoxic water-column conditions therefore vastly impedes ROL and weakens the rhizospheric oxic microshields; in turn rendering the seagrass more susceptible to H_2S intrusion (*Chapters 2, 3 & 9*).

(ii) Sediment re-suspension, leaf epiphyte overgrowth and/or leaf silt/clay covers have the potential to profoundly reduce the fitness of seagrass meadows, mainly as a result of reduced light availability/quality and by increasing the diffusive boundary layer thickness at the leaf surface, thereby impeding mass transfer across the leaf tissue. Such conditions may subsequently lead to severe seagrass die-backs, especially if combined with other environmental stressors such as high sediment O_2 demands (*Chapters 6 & 8*).

(iii) Seagrass-derived rhizospheric pH microheterogeneity may provide an additional chemical defence mechanism towards sediment-produced H_2S, as plant-mediated microniches of high rhizosphere pH leads to a shift in the chemical sulphide speciation towards tissue impermeable, and consequently non-phytotoxic, HS^- ions (*Chapters 2 & 4*). However, most seagrass-driven pH changes in the rhizosphere are caused by the spontaneous chemical reaction between H_2S and O_2 that produces sulphuric acid and thus reduces the rhizosphere pH, evidenced by a strong co-localisation between seagrass-generated rhizospheric oxic microzones and low-pH microniches (*Chapter 4*). Plant-derived rhizospheric low-pH microenvironments may be crucial for seagrasses colonizing carbonate-rich sediments in oligotrophic, tropical waters, where the high phosphate fixation capacity of calcium carbonates often leads to severe phosphorus-limitation (Short et al. 1990; Fourqurean et al. 1992; Jensen et al. 1998; Nielsen et al. 2007). The seagrass-mediated low-pH microniches results in carbonate dissolution, releasing the sediment-sequestered phosphate to the pore-water (*Chapter 7*).

(iv) Other important nutrients essential for seagrass growth and performance, such as nitrogen (NO_3^-, NH_3), may be largely facilitated by root-associated, diazotrophic (N_2-fixing) microorganisms such as some types of *Clostridia* (*Chapter 5*). *Clostridia* were found to be highly abundant and possibly selected for by the chemical conditions around the seagrass root apical meristems (*Chapter 5*), which are known to secrete dissolved organic carbon (DOC) and stimulate microbial activity (Moriarty et al. 1986; Pollard & Moriarty, 1991; Blaabjerg et al. 1998; Hansen et al. 2000; Nielsen et al. 2001; Badri & Vivanco, 2009).

Below, we provide detailed descriptions of each of the above-mentioned major findings, and discuss how the plants performance and the surrounding sediment characteristics were affected by changing environmental conditions. We conclude with a more general discussion of the future perspectives resulting out of my thesis work.

Intra-plant O_2 status and H_2S intrusion

The intra-plant O_2 status of seagrasses is known to be a complex and dynamic interaction between several O_2 sources and sinks, where the O_2 transport to the below-ground tissue is determined by the internal O_2 concentration gradient (Armstrong, 1979; Pedersen et al. 2004; Borum et al. 2006; Raun & Borum, 2013). However, little information exists on how the internal plant aeration is affected by changing environmental conditions such as sediment re-suspension, and thereby fluctuations in the water-column light availability and quality, in the field situation. In this thesis, we show that the internal meristematic O_2 concentration, determined at the basal leaf meristem of the common temperate seagrass species *Zostera muelleri* ssp*. capricorni* via microsensors *in situ*, is mainly driven by fluctuations in incident solar irradiance (*Chapters 8 & 9*). In the light, pronounced photosynthetically-derived internal O_2 evolution was observed at sunrise, resulting in an up to 40-fold increase in the internal O_2 partial pressure (pO_2), most likely facilitated by the accumulation of CO_2 within the aerenchymal tissue during night-time (*Chapter 8*). In darkness, when photosynthesis ceases seagrasses are completely dependent on a passive O_2 influx into the leaves from the surrounding water-column (Greve et al. 2003; Pedersen et al. 2004; Borum et al. 2005). This was further supported by our findings of strong correlations between the water-column O_2 conditions and the internal plant aeration during night-time (*Chapters 8 & 9*).

Dredging-induced sediment re-suspension and eutrophication has been shown to lead to enhanced seagrass mortality (e.g. Erftemeijer & Lewis, 2006; York et al. 2015). However, little is known of the adverse effects of epiphyte- and silt/clay covers on seagrass leaves in terms of potential reduced below-ground tissue oxidation capacity owing to reduced photosynthesis, and even less is known about what causes phytotoxic H_2S intrusion in seagrasses. In this thesis, we show that deposition of fine sediment particles (<63 µm sediment fraction) and leaf epiphyte overgrowth on seagrass leaves affects the intra-plant O_2 status by strongly regulating the plants performance through synergetic negative effects on (i) the light availability and quality for photosynthesis, (ii) the solute transfer across the leaf tissue surface owing to thicker DBLs, and (iii) as a result of high night-time respirations rates of leaf-associated microorganisms (*Chapters 6 & 8*). Leaf epiphyte- /silt-clay covers thus results in simultaneous adverse effects on the intra-plant O_2 status, reducing the

below-ground tissue oxidation capacity and thus rendering smothered plants more susceptible to phytotoxic H_2S intrusion (*Chapters 6 & 8)*. Recent studies by Hasler-Sheetal and Holmer (2014 & 2015) have shown that H_2S detoxification can also occur inside the plants as long as O_2 is present in the below-ground aerenchymal tissue. However, unfavourable environmental conditions, such as during water-column hypoxia at night-time (Pedersen et al. 2004; Borum et al. 2005) or caused by leaf silt/clay covers (*Chapter 8*), may result in inadequate internal tissue aeration, thus allowing intruding H_2S to freely diffuse to the vulnerable basal leaf meristem (Pedersen et al. 1998, 2004). It has recently been shown that H_2S in the below-ground tissue induce the production of reactive O_2 species (ROS), which eventually kills the basal leaf meristem and ultimately the whole plant (Pulido Pérez & Borum, 2010). Microbial-mediated oxidation of sulphide could be an efficient mean to remove intruded sulphide in seagrass, however, our *in situ* measurements revealed a degree of co-existence of H_2S and O_2 in the aerenchymal tissue (*Chapter 8*), which corroborate previous findings (Pedersen et al. 2004; Borum et al. 2005), and indicate negligible microbial-mediated aerenchymal H_2S re-oxidation. Generally rapid microbial H_2S re-oxidation would not allow for co-existence at such temporal extent (Jørgensen & Revsbech, 1983; Nelson et al. 1986). However, at sunrise, when active leaf photosynthesis supports steep internal O_2 concentration gradients and thus O_2 transport to below-ground tissues, over-night intruded H_2S is rapidly diminished within the aerenchyma as a result of chemical oxidation (*Chapter 8*), protecting the plants towards H_2S-induced suffocation.

Up until now, costal management of seagrass meadows has mainly focused on the effect of dredging and other activities on the water-column light availability over seagrass meadows. However, based on the evidence presented in chapter 6 and 8, we propose a widening of this perspective to include the consequences of enhanced silt/clay- and epiphyte covers on leaves, including: (i) increased thickness of leaf-insulating DBLs and (ii) competition with the epiphytic community for essential nutrients, CO_2 and O_2. These additional negative pressures may provide much longer lasting adverse effects on the health and performance of seagrass meadows in comparison to temporal light quality variation.

Seagrass-altered rhizospheric biogeochemistry

Oxic microshields and sediment detoxification

Seagrasses are known to release O_2 from the root-tips, especially from around the root apical meristem situated a few mm's behind the root-apex (e.g. Jensen et al. 2005; Frederiksen & Glud, 2006). Mature regions of roots generally possess barriers to ROL that vastly improve the effectivity of long-distance gas transport within the aerenchymal tissue of seagrasses (Barnabas, 1996; Colmer, 2003; Borum et al. 2006). Barriers to ROL seems to be of vital importance for seagrasses and the concomitantly enhanced internal tissue aeration may explain the immense success of seagrasses in coastal waters worldwide despite mainly colonizing strongly reduced, anoxic sediments (see e.g. Sand-Jensen et al. 2005; Jovanovic et al. 2015). However, it has often been indicated that ROL-generated rhizospheric oxic microzones may provide a below-ground chemical defence mechanism towards sediment-produced reduced phytotoxic compounds such as H_2S (e.g. Pedersen et al. 2004; Borum et al. 2005; Jensen et al. 2005; Borum et al. 2006). To explore this importance of ROL as protection against sediment toxicity, we developed a novel experimental approach applying a split flow-chamber wherein the seagrass plants were maintained in a de-oxygenated and reduced, artificial sediment matrix (*Chapter 1*). This allowed us to characterise the biogeochemical processes at the plant/sediment interface without continuously disturbing the geochemical conditions at the tissue surface (as performing microsensor measurements in natural sediment involves un-covering the roots from sediment when positioning the microsensors at the below-ground tissue surface) (*Chapters 1 & 2*). Using this technique we showed that seagrass-driven rhizospheric oxic microshields (i.e. a volume of sediment with an O_2 gradient reaching up to ~300 µm away from the tissue surface) can detoxify the surrounding sediment and thereby reduce the exposure of the below-ground biomass to phytotoxic H_2S (*Chapters 2 & 7*). The below-ground oxic microshields were most pronounced at the root/shoot junctions, including the basal leaf meristem with leaf sheath. This correlated with the areas in which we measured the highest rhizospheric H_2S re-oxidation rates (*Chapters 2, 5 & 7*), proving the efficiency of the oxic microshield in protecting the seagrass tissue. The below-ground tissue oxidation capacity was strongest in the light, with an up to ~3-fold increase in ROL at the root/shoot junction as compared to in darkness (*Chapters 2 & 5*). At the root-tips, light stimulation of

the leaf canopy resulted in an up to ~150-fold increase in ROL as compared to darkness (*Chapter 6*), albeit still >2 times lower than at the root/shoot junctions under equivalent incident photon irradiance. As such, the below-ground tissue ROL was clearly coupled to leaf photosynthesis, especially at the more distal parts of the plants (*Chapters 2, 5 & 6*), as also previously demonstrated for the internal plant tissue aeration (Greve et al. 2003; Pedersen et al. 2004; Borum et al. 2005; Borum et al. 2006). Seagrass below-ground tissue is residing within sediments characterised by high sulphate reduction rates and thus production of phytotoxic H_2S (Pollard & Moriarty, 1991; Isaksen & Finster, 1996: Blaabjerg et al. 1998; Blaabjerg & Finster, 1998; Hansen et al. 2000; Nielsen et al. 2001). As such the chemical defence mechanism of the below-ground tissue facilitates growth and survival within this hostile environment during non-stressful environmental conditions (*Chapters 2, 5 & 7*). However, during stressful environmental conditions, such as caused by over-night water-column hypoxia, the lower internal O_2 concentration results in diminished rhizospheric oxic microshields and thus increased exposure of the below-ground biomass to reduced phytotoxic compounds such as H_2S (*Chapters 2 & 3*). Inadequate internal aeration has previously been linked to severe H_2S intrusion and enhanced seagrass mortality (Plus et al. 2003; Pedersen et al. 2004; Borum et al. 2005). In this thesis, we show that epiphyte overgrowth on seagrass leaves also have adverse effects on ROL from the below-ground biomass and thus reduce the below-ground tissue oxidation capacity (*Chapter 6*). This was most pronounced in darkness where seagrasses with leaf epiphyte-covers lost their rhizospheric oxic microshields, initiating anaerobic metabolism in the below-ground tissue and thus rendering affected plants more vulnerable to chemical asphyxiation caused by H_2S intrusion (*Chapter 6*). We also show that ROL do not only occur from the root apical meristems (i.e. the root-tips) as previously assumed, but actually mainly from the root/shoot junctions, as well as from the rhizome (*Chapters 1-5, 7 & 9*). The O_2 distribution within the seagrass rhizosphere is thus much more prevalent than hitherto thought, which can explain the observed positive effects on the sediment redox potential, sulphide pools and microbial activity (Pollard & Moriarty, 1991; Nielsen et al. 2001; Holmer et al. 2006; Pagès et al. 2012) that all hardly could have been driven alone by the minor O_2 leakage from the small root apical meristems.

In summary, seagrass-derived rhizospheric oxic microzones thus serves as below-ground chemical microshields that oxidizes reduced phytotoxic compounds within the seagrass rhizosphere (mainly around the actively growing parts of the plants), and thereby greatly reduces the toxicity of the uppermost cm's of the anoxic sediment. The seagrass chemical defence mechanism is profoundly diminished during stressful environmental conditions such as water-column hypoxia and leaf epiphyte overgrowth, highlighting the importance of minimizing environmentally disturbing activities, such as dredging operations, nutrient loadings and coastal development, adjacent to these vital marine ecosystems.

Plant/microbe interactions

Seagrasses release dissolved organic carbon (DOC exudates) into the rhizosphere from their below-ground tissue (Moriarty, 1986; Pollard & Moriarty, 1991; Badri & Vivianco, 2009). Translocation of photosynthates to the below-ground biomass and subsequent secretion into the rhizosphere has been shown to enhance bacterial growth and productivity in the sediment (Pollard & Moriarty, 1991). This may benefit seagrasses in multiple ways, such as through bacterial-mediated H_2S re-oxidation. This oxidation process is much faster than the spontaneous chemical reaction between O_2 and H_2S (Jørgensen & Revsbech, 1983; Nelson et al. 1986) and thus rarely allows for appreciable co-localization between the two chemical species in the sediment. It is therefore intriguing to speculate on the existence of a symbiotic relationship between sulphide-oxidizing bacteria and seagrasses, such as previously suggested by Jensen et al. (2007). Given the potential importance of such relationship in the resilience of seagrasses to environmental perturbation, we applied our previously developed split flow-chamber system in combination with molecular techniques, including PCR sequencing and fluorescent staining; to investigate whether mutualistic relationships between seagrasses and their rhizosphere microbes exists. Combined with detailed microsensor measurements of O_2 and H_2S, we were able to probe the changes in the composition of the bacterial community in the rhizosphere as a result of the presence and activity of the seagrass host (*Chapter 5*). We found that plant-altered rhizospheric biogeochemistry controls the microbial community composition at the microscale level (*Chapter 5*). We detected a tendency towards enhanced relative mean abundance of

sulphide-oxidizing bacteria within seagrass-generated rhizospheric oxic microniches as compared to bulk sediment ($P>0.05$), with operational taxonomic units (OTUs) (i.e. clusters of similar 16S rRNA sequences) matching *Arcobacter* sp. and *Sulfurimonas* sp. (*Chapter 5*). However, comparisons of H_2S re-oxidation rates within a sterilized and microbe enriched environment, with ~34% of OTUs matching sulphide-oxidizing bacteria, showed no bacterial-mediated positive effects on sediment detoxification, thus indicating a weaker beneficial relationship between seagrasses and sulphide-oxidizing bacteria than previously anticipated (e.g. Jensen et al. 2007; Cúcio et al. 2016) (*Chapter 5*). Interestingly, around the root-tips we found significantly higher mean relative abundance (~57% of sequences; $p<0.05$) of the sulphate-reducing bacterial class *Clostridia*, with OTUs matching *Lachnospiraceae*. Many members of this class of bacteria are known to be capable of fixing nitrogen (diazotrophs), and these results therefore provide some support for the hypothesis of a mutual beneficial relationship between seagrasses and nitrogen fixing diazotrophs, where the seagrasses provides DOC to the diazotrophs in exchange for fixed nitrogen (e.g. Welsh, 2000; Devereux, 2005). Another way, in which seagrasses may benefit from boosting the microbial community, perhaps counterintuitively, is through the resulting increase in bacteria-mediated rhizospheric sulphide production that may lead to enhanced phosphorus solubilisation owing to H_2S reducing capacity through reductive Fe(III) dissolution, which is described in detail below (*Chapter 7*). In addition to changes to the sulphur cycling microbes, we also observed lower mean relative abundance of Bacteroidia within the plant-derived oxic microzone (~13% of sequences) compared to at the root apical meristems and within the bulk sediment (> 23% of sequences) albeit not significant ($p>0.05$; *Chapter 5*). The growth rate of *Bacteroidetes* is pH dependant (Thomas et al. 2011) and our results thus indicate that seagrass-derived reductions of rhizosphere pH (~2 pH units as compared to the bulk sediment) may impede growth of these potential plant pathogens (Thomas et al. 2011) (*Chapter 5*). The highly-motile *Spirochaetes* also seemed important rhizosphere colonizers (*Chapter 5*), which corresponds with results from previous studies showing that this bacterial class is often found in fluctuating chemical micro-gradients/interfaces (Berlanga et al. 2008).

As such, we have shown that seagrasses actively selects for a distinct microbial community composition at the plant/sediment interface, which may positively affect the nutrient

availability in the seagrass rhizosphere owing to enhanced nitrogen fixation by sulphate-reducing, diazotrophic bacteria such as *Lachnospiraceae* and *Desulfovibrio* sp. We therefore provide further evidence of a potential mutualistic beneficial relationship between seagrasses and rhizospheric, heterotrophic diazotrophs based on a mutual exchange of essential nutrients.

Rhizospheric pH microheterogeneity and nutrient mobilization

Seagrasses inhabiting carbonate-rich sediments e.g. in the Caribbean and around the Great Barrier Reef, Australia, are often phosphorus limited owing to the high phosphate fixation capacity of calcium carbonates (Short et al. 1990; Fourqurean et al. 1992; Jensen et al. 1998; Nielsen et al. 2007). Tropical seagrasses are thus generally challenged to mobilize nutrients such as phosphate and iron, around their below-ground tissues to accommodate growth in oligotrophic waters (e.g. Duarte et al. 1995). Dissolution of carbonates induced by seagrass-released organic acids has previously been suggested as a phosphorus mobilization mechanism in seagrass-vegetated carbonate rich sediments (Long et al. 2008); however, little evidence exists to support this. In this thesis, we have shown that the spontaneous chemical reaction between seagrass-released O_2 and sediment-produced H_2S leads to localised acidification of the rhizosphere owing to proton formation (*Chapters 2 & 4*). We further verified this finding via two-dimensional chemical imaging, showing a strong correlation between the seagrass-derived oxic microzones and the rhizospheric low-pH microniches (*Chapters 4 & 7*). This was demonstrated in high spatio-temporal resolution by means of both planar optodes and novel optical sensor nanoparticles incorporated into a reduced, artificial sediment matrix (*Chapters 4 & 7*). Interestingly, we also showed that the seagrass-derived rhizospheric low-pH microniches results in nutrient mobilization around the below-ground tissue of the tropical seagrass *Cymodocea serrulata* when colonizing carbonate-rich sediments (*Chapter 7*). As such, we found that tropical seagrasses mainly possess two biogeochemical mechanisms to mobilize nutrients around their below-ground tissue in carbonate-rich sediments (*Chapter 7*): (i) a direct acidification-induced phosphorus solubilisation mechanism that involves seagrass-generated rhizospheric low-pH microniches (down to pH of ~7 as compared to ~8 in the bulk natural sediment) leading to dissolution of

carbonates and concomitant release of calcium-bound phosphate to the pore-water, and (ii) an indirect sulphide-induced phosphorus and iron solubilisation mechanism based on seagrass-released DOC stimulating sulphate reducers in the rhizosphere and thereby enhancing the production of H_2S, which in turn leads to reduction of Fe(III)oxyhydroxides and concomitant release of (1) insoluble Fe(III)-phosphates, (2) Fe(III)oxyhydroxide adsorbed phosphate and (3) dissolved Fe(II) to the pore-water (*Chapter 7*). Tropical seagrasses have been shown to be Fe limited (Duarte et al. 1995) and an enhancement in the availability of dissolved iron (Fe(II)) in the pore-waters thus enables enhanced photo-pigment synthesis, such as Chl *a*, in the leaf epidermal tissues. The seagrass-derived rhizospheric nutrient mobilization mechanisms resulted in an up to 100-fold increase in the rhizospheric phosphorus availability and an up to 10-fold increase in the iron availability (*Chapter 7*). The revealed seagrass nutrient mobilization mechanisms thus explain the immense success of tropical seagrasses in oligotrophic, tropical waters (*Chapter 7*).

The thesis work has thus shown that the ability of seagrasses to alter the pH of their rhizosphere is an important biogeochemical process, where elevated rhizospheric pH microniches can alleviate the exposure of the vital meristematic tissue to phytotoxic H_2S through geochemical sulphide speciation shifts towards non-permeable HS^- ions, and where rhizospheric low-pH microniches mobilize essential nutrients around the below-ground biomass in carbonate-rich sediments.

Final conclusions

In order to proliferate, seagrasses rely on nutrients from both the water column and the sediment, but they also need to protect themselves against sediment-produced reduced phytotoxic compounds such as sulphide. Nutrient concentrations are often much higher in the sediment as compared to the water-column, but can be largely inaccessible to the plants due to various sediment fixation mechanisms. In this thesis, we show that seagrasses can alter their immediate rhizosphere biogeochemistry and thereby (i) detoxify the surrounding sediment, (ii) stimulate mutually beneficial rhizosphere microbes, such as sulphate-reducing diazotrophs, and (iii) enhance nutrient availability in the ambient pore-water. The plant-derived beneficial effects on the biogeochemical processes and chemical conditions within

the seagrass rhizosphere are strongly linked to the radial O_2 loss (ROL) from the below-ground tissue of seagrasses, and thus the intra-plant O_2 status. This underlines the importance for seagrasses to sustain positive internal O_2 budgets at any time. Inadequate internal tissue aeration may lead to severe phytotoxic H_2S intrusion, and/or inadequate nutrient mobilisation in carbonate-rich sediments causing nutrient starvation over the longer term, and thereby loss of crucial ecosystem services such as carbon capture and storage (i.e. “blue carbon”), coastal protection and marine biodiversity shelters. Our work has thus paved the way for better management strategies by increasing our knowledge on what determines seagrass health and thus what may result in seagrass die-offs. In light of the findings in this thesis, coastal managers are strongly advised to minimize the occurrence and duration of anthropogenic-induced environmental stressors leading to reduced internal plant aeration, including dredging-induced sediment re-suspension and agricultural-derived nutrient loadings, to preserve this vital marine ecosystem in future oceans.

Future research

The results from this thesis open up new avenues in the investigation of important plant/sediment interactions, which will further our knowledge of crucial rhizosphere dynamics such as how plants benefit from modifying the biogeochemistry of their rhizosphere. Specifically, the studies that have been carried out in this thesis and the techniques that we have developed may help direct molecular studies about where, when and at what scale to sample for molecular analyses. Too often, modern 'omics' approaches are carried out more or less "blindfolded", but in combination with microenvironmental analyses, such as chemical imaging and microsensor measurements, these studies can be improved upon and facilitate more hypothesis-driven approaches. As such, combining detailed microsensor measurements with molecular tools such as Fluorescence *In Situ* Hybridisation (FISH) to accurately link the below-ground chemical microenvironments with the activity and identity of specific microbial functional groups (such as sulphate-reducing bacteria and sulphide-oxidizing bacteria) at the plant-derived rhizospheric oxic/anoxic interfaces, deserves further attention.

In this thesis, several different techniques and novel methodologies were applied, all of which have different strengths and weaknesses. The combined use of *in situ* microsensor measurements with detailed laboratory measurements showed to be of great significance, as it enabled improved interpretation of results obtained *in situ*. For example, interpretation of the *in situ* work on how sediment re-suspension effects seagrass health was greatly facilitated by our prior knowledge based on detailed laboratory investigations determining the physiological response of seagrasses to sediment deposition on leaves. In addition, as discussed in chapter 3 and 4, employing optical sensor nanoparticles incorporated into artificial sediments to investigate below-ground biogeochemical processes on entire rhizosphere scale, provides an important supplement to other well-established microenvironmental analyzing techniques, such as planar optodes and microsensors. This includes, utilizing the high-resolution 2D chemical images provided by optical sensor nanoparticles to guide detailed 1D microsensor measurements to chemical hotspots within the rhizosphere that else would have been like "looking for a needle in a haystack" if only

applying microsensors. The main advantage of the optical nanoparticle-based sensors as compared to planar optodes is the fact that it is impossible to gain a good contact between the entire below-ground biomass and the planar optode at once. However, optical sensor nanoparticle measurements are limited to artificial sediments owing to the requirement for good optical properties in the investigated medium. Applying such artificial sediment matrix as compared to natural sediment obviously has its limitations due to the lower buffering capacity and microbial activity, some of which can be alleviated by enriching the applied artificial sediment with porewater microbes. The major benefit of employing a transparent artificial sediment matrix is, however, that it enables precise co-localization of the below-ground plant tissue structures with the rhizosphere biogeochemistry that is challenging to obtain in natural systems. Optical nanoparticle-based sensors thus have the potential to resolve important site-specific processes and interactions with the surrounding environment, which would otherwise be easy to overlook, especially when combined with other high-resolution measuring techniques, such as microsensors, and/or molecular studies.

Future studies of the dynamic and complex seagrass rhizosphere should include detailed descriptions of the seagrass microbiome, with special focus on potentially mutually beneficial relationships between the seagrass hosts and their rhizosphere and surface-associated microbial community, e.g., in terms of nutrient mobilization and sediment detoxification. Plant/microbe interactions at interfaces have often been shown to lead to enhanced plant fitness in terrestrial and aquatic environments, where in particular mycorrhizal fungi and rhizobia have been shown to be of great importance (e.g. Bolan, 1991; Jeffries et al. 2003; Denison & Kiers, 2004; Mohammadi et al. 2011); although some rhizospheric microbes can also act as pathogens (Thomas et al. 2011; Cúcio et al. 2016). Determining important seagrass/microbe relationships may help us better understand how seagrasses assimilate nutrients from the surrounding sediment and water-column, as well as the importance of microbes in providing protection towards reduced phytotoxic compounds produced in the sediment. During the last decades, seagrass meadows have been declining with alarming rates worldwide, mainly as a result of human-induced environmental stressors (Orth et al. 2006; Waycott et al. 2009) which are predicted to be intensified during

future climate change scenarios. A thorough understanding of rhizospheric seagrass/microbe interactions may provide us with important knowledge of how to protect seagrasses and thereby optimize carbon capture and sequestration in seagrass meadows to better manage this vital “blue carbon” ecosystem in a changing ocean.

REFERENCE LIST

Armstrong W. (1979). Aeration in higher plants. In: *Advances in Botanical Research* Vol. **7**. Academic Press, London.

Badri DV, Vivanco JM. (2009). Regulation and function of root exudates. *Plant, Cell and Environment* **32**: 666–681.

Barnabas AD. (1996). Casparian band-like structures in the root hypodermis of some aquatic angiosperms. *Aquatic Botany* **55**: 217-225.

Berlanga M, Aas JA, Paster BJ, Boumenna T, Dewhirst FE, Guerrero R. (2008). Phylogenetic diversity and temporal variation in the *Spirochaeta* populations from two Mediterranean microbial mats *International Microbiology* **11**: 267-274.

Blaabjerg V, Finster K. (1998). Sulphate reduction associated with roots and rhizomes of the marine macrophyte *Zostera marina*. *Aquatic Microbial Ecology* **15**(3): 311-314.

Blaabjerg V, Mouritsen KN, Finster K. (1998). Diel cycles of sulphate reduction rates in sediments of a *Zostera marina* bed (Denmark). *Aquatic Microbial Ecology* **15**(1): 97-102.

Bolan NS. (1991). A critical review on the role of mycorrhizal fungi in the uptake of phosphorus by plants. *Plant and Soil* **134**: 189-207.

Borum J, Pedersen O, Greve TM, Frankovich TA, Zieman JC, Fourqurean JW, Madden CJ. (2005). The potential role of plant oxygen and sulphide dynamics in die-off events of the tropical seagrass, *Thalassia testudinum*. *Journal of Ecology* **93**: 148-158.

Borum J, Sand-Jensen K, Binzer T, Pedersen O, Greve T. (2006). Oxygen movement in seagrasses. In: Larkum AWD, Orth JR & Duarte CM, eds. *Seagrasses: Biology, Ecology and Conservation.* Dordrecht, The Netherlands; Springer, Berlin: 255-270.

Colmer TD. (2003). Long-distance transport of gases in plants: a perspective on internal aeration and radial oxygen loss from roots. *Plant, Cell & Environment* **26**: 17-36.

Cúcio C, Engelen AH, Costa R, Muyzer G. 2016. Rhizosphere microbiomes of European seagrasses are selected by the plant, but are not species specific. *Frontiers in microbiology* **7**: 440.

Denison RF, Kiers ET. (2004). Why are most rhizobia beneficial to their plant hosts, rather than parasitic?. *Microbes and Infection* **6**: 1235-1239.

Devereux R. (2005). Seagrass rhizosphere microbial communities. In: Erik Kristensen, Ralf R. Haese & Joel E. Kostka, eds. *Coastal and estuarine studies: Interactions between macro- and microorganisms in marine sediments.* American Geophysical Union. Washington, USA.

Duarte CM, Merino M, Gallegos M. (1995). Evidence of iron deficiency in seagrasses growing above carbonate sediments. *Limnology and Oceanography* **40**(6): 1153-1158.

Erftemeijer PLA, Lewis RRR. (2006). Environmental impacts of dredging on seagrasses: a review. *Marine Pollution Bulletin* **52**(12): 1553-1572.

Fourqurean JW, Zieman JC, Powell GVN. (1992). Phosphorus limitation of primary production in Florida Bay: evidence from C:N:P ratios of the dominant seagrass *Thalassia testudinum*. *Limnology and Oceanography* **37**: 162–171.

Greve TM, Borum J, Pedersen O. (2003). Meristematic oxygen variability in eelgrass (*Zostera marina*). *Limnology and Oceanography* **48**(1): 210-216.

Hansen JW, Udy JW, Perry CJ, Dennison WC, Lomstein BA. (2000). Effect of the seagrass *Zostera capricorni* on sediment microbial processes. *Marine Ecology Progress Series* **199**: 83-96.

Hasler-Sheetal H, Holmer M. (2015). Sulfide Intrusion and Detoxification in the Seagrass *Zostera marina*. *PloS one* **10**(6): e0129136.

Holmer M, Hasler-Sheetal H. (2014). Sulfide intrusion in seagrasses assessed by stable sulfur isotopes—a synthesis of current results. *Frontiers in Marine Science* **1**: 64.

Holmer M, Pedersen O, Ikejima K. (2006). Sulfur cycling and sulfide intrusion in mixed Southeast Asian tropical seagrass meadows. *Botanica Marina* **49**: 91-102.

Isaksen MF, Finster K. (1996). Sulphate reduction in the root zone of the seagrass *Zostera noltii* on the intertidal flats of a coastal lagoon (Arcachon, France). *Marine Ecology Progress Series* **137**(1): 187-194.

Jeffries P, Gianinazzi S, Perotto S, Turnau K, Barea J-M. (2003). The contribution of arbuscular mycorrhizal fungi in sustainable maintenance of plant health and soil fertility. *Biology and Fertility of Soils* **37**: 1-16.

Jensen HS, McGlathery KJ, Marino R, Howarth RW. (1998). Forms and availability of sediment phosphorus in carbonate sand of Bermuda seagrass beds. *Limnology and Oceanography* **43**: 799–810.

Jovanovic Z, Pedersen MØ, Larsen M, Kristensen E, Glud RN. (2015). Rhizosphere O_2 dynamics in young *Zostera marina* and *Ruppia maritima*. *Marine Ecology Progress Series* **518**: 95-105.

Jørgensen BB, Revsbech NP. (1983). Colorless sulfur bacteria, *Beggiatoa* spp. & *Thiovulum* spp., in O_2 and H_2S microgradients. *Applied and Environmental Microbiology* **45**: 1261-1270.

Long MH, McGlathery KJ, Zieman JC, Berg P. (2008). The role of organic acid exudates in liberating phosphorus from seagrass-vegetated carbonate sediments. *Limnology and Oceanography* **53**(6): 2616-2626.

Margulis L. (1991). Symbiogenesis and symbionticism. In: Margulis L., editor. *Symbiosis as a source of evolutionary innovation: speciation and morphogenesis*. Cambridge, MIT press: 1-14.

Mohammadi K, Khalesro S, Sohrabi Y, Heidari G. (2011). A review: beneficial effects of the mycorrhizal fungi for plant growth. *Journal of Applied Environmental and Biological Sciences* **1**(9): 310-319.

Moriarty DJW, Iverson RL, Pollard PC. (1986). Exudation of organic carbon by the seagrass *Halodule wrightii* Aschers. and its effect on bacterial growth in the sediment. *Journal of Experimental Marine Biology and Ecology* **96**(2): 115-126.

Nelson DC, Jørgensen BB, Revsbech NP. (1986). Growth pattern and yield of a chemoautotrophic *Beggiatoa sp.* in oxygen-sulfide microgradients. *Applied and Environmental Microbiology* **52**(2): 225-233.

Nielsen LB, Finster K, Welsh DT, Donelly A, Herbert RA, De Wit R, Lomstein BA. (2001). Sulphate reduction and nitrogen fixation rates associated with roots, rhizomes and sediments from *Zostera noltii* and *Spartina maritima* meadows. *Environmental Microbiology* **3**(1): 63-71.

Nielsen OI, Koch MS, Madden CJ. (2007). Inorganic Phosphorus Uptake in a Carbonate-dominated Seagrass Ecosystem. *Estuaries and Coasts* **30**(5): 827–839.

Orth RJ, Carruthers TJB, Dennison WC, Duarte CM, Fourqurean JW, Heck Jr. KL, Hughes AR, Kendrick GA, Kenworthy WJ, Olyarnik S, et al. (2006). A global crisis for seagrass ecosystems. *BioScience* **56**(12): 987-996.

Pagès A, Welsh DT, Robertson D, Panther JG, Schäfer J, Tomlinson RB, Teasdale PR. (2012). Diurnal shifts in co-distributions of sulfide and iron(II) and profiles of phosphate and ammonium in the rhizosphere of *Zostera capricorni*. *Estuarine, Coastal and Shelf Science* **115**: 282-290.

Pedersen O, Binzer T, Borum J. (2004). Sulphide intrusion in eelgrass (*Zostera marina* L.). *Plant, Cell and Environment* **27**: 595-602.

Pedersen O, Borum J, Duarte CM, Fortes MD. (1998). Oxygen dynamics in the rhizosphere of *Cymodocea rotundata*. *Marine Ecology Progress Series* **169**: 283-288.

Plus M, Deslous-Paoli J-M, Dagault F. (2003). Seagrass (*Zostera marina* L.) bed recolonisation after anoxia-induced full mortality. *Aquatic Botany* **77**(2): 121-134.

Pollard PC, Moriarty D. (1991). Organic carbon decomposition, primary and bacterial productivity, and sulphate reduction, in tropical seagrass beds of the Gulf of Carpentaria, Australia. *Marine Ecology Progress Series* **69**(1): 149-159.

Pulido Pérez C, Borum J. (2010). Eelgrass (*Zostera marina*) tolerance to anoxia. *Journal of Experimental Marine Biology and Ecology* **385**: 8-13.

Raun AL, Borum J. (2013). Combined impact of water column oxygen and temperature on internal oxygen status and growth of *Zostera marina* seedlings and adult shoots. *Journal of Experimental Marine Biology and Ecology* **441**: 16–22.

Sand-Jensen K, Pedersen O, Binzer T, Borum J. (2005). Contrasting oxygen dynamics in the freshwater isoetid *Lobelia dortmanna* and the marine seagrass *Zostera marina*. *Annals of Botany* **96**(4): 613-623.

Short FT, Dennison WC, Capone DG. (1990). Phosphorus-limited growth of the tropical seagrass *Syringodium filiforme* in carbonate sediments. *Marine Ecology Progress Series* **62**(1): 169-174.

Thomas F, Hehemann J-H, Rebuffet E, Czjzek M, Michel G. (2011). Environmental and gut Bacteroidetes: the food connection. *Frontiers in microbiology* **2**: 93.

Waycott M, Duarte CM, Carruthers TJB, Orth RJ, Dennison WC, Olyarnik S, Calladine A, Fourqurean JW, Heck Jr. KL, Hughes AR, et al. (2009). Accelerating loss of seagrasses across the globe threatens coastal ecosystems. *PNAS* **106**: 12377–12381.

Welsh DT. (2000). Nitrogen fixation in seagrass meadows: regulation, plant–bacteria interactions and significance to primary productivity. *Ecology Letters* **3**(1): 58-71.

York PH, Carter AB, Chartrand K, Sankey T, Wells L, Rasheed MA. (2015). Dynamics of a deep-water seagrass population on the Great Barrier Reef: annual occurrence and response to a major dredging program. *Scientific reports* **5**: 13167.

APPENDICES

Appendix:

(i) Copies of published work
(ii) Poster presentations
(iii) Oral presentations
(iv) Additional manuscripts

Appendix 1

Copies of published work

Attached in the following order:

(1) Brodersen KE, Nielsen DA, Ralph PJ, Kühl M (2014). A split flow-chamber with artificial sediment to examine the below-ground microenvironment of aquatic macrophytes.
Marine Biology **161** (12): 2921-2930. doi: 10.1007/s00227-014-2542-3.

(2) Brodersen KE, Nielsen DA, Ralph PJ, Kühl M (2015). Oxic microshield and local pH enhancement protects *Zostera muelleri* from sediment-derived hydrogen sulphide.
New Phytologist **205** (3): 1264-1276. doi: 10.1111/nph.13124.

(3) Koren K*, Brodersen KE*, Jakobsen S, Kühl M (2015). Optical sensor nanoparticles in artificial sediments – a new tool to visualize O_2 dynamics around the rhizome and roots of seagrasses.
Environmental Science and Technology **49**(4): 2286-2292. doi: 10.1021/es505734b.

(4) Brodersen KE*, Koren K*, Lichtenberg M, Kühl M (2016). Nanoparticle-based measurements of pH and O_2 dynamics in the rhizosphere of *Zostera marina* L.: Effects of temperature elevation and light-dark transitions.
Plant, Cell & Environment (*First view*) (Accepted on March 22, 2016)

(5) Brodersen KE*, Lichtenberg M*, Paz LC, Kühl M (2015). Epiphyte-cover on seagrass (*Zostera marina* L.) leaves impedes plant performance and radial O_2 loss from the below-ground tissue.
Frontiers in Marine Science **2**:58. doi: 10.3389/fmars.2015.00058

Mar Biol (2014) 161:2921–2930
DOI 10.1007/s00227-014-2542-3

METHOD

A split flow chamber with artificial sediment to examine the below-ground microenvironment of aquatic macrophytes

Kasper Elgetti Brodersen · Daniel Aagren Nielsen · Peter J. Ralph · Michael Kühl

Received: 12 June 2014 / Accepted: 4 September 2014 / Published online: 16 September 2014

Abstract We present a new experimental set-up enabling fine-scale examination of how changing environmental conditions affect the below-ground biogeochemical microenvironment of aquatic macrophytes. By means of microsensor and planar optode technology, the influence of plant-mediated radial O_2 release on the below-ground chemical microenvironment of *Zostera muelleri* and *Halophila ovalis* was determined in high spatio-temporal resolution. The seagrass specimens were cultured in a new split flow chamber with artificial sediment made of a deoxygenated seawater–agar solution with added sulphide. Microelectrode measurements revealed radial O_2 release from the root–shoot junction of both *Z. muelleri* and *H. ovalis* during both light stimulation and darkness, resulting in a rapid decrease in H_2S concentration, and a significant drop in pH was observed within the plant-derived oxic microzone of *Z. muelleri*. No radial O_2 release was detectable from the below-ground tissue of *Z. muelleri* during conditions of combined water-column hypoxia and darkness, leaving the plants more susceptible to sulphide invasion. The spatial O_2 heterogeneity within the immediate rhizosphere of *Z. muelleri* was furthermore determined in two dimensions by means of planar optodes. O_2 images revealed a decrease in the spatial extent of the plant-derived oxic microzone surrounding the below-ground tissue during darkness, supporting the microelectrode measurements. This new experimental approach can be applied to all rooted aquatic plants, as it allows for direct visual assessment of the below-ground tissue surface during microprofiling, while enabling modification of the above-ground environmental conditions.

Communicated by M. Huettel.

Electronic supplementary material The online version of this article (doi:10.1007/s00227-014-2542-3) contains supplementary material, which is available to authorized users.

K. E. Brodersen (✉) · D. A. Nielsen · P. J. Ralph · M. Kühl
Plant Functional Biology and Climate Change Cluster, University of Technology, Sydney, 15 Broadway, Ultimo, Sydney, NSW 2007, Australia
e-mail: kasper.e.brodersen@student.uts.edu.au

M. Kühl
Marine Biological Section, Department of Biology, University of Copenhagen, Strandpromenaden 5, 3000 Helsingør, Denmark

M. Kühl
Singapore Centre on Environmental Life Sciences Engineering, School of Biological Sciences, Nanyang Technological University, Singapore, Singapore

Introduction

Seagrass meadows provide a diverse range of key ecosystem services such as coastal protection from erosion and enhancement of marine biodiversity (Larkum et al. 2006; Orth et al. 2006; Waycott et al. 2009), and they are ranked 2–4 times higher than mangroves/salt marshes and coral reefs in ecosystem service value (Costanza 1997). However, seagrass meadows are currently declining at an alarming rate worldwide, mainly as a result of anthropogenic stressors including eutrophication from land run-off and coastal developments such as harbour dredging and boating activities (Holmer et al. 2009; Orth et al. 2006; Ralph et al. 2006; Waycott et al. 2009). Inadequate internal aeration resulting in low meristematic (below-ground tissue) O_2 content is considered one of the key factors in seagrass die-off events (Borum et al. 2005; Greve et al. 2003; Pedersen et al. 2004; Raun and Borum 2013).

As seagrasses typically inhabit organically enriched, sulphidic sediments, they are challenged to provide their

below-ground tissue with sufficient O_2 in order to sustain aerobic metabolism in roots and rhizomes and provide protection against sediment-derived phytotoxic compounds (Borum et al. 2006). The internal O_2 supply mainly stems from photosynthesis in the leaves during daytime or from diffusive supply across the leaf surface from the surrounding water column during night-time or low light conditions. In the plant, O_2 is transported from the above-ground tissue to the below-ground tissue via low-resistance, intercellular gas-filled spaces (aerenchyma) (Borum et al. 2006; Greve et al. 2003; Jensen et al. 2005; Pedersen et al. 1998, 1999). The total amount of O_2 supplied to the root system is determined by the internal oxygen partial pressure (pO_2) of the shoots relative to the resistance of the below-ground tissue towards cross-tissue gas diffusion, as well as the consumption of O_2 via respiration and leakage along the diffusion path (Borum et al. 2006). The O_2 supply to the below-ground tissue is therefore strongly dependent on the environmental conditions and may be severely limited during the night when the water-column O_2 concentration is often reduced (Borum et al. 2006; Greve et al. 2003; Pedersen et al. 2004). Unusually, calm weather resulting in lowered flow as well as high water-column temperatures has also been shown to impede O_2 diffusion to the below-ground tissue (Binzer et al. 2005; Raun and Borum 2013).

Apart from directly restricting metabolic processes, inadequate internal aeration can also result in H_2S intrusion, leading to seagrass mortality from chemical asphyxiation (Holmer and Bondgaard 2001; Perez-Perez et al. 2012; Raven and Scrimgeour 1997). Previous studies have revealed that seagrasses often leak O_2 from their below-ground tissue to the surrounding rhizosphere, in particular from the area close to the root-apex (Frederiksen and Glud 2006; Jensen et al. 2005; Pedersen et al. 1998). Such radial O_2 loss (ROL) to the rhizosphere results in an oxidized microenvironment adjacent to the root surface, enabling chemical and/or microbial oxidation of reduced phytotoxic compounds (Jensen et al. 2005, 2007). In this way, healthy seagrasses may be actively modifying the geochemical microenvironment within the sediment to accommodate their growth (Brodersen et al. submitted).

The current understanding of the chemical microenvironment in the seagrass rhizosphere is largely based on microelectrode and planar optode measurements, which provide excellent means for describing internal and external O_2, H_2S and pH variability with high precision and high temporal and spatial resolution. (Brodersen et al. submitted; Borum et al. 2005; Frederiksen and Glud 2006; Greve et al. 2003; Jensen et al. 2005; Pedersen et al. 1998, 2004). Microelectrodes were introduced to seagrass research in the early 90 s (Caffrey and Kemp 1991) and have since revolutionized the understanding of the internal gas transport in seagrass tissue (Borum et al. 2005, 2006; Pedersen et al. 2004). Later these findings were supported by planar optode measurements (Frederiksen and Glud 2006; Jensen et al. 2005) enabling non-invasive imaging of the two-dimensional microdistribution of O_2 within the seagrass rhizosphere.

Microsensor techniques are limited by the difficulty of precise positioning of the microelectrode relative to roots and rhizomes. A commonly used method involves uncovering the root for microsensor positioning and subsequent covering with sediment. This limits the number of measuring points and can disturb redox conditions in natural sediment, especially when attempting microsensor measurements on actively growing roots (Jensen et al. 2005; Pedersen et al. 1998). Planar optodes provide a better overview of heterogeneity in the O_2 dynamics around the below-ground tissue, but the biomass must be closely associated with the planar optode, which can affect the distribution of solutes in the sediment by acting as a physical barrier to the diffusion of analyte compounds such as O_2 (Frederiksen and Glud 2006). Most studies of the below-ground chemical microenvironment of seagrasses have focused on the O_2 microdistribution in the rhizosphere, while knowledge about the microdistribution and dynamics of important chemical species such as H_2S and pH is very limited. Effects of changing environmental conditions on seagrass health are thus largely based on internal microelectrode measurements in the meristematic region of the rhizome (Binzer et al. 2005; Borum et al. 2005, 2006; Pedersen et al. 2004; Raun and Borum 2013), while knowledge about the dynamics of the external below-ground biogeochemical microenvironment is still lacking.

In order to address some of the experimental limitations in previous studies, we developed a new split flow chamber wherein seagrass specimens could be cultured in a transparent, sulphidic medium with properties mimicking those of typical reduced sediment. The set-up enables the use of both microsensors and planar optodes for rapid determination of changes in the below-ground tissue chemical microenvironment in response to changing environmental conditions in the leaf region (i.e. light/dark shifts and water-column O_2 content). This experimental approach allows for efficient analyses of the effect of combined environmental stressors, such as those predicted from climate changes or caused by human activity, on the health of seagrasses and other aquatic macrophytes. Hence, the aims of this study were to: (1) describe a new experimental approach that allows for measuring the dynamics of the chemical microenvironment around the tissue surface of aquatic macrophytes as a response to experimentally manipulated changing environmental conditions and (2) investigate whether results obtained with this method are comparable to below-ground chemical microdynamics previously reported in natural sediment.

Materials and methods

Flow chamber design

The flow chamber consisted of a "water phase" compartment and an adjoining "sediment" compartment, connected by a small slit (Fig. 1). The "water" compartment was designed as a conventional flow cell, in which water flows uniformly from an inlet towards an outlet on the opposite side of the chamber. Water flow was maintained with a submersible pump connected to the chamber via a silicon hose (Fig. 2). The "sediment" compartment was fully closed off except for the narrow opening (5 mm) to the "water" compartment, through which the seagrass leaves could reach the water phase. This narrow opening was closed off by a small polystyrene wedge after positioning of the seagrass specimen. To reduce influx of O_2 to the artificial sediment (described below), a silicon tube with numerous holes was positioned below the waterline in the compartment and continuously flushed with humidified N_2. The water phase in the "sediment" compartment was covered with parafilm to reduce evaporation and advection, and, lastly, a layer of aluminium foil was applied to further retain the N_2 in the chamber and to prevent roots being exposed to light. Microsensor measurements were performed through a small opening in the aluminium foil which could be closed off between measurements. In order to facilitate planar optode measurements (described below) from the underside of the sediment chamber, the bottom of the split flow chamber was made from 3-mm-thick, highly transparent polycarbonate. Detailed drawings of the flow chamber are provided as supplementary information (Fig. S1, S2, S3, S4 and S5).

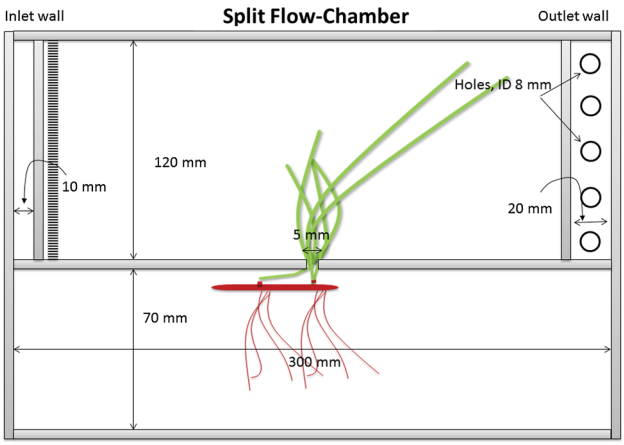

Fig. 1 Schematic drawing of the applied split flow chamber (*top view*) visualizing the position of the examined seagrass specimen, with leaves in the "water" compartment and roots/rhizome in the "sediment" compartment (detailed drawings are available in the supplementary information)

Transparent artificial sediment

Artificial sediment was constructed to mimic chemical conditions in natural sediment while enabling direct visual navigation when performing the below-ground microsensor measurements. The artificial sediment (in the "sediment" compartment) consisted of three functional layers: (1) a bottom layer (~3 mm) of Na_2S-enriched gauze (~1 mM H_2S) to ensure a continued diffusive supply of H_2S to the sediment, (2) a viscous, (~40 mm thick) anoxic layer of

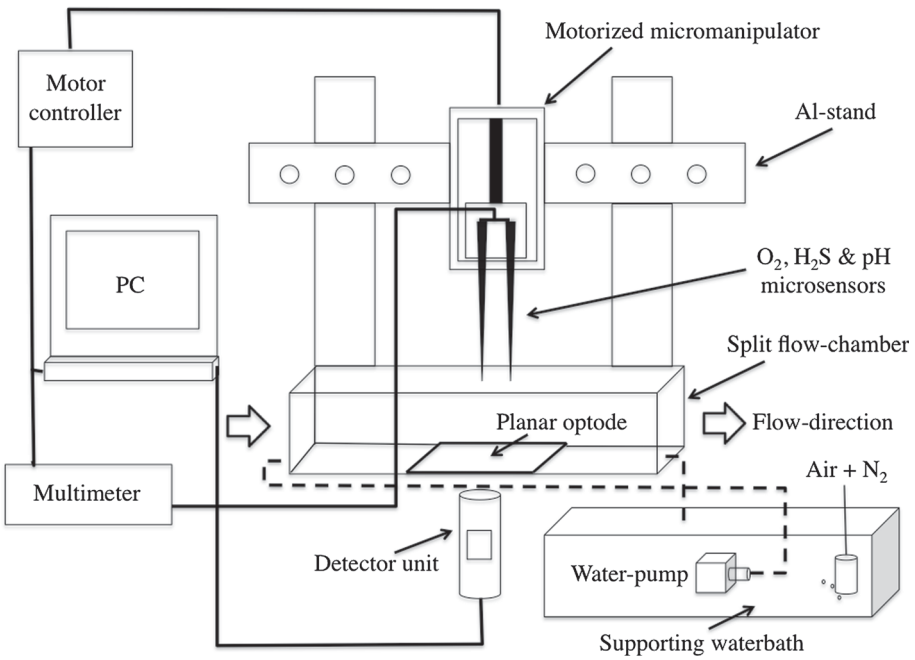

Fig. 2 Schematic diagram of the experimental set-up. Data acquisition and microsensor positioning were done with dedicated PC software (SensorTrace Pro, Unisense A/S, Denmark; VisiSens, PreSense, Germany)

a ~0.2–0.7 % agar–seawater solution deoxygenated via N_2 bubbling, buffered with HEPES buffer (10 mM) and amended with Na_2S to a final concentration of 50–200 µM H_2S and (3) a top layer (10–20 mm) of seawater kept hypoxic via continuous bubbling with humidified N_2 and thus functioning as an O_2 sink.

Filtered (0.22 µm) seawater was used throughout the experiment in order to ensure natural ratios of essential nutrients and avoid salinity gradients within the artificial sediment. For experiments involving planar optode measurements (see below), the gauze (layer 1) was excluded from the area above the planar optode to allow for direct visual inspection of the below-ground tissue from below the chamber. The separation of the different layers during casting of the artificial sediment was enabled by carefully pouring the upper medium with a plastic spoon to lower the impact force on the below medium.

Seagrass collection and maintenance

The seagrass specimens (i.e. *Halophila ovalis* and *Zostera muelleri* subsp. *capricorni*) were collected from shallow waters (less than 2 m depth) at Narrabeen Lagoon and Brisbane Waters, NSW, Australia. Specimens were transported to the University of Technology, Sydney, within 2 h of sampling, where the plants were maintained in a greenhouse under a natural light regime at a temperature of ~22 °C and a salinity of ~34. The below-ground tissue of the plants selected for measurements was gently washed free of adhering sediment particles and left in the water column attached with loose rubber bands to small glass jars filled with sand. The latter was done to remove any remaining sediment particles from the root surface and root hairs, without causing any damage to the root tissue. Furthermore, to obtain information on the natural chemical conditions in the sediment at the sampling site, a sediment core was collected at Narrabeen Lagoon adjacent to the seagrass meadow with a plastic tube (inner diameter 6.3 cm) used as corer.

Prior to each experiment, the seagrass plant was positioned horizontally in the split flow chamber with the leaves in the free-flowing "water" compartment and the rhizome and roots supported in the deoxygenated agar matrix. Each plant was acclimatized in the split flow chamber for several days prior to measurements and was acclimatized to the experimental conditions for a minimum of 3 h before each experiment to ensure steady-state conditions.

Experimental set-up

Illumination was provided by a tungsten halogen lamp fitted with a collimating lens (KL-2500, Schott GmbH, Germany). The downwelling photon irradiance (PAR, 400–700 nm) was measured with a scalar irradiance minisensor (US-SQS/L, Walz GmbH, Germany) connected to a calibrated quantum light meter (LI-250A, LI-COR, USA). The seagrass leaf canopy was positioned at the centre of the narrow light beam, thus limiting light exposure to the above-ground tissue. The plants were illuminated with an incident photon irradiance of 350–500 µmol photons m^{-2} s^{-1}. A constant flow (~1 cm s^{-1}) of aerated and thermostated seawater (22 °C; salinity of 34) was maintained in the free-flowing seawater compartment by the submerged pump. Hypoxic water-column conditions (see "Experimental treatments") were obtained by constantly flushing the supporting water bath with a mixture of atmospheric air and nitrogen. The O_2 concentration of the water bath was monitored via a Clark-type O_2 microsensor (OX-100, tip diameter of ~100 µm, Unisense A/S, Aarhus, Denmark). Plants were cultured in the flow chamber for more than 2 weeks under constant conditions (22 °C; Salinity of 34; 10:14 h light–dark cycle), and Chl *a* fluorometry was used to determine the longevity of seagrass plants held in the split flow chamber.

Experimental treatments

To demonstrate the potential of the novel experimental approach, we aimed to examine the impact of following treatments: (1) the effect of light exposure on the radial O_2 loss (ROL) from the below-ground tissue of *H. ovalis*; (2) the effect of light exposure and hypoxic (~50 % air saturation) conditions in the water column during darkness on ROL from the below-ground tissue of *Z. muelleri*; (3) the steady-state dynamics of the below-ground chemical microenvironment modified by *Z. muelleri*; and finally, (4) how the oxic microshield and the spatial O_2 heterogeneity within the rhizosphere of *Z. muelleri* is affected by a light–dark transition. The *H. ovalis* measurements are mainly included in this study to show that the experimental approach can be applied to different aquatic macrophytes with, e.g. highly different morphological appearance (i.e. the leaves of the *Z. muelleri* specimens were ~40 cm in length, as compared to *H. ovalis* only ~5 cm), thereby illustrating the wide applicability of the used methodology.

Microsensor measurements

We used Clark-type O_2 and H_2S microsensors (OX-50 and H2S-50, tip diameter of ~50 µm, Unisense A/S, Aarhus, Denmark; response time <5 and 10 s, respectively; stirring sensitivity <2 %) to measure the O_2 and H_2S concentrations of the below-ground microenvironment (Jeroschewski et al. 1996; Revsbech 1989). pH values were measured with pH microelectrodes (PH-50, Unisense A/S, Denmark; Kühl and Revsbech 2001). All microsensors were mounted on a

motorized micromanipulator and connected to a 4-channel multimeter (Unisense A/S, Denmark) both interfaced with a PC running data acquisition and positioning software (SensorTrace PRO, Unisense A/S, Denmark). The microsensors were linearly calibrated at experimental temperature and salinity before microprofiling commenced (further information on the calibration procedures is provided by the manufacture on www.unisense.com). The microsensors were positioned at the seagrass tissue surface (defined as 0 µm distance) by means of the micromanipulator. This was done by manually moving the microsensors while observing the microsensor tip and tissue surface through a stereomicroscope (AmScope, Irvine, CA, USA) equipped with a small observation device in the form of a custom-made polycarbonate plastic tube closed off by a clear window. The device was carefully submerged into the water column of the "sediment" compartment without disturbing the artificial sediment surface and enabled a less obstructed/distorted view through the microscope by excluding the air/water interface. Microprofiles around the below-ground tissue were measured in increments of 50–100 µm, whereas microprofiles describing the artificial sediment were measured in vertical step sizes of 1,000 µm.

Microsensor measurements within natural sediment

Vertical O_2 and H_2S microprofiles in natural sediment were obtained as described above. The sediment core was submerged into a cylinder-shaped aquarium (~2 L), and stirring was achieved via a constant flow of atmospheric air from an air-pump, applied onto the water surface through a Pasteur pipette (sediment surface at ~3 cm depth; ~22 °C; salinity of 34; incident irradiance of ~10 µmol photons m^{-2} s^{-1}).

Planar optode measurements

The spatial O_2 heterogeneity within the immediate rhizosphere of *Z. muelleri* was mapped with a transparent planar O_2 optode (Glud et al. 1996; Jensen et al. 2005) providing information on the two-dimensional O_2 distribution around the below-ground tissue. The planar optode consisted of an O_2 quenchable platinum(II)octaethylporphyrin luminophore (indicator dye) combined with a light harvesting antenna dye (Macrolex® fluorescence yellow 10GN) immobilized in polystyrene on a 125-µm-thick, transparent polyester support foil and covered with a semi-transparent silicon layer containing carbon powder (Larsen et al. 2011). The planar optode was imaged with a compact USB camera O_2 imaging system (VisiSens, PreSens, Germany) interfaced to a PC running the manufacturers imaging software system (VisiSens, PreSens, Germany). The detecting unit consisted of a digital camera equipped with a long-pass filter and violet-blue LEDs for excitation of the planar optode (VisiSens, PreSens, Germany).

The planar optode system used a colour ratiometric imaging approach (Larsen et al. 2011), where the LED excites both the reference and the O_2-sensitive dye causing dual emission, i.e. red luminescence from the O_2-quenchable indicator dye and green luminescence from the inert reference. The recorded intensity ratio between the recorded luminescence intensity in the red and green channel of the USB camera (i.e. Ratio = (Red − Green)/Green) provides a measure of the O_2 concentration at the surface of the planar optode. The planar optode was calibrated in anoxic (N_2 flushed) and air-saturated seawater before measurements commenced (further information on calibration procedures and image recordings are provided in Larsen et al. (2011)).

The planar optode was fixed on the bottom wall of the "sediment" compartment of the split flow chamber, using a thin layer of non-toxic silicone grease to "glue" the optode to the chamber bottom, carefully avoiding formation of air bubbles in between the chamber wall and optode. The sides of the optode were fixed with small pieces of tape. A seagrass plant was then positioned with the below-ground tissue touching the optode, where after the fluid, artificial sediment (~36 °C) was gently poured into the compartment followed by rapid cooling to air temperature (22 °C). Finally, a layer of anoxic seawater was established above the solidified artificial sediment by gently pouring nitrogen flushed seawater over the sediment as described above.

Flux calculations

A cylindrical version of Fick's first law of diffusion was used to calculate the radial O_2 fluxes from the root–shoot junctions (Steen-Knudsen 2002), assuming a perfect homogeneous and cylinder-shaped oxic microzone:

$$J(r)_{\text{below-ground tissue}} = \varphi Ds(C_1 - C_2)/r \ln (r_1/r_2)$$

where φ is the porosity, Ds is the apparent O_2 diffusion coefficient within the artificial sediment (here assumed similar to the molecular diffusion coefficient of O_2 in seawater, D_0), r is the tissue radius, and C_1 and C_2 are the measured O_2 concentrations at the distances r_1 and r_2, respectively (i.e. the inner and outer distance from the root centre). The porosity of the artificial sediment was calculated to be 0.95 from the weight loss of wet sediment (known initial volume) after drying in a 105 °C oven until a constant weight was reached. The radius of the root–shoot junction was defined under a stereo-microscope. D_0 at the experimental temperature and salinity was obtained from tables available from Unisense A/S (www.unisense.com).

Results

Chemical properties of the artificial sediment

The O_2 concentration of the seawater layer overlying the artificial sediment (i.e. the O_2 sink) was ~15 µmol L^{-1} owing to the continuous flushing with N_2 gas, which kept the artificial sediment anoxic for the duration of the experiments (Fig. 3a). In the first few mm of the artificial sediment, O_2 concentrations were low and decreased rapidly with depth as typical for natural marine sediment (Fig. 3a, b). The thin oxic zone was followed by an anoxic homogeneous zone, which extended to the bottom of the chamber. The seagrass below-ground tissue (i.e. root–shoot junction, rhizome and roots) was placed >20 mm below the artificial sediment surface to ensure no O_2 from the surface would reach the below-ground tissue, and all microsensor measurements were performed below this depth. In the anoxic part of the artificial sediment, we observed a rapid increase in the H_2S concentration with depth, reaching a maximum concentration of ~65 µmol L^{-1} at 3.6 cm depth (i.e. the deepest measured point within the artificial sediment ~10 mm below the below-ground tissue (Fig. 3a). The pH value of the artificial sediment decreased from ~7.5 at the surface of the sediment to pH 7 at the deepest point measured (~4 cm depth) (Fig. 3a). In comparison, the O_2 penetration depth within the natural marine sediment was ~1 mm and the H_2S concentration reached ~65 µmol L^{-1} at 4.5 cm depth (Fig. 3b).

Seagrass health during cultivation

Pulse amplitude-modulated (PAM) fluorometry measurements of photosynthetic performance (Beer et al. 1998; Ralph and Short 2002) confirmed that the plants were still healthy and photosynthetic competent after the 2-week incubation (F_v/F_m ~0.7; *Z. muelleri*). Furthermore, a complete new root bundle, internode and new leaves developed over a 7–8-day period in both species, signifying active growth in the flow chamber. Over the duration of the experiment, the new roots reached a length of 3 cm on average, corresponding to a growth rate of 0.4 cm day^{-1}, which is comparable to growth rates found for *Zostera marina* growing in natural sediment (Jensen et al. 2005).

Below-ground O_2 dynamics in the seagrass rhizosphere

Light exposure of the above-ground tissue of *Z. muelleri* resulted in a ~threefold increase in the radial O_2 loss from the root–shoot junction, increasing from 1.05 mmol O_2 m^{-2} h^{-1} in darkness to ~3.0 mmol O_2 m^{-2} h^{-1} under an incident irradiance of ~350 µmol photons m^{-2} s^{-1} (Fig. 4a). The radial O_2 loss from the root–shoot junction resulted in the establishment of a ~300-µm-thick oxic micro-niche in the surrounding sediment. Hypoxic conditions (~50 % air saturation) in the water column of the "water" compartment resulted in a complete disappearance of the oxic microzone surrounding the meristematic region of the rhizome, i.e. around the combined rhizome/basal leaf meristem area at the root–shoot junction (Fig. 4a). From the root–shoot junction of *H. ovalis,* we found a ~sixfold increase in the radial O_2 loss as a response to light stimuli, with O_2 fluxes increasing from 1.06 mmol O_2 m^{-2} h^{-1} in darkness to 6.5 mmol O_2 m^{-2} h^{-1} under an incident irradiance of ~500 µmol photons m^{-2} s^{-1} (Fig. 4b).

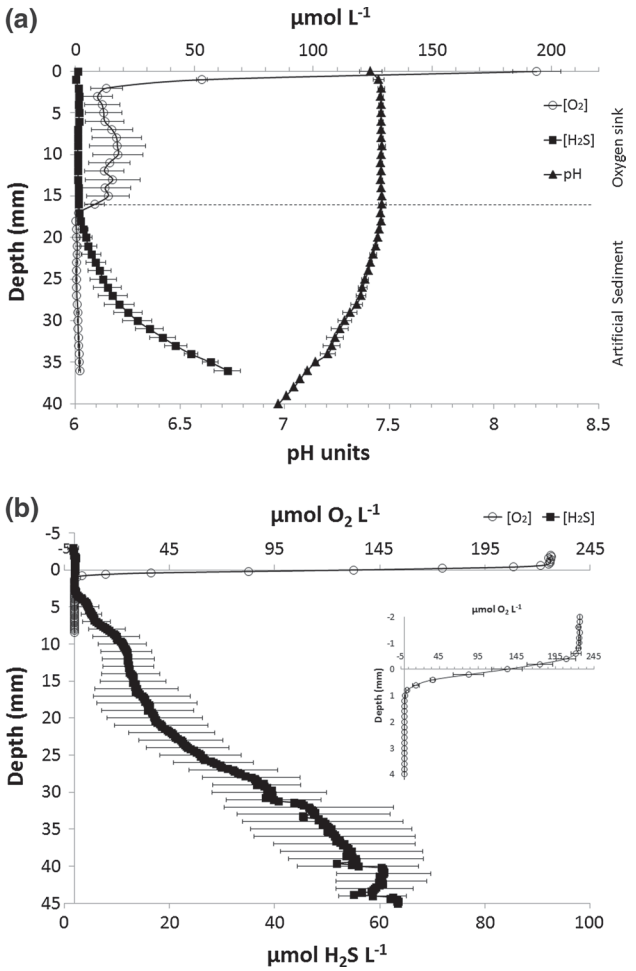

Fig. 3 **a** Vertical microprofiles of [O_2], [H_2S] and pH in the artificial sediment from the surface of the overlying O_2 sink (N_2 flushed seawater; ~16 mm deep) until ~10 mm below the below-ground tissue at a total vertical depth of ~4 cm. The *dotted line* represents the surface of the artificial sediment. All microsensor measurements were performed after the acclimatization period of the plants in the chamber, just prior to the experiments. **b** Vertical microprofiles of [O_2] and [H_2S] in natural sediment originating from Narrabeen Lagoon, NSW, Australia. An enlarged plot of the [O_2] microprofile across the water–sediment interface is inserted. Legends depict the different chemical species. *Symbols* and *error bars* indicate mean ± SD (n = 3–4)

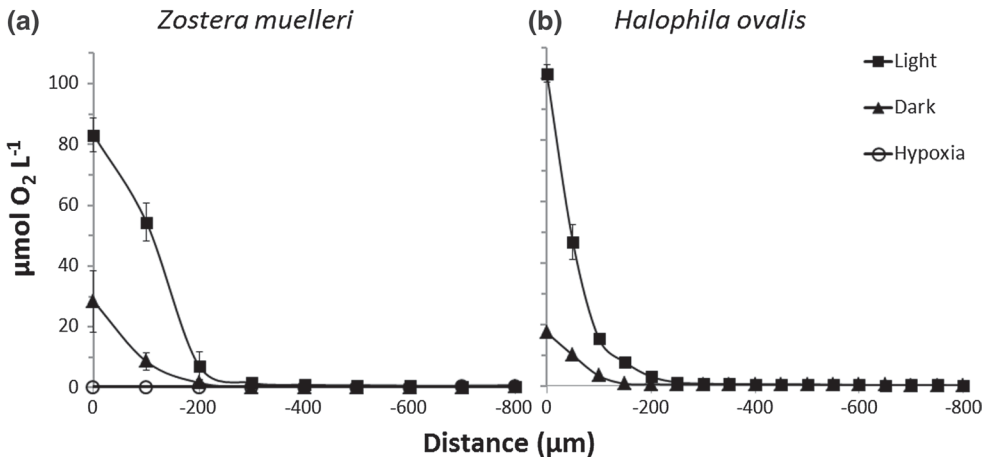

Fig. 4 **a** Radial O_2 loss from the root–shoot junction of *Z. muelleri* as measured with O_2 microelectrodes during darkness (*triangles*), under an incident irradiance of ~350 µmol photons m^{-2} s^{-1} (*squares*), and in darkness with hypoxic conditions (~50 % air saturation) in the water column surrounding the leaves (*empty circles*). $n = 3$. **b** Microelectrode measurements of the radial O_2 loss from the root–shoot junction of *H. ovalis* measured in darkness (*triangles*) and under an incident irradiance of ~500 µmol photons m^{-2} s^{-1} (*squares*). $n = 4$–5. Plants were investigated at the light intensity they were acclimatized to during cultivation/maintenance. Distance (in µm) refers to the distance from the below-ground tissue, where *x*-axis = 0 indicates the below-ground tissue surface. *Symbols* and *error bars* indicate mean ± SD

Chemical microenvironment at the below-ground tissue surface

The chemical microenvironment in the immediate rhizosphere of *Z. muelleri* at the root–shoot junction during darkness is shown in Fig. 5. Microelectrode measurements revealed a decrease in the H_2S concentration within the oxic microshield, decreasing from ~11.3 to 0 µmol H_2S L^{-1} at the below-ground tissue surface over a distance of ~1 mm, demonstrating complete re-oxidation and removal of phytotoxic H_2S at the tissue surface. The pH value decreased from 6.8 in the immediate rhizosphere to 4.7 at the tissue surface, likewise with a relatively steep gradient within the ~400-µm-thick oxic micro-niche (Fig. 5). The O_2 concentration at the below-ground tissue surface was ~65 µmol O_2 L^{-1} (Fig. 5).

Distribution of O_2 within the rhizosphere of *Zostera muelleri*

The planar optode images, visualizing the two-dimensional O_2 microdistribution at the root–shoot junction, revealed O_2 loss from the below-ground tissue of *Z. muelleri* both from roots of the first actively growing root bundle and from the root–shoot junction. This lead to the establishment of oxic microzones with O_2 concentrations reaching up to ~60 % air saturation in light (~300 µmol photons m^{-2} s^{-1}; Fig. 6). Light stimulation of the leaf canopy resulted in an expansion of the oxic microzones and enhanced O_2 leakage into the rhizosphere, as compared to in darkness (Fig. 6).

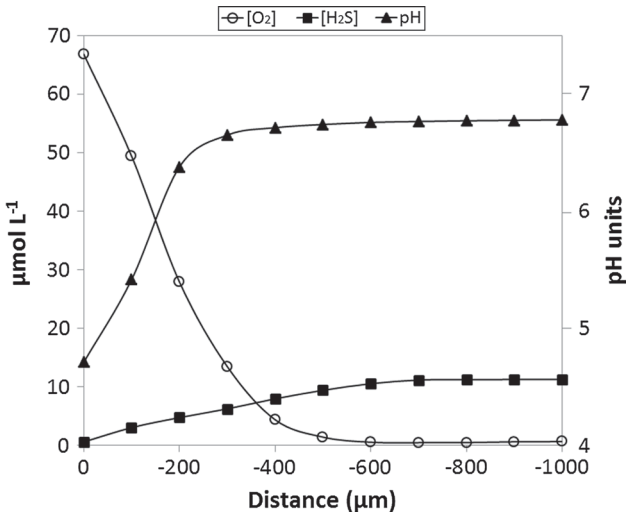

Fig. 5 The chemical microenvironment at the meristematic region of the rhizome of *Z. muelleri* measured with O_2, H_2S and pH microelectrodes. Legend depicts the different chemical species: O_2 concentration (*empty circles*); H_2S concentration (*squares*); pH values (*triangles*). Distance (in µm) refers to the distance from the below-ground tissue, where *x*-axis = 0 indicates the below-ground tissue surface. Average; no *error bars*. $n = 2$

Discussion

The new split flow chamber with transparent, artificial sediment enables investigations with high spatio-temporal resolution and replication to resolve effects of changing environmental conditions on seagrasses and their ability to modify the chemical microenvironment around their

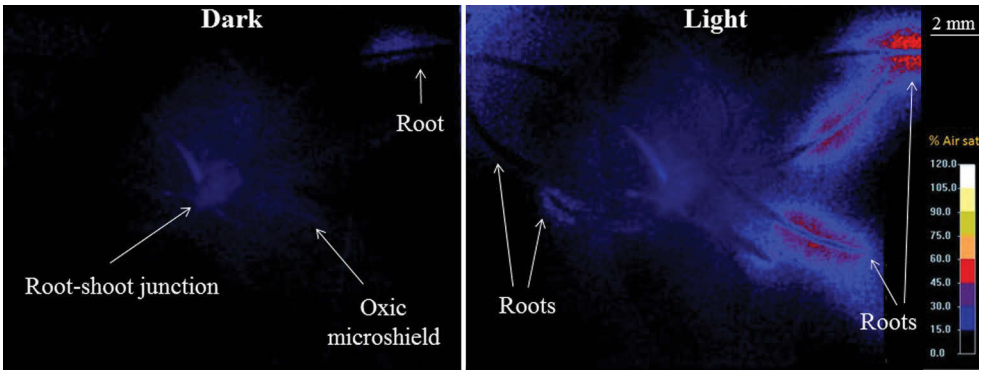

Fig. 6 The spatial O_2 heterogeneity within the rhizosphere of *Z. muelleri* mapped via planar optodes during light–dark transitions. Measurements were taken at quasi-steady state at a temperature of 22 °C, a salinity of 35 and a water-column flow velocity of 1 cm s^{-1}. The legend shows the O_2 concentration in % air saturation

below-ground tissue. We examined the effect of light–dark transitions and hypoxic water-column conditions on the oxidation capability of the below-ground tissue. The O_2 flux rates measured at the below-ground tissue of both seagrass species were similar to previous reported O_2 flux rates from the roots of *Cymodocea rotundata* in natural sediment (Pedersen et al. (1998); 2.3 and 5.3 mmol O_2 m^{-2} h^{-1} in darkness and light at equivalent incident irradiance, respectively). The radial O_2 loss (ROL) resulted in a 200–400-µm oxic microzone surrounding the root–shoot junction (Fig. 4), with a slight enhanced spatial distribution during light stimulation (~50 µm), owing to additional O_2 in the leaf aerenchyma due to photosynthesis (Fig. 4). The extent of the oxygenated microzones is defined by the balance between the rate of ROL and the total O_2 consumption rate of the surrounding sediment and was similar in extension to what has been found in previous studies in natural sediment (Jensen et al. 2005). Hence, the artificial sediment in the split flow chamber set-up appeared to mimic basic properties of natural sediment. Furthermore, seagrass sediments are generally very rich in organic matter and therefore exhibit high microbial activity, which in combination with a low O_2 solubility in water and low diffusion rate, results in very low O_2 penetration depths (often only a few mm; as seen on Fig. 3b). As such, by far most of the seagrass below-ground biomass resides in anoxic sediment, and therefore, we find that the chosen method to a reasonable extent replicates natural conditions. While the present study focuses on chemical dynamics, the set-up could be further modified to include natural sediment pore-water with its abundance of microbes. This would allow for the development and quantification of biogeochemical processes (such as microbial sulphide oxidation) in the set-up, which likely would influence the chemical microenvironment around the below-ground tissue. Such studies are underway.

When atmospheric O_2 was introduced to the seawater overlying the artificial sediment (O_2 sink) during measurements, the O_2 concentration of this sink depended on the total time that was spent on measuring during an experiment. During prolonged measurements (>4 h), the O_2 concentration reached a maximum of ~40 µmol O_2 L^{-1} (data not shown), whereas the O_2 concentration of the sink was ~0 µmol O_2 L^{-1} in between measurements, as a result of the covering of the "sediment" compartment containing the artificial sediment (based on initial measurements in the sink just after removing the cover; data not shown). Importantly, however, the increase in O_2 concentration did not extend to the deeper parts of the artificial sediment, where the seagrass rhizome and roots persisted in anoxia. Nevertheless, it is advisable to limit the measuring time and completely cover the "sediment" compartment of the split flow chamber between measurements to flush out the small amount of O_2 introduced during measurements. To avoid movement (wobbling) of the artificial sediment, the flow rate of N_2 had to be limited, resulting in the less than optimal O_2 removal efficiency during measurements. However, this issue may be alleviated by increasing the agar concentration of the artificial sediment at the cost of a significantly reduced visibility through the sediment.

The planar optode images revealed O_2 leakage from both the root–shoot junction and from the new and actively growing roots of *Z. muelleri* (Fig. 6). The spatial distribution of O_2 expanded during light stimulation of photosynthesis in the leaf canopy, thus supporting the microelectrode findings (Fig. 4). Both the microelectrode and planar optode measurements confirmed decreased oxidation capability of the below-ground tissue during darkness. In addition, hypoxic conditions in the water column resulted in an inability to sustain the external oxic microshield around the meristematic region of the rhizome, likely as a result of inadequate internal aeration (Fig. 4). This confirms a dependency of *Z. muelleri* on passive diffusion of O_2 from the water column during night-time, as previously reported in other seagrass species (e.g. Pedersen et al. 2004; Borum et al. 2005), particularly during summertime where plant respiration rates may be high, as a result of elevated seawater temperatures (Raun and Borum 2013).

The presence of the oxic microshield seemed to reduce the concentration of H_2S in the rhizosphere, most

likely as a result of chemical oxidation of H_2S with O_2 ($2O_2 + H_2S \rightarrow 2H^+ + SO_4^{2-}$). This process leads to formation of protons and can therefore explain the observed decrease in pH within the oxic microzone (Fig. 5). This phenomenon was also observed in a recent study, describing the dynamics of the chemical below-ground microenvironment of *Z. muelleri* under changing environmental conditions (Brodersen et al. submitted). Interestingly, a drop in pH within the oxic microzone towards the tissue surface (as seen on Fig. 5) would likely lead to dissolution of carbonates and concomitant release of sediment-bound phosphorus, which is generally a limiting nutrient in carbonate-rich sediments.

Prolonged periods of darkness thus have a significant negative impact on the oxidation capacity of the below-ground tissue, and in combination with decreased water-column O_2 content, this could leave seagrasses more sensitive to H_2S in the sediment as a result of inadequate internal aeration (Borum et al. 2005; Pedersen et al. 2004). Anthropogenic activities resulting in poor light conditions in the seagrass canopy, such as in the case of dredging operations where water-column turbidity is greatly increased (Erftemeijer and Lewis 2006), may thus have a substantial negative impact on the health of seagrass meadows, especially if enhanced respiration rates in the water column results in overnight hypoxia.

The presented experimental approach has broad applications within aquatic macrophyte ecophysiology and ecology. In this study, we focussed on the impact of environmental changes to the below-ground microenvironment, but effects on the above-ground microenvironment can easily be addressed as well. This could include investigations of: (1) how the thickness of the diffusive boundary layer around the leaves is affected by decreased water motion due to epiphyte growth on the leaf surface and (2) how the internal O_2 levels in leaves and rates of photosynthesis and respiration are affected by water turbidity. The main advantage of the presented experimental approach, as compared to previous used methodology (e.g. Jensen et al. 2005; Pedersen et al. 1998), is, however, that it simplifies the use of microsensors for measurements of the chemical microenvironment in the immediate rhizosphere, allowing for more frequent and detailed measurements with minimal risk of breaking the fragile microsensor tip. The artificial sediment allows for exact determination of the position of the microelectrode tip relative to the tissue surface, which is essential when doing quantitative calculations of fluxes and metabolic rates from microgradients. Such measurements can now be combined with planar optode measurements to get a more detailed mapping of the heterogeneity in the chemical microenvironment around the below-ground tissue, which otherwise would be challenging to obtain in natural sediment.

In summary, the experimental approach described in this paper has broad application within all micro-scale studies of aquatic macrophytes including plant–sediment interactions. A detailed understanding of how changing environmental conditions affect the health of aquatic macrophytes such as seagrasses, through its effect on the plants performance and its interaction with the surrounding sediment biogeochemistry, can lead to important new insight enabling better direction of coastal management resources, as well as provide a better understanding of the consequences of anthropogenic-induced stressors such as eutrophication and harbour dredging operations.

Acknowledgments We would like to thank technical officer Paul Brooks (UTS) for fruitful discussions and help during the development of the experimental set-up and Frederic Cadera (UTS) for helping with seagrass and sediment sampling. We thank Michael A. Rasheed for his intellectual contribution to the research in question. We acknowledge Ole Pedersen and Jens Borum for thoughtful initial discussions. This research was funded by the Australian Research Council (ARC) (MK, PJR), the Danish Council for Independent Research | Natural Sciences (MK) and through grants from the *Augustinus Foundation* and *Fabrikant P.A. Fiskers Foundation* (KEB).

References

Beer S, Vilenkin B, Weil A, Veste M, Susel L, Eshel A (1998) Measuring photosynthetic rates in seagrasses by pulse amplitude modulated (PAM) fluorometry. Mar Ecol Prog Ser 174:293–300

Binzer T, Borum J, Pedersen O (2005) Flow velocity affects internal oxygen conditions in the seagrass *Cymodocea nodosa*. Aquat Bot 83:239–247

Borum J et al (2005) The potential role of plant oxygen and sulphide dynamics in die-off events of the tropical seagrass, *Thalassia testudinum*. J Ecol 93:148–158

Borum J, Sand-Jensen K, Binzer T, Pedersen O, Greve T (2006) Oxygen movements in seagrasses. In: Larkum AWD, Orth JR, Duarte CM (eds) Seagrass Biology. Springer, Dordrecht, pp 255–270

Caffrey JM, Kemp WM (1991) Seasonal and spatial patterns of oxygen production, respiration and root-rhizome release in *Potamogeton perfoliatus L.* and *Zostera marina L.* Aquat Bot 40:109–128

Costanza REA (1997) The value of the world's ecosystem services and natural capital. Nature 387:253–260

Erftemeijer PLA, Lewis RRR (2006) Environmental impacts of dredging on seagrasses: a review. Mar Pollut Bull 52:1553–1572

Frederiksen MS, Glud RN (2006) Oxygen dynamics in the rhizosphere of *Zostera marina*: a two-dimensional planar optode study. Limnol Oceanogr 51:1072–1083

Glud RN, Ramsing NB, Gundersen JK, Klimat I (1996) Planar optodes: a new tool for fine scale measurements of two-dimensional O2 distribution in benthic communities. Mar Ecol Prog Ser 140:217–226

Greve TM, Borum J, Pedersen O (2003) Meristematic oxygen variability in eelgrass (Zostera marina). Limnol Oceanogr 48:210–216

Holmer M, Bondgaard EJ (2001) Photosynthetic and growth response of eelgrass to low oxygen and high sulfide concentrations during hypoxic events. Aquat Bot 70:29–38

Holmer M et al (2009) Sulfide intrusion in the tropical seagrasses *Thalassia testudinum* and *Syringodium filiforme*. Estuar Coast Shelf Sci 85:319–326

Jensen SI, Kühl M, Glud RN, Jorgensen LB, Prieme A (2005) Oxic microzones and radial oxygen loss from roots of *Zostera marina*. Mar Ecol Prog Ser 293:49–58

Jensen SI, Kühl M, Prieme A (2007) Different bacterial communities in the rhizoplane and bulk sediment of the seagrass *Zostera marina*. FEMS Microbiol Ecol 62:108–117

Jeroschewski P, Steuckart C, Kühl M (1996) An amperometric microsensor for the determination of H_2S in aquatic environments. Anal Chem 68:4351–4357

Kühl M, Revsbech NP (2001) Biogeochemical microsensors for boundary layer studies. In: Boudreau BP, Jorgensen BB (eds) The benthic boundary layer. Oxford University Press, New York, pp 180–210

Larkum AWD, Orth RJ, Duarte CM (2006) Seagrasses: biology, ecology, and conservation. Springer, Berlin

Larsen M, Borisov SM, Grunwald B, Klimant I, Glud RN (2011) A simple and inexpensive high resolution color ratiometric planar optode imaging approach: application to oxygen and pH sensing. Limnol Oceanogr Methods 9:348–360

Orth RJ et al (2006) A global crisis for seagrass ecosystems. Bioscience 56:987–996

Pedersen O, Borum J, Duarte CM, Fortes MD (1998) Oxygen dynamics in the rhizosphere of *Cymodocea rotundata*. Mar Ecol Prog Ser 169:283–288

Pedersen O, Borum J, Duarte CM, Fortes MD (1999) ERRATUM: oxygen dynamics in the rhizosphere of *Cymodocea rotundata*. Mar Ecol Prog Ser 178:310

Pedersen O, Binzer T, Borum J (2004) Sulphide intrusion in eelgrass (*Zostera marina* L.). Plant Cell Environ 27:595–602

Perez-Perez ME, Lemaire SD, Crespo JL (2012) Reactive oxygen species and autophagy in plants and algae. Plant Physiol 160:156–164

Ralph PJ, Short FT (2002) Impact of the wasting disease pathogen, *Labyrinthula zosterae*, on photobiology of eelgrass *Zostera marina*. Mar Ecol Prog Ser 226:265–271

Ralph PJ, Tomasko D, Seddon S, Moore K, Macinnis-Ng C (2006) Human impact on seagrasses: contamination and eutrophication in seagrass biology, ecology and conservation. Springer, Berlin, pp 567–593

Raun AL, Borum J (2013) Combined impact of water column oxygen and temperature on internal oxygen status and growth of *Zostera marina* seedlings and adult shoots. J Exp Mar Biol Ecol 441:16–22

Raven JA, Scrimgeour CM (1997) The influence of anoxia on plants of saline habitates with special reference to the sulfur cycle. Ann Bot 79:79–86

Revsbech NP (1989) An oxygen microsensor with a guard cathode. Limnol Oceanogr 34:474–478

Steen-Knudsen O (2002) Biological membranes: theory of transport, potentials and electric impulses. Cambridge University Press, Cambridge

Waycott M et al (2009) Accelerating loss of seagrasses across the globe threatens coastal ecosystems. PNAS 106:12377–12381

New Phytologist

Oxic microshield and local pH enhancement protects *Zostera muelleri* from sediment derived hydrogen sulphide

Kasper Elgetti Brodersen[1], Daniel Aagren Nielsen[1], Peter J. Ralph[1] and Michael Kühl[1,2,3]

[1]Plant Functional Biology and Climate Change Cluster, University of Technology Sydney (UTS), 15 Broadway, Ultimo, Sydney, NSW 2007, Australia; [2]Marine Biological Section, Department of Biology, University of Copenhagen, Strandpromenaden 5, DK-3000, Helsingør, Denmark; [3]Singapore Centre on Environmental Life Sciences Engineering, School of Biological Sciences, Nanyang Technological University, Singapore

Author for correspondence:
Kasper Elgetti Brodersen
Tel: +61 414 954 017
Email:
kasper.e.brodersen@student.uts.edu.au

Received: *7 April 2014*
Accepted: *15 September 2014*

New Phytologist (2015) **205:** 1264–1276
doi: 10.1111/nph.13124

Key words: biogeochemistry, microelectrodes, oxic microshield, plant–sediment interactions, radial oxygen release, rhizosphere, *Zostera muelleri*.

Summary

- Seagrass is constantly challenged with transporting sufficient O_2 from above- to belowground tissue via aerenchyma in order to maintain aerobic metabolism and provide protection against phytotoxins.
- Electrochemical microsensors were used in combination with a custom-made experimental chamber to analyse the belowground biogeochemical microenvironment of *Zostera muelleri* under changing environmental conditions.
- Measurements revealed high radial O_2 release of up to 500 nmol O_2 cm^{-2} h^{-1} from the base of the leaf sheath, maintaining a *c*. 300-μm-wide plant-mediated oxic microzone and thus protecting the vital meristematic regions of the rhizome from reduced phytotoxic metabolites such as hydrogen sulphide (H_2S). H_2S intrusion was prevented through passive diffusion of O_2 to belowground tissue from leaf photosynthesis in light, as well as from the surrounding water column into the flow-exposed plant parts during darkness. Under water column hypoxia, high belowground H_2S concentrations at the tissue surface correlated with the inability to sustain the protecting oxic microshield around the meristematic regions of the rhizome. We also found increased pH levels in the immediate rhizosphere of *Z. muelleri*, which may contribute to further detoxification of H_2S through shifts in the chemical speciation of sulphide.
- *Zostera muelleri* can modify the geochemical conditions in its immediate rhizosphere, thereby reducing its exposure to H_2S.

Introduction

Seagrasses (angiosperms) are considered to be crucial ecological engineers as they provide important ecosystem services that have a significant positive impact on their physical, chemical and biological surroundings (Costanza, 1997; Larkum *et al.*, 2006; Orth *et al.*, 2006; Waycott *et al.*, 2009). Over the past century, seagrass meadows have faced worldwide decline, mainly as a result of anthropogenic impacts such as eutrophication and coastal development (Orth *et al.*, 2006; Ralph *et al.*, 2006), resulting in an increasing number of seagrass die-off events (Seddon *et al.*, 2000; Plus *et al.*, 2003; Borum *et al.*, 2005), ranging from frequent small scale events (Carlson *et al.*, 1994; Zieman *et al.*, 1999) to isolated episodes of mass mortality (Robblee *et al.*, 1991). The exact causes leading to such die-offs remain largely unknown, but combined stressors such as high temperatures, high salinity, low flow-rates and water column hypoxia, causing plant tissue anoxia, in combination with hydrogen sulphide (H_2S) invasion from the surrounding sediment, have been suggested as likely causes (Carlson *et al.*, 1994; Zieman *et al.*, 1999; Borum *et al.*, 2005; Frederiksen *et al.*, 2006; Holmer *et al.*, 2009; Raun & Borum, 2013).

Because seagrasses mostly grow in highly reduced sediments (Borum *et al.*, 2006), they are constantly challenged to supply sufficient O_2 to their belowground tissue to sustain aerobic metabolism, as well as to provide protection against invasion of reduced phytotoxic compounds such as H_2S from the surrounding sediment (Armstrong, 1979; Borum *et al.*, 2005, 2006). To facilitate this, seagrasses have well-developed aerenchyma (lacunar system), which enable rapid internal gas-phase diffusion of O_2 to the roots, rhizomes and basal meristems. During daytime, photosynthesis in the seagrass leaves coupled with efficient gas transport in the aerenchyma ensures an adequate O_2 supply to the belowground tissues. At night-time, however, seagrasses are completely dependent upon passive diffusion of O_2 into leaves from the water column (Pedersen *et al.*, 1998; Borum *et al.*, 2006); this process is influenced by the O_2 concentration in the surrounding water, the thickness of the seagrass leaf diffusive boundary layer (DBL), and thereby the flow velocity of the surrounding water, as well as by the plant respiration rate itself (Pedersen *et al.*, 2004; Binzer *et al.*, 2005). This important physiological adaptation enables seagrasses to maintain an oxidized microzone (oxic microshield) around their roots (Pedersen *et al.*, 1998; Jensen *et al.*,

2005; Borum *et al.*, 2006; Frederiksen & Glud, 2006), typically originating from around the root apex/apical meristem (Jensen *et al.*, 2005; Borum *et al.*, 2006) and resulting in a temporally oxidized microzone 1–2 mm behind the root tip. The impact of such O_2 release on the biogeochemistry and microbial diversity in the seagrass rhizosphere is, however, still under-explored (e.g. Pedersen *et al.*, 1998, 1999; Jensen *et al.*, 2005, 2007).

The O_2 budget of seagrass, which determines the sulphide oxidation capability of the belowground tissue, is the result of complex interactions between several sources and sinks. Sources include photosynthetically derived O_2 evolution and passive diffusion of O_2 into the seagrass leaves from the ambient water column. The sinks consist of the sediment O_2 demand resulting from biotic and abiotic chemical reactions, as well as the plants' own respiration (Greve *et al.*, 2003; Borum *et al.*, 2005, 2006; Holmer *et al.*, 2006). Plant tissue respiration is strongly influenced by changes in water temperature, and increased respiration as a result of increasing temperature can lead to decreased O_2 supply to belowground tissue, resulting in inadequate internal aeration (Raun & Borum, 2013), which in turn may lead to H_2S intrusion.

Sulphide is produced by sulphate-reducing bacteria in anoxic marine sediment and exhibits a pH-dependent speciation where H_2S predominates at porewater pH < 7, and HS^- predominates at higher pH. As dissolved H_2S gas is the only form of sulphide that can freely permeate the cell membrane, the toxicity of sulphide in sediment not only relies on the overall sulphide concentration, but is also strongly affected by the sediment pH. High H_2S concentrations have a negative effect on the viability of submerged plants by reducing photosynthesis, reducing nutrient uptake, and by blocking the mitochondrial respiratory electron transport chain through its strong binding with iron in cytochrome *c* oxidase (Goodman *et al.*, 1995; Raven & Scrimgeour, 1997; Holmer & Bondgaard, 2001; Perez-Perez *et al.*, 2012). H_2S is thus considered a broad-spectrum toxin that leads to chemical asphyxiation and formation of reactive oxygen species (ROS), which can lead to protein degradation and peroxidation of membrane lipids (Raven & Scrimgeour, 1997; Eghbal *et al.*, 2004; Truong *et al.*, 2006; Perez-Perez *et al.*, 2012).

As H_2S can be chemically oxidised by O_2 (i.e. $2O_2 + H_2S \rightarrow 2H^+ + SO_4^{2-}$), the influx of H_2S into plant tissue seems to correlate with the inability to sustain a protective oxic microzone around the belowground tissue (Pedersen *et al.*, 2004; Borum *et al.*, 2005). The thickness and efficiency of such an oxic microshield depends on the rate of O_2 leakage to the rhizosphere relative to the O_2 consumption rate in the surrounding sediment. Bacterial sulphide oxidation in the immediate rhizosphere may also dramatically lower the half-life of H_2S in comparison to the spontaneous chemical oxidation alone (Cline & Richards, 1969; Chen & Morris, 1972; Almgren & Hagstrom, 1974; Jørgensen & Revsbech, 1983; Pedersen *et al.*, 2004), further alleviating the H_2S exposure of seagrass roots. Yet another potential chemical defence mechanism could involve a local increase of rhizosphere or root surface pH, shifting the sulphide speciation away from H_2S towards nonpermeable and thereby nonphytotoxic HS^- ions. A detailed description of the pH microheterogeneity within the seagrass rhizosphere is, however, still lacking.

Mature seagrass roots also exhibit a range of anatomical adaptations, including casparian band-like structures (Barnabes, 1996) and/or suberized lamellae (e.g. Enstone *et al.*, 2003) that reduce cross-tissue gas transport. This is likely to increase the efficiency with which O_2 is carried to the roots, thus facilitating the maintenance of aerobic metabolism and possibly also reducing H_2S intrusion (Armstrong, 1979; Armstrong & Armstrong, 2001; Jensen *et al.*, 2005). The presence of a strong barrier against cross-tissue gas transport has been shown to correlate with anaerobic conditions within the sediment, as well as the presence of phytotoxins (Colmer *et al.*, 1998; Armstrong & Armstrong, 2001).

In this study, we elucidate the dynamics of the chemical microenvironment in the rhizosphere of *Zostera muelleri* under changing environmental conditions. We present the first detailed microscale mapping of O_2, H_2S and pH gradients around the basal meristems with leaf sheath (BM), rhizome and roots of *Z. muelleri* and investigate whether local pH enhancement and sulphide oxidation contribute to H_2S detoxification in the rhizosphere.

Materials and Methods

Seagrass samples

Zostera muelleri ssp. *capricorni* (Asch.) S. W. L. Jacobs specimens were collected from a sheltered lagoon exposed to low flow rates (Narrabeen Lagoon, NSW, Australia). Specimens were sampled in shallow waters (*c.* 1 m depth) and transported in seawater from the sampling site to the laboratory within 1 h of sampling. Specimens were kept in a glasshouse under a natural light regime (*c.* 11 h : 13 h, light : dark cycle) for a minimum of 72 h before further handling. Three specimens with similar aboveground and belowground biomass (i.e. two shoots with intact root bundles and more than two internodes) were selected for this study. Rhizome and roots were gently washed and plants were left free of sediment over night to aerate roots and rhizomes before placing them in the split flow chamber (Fig. 1).

Split flow chamber and artificial sediment

A seagrass specimen was placed horizontally in a custom-made split flow chamber (Fig. 1), with the aboveground tissue positioned in the upper compartment with free-flowing seawater and the belowground tissue inserted in viscous, reduced artificial sediment consisting of: 0.19% anoxic seawater-agar (grade J3; Gelita, Beaudesert, Qld, Australia) solution amended with Na_2S to a final concentration of 250 μM H_2S and buffered with 10 mM anoxic HEPES buffer (*N*-2-hydroxyethylpiperazine-*N*′-2-ethanesulfonic acid; pH range 6.8–8.2). Natural seawater was used to ensure natural concentrations and ratios of essential nutrients. The artificial sediment was kept anoxic in the chamber by constantly flushing the overlying layer of seawater with humidified nitrogen (Fig. 1). To ensure a continuous supply of H_2S to the artificial sediment, pieces of gauze were soaked in anoxic and acidic (pH 4) 1 mM Na_2S solution and placed in the

bottom of the lower chamber before adding the artificial sediment. The O_2 demand of the reduced artificial sediment was kept relatively high in order to mimic natural sediment conditions. This was achieved through the combined effect of the added reducing agent (H_2S) constantly diffusing up into the artificial sediment from the bottom layer and the above-lying oxygen sink (further information on the experimental approach is provided in Brodersen *et al.* (2014)).

A constant flow (*c.* 1 cm s^{-1}) of seawater (21°C; salinity of 34) was maintained in the upper compartment via a pump submerged in an aerated, temperature-controlled water bath. Illumination in the upper compartment (with seagrass leaves) was provided by a fibre optic tungsten halogen lamp (KL-2500; Schott GmbH, Mainz, Germany). The downwelling quantum irradiance (PAR) was measured with a calibrated quantum irradiance meter (Li-250A; LiCor, Lincoln, NE, USA) equipped with an irradiance sensor (Walz GmbH, Effeltrich, Germany) kept at the same distance from the light source as the seagrass leaf canopy.

Plants were acclimatized to the split flow chamber under standard conditions (*c.* 250 µmol photons m^{-2} s^{-1}; 10 h : 14 h, light : dark cycle) for several days before measurements commenced. The seagrass specimens were then acclimatized to different treatment conditions: dark + air saturated water column; 260 µmol photons m^{-2} s^{-1} + air saturated water column; 350 µmol photons m^{-2} s^{-1} + air saturated water column; and dark + *c.* 50% air saturation in the water column (hypoxia). Treatments were applied for at least 3 h before measurements to ensure steady-state biogeochemical conditions (as confirmed by repeated microprofile measurements). The hypoxia treatment (i.e. *c.* 50% air saturation in the water column of the upper compartment) was achieved by simultaneously flushing the water in the supporting water bath with a mixture of N_2 and atmospheric air. The O_2 concentration in the water was constantly monitored by a calibrated Clark-type O_2 microsensor (OX-100, tip size *c.* 100 µm, 90% response time < 8 s, stirring sensitivity < 1.5%; Unisense A/S, Aarhus, Denmark). Thirty-six hours before the hypoxia experiment, additional sulphide (5 ml, 10 mM Na_2S) was injected into the bottom layer of the artificial sediment in order to re-establish H_2S concentrations, as preliminary experiments had shown that photosynthesis-induced O_2 release during the light treatment completely removed H_2S from the basal meristem microenvironment. The split flow chamber was left untouched for 36 h after the injection to ensure steady-state biogeochemical conditions as confirmed by repetitive vertical microsensor profiles. Before microelectrode measurements commenced, O_2 microprofiles were performed at the cut end of the rhizome to ensure that no O_2 release was detectable, indicating intact plants and thereby an enclosed aerenchyma.

Microsensor measurements

Precontaminated (i.e. pre-exposed to H_2S) Clark-type O_2 microsensors (OX-50, tip diameter *c.* 50 µm; Unisense A/S; Revsbech, 1989), with a fast 90% response time of < 5 s and a low stirring sensitivity of < 2% were used to measure the radial O_2 release from the belowground tissue. Oxygen microelectrodes were linearly calibrated from signal readings in 100% air saturated seawater and anoxic seawater (seawater amended with the O_2

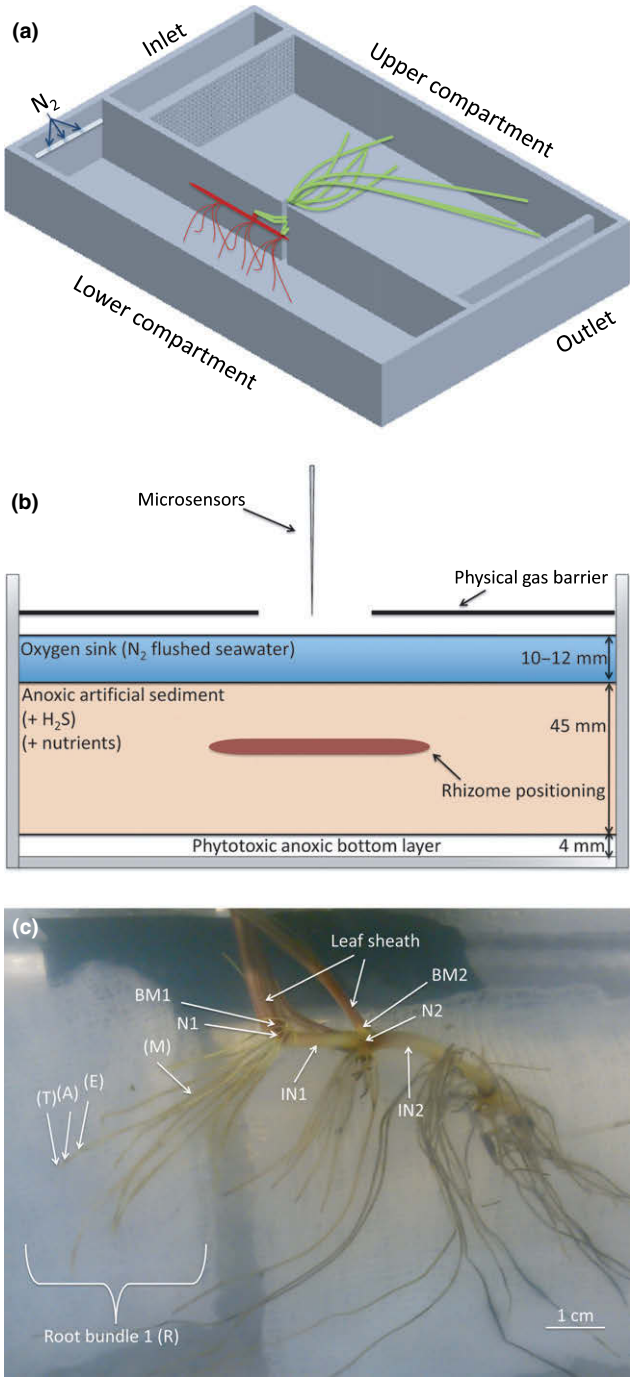

Fig. 1 (a) Split flow chamber shown from above, with the free-flowing water section (upper chamber) and the anoxic artificial sediment compartment (lower chamber) (split flow chamber illustration provided by Dotmar EPP, Australia). (b) Median section of lower part of split flow chamber illustrating the three layers of the artificial sediment. (c) Schematic illustration of *Zostera muelleri* belowground tissue, visualizing the spatial distribution of the microsensor measurements within the immediate rhizosphere. T, root tip/root cap; A, apical meristem region; E, elongation zone; M, mature zone (i.e. formation of root hairs); BM, basal meristem with leaf sheath; N, node; IN, internode.

scavenger sodium dithionite) at experimental temperature and salinity.

H_2S concentrations were measured with Clark-type H_2S microelectrodes (H_2S-50, tip diameter *c.* 50 μm, 90% response time < 10 s, stirring sensitivity < 2%; Unisense A/S; Jeroschewski *et al.*, 1996; Kühl *et al.*, 1998) that were linearly calibrated (three-points) in anoxic, acidic Na_2S (pH 4) solutions of known H_2S concentrations (i.e. 0, 50 and 100 μM, at experimental temperature and salinity). The microelectrode is only sensitive to H_2S (Jeroschewski *et al.*, 1996), which is the only sulphide species that is able to penetrate plant tissue by liquid solution permeation of the plasmalemma (Raven & Scrimgeour, 1997).

pH measurements were done with pH microelectrodes (PH-50, tip diameter *c.* 50 μm, linear range pH 4–9; Unisense A/S; Kühl & Revsbech, 2001) with a 90% response time < 10 s and a detection limit of 0.05–0.1 pH units. The pH microelectrodes were used in combination with a reference electrode (REF-RM, tip diameter of *c.* 5 mm; Unisense A/S) immersed in the seawater in the flow through chamber in which measurements were taken. The pH microelectrode was calibrated from sensor readings in three pH buffers (pH 4, 7 and 9, at experimental temperature and salinity) and responded linearly to pH over the calibration range with a signal to pH ratio of *c.* 52 mV/pH unit.

All microsensors were connected to a four channel multimeter (Unisense A/S) interfaced with a PC running data acquisition software (SensorTrace PRO; Unisense A/S). During operation, the microsensors were mounted on a PC-interfaced motorized micromanipulator (MM33-2, MC-232; Unisense A/S) controlled by dedicated positioning software (SensorTrace PRO; Unisense A/S). All microprofiles were measured in steps of 100 μm (except vertical profiles describing the relative difference between the rhizosphere and the artificial sediment that were performed in 1000 μm step sizes). Before each microprofile measurement commenced, the microsensors were positioned at the tissue surface (indicated as 0 μm on graphs) by means of the micromanipulator, while observing the plant tissue surface and microsensor tip in the transparent, artificial sediment through a stereomicroscope mounted on an articulating arm (SM-6TZ; Amscope, Irvine, CA, USA) equipped with a handheld lens (further described in Brodersen *et al.*, 2014).

Mapping the chemical microenvironment

Microelectrode measurements were performed at the basal meristems with leaf sheath (meristematic regions of the rhizome; base of leaf sheath), at the nodes (meristematic regions of the rhizome; root–shoot junctions), on the internodes (three points/locations along the latitude direction), as well as on the first root bundle ($n = 2$–4, where 'n' represents numbers of technical replicates). Note that the meristematic region of the rhizome is a combined basal leaf/rhizome meristem area located between the leaf bundle and rhizome (Short & Duarte, 2001); in this study divided up in two regions, namely the nodium and the basal meristem with leaf sheath *c.* 1 mm apart. The first root bundle was divided into four areas: root mature zone (with completely developed root hairs; RM), root elongation zone (RE), root apical meristem region (area of root cell division; RA) and root tip (RT) based on observations under a stereo microscope (see Fig. 1).

Flux calculations

The radial oxygen flux ($J(r)$; nmol O_2 cm^{-2} h^{-1}) from the below-ground tissue was calculated via a cylindrical version of Fick's first law of diffusion, assuming homogeneous O_2 release from a perfect cylinder (Steen-Knudsen, 2002):

$$J(r)_{root-system} = \phi D_s(C_1 - C_2)/r \ln(r_1/r_2) \quad \text{Eqn 1}$$

(ϕ, porosity; D_s, diffusion coefficient for oxygen in the artificial sediment; r, radius of the given root/rhizome, ΔC, oxygen concentration gradient through the oxic microzone (i.e. from the tissue surface to the last point of the linear concentration gradient *c.* 300 μm away from the tissue surface); r_1 and r_2, distance from the root centre (i.e. radius of inner and outer cylinder shell) equivalent to the measured O_2 concentrations C_1 and C_2, respectively). Radial H_2S consumption rates ($J(r)_{H_2S}$; in nmol H_2S cm^{-2} h^{-1}) were calculated in a similar manner only replacing the respective diffusion coefficient (see next paragraph).

The porosity, ϕ, of the artificial sediment was 0.95, and was determined after drying the sediment at 105°C in an oven until a constant weight was reached (known initial volume and wet weight). The following equation was used for the calculation:

$$\phi(\%) = ((M_w/D_w) \cdot 100)/((M_w/D_w) + (M_a/D_a)) \quad \text{Eqn 2}$$

(M_w, weight of seawater; D_w, density of seawater; M_a, weight of agar; D_a, density of agar). The respective diffusion coefficients within the sediment were calculated to be $D_{S,H_2S} = 1.5251 \times 10^{-5}$ cm^2 s^{-1} and $D_{S,O_2} = 2.0138 \times 10^{-5}$ cm^2 s^{-1} at experimental temperature and salinity (assuming similar diffusion rates as in seawater). The molecular diffusion coefficient for O_2 in seawater, D_0, and the multiplication factor for calculating the molecular diffusion coefficient of H_2S at experimental temperature and salinity, were taken from tables available at www.unisense.com (Ramsing & Gundersen, 2014).

Measurements of seagrass health and photosynthetic capacity during cultivation

Maximum and effective quantum yields of photosystem II (PSII) in *Z. muelleri* were measured by pulse amplitude modulated (PAM) fluorometry (PocketPAM equipped with an optical fiber; PAM settings: saturating intensity 6, saturating width 0.6 s, $F > 100$). The measurements were used as a general indicator of seagrass health. Light energy absorbed by chlorophylls can either be used for photochemistry, re-emitted as fluorescence (i.e. as longer wavelengths) or dissipated as heat (nonphotochemical quenching (NPQ)). The relative proportions of energy directed through each of these different pathways define the health of the photosystems, and can be used to determine maximum PSII

quantum yield as:

$$F_v/F_m = (F_m - F_o)/F_m \quad \text{Eqn 3}$$

and the effective quantum yield of PSII as:

$$\Delta F/F_m' = (F_m' - F)/F_m' \quad \text{Eqn 4}$$

(F_m, maximal fluorescence yield for dark-acclimated plants; F_o, minimum fluorescence yield; F_m', light-adapted maximum fluorescence yield). As quantum yields are ratios of fluorescence yield measurements, they have no units (Beer *et al.*, 1998; Ralph & Short, 2002). The maximum quantum yield provides a measure of PSII photochemical efficiency (after a minimum dark adaptation period of 10 min) and the effective quantum yield is a measure of PSII photosynthetic activity (measured under experimented irradiance intensities, i.e. 260 and 350 μmol photons m^{-2} s^{-1}). Seagrass specimens were maintained in the artificial sediment for > 14 d before experiments (similar conditions as used during the microsensor measurements), to verify the long-term health of the plants under the experimental conditions. This was confirmed by the observation of active growth in both above- and belowground biomass during cultivation, as well as by measured effective and maximum quantum yields. A complete new root bundle, internode and bundle of leaves were developed during cultivation. The rhizome was growing *c.* 0.8 cm and the new root bundle reached an average root length of 2.6 cm over a 7 d period.

Histology

The base of the leaf sheath of the first shoot and the first internode of each plant were cut into 20–40 μm transverse tissue sections by means of a cryotome after prefixation in cryo-gel (Tissue-Tek®; ProSciTech, Kirwan, Qld, Australia). The samples were left embedded in the cryo-gel at *c.* 4°C for 24 h before the cutting process, to ensure efficient tissue penetration. The obtained sections of the belowground tissue were then transferred to microscope glass slides where they were gently washed to remove any remaining cryo-gel. The cleaned sections were then examined under a stereo microscope and photographed with a digital camera (Coolpix 995; Nikon, Tokyo, Japan).

Results

The detailed mapping of the belowground chemical microenvironment presented in the following originates from three *Zostera muelleri* plants exposed to similar experimentally manipulated environmental conditions, as well as above- and belowground microenvironmental conditions. Results are shown from the two plants examined in most detail.

Chemical conditions in the immediate rhizosphere

Photosynthetic O_2 evolution, as well as diffusion of O_2 from the ambient water column into the aerenchyma, resulted in high radial O_2 release to the immediate rhizosphere of *Z. muelleri* (Fig. 2; Table 1). The O_2 release originating from the base of the leaf sheath, as well as the rhizome (i.e. node and internodes), resulted in the establishment of a *c.* 300-μm-thick oxic microshield around the basal meristems with leaf sheath (BM), nodes (during light and dark treatments; Fig. 2) and internodes (during light treatments only; Fig. 2). Furthermore, a slightly deeper O_2 penetration depth was observed within the immediate rhizosphere of *Z. muelleri*, here defined as from the oxic microshield/reduced sediment interface to the last measured point in the rhizosphere (i.e. *c.* 0.3–5 mm distance away from the belowground tissue) as compared to the bulk artificial sediment (Supporting Information Figs S1–S3; except during hypoxic water column conditions (further described in Notes S1)). H_2S was completely removed from the artificial sediment surrounding the BM, as well as from the first sections of the rhizome (until internode 2), and the H_2S concentration was generally highly reduced (up to 20-fold) within the immediate rhizosphere, as compared to the bulk artificial sediment concentrations measured at a similar depth (Figs 2, S1, S2; except during hypoxic water column conditions). As a reference to the measurements at the BM, H_2S microprofiles were performed at the same vertical depth but *c.* 5 mm away from the meristematic regions of the rhizome, and confirmed that H_2S was present at concentrations up to 23 μmol H_2S l^{-1} just outside the immediate rhizosphere (Fig. S4).

No or low radial O_2 release was detectable from the root bundles as well as further down the rhizome – that is, away from the growing direction (Fig. 3; data from root bundle 2 not shown). This correlated with the relatively high H_2S concentrations (> 200 μmol H_2S l^{-1}) measured in the artificial sediment surrounding the root tips (Fig. 3; dark treatment).

In the immediate rhizosphere of the meristematic tissue, pH values reached up to *c.* 7.9 as compared to pH *c.* 6.2 in the bulk of the artificial sediment at similar vertical depth (Figs 2, S1, S2). Within the immediate rhizosphere, pH decreased towards the root tips (Fig. 3), reaching pH values of *c.* 6.0 at the root tip surface. Due to the horizontal orientation of the belowground tissue in the flow chamber, these findings could not have been simply a result of the vertical pH microgradient present in the reduced artificial sediment (Figs 1, S1, S2).

Microgradients and oxic microshield

At an incident irradiance of 350 μmol photons m^{-2} s^{-1}, radial O_2 release rates reached local maxima of *c.* 500 nmol O_2 cm^{-2} h^{-1} at the base of the leaf sheath, located at the meristematic region of the rhizome (Fig. 2; plant 2, node 1; Table 1). This correlated with a complete removal of H_2S in the same region (Fig. 2). The highest re-oxidation rate of H_2S was measured at the second internode of plant 2 during the dark treatment, reaching *c.* 48 nmol H_2S cm^{-2} h^{-1}. This somewhat unexpected region of the rhizome consuming most H_2S per unit time was likely a result of the almost complete re-oxidation and consequent removal of H_2S in the immediate rhizosphere of the meristematic regions of the rhizome (Fig. 2; Table 1). Hence, flux calculation from this region with the highest O_2 leakage was

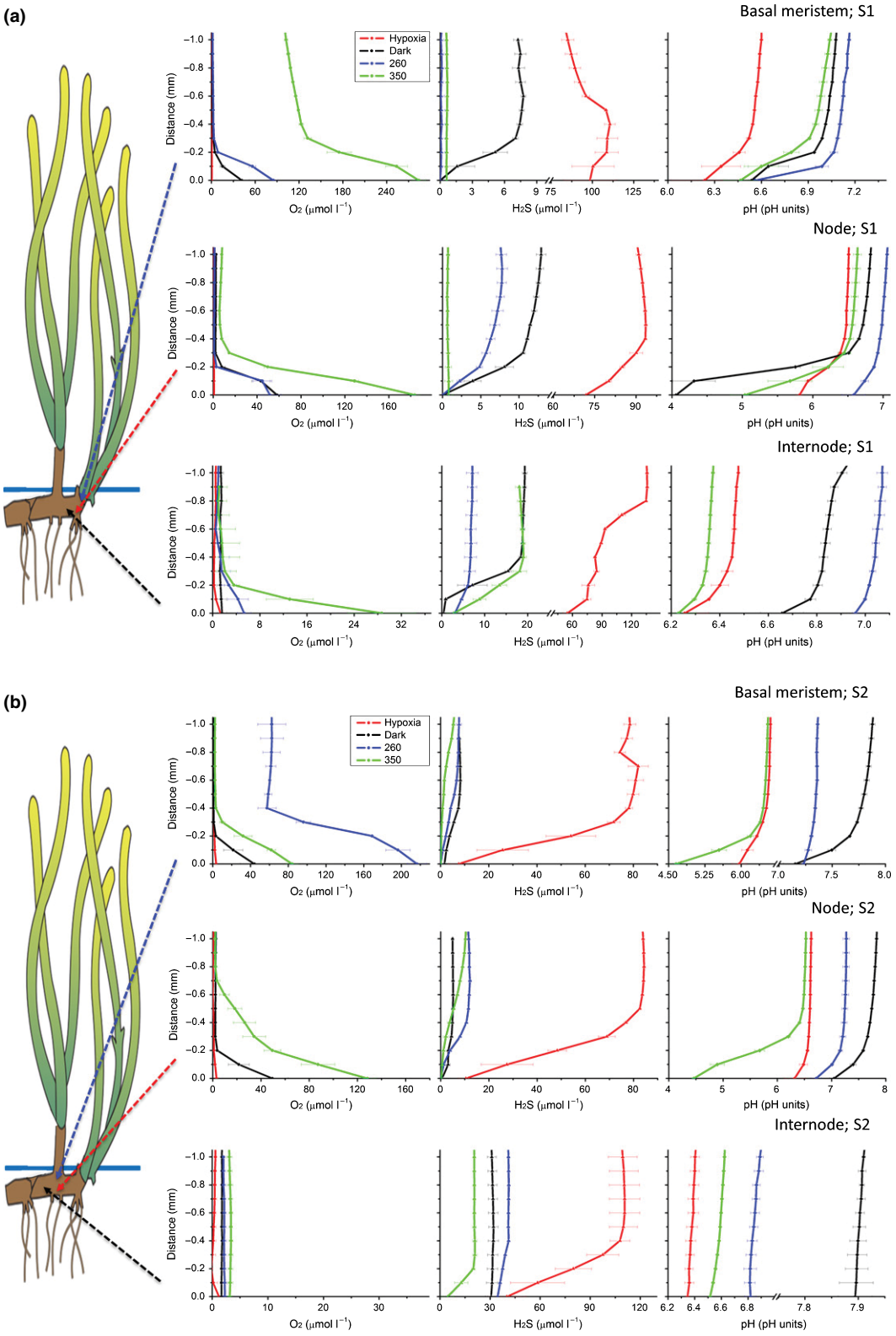

Fig. 2 The dynamics of the belowground chemical microenvironment of *Zostera muelleri* under experimentally changed environmental conditions as mapped with microelectrodes, illustrating the rhizome region including basal meristems with leaf sheath: (a) shoot 1; (b) shoot 2. The *x*- and *y*-axis are organized spatially, thus reflecting the actual orientation of the belowground microsensor measurements. Y = 0 indicate the belowground tissue surface. Error bars are ± SD. $n = 2–4$. The illustration of *Z. muelleri* originates from the IAN/UMCES symbol and image libraries (Diana Kleine, Integration and Application Network (IAN), University of Maryland Center for Environmental Science (ian.umces.edu/imagelibrary/)).

New Phytologist (2015) 205: 1264–1276
www.newphytologist.com

Table 1 Radial oxygen release (O_2 flux), oxygen concentration at the belowground tissue surface, H_2S consumption within the oxic microshield, total sulphide concentration at the tissue surface (S) and at the oxic microzone-reduced sediment interface (I), and ΔpH through the oxic microshield in *Zostera muelleri*

Treatment (μmol photons m^{-2} s^{-1})		O_2 flux (nmol O_2 cm^{-2} h^{-1})	O_2 at surface (μM)	H_2S consumption (nmol H_2S cm^{-2} h^{-1})	Total sulphide: surface & interface (S: I) (μM)	ΔpH (pH units)
0	BM	170.8 ± 34	68.8 ± 21	15.8 ± 1.6	1.2:24.8	0.90 ± 0.4
	N	125.4 ± 29	45.5 ± 8.8	16.5 ± 4.3	0.7:20.5	1.69 ± 0.4
	IN	0.5 ± 0.5	1.5 ± 0.7	37.3 ± 9	0.5:27.8	0.56 ± 0.5
	IN2	0.6 ± 0.5	2.1 ± 0.4	25.2 ± 23	221.3:251.9	0.02 ± 0.0
	RM	(–)	2.0 ± 0.3	(–)	(S: 253.5)	0.03
	RA	(–)	0.8 ± 0.1	(–)	(S: 271.0)	0.00
260	BM	355.2 ± 66	150.6 ± 66	3.9 ± 3.9	0.0:9.6	0.33 ± 0.2
	N	312.5 ± 123	134.0 ± 82	19.5 ± 5.3	0.0:27.5	0.44 ± 0.1
	IN	9.9	5.3 ± 1.2	8.8	7.5:18.4	0.08
	IN2	0.4	2.3 ± 0.4	12.1	70.9:85.7	0.01
	RM	(–)	1.3 ± 0.1	(–)	(S: 77.2)	0.01
	RA	(–)	0.7 ± 0.0	(–)	(S: 156.1)	0.00
350	BM	304.6 ± 108	184.1 ± 100	5.3 ± 5.3	0.5:1.4	1.14 ± 0.7
	N	395.0 ± 102	155.9 ± 28	5.9 ± 5.9	0.5:3.1	1.72 ± 0.2
	IN	92.8	28.7 ± 5.8	29.9	3.5:25.8	0.12
	IN2	0.0	3.1 ± 0.5	42.7	7.0:33.6	0.07
	RM	(–)	1.1 ± 2.3	(–)	(S: 63.7)	0.01
	RA	(–)	1.8 ± 0.4	(–)	(S: 123.9)	0.00
Hypoxia	BM	1.8 ± 1.7	1.4 ± 0.7	86.4 ± 57	67.1:145.8	0.29 ± 0.1
	N	2.0 ± 2.0	1.3 ± 0.6	81.2 ± 44	46.6:130.0	0.30 ± 0.1
	IN	2.0 ± 2.0	1.0 ± 0.1	59.8	70.4:120.2	0.26 ± 0.1
	IN2	2.5 ± 2.5	0.6 ± 0.4	110.6	54.3:148.2	0.02 ± 0.0
	RM	(–)	0.7 ± 0.2	8.7	(S: 113.5)	0.01
	RA	(–)	0.7 ± 0.1	(–)	(S: 102.3)	0.00

Calculated for each of the four different treatments: dark, 260 μmol photons m^{-2} s^{-1}, 350 μmol photons m^{-2} s^{-1} and hypoxia, at the basal meristem with leaf sheath (BM); node (N); internode (IN); mature zone of roots (RM); and apical meristem region of roots (RA). Mean values ± SE (except internode and root values which are given as mean ± SD); and the total sulphide concentration which is given as a mean (n = 3–15). As flux rates are calculated from mean values, only SE are provided. –, zero flux rate. Additional statistical information confirming the resemblance between the examined plants is provided in Supporting Information Fig. S5.

New Phytologist

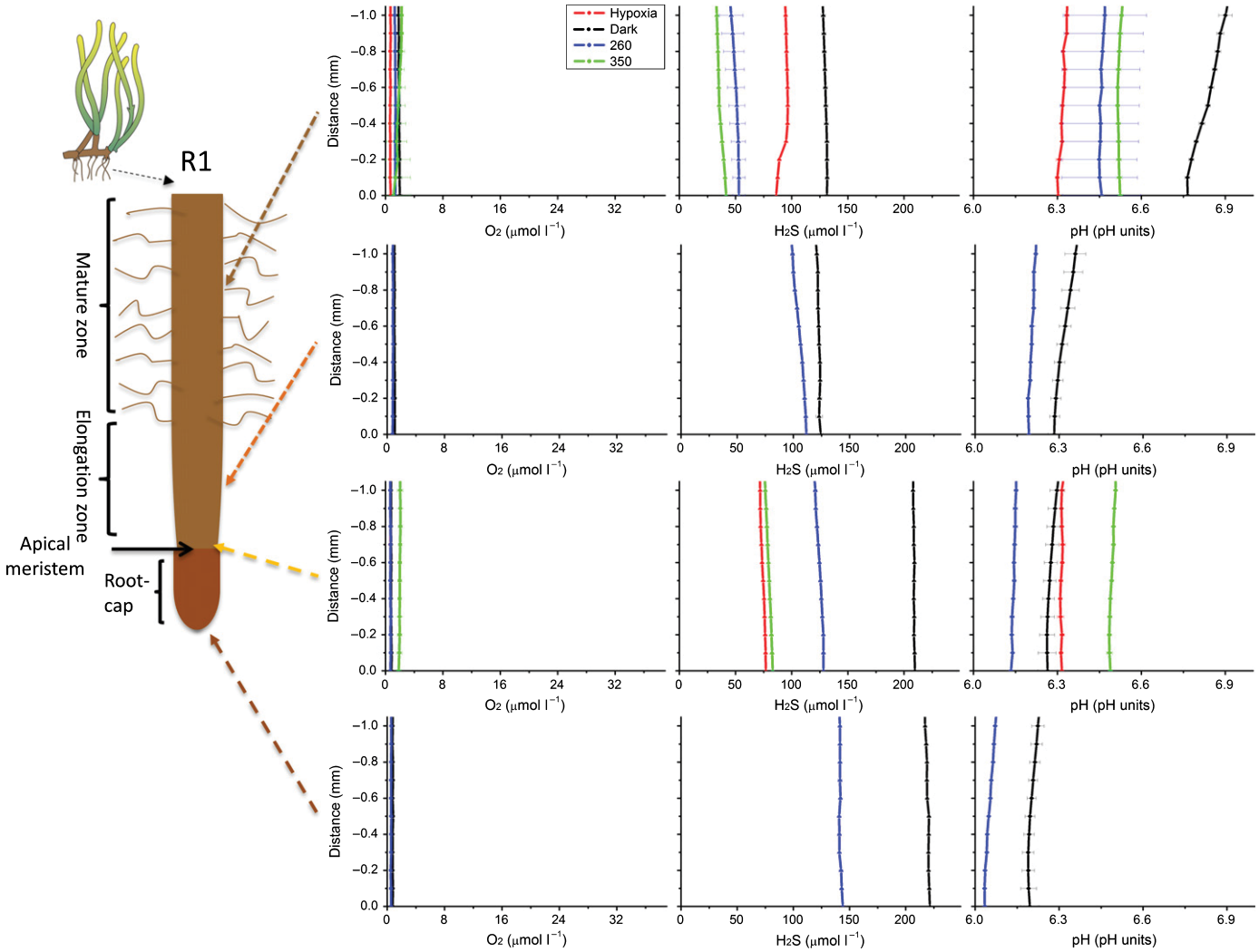

Fig. 3 Microprofiles showing the belowground microenvironment surrounding the roots of the first root-bundle (R1) in *Zostera muelleri*. Y = 0 indicates the belowground tissue surface. Error bars are ± SD. $n = 2–4$. Abbreviations are explained in the main text. Seagrass illustration from ian.umces.edu/imagelibrary/.

impossible. The highest O_2 release rates were measured at the meristematic regions of the rhizome (i.e. BM and nodes), with > 3-fold higher release rates as compared to any other regions of the belowground tissue (Table 1; expect during hypoxia conditions). Inside the oxic microshield, pH levels decreased towards the tissue surface with an average of *c.* 1 pH unit (Table 1). A close-up of the oxic microshield and the overall dynamics of the chemical microenvironment within the immediate rhizosphere, as well as throughout the oxic microzone is shown in Fig. 4.

Changing environmental conditions

The main difference between the light and dark treatments was the establishment of an oxic microshield around the first internode during illumination, as a result of radial O_2 release from this section of the plant (Fig. 2). At the tissue surface of the first internode, an average radial O_2 release rate of 93 nmol O_2 cm^{-2} h^{-1} and an average H_2S consumption rate of 30 nmol H_2S cm^{-2} h^{-1} was found, under an incident irradiance of 350 μmol photons m^{-2} s^{-1} (Table 1).

The radial O_2 release from the meristematic regions of the rhizome increased from 2 nmol O_2 cm^{-2} h^{-1} during hypoxia to 395 nmol O_2 cm^{-2} h^{-1} at an incident irradiance of 350 μmol photons m^{-2} s^{-1} in an air-saturated water column (Table 1).

The H_2S concentration at the surface of this region varied between 0 and *c.* 2 μmol H_2S l^{-1} in darkness, and between 0 and 1 μmol H_2S l^{-1} under the highest experimental incident irradiance (350 μmol photons m^{-2} s^{-1}; Fig. 2). During water column hypoxia, the H_2S concentration increased to between 8 and 99 μmol H_2S l^{-1} (Fig. 2).

The low or lacking radial O_2 release from the belowground tissue during and after water column hypoxia thus resulted in relatively high H_2S concentrations at the belowground tissue surface averaging 56 μmol H_2S l^{-1} (Figs 2, 3; Table 1). These findings suggest very limited consumption and removal of H_2S

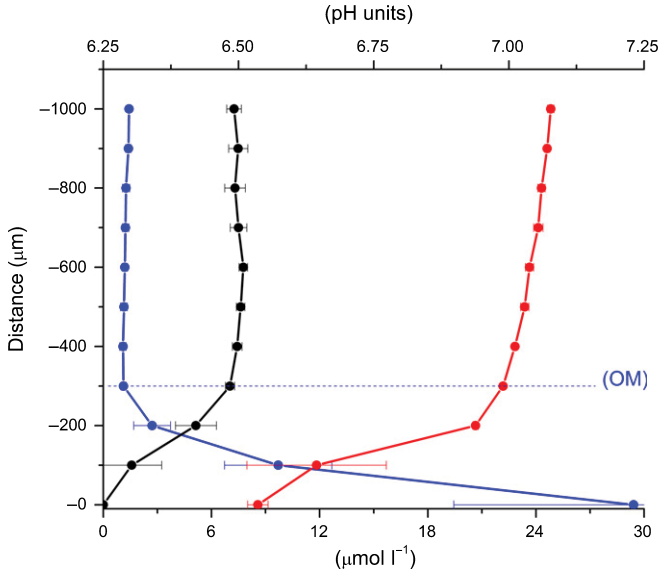

Fig. 4 Selected microprofiles showing the oxic microshield (OM) at the basal meristem with leaf sheath in *Zostera muelleri*. [O_2] (blue circles), [H_2S] (black circles) and pH (red circles) values measured at increasing distance away from the belowground tissue (base of the leaf sheath), illustrating the dynamics of the belowground chemical microenvironment across the oxygen–sulphide interface as well as throughout the oxic microzone. Y = 0 indicates the belowground tissue surface. Error bars are ± SD (n = 3). The microprofiles shown are from the dark treatment.

during the hypoxia treatment as a result of the much lower oxidation capability of the belowground tissue. Furthermore, *Z. muelleri* specimens showed low recovery after the hypoxia treatment, where no belowground radial O_2 release was detectable for a period of 48 h after the exposure (12 h : 12 h, light : dark cycle; leaf canopy exposed to 100% air saturated water column during the recovery time), and a loss of aboveground biomass was observed (i.e. detachment of leaves; data not shown).

Oxygen source and rhizome histology

Histological studies of the BM and the surrounding leaf sheath revealed extensive internal gas channels (lacunar system) in the tissue of the leaf sheath at the meristematic region of the rhizome, in addition to gas channels in the meristematic tissue (Fig. 5). The transverse sections of the first internode, that is, further away from the growth direction, also showed well-developed aerenchyma situated in the cortex in a circular orientation close to the tissue centre (Fig. 5). Moreover, a central stele was distinct in the cross-tissue section of the internode, and a newly formed root bundle, clearly impeding the distribution of the aerenchyma, was visible in the cross-tissue section of the basal meristem area (Fig. 5).

PAM fluorometry measurements

The maximum quantum yields of PSII measured at the centre of each leaf in the middle of the leaf canopy was *c.* 0.67 for both plants (Table 2). After exposure to hypoxic conditions in the water column, the maximum quantum yield decreased 6% to

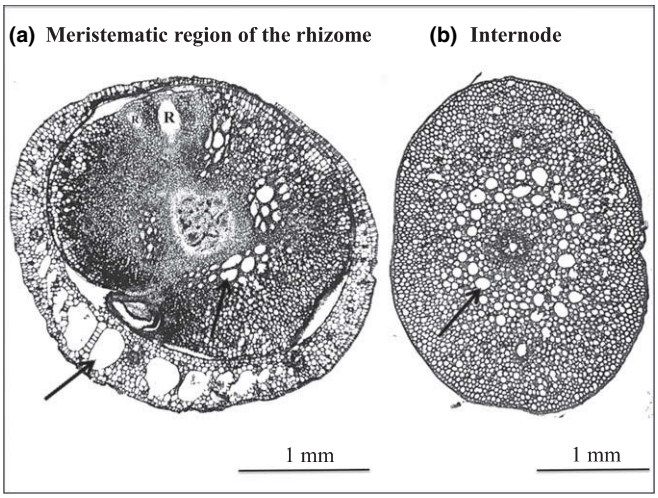

Fig. 5 Transverse sections of the rhizome in *Zostera muelleri*. (a) Meristematic region of the rhizome, including the surrounding leaf sheath; (b) internode. Black arrows show aerenchyma (internal lacunar system). Note the extensive distribution of the internal gas channels in the leaf sheath. R, initial formation of a root bundle.

0.61 (measured on plant 2, n = 4; Table 2). The effective quantum yield increased 23% (from 0.43 to 0.53) when the light intensity was increased from 260 to 350 µmol photons m^{-2} s^{-1}, but decreased by > 50% (to 0.27) after exposure to hypoxic conditions under an incident irradiance of 350 µmol photons m^{-2} s^{-1} (Table 2). These results verify that the measured microprofiles of the chemical microenvironment represent the dynamics of healthy and photosynthetic competent seagrasses (under the light : dark treatments) and that the seagrass photosynthetic quantum efficiency was affected by the hypoxic conditions (measured after a 24 h recovery time; 12 h : 12 h, light : dark cycle).

Discussion

Our results show that the seagrass *Zostera muelleri* can modify the biogeochemical conditions of its immediate rhizosphere, via O_2 release from belowground tissue, resulting in an almost complete re-oxidation of phytotoxic H_2S around the basal meristems with leaf sheath (BM) and rhizome in the growing direction (Figs 2, 6). This supports earlier findings in studies of *Thalassia* sp., showing significantly decreased sulphate reduction rates and H_2S pools in seagrass-vegetated sediment as compared to nonvegetated areas (Borum *et al.*, 2005; Holmer *et al.*, 2006). The continuous release of O_2 from the belowground tissue of *Z. muelleri* likely ensures the maintenance of an oxic microshield around vital and metabolically active parts of the plant (Figs 2, 4). The oxic microshield was widest at the base of the leaf sheath (Fig. 2; Table 1), which likely protects this important but vulnerable part of the plant from H_2S intrusion. The leaf sheath surrounds the meristematic plant tissue that, owing to its compact anatomy, has poorly developed aerenchyma, wherefore O_2 transport and supply to this sensitive area is impeded (Raun & Borum, 2013). This is supported by our observations of the morphological characteristics of the aerenchyma in the leaf sheath (Fig. 5), showing a

Table 2 Maximum and effective quantum yields of photosystem II (PSII) measured at the centre of the leaf in the middle of the leaf canopy of both vertical shoots in *Zostera muelleri*

	F_v/F_m max	$\Delta F/F_m'$ effective	Incident irradiance (μmol photons m^{-2} s^{-1})
Plant 1	0.67 ± 0.1	0.43 ± 0.1	260
Plant 2	0.67 ± 0.1	0.53 ± 0.1	350
Plant 2 (after HYPOXIA)	0.61 ± 0.1	0.26 ± 0.1	350

The after hypoxia measurements were conducted after a 24 h, 12 h : 12 h, light : dark cycle. Leaves were exposed to a 100% air saturated water column during the 24 h recovery time. Means ± SD (n = 2–4).

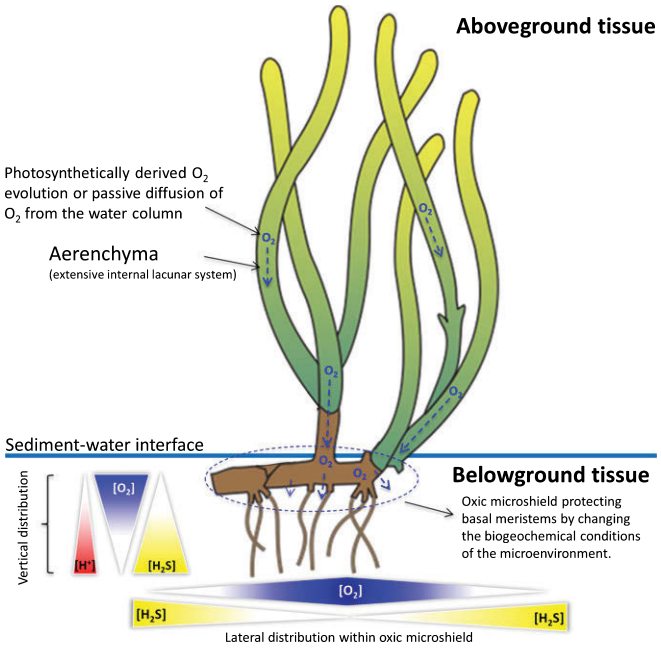

Fig. 6 Conceptual diagram visualizing the results of the microelectrode measurements performed in the belowground microenvironment of *Zostera muelleri* and presented here in this study. The colour gradient in the immediate rhizosphere indicates the relative concentration of the chemical species (blue, oxygen; yellow, H_2S; red, pH value (indicated as the relative amount of hydrogen ions)). Seagrass illustration from ian.umces.edu/imagelibrary/.

well-developed lacunar system at the basal meristems with large internal gas channels, thus enabling rapid and extensive O_2 release to the rhizosphere. Furthermore, a slightly deeper O_2 penetration and a downward movement of the H_2S front were found within the immediate rhizosphere as compared to the bulk artificial sediment (Figs S1, S2), a result of plant-mediated alterations of the belowground biogeochemical microenvironment, whereby the plants accommodate their own growth.

The radial O_2 fluxes from the meristematic regions of the rhizome (up to *c.* 5 mmol O_2 m^{-2} h^{-1} in light and 3.32 mmol O_2 m^{-2} h^{-1} in darkness; Fig. 2; Table 1) are similar to previously reported rates measured in the rhizosphere of *Cymodocea rotundata* (5.25 mmol O_2 m^{-2} h^{-1} in light and 2.28 mmol O_2 m^{-2} h^{-1} in darkness; Pedersen *et al.*, 1998). Earlier studies have shown that photosynthetically derived O_2 evolution during illumination results in an enhanced O_2 partial pressure in the internal gas channels of the plant. In darkness, on the other hand, the belowground tissue is supported only by passive diffusion from the surrounding water column through the leaf tissue and into the lacunar system (Greve *et al.*, 2003; Sand-Jensen *et al.*, 2005; Borum *et al.*, 2006). This is supported by our findings of higher O_2 release during light exposure, as well as the formation of an oxic microshield around the first internode as a result of O_2 release from the rhizome under an incident irradiance of 350 μmol photons m^{-2} s^{-1} (Fig. 2). The thickness of the oxic microshield (*c.* 300 μm; Figs 2, 4) surrounding the rhizome of *Z. muelleri* was similar to previous measurements around *Z. marina* in natural sediment, where Jensen *et al.* (2005) found an *c.* 500-μm-thick O_2 microzone surrounding the root tip. The O_2 demand of the reduced artificial sediment in our experimental setup was thus of similar magnitude as in natural settings. Previous O_2 microelectrode and planar optode studies of *Z. marina* roots (Jensen *et al.*, 2005; Frederiksen & Glud, 2006) demonstrated a heterogeneous microdistribution of O_2 along the first actively growing root bundle, with O_2 mainly leaking out from around the apical meristem of the root tip (i.e. 1–2 mm away from root apex). Low rates of O_2 release were also observed from the meristematic region of the rhizome of *Z. marina* by Jensen *et al.* (2005), indicating an analogous protection mechanism provided by the leaf sheath to the diminished gas channels in the compact meristematic tissue in this particular *Zostera* species. This is also supported by findings by Caffrey & Kemp (1991), who detected O_2 release to the rhizosphere from both roots and rhizomes of *Z. marina*.

The observed co-existence of H_2S and O_2 within the oxic microzone (Figs 2, 4) suggests that spontaneous chemical re-oxidation was the dominant sulphide oxidizing mechanism in this experiment, as bacteria-mediated oxidation is 10^4–10^5 times faster than chemical oxidation and thus rarely allows for co-existence to such temporal and spatial extents (Jørgensen & Revsbech, 1983; Nelson *et al.*, 1986; Pedersen *et al.*, 2004). However, microbially mediated oxidation of H_2S is likely more important in natural sediments in which the bacterial abundance is much higher than in the artificial sediment employed in this study. As such, the presence of sulphide-oxidizing bacteria would lead to shorter turnover time of H_2S and decrease the likelihood of H_2S to reach the rhizome in the presence of O_2 (Jørgensen & Revsbech, 1983; Nelson *et al.*, 1986).

The decreased pH levels found within the oxic microshield of the meristematic regions of the rhizome may be a result of the formation of sulphuric acid as a byproduct of the spontaneous chemical reactions between O_2 and H_2S (Figs 2, 4). Interestingly, such locally decreased pH levels could lead to the release of sediment bound phosphorus, which is often considered a limiting nutrient in carbonate-rich marine sediments (Fourqurean & Zieman, 2002; Holmer *et al.*, 2006), thus allowing for these plants to grow in phosphorus-limited regions (Holmer *et al.*, 2006). The increased pH just outside the oxic microshield, as compared to the bulk artificial sediment (Figs 2, 4), indicates that *Z. muelleri* may secrete chemical substances (allelochemicals) to

compensate for the generally decreased pH levels in the oxic microzone. An increase in the sediment pH would furthermore lead to a decrease in the H_2S concentrations in the immediate rhizosphere as a result of a pH-induced change in the sulphide equilibrium towards nonphytotoxic HS^- ions, thus acting as a counterbalance to the supposedly plant-induced formation of sulphuric acid. The enhanced pH level in the rhizosphere could consequently act as an additional chemical defence mechanism against toxic H_2S. This potential importance of pH changes in the rhizosphere of aquatic macrophytes has largely been overlooked in previous studies (Caffrey & Kemp, 1991; Pedersen *et al.*, 1998; Jensen *et al.*, 2005).

The limited O_2 release during water column hypoxia (Fig. 2) resulted in the deterioration of the oxic microshield and a concomitant increase in the flux of H_2S towards the tissue surface (Table 1). This likely enhanced the risk of H_2S intrusion into the plant tissue as H_2S reaches the tissue surface as a consequence of inadequate internal aeration (Table 1; Fig. 2). Particularly interesting is the observation of H_2S intrusion into the mature zone of roots when exposed to hypoxic conditions (Fig. 3). This was not observed in any of the other treatments (i.e. an influx of H_2S) and thus strongly suggests that this happened as a result of lowered O_2 release from the rhizome and less O_2 support to the roots (Fig. 3). These results are supported by the findings of Pedersen *et al.* (2004), showing H_2S intrusion into seagrass meristem tissue at low–moderate water column O_2 concentrations (*c.* 35% of air saturation). In our study, we found a slightly enhanced O_2 compensation point of *c.* 50% of air saturation in the water column – that is, the O_2 concentration where the total O_2 demand exceeds the rate of passive O_2 diffusion from the surrounding water column. This can most likely be explained by relatively thicker diffusive boundary layers over the leaves (Binzer *et al.*, 2005), although enhanced plant respiration and a higher O_2 demand of the artificial sediment are also possible explanations.

A recent study by Raun & Borum (2013) showed that internal meristematic anoxia (or hypoxia) occurred in *Z. marina* at a water column O_2 concentration of *c.* 30% air saturation at 15°C, but also at *c.* 60% air saturation at 25°C. High temperatures can thus have a substantial negative impact on the O_2 concentrations of the meristematic tissue as a result of increased plant tissue respiration. The experiments of Raun & Borum (2013) were conducted in water-filled jars – that is with the above- and belowground tissue experiencing exactly the same conditions – and did not take into account the potential importance of bacterial respiration and spontaneous chemical reactions such as H_2S re-oxidation. Hence, a slight decrease or increase in one of the numerous sinks or sources of O_2 could explain the higher O_2 compensation point seen in our experiment (Fig. 2; Table 1).

No radial O_2 release was found from the roots of *Z. muelleri* (Fig. 3). A barrier to radial O_2 release from the root-region of seagrasses has previously been shown to be restricted to the mature zone of the roots of *Z. marina*, with O_2 leaking out from around the root cap (Jensen *et al.*, 2005). Roots growing in reduced environments rely on a continued supply of O_2 to the active apical meristem during elongation. A barrier to O_2 release, such as that provided by casparian band-like structures composed of suberin (Barnabes, 1996), can ensure an efficient transport of O_2 to the roots, as well as provide protection against intrusion of phytotoxic compounds such as H_2S. Additionally, the oxic microzone described in this study results in a protective oxidized zone, in which new roots can form and reach maturity with developed barriers to O_2 release and H_2S intrusion (Fig. 7).

Loss of seagrass meadows has been related to H_2S poisoning during water column hypoxia (Pedersen *et al.*, 2004; Borum *et al.*, 2005), as the internal O_2 partial pressure of the aerenchyma has been found to be highly correlated with the water column O_2 content (Pedersen *et al.*, 2004; Borum *et al.*, 2005). Water column hypoxia leads to inadequate internal aeration, which in turn may result in H_2S intrusion. Our results strongly support these previous findings showing that seagrass is more sensitive to water column hypoxia during night-time, where there is no photosynthesis-driven O_2 supply to the rhizosphere. This underlines the importance of the diffusive supply of water column O_2 over the seagrass leaf DBL during the night. Sufficient oxygen support from the water column in darkness ensures the maintenance of a protective oxic microshield around meristematic regions of the rhizome, and is thus vital for seagrass survival in highly reduced sediments.

In conclusion, we found that *Z. muelleri* is able to modify the chemical conditions of its immediate rhizosphere, resulting from high radial O_2 release from the base of the leaf sheath surrounding the meristematic regions of the rhizome. This enables oxidation of ambient phytotoxic H_2S, and thereby acts as a chemical defence mechanism, protecting the most vulnerable meristematic tissue. In addition, plant-mediated pH increase in the immediate rhizosphere likely reduces the concentration of phytotoxic H_2S by shifting the speciation of sulphide towards nonphytotoxic HS^- ions, thus leading to further detoxification of the belowground microenvironment. Water column hypoxia may lead to an inadequate internal O_2 supply to the belowground tissues,

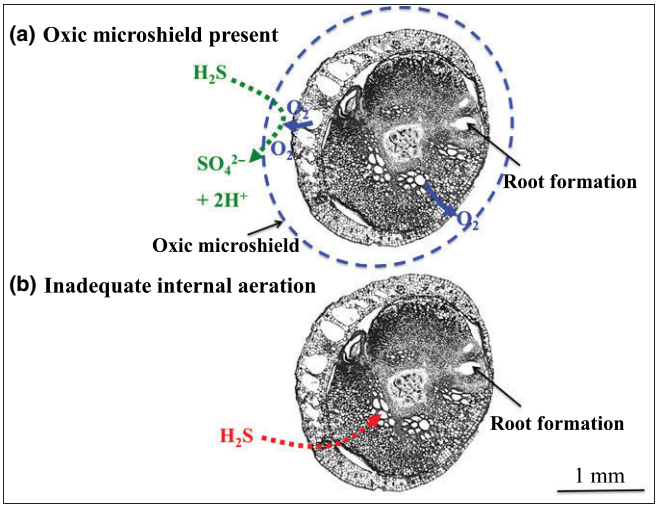

Fig. 7 Conceptual diagram illustrating the protecting oxic microshield at the meristematic region of the rhizome (cross tissue section of the basal meristem with leaf sheath) in *Zostera muelleri*. The presence of the oxic microshield leads to a plant-derived oxidation of sediment produced H_2S (a). Inadequate internal aeration may result in H_2S intrusion (b).

resulting in H_2S intrusion as a consequence of the degradation of the protecting oxic microshield. Prolonged or sudden degradation of the oxic microshield protecting the vital basal meristems may thus be the initial external chemical mechanism behind sudden seagrass die-off events in highly reduced marine sediments.

Acknowledgements

We thank Jens Borum and Ole Pedersen (University of Copenhagen) for helpful discussions during the outline and design process of the experimental setup. We thank Dr Milan Szabo and Dr Verena Schrameyer (UTS) for help and discussions during PAM measurements. We acknowledge Dr Ingo Burghardt, Jacqueline Loyola-Echeverria and Dr Mathieu Pernice for fruitful discussions during the preparation of our histology samples. This research was funded by grants from Augustinus Fonden, Fabrikant P.A. Fiskers Fond (K.E.B.), and the Danish Council for Independent Research, Natural Sciences (M.K.), the Australian Research Council (P.J.R., M.K.) and the University of Technology, Sydney (K.E.B.).

References

Almgren T, Hagstrom I. 1974. The oxidation rate of sulphide in sea water. *Water Research* **8**: 395–400.

Armstrong J, Armstrong W. 2001. Rice and *Phragmites*: effects of organic acids on growth, root permeability, and radial oxygen loss to the rhizosphere. *American Journal of Botany* **88**: 1359–1370.

Armstrong W. 1979. *Aeration in higher plants*. London, UK: Academic Press.

Barnabes AD. 1996. Casparian band-like structures in the root hypodermis of some aquatic angiosperms. *Aquatic Botany* **55**: 217–225.

Beer S, Vilenkin B, Weil A, Veste M, Susel L, Eshel A. 1998. Measuring photosynthetic rates in seagrasses by pulse amplitude modulated (PAM) fluorometry. *Marine Ecology Progress Series* **174**: 293–300.

Binzer T, Borum J, Pedersen O. 2005. Flow velocity affects internal oxygen conditions in the seagrass *Cymodocea nodosa*. *Aquatic Botany* **83**: 239–247.

Borum J, Pedersen O, Greve TM, Frankovich TA, Zieman JC, Fourqurean JW, Madden CJ. 2005. The potential role of plant oxygen and sulphide dynamics in die-off events of the tropical seagrass, *Thalassia testudinum*. *Journal of Ecology* **93**: 148–158.

Borum J, Sand-Jensen K, Binzer T, Pedersen O, Greve T. 2006. Oxygen movement in seagrasses. In: Larkum AWD, Orth JR, Duarte CM, eds. *Seagrasses: biology, ecology and conservation*. Dordrecht, the Netherlands: Springer, 255–270.

Brodersen KE, Nielsen DA, Ralph PJ, Kühl M. 2014. A split flow chamber with artificial sediment to examine the below-ground microenvironment of aquatic macrophytes. *Marine Biology*. doi: 10.1007/s00227-014-2542-3.

Caffrey JM, Kemp WM. 1991. Seasonal and spatial patterns of oxygen production, respiration and root-rhizome release in *Potamogeton perfoliatus* L. and *Zostera marina* L. *Aquatic Botany* **40**: 109–128.

Carlson J, Paul R, Yarbro LA, Barber TR. 1994. Relationship of sediment sulfide to mortality of *Thalassia testudinum* in Florida Bay. *Bulletin of Marine Science* **54**: 733–746.

Chen KY, Morris JC. 1972. Kinetics of oxidation of aqueous sulfide by O_2. *Environmental Science and Technology* **6**: 529–537.

Cline JD, Richards RA. 1969. Oxygenation of hydrogen sulfide in seawater at constant salinity, temperature, and pH. *Environmental Science and Technology* **3**: 838–843.

Colmer TD, Gibberd MR, Wiengweera A, Thin TK. 1998. The barrier to radial oxygen loss from roots of rice (*Oryza sativa* L.) is induced by growth in stagnant solution. *Journal of Experimental Botany* **49**: 1431–1436.

Costanza R. 1997. The value of the world's ecosystem services and natural capital. *Nature* **387**: 253–260.

Eghbal MA, Pennefather PS, O'Brien PJ. 2004. H_2S cytotoxicity mechanism involves reactive oxygen species formation and mitochondrial depolarisation. *Toxicology* **203**: 69–76.

Enstone DE, Peterson CA, Ma F. 2003. Root endodermis and exodermis: structure, function, and responses to the environment. *Journal of Plant Growth Regulation* **21**: 335–351.

Fourqurean JW, Zieman JC. 2002. Nutrient content of the seagrass *Thalassia testudinum* reveals regional patterns of relative availability of nitrogen and phosphorus in the Florida Keys, USA. *Biogeochemistry* **61**: 229–245.

Frederiksen MS, Glud RN. 2006. Oxygen dynamics in the rhizosphere of *Zostera marina*: a two-dimensional planar optode study. *Limnology and Oceanography* **51**: 1072–1083.

Frederiksen MS, Holmer M, Borum J, Kennedy H. 2006. Temporal and spatial variation of sulfide invasion in eelgrass (*Zostera marina*) as reflected by its sulfur isotopic composition. *Limnology and Oceanography* **51**: 2308–2318.

Goodman JL, Moore KA, Dennison WC. 1995. Photosynthetic responses of eelgrass (*Zostera marina* L.) to light and sediment sulfide in a shallow barrier island lagoon. *Aquatic Botany* **50**: 37–47.

Greve TM, Borum J, Pedersen O. 2003. Meristematic oxygen variability in eelgrass (*Zostera marina*). *Limnology and Oceanography* **48**: 210–216.

Holmer M, Bondgaard EJ. 2001. Photosynthetic and growth response of eelgrass to low oxygen and high sulfide concentrations during hypoxic events. *Aquatic Botany* **70**: 29–38.

Holmer M, Pedersen O, Ikejima K. 2006. Sulfur cycling and sulfide intrusion in mixed Southeast Asian tropical seagrass meadows. *Botanica Marina* **49**: 91–102.

Holmer M, Pedersen O, Krause-Jensen D, Olesen B, Hedegård Petersen M, Schopmeyer S, Koch M, Lomstein BA, Jensen HS. 2009. Sulfide intrusion in the tropical seagrasses *Thalassia testudinum* and *Syringodium filiforme*. *Estuarine, Coastal and Shelf Science* **85**: 319–326.

Jensen SI, Kühl M, Glud RN, Jørgensen LB, Prieme A. 2005. Oxic microzones and radial oxygen loss from roots of *Zostera marina*. *Marine Ecology Progress Series* **293**: 49–58.

Jensen SI, Kühl M, Prieme A. 2007. Different bacterial communities in the rhizoplane and bulk sediment of the seagrass *Zostera marina*. *FEMS Microbiology Ecology* **62**: 108–117.

Jeroschewski P, Steuckart C, Kühl M. 1996. An amperometric microsensor for the determination of H_2S in aquatic environments. *Analytical Chemistry* **68**: 4351–4357.

Jørgensen BB, Revsbech NP. 1983. Colorless sulfur bacteria, *Beggiatoa* spp. & *Thiovulum* spp., in O_2 and H_2S microgradients. *Applied and Environmental Microbiology* **45**: 1261–1270.

Kühl M, Revsbech NP. 2001. Biogeochemical microsensors for boundary layer studies. In: Boudreau BP, Jørgensen BB, eds. *The benthic boundary layer*. New York, NY, USA: Oxford University Press, 180–210.

Kühl M, Steuckart C, Eickert G, Jeroschewski P. 1998. A H_2S microsensor for profiling sediments and biofilms: application in acidic sediment. *Aquatic Microbial Ecology* **15**: 201–209.

Larkum AWD, Orth RJ, Duarte CM. 2006. *Seagrasses: biology, ecology and conservation*. Berlin, Germany: Springer.

Nelson DC, Jørgensen BB, Revsbech NP. 1986. Growth pattern and yield of a chemoautotrophic *Beggiatoa* sp. in oxygen-sulfide microgradients. *Applied and Environmental Microbiology* **52**: 225–233.

Orth RJ, Carruthers TJB, Dennison WC, Duarte CM, Fourqurean JW, Heck KL Jr, Hughes AR, Kendrick GA, Kenworthy WJ, Olyarnik S *et al.* 2006. A global crisis for seagrass ecosystems. *BioScience* **56**: 987–996.

Pedersen O, Binzer T, Borum J. 2004. Sulphide intrusion in eelgrass (*Zostera marina* L). *Plant, Cell & Environment* **27**: 595–602.

Pedersen O, Borum J, Duarte CM, Fortes MD. 1998. Oxygen dynamics in the rhizosphere of *Cymodocea rotundata*. *Marine Ecology Progress Series* **169**: 283–288.

Pedersen O, Borum J, Duarte CM, Fortes MD. 1999. ERRATUM: oxygen dynamics in the rhizosphere of *Cymodocea rotundata*. *Marine Ecology Progress Series* **178**: 310.

Perez-Perez ME, Lemaire SD, Crespo JL. 2012. Reactive oxygen species and autophagy in plants and algae. *Plant Physiology* **160**: 156–164.

Plus M, Deslous-Paoli J-M, Dagault F. 2003. Seagrass (*Zostera marina* L.) bed recolonisation after anoxia-induced full mortality. *Aquatic Botany* **77**: 121–134.

Ralph PJ, Short FT. 2002. Impact of the wasting disease pathogen, *Labyrinthula zosterae*, on photobiology of eelgrass *Zostera marina*. *Marine Ecology Progress Series* **226**: 265–271.

Ralph PJ, Tomasko D, Moore K, Seddon S, Macinnis-Ng CMO. 2006. Human impacts on seagrasses: eutrophication, sedimentation and contamination. In: Larkum AWD, Orth RJ, Duarte CM, eds. *Seagrasses: biology, ecology and conservation*. Berlin, Germany: Springer, 567–593.

Ramsing NB, Gundersen JK. 2014. *Seawater and gasses: tabulated physical parameters of interest to people working with microsensors in marine systems: unisense data tables*. Available from Unisense A/S, Denmark. [WWW document] URL http://www.unisense.com/files/PDF/Diverse/Seawater & Gases table.pdf [accessed 17 September 2014].

Raun AL, Borum J. 2013. Combined impact of water column oxygen and temperature on internal oxygen status and growth of *Zostera marina* seedlings and adult shoots. *Journal of Experimental Marine Biology and Ecology* **441**: 16–22.

Raven JA, Scrimgeour CM. 1997. The influence of anoxia on plants of saline habitates with special reference to the sulfur cycle. *Annals of Botany* **79**: 79–86.

Revsbech NP. 1989. An oxygen microsensor with a guard cathode. *Limnology and Oceanography* **34**: 474–478.

Robblee MB, Barber TR, Carlson PR Jr, Durako MJ, Fourqurean JW, Muehlstein LK, Prorter D, Yarbro LA, Zieman RT, Zieman JC. 1991. Mass mortality of the tropical seagrass *Thalassia testudinum* in Florida Bay (USA). *Marine Ecology Progress Series* **71**: 297–299.

Sand-Jensen K, Pedersen O, Binzer T, Borum J. 2005. Contrasting oxygen dynamics in the freshwater isoetid *Lobelia dortmanna* and the marine seagrass *Zostera marina*. *Annals of Botany* **96**: 613–623.

Seddon S, Connolly R, Edyvane KS. 2000. Large-scale seagrass dieback in northern Spencer Gulf, South Australia. *Aquatic Botany* **66**: 297–310.

Short FT, Duarte CM. 2001. Methods for the measurement of seagrass growth and production. In: Short FT, Coles RG, eds. *Global seagrass research methods*. Amsterdam, the Netherlands: Elsevier, 155–182.

Steen-Knudsen O. 2002. *Biological membranes: theory of transport, potentials and electric impulses*. Cambridge, UK: Cambridge University Press.

Truong DH, Eghbal MA, Hindmarsh W, Roth SH, O'Brien PJ. 2006. Molecular mechanisms of hydrogen sulfide toxicity. *Drug Metabolism Reviews* **38**: 733–744.

Waycott M, Duarte CM, Carruthers TJB, Orth RJ, Dennison WC, Olyarnik S, Calladine A, Fourqurean JW, Heck KL Jr, Hughes AR *et al.* 2009. Accelerating loss of seagrasses across the globe threatens coastal ecosystems. *Proceedings of the National Academy of Sciences, USA* **106**: 12377–12381.

Zieman JC, Fourqurean JW, Frankovich TA. 1999. Seagrass die-off in Florida Bay: long-term trends in abundance and growth of turtle grass, *Thalassia testudinum*. *Estuaries* **22**: 460–470.

Supporting Information

Additional supporting information may be found in the online version of this article.

Figs S1 and S2 The vertical distribution of O_2, H_2S and pH in the immediate rhizosphere of *Zostera muelleri* as compared to the reduced, bulk artificial sediment in plants 1 and 2, respectively.

Fig. S3 Conceptual diagram roughly illustrating the position of the microprofile measurements, as well as the defined zones of interest within the artificial sediment in this study.

Fig. S4 Microprofile of the H_2S concentration in the 'bulk' artificial sediment (at a *c.* 5 mm horizontal distance away from the basal meristem with leaf sheath of *Zostera muelleri*), thus serving as a reference to the H_2S measurements just at and at increasing distance away from the belowground tissue surface.

Fig. S5 The O_2 concentration at the meristematic tissue surface (in μM) under three different treatments.

Note S1 Additional methods, results and discussion.

Please note: Wiley Blackwell are not responsible for the content or functionality of any supporting information supplied by the authors. Any queries (other than missing material) should be directed to the *New Phytologist* Central Office.

Environmental Science & Technology

Article

pubs.acs.org/est

Optical Sensor Nanoparticles in Artificial Sediments—A New Tool To Visualize O_2 Dynamics around the Rhizome and Roots of Seagrasses

Klaus Koren,[†,#] Kasper E. Brodersen,[‡,#] Sofie L. Jakobsen,[†] and Michael Kühl*[,†,‡,§]

[†]Marine Biological Section, Department of Biology, University of Copenhagen, Helsingør DK-3000, Denmark

[‡]Plant Functional Biology and Climate Change Cluster, University of Technology Sydney, Ultimo, New South Wales 2007, Australia

[§]Singapore Centre on Environmental Life Sciences Engineering, School of Biological Sciences, Nanyang Technological University, Singapore 639798, Singapore

Supporting Information

ABSTRACT: Seagrass communities provide important ecosystems services in coastal environments but are threatened by anthropogenic impacts. Especially the ability of seagrasses to aerate their below-ground tissue and immediate rhizosphere to prevent sulfide intrusion from the surrounding sediment is critical for their resilience to environmental disturbance. There is a need for chemical techniques that can map the O_2 distribution and dynamics in the seagrass rhizosphere upon environmental changes and thereby identify critical stress thresholds of e.g. water flow, turbidity, and O_2 conditions in the water phase. In a novel experimental approach, we incorporated optical O_2 sensor nanoparticles into a transparent artificial sediment matrix consisting of pH-buffered deoxygenated sulfidic agar. Seagrass growth and photosynthesis was not inhibited in the experimental setup when the below-ground biomass was immobilized in the artificial sulfidic sediment with nanoparticles and showed root growth rates (~5 mm day^{-1}) and photosynthetic quantum yields (~0.7) comparable to healthy seagrasses in their natural habitat. We mapped the real-time below ground O_2 distribution and dynamics in the whole seagrass rhizosphere during experimental manipulation of light exposure and O_2 content in the overlaying water. Those manipulations showed that oxygen release from the belowground tissue is much higher in light as compared to darkness and that water column hypoxia leads to diminished oxygen levels around the rhizome/roots. Oxygen release was visualized and analyzed on a whole rhizosphere level, which is a substantial improvement to existing methods relying on point measurements with O_2 microsensors or partial mapping of the rhizosphere in close contact with a planar O_2 optode. The combined use of optical nanoparticle-based sensors with artificial sediments enables imaging of chemical microenvironments in the rhizosphere of aquatic plants at high spatiotemporal resolution with a relatively simple experimental setup and thus represents a significant methodological advancement for studies of environmental impacts on aquatic plant ecophysiology.

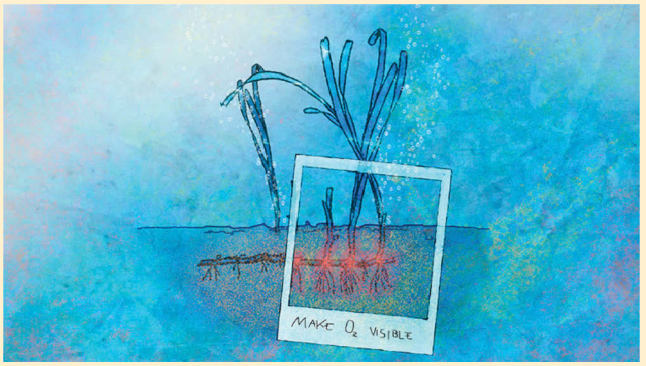

INTRODUCTION

Seagrasses are marine flowering plants that provide a range of essential eco-engineering services, such as facilitating carbon sequestration, improving water clarity, and protecting coastal areas against erosion.[1] Despite being considered as a high-value ecosystem, providing nursery areas and feeding grounds to numerous important commercial marine fish and crustacean species, seagrass meadows are currently declining with an alarming rate mainly due to human activity.[2,3] Seagrass plants mostly inhabit shallow coastal sediments, where they form an important coastal ecosystem with high productivity and biodiversity.[1,2] However, the below-ground biomass of seagrasses is anchored and grows in organic rich, reduced and often sulfidic sediments, which present a challenge to the plants and can potentially be involved in die-off events.[4,5] Sulfide, and especially dissolved H_2S, is highly toxic for seagrasses[6,7] that have developed a variety of structural defense mechanisms such as the presence of an intracellular gas-filled lacunar system (aerenchyma) enabling rapid and low-resistance exchange of gases between the above- and below-ground tissue and rhizosphere.[8] However, our understanding of the function of this system and its role for the survival of seagrasses under environmental stress is still incomplete. The chemical microenvironment in the seagrass rhizosphere exhibits a high spatiotemporal heterogeneity that remains to be studied in detail. Especially the O_2 dynamics in the rhizosphere is of importance as radial O_2 loss from the below-ground biomass can act as a microshield against toxic H_2S from the surrounding sediment.[9−11] Inadequate O_2 transport from seagrass leaves to

Received: November 24, 2014
Revised: January 15, 2015
Accepted: January 22, 2015

DOI: 10.1021/es505734b
Environ. Sci. Technol. XXXX, XXX, XXX−XXX

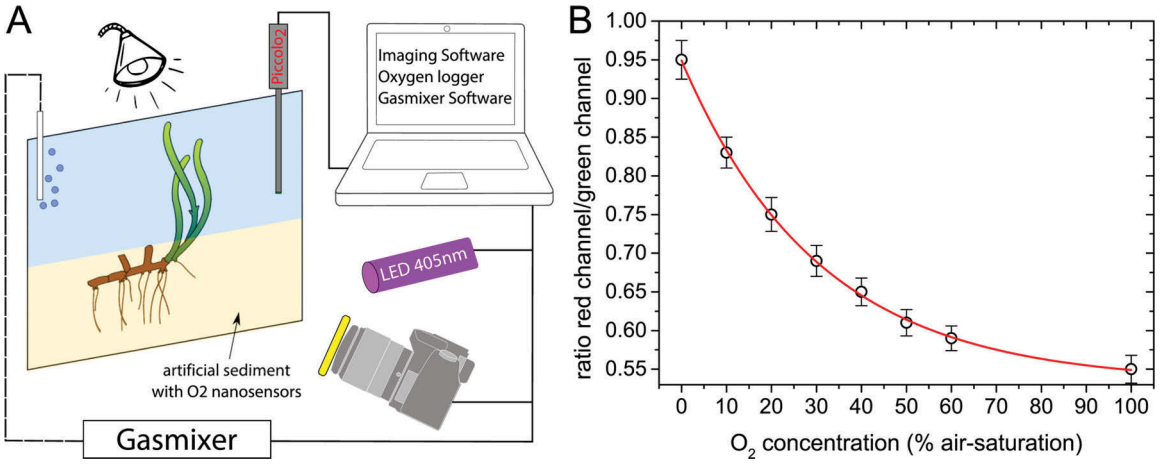

Figure 1. A: Experimental setup. The below-ground tissue of the seagrass is embedded in the artificial sediment containing the O_2 sensitive nanoparticles. A SLR camera and LED are mounted perpendicular to the transparent chamber wall. Gas supply and reference optode are immersed in the overlaying water. B: Calibration curve of the sensor nanoparticles in the artificial sediment. Symbols and error bars represent means ± SD (n = 3). The red curve shows a fit of an exponential decay function to the calibration data ($R^2 > 0.999$).

the below-ground tissue is regarded as a key mechanism in seagrass die-off events[12,13] upon anthropogenic impacts such as dredging and eutrophication affecting the transparency and/or O_2 level in the overlaying water.[14]

It has recently been shown that O_2 released from the meristematic region of the rhizome of the seagrass species *Zostera muelleri* subsp. *capricorni* alters the local below-ground chemical microenvironment by chemically reoxidizing H_2S and thereby detoxifying the surrounding sediment.[11] This chemical defense mechanism is highly affected by hypoxic water-column conditions during darkness, as the oxidation capacity of the below-ground tissue of seagrasses is completely dependent on passive diffusion of O_2 from the surrounding water-column, across diffusive boundary layers and into the aerenchyma when no O_2 is evolved via photosynthesis.[11−13]

Most studies of the O_2 dynamics in the seagrass rhizosphere have used electrochemical or optical microsensors[9−11,15] that enable measurements with a very high spatiotemporal resolution but only at a limited set of measuring points. Therefore, studying different regions of the rhizome is very tedious, and it is impossible to account for the complete O_2 distribution around the below-ground biomass. There is thus a need for techniques that can map the heterogeneous O_2 microdistribution and dynamics around the rhizome and roots of seagrasses over larger spatial scales.

Imaging of chemical parameters using planar optical sensor foils, i.e., planar optodes, is a powerful alternative to microsensor measurements.[16] While planar optodes are excellent tools for visualizing dynamic processes in sediments,[17−19] this approach is not as straightforward for investigations of the rhizosphere, where a good contact between the sensor foil and the plant tissue is needed. Achieving such a good contact is not easy and obviously only possible for selected parts of the roots at once.[20,21] Depending on the root geometry and the planar sensor layer thickness, diffusive smearing of the true O_2 distribution can also be induced due to the presence of the O_2-impermeable sensor foil up against the biomass.[22]

In the present study we used O_2 sensitive optical nanosensors[23] in combination with an artificial, semitransparent sulfidic sediment matrix to simultaneously map the O_2 dynamics in the whole rhizosphere of the seagrass *Zostera muelleri*. We present the new methodology and show its application for mapping responses in the rhizosphere O_2 microenvironment due to changes in irradiance and O_2 content in the overlaying water.

MATERIALS AND METHODS

Materials for the Nanosensors. Platinum(II) meso-(2,3,4,5,6-pentafluoro)phenyl porphyrin (PtTFPP) was bought from Frontier Scientific (www.frontiersci.com); Macrolex fluorescence yellow 10GN (MY) was obtained from Kremer Pigments (http://kremerpigments.com). The styrene maleic anhydride copolymer (PSMA with 8% MA, Mw: 250000 g*mol^{-1}) XIRAN was generously provided by Polyscope (http://www.polyscope.eu). Tetrahydrofuran (THF) was obtained by Sigma-Aldrich.

Materials for the Transparent, Artificial Sediment. Agar powder for microbiology (gel point ∼35 °C; gel strength >300 g cm^{-2}), HEPES buffer (*N*-(2-hydroxyethyl)piperazine-*N*′-(2-ethanesulfonic acid); pK_a (at 25 °C) = 7.48; useful pH range = 6.8−8.2), and sodium sulfide nonahydrate ($Na_2S·9H_2O$) were purchased from Sigma-Aldrich (www.sigmaaldrich.com).

Nanosensor Preparation. The sensor nanoparticles were prepared according to the previously described method by Mistlberger et al.[24] Briefly, 200 mg of PSMA, 3 mg of MY (reference dye), and 3 mg of PtTFPP (O_2 indicator) were dissolved in 20 g of THF. This mixture was quickly poured into 200 mL of vigorously stirred distilled water. After evaporating the THF under an air stream, the particle suspension was concentrated at elevated temperature (60 °C) until a concentration of 5 mg per mL was reached. The concentration was checked by drying and subsequent weighing of 1 mL of the particle suspension. The obtained particles have a size of several hundred nm and a strongly negative zeta potential of around −30 mV as shown elswhere.[24] The particle suspension could be stored over several weeks without any signs of sedimentation, color change, or change in the calibration characteristics.

Seagrass Collection. Seagrass specimens of *Zostera muelleri* subsp. *capricorni* (Asch.) S.W.L.Jacobs were collected from a shallow (<1 m deep) coastal site at Brisbane Waters, NSW, Australia. The plants were transported (in water from the sampling site) to a greenhouse facility at the University of

DOI: 10.1021/es505734b
Environ. Sci. Technol. XXXX, XXX, XXX−XXX

Technology Sydney, where they were kept under natural light at a salinity of ~34 ppt and a temperature of ~22 °C. Prior to the experiments, specimens were gently washed free of any adhering sediment particles before transferring them to the experimental chamber.

Experimental Setup. The experimental chamber (inner dimensions 10 × 130 × 120 mm) consisted of a custom-made narrow, transparent acrylic chamber with a removable front window made of polycarbonate for ease of access when casting the sediment and improved optical properties during imaging, respectively (see Figure 1 and the Supporting Information video). Illumination of the plant leaves was provided by a tungsten halogen lamp equipped with a collimating lens (KL-2500, Schott GmbH, Germany). Stirring and aeration of the water-column was obtained via a submerged Pasteur pipet connected to an air pump or a gas mixer (Sensorsense, The Netherlands).

Preparation of the Artificial Sediment. The transparent, artificial sediment consisted of a deoxygenated ~0.5% (w/w) agar-seawater solution (100 mL), buffered with HEPES (final concentration of 10 mM) and amended with O_2-sensitive nanoparticles (2% w/w) and Na_2S to a final H_2S concentration of 250 μM (at pH 7). Prior to casting the sediment, the agar powder had been prewashed overnight in cold seawater to improve clarity. The reduced, artificial sediment was thus constructed to mimic chemical settings in natural sediment while allowing for direct visual investigation of the below-ground tissue during measurements.

The sensor nanoparticles were added to the heated artificial sediment mixture during the preparation. Oxygen sensor nanoparticles could be homogeneously incorporated into the artificial sediment matrix with no visible formation of larger sensor particle aggregates in the agar. To ensure this, the timing of the nanoparticle addition to the agar is important, and this should be done shortly before the artificial sediment is poured into the chamber (i.e., at ~38 °C). The concentration of nanoparticles in the agar ensured a good measuring signal, while preserving a good visual transparency. To further avoid potential limitations of transparency, we placed the seagrass rhizome close to (without touching) the polycarbonate plate of the experimental chamber when pouring the agar with nanoparticles into the chamber (at an agar matrix temperature of ~36 °C that rapidly cooled to room temperature upon contact with the experimental chamber wall). The chamber could then be sealed and positioned in front of the imaging system. Gas supply from a gas mixer was ensured, and a fiber-optic optode (Pyro-Science GmbH, Germany) was introduced to continuously monitor the O_2 concentration in the water column. The leaf canopy was kept in the upper stirred water-phase. A schematic of the setup can be seen in Figure 1. A detailed video documentation of these preparation steps can be found in the Supporting Information.

Imaging Setup. We used a ratiometric RGB camera setup for O_2 imaging.[25] The system consisted of a SLR camera (EOS 1000D, Canon, Japan) combined with a macro objective (Macro 100 f2,8 D, Tokina, Japan) equipped with a 455 nm long pass filter (Uqgoptics.com). Excitation of sensor particles was achieved with a 405 nm multichip LED equipped with a bandpass filter (NT43-156, Edmundoptics.com). The LED was powered by a USB-controlled LED driver unit for fluorescence imaging applications (available from http://imaging.fish-n-chips.de). Image acquisition control of the SLR and LED was done with the software look@RGB (http://imaging.fish-n-chips.de).

Image Analysis and Calibration. Acquired images were split into red, green, and blue channels and analyzed using the freely available software ImageJ (http://rsbweb.nih.gov/ij/). In order to obtain O_2 concentration images the following steps were performed: First the red channel (O_2 sensitive emission of PtTFPP) and green channel (emission of the reference dye MY) images were divided using the ImageJ plugin Ratio Plus (http://rsb.info.nih.gov/ij/plugins/ratio-plus.html). Afterward, the obtained ratio-image was fitted with the previously obtained calibration curve using the Curve Fitting tool of ImageJ (exponential decay). The calibration curve was generated as follows. A small piece of nanosensor-containing nonsulfidic agar was immobilized in the chamber. Oxygen levels of the water on top of the agar were altered with the help of compressed air and nitrogen, which were mixed by a PC-controlled gas mixer (SensorSense, The Netherlands). Simultaneously, the O_2 level in the water column was monitored by means of a calibrated O_2 optode system (Oxygen dipping probe connected to Piccolo2 m; PyroScience GmbH, Aachen, Germany). To ensure that equilibrium was reached, each calibration step was held for 60 min. The calibration was obtained by linking the measured image ratios to the measured O_2 level (Figure 1). A visualization of the calibration process can be found in the Supporting Information (Figure S1).

Seagrass Photosynthetic Performance. We assessed the photosynthetic competence of various parts of the seagrasses using a fiber-optic pulse amplitude modulated (PAM) fluorometer (PocketPAM, Walz GmbH, Germany) measuring the quantum yield of the PSII photosynthetic electron transport in the dark adapted state (F_v/F_m = the maximal quantum yield) and in the presence of actinic light (YII = the effective quantum yield).[26]

Experimental Treatments. We monitored the O_2 distribution around the seagrass roots under 2 experimental manipulations:

i) During a light-dark transition, where the plant leaves were first illuminated with an incident photon irradiance of ~500 μmol photons m^{-2} s^{-1} for 90 min to ensure that equilibrium conditions were reached in the light. Thereafter, the external illumination was switched off, and the plant was left in the dark for 3 h. During the dark incubation, the image acquisition could be automated, while measurements in light required switching the external light source off for a brief period just before and during image acquisition.

ii) During decreasing O_2 contents in the water-column, from 100% air saturation down to ~0% air saturation. The plant was first kept at an irradiance of ~500 μmol photons m^{-2} s^{-1} for 90 min in air saturated water to ensure that equilibrium conditions was reached. Then the external illumination was switched off, and the overlaying water was flushed with N_2 gas for 2.5 h to simulate water column hypoxia. Finally the water-column was again bubbled with air, and the plant was still kept in the dark for another 4.5 h. The O_2 concentration in the water-column was monitored simultaneously by the above-mentioned fiber-optic O_2 optode. Image acquisition was performed as described above.

RESULTS AND DISCUSSION

Introduction of optical sensor nanoparticles into the artificial sediment did not affect the sensor performance. The calibration curve of the agar-immobilized O_2 nanoparticles showed the

DOI: 10.1021/es505734b
Environ. Sci. Technol. XXXX, XXX, XXX−XXX

expected exponential decay typical for optical O_2 sensors based on luminescence quenching[27] (Figure 1).

Obviously, it is important to assess potential effects of the artificial sediment with nanosensors on the seagrass health. In this study, we evaluated two plants of the species *Z. muelleri*. Both plant specimens tolerated the artificial sediment with nanoparticles well, and new root growth (at a rate of ~5 mm d^{-1}) was actually observed in both plants after a few days. Good plant health was also confirmed by measurements of photosynthetic performance of the two plants (Table 1). PAM fluorometry measurements in both plants revealed a high quantum efficiency of photosynthesis in the leaf canopy (shoot 1); i.e., maximum and effective quantum yields of PSII ~0.7 and ~0.6 (at a light intensity of 500 μmol photons m^{-2} s^{-1}), respectively. As seagrasses are considered healthy when maximum PSII quantum yields of the shoot are around 0.7,[28] we concluded that the two studied plants cultivated in the artificial sediment were healthy. Besides the shoot, the photosynthetic performance of the prophyllum, i.e., single leaves originating from the horizontal rhizome, was also evaluated. Whereas plant 1 had photosynthetically active prophyllums, albeit with a lower photosynthetic quantum efficiency than the fresh leaves, plant 2's prophyllums showed no photosynthetic activity (Table 1); these observations were also supported by the respective images of O_2 concentration around these structures (see Figure 2). The presence of photosynthetically active prophyllums was a surprising finding, as these older plant structures are typically considered inactive. A more detailed investigation of this finding was, however, beyond the scope of this study and will be examined in future work.

Table 1. Maximum (F_v/F_m) and Effective (Y(II)) Quantum Yields of PSII-Related Photosynthetic Electron Transport in Seagrass Leaves of Plants Mounted in the Experimental Setup with Artificial Sediment + O_2 Nanoparticles[a]

	shoot	prophyllum	prophyllum
plant 1	nodium 1	nodium 5	nodium 8
F_v/F_m	0.74 ± 0.01	0.61 ± 0.02	0.59 ± 0.02
Y(II)	0.60 ± 0.01	0.48 ± 0.02	0.39 ± 0.01
	shoot	prophyllum	prophyllum
plant 2	nodium 1	nodium 2	nodium 5
F_v/F_m	0.73 ± 0.01	(−)	(−)
Y(II)	0.58 ± 0.02	(−)	(−)

[a]Mean ± SD; n = 4–6. (−) indicates no photosynthetic activity.

While the presented O_2 nansosensor methodology is not applicable to natural nontransparent sediments, it is well suited to investigate the below-ground chemical microenvironment of seagrasses embedded in artificial transparent sediment matrices that mimic key aspects of the sediment biogeochemistry such as high sulfide contents.[11] With the experimental setup, both structural images of the two plants as well as images of O_2 concentration surrounding their below-ground biomass could be recorded (Figure 2). Both images were taken after exposing the plants to an irradiance of 500 μmol photons m^{-2} s^{-1} for 90 min. The O_2 distribution in the below-ground environment was evidently very different between the two investigated specimens. In plant 1, photosynthetically active prophyllums (one marked as P in each picture) oxidized the sediment, while plant 2 mainly showed O_2 leakage around the nodiums (marked as N), the basal meristem (B), and at the root tips. One of the benefits of the method presented here is that aligned structural and chemical (O_2 concentration) images can easily be obtained. While the chamber is illuminated by an external light source a structural image can be taken and by switching off the external light source and triggering the LED illumination, a luminescence image can be acquired that leads to an O_2 concentration image. In this way the position of structural elements (e.g., roots, rhizome) can be precisely aligned with the chemical information. A slight drawback is that due to the emission filter in front of the SLR camera, the structural picture appears slightly yellow.

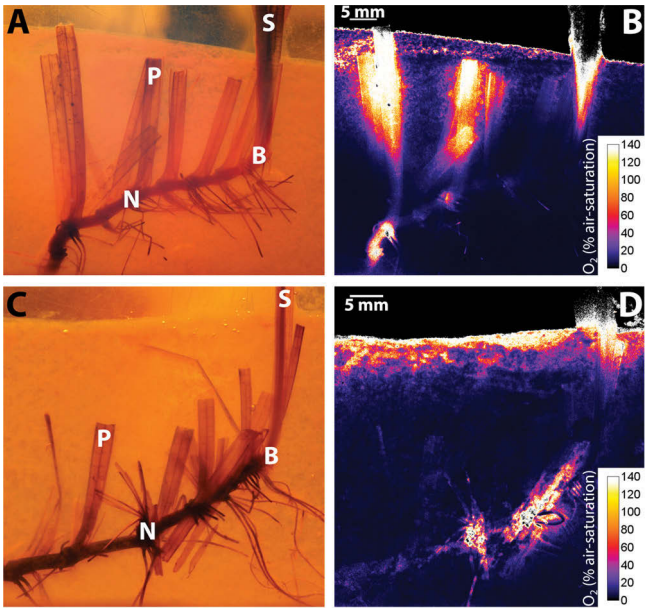

Figure 2. Structural images of the seagrass *Z. muelleri* mounted in the artificial sediment (A, C) and the respective false color images of the O_2 concentration distribution (B, D) around plant 1 (top) and plant 2 (bottom) recorded after 90 min illumination of the leaves with 500 μmol photons m^{-2} s^{-1}. Several plant structural elements are pointed out: S – shoot, N – nodium, P – prophyllum, B – basal meristem.

The O_2 imaging showed that it is possible to simultaneously map the O_2 distribution within the entire seagrass rhizosphere (Figure 2, 3), and the method is well suited to observe changes in sediment oxygenation under different environmental conditions. Light exposure of the leaf canopy thus dramatically changed the O_2 status around the roots and rhizome (Figure 3). Under high irradiance, seagrass leaf photosynthesis produced O_2 that was transported to the below-ground biomass of the plant, where it supported aerobic metabolism and leaked into the immediate rhizosphere leading to locally increasing O_2 levels during illumination (Figure 3A, 3C; region of interest (ROI), 1–3). During illumination, leakage of O_2 was also observed at the node region (ROI 2) and the basal meristem (ROI 3). In contrast to the area on top of one of the prophyllums (ROI 1), this leakage did not originate from photosynthesis at the spot but was due to diffusive transport through the aerenchyma.

In darkness, O_2 diffuses into the leaves from the surrounding water, across the diffusive boundary layer (DBL), and is then transported to the below-ground tissue. This caused less oxygenation of the rhizosphere, due to a relatively lower O_2 supply from the above-ground tissue and owing to O_2 consumption along the diffusive transport path (Figure 3;

DOI: 10.1021/es505734b
Environ. Sci. Technol. XXXX, XXX, XXX–XXX

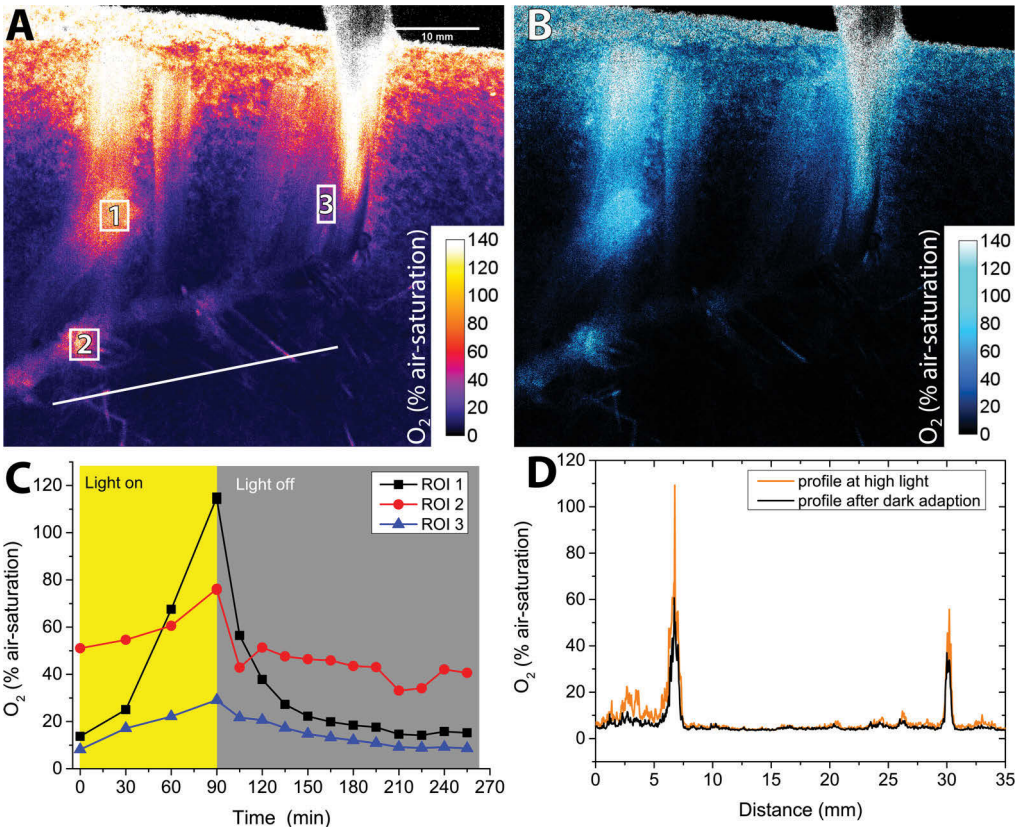

Figure 3. A: False color image of the O_2 concentration around the seagrass roots taken after 90 min illumination of the leaves with 500 μmol photons m^{-2} s^{-1}. B: An O_2 depletion image visualizing the change in O_2 concentration between the end of the light period (i.e., onset of darkening) and 130 min later. C: time profile of the 3 regions of interest (ROIs) over the light-dark exposure experiment. D: line profile (line shown in A) across some small roots at the time points 90 and 240 min.

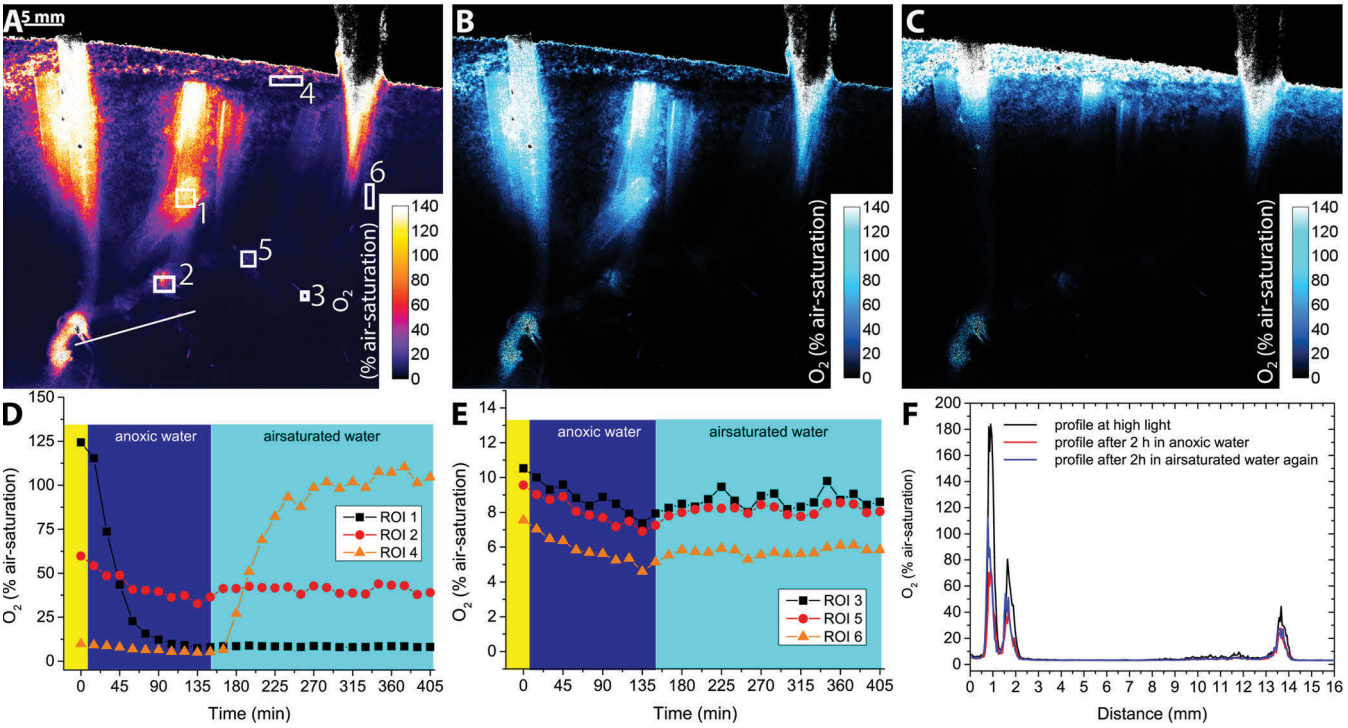

Figure 4. A: False color image of the O_2 concentration around the seagrass roots taken after 90 min illumination of the leaves at 500 μmol photons m^{-2} s^{-1}. Oxygen dynamics pictures visualizing the change in oxygenation between the time points 0 min (light) and 135 min (anoxic water) (B) and between the time points 135 min (anoxic water) and 405 min (air saturated water) (C). D–E: time profile of the 6 ROIs. F: line profile across some small roots at the time points 0, 120, and 240 min.

DOI: 10.1021/es505734b
Environ. Sci. Technol. XXXX, XXX, XXX–XXX

ROI 1−3 and line profile). To visualize the changes between high light and dark conditions, we calculated an O_2 concentration difference picture by subtracting the dark O_2 image (time point 240 min) from the high light O_2 image (time point 90) (Figure 3B). This showed that the O_2 production in the prophyllum had a high local impact, but clear differences were also evident at the root tips, close to the nodium and the basal meristem. Such O_2 leakage into the rhizosphere can protect the seagrass from H_2S intrusion through development of an oxic microshield around the below-ground tissue that prevents H_2S from reaching the tissue surface, via chemical oxidation with O_2 (i.e., $2O_2 + H_2S \rightarrow 2H^+ + SO_4^{2-}$).[11] Furthermore, the line profile in Figure 3D showed significant O_2 leakage around the root tips. This leakage may have a particular important defense role for the plant as this may enable intermittent root growth through relatively oxidized microzones.

While light-dark shifts appear on a diel basis, other environmental changes such as O_2 depletion in the water column appear more rarely in the natural environment. Hypoxic water-column conditions may be caused by anthropogenic impacts such as eutrophication (e.g., due to land runoff and nutrient loadings) and/or by dredging operations in areas close to the seagrass meadows. During the latter, resuspended anoxic sediment attenuates light and consumes O_2 in the water column leading to hypoxia (or even anoxia).[14] This is especially critical for seagrasses during night-time, where photosynthetic O_2 supply in the leaves is absent. To investigate such effects, we monitored how defined changes in the O_2 content of the water column affected the rhizosphere O_2 microenvironment of the seagrass (Figure 4). In 5 of the selected ROIs, O_2 was rapidly depleted in the seagrass rhizosphere under dark anoxic conditions in the overlaying water. After re-establishing full atmospheric saturation in the water column, O_2 diffusion from the water column into above-ground tissue resulted in increased below-ground O_2 levels in the rhizosphere that approached steady state (Figure 4; ROI 2, 3, 5, and 6). This was further confirmed by measuring line profiles of the O_2 concentration across some smaller roots (Figure 4F). Notably, ROI 1 in Figure 4 showed no increase in O_2 concentration indicating that the prophyllums were not supplied with O_2 via the aerenchyma. The presented experimental setup thus provides important information about the oxidation capability of the below-ground tissue of seagrasses under various environmental scenarios. Spatially explicit investigations are important, especially seen in light of recent studies linking seagrass die-backs with hypoxic water-column conditions, leading to internal anoxia, and thereby making the plants more susceptible to sulfide intrusion.[11−13]

In Figure 4, ROI 4 was chosen to follow the O_2 dynamics in the artificial sediment in close proximity to the artificial sediment surface. This area showed efficient O_2 diffusion into the uppermost few mm's within the time frame of the experiments. The sulfide in the top layer of the artificial sediment thus gets depleted over time, when O_2 is present in the overlaying water and such depletion has to be considered as this limits the long-term applicability of the experimental setup. Possible ways to avoid such oxygenation over longer incubation times are presented elsewhere.[29] The O_2 concentration difference images comparing high light and darkness (under water column anoxia) showed pronounced changes around the photosynthetic prophyllum (Figure 4B), while O_2 leakage was predominantly observed at the root tips and the nodiums when diffusion from the water column was the only supply mechanism (Figure 4C).

While planar optrodes only generate luminescence images when the focal plane of the camera matches with the plane of the optrode, the method presented here enables imaging at different focal planes. As the entire artificial sediment is stained with optical sensor nanoparticles it is in principle possible to image at different focal planes. In the Supporting Information O_2 distribution images at six different focal plains within the artificial sediment are shown (Figure S2). Only in one of the pictures is the rhizome in focus; the others present focal planes in front and in the back of the rhizome. The further away from the actual roots the picture is taken the lower the O_2 concentration. This explains why close contact to the roots is required when working with planar optrodes. When the sensor film is further away from the roots, only a blurry image can be observed.

In conclusion, the use of O_2 sensitive nanoparticles in artificial transparent sediment represents a powerful new tool to analyze the microenvironment around the below-ground biomass of seagrasses and to quantify O_2 dynamics at high spatiotemporal resolution in the whole rhizosphere upon environmental changes. The possibility of mapping the whole below-ground O_2 distribution and dynamics in the seagrass rhizosphere enables identification of particular hot spots with different O_2 supply mechanisms. In contrast to microsensor measurements, this method can thus generate data for multiple parts of the plant simultaneously significantly accelerating studies of the chemical dynamics in the rhizosphere of aquatic plants. In future studies, O_2 mapping can be easily supplemented with detailed spot measurements with microsensors for O_2 and other chemical parameters such as pH and H_2S,[11,29] where the selection of specific measuring sites can be guided by O_2 sensitive nanoparticle maps. The application of this new experimental approach is not limited to seagrasses and can easily be adapted to studies of other waterlogged plants and environments. For example, studies of O_2 dynamics in rice with the new approach presented here could easily be combined with other techniques for monitoring metal concentrations around the roots.[30]

■ ASSOCIATED CONTENT

Supporting Information

Visualization of the image analysis and O_2 concentration images obtained in different focal planes. A detailed video documentation of the O_2 sensitive sediment preparation and mounting of seagrass in the experimental chamber. This material is available free of charge via the Internet at http://pubs.acs.org.

■ AUTHOR INFORMATION

Corresponding Author

*E-mail: mkuhl@bio.ku.dk.

Author Contributions

[#]K.K. and K.E.B. contributed equally.

K.K., K.E.B., and M.K. designed the research. K.K., K.E.B., M.K., and S.L.J. conducted experiments. K.K., K.E.B., and M.K. analyzed the data. K.K. wrote the manuscript with editorial help from K.E.B. and M.K. All authors have given approval to the final version of the manuscript.

Notes

The authors declare no competing financial interest.

DOI: 10.1021/es505734b
Environ. Sci. Technol. XXXX, XXX, XXX−XXX

■ ACKNOWLEDGMENTS

We thank Dr. Daniel A. Nielsen for help with the experimental setup and for fruitful discussions, Josua Hösch for help with video editing, and Sabrina Kapus for providing the TOC picture. This study was funded by research grants from the Australian Research Council (M.K.), the Danish Council for Independent Research | Natural Sciences (M.K.), the Villum Foundation (M.K., K.K.), the Augustinus Foundation (K.E.B.), and the PA Fiskers Fund (K.E.B.).

■ REFERENCES

(1) Orth, R. J.; Carruthers, T. J. B.; Dennison, W. C.; Duarte, C. M.; Fourqurean, J. W.; Heck, K. L., Jr.; Hughes, A. R.; Kendrick, G. A.; Kenworthy, W. J.; Olyarnik, S.; et al. A Global Crisis for Seagrass Ecosystems. *BioScience* **2006**, *56*, 987−996.

(2) Larkum, A. W. D.; Orth, R. J.; Duarte, C. M. *Seagrasses: biology, ecology and conservation*; Springer: Dordrecht, Netherlands, 2006.

(3) Waycott, M.; Duarte, C. M.; Carruthers, T. J. B.; Orth, R. J.; Dennison, W. C.; Olyarnik, S.; Calladine, A.; Fourqurean, J. W.; Heck, K. L.; Hughes, A. R.; et al. Accelerating loss of seagrasses across the globe threatens coastal ecosystems. *Proc. Natl. Acad. Sci. U. S. A.* **2009**, *106*, 12377−12381.

(4) Holmer, M.; Bondgaard, E. J. Photosynthetic and growth response of eelgrass to low oxygen and high sulfide concentrations during hypoxic events. *Aquat. Bot.* **2001**, *70*, 29−38.

(5) Holmer, M.; Frederiksen, M. S.; Møllegaard, H. Sulfur accumulation in eelgrass (*Zostera marina*) and effect of sulfur on eelgrass growth. *Aquat. Bot.* **2005**, *81*, 367−379.

(6) Pérez-Pérez, M. E.; Lemaire, S. D.; Crespo, J. L. Reactive oxygen species and autophagy in plants and algae. *Plant Physiol.* **2012**, *160*, 156−164.

(7) Lamers, L. P. M.; Govers, L. L.; Janssen, I. C. J. M.; Geurts, J. J. M.; Van der Welle, M. E. W.; Van Katwijk, M. M.; Van der Heide, T.; Roelofs, J. G. M.; Sumolders, A. J. P. Sulfide as a soil phytotoxin-a review. *Front. Plant Sci.* **2013**, *4*, 268.

(8) Borum, J.; Sand-Jensen, K.; Binzer, T.; Pedersen, O.; Greve, T. M. Oxygen Movement in Seagrasses. In *Seagrasses: Biology, Ecology and Conservation*; Springer: Dordrecht, Netherlands, 2006; pp 255−270.

(9) Jensen, S.; Kühl, M.; Glud, R.; Jørgensen, L.; Priemé, A. Oxic microzones and radial oxygen loss from roots of *Zostera marina*. *Mar. Ecol.: Prog. Ser.* **2005**, *293*, 49−58.

(10) Connell, E. L.; Colmer, T. D.; Walker, D. I. Radial oxygen loss from intact roots of *Halophila ovalis* as a function of distance behind the root tip and shoot illumination. *Aquat. Bot.* **1999**, *63*, 219−228.

(11) Brodersen, K. E.; Nielsen, D. A.; Ralph, P. J.; Kühl, M. Oxic microshield and local pH enhancement protects *Zostera muelleri* from sediment derived hydrogen sulphide. *New Phytol.* **2015**, *205*, 1264−1276.

(12) Borum, J.; Pedersen, O.; Greve, T. M.; Frankovich, T. A.; Zieman, J. C.; Fourqurean, J. W.; Madden, C. J. The potential role of plant oxygen and sulphide dynamics in die-off events of the tropical seagrass *Thalassia testudinum*. *J. Ecol.* **2005**, *93*, 148−158.

(13) Pedersen, O.; Binzer, T.; Borum, J. Sulphide intrusion in eelgrass (*Zostera marina* L.). *Plant, Cell Environ.* **2004**, *27*, 595−602.

(14) Erftemeijer, P. L. A.; Lewis, R. R. R. Environmental impacts of dredging on seagrasses: a review. *Mar. Pollut. Bull.* **2006**, *52*, 1553−1572.

(15) Pedersen, O.; Borum, J.; Duarte, C. M. Oxygen dynamics in the rhizosphere of *Cymodocea rotundata*. *Mar. Ecol.: Prog. Ser.* **1998**, *169*, 283−288.

(16) Schäferling, M. The art of fluorescence imaging with chemical sensors. *Angew. Chem., Int. Ed. Engl.* **2012**, *51*, 3532−3554.

(17) Glud, R. N.; Tengberg, A.; Kühl, M.; Hall, P.; Klimant, I. An in situ instrument for planar O 2 optode measurements at benthic interfaces. *Limnol. Oceanogr.* **2001**, *46*, 2073−2080.

(18) Kühl, M.; Polerecky, L. Functional and structural imaging of phototrophic microbial communities and symbioses. *Aquat. Microb. Ecol.* **2008**, *53*, 99−118.

(19) Polerecky, L.; Volkenborn, N.; Stief, P. High Temporal Resolution Oxygen Imaging in Bioirrigated Sediments. *Environ. Sci. Technol.* **2006**, *40*, 5763−5769.

(20) Frederiksen, M. S.; Glud, R. N. Oxygen dynamics in the rhizosphere of *Zostera marina*: A two-dimensional planar optode study. *Limnol. Oceanogr.* **2006**, *51*, 1072−1083.

(21) Jovanovic, Z.; Pedersen, M.; Larsen, M.; Kristensen, E.; Glud, R. Rhizosphere O_2 dynamics in young *Zostera marina* and *Ruppia maritima*. *Mar. Ecol.: Prog. Ser.* **2015**, *518*, 95−105.

(22) Meysman, F. J. R.; Galaktionov, O. S.; Glud, R. N.; Middelburg, J. J. Oxygen penetration around burrows and roots in aquatic sediments. *J. Mar. Res.* **2010**, *68*, 309−336.

(23) Borisov, S. M.; Mayr, T.; Mistlberger, G.; Waich, K.; Koren, K.; Chojnacki, P.; Klimant, I. Precipitation as a simple and versatile method for preparation of optical nanochemosensors. *Talanta* **2009**, *79*, 1322−1330.

(24) Mistlberger, G.; Koren, K.; Scheucher, E.; Aigner, D.; Borisov, S. M.; Zankel, A.; Pölt, P.; Klimant, I. Multifunctional Magnetic Optical Sensor Particles with Tunable Sizes for Monitoring Metabolic Parameters and as a Basis for Nanotherapeutics. *Adv. Funct. Mater.* **2010**, *20*, 1842−1851.

(25) Larsen, M.; Borisov, S. M.; Grunwald, B.; Klimant, I.; Glud, R. N. A simple and inexpensive high resolution color ratiometric planar optode imaging approach: application to oxygen and pH sensing. *Limnol. Oceanogr.: Methods* **2011**, *9*, 348−360.

(26) Ralph, P. J.; Short, F. T. Impact of the wasting disease pathogen, *Labyrinthula zosterae*, on the photobiology of eelgrass *Zostera marina*. *Mar. Ecol.: Prog. Ser.* **2002**, *226*, 265−271.

(27) Meier, R. J.; Fischer, L. H.; Wolfbeis, O. S.; Schäferling, M. Referenced luminescent sensing and imaging with digital color cameras: A comparative study. *Sens. Actuators, B* **2013**, *177*, 500−506.

(28) Macinnis-Ng, C. M. .; Ralph, P. J. Short-term response and recovery of *Zostera capricorni* photosynthesis after herbicide exposure. *Aquat. Bot.* **2003**, *76*, 1−15.

(29) Brodersen, K. E.; Nielsen, D. A.; Ralph, P. J.; Kühl, M. A split flow chamber with artificial sediment to examine the below-ground microenvironment of aquatic macrophytes. *Mar. Biol.* **2014**, *161*, 2921−2930.

(30) Williams, P. N.; Santner, J.; Larsen, M.; Lehto, N. J.; Oburger, E.; Wenzel, W.; Glud, R. N.; Davison, W.; Zhang, H. Localized Flux Maxima of Arsenic, Lead, and Iron around Root Apices in Flooded Lowland Rice. *Environ. Sci. Technol.* **2014**, *48*, 8498−8506.

DOI: 10.1021/es505734b
Environ. Sci. Technol. XXXX, XXX, XXX−XXX

Plant, Cell & Environment

Plant, Cell and Environment (2016) doi: 10.1111/pce.12740

Original Article

Nanoparticle-based measurements of pH and O_2 dynamics in the rhizosphere of *Zostera marina* L.: effects of temperature elevation and light-dark transitions

Kasper Elgetti Brodersen[1†], Klaus Koren[2†], Mads Lichtenberg[2] & Michael Kühl[1,2]

[1]*Plant Functional Biology and Climate Change Cluster, University of Technology Sydney, 15 Broadway, Ultimo, Sydney, New South Wales 2007, Australia and* [2]*Marine Biological Section, Department of Biology, University of Copenhagen, Strandpromenaden 5, DK-3000 Helsingør, Denmark*

ABSTRACT

Seagrasses can modulate the geochemical conditions in their immediate rhizosphere through the release of chemical compounds from their below-ground tissue. This is a vital chemical defence mechanism, whereby the plants detoxify the surrounding sediment.

Using novel nanoparticle-based optical O_2 and pH sensors incorporated in reduced and transparent artificial sediment, we investigated the spatio-temporal dynamics of pH and O_2 within the entire rhizosphere of *Zostera marina* L. during experimental manipulations of light and temperature. We combined such measurements with O_2 microsensor measurements of the photosynthetic productivity and respiration of seagrass leaves.

We found pronounced pH and O_2 microheterogeneity within the immediate rhizosphere of *Z. marina*, with higher below-ground tissue oxidation capability and rhizoplane pH levels during both light exposure of the leaf canopy and elevated temperature, where the temperature-mediated stimuli of biogeochemical processes seemed to predominate. Low rhizosphere pH microenvironments appeared to correlate with plant-derived oxic microzones stimulating local sulphide oxidation and thus driving local proton generation, although the rhizoplane pH levels generally where much higher than the bulk sediment pH.

Our data show that *Z. marina* can actively alter its rhizosphere pH microenvironment alleviating the local H_2S toxicity and enhancing nutrient availability in the adjacent sediment via geochemical speciation shift.

Key-words: microbial metabolism; nanoparticles; O_2; pH; plant-sediment interactions; seagrass; temperature elevation.

Correspondence: Kasper Elgetti Brodersen and Michael Kühl. Phone: +61 414 954 017; +45 4047 6304; e-mail: kasper.e.brodersen@student.uts.edu.au; mkuhl@bio.ku.dk

[†]*These authors contributed equally to this work.*

INTRODUCTION

To accommodate growth in often highly reduced, sulphidic sediment environments, seagrasses possess aerenchymal tissue composed of a system of interconnected gas channels facilitating rapid transport of O_2 from the seagrass leaves to the below-ground tissue (Larkum *et al.* 1989; McComb *et al.* 1999). Aerenchymal O_2 supply supports aerobic metabolism at the root apical meristems, and also facilitates radial O_2 loss (ROL) to the immediate rhizosphere from the basal meristems with leaf sheath, rhizome and the root apical meristems (Pedersen *et al.* 1998, 1999; Jensen *et al.* 2005; Frederiksen & Glud 2006; Brodersen *et al.* 2014, 2015a; Koren *et al.* 2015). The below-ground ROL drives local chemical oxidation of the surrounding sediment in plant-derived oxic microniches, wherein new actively growing roots can form and reach maturity with protective barriers to ROL and sulphide intrusion (Barnabas 1996; Enstone *et al.* 2003; Brodersen *et al.* 2014, 2015a). Most of these barriers to ROL are induced by anoxic, sulphidic conditions (Armstrong & Armstrong 2001, 2005) and inhibit gas-exchange over most of the root surface area ensuring an efficient internal gas transport to the apical parts of growing roots (Colmer 2003).

Seagrasses can thus actively alter their rhizosphere microenvironment through the release of O_2 from their below-ground tissue, thereby enhancing the redox potential of the immediate rhizosphere and stimulating re-oxidation of sediment-produced reduced phytotoxins, such as H_2S (Lamers *et al.* 2013; Brodersen *et al.* 2014, 2015a). The oxidation capacity of the below-ground tissue is determined by numerous O_2 sources and sinks (Borum *et al.* 2006), where the most important regulating parameters include the O_2 conditions in the water column during night-time as the plants are completely dependent on passive diffusion of O_2 into their leaves when photosynthesis ceases (O_2 source) (Greve *et al.* 2003; Pedersen *et al.* 2004; Borum *et al.* 2005; Frederiksen & Glud 2006; Brodersen *et al.* 2015a), the light availability and quality during day-time strongly regulating rates of shoot photosynthesis (O_2 source) (Brodersen *et al.* 2015a,2015b), the ambient water temperature affecting plant and sediment respiratory needs and reaction kinetics (mainly regulating the O_2 sinks, but also affects rates of leaf photosynthesis) (Raun & Borum 2013), as

well as the thickness of the seagrass leaf diffusive boundary layer impeding gas and nutrient exchange with the surrounding water-column and thereby the water flow (thus negatively affecting the O_2 source) (Binzer *et al.* 2005; Brodersen *et al.* 2015b).

Recently, Brodersen *et al.* (2015a) showed that the seagrass *Zostera muelleri* subsp. *capricorni* can modulate the pH microenvironment in its immediate rhizosphere, further alleviating the risk of H_2S intrusion through local sediment pH enhancements. This chemical defence mechanism, whereby pH enhancement changes the sulphide speciation in the rhizosphere towards non-permeable HS^- ions, is still poorly understood and there is therefore a need to elucidate the sediment pH microheterogeneity on a whole rhizosphere-scale.

Possible mechanisms behind such pH changes in the immediate rhizosphere are plant-derived allelochemicals. Rhizome/root exudation of organic carbon to the rhizosphere, as a result of internal carbon translocation, leads to enhanced bacterial productivity and growth in the seagrass rhizosphere (Moriarty *et al.* 1986). Rates of sulphate reduction have been coupled to plant photosynthesis and below-ground biomass (Pollard & Moriarty 1991; Blaabjerg & Finster 1998; Blaabjerg *et al.* 1998; Hansen *et al.* 2000; Nielsen *et al.* 2001) and young seagrass roots have also been found to stimulate the growth of *epsilon-* and *gamma-proteobacteria* that can utilize O_2 and nitrate as electron acceptors to re-oxidize sulphide (Jensen *et al.* 2007). Interestingly, the younger plant structures often leak O_2 from around the root-cap, where the presence of sulphide oxidizers overlaps with the plant-derived oxygenated microniches (Jensen *et al.* 2005; Frederiksen & Glud 2006; Brodersen *et al.* 2014).

The root-shoot junctions (including the basal leaf meristem) and the root apical meristems (Moriarty *et al.* 1986) have been suggested as sites of exudation, with rhizome/root organic carbon exudation amounting up to 18% of the total carbon fixed by the seagrass host (Hansen *et al.* 2000). The highest sulphate reduction rates in the seagrass rhizosphere have correspondingly been observed at the seagrasses rhizomes and roots, where, for example, Pollard & Moriarty (1991) found 6 times higher sulphate reduction rates in seagrass-vegetated sediment as compared to non-vegetated areas. Sulphate reducing bacteria associated with the below-ground tissue of seagrasses show high O_2 tolerance (Blaabjerg & Finster 1998), and several studies have shown that increasing temperature and light exposure of the seagrass leaf canopy has a pronounced positive impact on the rhizosphere sulphate reduction rate (Isaksen & Jørgensen 1994; Isaksen & Finster 1996; Blaabjerg *et al.* 1998). Sulphate reduction can have a positive impact on the availability of phosphate in marine sediment owing to its reducing properties (Pollard & Moriarty 1991), adding to the growing evidence of a specific relationship between the seagrass host and sulphate reducing bacteria based on a reciprocal exchange of nutrients (Moriarty *et al.* 1986; Blaabjerg *et al.* 1998; Hansen *et al.* 2000; Nielsen *et al.* 2001).

The consumption or production of protons as a result of microbial metabolisms and/or plant-derived allelochemicals plays an important role in the determination of sediment pH (Srinivasan & Mahadevan 2010; Brodersen *et al.* 2015a). Such sediment pH alterations can influence the chemical speciation and availability of vital nutrients (e.g. ammonium and phosphate) at the plant/sediment interfaces (Pollard & Moriarty 1991; Pagès *et al.* 2011, 2012; Brodersen *et al.* 2015a). Yet the understanding of rhizosphere pH dynamics in seagrasses is underexplored and data on pH microheterogeneity at plant/sediment interfaces are lacking.

In present study, we used novel O_2 and pH sensitive optical nanosensors incorporated in artificial, transparent sediment to investigate the pH and O_2 microdynamics in the rhizosphere of *Zostera marina* L. during light/dark transitions and temperature elevations. Our results provide new insights into the pH microheterogeneity and O_2 distribution in the *Zostera marina* L. rhizosphere during changing environmental conditions. We discuss how such pH and O_2 microgradients may alter the geochemical speciation of vital chemical species at plant/sediment- and oxic/anoxic interfaces.

MATERIALS AND METHODS

Seagrass sampling

Zostera marina L. specimens were collected in shallow waters (less than 2 m depth) near Rungsted Harbour, Denmark and were transported in seawater from the sampling site to the laboratory within 1 h of sampling. The collected seagrass specimens were transplanted into sieved sediment from the sampling site to exclude burrowing animals from the holding tank. Specimens were held in a 30 L aquarium continuously flushed with aerated seawater (5 L h^{-1}; salinity of 34‰; temperature of ~12 °C) under a 14:10 h light/dark cycle. Illumination with a photon irradiance (400-700 nm) of ~200 µmol photons m^{-2} s^{-1} was provided by a combination of fluorescent and halogen lamps. Prior to experiments, selected plants were gently washed free of any adhering sediment particles and rhizome ends were carefully sealed with petroleum jelly to avoid gas leakage from damaged older rhizome parts, before placement in the custom-made, narrow split flow chamber (described below; Fig. 1). Relative small *Z. marina* specimens were used owing to the chamber dimension restrictions.

Experimental setup and artificial, transparent sediment

The applied experimental chamber consisted of a custom-made narrow, transparent acrylic split flow chamber attached to the side of a 30 L aquarium (inner dimensions 1 × 13 × 12 cm; Fig. 1). The split flow chamber was divided into an upper and lower compartment by means of an acrylic wall with numerous holes (inner diameter of ~1 mm) and was equipped with a removable front window for ease of access when casting the sediment and positioning the seagrass. A seagrass specimen was positioned in the upper compartment with the above-ground tissue in the free-flowing seawater phase and the below-ground tissue embedded in reduced, artificial sediment (Fig. 1). The artificial, transparent sediment with embedded nanosensors was designed to mimic chemical settings in natural marine sediment (Brodersen *et al.* 2014),

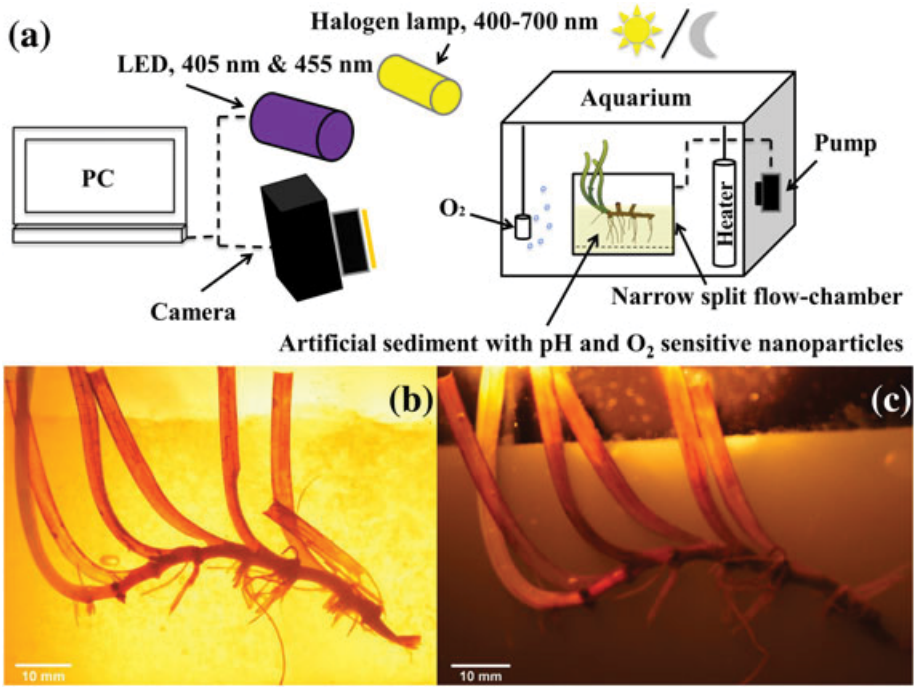

Figure 1. Schematic diagram of the experimental setup, showing the aquarium equipped with the custom-made narrow split flow-chamber and the ratiometric bio-imaging camera system (a). Image of the below-ground plant tissue structure during O_2 measurements (b). Image visualising the below-ground plant tissue structure during pH measurements (c). Note that the difference in brightness seen on the structural images (b, c) is due to the specific long pass filters used for luminescence imaging.

while enabling direct visual assessment of the below-ground tissue during measurements (Fig. 1; further described in Koren *et al.* 2015). The transparent artificial sediment consisted of a deoxygenated ~0.5% (w/v) agar-seawater gel, buffered with HEPES (final concentration of 10 mM; pH ~7), amended with O_2 or pH sensitive nanoparticles (~3 and 7 % v/v, respectively) and Na_2S*9H_2O to a final H_2S concentration of 500 µM (at pH 7). The agar powder was pre-washed in continuously stirred cold seawater to improve clarity. The lower compartment of the split flow chamber contained a highly sulphidic (final H_2S concentration of 2500 µM) deoxygenated ~0.5% (w/v) agar-seawater solution buffered with HEPES (10 mM), ensuring a continuous supply of H_2S to the above artificial sediment with nanosensors during experiments, thereby maintaining a constantly high O_2 demand in the sediment (Brodersen *et al.* 2014, 2015a). After positioning of the plant and casting the sediments, the chamber was sealed and placed in front of the imaging system (described below).

Illumination of the leaf canopy was provided by a fibre-optic tungsten halogen lamp (KL-2500; Schott GmbH, Mainz, Germany) equipped with a collimating lens. The incident photon irradiance (PAR, 400-700 nm) at the level of the seagrass leaf canopy was measured with a calibrated irradiance sensor (Walz GmbH, Effeltrich, Germany) connected to a quantum irradiance meter (LI-250; LiCor, Lincon, NE, USA). A constant flow of seawater (salinity of 34‰) was maintained in the water-column of the upper flow chamber compartment via a connected pump submerged in an aerated and temperature-controlled seawater tank. The below-ground pH and O_2 microenvironment within the *Zostera marina* L. rhizosphere was investigated during light/dark transitions (incident photon irradiance of 500 µmol photons m^{-2} s^{-1}) and at two different experimental temperatures (~16 and 24 °C). Plants were acclimatized to the experimental conditions for a minimum of 4 h prior to start of measurements to ensure steady-state biogeochemical conditions in the rhizosphere (as confirmed from repetitive image recordings). Temperature changes were induced by slowly increasing the temperature of the seawater reservoir for ~3 h until the desired temperature was reached and the plants were then allowed to acclimatize to the experimental temperature and irradiance for another 4 h before image recordings commenced.

Optical nanoparticle-based sensors

The optical nanoparticle-based pH sensors were prepared based on a modified literature method (Wang *et al.* 2012; Xie *et al.* 2013). Briefly, 1 mg of perylene (Sigma-Aldrich), 1 mg of lipophilic indicator1-hydroxypyrene-3,6,8-tris-bis(2-ethylhexyl)sulfonamide (lipo-HPTS) (generously provided by Dr. Sergey Borisov TU Graz; Borisov *et al.* 2009) and 100 mg of the triblock copolymer Pluronic® F-127 (Sigma-Aldrich) were dissolved in 15 mL of tetrahydrofuran (THF). The mixture was poured into 100 mL of continuously stirred distilled water, the THF was evaporated under an air stream, and the particle suspension was concentrated to a final concentration of 5 mg mL^{-1} at 60 °C. The obtained pH sensor nano particles had an average size of <100 nm as shown in the literature (Xie *et al.* 2013). The pH sensor nanoparticles were added to the pre-heated and previously deoxygenated artificial sediment in the last stage of the

casting procedure, i.e., during cooling at ~38 °C to obtain a final concentration of ~7 % (v/v) in the agar matrix.

A detailed description of the optical nanoparticle-based pH sensors, including optical properties and calibration procedures is provided in the Supporting Information (Fig. S1–4 and S6; Notes S1).

Artificial sediment with optical O_2 sensor nanoparticles was prepared according to Koren *et al.* (2015). Briefly, 3 mg of platinum(II) meso-(2,3,4,5,6-pentafluoro)phenyl porphyrin (PtTFPP; indicator dye), 3 mg of Macrolex fluorescence yellow 10GN (MY; reference dye) and 200 mg of the styrene maleic anhydride copolymer (PSMA with 8% MA) XIRAN were dissolved in 20 g of Tetrahydrofuran (THF). This mixture was then poured into 200 mL of continuously stirred distilled water. THF was evaporated under an air stream, and the particle suspension was concentrated to a final concentration of 5 mg mL^{-1} at 60 °C. The optical O_2 sensor nanoparticles were added to the pre-heated and previously deoxygenated artificial sediment in the last stage of the casting procedure at an agar temperature of ~38 °C to obtain a final concentration of ~ 3% (v/v) in the agar matrix.

Calibration curves of the optical O_2 sensor nano particles at the two different experimental temperatures are provided in the Supporting Information (Fig. S5).

Imaging setup and data acquisition

A RGB camera setup (Larsen *et al.* 2011) was used for ratiometric pH and O_2 imaging (Fig. 1). The imaging system consisted of a SLR camera (EOS 1000D, Canon, Japan) mounted on a tripod and equipped with a macro objective lens (Macro 100 f2,8 D, Tokina, Japan) and a long pass filter (pH imaging, 455 nm; O_2 imaging, 530 nm; Uqgoptics.com). Excitation of the luminescent sensor nano particles was achieved by means of a multichip LED (LedEngin Inc, RS Components Ltd, Corby, UK) combined with a bandpass filter (pH imaging, 405 nm; O_2 imaging, 455 nm). The applied LEDs were powered by a USB-controlled LED driver unit designed for luminescence imaging applications (imaging.fish-n-chips.de). Data acquisition and control of the SLR exposure and LED light were achieved with a PC running custom software "look@RGB" (imaging.fish-n-chips.de).

Image calibration and analysis

The obtained SLR images were first split into red, green and blue channels and were then analysed via the Java-based image processing software ImageJ (rsbweb.nih.gov/ij/). In order to achieve images of pH and O_2 dependent ratios, raw images were divided using the ImageJ plugin Ratio Plus (rsb.info.nih.gov/ij/plugins/ratio-plus.html). For O_2 imaging, this implied dividing the red channel (emission of the O_2 sensitive dye) with the green channel (emission of the reference dye). For pH imaging, the red channel (indicator dye) was divided with the blue channel (reference dye). The obtained ratio images were fitted with previously obtained calibration curves (Fig. S4 and S5) using the Curve Fitting function in ImageJ, by means of linking the ratio images to the respective O_2 concentrations or pH units (see further details in Larsen *et al.* 2011; Koren *et al.* 2015).

Net photosynthesis and plant respiration rates

A seagrass leaf was positioned in a custom-made sample holder consisting of two 2 mm plexiglass plates to ensure a steady sample during microsensor measurements. Profiles were made through a hole in the plates (ø = 3 mm) towards the seagrass leaf surface. The sample holder was positioned in a flow chamber (25 × 8 × 5 cm), which was connected to an aquarium pump ensuring a steady flow of ~3 cm s^{-1} of aerated seawater (salinity = 34) from a 25 L aquarium, wherein the temperature was kept constant at either ~16 or 24 °C by a thermostate (F25-HD, Julabo GmbH, Germany). Light was provided with a fiber-optic tungsten halogen lamp (KL-2500 LCD, Schott GmbH, Germany) positioned at a 45° angle above the sample. The experimental photon irradiance (PAR) was 500 µmol photons m^{-2} s^{-1}, measured at the position of the sample, i.e., the leaf canopy, with a calibrated quantum irradiance meter (ULM-500, Walz GmbH, Germany) connected to an submersible spherical micro-quantum-sensor (US-SQS/L, Walz Gmbh, Germany).

Vertical profiles of O_2 concentration were measured in 50 µm increments from 0.5 mm above the leaf towards the tissue surface, using a Clark-type O_2 microsensor with a tip diameter of <25 µm (OX-25, Unisense, Denmark; Revsbech 1989), with a fast response time ($t_{90} < 0.5$ s) and a low stirring sensitivity (1-2%). The microsensor was mounted on a motorized micromanipulator (MU-1, PyroScience GmbH, Germany) and connected to a pA-meter (OXY-meter, Unisense, Denmark) that was interfaced to a PC via an A/D converter (DCR-16, PyroScience GmbH, Germany). Microsensor positioning and data acquisition were controlled by dedicated software (Profix, PyroScience GmbH, Germany).

Net photosynthesis and dark respiration rates were calculated from Fick's 1st law of diffusion:

$$J_{O_2} = -D_0 \frac{\partial C}{\partial z}$$

where D_0 is the salinity and temperature dependent diffusion coefficient of O_2 in seawater (www.unisense.com) and dC/dz is the linear concentration gradient of O_2 in the diffusive boundary layer.

RESULTS

Rates of photosynthesis and respiration

The net photosynthesis and respiration rates of *Zostera marina* L. at the two experimental temperatures were determined via O_2 concentration microprofiles measured towards the leaf tissue surface (Fig. 2). Measurements revealed a 2.2 times higher net photosynthesis rate at 24 °C as compared to 16 °C, amounting to an increase in O_2 efflux from 0.117 to 0.252 nmol O_2 cm^{-2} s^{-1}; and a 1.4 times higher respiration rate at 24 °C as compared to 16 °C, which amounted to an increase in O_2 influx from −0.116 to −0.159 nmol O_2 cm^{-2} s^{-1}. The measured temperature-induced enhancement in the rate

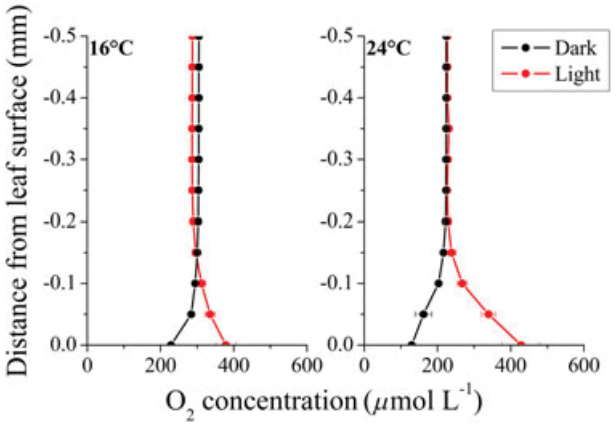

Figure 2. Vertical O_2 concentration microprofiles measured towards the leaf tissue surface of *Z. marina* during light-dark transitions (incident irradiance (PAR) of 500 µmol photons m^{-2} s^{-1}) at the two experimental temperatures (~16 and 24 °C). Y = 0 indicate the leaf tissue surface. Symbols with error bars represent the mean ± SD. n = 3; leaf level replicates.

of net photosynthesis and respiration corresponded to Q_{10} temperature coefficients of 2.6 and 1.5, respectively.

O_2 distribution and microdynamics

The two-dimensional O_2 distribution in the *Z. marina* L. rhizosphere at 16 and 24 °C during light-dark transitions is shown in Fig. 3. The O_2 images showed an O_2 release, i.e., radial oxygen loss, especially from the root-shoot junctions (nodiums) and the rhizome, leading to several oxic microniches in the immediate rhizosphere of *Z. marina* L. The seagrass was able to maintain oxic conditions around the rhizome even without photosynthetic activity (Fig. 3).

The O_2 concentration images revealed a distinct increase in the belowground tissue oxidation capacity at 24 °C as compared to 16 °C; this temperature effect slightly predominated over light stimulation of the plants photosystems (Fig. 3). The extent of oxygenated regions and the below-ground tissue surface O_2 concentration did only increase slightly during light exposure of the leaf canopy at 16 °C (incident irradiance of 500 µmol photons m^{-2} s^{-1}; Fig. 3), whereas the effect of light stimulation on ROL was more pronounced at 24 °C. Some of the prophyllums (single leaves originating from the rhizome at the nodiums), as well as the leaf sheath at the base of the shoot also released O_2 to the rhizosphere. The maximal width of the oxic microniches around the rhizome was ~5.0 mm at nodium 7 during light exposure at a temperature of 24 °C, corresponding to an oxic microshield thickness of ~0.75 mm surrounding the respective root-shoot junction (data obtained by subtracting the diameter of the rhizome), which is similar to previous findings in natural sediment (e.g. Pedersen *et al.* 1998; Jensen *et al.* 2005). The O_2 concentrations determined within selected regions of interest (ROIs) in the *Z. marina* rhizosphere confirmed these observations (Fig. 4; Table 1). Based on O_2 concentration measurements in ROI 1-7, we calculated a mean of a 1.1-fold increase in the oxidation capability of the belowground tissue as a result of the dark/light transitions as compared to a 1.3-fold increase in response to the 8 °C temperature elevation. The highest rhizome surface O_2 levels were found at the root-shoot junctions (nodium 4, 5 and 7) corresponding to O_2 concentrations reaching up to 122 µmol L^{-1} (ROI 3, 4 and 5 in Fig. 4; Table 1). The O_2 imaging thus documented pronounced spatial microheterogeneity and high spatio-temporal microdynamics of the belowground oxic microzones around the rhizome of *Z. marina* that was modulated by changes in light and temperature.

pH heterogeneity and dynamics

We found a high degree of pH heterogeneity within the seagrass rhizosphere, with distinct microzones of very low pH (down

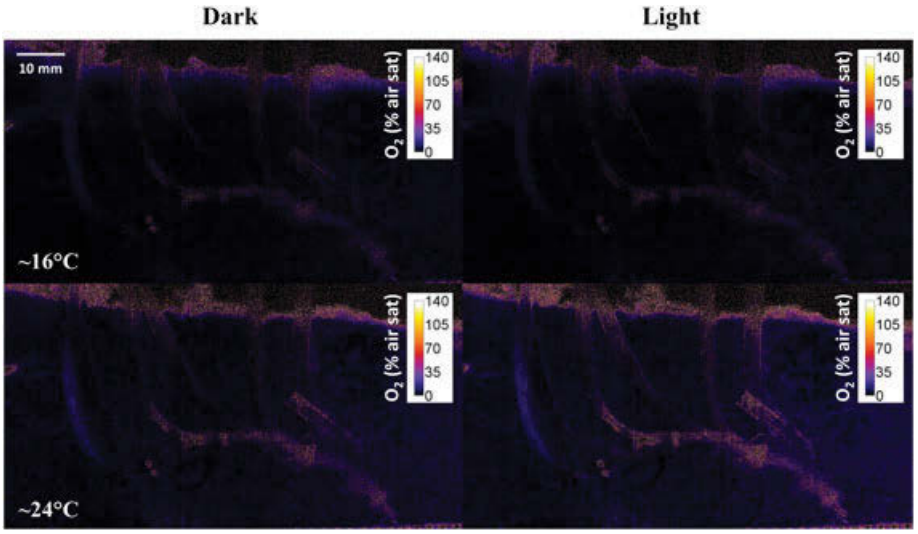

Figure 3. O_2 distribution and microdynamics within the rhizosphere of *Zostera marina* L. determined via optical nanoparticle-based O_2 sensors (O_2 colour coded image). The steady-state O_2 images were obtained at two different temperatures (16 and 24 °C) during light-dark transitions (photon irradiance (PAR) of 500 µmol photons m^{-2} s^{-1}). Legends depict the O_2 concentration in % air saturation. The presented images represent an average of 2 images.

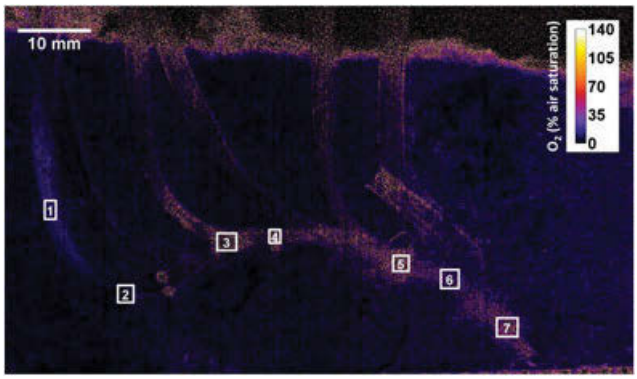

Figure 4. Selected regions of interest (ROI) within the immediate rhizosphere of *Zostera marina* L. used to determine the O_2 distribution during light/dark transitions (incident irradiance (PAR) of 500 µmol photons m^{-2} s^{-1}) at the experimental temperatures (~16 and 24 °C). Boxes and numbers indicate the measured ROI. Mean O_2 concentration values representing the entire ROI are presented in Table 1.

to ~ pH 4), as well as rhizome/rhizoplane pH levels well above the pH of the surrounding bulk sediment (up to pH > 8; Fig. 5). Comparison of O_2 and pH images revealed that areas of low pH overlapped with oxic microniches in the seagrass rhizosphere, whereas the high pH levels predominantly were measured on the surface of the mature part of the roots, the prophyllums and at the end of the rhizome, although patchy distributions of relatively high pH levels (as compared to bulk sediment pH levels) were observed on the surface of the entire belowground tissue. Selected regions of interest (ROIs) within the immediate rhizosphere of *Z. marina* exhibited higher pH levels (ΔpH of 0.02 - 0.31) in the rhizoplane during light exposure of the leaf canopy as compared to dark conditions at both experimental temperatures (ROI 1-7; Fig. 6; Table 2). The light-driven pH microdynamics was surpassed by the effect of the 8 °C temperature elevation showing much higher pH levels (ΔpH of 0.46 – 0.88) in the rhizoplane of *Zostera marina* L. at 24 °C as compared to 16 °C during both light exposure and darkness (ROI 1-3 and 5-7; Fig. 6; Table 2). A distinct hotspot of low pH was measured in the region of nodium 7, internode 7 and nodium 8 with an up to 5.2 mm wide zone of pH <5. The lowest rhizosphere pH levels were measured within this distinct zone with pH levels reaching the lower detection limit (pH 4) of the pH indicator (Fig. 5 & 6). The region of the belowground tissue with the highest pH levels was also found adjacent to nodium 7, corresponding to ROI 7 in Fig. 6 (Table 2).

pH microheterogeneity at interfaces

Extraction of cross-tissue pH values along line profiles in the pH images revealed pronounced pH microheterogeneity at interfaces (Fig. 7). The pH increased relative to the ambient sediment across internode 3 with the surrounding prophyllum, reaching pH levels of up to 8.3 on the rhizome surface and correlating with rapidly increasing pH levels at the rhizome/sediment interface (Fig. 7b; CTS 1). Interestingly, the cross tissue pH profile across internode 4 with prophyllum close to nodium 4 showed increasing pH levels at the approximate position of the oxic/anoxic interface with pH levels reaching up to 8.0 during light exposure of the leaf canopy (Fig. 7c; CTS2). This was contrary to the rhizome/sediment interface where decreasing pH levels down to 4.1 were observed on the rhizome surface (measured during light exposure at 16 °C), thus indicative of proton consuming and producing biogeochemical processes altering the geochemical microenvironment at this specific belowground oxic microniche (Fig. 7c; CTS2).

A line microprofile across a root from root-bundle 6 showed similar microheterogeneity as found at internode 3, with increasing pH levels at the root/sediment interface, and root surface pH levels of up to 7.6 (Fig. 7d; CTS 3). Cross tissue microprofile 4 across internode 7 with prophyllum showed a pronounced decrease in pH at the approximate position of the oxic/anoxic interface with pH levels within the low pH hotspot approaching the lower detection limit of the pH indicator (Fig. 7e; CTS 4). Across nodium 9 at the end of the rhizome with a degraded prophyllum, pH increased at the approximate position of the rhizome up to pH 8.7 (Fig. 7f; CTS5). These observations were

Table 1. O_2 concentrations at selected regions of interest (ROI) within the immediate rhizosphere of *Zostera marina* L. Boxes and numbers indicate the measured ROI. O_2 concentrations are given in both % air saturation and µmol L^{-1} at ~16 and 24 °C during light-dark transitions

	~16 °C				~24 °C			
	Dark		Light		Dark		Light	
$[O_2]$	% air sat.	µmol L^{-1}	% air sat.	µmol L^{-1}	% air sat.	µmol L^{-1}	% air sat.	µmol L^{-1}
ROI 1	5.8	(14.6)	6.2	(15.4)	11.8	(25.5)	14.2	(30.6)
ROI 2	8.9	(22.3)	9.0	(22.5)	10.7	(23.1)	13.2	(28.6)
ROI 3	37.2	(93.2)	37.5	(94.0)	49.3	(106.6)	54.9	(118.6)
ROI 4	32.3	(81.0)	36.1	(90.6)	50.3	(108.7)	52.7	(113.9)
ROI 5	34.6	(86.7)	35.1	(88.0)	47.3	(102.3)	56.3	(121.8)
ROI 6	12.2	(30.6)	12.5	(31.3)	18.2	(39.3)	23.2	(50.3)
ROI 7	24.0	(60.2)	25.6	(64.3)	35.2	(76.0)	42.3	(91.5)

ROI 1 represents measurements at the non-illuminated part of the shoot; ROI 2 = at the root-shoot junction (nodium 2); ROI 3 = at the base of the prophyllum close to the root-shoot junction (nodium 4); ROI 4 = at the root-shoot junction (nodium 5); ROI 5 = at the root-shoot junction (nodium 7); ROI 6 = internode 7 with prophyllum; ROI 7 = at the rhizome-end.

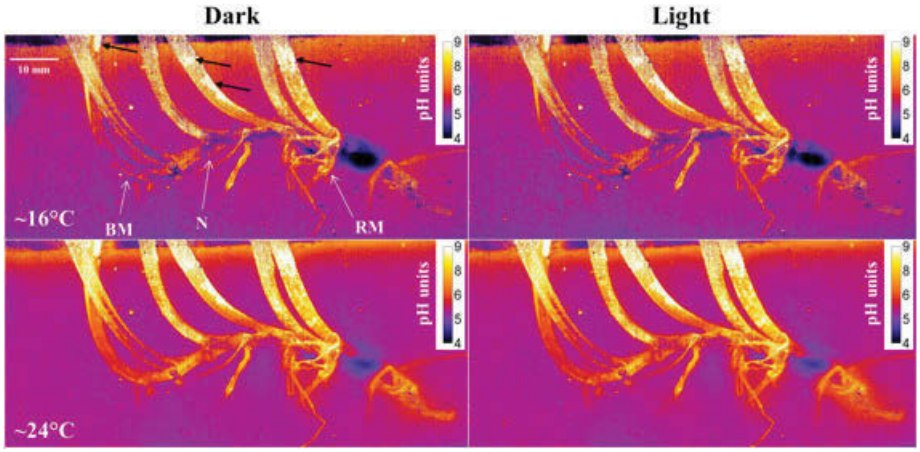

Figure 5. pH heterogeneity and microdynamics within the rhizosphere of *Zostera marina* L. determined via optical nanoparticle-based pH sensors (pH colour coded image). The steady-state pH images were obtained at two different temperatures (i.e. ~16 and 24 °C) during light-dark transitions (incident light intensity (PAR) of 500 µmol photons m^{-2} s^{-1}). Legends depict the pH value. BM indicates the basal leaf meristem; N indicates nodium 4; RM indicates the mature zone of roots in root-bundle 7. Images represent the average of 3 measurements. Note that white areas on leaves/prophyllums (marked with black arrows on the figure) should be interpreted with caution as some of these high pH microniches (pH of ≥9) seemed to be caused by epiphyte-derived red background luminescence (for further information see Notes S1; Figure S6).

supported by vertical pH microprofiles measured from the seawater/sediment interface down to the bottom of the pH sensitive sediment (Fig. 8). A rapid decrease in pH was observed within the uppermost 5 mm as typically observed in natural marine sediments (Stahl *et al.* 2006; Zhu *et al.* 2006), with pH levels decreasing from about ~ 7 at the water/sediment interface down to pH ~6 at 5 mm depth where after it stabilised.

A vertical pH microprofile extracted from pH images (VM1; Fig. 8b) showed the pH microdynamics and microheterogeneity at the interfaces between the sediment and the first prophyllum, as well as between the sediment and the basal meristem with leaf sheath. An increase in pH was measured at the position of the basal meristem with leaf sheath, i.e., the meristematic region of the rhizome, and along roots of the first root bundle (Fig. 8b). This was in contrast to pH conditions at the prophyllum/sediment interface, where we observed a rapid increase in pH towards the leaf tissue surface followed by a rapid decrease across the prophyllum, possibly due to oxic conditions and/or biological re-oxidation of H_2S (Fig. 8b; VM1). Another vertical pH microprofile (Fig. 8c; VM2) showed a rapid pH decrease at the interface between the sediment and the base of the fifth prophyllum/internode 7. At nodium 8 (root-shoot junction), a rapid increase in pH was seen at the approximate position of the oxic/anoxic interface with pH levels up to 8.4, followed by a strong decrease in pH across the rhizome tissue with pH levels decreasing to ~4.6 (Fig. 8d; VM3). A root from root-bundle 8 may have interfered with the interpretation of the pH microdynamics at nodium 8 (see Fig. 8d; VM3; ~26 mm depth). Nevertheless, our results clearly showed that plant-derived alterations of the belowground chemical microenvironment caused pH changes in the rhizosphere with a high degree of spatial microheterogeneity.

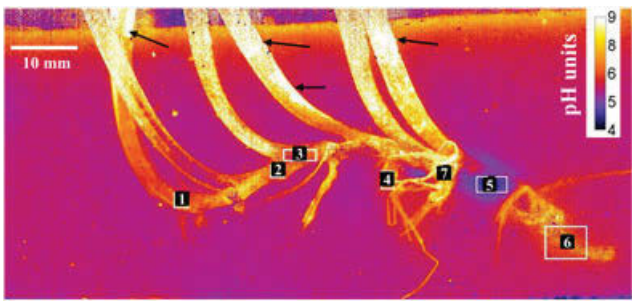

Figure 6. Selected regions of interest (ROI) within the immediate rhizosphere of *Zostera marina* L. used to determine the pH heterogeneity and dynamics during light-dark transitions (incident irradiance (PAR) of 500 µmol photons m^{-2} s^{-1}) at the two experimental temperatures (~16 and 24 °C). Boxes and numbers indicate the measured ROI. Mean pH values representing the entire ROI are presented in Table 2. Note that the white areas on leaves/prophyllums (marked with black arrows on the figure) should be interpreted with caution as some of these high pH microniches (pH of ≥9) seemed to be caused by epiphyte-derived red background luminescence (Notes S1; Figure S6).

DISCUSSION

Our results showed a high spatio-temporal pH and O_2 microheterogeneity in the rhizosphere of *Z. marina*, where the chemical conditions in the immediate rhizosphere were highly affected by the plant (Fig. 3 and 5). Radial O_2 loss (ROL) from the belowground tissue of *Z. marina* resulted in oxic microniches around the root-shoot junctions and the rhizome (Fig. 3 & 4). Such oxic microniches have recently been shown to facilitate chemical re-oxidation of sediment-produced H_2S, and ROL is therefore an important chemical defence mechanism whereby the plants can actively detoxify phytotoxins in the surrounding sediment (Brodersen *et al.* 2014, 2015a).

Oxidation capacity of the below-ground tissue

The higher oxidation capacity of the below-ground tissue observed at 24 °C as compared to 16 °C (Fig. 4; Table 1) was

Table 2. pH values in selected regions of interest (ROI) within the immediate rhizosphere of *Zostera marina* L. Values are given as a mean of the entire ROI ± S.E; and as the relative difference in pH between the experimentally changed environmental conditions (ΔpH). n = 5–18. The average pH of the bulk, artificial sediment at similar vertical depth as the below-ground biomass was ~ 5.7 ± 0.0 (includes all treatments)

	16 °C		24 °C		16 °C	24 °C	dark	light
	dark	light	dark	light	dark/light	dark/light	16/24 °C	16/24 °C
	pH	pH	pH	pH	ΔpH	ΔpH	ΔpH	ΔpH
ROI 1	5.8 ± 0.0	5.8 ± 0.0	6.4 ± 0.0	6.4 ± 0.0	0.0	0.1	0.6	0.6
ROI 2	5.6 ± 0.0	5.7 ± 0.1	6.3 ± 0.0	6.5 ± 0.1	0.1	0.2	0.7	0.8
ROI 3	5.6 ± 0.0	5.7 ± 0.1	6.3 ± 0.0	6.4 ± 0.1	0.1	0.2	0.7	0.7
ROI 4	6.7 ± 0.0	6.7 ± 0.1	6.6 ± 0.0	6.8 ± 0.0	0.0	0.2	-0.1	0.1
ROI 5	3.9 ± 0.0	4.2 ± 0.1	4.8 ± 0.0	4.9 ± 0.0	0.3	0.1	0.9	0.7
ROI 6	5.9 ± 0.0	6.0 ± 0.1	6.3 ± 0.0	6.6 ± 0.1	0.1	0.3	0.5	0.7
ROI 7	6.6 ± 0.1	6.9 ± 0.2	7.1 ± 0.0	7.4 ± 0.1	0.2	0.2	0.5	0.5

ROI 1 represents measurements at the basal leaf meristem (nodium 1); ROI 2 = the root-shoot junction (nodium 4); ROI 3 = at the base of the prophyllum close to the root-shoot junction (nodium 4); ROI 4 = root-bundle at nodium 6; ROI 5 = internode 7 with prophyllum; ROI 6 = at the rhizome-end; ROI 7 = root-shoot junction (nodium 7).

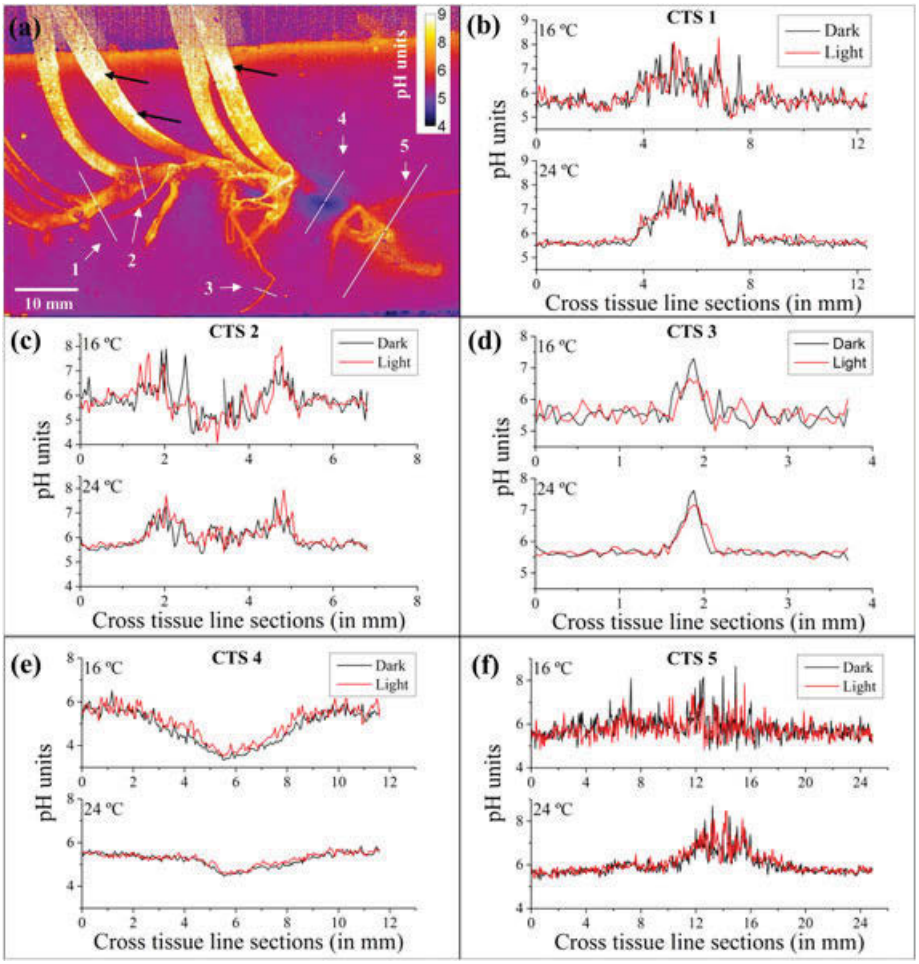

Figure 7. Cross tissue line sections (CTS) determining the pH microdynamics at the plant/rhizosphere interface and on the plant tissue surface. The steady-state cross tissue line sections were determined at the two experimental temperatures (i.e. ~16 and 24 °C) during light-dark transitions (under an incident photon irradiance (PAR) of 500 µmol photons m^{-2} s^{-1}). (a) Structural image of the seagrass *Z. marina* L. embedded in the artificial, transparent sediment with pH sensitive nanoparticles (pH colour coded image), illustrating the positions of the respective cross tissue line sections (CTS1-5). (b) Line microprofile across internode 3 with attached prophyllum (CTS1). (c) Line microprofile across internode 4 with prophyllum close to nodium 4 (CTS2). (d) Line microprofile across root from root-bundle 6 (CTS3). (e) Line microprofile across internode 7 with propyllum at the base of the prophyllum (CTS4). (f) Line microprofile across nodium 9 at the end of the rhizome with degraded prophyllum (CTS5). n = 3. Note that the white areas on leaves/prophyllums (marked with black arrows on the figure) should be interpreted with caution, as some of these high pH microniches (pH of ≥9) seemed to be caused by epiphyte-derived red background luminescence (Notes S1; Figure S6).

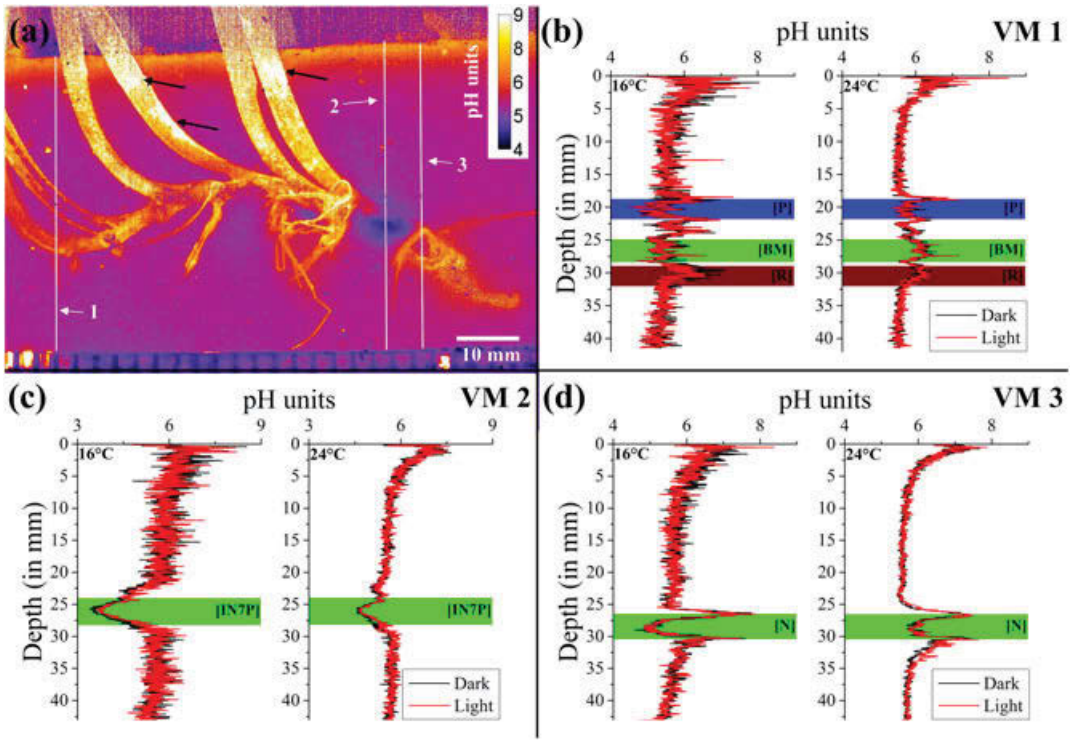

Figure 8. Vertical pH microprofiles (VM) illustrating the pH heterogeneity and microdynamics in the rhizosphere of *Z. marina* L. The vertical pH microprofiles were determined at steady-state conditions during light-dark transitions (photon irradiance (PAR) of 500 µmol photons m^{-2} s^{-1}) at ~16 and 24 °C. (a) Structural image of the *Z. marina* L. plant illustrating the spatial positions of the vertical pH microprofiles (colour coded image). (b) Vertical pH microprofile from the water/sediment interface across the first prophyllum and the basal meristem with leaf sheath to the bottom of the artificial sediment (VM1). (c) Vertical pH microprofile from the water/sediment interface across the base of the fifth prophyllum and the rhizome (internode 7) to the bottom of the artificial sediment (VM2). (d) Vertical pH microprofile from the water/sediment interface across the root-shoot junction at nodium 8 to the bottom of the artificial sediment (VM3). Y-axis = 0 indicate the artificial sediment surface. The approximate position of the below-ground tissue is indicated on the graphs by means of colour coded boxes (i.e. P = Prophyllum (blue), BM = Basal meristem with leaf sheath (green), R = Roots (brown); IN7P = Internode 7 at the base of the prophyllum (green); N = Nodium 8 (green)). n = 3. Note that the white areas on leaves/prophyllums (marked with black arrows on the figure) should be interpreted with caution, as some of these high pH microniches (pH of ≥9) seemed to be caused by epiphyte-derived red background luminescence (Notes S1; Figure S6).

due to a relatively higher rate of shoot photosynthesis (Fig. 2). The light-independent reactions, i.e., the enzyme-controlled reactions in the photosystems, are highly temperature dependent and the rate of photosynthesis, therefore, increases in direct proportion to temperature until it reaches a temperature optimum for the given plant, where after it rapidly decreases e.g. due to enzyme denaturation (Staehr & Borum 2011). The optimum temperature for oxygenic photosynthesis in summer acclimated *Z. marina* plants is ~24 °C (Staehr & Borum 2011). The higher ROL from the rhizome in darkness at 24 °C as compared to 16 °C (Fig. 3 & 4) may be explained by a significantly higher O_2 diffusion coefficient in the temperature elevated water. As a water column temperature elevation of 8 °C results in a ~25% increase in the rate of O_2 diffusion across the diffusive boundary layer (DBL) and into the above-ground tissue from the surrounding aerated water column (Ramsing & Gundersen 2015), thus allowing enhanced internal O_2 supply through the aerenchyma (low-resistance internal gas channels) to the below-ground tissue during darkness. This enhancement of the internal O_2 concentration gradient may be supported by a simultaneous temperature-induced increase in ROL owing to (i) the relatively increased lateral molecular O_2 diffusion rate across the epidermal layer of the belowground tissue at higher temperatures (although this might be counter-balanced by the higher tissue respiration), and (ii) the high leaf surface-to-volume ratio of the small *Z. marina* specimens used in this study leading to a relatively high efflux of O_2 from the leaves into the water column in light and a relatively high influx of O_2 from the water column into leaves in darkness.

Most prophyllums seemed to release O_2 into the rhizosphere (Fig. 3), and where prophyllum 1-5 potentially could be fueled by O_2 from the water-column, the fully buried prophyllum 6 at nodium 9 must be supplied with O_2 from the rhizome. Only a minor O_2 leakage was detected from the roots of the 2nd root-bundle close to the basal leaf meristem during light exposure and a temperature of 24 °C (Fig. 3). Structural tissue barriers to ROL (e.g. suberin; Barnabas 1996) minimize cross tissue gas permeability of mature roots (e.g. Colmer 2003; Jensen *et al.* 2005; Frederiksen & Glud 2006; Brodersen *et al.* 2015a). Frederiksen & Glud (2006) found that the root oxygenated zones diminished with root age and suggested that O_2 leakage from *Z. marina* roots eventually ceased. Our results further support such anatomical root adaptation of *Z. marina* to a life in a hostile reduced sediment environment. Barriers

to ROL protect the plants against exposure to sediment-derived reduced phytotoxins such as H_2S and increase the amount of internal O_2 transported to the apical root meristems ensuring aerobic metabolism in distal parts of the plants.

pH microheterogeneity in the rhizosphere

The novel pH sensitive nanosensors incorporated in the transparent sediment matrix enabled the first detailed mapping of the spatio-temporal pH microheterogeneity in the whole rhizosphere of *Z. marina* (Fig. 5). A similar pattern was recently observed in the rhizosphere of *Zostera muelleri spp. capricorni* by means of point measurements using electrochemical microsensors (Brodersen *et al.* 2015a). Regions in the immediate rhizosphere of *Z. marina* with very low pH levels (pH <5) seemed to correlate with the plant-derived oxic microniches. Such acidification could be due to proton formation as a byproduct of the spontaneous chemical reactions between plant-released O_2 and sediment H_2S within the oxic microzone (Fig. 5 & 6). We also measured slightly lower pH values in the immediate rhizosphere during darkness as compared to in light (Fig. 5 & 6), owing to plant and sediment respiration processes in addition to the aforementioned plant-derived spontaneous chemical re-oxidation of H_2S.

At the end of the rhizome around nodium 9, the pH imaging revealed high pH levels in the adjacent sediment (Fig. 7f). We speculate that such local pH enhancement may be due to high levels of accessible organic carbon in this specific region of the rhizoplane, as a result of tissue degradation and rhizome exudates, leading to proton consumption through microbial metabolisms such as sulphate reduction (Isaksen & Finster 1996; Blaabjerg *et al.* 1998; Hansen *et al.* 2000; Nielsen *et al.* 2001). These plant-microbial mediated local changes in the rhizosphere pH microenvironment are potentially very important for seagrasses as enhanced pH levels in the immediate rhizosphere lead to a shift in the sulphide speciation away from H_2S and towards non-permeable and thus non-phytotoxic HS^- ions. Besides formation of oxic microniches due to ROL (see above), rhizosphere pH changes represent another chemical defense mechanism, whereby the plants further detoxify the surrounding sediment to accommodate their own growth in the often reduced, anoxic environments (Brodersen *et al.* 2015a).

Biogeochemical processes

The enhanced photosynthetic activity of *Z. marina* L. at its photosynthetic temperature optimum (~24 °C) (Fig. 2), positively affects the production of photosynthates and thereby lead to diurnal increases in the secretion of root/rhizome exudates and ROL (Moriarty *et al.* 1986; Blaabjerg *et al.* 1998; Nielsen *et al.* 2001) that may stimulate the microbial activity (such as sulphate reduction and sulphide oxidation, respectively) on the root/rhizome surface and in the immediate rhizosphere. The overall higher pH levels measured in the immediate rhizosphere at 24 °C as compared to 16 °C (Fig. 5 & 6), may thus be a result of a temperature-induced enhancement in the plants photosynthetic activity leading to increased rhizome/root exudation of organic carbon to the rhizosphere (Moriarty *et al.* 1986; Blaabjerg *et al.* 1998). Such exudation could either directly increase the pH levels in the immediate rhizosphere and on the below-ground tissue surface through secreted allelochemicals like amines (although this would be an expensive chemical defence mechanism for the plants) and other alkaline substances, and/or indirectly via stimulation of microbial processes such as sulphate reduction (as indicated at the plant-derived oxic/anoxic interfaces (Fig. 7c & 8d)), in combination with the generally temperature-mediated increase of the sulphate reduction rates owing to reaction kinetics (Isaksen & Finster 1996; Blaabjerg *et al.* 1998). Sulphate reduction rates associated with rinsed *Zostera muelleri spp. capricorni* roots/rhizomes have been found to be up to 11 times higher than in the bulk sediment (Hansen *et al.* 2000), and both rhizome and roots have been shown to be important habitats for sulphate-reducing and N_2-fixing bacteria (Blaabjerg & Finster 1998; Nielsen *et al.* 2001). Sulphate-reducing bacteria associated with rhizomes/roots possess a high N_2-fixing activity that can cover up to 65% of the nitrogen needed by the seagrass plants (Hansen *et al.* 2000; Nielsen *et al.* 2001).

Notably, high sulphate reduction rates in the seagrass rhizosphere, furthermore, leads to a sulphide-induced release of sediment-bound phosphorus, as the reduction of Fe(III) (oxyhydroxides) to Fe(II) results in phosphate release to the pore water, which then becomes available for plant growth (Pollard & Moriarty 1991; Pagès *et al.* 2011, 2012). A mutual beneficial relationship between the *Zostera marina* L. plant host and sulphate reducing bacteria in the rhizoplane seems therefore likely during non-stressed environmental conditions, where the sulphate reducing bacteria provides nutrients in the form of nitrogen and phosphate to the plant host as a response to plant-mediated rhizome/root exudates. However, we note that this hypothesis remains speculative and needs further experimental support. Our study did not aim to investigate the role of sulphate reducing bacteria in the *Z. marina* rhizosphere, and as we have used a sterile artificial sediment any sulphate reducing bacteria in the immediate rhizosphere must have originated from the non-sterile plant tissue. Future studies could e.g. involve artificial sediment based on extracted pore water or even cultures of sulphate reducing bacteria in combination with quantification of bacteria around the root biomass, e.g. using FISH with group-specific probes.

In other microniches associated with the formation of oxic microzones (Fig. 7c & 8d) biological and/or spontaneous chemical sulphide re-oxidation processes reduced the rhizoplane pH levels (Fig. 5). Such hotspots of low pH may well be due to a relatively higher abundance of sulphide oxidizing bacteria at that specific region, as microbes associated with the below-ground tissue of seagrass show a patchy distribution (Nielsen *et al.* 2001).

Optical nanoparticle-based sensors incorporated into transparent artificial sediment

The combined use of O_2 and pH sensitive nanoparticles with transparent artificial sediments enabled combined chemical

and structural imaging on the whole rhizosphere level. This novel application of optical nanoparticle-based sensors represents an important supplement to existing methods, such as planar optodes and microsensors, when elucidating the rhizosphere of aquatic macrophytes, as the former rarely allows close contact to the entire belowground tissue at once and the latter rely on precise point measurements, which makes mapping the entire rhizosphere extremely tedious if not impossible. In addition, the optical nanoparticle-based sensors enable close spatial alignment of pH and O_2 concentration mapping thus facilitating co-localization of these important chemical parameters relative to particular plant/sediment and oxic/anoxic interfaces within the rhizosphere. However, at the current state, the present nanoparticle methodology only allows for O_2 and pH imaging in artificial sediments.

The strengths of employing such reduced artificial sediment, as compared to natural sediment, encompass: (i) significantly improved visual assessment within the investigated rhizosphere, thus allowing for determination of the exact position of the entire below-ground tissue during imaging, which is a necessity when determining the effects of plant/sediment interactions on the rhizosphere biogeochemistry, and (ii) changes observed within the homogenous artificial sediment can be assigned to plant-mediated alterations, which can be difficult to conclude in highly heterogeneous natural sediment. Weaknesses of using an artificial sediment matrix, as compared to natural sediment, include: (i) a significantly reduced microbial abundance in the bulk sediment, and (ii) a potential lower sediment pH buffering capacity, which may lead to slightly overestimated responses. Moreover, a minor limitation of current ratiometric pH imaging is that high energy excitation light has to be used when exciting the pH sensitive indicator dyes, potentially causing artefacts in the pH images owing to, for example, chlorophyll-derived red background luminescence. Further information on how to avoid/limit such potential artefacts in the pH images is available in the supporting information (Notes S1; Fig. S6). Nevertheless, nanoparticle-based imaging provides detailed information about the geochemical conditions and dynamics in the rhizosphere of aquatic macrophytes at high spatio-temporal resolution without the potential smearing effects seen with planar optodes and allows the first investigations of pH and O_2 dynamics in the entire seagrass rhizosphere in real-time and at all below-ground tissue/sediment interfaces. Nanoparticle-based imaging thus has the potential to further resolve important plant-sediment interactions, such as, for example, plant-derived sediment detoxification processes, in addition to, simply directing precise microsensor measurements to biogeochemical hotspots within natural sediment.

In conclusion, novel optical nanoparticle-based imaging revealed a pronounced spatio-temporal pH and O_2 microheterogeneity in the immediate rhizosphere of *Z. marina* L. Light stimulation of the leaf canopy and temperature elevation to the plants photosynthetically temperature optimum, i.e., from ~16 to 24 °C, lead to higher oxidation capacity of the belowground tissue and higher pH levels in the immediate rhizoplane, where the temperature-induced stimulation seemed to predominate. Low rhizosphere pH levels correlated with the plant-derived oxic microniches. Patchy distributions of high rhizosphere pH levels were found on the tissue surface, and cross tissue pH microprofiles revealed enhanced pH levels at selected oxic/anoxic interfaces. We speculate that the higher pH levels on the tissue surface and at the oxic/anoxic interface may be due to a plant-derived stimulation of proton consuming microbial metabolisms such as sulfate reduction and excretion of alkaline substances. Protons produced or consumed during microbial metabolisms, in addition to plant-mediated allelochemicals and chemical re-oxidation of H_2S, thus seemed responsible for the photosynthesis/temperature-driven alterations of the geochemical microenvironment determined in the *Zostera marina* L. rhizosphere.

CONFLICT OF INTEREST

The authors declare no conflict of interest and no competing financial interest.

ACKNOWLEDGMENTS

We would like to thank Egil Nielsen, University of Copenhagen (KU) for manufacturing the applied aquarium and experimental split flow chamber. We thank Sofie Lindegaard Jakobsen (KU) for technical assistance and Dr. Sergey Borisov (Graz University of Technology) for generously providing the used pH indicator. The study was funded by research grants from the Augustinus Foundation (KEB); Fab. P.A. Fiskers Fund (KEB); the Danish Council for Independent Research | Natural Sciences (MK); the Villum Foundation (MK, KK); and the Australian Research Council [ARC Linkage, LP 110200454] (MK).

REFERENCE

Armstrong J. & Armstrong W. (2001) Rice and *Phragmites*: effects of organic acids on growth, root permeability, and radial oxygen loss to the rhizosphere. *American Journal of Botany* **88**, 1359–1370.

Armstrong J. & Armstrong W. (2005) Rice: Sulfide-induced Barriers to Root Radial Oxygen Loss, Fe^{2+} and Water Uptake, and Lateral Root Emergence. *Annals of Botany* **96**, 625–638.

Barnabas A.D. (1996) Casparian band-like structures in the root hypodermis of some aquatic angiosperms. *Aquatic Botany* **55**, 217–225.

Binzer T., Borum J. & Pedersen O. (2005) Flow velocity affects internal oxygen conditions in the seagrass *Cymodocea nodosa*. *Aquatic Botany* **83**, 239–247.

Blaabjerg V. & Finster K. (1998) Sulphate reduction associated with roots and rhizomes of the marine macrophyte *Zostera marina*. *Aquatic Microbial Ecology* **15**, 311–314.

Blaabjerg V., Mouritsen K.N. & Finster K. (1998) Diel cycles of sulphate reduction rates in sediments of a *Zostera marina* bed (Denmark). *Aquatic Microbial Ecology* **15**, 97–102.

Borisov S.M., Herrod D.L. & Klimant I. (2009) Fluorescent poly(styrene-block-vinylpyrrolidone) nanobeads for optical sensing of pH. *Sensors and Actuators B: Chemical* **139**, 52–58.

Borum J., Pedersen O., Greve T.M., Frankovich T.A., Zieman J.C., Fourqurean J. W. & Madden C.J. (2005) The potential role of plant oxygen and sulphide dynamics in die-off events of the tropical seagrass, *Thalassia testudinum*. *Journal of Ecology* **93**, 148–158.

Borum J., Sand-Jensen K., Binzer T., Pedersen O. & Greve T.M. (2006) Oxygen movement in seagrasses. In *Seagrasses: Biology, Ecology and Conservation* (eds Larkum A.W.D., Orth J.R. & Duarte C.M.), pp. 255–270. Dordrecht, The Netherland Springer, Berlin.

Brodersen K.E., Nielsen D.A., Ralph P.J. & Kühl M. (2014) A split flow chamber with artificial sediment to examine the below-ground microenvironment of

aquatic macrophytes. *Marine Biology* **161**, 2921–2930. DOI:10.1007/s00227-014-2542-3.
Brodersen K.E., Nielsen D.A., Ralph P.J. & Kühl M. (2015a) Oxic microshield and local pH enhancement protects *Zostera muelleri* from sediment derived hydrogen sulphide. *New Phytologist* **205**, 1264–1276. DOI:10.1111/nph.13124.
Brodersen K.E., Lichtenberg M., Paz L.-C. & Kühl M. (2015b) Epiphyte-cover on seagrass (*Zostera marina* L.) leaves impedes plant performance and radial O_2 loss from the below-ground tissue. *Frontiers in Marine Science* **2**, 58. DOI:10.3389/fmars.2015.00058.
Colmer T.D. (2003) Long-distance transport of gases in plants: a perspective on internal aeration and radial oxygen loss from roots. *Plant, Cell & Environment* **26**, 17–36.
Enstone D.E., Peterson C.A. & Ma F. (2003) Root endodermis and exodermis: structure, function, and responses to the environment. *Journal of Plant Growth Regulation* **21**, 335–351.
Frederiksen M.S. & Glud R.N. (2006) Oxygen dynamics in the rhizosphere of *Zostera marina*: A two-dimensional planar optode study. *Limnology and Oceanography* **51**, 1072–1083.
Greve T.M., Borum J. & Pedersen O. (2003) Meristematic oxygen variability in eelgrass (*Zostera marina*). *Limnology and Oceanography* **48**, 210–216.
Hansen J.W., Udy J.W., Perry C.J., Dennison W.C. & Lomstein B.A. (2000) Effect of the seagrass *Zostera capricorni* on sediment microbial processes. *Marine Ecology Progress Series* **199**, 83–96.
Isaksen M.F. & Finster K. (1996) Sulphate reduction in the root zone of the seagrass *Zostera noltii* on the intertidal flats of a coastal lagoon (Arcachon, France). *Marine Ecology Progress Series* **137**, 187–194.
Isaksen M.F. & Jørgensen B.B. (1994) Thermophilic sulfate-reducing bacteria in cold marine sediment. *FEMS Microbiology Ecology* **14**, 1–8.
Jensen S.I., Kühl M., Glud R.N., Jørgensen L.B. & Prieme A. (2005) Oxic microzones and radial oxygen loss from roots of *Zostera marina*. *Marine Ecology Progress Series* **293**, 49–58.
Jensen S.I., Kühl M. & Prieme A. (2007) Different bacterial communities in the rhizoplane and bulk sediment of the seagrass *Zostera marina*. *FEMS Microbiology Ecology* **62**, 108–117.
Koren K., Brodersen K.E., Jakobsen S.L. & Kühl M. (2015) Optical sensor nanoparticles in artificial sediments – a new tool to visualize O_2 dynamics around the rhizome and roots of seagrasses. *Environmental Science and Technology* **49**, 2286–2292. DOI:10.1021/es505734b.
Lamers L.P., Govers L.L., Janssen I.C., Geurts J.J., Van der Welle M.E., Van Katwijk M.M., … Smolders A.J. (2013) Sulfide as a soil phytotoxin—a review. *Frontiers in plant science* **4**, 268. DOI:10.3389/fpls.2013.00268.
Larkum A.W.D., McComb A.J. & Shepherd S.A. (1989) *Biology of seagrass*. Elsevier, Amsterdam.
Larsen M., Borisov S.M., Grunwald B., Klimant I. & Glud R.N. (2011) A simple and inexpensive high resolution color ratiometric planar optode imaging approach: application to oxygen and pH sensing. *Limnology and Oceanography: Methods* **9**, 348–360.
McComb A.J., Dennison W.C. & Atwell B. (1999) Seagrasses: angiosperms adapted to sea floors. In *Plants in action*: *Adaptation in nature*, *performance in cultivation* (eds Kriedemann P.E., Atwell B.J. & Turnbull C.G.N.). Macmillan Education Australia Pty Ltd, Melbourne, Australia.
Moriarty D.J.W., Iverson R.L. & Pollard P.C. (1986) Exudation of organic carbon by the seagrass *Halodule wrightii* Aschers. and its effect on bacterial growth in the sediment. *Journal of Experimental Marine Biology and Ecology* **96**, 115–126.
Nielsen L.B., Finster K., Welsh D.T., Donelly A., Herbert R.A., De Wit R. & Lomstein B.A. (2001) Sulphate reduction and nitrogen fixation rates associated with roots, rhizomes and sediments from *Zostera noltii* and *Spartina maritima* meadows. *Environmental Microbiology* **3**, 63–71.
Pagès A., Teasdale P.R., Robertson D., Bennett W.W., Schäfer J. & Welsh D.T. (2011) Representative measurement of two-dimensional reactive phosphate distributions and co-distributed iron(II) and sulfide in seagrass sediment porewaters. *Chemosphere* **85**, 1256–1261.
Pagès A., Welsh D.T., Robertson D., Panther J.G., Schäfer J., Tomlinson R.B. & Teasdale P.R. (2012) Diurnal shifts in co-distributions of sulfide and iron(II) and profiles of phosphate and ammonium in the rhizosphere of *Zostera capricorni*. *Estuarine, Coastal and Shelf Science* **115**, 282–290.
Pedersen O., Binzer T. & Borum J. (2004) Sulphide intrusion in eelgrass (*Zostera marina* L.). *Plant. Cell and Environment* **27**, 595–602.
Pedersen O., Borum J., Duarte C.M. & Fortes M.D. (1998) Oxygen dynamics in the rhizosphere of *Cymodocea rotundata*. *Marine Ecology Progress Series* **169**, 283–288.
Pedersen O., Borum J., Duarte C.M. & Fortes M.D. (1999) ERRATUM: Oxygen dynamics in the rhizosphere of *Cymodocea rotundata*. *Marine Ecology Progress Series* **178**, 310.
Pollard P.C. & Moriarty D. (1991) Organic carbon decomposition, primary and bacterial productivity, and sulphate reduction, in tropical seagrass beds of the Gulf of Carpentaria, Australia. *Marine Ecology Progress Series* **69**, 149–159.
Ramsing N.B. & Gundersen J.K. (2015) Seawater and Gasses: Tabulated physical parameters of interest to people working with microsensors in marine systems: Unisense data tables. Available at: www.unisense.dk. Accessed March 30, 2016.
Raun A.L. & Borum J. (2013) Combined impact of water column oxygen and temperature on internal oxygen status and growth of *Zostera marina* seedlings and adult shoots. *Journal of Experimental Marine Biology and Ecology* **441**, 16–22.
Revsbech N.P. (1989) An oxygen microsensor with a guard cathode. *Limnology and Oceanography* **34**, 474–478.
Staehr P. & Borum J. (2011) Seasonal acclimation in metabolism reduces light requirements of eelgrass (*Zostera marina*). *Journal of Experimental Marine Biology and Ecology* **407**, 139–146.
Stahl H., Glud A., Schröder C.R., Klimant I., Tengberg A. & Glud R.N. (2006) Time-resolved pH imaging in marine sediments with a luminescent planar optode. *Limnology and Oceanography: Methods* **4**, 336–345.
Srinivasan K. & Mahadevan R. (2010) Characterization of proton production and consumption associated with microbial metabolism. *BMC Biotechnology* **10**, 2. DOI:10.1186/1472-6750-10-2.
Wang X., Stolwijk J.A., Lang T., Sperber M., Meier R.J., Wegener J. & Wolfbeis O.S. (2012) Ultra-small, highly stable, and sensitive dual nanosensors for imaging intracellular oxygen and pH in cytosol. *Journal of the American Chemical Society* **134**, 17011–17014.
Xie X., Mistlberger G. & Bakker E. (2013) Ultrasmall fluorescent ion-exchanging nanospheres containing selective ionophores. *Analytical Chemistry* **85**, 9932–9938.
Zhu Q., Aller R.C. & Fan Y. (2006) Two-dimensional pH distributions and dynamics in bioturbated marine sediments. *Geochimica et Cosmochimica Acta* **70**, 4933–4949.

Received 21 August 2015; received in revised form 29 February 2016; accepted for publication 3 March 2016

SUPPORTING INFORMATION

Additional Supporting Information may be found in the online version of this article at the publisher's web-site.

Figure S1. Luminescence spectra of the optical pH nanosensors.
Figure S2. Calibration of pH nanosensor luminescence.
Figure S3. Calibration curves for optical pH nanoparticle-based sensors.
Figure S4. pH microprofiles in the bulk, artificial sediment containing pH sensitive nanoparticles measured with both a calibrated pH microelectrode and the optical nanoparticle-based pH sensors.
Figure S5. Calibration curves of optical O2 nanoparticle-based sensors.
Figure S6. Potential artefacts in pH images.
Notes S1. Luminescence imaging.

frontiers in Marine Science

ORIGINAL RESEARCH
published: 20 August 2015
doi: 10.3389/fmars.2015.00058

Epiphyte-cover on seagrass (*Zostera marina* L.) leaves impedes plant performance and radial O_2 loss from the below-ground tissue

Kasper E. Brodersen[1*†], *Mads Lichtenberg*[2†], *Laura-Carlota Paz*[3] *and Michael Kühl*[1,2]

[1] *Plant Functional Biology and Climate Change Cluster, University of Technology, Sydney, Sydney, NSW, Australia,* [2] *Marine Biological Section, Department of Biology, University of Copenhagen, Helsingør, Denmark,* [3] *Department of Bioscience - Microbiology, Aarhus University, Aarhus, Denmark*

OPEN ACCESS

Edited by:
Christos Dimitrios Arvanitidis, Hellenic Centre for Marine Research, Greece

Reviewed by:
Jose M. Riascos, Universidad de Antofagasta, Chile
Eugenia T. Apostolaki, Hellenic Centre for Marine Research, Greece

***Correspondence:**
Kasper E. Brodersen, Plant Functional Biology and Climate Change Cluster (C3), Faculty of Science, University of Technology Sydney, PO Box 123, Broadway, NSW 2007, Australia
kasper.e.brodersen@student.uts.edu.au;
Website: elgetti.wordpress.com

[†] *These authors have contributed equally to this work.*

Specialty section:
This article was submitted to Marine Ecosystem Ecology, a section of the journal Frontiers in Marine Science

Received: *15 May 2015*
Accepted: *03 August 2015*
Published: *20 August 2015*

Citation:
Brodersen KE, Lichtenberg M, Paz L-C and Kühl M (2015) Epiphyte-cover on seagrass (Zostera marina L.) leaves impedes plant performance and radial O_2 loss from the below-ground tissue. Front. Mar. Sci. 2:58. doi: 10.3389/fmars.2015.00058

The O_2 budget of seagrasses is regulated by a complex interaction between several sources and sinks, which is strongly regulated by light availability and mass transfer over the diffusive boundary layer (DBL) surrounding the plant. Epiphyte growth on leaves may thus strongly affect the O_2 availability of the seagrass plant and its capability to aerate its rhizosphere as a defense against plant toxins. We used electrochemical and fiber-optic microsensors to quantify the O_2 flux, DBL, and light microclimate around leaves with and without filamentous algal epiphytes. We also quantified the below-ground radial O_2 loss (ROL) from roots (~1 mm from the root-apex) to elucidate how this below-ground oxic microzone was affected by the presence of epiphytes. Epiphyte-cover on seagrass leaves (~21% areal cover) resulted in reduced light quality and quantity for photosynthesis, thus leading to reduced plant fitness. A ~4 times thicker DBL around leaves with epiphyte-cover impeded gas (and nutrient) exchange with the surrounding water-column and thus the amount of O_2 passively diffusing down to the below-ground tissue through the aerenchyma in darkness. During light exposure of the leaves, radial oxygen loss from the below-ground tissue was ~2 times higher from plants without epiphyte-cover. In contrast, no O_2 was detectable at the surface of the root-cap tissue of plants with epiphyte-cover during darkness, leaving the plants more susceptible to sulfide intrusion. Epiphyte growth on seagrass leaves thus has a negative effect on the light climate during daytime and O_2 supply in darkness, hampering the plants performance and thereby reducing the oxidation capability of its below-ground tissue.

Keywords: epiphyte-cover, light, diffusive boundary layer, radial O_2 loss, oxic microshield, microenvironment

Introduction

Seagrasses are angiosperms that form coastal habitats of prime importance for marine biodiversity and carbon sequestration (Duarte, 2001; Duarte et al., 2005). Over the past century, seagrasses have faced an alarming global decline, owing to both direct and indirect human interference (Robblee et al., 1991; Zieman et al., 1999; Seddon et al., 2000; Plus et al., 2003; Orth et al., 2006). Seagrasses inhabit organic rich, reduced sediments and the exposure of their below-ground biomass to sediment-derived hydrogen sulfide (H_2S), as a result of inadequate internal aeration due to low

water-column O_2 levels during darkness, has been identified as a key factor in seagrass die-back events (Greve et al., 2003; Borum et al., 2005; Brodersen et al., 2015). Hydrogen sulfide is produced in reduced sediment through bacterial sulfate reduction, which is considered the quantitatively most important anaerobic degradation process in coastal marine sediment (Jørgensen, 1982). H_2S is a phytotoxin that leads to chemical asphyxiation, due to a strong chemical binding with cytochrome *c* in the mitochondrial electron transport chain (Eghbal et al., 2004; Pérez-Pérez et al., 2012; Lamers et al., 2013). If H_2S reaches the root tissue surface it may enter the lacunar system of the seagrass plant via lipid-solution permeation of the plasmalemma (Raven and Scrimgeour, 1997). Such H_2S intrusion into the below-ground tissue of seagrasses has mainly been related to inadequate internal aeration during night-time, as a result of a low water-column O_2 content and thus a decrease in the diffusive O_2 supply from the surrounding water-column (Pedersen et al., 2004; Borum et al., 2005). The amount of O_2 passively diffusing into the leaves from the water-column during darkness, is thus highly dependent on the water-column O_2 content, but is also strongly affected by other factors such as the DBL thickness (Binzer et al., 2005; Borum et al., 2006) and the leaf surface area. The DBL surrounds all aquatic surfaces, such as seagrass leaves, and functions as a diffusive barrier to the exchange of gasses and nutrients with the surrounding water-column by impeding water motions toward the leaf tissue surface (Jørgensen and Revsbech, 1985). The width and thus the mass transfer impedance of the DBL depends on factors such as the surface topography and the flow velocity, where e.g., relative low flow rates and uneven surfaces increases the thickness of the DBL (Jørgensen and Des Marais, 1990); both parameters are highly affected by epiphyte growth on the leaf surface.

Light availability is the key environmental factor regulating photosynthesis and thus the O_2 supply during day-time, and small decreases in irradiance can cause significant declines in the growth and distribution of seagrasses (Burkholder et al., 2007; Ralph et al., 2007). In eutrophic coastal waters, light can be attenuated up to 100-fold in the upper 1–4 m of the water column, often with dramatic changes in the spectral composition (Sand-Jensen and Borum, 1991). Therefore, rooted macrophytes are often spatially limited to biotopes with sufficient light exposure, i.e., water depths experiencing a minimum of 10% of surface irradiance for temperate seagrasses (Borum, 1983; Duarte, 1991). Eutrophication can stimulate epiphyte colonization on seagrass leaves (Richardson, 2006) potentially affecting the light availability for the plant. Epiphytes may thus have a major impact on the photosynthetic O_2 evolution of rooted macrophytes, such as seagrasses (Sand-Jensen, 1977).

The O_2 budget of seagrass plants is regulated by a complex interaction between several sources and sinks. Sources encompass photosynthetic O_2 evolution in leaves during day-time and passive diffusion of O_2 into the leaves from the water-column in darkness. Sinks encompass the total O_2 demand of the surrounding sediment, including bacterial respiration and chemical reactions with reduced compounds, as well as the plants own respiratory needs. The amount of O_2 produced or passively diffusing into the leaves is affected by external physical factors such as the light availability for underwater photosynthesis, the flow-dependent thickness of the DBL and the water-column O_2 content, whereas the sinks are highly affected by elevated seawater temperatures and the quantity of accessible organic matter in the rhizosphere (Pedersen et al., 2004; Binzer et al., 2005; Borum et al., 2006; Raun and Borum, 2013).

The O_2 is transported from the above-ground tissue to the below-ground tissue through the aerenchyma, i.e., an internal gas-filled lacunar system, whereby plants support aerobic metabolism in their root-system and provide protection against reduced toxic compounds such as H_2S and Fe^{2+} (Armstrong, 1979; Borum et al., 2006). Some of the transported O_2 is leaked to the rhizosphere as the so-called radial oxygen loss (ROL), especially at the basal leaf meristems, root-shoot junctions and root-caps (Koren et al., 2015). During non-stressful environmental conditions, ROL maintains a ~0.5 mm wide oxic microzone around the leaking areas that continuously oxidizes the surrounding sediment and thus alters the immediate sediment biogeochemistry in the seagrass rhizosphere (Pedersen et al., 1998; Jensen et al., 2005; Brodersen et al., 2015). This chemical defense mechanism is, however, negatively affected by over-night water-column hypoxia (Brodersen et al., 2015).

Seagrass morphology is an important controlling factor affecting the likelihood of H_2S intrusion into seagrasses, where a higher above- to below-ground biomass ratio positively affects the seagrasses oxidation capacity and reduces the risk of H_2S intrusion (Frederiksen et al., 2006). Seagrass roots possess structural barriers to ROL in mature root tissue regions such as Casparian band-like structures of suberin in the hypodermis (Barnabas, 1996). Such barriers to ROL in the basal-parts of seagrass roots increase the intra-plant O_2 transport to the active apical root meristem and therefore are very important for seagrass root metabolism.

In this study, we used electrochemical and fiber-optic microsensors to investigate effects of epiphyte-cover on seagrass leaves on the below-ground aeration of the rhizosphere of the seagrass *Zostera marina* kept in a custom-made split flow-chamber with natural sediment. This microenvironmental approach allowed us to (i) analyse the DBL and light microclimate around seagrass leaves with- and without epiphytes, and (ii) correlate changes in these above-ground micro-environmental parameters with changes in the ROL from the root-caps, and thereby, the oxidation capacity of the below-ground tissue.

Materials and Methods

Seagrass and Sediment Sampling

Marine sediment and *Z. marina* specimens with and without leaf epiphyte-cover were collected from shallow coastal waters (<2 m depth) at Aggersund, Limfjorden, Denmark. After sampling, plants and sediment were transported to a nearby field station (Rønbjerg Marine Biological Station, Aarhus University, Denmark), where they were kept in constantly aerated water reservoirs prior to experiments. Seagrass specimens with similar above- and below-ground biomass ratios were selected from the reservoirs and gently washed free of adhering sediment before

transferred to the experimental split flow-chamber (see below; Brodersen et al., 2014). In the following, seagrasses with epiphyte-cover refer to plants with ∼21% areal cover of filamentous algal epiphytes on leaves in contrast to seagrasses without visible leaf epiphyte-cover. The above- to below-ground biomass ratio was 1.0 and 0.8 of selected plants with and without leaf epiphyte-cover, respectively, based on g DW values obtained after drying the plants in an oven at 60°C until a constant weight was reached.

Experimental Setup

Plants were horizontally positioned in the flow-chamber (one plant at a time) with the leaf canopy in the free flowing water phase compartment and the below-ground biomass transplanted in homogenized sediment from the sampling site in the adjoining "sediment" compartment (**Figure 1**). An anoxic water column (∼2 cm depth) functioned as a liquid-phase diffusion barrier to O_2 intrusion over the sediment compartment of the flow chamber, as preliminary studies had shown a constant loss/efflux of reduced compounds such as H_2S from the sediment during incubation. Illumination of the leaf canopy was provided by a fiber-optic tungsten halogen lamp (KL-2500LCD, Schott GmbH, Germany). The downwelling photon irradiance (PAR, 400–700 nm) at the leaf surface was measured with a spherical quantum sensor (US-SQS/L, Walz GmbH, Germany) connected to a calibrated quantum irradiance meter (ULM-500, Walz GmbH, Germany). A constant flow (∼0.5 cm s^{-1}) of aerated seawater (∼22°C, Salinity = 30) was maintained in the seawater compartment of the flow chamber by means of a pump submersed in an aerated seawater reservoir (**Figure 1**).

Light and O_2 Measurements

We used scalar irradiance microprobes (sphere diameter 50 µm; manufactured by a modified procedure of Lassen et al., 1992; Rickelt et al., submitted) to quantify the light microenvironment around leaves of *Z. marina* with- and without epiphyte cover under two different irradiance levels (50 and 200 µmol photons m^{-2} s^{-1}; **Figure 1A**). The scalar irradiance microprobe was connected to a fiber-optic spectrometer (USB 2000+, Ocean Optics, USA), interfaced to a PC running spectral acquisition software (SpectraSuite, Ocean Optics, USA). We measured vertical profiles of spectral scalar irradiance in 0.1 mm steps from the leaf surface to 1 mm above the leaf surface, and in 1 mm steps from 1 to 10 mm from the leaf surface. To quantify the downwelling irradiance, we recorded spectra of the vertically incident light with the scalar irradiance microprobe tip positioned over a black non-reflective light well at the same position and distance in the light beam as the seagrass tissue surface; in a collimated light field the downwelling- and scalar irradiance are identical (Kühl and Jørgensen, 1994).

Clark-type O_2 microsensors (OX-10 and OX-50, Unisense A/S, Aarhus, Denmark; Revsbech, 1989) with a fast response

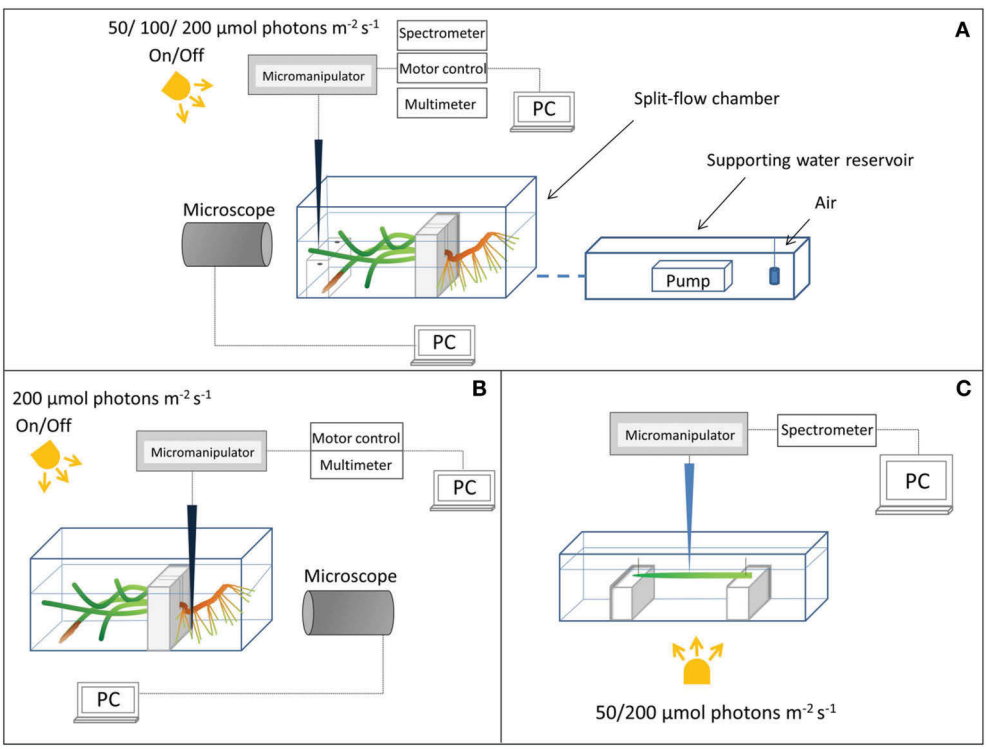

FIGURE 1 | Schematic diagram of the experimental setups. (A) Above-ground light and O_2 microsensor measurements. **(B)** Measurements on the below-ground chemical microenvironment with Clark-type O_2 microsensors. **(C)** Measuring light transmission spectra at the seagrass leaf surface.

time (<0.5 s) and low stirring sensitivity (<2–3%) were used to measure (i) the radial O_2 loss (ROL) from the below-ground biomass of *Z. marina* (∼1 mm from the root-apex; **Figure 1B**), and (ii) the O_2 concentration at and toward the leaf surface (**Figure 1A**). The O_2 microsensors were linearly calibrated from signal readings in 100% air saturated seawater and anoxic seawater (by addition of ascorbate) at experimental temperature and salinity; prior to calibrations and measurements in natural sediment, the microsensors were pre-contaminated with sulfide, i.e., they were pre-polarized in a Na_2S solution, to avoid drifting calibrations during experiments.

Microsensors were mounted on a motorized micromanipulator (Unisense A/S, Denmark) and connected to a PC-interfaced microsensor multimeter (Unisense A/S, Denmark); both were controlled by dedicated data acquisition and positioning software (SensorTrace Pro, Unisense A/S, Denmark). Microsensors and microprobes were carefully positioned at the tissue surface (defined as 0 μm) by manual operation of the micromanipulator, while observing the microsensor tip and tissue surface with a USB microscope (AD7013MZT, DinoLite, AnMo Electronics Corp., Taiwan). When positioning the O_2 microsensors at the below-ground tissue surface, a root from the first root-bundle was first gently un-covered from sediment before manually moving the microsensor to the surface of the root-cap, where after the root was gently covered again with sediment. Steady state O_2 levels at the below-ground tissue surface were re-established after ∼3 h (data not shown). Microprofiles of O_2 concentration were measured in depth increments of 50 μm.

Light Calculations

To quantify PAR, we integrated the measured scalar irradiance spectra over 400–700 nm and calculated the fractions of incident PAR irradiance for each measured depth position. By multiplying with the known incident photon irradiance (in μmol photons m^{-2} s^{-1}), measured with a calibrated quantum irradiance meter (ULM-500, Walz GmbH, Germany) equipped with a spherical quantum sensor (US-SQS/L, Walz GmbH, Germany), absolute photon scalar irradiance levels in each depth could be calculated as:

$$E(PAR)_z = \left(\frac{A_z}{A_D}\right) E_d$$

where $E(PAR)_z$ is the *PAR* photon scalar irradiance in depth z, A_z is the wavelength integrated signal in depth z, A_D is the wavelength integrated downwelling irradiance, and E_d is the downwelling photon irradiance (in μmol photons m^{-2} s^{-1}).

Since the leaves of *Z. marina* were ∼50 μm thick, it was not possible to measure internal light gradients in the leaves with microprobes. Instead we measured the spectral attenuation of light through leaves with and without epiphyte cover. A leaf, with- or without epiphytes, was positioned in a transparent acrylate chamber illuminated from below and with the incident irradiance determined as above (**Figure 1C**). Concomitantly, the microprobe was positioned at the abaxial surface of the leaf and the transmitted spectra were recorded on leaves with- and without epiphytes.

Flux Calculations

The O_2 flux between the leaf surface and the surrounding seawater was calculated using Fick's first law of diffusion:

$$J_{O_2} = -D_0 \frac{\partial C}{\partial z}$$

where D_0 is the molecular diffusion coefficient of O_2 in seawater at experimental temperature and salinity ($2.0845 \cdot 10^{-5}$ cm^{-2} s^{-1}; tabulated values available at www.unisense.com), and $\frac{\partial C}{\partial z}$ is the slope of the linear O_2 concentration gradient within the DBL.

A cylindrical version of Fick's first law of diffusion, described by Steen-Knudsen (2002), was used to calculate the ROL from the below-ground tissue surface (assuming a homogenous and cylinder-shaped O_2 loss from the roots):

$$J(r)_{root-cap} = \varphi D_0 (C_1 - C_2) / rln(\frac{r_1}{r_2})$$

where φ is the porosity of the sediment and φD_0 estimates the diffusivity of O_2 within the sediment at experimental temperature and salinity, r is the radius of the root, and C_1 and C_2 are the O_2 concentrations measured at the radial distances r_1 and r_2, respectively. Porosity was determined from the weight loss of wet sediment from the sampling site (known initial volume and weight) after drying at 60°C until a constant weight was reached (Porosity = 0.51).

Statistical Procedures

Data were tested for normality (Shapiro-Wilk) and equal variance prior to statistical analysis. Student's *t*-tests were used to compare treatments (with- or without leaf epiphytes) on data that met the above-mentioned assumptions. Mann-Whitney Rank Sum tests were used on data lacking normality and/or equal variance. A Two-Way ANOVA was performed to examine the influence of leaf epiphyte-cover and incident irradiance on O_2 fluxes across the leaf tissue surface (Table S1). Analysis of covariance (ANCOVA) was used to examine the effect of leaf epiphytes on scalar irradiance with distance from the leaf surface as a covariant. The significance level was set to $p < 0.05$. Statistical tests were performed in SigmaPlot and SPSS.

Results

Light Climate

Our observations on the light microclimate around the leaves of *Z. marina* revealed that epiphyte cover affect the quantity and quality of light reaching the seagrass leaf.

In the presence of epiphytes, photon scalar irradiance (PAR, 400–700 nm) on the surface of seagrass leaves was reduced by 54 and 92% under a downwelling photon irradiance of 50 and 200 μmol photons m^{-2} s^{-1}, respectively (**Figure 2**). Without epiphytes, we observed a 3 and 4% increase in photon scalar irradiance at incident irradiance levels of 50 and 200 μmol photons m^{-2} s^{-1}, respectively. Analysis of covariance (ANCOVA) confirmed significant difference in the scalar irradiance at the leaf tissue surface of plants with leaf epiphyte cover as compared to plants without leaf epiphyte cover

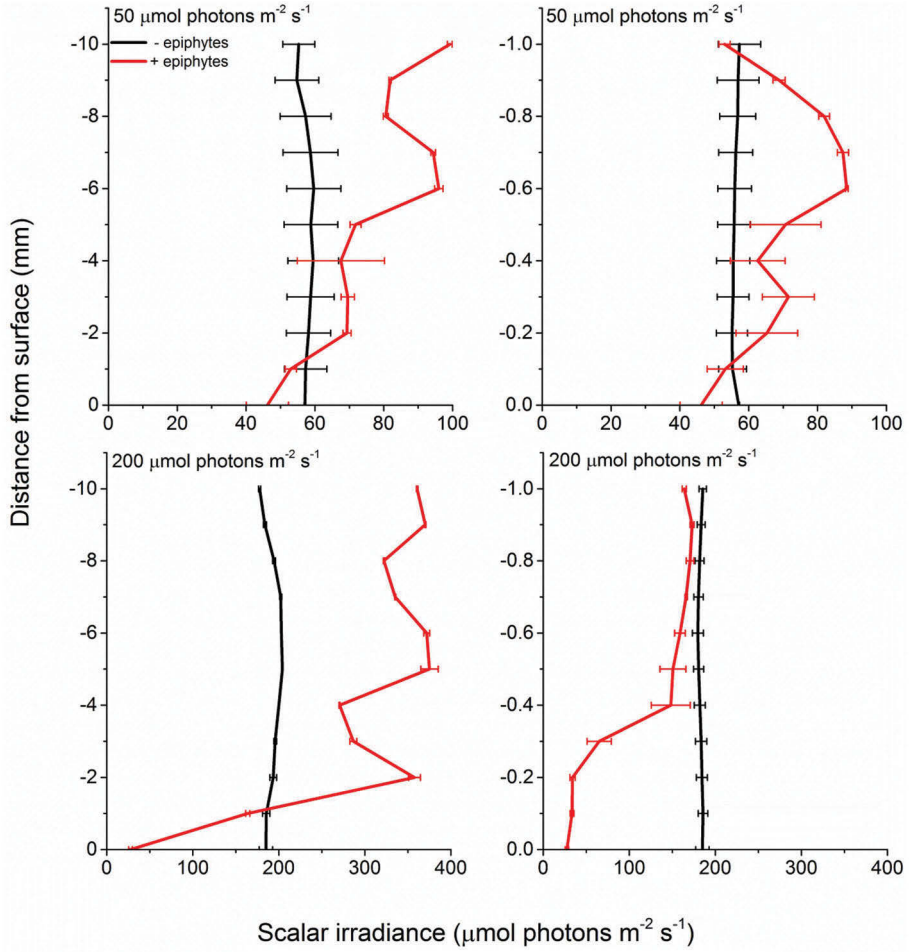

FIGURE 2 | Profiles of photon scalar irradiance measured at two different downwelling photon irradiances (50- and 200 μmol photons m^{-2} s^{-1}) on *Z. marina* leaves with- and without epiphyte cover. Left panels show the scalar irradiance 0–10 mm from the leaf surface measured in 1 mm steps. Right panels show the scalar irradiance 0–1 mm from the leaf surface measured in 0.1 mm steps (enlarged plots of the scalar irradiance showed in the left panels). Data points represents means ± S.D. $n = 3$; leaf level replicates.

($p < 0.01$), as well as between photon scalar irradiance measured at $z = 10$ mm and $z = 0$ mm for plants with leaf epiphyte cover ($p < 0.01$). No significant difference was found between photon scalar irradiance measured at $z = 10$ mm and $z = 0$ mm for plants without leaf epiphyte cover ($p > 0.05$).

The decrease in scalar irradiance in the upper canopy (1–10 mm above the leaf surface) was uniform across wavelengths in the PAR region, while a spectral shift became evident in the lower canopy (0–1 mm above the leaf surface) with blue light and light around 675 nm being absorbed preferentially (**Figure 3**). However, approaching the surface of the seagrass leaf we also observed an enhanced absorption around 625 nm indicative of phycocyanin found in cyanobacteria.

This was further clarified in the seagrass light transmission spectra (**Figure 4**) where, in the absence of epiphytes, mainly actinic light and light around 675 nm were absorbed, corresponding to the absorption spectrum of Chl *a*. In the presence of epiphytes there was a profound decrease in all wavelengths in the PAR region leading to a reduction in the transmitted light with 71 and 88% (downwelling photon irradiance of 50 and 200 μmol photons m^{-2} s^{-1}, respectively). Students *t*-tests performed at 425, 560, and 675 nm (except at 425 nm under an incident irradiance of 50 μmol photons m^{-2} s^{-1}, where a Mann-Whitney test was performed due to data lacking normality; $p < 0.05$) confirmed significant difference in the transmitted light spectra between plants with leaf epiphyte cover and plants without leaf epiphyte cover ($p < 0.01$). In addition there was a relatively larger absorption of green light in the presence of epiphytes, evident from a change in the ratio of wavelengths 560:675 nm from six without epiphytes to three with epiphytes suggesting absorption from accessory epiphyte pigments.

Diffusive Boundary Layer and Photosynthesis

The O_2 concentration microprofiles at the *Z. marina* leaf tissue surface revealed a ∼4 times thicker DBL around leaves with

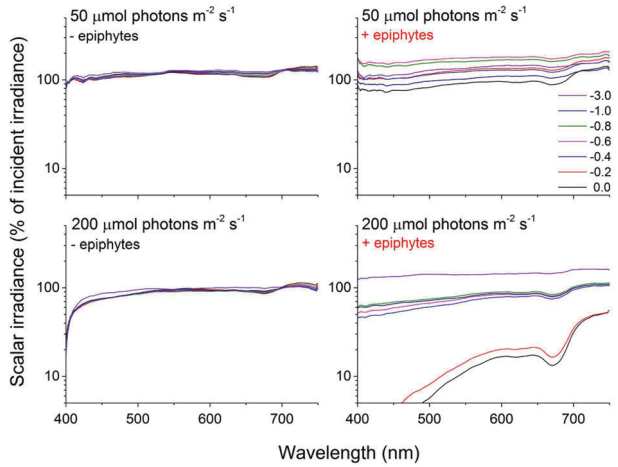

FIGURE 3 | Spectral scalar irradiance measured over *Z. marina* leaves under an incident irradiance of 50 and 200 µmol photons m^{-2} s^{-1} with- (right panels) and without epiphytes (left panels). Colored lines represents spectra collected at the given depths in mm above the leaf surface expressed as % of incident irradiance on a log-scale. $n = 3$; leaf level replicates.

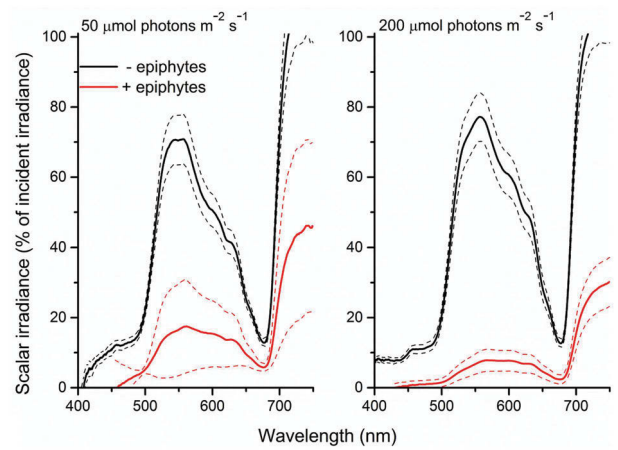

FIGURE 4 | Spectra of scalar irradiance transmitted through *Z. marina* leaves with- (red line) and without (black line) epiphyte cover and at two different downwelling photon irradiances (50- and 200-µmol photons m^{-2} s^{-1}). Dashed lines represents ± S.D. $n = 4$; leaf level replicates.

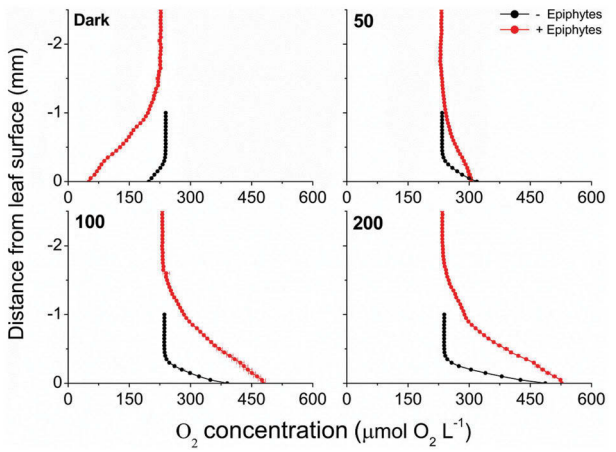

FIGURE 5 | Vertical microprofiles of the O_2 concentration measured toward the leaf surface under four different incident photon irradiances (0, 50, 100, and 200 µmol photons m^{-2} s^{-1}). Red symbols and lines represent leaves with 21% epiphyte-cover, Black symbols and lines represent leaves without epiphyte-cover. $y = 0$ indicates the leaf surface. Symbols and errors bars represent means ± SD. $n = 3$–4; leaf level replicates.

epiphyte-cover as compared to leaves without epiphyte-cover, i.e., an increase in the DBL thickness from ∼350 to 1400 µm (**Figure 5**). During darkness, passive diffusion of O_2 from the surrounding water-column resulted in a constant influx of O_2 into leaves both with and without epiphyte-cover, supporting the below-ground tissue with O_2 (**Figure 5**; **Table 1**). However, the thick DBL around leaves with epiphyte-cover impeded the diffusive O_2 supply in darkness as compared to plants without epiphyte-cover [seen as a reduction in the seagrass leaf surface O_2 concentration from ∼198 to 51 µmol L^{-1} (Student's *t*-test, $p < 0.001$); **Figure 5**], leaving these plants more vulnerable to low water-column O_2 contents at night-time.

Net O_2 production increased with increasing photon irradiance, as a result of enhanced shoot photosynthesis (**Figure 5**). The lower light availability for plants with epiphyte-cover resulted in relatively lower net photosynthesis rates, and the compensation irradiance increased from ∼12 to 27 µmol photons m^{-2} s^{-1} for plants with epiphyte-cover (**Figure 6**; **Table 1**). Despite the lower net photosynthesis in plants with leaf epiphyte-cover, there was a higher build-up of O_2 on the tissue surface under moderate photon irradiances (100 µmol photons m^{-2} s^{-1}) as compared to plants without leaf epiphyte-cover, owing to limited gas exchange with the surrounding water-column as a result of the enhanced DBL thickness.

Radial O_2 Loss

We used the measured steady state O_2 microprofiles around the root-cap of *Z. marina* with and without leaf epiphyte-cover (**Figure 7**), to calculate the radial O_2 flux into the surrounding sediment. In light, we calculated the ROL from the root-cap to be 65.7 nmol O_2 cm^{-2} h^{-1} from plants with leaf epiphyte-cover as compared to 152.7 nmol O_2 cm^{-2} h^{-1} from plants without leaf epiphyte-cover (**Table 1**). The ROL maintained a ∼300 µm thick oxic microzone around the root-cap of *Z. marina* (**Figure 7**). In darkness, the ROL from the root-cap dramatically decreased to 0 nmol O_2 cm^{-2} h^{-1} in plants with leaf epiphyte-cover (i.e., no O_2 was detectable at the root surface during darkness; **Figure 7**), and 0.8 nmol O_2 cm^{-2} h^{-1} in plants without leaf epiphyte-cover (**Table 1**). Epiphyte-covered plants did thus lose their oxic microshield against H_2S intrusion in darkness.

Discussion

Our results provide clear experimental evidence that epiphyte growth on *Z. marina* leaves reduces both light quantity and quality reaching the seagrass leaf, thereby impeding the overall

TABLE 1 | O_2 fluxes across the leaf surface and radial O_2 loss from the root-cap (~1 mm from the root-apex).

Downwelling photon irradiance μmol photons m^{-2} s^{-1}	Leaves (+ Epiphytes) nmol O_2 cm^{-2} h^{-1}	Leaves (– Epiphytes) nmol O_2 cm^{-2} h^{-1}	Root-cap (+ Epiphytes) nmol O_2 cm^{-2} h^{-1}	Root-cap (- Epiphytes) nmol O_2 cm^{-2} h^{-1}
0	−106.4 ± 1.8	−107.1 ± 1.0	0	0.8 ± 0.1
50	60.6 ± 4.0[a]	271.9 ± 3.3	(–)	(–)
100	164.7 ± 4.9[a]	520.7 ± 12.8	(–)	(–)
200	221.2 ± 27.8[a]	800.9 ± 14.7	65.7 ± 21.0[b]	152.7 ± 7.5

(-) indicate no data points. Negative values denote net O_2 uptake. Rates are mean ± S.D. n = 3–5; leaf/root level replicates.
[a,b]Indicates significant difference between seagrasses with leaf epiphyte cover as compared to seagrasses without leaf epiphyte cover (control plants) ([a]Two-Way ANOVA, $F_{3,\ 3\ (PAR)} = 2931.2$, $F_{1,\ 3\ (epiphytes)} = 3555.1$, $p < 0.01$; [b]Mann-Whitney test, $p < 0.05$).

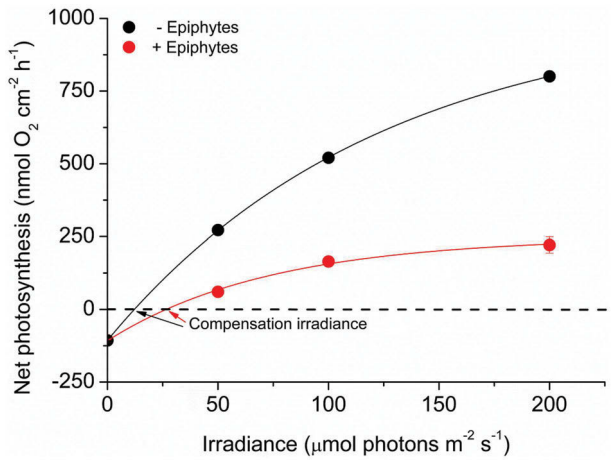

FIGURE 6 | Net photosynthesis rates as a function of downwelling photon irradiance. Rates were calculated for the four different incident irradiances (0, 50, 100, and 200 μmol photons m^{-2} s^{-1}) and were fitted with a hyperbolic tangent function (Webb et al., 1974) with an added term to account for respiration (Spilling et al., 2010) ($R^2 = 0.99$). Red symbols and line represent leaves with ~21% epiphyte-cover. Black symbols and line represent leaves without epiphyte-cover. Error bars are ±SD. $n = 3–4$; leaf level replicates.

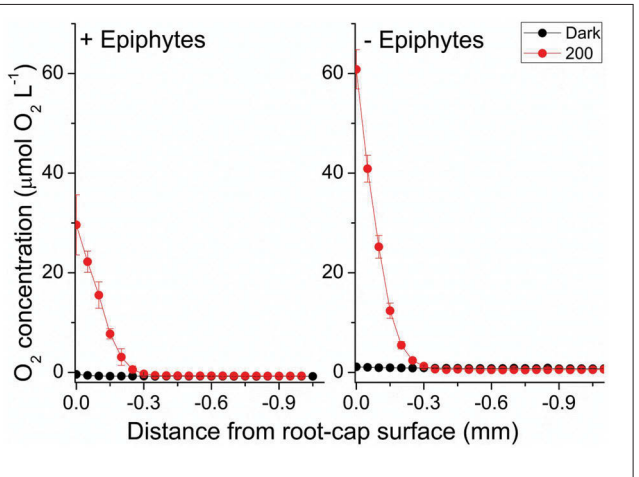

FIGURE 7 | Radial O_2 loss from the root-cap of *Z. marina* (~1 mm from the root-apex) to the immediate rhizosphere measured at two different photon irradiances (0 and 200 μmol photons m^{-2} s^{-1}). Left panel show radial O_2 loss from seagrass with leaf epiphyte-cover, right panel show radial O_2 loss from seagrass without leaf epiphyte-cover. $X = 0$ indicates the root surface. Error bars are ±SD. $n = 3–5$; root level replicates.

plant performance during day-time. Furthermore, leaf epiphyte-cover lead to an enhanced thickness of the DBLs surrounding the leaves, thus impeding the exchange of gasses and essential nutrients with the ambient water-column. In darkness, this resulted in a negative effect on the intra-plant O_2 status that subsequently reduced the oxidation capability of the below-ground tissue, thereby rendering plants more vulnerable to sediment-produced reduced phytotoxic compounds, such as H_2S.

Light Microenvironment and Shoot Photosynthesis

Light availability on the surface of the leaves of *Z. marina* covered by epiphytes was dramatically decreased compared to leaves without epiphytes in agreement with previous studies (Drake et al., 2003; Pedersen et al., 2014). Effectively, this means that a higher downwelling photon irradiance is needed to meet the compensation irradiance for the epiphyte covered leaf (**Figure 6**). We expected a larger change in the spectral quality of light reaching the leaf surface through the epiphyte canopy, but as the generation time of unicellular and filamentous algae colonizing the seagrass are short relative to the seagrass leaves, there might have been a large proportion of dead epiphytes thus acting as particulate organic matter with a more uniform light attenuation (**Figure 3**, upper right). However, in the lower epiphyte canopy (0–1 mm above the seagrass surface) there was a non-uniform attenuation of light leading to a strong reduction in blue light reaching the seagrass surface (**Figure 3**, lower right). In the transmittance spectra, we saw a disproportionate large amount of green light being attenuated in the presence of epiphytes indicating the presence of a community possessing accessory pigments able to utilize green light, such as red algal or cyanobacterial phycobiliproteins.

Although a large proportion of the green light was attenuated by epiphytes, blue and red light were almost completely removed, leaving the plant in a light environment with predominately green light which is less effectively absorbed by Chl *a*. Thus, both quality and especially the quantity of light were diminished in the presence of epiphytes thereby leaving the plant for longer periods near the minimal light requirement for growth, which

is high in *Z. marina* (∼20% of surface irradiance; Dennison et al., 1993). A recent study showed ∼90% reduction in biomass under prolonged diminished light conditions, comparable to the decrease in light shown here (Kim et al., 2015). It has been speculated that the high minimum light requirement for growth reflects that seagrasses often grow in anoxic, sulfide-rich sediments (Ralph et al., 2007). The presence of sulfide results in decreased photosynthesis and increased O_2 consumption in the dark (Goodman et al., 1995; Holmer and Bondgaard, 2001), which means that more light is needed to drive a sufficient photosynthetic O_2 supply to maintain positive growth. Diminished light conditions due to epiphyte cover can thus reduce the fitness of the plant.

The ∼4 times enhanced DBL thickness around leaves with epiphyte-cover adversely affected the internal O_2 supply to the below-ground tissue at night-time. In addition, it lead to a build-up of O_2 at the leaves surface under high incident photon irradiance (≥100 μmol photons m^{-2} s^{-1}; **Figure 5**), which potentially could lead to enhanced photorespiration (as surplus internal O_2 molecules may bind competitively to RuBisCO instead of CO_2 resulting in decreased CO_2 fixation and reduced photosynthetic efficiency) and/or internal oxidative stress (Maberly, 2014). At low photon irradiance (50 μmol photons m^{-2} s^{-1}), the reduced light availability and lower photosynthetic activity, seemed to counter-balance this internal O_2 build-up caused by the insulating DBL (**Figure 5**). Furthermore, the epiphytes themselves, i.e., filamentous algal epiphytes and most probably leaf- and filamentous algal epiphyte-associated bacterial communities, contribute with oxygenic photosynthesis and respiration, thereby further enhancing the O_2 consumption at the leaf surface during night-time. Correspondingly, we found a ∼2 times higher compensation irradiance of plants with leaf epiphyte-cover, as compared to plants without epiphyte-cover (**Figure 6**). This may be a very important factor during prolonged events of poor light conditions, such as during dredging operations and eutrophication, making plants with leaf epiphyte-cover more prone to sulfide invasion as a result of inadequate internal aeration (Pedersen et al., 2004; Borum et al., 2005). The generally reduced net photosynthesis rates of plants with epiphyte-cover (**Figure 6**), was most likely a combined result of the poor light conditions and a limited influx of CO_2 from the surrounding water-column. Such DBL-induced limited gas exchange with the ambient water-column can lead to inorganic carbon limitation enhancing photorespiration (e.g., Maberly, 2014) thereby impeding shoot photosynthesis.

Light-driven O_2 Microdynamics in the Rhizosphere

Photosynthetic O_2 evolution resulted in the establishment of a ∼300 μm wide oxic microzone around the root-cap of *Z. marina* at the approximate position of the apical root meristem (**Figure 7**). Plants with epiphyte-cover exhibited a negative effect on the below-ground tissue oxidation capacity with ∼2 times lower ROL from the root-apex during light stimulation of the leaf canopy, as compared to plants without leaf epiphyte-cover. Although the ROL in light from the root-cap of plants with and without epiphyte-cover were of similar magnitude to fluxes previously reported by Jensen et al. (2005; Table 1), a lower oxidation capability of the below-ground tissue will almost certainly have a negative effect on the overall plants performance. ROL has been shown to improve the chemical conditions in the immediate rhizosphere of seagrasses due to enhanced sulfide reoxidation (Brodersen et al., 2015). The oxic microshield at the root-cap surface can thus protect the apical root meristem from reduced phytotoxic compounds, such as H_2S, through chemical re-oxidation with O_2.

Dark O_2 Microdynamics in the Rhizosphere

During darkness, no O_2 was detected at the root-cap surface of plants with leaf epiphyte-cover, indicative of inadequate internal aeration in contrast to plants without leaf epiphyte-cover, where low levels of O_2 were detectable at the root-cap surface during darkness (**Figure 7**; **Table 1**). Such breakdown of the oxic microshield in presence of epiphytes on seagrass leaves can be of great importance, as a shift to anaerobic metabolism in the root-system results in a much less efficient energy utilization than with aerobic metabolism, as anaerobic conditions inhibit the translocation of carbohydrates supporting plant metabolism (Zimmerman and Alberte, 1996; Greve et al., 2003). Previous studies of *Z. marina* have shown that the ROL from the root-apex persists during darkness at a much higher flux rate (up to 16.2 nmol O_2 cm^{-2} h^{-1} measured 2 mm behind the root-apex) than reported in this study (Jensen et al., 2005; Frederiksen and Glud, 2006). This apparent discrepancy may be explained by bacterial colonization of the root-cap surface consuming the small amounts of leaked O_2 through microbial respiration and/or by ferrous sulfide (FeS) and iron plaques. Sulfate reducing bacteria have thus previously been isolated from surface-sterilized roots of *Z. marina* (Nielsen et al., 1999; Finster et al., 2001).

Interestingly, the root-cap mediated O_2 leakage to the rhizosphere may also be important for plant-beneficial root-associated microbial processes, such as H_2S re-oxidation, in addition to simply detoxifying reduced substances in the immediate rhizosphere through spontaneous chemical reactions. Bacterially-mediated H_2S oxidation is about 10.000–100.000 times faster than the chemical reaction alone (Jørgensen and Postgate, 1982) and therefore has potential to be of high value for the plants. It has been suggested that H_2S oxidation also takes place inside the plant (Holmer et al., 2005; Holmer and Hasler-Sheetal, 2014), as seagrass exposed to high sediment H_2S levels showed internal accumulation of elemental sulfur that is an intermediate in the sulfide oxidation. This process is, however, driven by simple chemical reactions between H_2S and O_2 and is not mediated by intra-plant enzymes or bacteria (Pedersen et al., 2004) as seen in some marine invertebrates (Grieshaber and Völkel, 1998).

The lower light availability for photosynthesis of plants with filamentous algal epiphyte-cover seemed to be the key factor behind the lower ROL from the root-cap (**Figure 7**), as a result of the relative lower net photosynthesis rates and thereby lower O_2 production in leaves, as compared to plants without epiphyte-cover (**Figure 6**). This might seem obvious, but the DBL-induced impedance of O_2 exchange with the water-column of plants with

epiphyte-cover, could also have resulted in an enhancement in the aerenchymal O_2 level (seen as the build-up in the surface O_2 concentration on **Figure 5**) and thereby a concomitant higher ROL from the root-apex, but this effect was apparently overruled by lower seagrass photosynthesis due to epiphyte shading and/or inorganic carbon limitation due to increased DBL thickness.

Burnell et al. (2014) recently demonstrated that high incident photon irradiance (∼200 μmol photons m^{-2} s^{-1}) in combination with elevated water-column CO_2 concentrations (up to 900 μl L^{-1}, representing future predictions of enhanced water-column CO_2 levels) had a negative effect on seagrass biomass and leaf growth, as compared to low light conditions. The observed negative growth response to combined high CO_2 and light conditions appeared to be closely related to overgrowth of seagrass leaves with filamentous algal epiphytes. This finding supports our microsensor measurements demonstrating the negative effects of leaf epiphyte-cover on the intra-plant O_2 status and the below-ground tissue oxidation capacity. Epiphyte-impeeded O_2 evolution in seagrass leaves causing reduced internal aeration and increased H_2S intrusion may result in enhanced seagrass mortality if unfavorable light conditions persist for longer periods of time. This emphasizes the importance of minimizing nutrient loading into seagrass inhabited marine coastal waters, as eutrophication often leads to poor light conditions, low water quality, algal blooms and enhanced night-time O_2 consumption in the water column.

In conclusion, the present study shows that epiphyte-cover of seagrass leaves leads to reduced oxidation capability of the below-ground tissue, due to a combined result of lower light availability and thicker DBLs around leaves, impeding seagrass photosynthesis. This synergetic negative effect on the plants performance, resulted in a ∼2 times higher compensation irradiance in *Z. marina* leaving epiphyte-covered seagrasses more vulnerable to H_2S invasion during prolonged events of poor light conditions in the surrounding water-column. Seagrasses with leaf epiphyte-cover are thus more prone to anthropogenic impacts and activity in coastal environments, as leaf epiphytes reduce their resilience toward environmental disturbances.

Author Contributions

KB, ML, LP, and MK designed the research. KB, ML, and LP conducted the experiments. KB, ML, LP, and MK analyzed the data. KB and ML wrote the manuscript with editorial help from MK. All authors have given approval to the final version of the manuscript. The authors declare no competing financial interest.

Acknowledgments

We thank Unisense A/S, the microbiology group at Aarhus University and Johan F. Kraft for providing the microsensor equipment used in this study. We thank Lars F. Rickelt for manufacturing the scalar irradiance microsensors and Peter Ralph (UTS) for financial support of KB. The research was funded by grants from the *Augustinus Foundation*, *P. A. Fiskers Fund* and *Jorck and Wife's Fund* (KB), the *Danish Council for Independent Research |Natural Sciences* (MK), and the *Australian Research Council* (ARC LP 110200454) (MK).

Supplementary Material

The Supplementary Material for this article can be found online at: http://journal.frontiersin.org/article/10.3389/fmars.2015.00058

References

Armstrong, W. (1979). *Aeration in Higher Plants*. London: Academic Press.

Barnabas, A. D. (1996). Casparian band-like structures in the root hypodermis of some aquatic angiosperms. *Aquat. Bot.* 55, 217–225. doi: 10.1016/S0304-3770(96)01072-8

Binzer, T., Borum, J., and Pedersen, O. (2005). Flow velocity affects internal oxygen conditions in the seagrass *Cymodocea nodosa*. *Aquat. Bot.* 83, 239–247. doi: 10.1016/j.aquabot.2005.07.001

Borum, J. (1983). "The quantitative role of macrophytes, epiphytes, and phytoplankton under different nutrient conditions in Roskilde Fjord, Denmark," in *Proceedings of the International Symposium on Aquatic Macrophytes* (Nijmegen), 35–40.

Borum, J., Pedersen, O., Greve, T. M., Frankovich, T. A., Zieman, J. C., Fourqurean, J. W., et al. (2005). The potential role of plant oxygen and sulphide dynamics in die-off events of the tropical seagrass, *Thalassia testudinum*. *J. Ecol.* 93, 148–158. doi: 10.1111/j.1365-2745.2004.00943.x

Borum, J., Sand-Jensen, K., Binzer, T., Pedersen, O., and Greve, T. (2006). "Oxygen movement in seagrasses," in *Seagrasses: Biology, Ecology and Conservation*, eds A. W. D. Larkum, J. R. Orth, and C. M. Duarte (Dordrecht; Berlin: Springer), 255–270.

Brodersen, K. E., Nielsen, D. A., Ralph, P. J., and Kühl, M. (2014). A split flow chamber with artificial sediment to examine the below-ground microenvironment of aquatic macrophytes. *Mar. Biol.* 161, 2921–2930. doi: 10.1007/s00227-014-2542-3

Brodersen, K. E., Nielsen, D. A., Ralph, P. J., and Kühl, M. (2015). Oxic microshield and local pH enhancement protects *Zostera muelleri* from sediment derived hydrogen sulphide. *New Phytol.* 205, 1264–1276. doi: 10.1111/nph.13124

Burkholder, J. M., Tomasko, D. A., and Touchette, B. W. (2007). Seagrasses and eutrophication. *J. Exp. Mar. Biol. Ecol.* 350, 46–72. doi: 10.1016/j.jembe.2007.06.024

Burnell, O. W., Russell, B. D., Irving, A. D., and Connell, S. D. (2014). Seagrass response to CO_2 contingent on epiphytic algae: indirect effects can overwhelm direct effects. *Oecologia* 176, 871–882. doi: 10.1007/s00442-014-3054-z

Dennison, W. J., Orth, R. J., Moore, K. A., Stevenson, J. C., Carter, V., Kollar, S., et al. (1993). Assessing water quality with submerged aquatic vegetation. *Bioscience* 43, 86–94. doi: 10.2307/1311969

Drake, L. A., Dobbs, F. C., and Zimmerman, R. C. (2003). Effects of epiphyte load on optical properties and photosynthetic potential of the seagrasses *Thalassia testudinum* Banks ex König and *Zostera marina* L. *Limnol. Ocenogr.* 48, 456–463. doi: 10.4319/lo.2003.48.1_part_2.0456

Duarte, C. M. (1991). Seagrass depth limits. *Aquat. Bot.* 40, 363–377. doi: 10.1016/0304-3770(91)90081-F

Duarte, C. M. (2001). "Seagrass ecosystems," in *Encyclopedia of Biodiversity,* Vol 5, ed S. L. Leven (San Diego, CA: Academic Press), 254–268. doi: 10.1016/B0-12-226865-2/00241-8

Duarte, C. M., Middelburg, J. J., and Caraco, N. (2005). Major role of marine vegetation on the oceanic carbon cycle. *Biogeosciences* 2, 1–8. doi: 10.5194/bg-2-1-2005

Eghbal, M. A., Pennefather, P. S., and O'Brien, P. J. (2004). H_2S cytotoxicity mechanism involves reactive oxygen species formation and mitochondrial depolarisation. *Toxicology* 203, 69–76. doi: 10.1016/j.tox.2004.05.020

Finster, K., Thomsen, T. R., and Ramsing, N. B. (2001). *Desulfomusa hansenii* gen. nov., sp. nov., a novel marine propionate-degrading, sulfate-reducing bacterium isolated from *Zostera marina* roots. *Int. J. Syst. Evol. Microbiol.* 51, 2055–2061. doi: 10.1099/00207713-51-6-2055

Frederiksen, M. S., and Glud, R. N. (2006). Oxygen dynamics in the rhizosphere of *Zostera marina*: a two-dimensional planar optode study. *Limnol. Oceanogr.* 51, 1072–1083. doi: 10.4319/lo.2006.51.2.1072

Frederiksen, M. S., Holmer, M., Borum, J., and Kennedy, H. (2006). Temporal and spatial variation of sulfide invasion in eelgrass (*Zostera marina*) as reflected by its sulfur isotopic composition. *Limnol. Oceanogr.* 51, 2308–2318. doi: 10.4319/lo.2006.51.5.2308

Goodman, J. L., Moore, K. A., and Dennison, W. C. (1995). Photosynthetic responses of eelgrass (*Zostera marina* L.) to light and sediment sulfide in a shallow barrier island lagoon. *Aquat. Bot.* 50, 37–47. doi: 10.1016/0304-3770(94)00444-Q

Greve, T. M., Borum, J., and Pedersen, O. (2003). Meristematic oxygen variability in eelgrass (*Zostera marina*). *Limnol. Oceanogr.* 48, 210–216. doi: 10.4319/lo.2003.48.1.0210

Grieshaber, M. K., and Völkel, S. (1998). Animal adaptations for tolerance and exploitation of poisonous sulfide. *Annu. Rev. Physiol.* 60, 33–53. doi: 10.1146/annurev.physiol.60.1.33

Holmer, M., and Bondgaard, E. J. (2001). Photosynthetic and growth response of eelgrass to low oxygen and high sulfide concentrations during hypoxic events. *Aquat. Bot.* 70, 29–38. doi: 10.1016/S0304-3770(00)00142-X

Holmer, M., Frederiksen, M., and Møllegaard, H. (2005). Sulfur accumulation in eelgrass (*Zostera marina*) and effect of sulfur on eelgrass growth. *Aquat. Bot.* 81, 367–379. doi: 10.1016/j.aquabot.2004.12.006

Holmer, M., and Hasler-Sheetal, H. (2014). Sulfide intrusion in seagrasses assessed by stable sulfur isotopes – a synthesis of current results. *Front. Mar. Sci.* 1:64. doi: 10.3389/fmars.2014.00064

Jensen, S. I., Kühl, M., Glud, R. N., Jørgensen, L. B., and Prieme, A. (2005). Oxic microzones and radial oxygen loss from roots of *Zostera marina*. *Mar. Ecol. Prog. Ser.* 293, 49–58. doi: 10.3354/meps293049

Jørgensen, B. B. (1982). Mineralization of organic matter in the sea bed - the role of sulfate reduction. *Nature* 296, 643–645. doi: 10.1038/296643a0

Jørgensen, B. B., and Des Marais, D. J. (1990). The diffusive boundary layer of sediments: oxygen microgradients over a microbial mat. *Limnol. Oceanogr.* 35, 1343–1355. doi: 10.4319/lo.1990.35.6.1343

Jørgensen, B. B., and Postgate, J. R. (1982). Ecology of the bacteria of the Sulfur cycle with special reference to anoxic oxic interface environments. *Philos. Trans. R. Soc. Lond. B Biol. Sci.* 298, 543–561. doi: 10.1098/rstb.1982.0096

Jørgensen, B. B., and Revsbech, N. P. (1985). Diffusive boundary layers and the oxygen uptake of sediments and detritus. *Limnol. Oceanogr.* 30, 111–122. doi: 10.4319/lo.1985.30.1.0111

Kim, Y. K., Kim, S. H., and Lee, K. S. (2015). Seasonal growth responses of the seagrass *Zostera marina* under severely diminished light conditions. *Estuar. Coasts* 38, 558–568. doi: 10.1007/s12237-014-9833-2

Koren, K., Brodersen, K. E., Jakobsen, S. L., and Kühl, M. (2015). Optical sensor nanoparticles in artificial sediments – a new tool to visualize O_2 dynamics around the rhizome and roots of seagrasses. *Environ. Sci. Technol.* 49, 2286–2292. doi: 10.1021/es505734b

Kühl, M., and Jørgensen, B. B. (1994). The light-field of microbenthic communities - radiance distribution and microscale optics of sandy coastal sediments. *Limnol. Oceanogr.* 39, 1368–1398. doi: 10.4319/lo.1994.39.6.1368

Lamers, L. P., Govers, L. L., Janssen, I. C., Geurts, J. J., Van der Welle, M. E., Van Katwijk, M. M., et al. (2013). Sulfide as a soil phytotoxin—a review. *Front. Plant Sci.* 4:268. doi: 10.3389/fpls.2013.00268

Lassen, C., Ploug, H., and Jørgensen, B. B. (1992). A fiberoptic scalar irradiance microsensor - application for spectral light measurements in sediments. *FEMS Microbiol. Ecol.* 86, 247–254. doi: 10.1111/j.1574-6968.1992.tb04816.x

Maberly, S. C. (2014). The fitness of the environments of air and water for photosynthesis, growth, reproduction and dispersal of photoautotrophs: an evolutionary and biogeochemical perspective. *Aquat. Bot.* 118, 4–13. doi: 10.1016/j.aquabot.2014.06.014

Nielsen, J. T., Liesack, W., and Finster, K. (1999). *Desulfovibrio zosterae* sp. nov., a new sulphate reducer isolated from surface-sterilized roots of the seagrass *Zostera marina*. *Int. J. Syst. Evol. Microbiol.* 49, 859–865.

Orth, R. J., Carruthers, T. J., Dennison, W. C., Duarte, C. M., Fourqurean, J. W., Heck, K. L., et al. (2006). A global crisis for seagrass ecosystems. *Bioscience* 56, 987–996. doi: 10.1641/0006-3568(2006)56[987:AGCFSE]2.0.CO;2

Pedersen, M. F., Nejrup, L. B., Pedersen, T. M., and Frederiksen, S. (2014). Sub canopy light conditions only allow low annual net productivity of epiphytic algae on kelp *Laminaria hyperborea*. *Mar. Ecol. Prog. Ser.* 516, 163–176. doi: 10.3354/meps11019

Pedersen, O., Binzer, T., and Borum, J. (2004). Sulphide intrusion in eelgrass (*Zostera marina* L.). *Plant Cell Environ.* 27, 595–602. doi: 10.1111/j.1365-3040.2004.01173.x

Pedersen, O., Borum, J., Duarte, C. M., and Fortes, M. D. (1998). Oxygen dynamics in the rhizosphere of *Cymodocea rotundata*. *Mar. Ecol. Prog. Ser.* 169, 283–288. doi: 10.3354/meps169283

Pérez-Pérez, M. E., Lemaire, S. D., and Crespo, J. L. (2012). Reactive oxygen species and autophagy in plants and algae. *Plant Physiol.* 160, 156–164. doi: 10.1104/pp.112.199992

Plus, M., Deslous-Paoli, J.-M., and Dagault, F. (2003). Seagrass (*Zostera marina* L.) bed recolonisation after anoxia-induced full mortality. *Aquat. Bot.* 77, 121–134. doi: 10.1016/S0304-3770(03)00089-5

Ralph, P. J., Durako, M. J., Enriquez, S., Collier, C. J., and Doblin, M. A. (2007). Impact of light limitation on seagrasses. *J. Exp. Mar. Biol. Ecol.* 350, 176–193. doi: 10.1016/j.jembe.2007.06.017

Raun, A. L., and Borum, J. (2013). Combined impact of water column oxygen and temperature on internal oxygen status and growth of *Zostera marina* seedlings and adult shoots. *J. Exp. Mar. Biol. Ecol.* 441, 16–22. doi: 10.1016/j.jembe.2013.01.014

Raven, J. A., and Scrimgeour, C. M. (1997). The influence of anoxia on plants of saline habitats with special reference to the Sulfur cycle. *Ann. Bot.* 79, 79–86. doi: 10.1093/oxfordjournals.aob.a010309

Revsbech, N. P. (1989). An oxygen microsensor with a guard cathode. *Limnol. Oceanogr.* 34, 474–478. doi: 10.4319/lo.1989.34.2.0474

Richardson, S. L. (2006). Response of epiphytic foraminiferal communities to natural eutrophication in seagrass habitats off Man O'War Cay, Belize. *Mar. Ecol.* 27, 404–416. doi: 10.1111/j.1439-0485.2006.00096.x

Robblee, M. B., Barber, T. R., Carlson, P. R. Jr., Durako, M. J., Fourqurean, J. W., Muehlstein, L. K. et al. (1991). Mass mortality of the tropical seagrass *Thalassia testudinum* in Florida Bay (USA). *Mar. Ecol. Prog. Ser.* 71, 297–299.

Sand-Jensen, K. (1977). Effect of epiphytes on eelgrass photosynthesis. *Aquat. Bot.* 3, 55–63. doi: 10.1016/0304-3770(77)90004-3

Sand-Jensen, K., and Borum, J. (1991). Interactions among phytoplankton, periphyton, and macrophytes in temperate freshwaters and estuaries. *Aquat. Bot.* 41, 137–175. doi: 10.1016/0304-3770(91)90042-4

Seddon, S., Connolly, R., and Edyvane, K. S. (2000). Large-scale seagrass dieback in northern Spencer Gulf, South Australia. *Aquat. Bot.* 66, 297–310. doi: 10.1016/S0304-3770(99)00080-7

Spilling, K., Titelman, J., Greve, T. M., and Kühl, M. (2010). Microsensor measurements of the external and internal microenvironment of *Fucus vesiculosus* (Phaeophyceae). *J. Phycol.* 46, 1350–1355. doi: 10.1111/j.1529-8817.2010.00894.x

Steen-Knudsen, O. (2002). *Biological Membranes: Theory of Transport, Potentials and Electric Impulses*. Cambridge, UK: Cambridge University Press.

Webb, W. L., Newton, M., and Starr, D. (1974). Carbon-dioxide exchange of *Alnus-rubra* - mathematical-model. *Oecologia* 17, 281–291. doi: 10.1007/BF00345747

Zieman, J. C., Fourqurean, J. W., and Frankovich, T. A. (1999). Seagrass die-off in Florida Bay: long-term trends in abundance and growth of turtle grass, *Thalassia testudinum*. *Estuaries* 22, 460–470. doi: 10.2307/1353211

Zimmerman, R. C., and Alberte, R. S. (1996). Effect of light/dark transition on carbon translocation in eelgrass *Zostera marina* seedlings. *Mar. Ecol. Prog. Ser.* 136, 305–309. doi: 10.3354/meps136305

Conflict of Interest Statement: The authors declare that the research was conducted in the absence of any commercial or financial relationships that could be construed as a potential conflict of interest.

Appendix 2

Poster Presentations

Attached in the following order:

(i) The 11th International Seagrass Biology Workshop (ISBW11), held in Sanya, China (2014). Winner of poster award.

(ii) The annual PhD day at BIO, University of Copenhagen, held in Copenhagen, Denmark (2015).

(iii) EUROPT[R]ODE XIII conference on optical chemical sensors and biosensors, held in Graz, Austria (2016).

ISBW11, 2014

UTS: C3 PLANT FUNCTIONAL BIOLOGY & CLIMATE CHANGE CLUSTER

UNIVERSITY OF TECHNOLOGY SYDNEY

Seagrasses actively modify their below-ground geochemical microenvironment: a microsensor study of *Zostera muelleri*

Kasper Elgetti Brodersen[1], Daniel A. Nielsen[1], Peter J. Ralph[1] and Michael Kühl[1,2]

[1] Plant Functional Biology and Climate Change Cluster, University of Technology, Sydney, Australia
[2] Marine Biological Section, University of Copenhagen, Denmark

Background

- Seagrass meadows constitute globally important marine ecosystems; supporting high marine biodiversity and protecting coastal areas from erosion.
- Over the past century, the worldwide extent of seagrass meadows have declined with an alarming rate, and in order to better manage these vital marine habitats for long-term preservation, new insight into the possible geochemical mechanisms behind these die-backs is crucial.

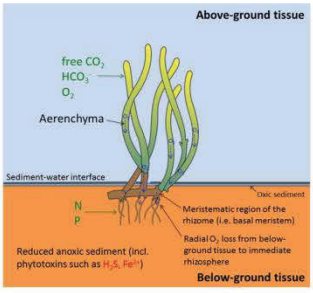

Fig. 1 Conceptual diagram illustrating the biogeochemical processes of *Zostera muelleri* spp. *capricorni*. Passive (night-time) or actively (day-time) evolved O_2 is transported down to the below-ground tissue through low-resistance internal gas channels (i.e. the aerenchyma) and is subsequently lost to the immediate rhizosphere. Thus potentially providing protection against sediment-produced reduced, phytotoxic compounds.

Aim & Hypothesis

- Can seagrasses actively alter their below-ground biogeochemical microenvironment through the release of chemical compounds?

Materials & Methods

- Electrochemical microsensors and planar optodes were used in combination with a custom-made split flow-chamber with artificial, transparent sediment, to investigate the below-ground chemical microenvironment of *Zostera muelleri ssp. capricorni* under changing environmental conditions.

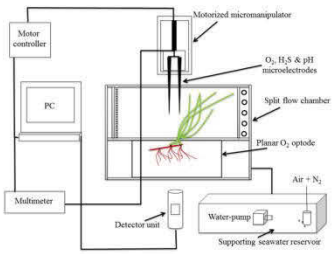

Fig. 2 Experimental setup. Microsensor positioning and data acquisition was achieved via dedicated PC software (SensorTracePro, Unisense A/S; VisiSens, PreSens).

Results: Chemical microenvironment

- Oxic microshield & local pH enhancement provide protection against sediment-produced reduced phytotoxins, such as H_2S.
- During water-column hypoxia, the oxic microzone around the meristematic tissue was significantly reduced, resulting in high levels of H_2S reaching the tissue surface and a concomitant decrease in the plants overall viability

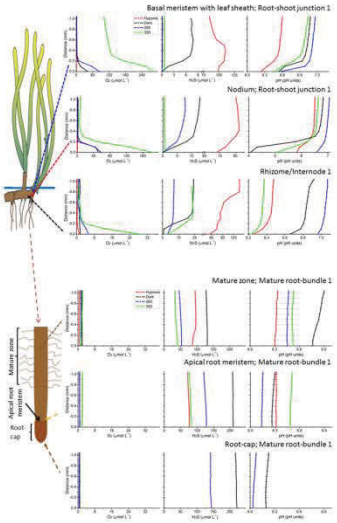

Fig. 3 Dynamics of the below-ground chemical microenvironment determined during light-dark transitions, as well as during an over-night water-column hypoxia event. Legend depicts the different experimentally manipulated treatments (light intensity in $\mu E\ m^{-2}\ s^{-1}$). Y-axis = 0 indicate the below-ground tissue surface. n=3.

Oxic microshield

- Radial O_2 loss from the basal meristem with leaf sheath lead to the formation of a ~300 µm wide oxic microzone around the meristematic tissue, wherein no (or very low levels of) H_2S could be observed at the tissue surface despite high concentrations in the surrounding artificial sediment (i.e. >200 µmol $H_2S\ L^{-1}$).
- A significant decrease in pH within the oxic microzone was also detected which could play an important role in the release of sediment-bound phosphorus in natural systems.

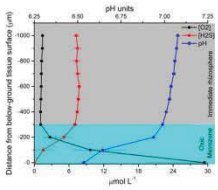

Fig. 4 Microelectrode measurements towards the below-ground tissue surface (at y-axis = 0) visualising the protecting oxic microshield and a concomitant decrease in pH and H_2S. The latter was most likely due to the formation of sulphuric acid produced via the chemical reaction between plant-mediated O_2 and sediment-produced H_2S. n=3

2D O_2 microdistribution

- Actively growing roots leak O_2 from around the apical root meristem, thereby oxidizing the surrounding below-ground microenvironment, as they grow through the reduced sediment.

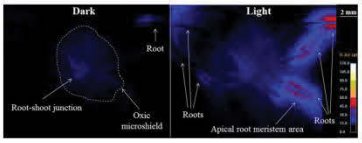

Fig. 5 Two-dimensional O_2 image of actively growing *Z. muelleri* roots (colour coded). The O_2 distribution was determined during a light-dark transition. Legend depicts the O_2 concentration in % air saturation.

Conclusion: Chemical defence mechanism revealed

Below-ground geochemical microenvironment

- Seagrasses actively alter their below-ground geochemical microenvironment through the release of chemical compounds, such as O_2, and thereby accommodate their own growth.

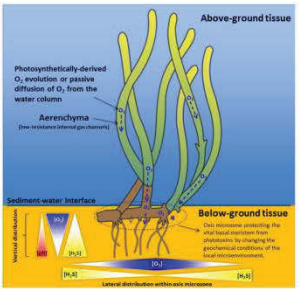

Fig. 6 Conceptual diagram visualising the major findings of the present study. Hence, a local oxic microzone around the root-shoot junctions protecting the active parts of the below-ground tissue from reduced, toxic compounds produced in the surrounding sediment through microbial metabolisms.

Chemical defence mechanism

- *Z. muelleri* can thus protect itself against phytotoxic H_2S by modifying its below-ground geochemical microenvironment through the release of chemical compounds, a vital chemical defence mechanism that becomes highly inefficient during over-night water-column hypoxia.

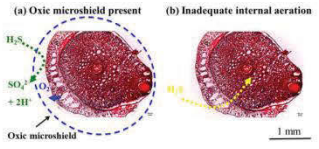

Fig. 7 Cross tissue sections from the basal meristem region. (a) Protecting (external) oxic microshield present. (b) Inadequate internal aeration may lead to sulphide intrusion.

Acknowledgements: We thank Ole Pedersen, Jens Borum, Verena Schrameyer, Milan Szabo and Mathieu Pernice. This project was funded by the Australian Research Council (ARC) and the Danish Council for Independent Research | Natural sciences.

Corresponding author: kasper.e.brodersen@student.uts.edu.au

Publications: Brodersen et al. 2014. A split flow-chamber with artificial sediment to examine the below-ground microenvironment of aquatic macrophytes. *Marine Biology* DOI: 10.1007/s00227-014-2542-3

Brodersen et al. 2014. Oxic microshield and local pH enhancement protects *Zostera muelleri* from sediment derived hydrogen sulphide. *New Phytologist* DOI: 10.1111/nph.13124

Seagrass illustration in Fig 1 and 6 originate from the IAN Image library. Diana Kleine, Integration and Application Network, University of Maryland, Center for Environmental Science (ian.umces.edu/imagelibrary/).

PhD Day at BIO, 2015

Epiphytic microalgae on seagrass leaves impede photosynthesis and radial O_2 loss from the roots

Mads Lichtenberg, Kasper Elgetti Brodersen, Laura-Carlota Paz, Michael Kühl
Marine Biological Section, Department of Biology, University of Copenhagen

UNIVERSITY OF COPENHAGEN

Background

- Seagrass leaves are often covered by epiphytic algae and bacteria that change the surface topography and physico-chemical environment on the leaf.
- Heavy epiphyte load has been correlated with eutrophication and seagrass beds are declining globally due to direct and indirect human interference.
- We investigated direct effects of epiphyte cover on the light microclimate, photosynthesis, and rhizosphere O_2 microenvironment of the seagrass *Zostera marina*, where the latter plays an important role in the chemical defense against intrusion of phyto-toxic H_2S from the surrounding sediment.

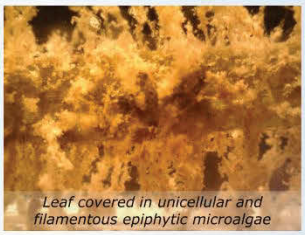

Leaf covered in unicellular and filamentous epiphytic microalgae

Results

- Light was reduced by 92% at the seagrass surface compared to the irradiance level above the epiphyte canopy.
- The diffusive boundary layer (DBL) was about 4 times thicker in the presence of epiphytes, impeding the O_2 exchange between seagrass leaves and the seawater.
- Under epiphyte cover, seagrass net photosynthesis was lower at all irradiances, resulting in a 2-fold increase in compensation irradiance compared to epiphyte free leaves.
- Lower seagrass photosynthesis resulted in a decreased aerenchymatic transport of O_2 to the rhizome and a reduced flux of O_2 into the rhizosphere.
- In darkness no O_2 was detectable at the root surface of plants with epiphyte cover.

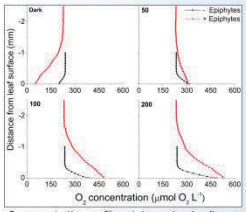

*O_2 concentration profiles at increasing irradiances (Dark, 50, 100, 200 µmol photons m^{-2} s^{-1}) measured on leaves **with** and **without** epiphyte cover.*

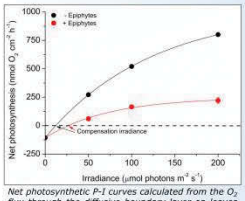

*Net photosynthetic P-I curves calculated from the O_2 flux through the diffusive boundary layer on leaves **with** and **without** epiphyte cover.*

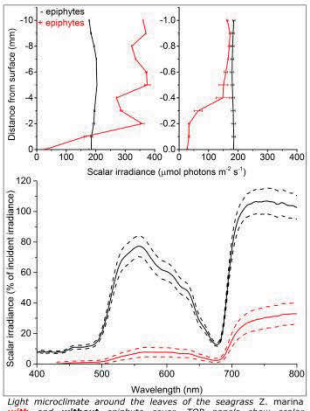

*Light microclimate around the leaves of the seagrass Z. marina **with** and **without** epiphyte cover. TOP panels show scalar irradiance profiles towards the surface of the leaves and BOTTOM panel show the light transmitted through a leaf **with** and **without** epiphyte cover.*

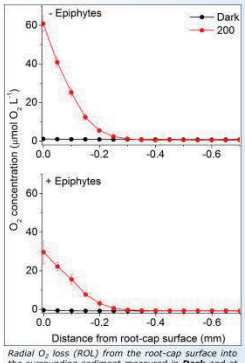

*Radial O_2 loss (ROL) from the root-cap surface into the surrounding sediment measured in **Dark** and at **200 µmol photons m^{-2} s^{-1}** in plants with- and without epiphyte cover.*

Conclusion

- Reduced light conditions at the leaf surface of the seagrass *Zostera marina* impeded overall plant performance during daytime.
- Epiphyte cover increases the DBL thickness impeding mass transfer.
  - In light this creates a build up of O_2 at the leaf surface → increased risk of photorespiration.
  - In dark this negatively affects the intra-plant O_2 status.
- Higher compensation irradiance → longer time of net O_2 consumption in the whole plant.
- Lower photosynthesis in epiphyte covered seagrass leaves results in much lower oxidation capability of below-ground tissues
- Under epiphyte-cover, the plant is thus more vulnerable to H_2S intrusion via the roots, causing reduced plant fitness.

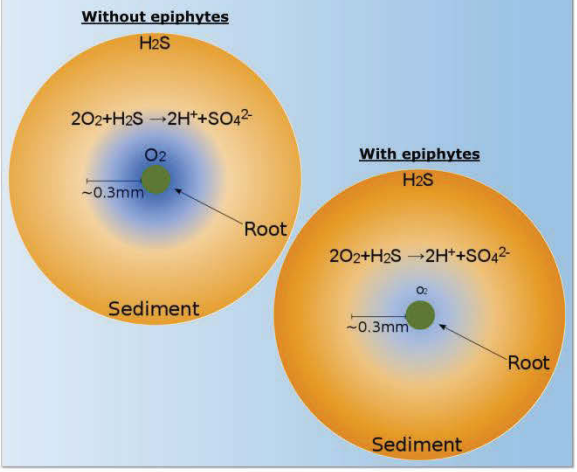

Methods

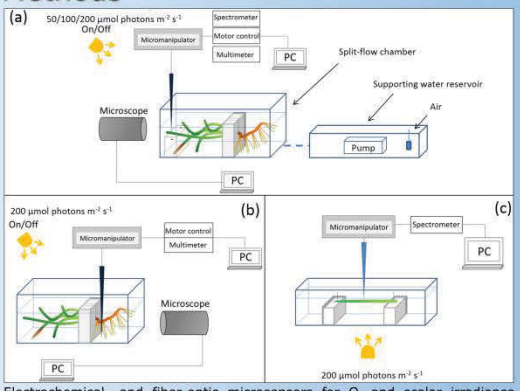

Electrochemical- and fiber-optic microsensors for O_2 and scalar irradiance were used to quantify the impact of epiphytes on the leaf surface light-microclimate, plant photosynthesis, and radial O_2 loss from the roots of the seagrass *Z. marina*. A custom-made split flow chamber allowed microsensor measurements in the leaf canopy and in the sediment covered rhizosphere.

Brodersen KE*, Lichtenberg M*, Paz L-C and Kühl M (2015) Epiphyte-cover on seagrass (*Zostera marina* L.) leaves impedes plant performance and radial O_2 loss from the below-ground tissue. *Frontiers in Marine Science* **2:58**. doi: 10.3389/fmars.2015.00058

EUROPT[R]ODE XIII, 2016

faculty of science
university of copenhagen

Optical Sensor Nanoparticles in Artificial Sediments – a New Tool to Visualize O_2 and pH Dynamics Around the Rhizome and Roots of Seagrasses

Klaus Koren[a], Kasper E. Brodersen[b], and Michael Kühl[ab]

a Marine Biology Section, Department of Biology, University of Copenhagen, 3000 Helsingør, Denmark
b Plant Functional Biology and Climate Change Cluster, University of Technology Sydney, Australia

porphyrin24@gmail.com

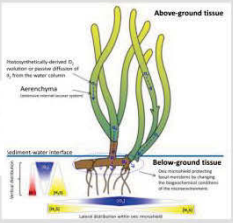

Abstract

Seagrasses are flowering aquatic plants that have adapted to growing in H_2S rich sediments. As part of this adaptation, seagrasses can alter the chemical microenvironment around their below-ground tissue e.g. by releasing O_2 from the roots and other parts of the rhizome to provide protection against H_2S intrusion [1]. In order to visualize and quantify such microenvironmental dynamics, optical O_2 and pH sensor nanoparticles were incorporated into an artificial, optically transparent sediment [2, 3]. The sensor nanoparticles contained both an analyte-sensitive indicator dye and an inert reference dye, enabling sensor readout via the use of ratiometric RGB imaging with a normal SLR camera.

Results

Imaging Setup

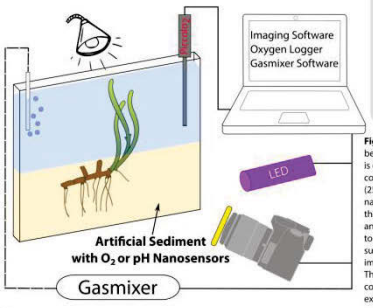

Figure 1: Experimental setup. The below-ground tissue of the seagrass is embedded in an artificial sediment consisting of buffered H_2S rich (250µM) agar. The O_2 or pH sensitive nanoparticles are dispersed within this artificial sediment. A SLR camera and LED are mounted perpendicular to the transparent chamber wall. Gas supply and reference optode are immersed in the overlaying water. The temperature of the setup is controlled by a immersed heater and external illumination is provided.

Nanosensors - Materials and Calibrations

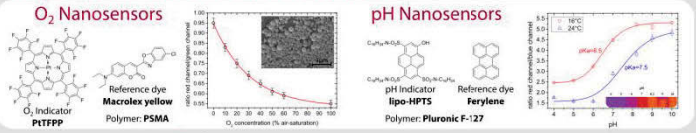

O_2 Imaging

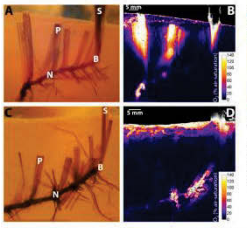

Figure 3: Structural images of the seagrass *Z. muelleri* mounted in the artificial sediment (A, C) and the respective false color images of the O_2 concentration distribution (B, D). Several plant structural elements are pointed out: S – shoot, N - nodium, P – prophyllum, B - basal meristem

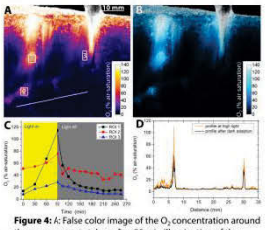

Figure 4: A: False color image of the O_2 concentration around the seagrass roots taken after 90 min illumination of the leaves B: As O_2 depletion image visualizing the change in O_2 concentration between the end of the light period and 130 min in the dark. C: time profile of the 3 ROIs over the light-dark exposure experiment. D: line profile (line shown in A) across some small roots

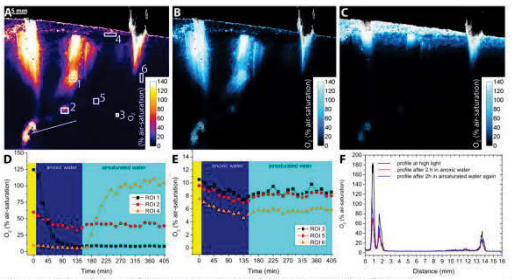

Figure 5: A: False color image of the O_2 concentration around the seagrass roots taken after 90 min illumination of the leaves at 500 µmol photons $m^{-2}s^{-1}$. Oxygen dynamics pictures visualizing the change in oxygenation between the time points 0 min (light) and 135 min (anoxic water) (B) and between the time points 135 min (anoxic water) and 405 min (airsatu-rated water) (C). D-E: time profile of the 6 ROIs. F: line profile across some small roots at the time points 0, 120 and 240 min

pH Imaging

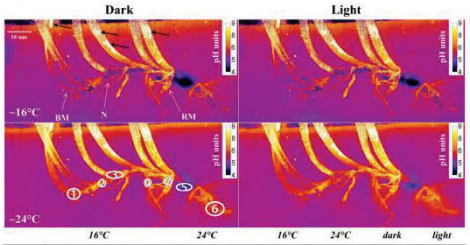

	16°C		24°C		16°C	24°C	dark	light
	dark	light	dark	light	dark/light	dark/light	16/24°C	16/24°C
	pH	pH	pH	pH	ΔpH	ΔpH	ΔpH	ΔpH
ROI 1	5.8±0.0	5.8±0.0	6.4±0.0	6.4±0.0	0.0	0.1	0.6	0.6
ROI 2	5.6±0.0	5.7±0.1	6.3±0.0	6.5±0.1	0.1	0.2	0.7	0.8
ROI 3	5.6±0.0	5.7±0.1	6.3±0.0	6.4±0.1	0.1	0.2	0.7	0.7
ROI 4	6.7±0.0	6.7±0.1	6.6±0.0	6.8±0.0	0.0	0.2	-0.1	0.1
ROI 5	3.9±0.0	4.2±0.1	4.8±0.0	4.9±0.0	0.3	0.1	0.9	0.7
ROI 6	5.9±0.0	6.0±0.1	6.3±0.0	6.6±0.1	0.1	0.3	0.5	0.7
ROI 7	6.6±0.1	6.9±0.2	7.1±0.0	7.4±0.1	0.2	0.2	0.5	0.5

Figure 2: pH images of the rihizome of seagrass *Zostera marina L.* exposed to darkness and light at two temperatures (16 and 24°C). The table presents values in selected regions of interest (ROI) within the immediate rhizosphere. Values are given as a mean of the entire ROI ± S.E; and as the relative difference in pH between the experimentally changed environmental conditions (ΔpH). n = 5-18

Conclusion

Using this setup, it was possible to localize chemical hotspots in the rhizosphere and to resolve changes in belowground O_2 and pH levels at high spatio-temporal resolution. Light/dark shifts yielded pronounced changes in the chemical microenvironment that could be analyzed in detail via dedicated analysis and processing software. The novel imaging setup enabled the investigation of effects caused by changing water-column temperature and O_2 content on the chemical below-ground microenvironment; an important factor in understanding the plants ability to cope with environmental stressors in a changing world.

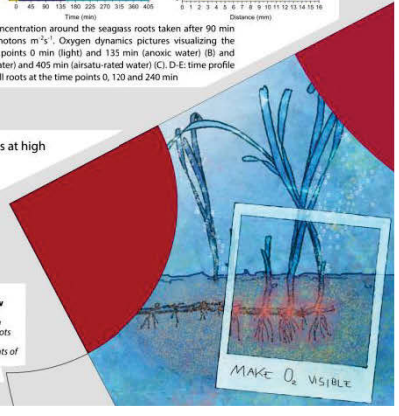

Acknowledgement

We thank Dr. Daniel A. Nielsen for helping with the experimental setup and for fruitful discussions and Sofie Jakobsen for technical assistance. This study was funded by research grants from the Australian Research Council (MK), the Danish Council for Independent Research | Natural Sciences (MK), the Villum Foundation (MK, KK), the Augustinus Foundation (KEB) and PA Fiskers Fund (KEB).

VILLUM FONDEN
DET FRIE FORSKNINGSRÅD
DANISH COUNCIL FOR INDEPENDENT RESEARCH

References

1: K. E. Brodersen, D. A. Nielsen, P. J. Ralph, M. Kühl. *Oxic microshield and local pH enhancement protects Zostera muelleri from sediment derived hydrogen sulphide* **New Phytol.** 2015, 205, 1264–1276.
2: Koren, K.; Brodersen, K. E.; Jakobsen, S. L.; Kühl, M. *Optical Sensor Nanoparticles in Artificial Sediments-A New Tool To Visualize O2 Dynamics around the Rhizome and Roots of Seagrasses* **Environ. Sci. Technol.** 2015, 49, 2286–2292.
3: Brodersen K. E, Koren K, Lichtenberg M, Kühl M. *Nanoparticle-based measurements of pH and O2 dynamics in the rhizosphere of Zostera marina L.: Effects of temperature elevation and light-dark transitions* **Plant Cell Environ.** in press

Appendix 3

Oral presentation

The 52nd Australian Marine Science Association (AMSA) conference, held in Geelong, Australia (2015).

O_2 and pH microdynamics around the rhizome and roots of seagrasses determined via novel optical nanoparticle-based sensors

Kasper Elgetti Brodersen, Klaus Koren & Michael Kühl

Abstract

Seagrasses provide important eco-engineering services in coastal environments but have over the past century been declining with alarming rates mainly due to anthropogenic activity. Seagrasses are constantly challenged to aerate their belowground tissue and the surrounding sediment to prevent intrusion of reduced, phytotoxic compounds, such as hydrogen sulfide (H_2S), and to ensure aerobic metabolism. In present study, we developed a novel bioimaging approach to determine O_2 and pH microdynamics and distributions around the belowground tissue of seagrasses by means of optical nanoparticle-based O_2 and pH sensors incorporated into transparent, artificial sediments consisting of a deoxygenated, pH-buffered, sulphidic seawater/agar matrix. Seagrass growth and photosynthetic activity did not seem affected by the experimental setup/conditions based on root growth rates (~5 mm d^{-1}) and photosynthetic quantum yields (~0.7); which both were comparable to healthy seagrasses growing in their natural habitat. Oxygen release and the pH heterogeneity were visualised and analysed on a whole rhizosphere level, which is a substantial improvement to existing methods such as via microsensors and/or planar optodes. Our images determined higher O_2 release from the belowground tissue in light as compared to darkness, and that water-column hypoxia leads to reduced O_2 levels around the rhizome and roots. We found

pronounced spatial pH microheterogeneity within the immediate rhizosphere of *Z. marina L*. Light exposure of the leaf canopy and elevated temperature resulted in higher rhizosphere pH levels (rhizome/roots surface ΔpH of up to 0.9 pH units). Low rhizosphere pH microenvironments (pH levels down to ~4) appeared to correlate with the plant-mediated oxic microniches, although the rhizoplane/tissue surface pH levels overall were much higher than the pH of the surrounding sediment (~0.4 pH units higher). Seagrasses thus alters the pH levels of their immediate rhizosphere, an important chemical defence mechanism that further alleviates the H_2S toxicity in the rhizosphere through geochemical speciation shift of sulphide towards non-tissue-permeable HS^- ions, as well as the plant-derived low pH microenvironments may lead to nutrient mobilization that then becomes available for plant assimilation.

Appendix 4

Additional manuscripts

Abstracts from additional manuscripts which represent work performed during my PhD are attached in the following order:

(i) **Paul York *et al*.** Identifying knowledge gaps in seagrass research and management: an Australian perspective. (Submitted).

(ii) **Anthony W. D. Larkum *et al*.** Photosynthesis and metabolism of Seagrasses. In: AWD Larkum, G Kendrick, PJ Ralph, eds. *Seagrasses of Australia*. Book chapter 16. (In review).

(iii) **Mikael Kim *et al*.** Low oxygen affects photorespiration and the level of expression of two carbon metabolism genes in the seagrass *Zostera muelleri*. (In prep.).

(iv) **Verena Schrameyer *et al*.** Shading effects on O_2 and H_2S conditions in sandy sediments inhabited by tropical seagrasses: comparison of deep and shallow water meadows (In prep.).

Identifying knowledge gaps in seagrass research and management: an Australian perspective

Paul H. York*, Timothy M. Smith, Rob G. Coles, Skye A. McKenna, Rod M. Connolly, Andrew D. Irving, Emma L. Jackson, Kathryn McMahon, John W. Runcie, Craig D. H. Sherman, Brooke K. Sullivan, Stacy M. Trevathan-Tackett, **Kasper E. Brodersen**, Alex B. Carter, Carolyn J. Ewers, Paul S. Lavery, Chris M. Roelfsema, Elizabeth A. Sinclair[1], Simone Strydom, Jason E. Tanner, Kor-jent van Dijk, Fiona Y. Warry, Michelle Waycott, Sam Whitehead

*Corresponding author: Paul York (TropWATER, JCU, Cairns), email: paul.york@jcu.edu.au

Abstract

Seagrass species form important marine and estuarine habitats providing valuable ecosystem services and functions. Coastal zones that are increasingly impacted by anthropogenic development have experienced substantial declines in seagrass abundance around the world. Australia, which has some of the world's largest seagrass meadows and is home to over half of the known species, is not immune to these losses. In 1999 a review of seagrass ecosystems knowledge was conducted in Australia and strategic research priorities were developed to provide research direction for future studies and management. Subsequent rapid evolution of seagrass research and scientific methods has led to more than 70% of peer reviewed seagrass literature being produced since that time. A workshop was held as part of the Australian Marine Sciences Association conference in July 2015 in Geelong, Victoria, to update and redefine strategic priorities in seagrass research. Participants identified 40 research questions from 10 research fields (taxonomy and systematics, physiology, population biology, sediment biogeochemistry and microbiology, ecosystem function, faunal habitats, threats, rehabilitation and restoration, mapping and monitoring, management tools) as priorities for future research on Australian seagrasses. Progress in research will rely on advances in areas such as remote sensing, genomic tools, microsensors, computer modeling, and statistical analyses. A more interdisciplinary approach will be needed to facilitate greater understanding of the complex interactions among seagrasses and their environment.

Chapter 16: Seagrasses of Australia

Photosynthesis and metabolism of Seagrasses

Anthony W. D. Larkum, Gaurav Sablok, Mathieu Pernice, Martin Schliep, Peter Davey, Milan Szabo, John A. Raven, Mads Lichtenberg, **Kasper E. Brodersen**, Peter J. Ralph

Conclusions

Previous reviews (see e.g. Larkum et al. 2006) have dealt extensively with several topics and for this reason this chapter has dealt on a narrower range of topics. These are:

a) the uptake of inorganic carbon by the leaves of seagrasses,
b) the biochemistry of carbon fixation in photosynthesis,
c) the influence of anatomy on photosynthesis and gaseous transport to the rhizome and roots, and,
d) the effect of epiphytes on photosynthesis.

Of these four topics the one most extensively treated here is the first, the uptake of inorganic carbon from the ambient seawater. This is because there are large lacunae in our knowledge of these processes, which are so profoundly important to our understanding of how seagrasses have become so successful in our seas over the last 100 million years or so and how today they are so important for the production of “blue carbon”. The second topic (b) is noteworthy because modern “omics” and real-time PCR approaches promises to throw light on a topic that has defied research efforts over a long period. However, we will have to wait to see whether the actuality of a C4 type of photosynthetic metabolism is eventually proved in seagrasses.

Low oxygen affects photorespiration and the level of expression of two carbon metabolism genes in the seagrass *Zostera muelleri*

Mikael Kim, Mathieu Pernice*, **Kasper Elgetti Brodersen**, Milan Szabo, Gaurav Sablok, Anthony W. D. Larkum, John A. Raven, and Peter J. Ralph

*Corresponding author: Mathieu Pernice (UTS), email: mathieu.pernice@uts.edu.au

Abstract

Seagrasses are a group of marine angiosperms that evolved approximately 100 million years ago to live in shallow coastal waters, an environment regularly subjected to changes in oxygen and irradiance. Of the 72 identified species of seagrass, *Zostera muelleri* is the dominant species in south-eastern Australia, and is critical for healthy coastal ecosystems, which underpin tourism, substance gathering and fishing for coastal population in Australia. Despite its important role as ecological engineer and carbon sink, little is known about the pathways of carbon fixation in *Z. muelleri* and their regulation in response to environmental changes. Further, there is no consensus in the scientific community as to whether *Z. muelleri* is strictly a C3 plant or a C3-C4 intermediate. In this study, the response of *Z. muelleri* exposed to anoxic conditions was investigated by using (i) O_2 microsensors in combination with custom made flow chamber to measure changes in photosynthetic rates (i.e. photosynthetic efficiency, maximum photosynthetic rate, compensation irradiance, saturating irradiance and dark respiration rate) and (ii) Reverse Transcription quantitative real-time PCR (RT-qPCR) to measure changes in expression levels of key genes in C4 metabolism (i.e. genes coding for phospho*enol*pyruvate carboxylase and carbonic anhydrase). We found that lower levels of oxygen (i) increased photosynthetic efficiency in *Z. muelleri*, a characteristic of C3 mechanism of carbon assimilation, and (ii) decreased the expression level of key genes in C4 metabolism (i.e. genes coding for phospho*enol*pyruvate carboxylase and carbonic anhydrase). These results suggest that regulation of photosynthesis in *Z. muelleri* might involve a close collaboration between the C3 and C4 metabolic pathways. Overall, this study highlights that the photosynthetic response of *Z. muelleri* to changing oxygen is highly dynamic and should be considered when assessing seagrass primary production in shallow coastal waters.

Shading effects on O_2 and H_2S conditions in sandy sediments inhabited by tropical seagrasses: comparison of deep and shallow water meadows

Verena Schrameyer[#], Paul York[#], Katie Chartrand, Peter J. Ralph, Michael Kühl, **Kasper Elgetti Brodersen**[*], Michael A. Rasheed

[#]These authors contributed equally to this work and therefore share the first authorship

*Corresponding author: elgetti@hotmail.com (Kasper Elgetti Brodersen)

Abstract

Seagrass meadows increasingly experience reduced light quality and availability, as a result of anthropogenic impacts owing to coastal development, agricultural practices, but also due to climate change induced increased rainfall resulting silt plumes. This study examined the impact of reduced incoming photon irradiance upon seagrass biomass and sediment biogeochemistry within shallow- and deep-water seagrass meadows at Green Island, Australia. We also compared un-vegetated versus seagrass vegetated sites at both depths. Artificial shading (down to ~20% of incoming solar irradiance) was applied in shallow- and deep-water sites for up to two weeks. Sediment cores were sampled and analysed using O_2 and H_2S microsensors. Higher diffuse O_2 uptake (DOU) rates, volume-specific O_2 consumption (R) rates and lower O_2 penetration depths were found in seagrass vegetated areas as compared to un-vegetated areas at the shallow-water sites. Sediment characteristics at the deep-water sites did not differ between un-vegetated and vegetated sites. At the shallow-water site, shading resulted in slightly decreased biomass albeit not significant, and significantly lower hydrogen sulphide (H_2S) levels in the sediment. No shading effects on sediment biogeochemistry were found at deep-water site. Overall our results show that the below-ground sediment biogeochemistry of shallow- and deep-water seagrass meadows differ in dependency on incident photon irradiance, where our findings indicate that the microbial community in shallow-water sites are much more abundant and directly linked to the seagrass productivity and health.

Keywords: carbonate sediment, hydrogen sulphide, light, O_2 demand, seagrass, shading, tropical

"To love you must understand

To understand you must explore

Every journey begins with an idea

Let's hunt some microbes"

The End